THE FUNCTION OF PHAGOCYTES IN NON-MAMMALS

EDITED BY: Xinjiang Lu, Qing Deng and Kim Dawn Thompson
PUBLISHED IN: Frontiers in Immunology

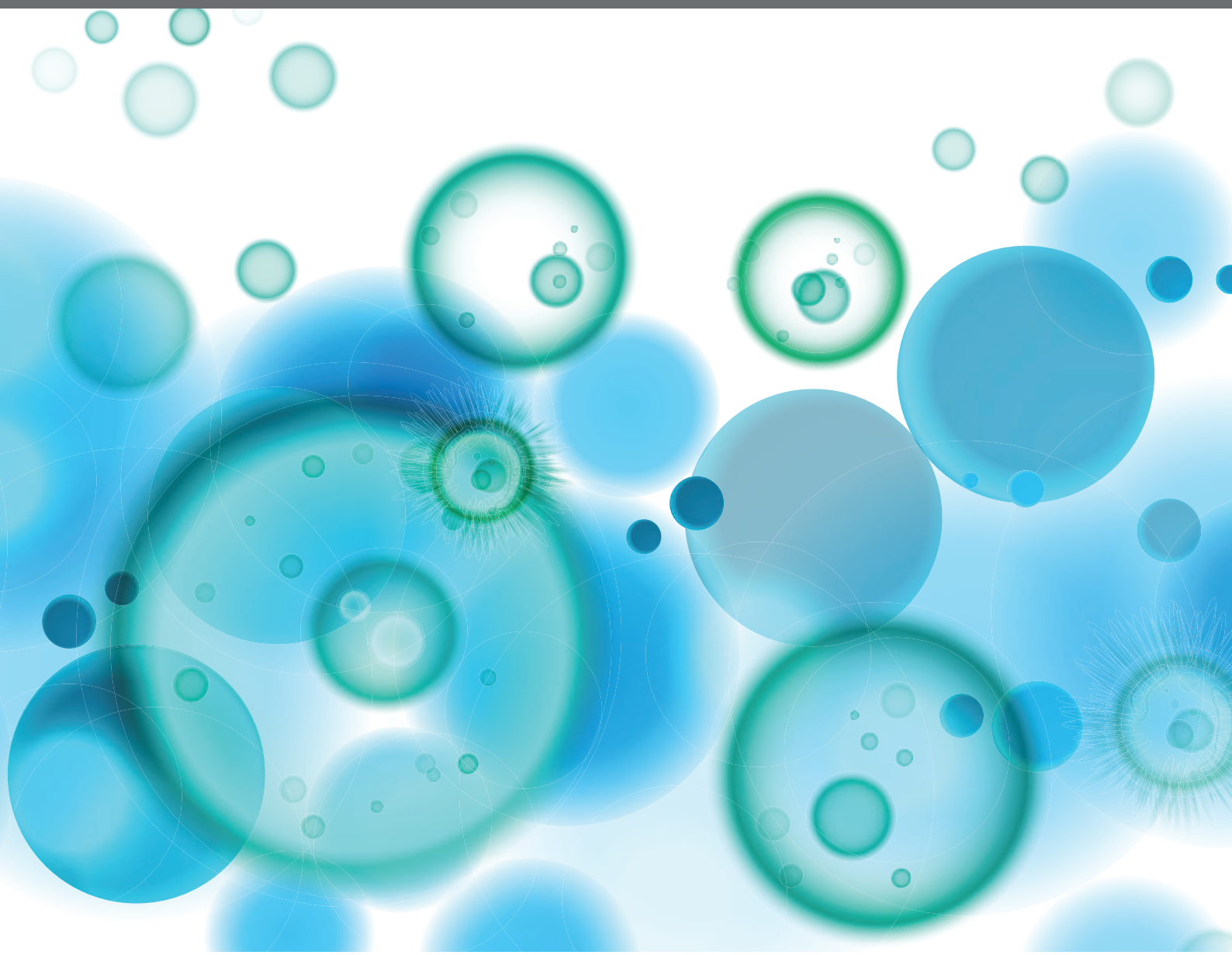

frontiers Research Topics

frontiers

ISSN 1664-8714
ISBN 978-2-88966-438-2
DOI 10.3389/978-2-88966-438-2

About Frontiers

Frontiers is more than just an open-access publisher of scholarly articles: it is a pioneering approach to the world of academia, radically improving the way scholarly research is managed. The grand vision of Frontiers is a world where all people have an equal opportunity to seek, share and generate knowledge. Frontiers provides immediate and permanent online open access to all its publications, but this alone is not enough to realize our grand goals.

Frontiers Journal Series

The Frontiers Journal Series is a multi-tier and interdisciplinary set of open-access, online journals, promising a paradigm shift from the current review, selection and dissemination processes in academic publishing. All Frontiers journals are driven by researchers for researchers; therefore, they constitute a service to the scholarly community. At the same time, the Frontiers Journal Series operates on a revolutionary invention, the tiered publishing system, initially addressing specific communities of scholars, and gradually climbing up to broader public understanding, thus serving the interests of the lay society, too.

Dedication to Quality

Each Frontiers article is a landmark of the highest quality, thanks to genuinely collaborative interactions between authors and review editors, who include some of the world's best academicians. Research must be certified by peers before entering a stream of knowledge that may eventually reach the public - and shape society; therefore, Frontiers only applies the most rigorous and unbiased reviews.
Frontiers revolutionizes research publishing by freely delivering the most outstanding research, evaluated with no bias from both the academic and social point of view. By applying the most advanced information technologies, Frontiers is catapulting scholarly publishing into a new generation.

What are Frontiers Research Topics?

Frontiers Research Topics are very popular trademarks of the Frontiers Journals Series: they are collections of at least ten articles, all centered on a particular subject. With their unique mix of varied contributions from Original Research to Review Articles, Frontiers Research Topics unify the most influential researchers, the latest key findings and historical advances in a hot research area! Find out more on how to host your own Frontiers Research Topic or contribute to one as an author by contacting the Frontiers Editorial Office: frontiersin.org/about/contact

THE FUNCTION OF PHAGOCYTES IN NON-MAMMALS

Topic Editors:
Xinjiang Lu, Ningbo University, China
Qing Deng, Purdue University, United States
Kim Dawn Thompson, Moredun Research Institute, United Kingdom

Citation: Lu, X., Deng, Q.,Thompson, K. D., eds. (2021). The Function of Phagocytes in Non-Mammals. Lausanne: Frontiers Media SA.
doi: 10.3389/978-2-88966-438-2

Table of Contents

frontiers in Immunology

EDITORIAL
published: 11 December 2020
doi: 10.3389/fimmu.2020.628847

Editorial: The Function of Phagocytes in Non-Mammals

Xin-Jiang Lu[1,2,3,4]*, *Qing Deng*[5]* and *Kim Dawn Thompson*[6]*

[1] State Key Laboratory for Managing Biotic and Chemical Threats to the Quality and Safety of Agro-products, Ningbo University, Ningbo, China, [2] Laboratory of Biochemistry and Molecular Biology, School of Marine Sciences, Ningbo University, Ningbo, China, [3] Key Laboratory of Applied Marine Biotechnology of Ministry of Education, Ningbo University, Ningbo, China, [4] Laboratory for Marine Biology and Biotechnology, Pilot National Laboratory for Marine Science and Technology, Qingdao, China, [5] Department of Biological Sciences, Purdue University, West Lafayette, IN, United States, [6] Aquaculture Research Group, Moredun Research Institute, Penicuik, United Kingdom

Keywords: phagocytes, non-mammals, macrophages, neutrophils, B cells, macrophage polarization, hemocytes, teleost

Editorial on the Research Topic

The Function of Phagocytes in Non-Mammals

Non-mammalian animals are useful models for understanding the evolution of the immune system and studying the underlying mechanisms of cellular and molecular responses in mammalian immunity. Recent literature has expanded the function of phagocytes beyond pathogen killing to tissue-supporting activities (1). In humans, many diseases that stem from dysregulated phagocyte function, such as congenital neutropenia, familial Mediterranean fever, and sepsis (2–4), still lack satisfactory treatment regimens. Because of the high degree of conservation present in basic functions of the innate immune system, it is our opinion that research on non-mammalian phagocytes will provide novel insight into new paradigms for mammalian phagocyte counterparts. For example, extracellular chromatin from phagocytes participates in host defenses found in both invertebrates and vertebrates (5). Indeed, the use of zebrafish models has advanced our understanding of phagocyte functions, in human tuberculosis, for example (6). The composition of phagocytes in non-mammals is more diverse. Phagocytes in mammals consist mainly of macrophages and neutrophils, while in teleosts, B lymphocytes and thrombocytes from peripheral blood also have potent phagocytic activity (7, 8). Teleost-specific genome duplication events produce genes with overlapping functions, potentially resulting in sub-functionalization in the teleost immune system. An example of this is CXCR3.1 and CXCR3.2 in teleosts, which differentially contribute to macrophage polarization (9).

The collection of 14 papers within this Research Topic contributes substantially to the development of research tools and improved understanding of the function and regulation of phagocytes in non-mammals. Wu et al. reviewed recent advances of phagocytic B cells and their microbicidal ability in teleosts. Experimental evidence demonstrated that in both teleosts and mammals, phagocytic B cells could recognize, take up, and destroy particulate antigens and then present those processed antigens to $CD4^+$ T cells to elicit adaptive immune responses. Future prospective studies will focus on the fundamental differences in phagocytic processes between B cells and classical phagocytes, such as macrophages and neutrophils. Linnerz et al. reviewed new findings of underlying cellular and molecular mechanisms for a variety of phagocyte responses in zebrafish. They also described signaling pathways that controlled the recruitment and fate of phagocytes at inflammatory sites of zebrafish. Furthermore, they demonstrated the limitations and opportunities for studying phagocytes in zebrafish, which found early embryonic and larval stages to be a good model for studying the innate immune response without

OPEN ACCESS

Edited and reviewed by:
Miki Nakao,
Kyushu University, Japan

***Correspondence:**
Xin-Jiang Lu
lxj711043@163.com
Qing Deng
deng67@purdue.edu
Kim Dawn Thompson
kim.thompson@moredun.ac.uk

Specialty section:
This article was submitted to Comparative Immunology, a section of the journal Frontiers in Immunology

Received: *13 November 2020*
Accepted: *20 November 2020*
Published: *11 December 2020*

Citation:
Lu X-J, Deng Q and Thompson KD (2020) Editorial: The Function of Phagocytes in Non-Mammals. Front. Immunol. 11:628847. doi: 10.3389/fimmu.2020.628847

interference of adaptive immunity. Sommer et al. reviewed the role of two main classes of chemokine receptors, the CC and CXC subtypes, in phagocyte migration in zebrafish models for cancer, infectious disease, and inflammation, with special emphasis on chemokine receptors and atypical chemokine receptors in shaping self-generated chemokine gradients. In addition, they used the functional antagonism between two paralogs of the CXCR3 family as an example to illustrate divergence and sub-functionalization of chemokine receptors in zebrafish.

Wentzel et al. described the metabolic signatures associated with macrophage polarization. They found decreased oxidative phosphorylation and increased glycolysis in M1 macrophages, while similar oxidative phosphorylation and glycolysis were found between M2 and control macrophages. Their results suggest that immunometabolic reprogramming determined the inflammatory phenotype of polarized macrophages in teleost fish such as carp, similar to what happens in mammals. Ultimately, this helps to improve our understanding of the fundamental mechanisms underlying energy metabolism and metabolic reprogramming of immune cells in teleost fish.

Liu S. et al. reviewed the current knowledge of hemocyte phagocytosis in crustaceans. The authors summarized phagocytosis related receptors for recognition and internalization of pathogens, as well as the downstream signal pathways and intracellular regulators involved in phagocytosis in crustaceans. Different subpopulation of hemocytes in diverse species of crustaceans exhibited variable phagocytic activities. Further investigation is necessary to reveal phagosome formation and maturation, as well as microbe destruction in the hemocytes of crustaceans. Liu C. et al. identified CD63 as a receptor that participates in immune recognition and hemocyte phagocytosis in oyster, and found CD63 to be recruited to the phagosomes after *Yarrowia lipolytica* stimulation. The CD63 receptor showed binding capacity to glucan, peptidoglycan, and lipopolysaccharide. Their work indicates that CD63 may function as a gateway between the pattern recognition of foreign invaders and the immune response of oysters. Lin et al. established a facile magnetic cell sorting method to enrich professional phagocytes from hemocytes of Hong Kong oyster. Pathway annotation of phagocytic processes of these hemocytes revealed that focal adhesion and extracellular matrix–receptor interactions were the most conspicuously enriched pathways in phagocytes by transcriptomic analysis. Focal adhesion kinase and heparan sulfate proteoglycans were identified as major regulators in anti-bacterial defense of hemocytes. Mao et al. isolated granulocytes and hyalinocytes by flow cytometry from Pacific oyster hemocytes. Cdc42 was identified as a core regulator of phagocytic pathways in these cells through an array of differentially expressed genes. The AP-1 transcription factor Fos was confirmed to facilitate functional differentiation of hemocytes in an assay on binding to target genes by the AP-1 binding site. Their works provide mechanistic underpinnings of functional differentiation of hemocytes in a marine invertebrate Pacific oyster.

Yaparla et al. investigated the production of phagocytes in amphibians. They confirmed that while the liver periphery of *Xenopus laevis* hosts hematopoietic stem cells and megakaryocyte/erythroid potentials, their bone marrow contains granulocyte/macrophage potentials. They also demonstrated that condition medium from *X. laevis* bone marrow cells chemo-attracts liver periphery and peripheral blood cells, supporting the concept that cells bearing granulocyte/macrophage potentials originate from the frog liver periphery. Sreekantapuram et al. established an *ex vivo* chicken whole-blood infection assay to analyze interactions between host cells and several model pathogens. Monocytes, and to a lesser extent heterophils, were shown to be associated with pathogens. They provide the first insight into quantitative interactions of three model pathogens with different immune cell populations in avian blood, demonstrating a broad spectrum of different characteristics during the immune response that depends on the pathogen and the chicken line. More-Bayona et al. evaluated the impact of xenobiotic mixtures on chicken immunity. An increase in resident macrophages and a decrease in $CD8^+$ lymphocytes were observed in the abdominal cavity after acute exposure to contaminated water. Leukocyte recruitment into the challenge site and activation of phagocyte antimicrobial responses were also affected. They emphasize that it is necessary to consider the impact of xenobiotic mixtures in the assessments of water quality.

Soto-Dávila et al. evaluated the effects of Vitamins D2 and D3 on the phagocytic response of Atlantic salmon (*Salmo salar* L.) primary macrophage cultures to *Aeromonas salmonicida*. Vitamin D is an essential nutrient for finfish aquafeeds, although its role in fish cell immunity is unknown. The authors found vitamin D3 to induce anti-bacterial innate immunity pathways in macrophages, affecting bacterial attachment, infection, and growth within the macrophage cultures. Vitamin D2, on the other hand, had no effect. Pérez-Stuardo et al. treated Atlantic salmon macrophage-enriched cell cultures, infected with *Piscirickettsia salmonis*, with non-specific IgM-enriched beads and evaluated the effect that this treatment had on lysosomal (pH change) and proteolytic activity. Treatment with the IgM-beads reversed the modulation of lysosomal activity induced by the bacterial infection and promoted macrophage survival and bacterial elimination. Park et al. highlighted the usefulness of imaging flow cytometry (IFC) in phagocyte research —a technique combining flow cytometry with digital microscopy to generate quantitative high-throughput imaging data. The authors used IFC to study phagocytic cells from Atlantic salmon, Nile tilapia (*Oreochromis niloticus*), and blue mussel (*Mytilus edulis*), including the effects of incubation temperature on their ability to phagocytose degradable particles *in vitro*. While phagocytosis by fish phagocytes was affected by the incubation temperature, no effect of temperature was noted on the activity of blue mussel phagocytes.

Overall, the content of this Research Topic reflects the significant growth and advances in the field of phagocytes in non-mammals. It contributes to improved mechanistic understanding, which is interrelated with evaluating both cellular and molecular biological approaches to investigate the function, mechanism, and production of phagocytes. Further characterization of phagocytes in non-mammals will be focused on more detail mechanisms and new methods, which is invaluable to understand the evolution of phagocytes.

AUTHOR CONTRIBUTIONS

All authors listed have made a substantial, direct, and intellectual contribution to the work and approved it for publication.

FUNDING

This project was supported by the Program for the Natural Science Foundation of China (41776151; 31972821), the Zhejiang Provincial Natural Science Foundation of China (LR18C040001; LZ18C190001), the Fundamental Research Funds for the Provincial Universities of Zhejiang (SJLZ2020002), and the National Institutes of Health (Grant R35GM119787 to QD).

ACKNOWLEDGMENTS

We would like to thank all authors for their contribution to this Research Topic.

REFERENCES

1. Bleriot C, Chakarov S, Ginhoux F. Determinants of resident tissue macrophage identity and function. *Immunity* (2020) 52:957–70. doi: 10.1016/j.immuni.2020.05.014
2. Muench DE, Olsson A, Ferchen K, Pham G, Serafin RA, Chutipongtanate S, et al. Mouse models of neutropenia reveal progenitor-stage-specific defects. *Nature* (2020) 582:109–14. doi: 10.1038/s41586-020-2227-7
3. Akula MK, Shi M, Jiang Z, Foster CE, Miao D, Li AS, et al. Control of the innate immune response by the mevalonate pathway. *Nat Immunol* (2016) 17:922–9. doi: 10.1038/ni.3487
4. Delano MJ, Ward PA. Sepsis-induced immune dysfunction: can immune therapies reduce mortality? *J Clin Invest* (2016) 126:23–31. doi: 10.1172/JCI82224
5. Robb CT, Dyrynda EA, Gray RD, Rossi AG, Smith VJ. Invertebrate extracellular phagocyte traps show that chromatin is an ancient defence weapon. *Nat Commun* (2014) 5:4627–7. doi: 10.1038/ncomms5627
6. Saralahti AK, Uusi-Mäkelä MIE, Niskanen MT, Rämet M. Integrating fish models in tuberculosis vaccine development. *Dis Model Mech* (2020) 13: dmm045716. doi: 10.1242/dmm.045716
7. Li J, Barreda D, Zhang YA, Boshra H, Gelman A, Lapatra S, et al. B lymphocytes from early vertebrates have potent phagocytic and microbicidal abilities. *Nat Immunol* (2006) 7:1116–24. doi: 10.1038/ni1389
8. Nagasawa T, Nakayasu C, Rieger AM, Barreda DR, Somamoto T, Nakao M. Phagocytosis by thrombocytes is a conserved innate immune mechanism in lower vertebrates. *Front Immunol* (2014) 5:445. doi: 10.3389/fimmu.2014.00445
9. Lu XJ, Chen Q, Rong YJ, Chen F, Chen J. CXCR3.1 and CXCR3.2 differentially contribute to macrophage polarization in teleost fish. *J Immunol* (2017) 198:4692–706. doi: 10.4049/jimmunol.1700101

Conflict of Interest: The authors declare that the research was conducted in the absence of any commercial or financial relationships that could be construed as a potential conflict of interest.

frontiers in Immunology

ORIGINAL RESEARCH
published: 14 January 2020
doi: 10.3389/fimmu.2019.03011

Effects of Vitamin D_2 (Ergocalciferol) and D_3 (Cholecalciferol) on Atlantic Salmon (*Salmo salar*) Primary Macrophage Immune Response to *Aeromonas salmonicida* subsp. *salmonicida* Infection

*Manuel Soto-Dávila[1], Katherinne Valderrama[1], Sabrina M. Inkpen[2], Jennifer R. Hall[3], Matthew L. Rise[2] and Javier Santander[1]**

[1] Marine Microbial Pathogenesis and Vaccinology Lab, Department of Ocean Sciences, Memorial University of Newfoundland, St. John's, NL, Canada, [2] Department of Ocean Sciences, Memorial University of Newfoundland, Ocean Science Centre, St. John's, NL, Canada, [3] Aquatic Research Cluster, CREAIT Network, Ocean Sciences Centre, Memorial University of Newfoundland, St. John's, NL, Canada

OPEN ACCESS

Edited by:
Kim Dawn Thompson, Moredun Research Institute, Norway

Reviewed by:
Jorge Galindo-Villegas, Nord University, Norway
Nawroz Kareem, Keele University, United Kingdom

***Correspondence:**
Javier Santander
jsantander@mun.ca

Specialty section:
This article was submitted to Comparative Immunology, a section of the journal Frontiers in Immunology

Received: *24 September 2019*
Accepted: *09 December 2019*
Published: *14 January 2020*

Citation:
Soto-Dávila M, Valderrama K, Inkpen SM, Hall JR, Rise ML and Santander J (2020) Effects of Vitamin D_2 (Ergocalciferol) and D_3 (Cholecalciferol) on Atlantic Salmon (Salmo salar) Primary Macrophage Immune Response to Aeromonas salmonicida subsp. salmonicida Infection. Front. Immunol. 10:3011. doi: 10.3389/fimmu.2019.03011

Vitamin D_2 (ergocalciferol) and vitamin D_3 (cholecalciferol) are fat-soluble secosteroid hormones obtained from plant and animal sources, respectively. Fish incorporates vitamin D_2 and D_3 through the diet. In mammals, vitamin D forms are involved in mineral metabolism, cell growth, tissue differentiation, and antibacterial immune response. Vitamin D is an essential nutrient in aquafeeds for finfish. However, the influence of vitamin D on fish cell immunity has not yet been explored. Here, we examined the effects of vitamin D_2 and vitamin D_3 on *Salmo salar* primary macrophage immune response to *A. salmonicida* subspecies *salmonicida* infection under *in vitro* conditions. We determined that high concentrations of vitamin D_2 (100,000 ng/ml) and D_3 (10,000 ng/ml) affect the growth of *A. salmonicida* and decrease the viability of *S. salar* primary macrophages. In addition, we determined that primary macrophages pre-treated with a biologically relevant concentration of vitamin D_3 for 24 h showed a decrease of *A. salmonicida* infection. In contrast, vitamin D_2 did not influence the antibacterial activity of the *S. salar* macrophages infected with *A. salmonicida*. Vitamin D_2 and D_3 did not influence the expression of canonical genes related to innate immune response. On the other hand, we found that *A. salmonicida* up-regulated the expression of several canonical genes and suppressed the expression of *leukocyte-derived chemotaxin 2* (*lect-2*) gene, involved in neutrophil recruitment. Primary macrophages pre-treated for 24 h with vitamin D_3 counteracted this immune suppression and up-regulated the transcription of *lect-2*. Our results suggest that vitamin D_3 affects *A. salmonicida* attachment to the *S. salar* primary macrophages, and as a consequence, the *A. salmonicida* invasion decreased. Moreover, our study shows that the positive effects of vitamin D_3 on fish cell immunity seem to be related to the *lect-2* innate immunity mechanisms. We did not identify positive effects of

vitamin D_2 on fish cell immunity. In conclusion, we determined that the inactive form of vitamin D_3, cholecalciferol, induced anti-bacterial innate immunity pathways in Atlantic salmon primary macrophages, suggesting that its utilization as a component of a healthy aquafeed diet in Atlantic salmon could enhance the immune response against *A. salmonicida*.

Keywords: Atlantic salmon, vitamin D_3, vitamin D_2, innate immunity, primary macrophages, *Aeromonas salmonicida*, Gram-negative

INTRODUCTION

Vitamin D is a fat-soluble secosteroid hormone that plays a crucial role in calcium and phosphorus homeostasis, cardiovascular physiology, cell proliferation and differentiation, among other functions (1–6). In fish, vitamin D is involved in the endocrine control of calcium and phosphorus homeostasis, similar to mammals (4). Also, it has been shown that vitamin D can act as an immunomodulatory agent in mammals (7, 8).

In contrast to terrestrial vertebrates, fish are not able to obtain vitamin D through the photochemical pathway, thus fish must ingest vitamin D from dietary sources (9). In freshwater and marine environments, the main dietary sources of vitamin D are phytoplankton and zooplankton (9). Phytoplankton provide fish with vitamin D_2 (ergocalciferol), while zooplankton provide them with vitamin D_3 (cholecalciferol) (10).

The beneficial stimulatory effects of vitamins D_2 and D_3 on innate immunity have been described in humans and other mammals (5, 8, 11–14). The positive effects of vitamins in fish are well-established, and currently vitamins D_2 and D_3 are essential components of aquafeed diets (4). Additionally, vitamin D is utilized as an adjuvant in aqua-vaccine preparations (15). However, the role of vitamin D in fish physiology is still enigmatic, and the immune stimulant mechanisms against infectious diseases are unknown.

Atlantic salmon (*Salmo salar*) is a high-value cultured finfish species, and the main species cultured in Canada, Chile, UK, and Norway (16–18). Infectious diseases caused by bacterial pathogens such as *Renibacterium salmoninarum*, *Piscirickettsia salmonis*, *Vibrio anguillarum*, and *Aeromonas salmonicida* subsp. *salmonicida* (19–24), have affected this industry since its origin (25, 26). Currently, several measures are utilized to prevent infectious diseases in the Atlantic salmon aquaculture industry, including a healthy diet that includes immunostimulants (27–29).

Functional constituents of healthy aquafeed diets like essential nutrients (such as vitamins, probiotics, prebiotics, and immunostimulants) are currently being considered to improve not only fish growth and stress tolerance, but also the resistance to diseases by enhancing non-specific defense mechanisms (30, 31). These essential nutrients are capable of directly activating immune mechanisms, such as phagocytic activity (e.g., macrophages and neutrophils), complement system, lysozyme activity, and others (32–34). Phagocytosis is an active host defense mechanism, involving the action of monocytes, dendritic cells, neutrophils, and macrophages (34–36). From these phagocytic leukocytes, the macrophages play an important role linking the innate and adaptive immune responses, and previous studies have shown that immunostimulants (i.e., fructooligosaccharides, mannanoligosaccharides) can successfully enhance the phagocytic activity in rainbow trout and European sea bass (34, 37, 38).

Immunostimulants are natural compounds that have been shown to be safe and effective for fish (30, 33, 39). In humans, vitamin D plays an important role in the suppression of pro-inflammatory cytokines such as *il-17*, *il-1b*, and *tnf-α* in individuals affected by type 2 diabetes and autoimmune diseases, preventing chronic inflammation (40, 41). Additionally, vitamin D significantly reduces *Staphylococcus aureus* infection in pre-treated bovine epithelial cells and modulates the expression of innate immune related genes (8, 13, 14). These studies suggest that vitamin D could trigger similar protective effects in fish. Here, we evaluate the effects of vitamins D_2 and D_3 on the innate immune responses of Atlantic salmon primary macrophages to *A. salmonicida* infection.

MATERIALS AND METHODS

Aeromonas salmonicida Growth Conditions

A. salmonicida was grown in accordance to the protocol used by Soto-Dávila et al. (42). Briefly, a single colony of *A. salmonicida* J223 (24) was incubated in 3 ml of Trypticase Soy Broth (TSB, Difco, Franklin Lakes, NJ) at 15°C in a 16 mm diameter glass tube and placed in a roller for 24 h. After growth, 300 μl of the overnight culture was added to 30 ml of TSB media using a 250 ml flask and incubated for 24 h at 15°C with aeration (180 rpm). After bacteria reached an O.D. 600 nm ∼0.7 (1×10^8 CFU ml^{-1}), the bacterial culture was centrifuged at 6,000 rpm at room temperature for 10 min. The pellet was washed twice with phosphate buffered saline [PBS; 136 mM NaCl, 2.7 mM KCl, 10.1 mM Na_2HPO_4, 1.5 mM KH_2PO_4 (pH 7.2)] and centrifuged at 6,000 rpm at room temperature for 5 min, and finally resuspended in 300 μl of PBS (∼5×10^{10} CFU ml^{-1}). The concentrated bacterial inoculum was serially diluted and quantified by plating onto TSA supplemented with Congo red (50 μg ml^{-1}) for 4 days.

Vitamin D_2 and D_3 Inhibitory Effects on *A. salmonicida* Growth

To determine whether vitamin D_2 or vitamin D_3 have inhibitory effect on *A. salmonicida* growth, 30 μl of the overnight growth bacteria were placed in 3 ml of TBS containing different

concentrations of vitamin D_2 (10; 100; 1,000; 10,000; and 100,000 ng ml^{-1}; Sigma-Aldrich) or vitamin D_3 (10; 100; 1,000; and 10,000 ng ml^{-1}; Sigma-Aldrich). Bacterial growth was measured by O.D. 600 nm until 48 h. The effect of each vitamin concentration on *A. salmonicida* growth was measured in triplicate, and TSB media containing the respective vitamin D concentration was utilized as a blank.

Fish Holding

Adult specimens of Atlantic salmon 4.0 ± 0.1 kg (mean ± SE) were obtained from the Dr. Joe Brown Aquatic Research Building (JBARB) at the Department of Ocean Sciences, Memorial University of Newfoundland, Canada. The animals were kept in 37 m^3 tanks, with flow-through (100 l min^{-1}) seawater (6.5°C) and ambient photoperiod. The individuals were fed twice per day with commercial salmonid dry pellets (Skretting Optiline Microbalance 3000 EP, 12.0 mm pellets: 38% protein, 33% fat, 1.6% calcium, 1.5% fiber, 1% phosphorus) with a ration of 0.5% of body weight per day. The experiment was performed in accordance with the guidelines of the Canadian Council on Animal Care and approved by Memorial University of Newfoundland's Institutional Animal Care Committee (protocols #17-01-JS; #17-02-JS).

Macrophage Isolation

Primary macrophages were isolated from Atlantic salmon head kidney. Tissues from 6 fish were aseptically removed and individually minced through 100 μm nylon sterile cell strainers (Fisher Scientific, Thermo Fisher Scientific, Waltham, MA, USA) in isolation media [(Leibovitz-15 (Gibco®, Gran Island, NY, USA) supplemented with 250 μg ml^{-1} heparin, 100 U ml^{-1} penicillin, 100 μg ml^{-1} streptomycin, and 0.1% Fetal Bovine Serum (FBS)]. After this period, 4 ml of cell suspension were centrifuged (1,000 × g at 4°C) for 30 min in a 34/51% Percoll gradient (GE Healthcare, Uppsala, Sweden). Macrophages collected from the macrophage-enriched interface were washed with PBS twice and the number and viable cells were determined using the Countness™ cell counter (Invitrogen), and trypan blue stain (Invitrogen). After determining the cell concentration (number of cells per ml^{-1}) of each sample, the primary macrophages were seeded in 22 mm 12-well or 35 mm 6-well cell-culture multidishes (Thermo Scientific, Roskilde, Denmark) at a concentration of 1 x 10^7 cells ml^{-1}. The plates were incubated at 15°C for 24 h in isolation media. After this period the cells were washed with PBS and incubated at 15°C for an additional 4 days in 1 ml of culture media (Leibovitz-15 (Gibco®), supplemented with 0.1% 2-Mercaptoethanol, 100 U ml^{-1} penicillin, 100 μg ml^{-1} streptomycin, and 5% FBS) to allow cell attachment until the assays were performed.

Vitamin D_2 and D_3 Toxicity in Atlantic Salmon Primary Macrophages

Atlantic salmon primary macrophages were seeded in 12-well cell-culture multidishes at a concentration of 1 x 10^7 cells ml^{-1}. After 4 days of incubation the culture media was removed, cells washed with PBS, and 1 ml of culture media containing different concentrations of vitamin D_2 (10; 100; 1,000; 10,000; and 100,000 ng ml^{-1}) or vitamin D_3 (10; 100; 1,000; and 10,000 ng ml^{-1}) was added. Twenty-four hours and 48 h post-vitamin treatment, cells were treated with 500 μl of trypsin-EDTA (0.5%; Gibco) for 10 min, and then trypsin was inactivated with 500 μl of culture media. The cells were stained with trypan blue (0.4%; Invitrogen) in a ratio of 1:1 (10 μl: 10 μl) and quantified using Countess™ Cell Counting Chamber Slides (Invitrogen) and Countess® Automated Cell Counter (Invitrogen) according to the manufacturer's instructions. Viability of cells was determined for each vitamin D_2 and D_3 concentration and the control group. All samples were taken from 6 individual fish.

Gentamicin Exclusion Assay

Infections of primary macrophages with *A. salmonicida* were performed according to the protocol used by Soto-Dávila et al. (42) with modifications. Briefly, after 4 days, the primary macrophages were washed with 1 ml of PBS and inoculated with 1 ml of culture media without antibiotics containing either 100 ng ml^{-1} of vitamin D_2 or D_3 for 24 h. After this period, media was removed, cells washed with 1 ml of PBS, and pre-treated primary macrophage monolayers were infected with 10 μl of bacterial suspension [∼1 × 10^7 cells ml^{-1}; Multiplicity of Infection (MOI) 1:1 (bacteria:macrophage)] and incubated at 15°C. For attachment, after 1 h of infection, the infected primary macrophage monolayers were washed twice with 1 ml of PBS and then lysed using 400 μl of Triton X100 (0.01%; Sigma) for 10 min (43). After this 600 μl of PBS was added to complete 1 ml of lysed macrophage suspension. Then, the lysed macrophage suspensions were serially diluted (1:10) and plate/counted on TSA plates supplemented with Congo red to determine the number of viable *A. salmonicida* per monolayer. The plates were incubated at 15°C for 5 days to determine the CFU per well.

For invasion, the primary macrophages were infected for 1 h, washed twice with 1 ml of PBS, and 1 ml of fresh culture media supplemented with gentamicin (10 μg ml^{-1}, a higher concentration than the minimal inhibitory concentration) (24) was added. Gentamicin treatment was applied to kill remaining extracellular bacteria. After 2, 3, and 4 h of infection, the infected primary macrophage monolayers were washed twice with PBS and then lysed using 400 μl of Triton X100 (0.01%) for 10 min (43). After this, 600 μl of PBS was added to complete 1 ml of lysed macrophage suspension. Then, the lysed macrophage suspensions were serially diluted (1:10) and plate/counted on TSA plates supplemented with Congo red to determine the number of viable intracellular *A. salmonicida* per monolayer. The plates were incubated at 15°C for 5 days to determine the CFU per well. All samples were taken from 6 individual fish.

Vitamin D_2 and D_3 Pre-treated Primary Macrophage Viability After *A. salmonicida* Infection

To determine the viability of infected primary macrophages, the cells were seeded in 12 wells plates, pre-treated with 100 ng ml^{-1} of vitamin D_2 or vitamin D_3, infected with *A. salmonicida*, and processed following the method used during the gentamicin exclusion assay. Cells were washed with 1 ml of PBS and then

treated with 500 µl of trypsin-EDTA (0.5%; Gibco) for 10 min. After this period, the trypsin was inactivated with 500 µl of culture media. The primary macrophages were stained using trypan blue (0.4%; Invitrogen) in a ratio of 1:1 (10 µl: 10 µl) and quantified using Countess™ Cell Counting Chamber Slides (Invitrogen) and the Countess® Automated Cell Counter (Invitrogen) according to the manufacturer's instructions. The numbers of alive and dead cells were determined at each time point post-infection. All the primary macrophages were isolated from 6 individual fish and technical triplicates were utilized.

RNA Extraction

RNA samples were obtained from head kidney primary macrophages inoculated with either PBS; live *A. salmonicida* (J223); formalin-killed *A. salmonicida* (FK J223); 100 ng ml^{-1} vitamin D_2 or D_3; 1,000 ng ml^{-1} vitamin D_2 or D_3, or 100 ng ml^{-1} vitamin D_2 or D_3 + live *A. salmonicida* (J223). The treatments that included vitamin D (D_2 or D_3) were pre-treated with the respective concentration 24 h before the challenge, meanwhile treatments without vitamin D were pre-treated only with the control vehicle 24 h before the challenge. Each sample was obtained 3 h post-inoculation.

Total RNA from Atlantic salmon primary macrophages was extracted using 1 ml of TRIzol Reagent (Invitrogen), and purified using the RNeasy® Mini Kit (QIAGEN) following the manufacturer's instructions (44). RNA samples were treated with 2 U of TURBO DNase (TURBO DNA-free™ Kit, Invitrogen) following the manufacturer's instructions to degrade any residual genomic DNA. Briefly, samples were incubated at 37°C for 30 min, 2.5 µl of DNase Inactivation Reagent was added, and samples incubated 5 min at room temperature. Then, samples were centrifuged at 10,000 x g for 1.5 min and the supernatant containing the RNA carefully transferred to a new tube. Purified RNA samples were quantified and evaluated for purity (A260/280 and A260/230 ratios) using a Nano-quant spectrophotometer (Genway, UK), and evaluated for integrity using 1% agarose gel electrophoresis (45). Column purified RNA samples had A260/280 ratios between 1.9 and 2.1 and A260/230 ratios between 1.9 and 2.2. A PCR test was conducted using the reference genes' primers [*60S ribosomal protein L32 (rpl32)* and *β-actin*] and the RNA as template to rule out the presence of DNA. All RNA samples did not show presence of DNA.

First-strand cDNA templates for qPCR were synthesized from 500 ng of DNaseI-treated, column-purified total RNA using SuperScript™ IV VILO™ Master Mix (Invitrogen) following the manufacturer's instructions. Each sample was incubated at 25°C for 10 min, at 50°C for 10 min, and at 85°C for 5 min.

Gene Paralogue Discovery and qPCR

All qPCR reactions were performed in a 20 µl reaction, containing 1× PowerUp SYBR Green Master Mix (Applied BioSystems, Foster City, CA, USA), 500 nM (final concentration) of both the forward and reverse primer and the indicated cDNA quantity. All samples were amplified and detected using the QuantStudio 3 Real Time PCR System (Applied BioSystems). The reaction mixtures were incubated for 2 min at 50°C, then 2 min at 95°C, followed by 40 cycles of 1 s at 95°C, 30 s at 60°C, and finally 15 s at 95°C, 1 min at 60°C, and 15 s at 95°C.

The primer sequences of *interleukin 1 beta* (*il-1b*), *interleukin 8 (il-8)*, *tumor necrosis factor alpha (tnf-α)*, *soluble toll-like receptor 5* (*stlr5*), and *leukocyte-derived chemotaxin 2* (*lect-2*) are listed in **Table 1**. Gene paralogue discovery, qPCR primer design and initial quality testing were performed as described in Caballero-Solares et al. (49). Since the reagents, cycling conditions and samples were different in the current study, primer efficiencies (**Table 1**) were reassessed. Briefly, a 7-point 1:3 dilution series starting with cDNA representing 40 ng of input total RNA was generated, and efficiencies then calculated using the formula $E=10^{(-1/slope)}$ (50).

Transcripts levels of the genes of interest (*il-1b*, *il-8*, *tnf-α*, *stlr5*, and *lect-2*) were normalized to transcript levels of two endogenous control genes. Levels of five candidate normalizers (*60S ribosomal protein 32*; *β-actin*, *18S*, *elongation factor 1 alpha*, and *hypoxanthine phosphoribosyl transferase 1*) were assessed in 50% of the samples (i.e., in 3 random samples per treatment) using cDNA representing 40 ng of input total RNA. Reference gene stability was then analyzed using both geNorm and BestKeeper (**Supplementary Table 1**). Both analyses identified *β-actin* (geNorm M = 0.592; BestKeeper value = 0.263) and *60S ribosomal protein L32* (geNorm M = 0.592; BestKeeper value = 0.364) and as the most stably expressed genes (**Supplementary Table 1**).

After normalizer testing was completed, transcript levels of the genes of interest were analyzed in the individual study samples, with normalization to both *β-actin* and *60S ribosomal protein L32*. In all cases, levels were assessed (in triplicate) in six individuals per treatment using cDNA representing 40 ng of input total RNA. On each gene a no RT control was included. Gene expression was determined using the comparative $2^{-\Delta\Delta Ct}$ method (51).

Phagocytosis Assay

The phagocytosis assay was performed following the protocol used by Smith et al. (39) with modifications. Cells were incubated for 3 days and inoculated with vehicle control (2 µl of ethanol in 1 ml of culture media without antibiotics), 100; 1,000; or 10,000 ng ml^{-1} of either vitamin D_2 or D_3 for 24 h. After this time, cells were washed twice with PBS, and inoculated with 1 µm of Fluoresbrite YG microspheres at a ratio of ∼1:30 macrophage:microsphere (Polysciences, Warrington, PA, USA) (39, 52). Twenty-four hours after microsphere addition, primary macrophages were washed with PBS and posteriorly cells treated with trypsin-EDTA (0.5%; Gibco) for 10 min. Then, cells were resuspended in 500 µl of FACS buffer (PBS + 1% FBS). Fluorescence was detected from 10,000 cells using a BD FACS Aria II flow cytometer and analyzed using BD FACS Diva v7.0 software (BD Biosciences, San Jose, CA, USA). The control pre-treated macrophages were used to compare with the FITC positive cells in vitamin D pre-treated cells. Percentages of FITC positive cells were determined for each condition. The experiments were conducted using macrophages isolated from 3 independent fish.

TABLE 1 | Primers used in qPCR studies.

Gene name (symbol) (GenBank acc. no.)	Nucleotide sequence (5′-3′)	[c]Efficiency (%)	Amplicon size (bp)	References
interleukin 1 beta (*il-1b*) (AY617117)	F: GTATCCCATCACCCCATCAC	99.7	119	This study
	R: TTGAGCAGGTCCTTGTCCTT			
interleukin 8 (*il-8*) (BT046706)	F: GAAAGCAGACGAATTGGTAGAC	100.7	99	This study
	R: GCTGTTGCTCAGAGTTGCAAT			
tumor necrosis factor alpha (*tnf-α*) (AY929386)	F: GGATGGAATGGAGCATCAGC	106.4	141	(39)
	R: TGCACGGTGTTAGCGGTAAG			
leukocyte cell derived chemotaxin 2 (*lect-2*) (BT059281)	F: CAGATGGGGACAAGGACACT	101.1	150	(39)
	R: GCCTTCTTCGGGTCTGTGTA			
toll-like receptor 5 (soluble) (*stlr5*) (AY628755)	F: ATCGCCCTGCAGATTTTATG	94.1	103	(39)
	R: GAGCCCTCAGCGAGTTAAAG			
[a]β-actin (*actb*) (BG933897)	F: CCAAAGCCAACAGGGAGAAG	104.4	91	(46)
	R: AGGGACAACACTGCCTGGAT			
[a]60S ribosomal protein *L32* (*rpl32*) (BT043656)	F: AGGCGGTTTAAGGGTCAGAT	100.7	119	(46)
	R: TCGAGCTCCTTGATGTTGTG			
[b]18S (*18S*)	F: GTCCGGGAAACCAAAGTC	91.0	Not provided	(47)
	R: TTGAGTCAAATTAAGCCGCA			
[b]elongation factor 1 alpha (*EF-1α*) (AF321836)	F: TGGCACTTTCACTGCTCAAG	96.3	197	(39)
	R: CAACAATAGCAGCGTCTCCA			
[b]hypoxanthine phosphoribosyl transferase 1 (*HPRT1*) (EG866745)	F: CCGCCTCAAGAGCTACTGTAAT	94.7	255	(48)
	R: GTCTGGAACCTCAAACCCTATG			

[a]*Normalizers used in experimental qPCR analyses.*
[b]*Candidate normalizer genes.*
[c]*Amplification efficiencies were calculated using a 7-point 1:3 dilution series starting with cDNA representing 40 ng of input total RNA. See methods for details.*

Statistical Analysis

All data are shown as the mean ± standard error (SE). Assumptions of normality and homoscedasticity were tested for the detected variances. A Kruskal-Wallis non-parametric test was performed for *A. salmonicida* growth curve and gene expression results. Macrophages viability, gentamicin exclusion assay, and phagocytosis assay data were analyzed using a repeated measures two-way ANOVA test, followed by Sidak multiple comparisons *post hoc* test to identify significant differences of each treatment in different times or concentrations and between treatments in the same time point. Differences were considered significant at $P < 0.05$. All statistical analyses were performed using GraphPad Prism (GraphPad Software, La Jolla California USA, www.graphpad.com).

RESULTS

Inhibitory Effects of Vitamin D_2 and D_3 on *A. salmonicida* Growth

Growth of *A. salmonicida* at different concentrations of vitamin D_2 and D_3 was determined by O.D. 600 nm at different time points until 48 h. Bacteria growth was not affected in concentrations of 10, 100, 1,000, and 10,000 ng ml^{-1} of vitamin D_2 (vitamin D_2) (**Figure 1A**). In contrast, *A. salmonicida* growth was significantly reduced in the presence of 100,000 ng ml^{-1} of vitamin D_2 (**Figure 1A**). *A. salmonicida* growth was not affected by 10 and 100 ng ml^{-1}of vitamin D_3 (vitamin D_3) (**Figure 1B**). However, *A. salmonicida* growth was significantly affected by 1,000 and 10,000 ng ml^{-1} of the vitamin D_3 (**Figure 1B**).

Evaluation of the Toxicity of Vitamin D_2 and D_3 in Atlantic Salmon Primary Macrophages

Atlantic salmon primary macrophage viability was determined after 24 and 48 h of exposure to concentrations of 0, 10, 100, 1,000, 10,000, and 100,000 ng ml^{-1} of vitamin D_2. Results obtained did not show significant differences in viability between the control group, compared with the cells treated with 10, 100, 1,000, and 10,000 ng ml^{-1} of vitamin D_2. However, a significant difference was observed in cells inoculated with the media containing a concentration of 100,000 ng ml^{-1} of vitamin D_2 after 24 h ($1.67 \times 10^4 \pm 6.67 \times 10^3$) and 48 h ($6.67 \times 10^3 \pm 6.67 \times 10^3$) (**Figure 2A**).

The percentage of viability did not show significant differences between the control group and the primary macrophages treated with 10, 100, 1,000, and 10,000 ng ml^{-1} of vitamin D_2. Nevertheless, a highly significant decrease in macrophage viability was observed at a concentration of 100,000 ng ml^{-1} of vitamin D_2 after 24 h (13.33 ± 4.48%) and 48 h (5.67 ± 5.67%) (**Figure 2B**).

The viability of Atlantic salmon primary macrophages was also determined at 24 and 48 h post-treatment with vitamin D_3 in concentrations of 10, 100, 1,000, and 10,000 ng ml^{-1}. The number of live cells per ml did not show significant differences

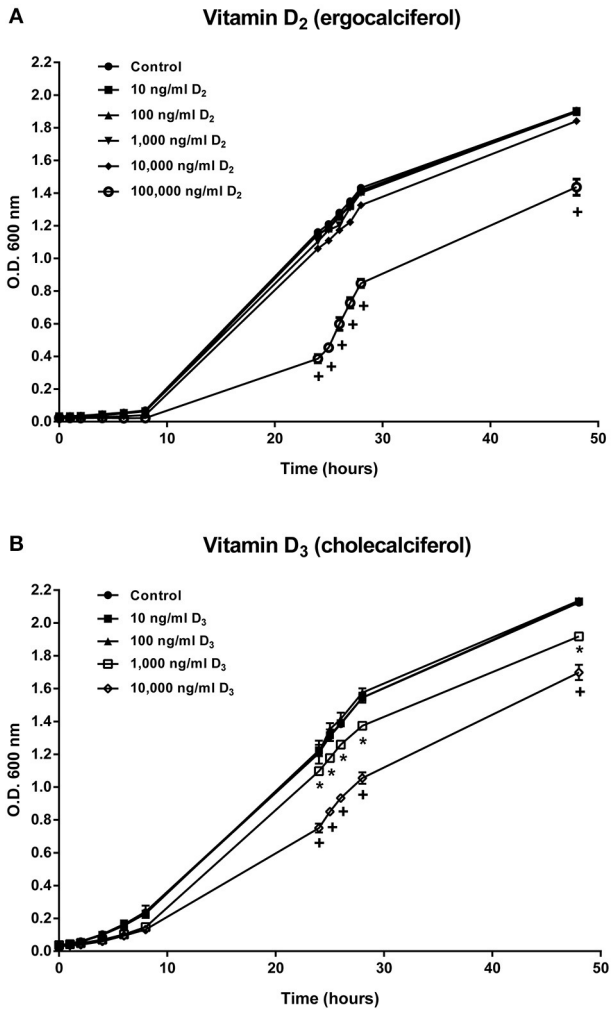

FIGURE 1 | *Aeromonas salmonicida* subsp. *salmonicida* growth curve in TSB media supplemented with **(A)** 10, 100, 1,000, 10,000, and 100,000 ng ml^{-1} of vitamin D_2 and **(B)** 10, 100, 1,000, and 10,000 ng ml^{-1}of vitamin D_3. Growth was determined by reading O.D. 600 nm at different time points until 48 h. Each value is the mean ± S.E.M ($n = 3$). Symbols (*, +) indicate differences between each group at different time points of measure, $p < 0.05$.

in primary macrophages treated with 10, 100, and 1,000 ng ml^{-1} (**Figure 2C**). Moreover, no significant differences were observed in the viability of primary macrophages treated with 10,000 ng ml^{-1} of vitamin D_3 after 24 h compared with the control (**Figure 2C**). Nevertheless, in cells exposed to 10,000 ng ml^{-1} of vitamin D_3, a significant decrease in the viability was observed after 48 h of treatment ($2.85 \times 10^5 \pm 1.44 \times 10^4$) (**Figure 2C**).

The percentage of viability in vitamin D_3 treated cells did not show significant differences after 24 h of exposure to concentrations of 10, 100, 1,000, and 10,000 ng ml^{-1} compared with the control group (**Figure 2D**). Also, no significant differences were observed in Atlantic salmon macrophages treated during 48 h with vitamin D_3 in a concentration of 10, 100, and 1,000 ng ml^{-1} compared with the control (**Figure 2D**). However, a significant decrease was observed in cells incubated with a concentration of 10,000 ng ml^{-1} of vitamin D_3 compared with the control and all the lower doses of vitamin D_3 at the 48 h time point (59.00 ± 1.15%) (**Figure 2D**). Moreover, in the group incubated at a concentration of 1,000 ng ml^{-1} of vitamin D_3, a significant higher percentage of viability was observed in cells treated for 48 h compared with the 24 h group (**Figure 2D**). Also, in the primary macrophages treated with 10,000 ng ml^{-1} of vitamin D_3, a significant difference was observed at different times, showing a decrease in the viability of cells treated for 48 h with vitamin D_3 compared with the cells incubated for only 24 h (**Figure 2D**).

Gentamicin Exclusion Assay in Vitamin D_2 and D_3 Pre-treated Cells Infected With *A. salmonicida*

The effects of vitamins D_2 and D_3 on the growth of *A. salmonicida* (**Figure 1**) and the effects on the viability of primary macrophages (**Figure 2**) were used to determine the concentration to be utilized in the gentamicin exclusion assays. Based on these results, the primary macrophages were pre-treated with 100 ng ml^{-1} (vitamin D_2 or D_3) for the gentamicin exclusion assay.

Cells pre-treated for 24 h with 100 ng ml^{-1} of vitamin D_2 and then infected with *A. salmonicida*, did not show significant differences in cell numbers at 1, 2, 3, and 4 h post-infection compared with the control group (**Figure 3A**). Also, no significant differences were observed in the viability of primary macrophages pre-treated and then infected with *A. salmonicida* at 1, 2, 3, and 4 h post-infection compared with the control group (**Figure 3B**).

The primary macrophages were infected with a total of 4.3×10^6 CFU per ml at a MOI of 1. The percentage of *A. salmonicida* attached was significantly higher in primary macrophages pre-treated with vitamin D_2 (49.09 ± 2.76%) compared with the control group (34.39 ± 2.12%) (**Figure 3D**). At invasion time-points, after 2 h of infection no significant differences were observed in cells pre-treated with vitamin D_2 compared with the control group at the same time point (**Figure 3D**). Moreover, no significant differences were observed in the control group and the vitamin D_2 pre-treated primary macrophages after 3 h of infection with *A. salmonicida* (**Figure 3D**). No significant differences were also found between the control and the vitamin D_2 treatment 4 h post-infection. However, a significant decrease in bacterial invasion was observed between 2 and 4 h in the primary macrophages pre-treated with vitamin D_2 (**Figure 3D**).

A similar response was obtained in cells pre-treated for 24 h with vitamin D_3 and then infected with *A. salmonicida*. For instance, no significant differences were found in the percentage of viability between the control group after 1, 2, 3, and 4 h of infection and the vitamin D_3 pre-treated macrophages at 1, 2, 3, and 4 h (**Figure 3F**).

Atlantic salmon primary macrophages pre-treated with vitamin D_3 were infected with a total of 2.56×10^6 bacterial cells per ml^{-1} (**Figure 3G**). The percentage of attachment (1 h post-infection) was significantly lower in the primary macrophages pre-treated for 24 h with vitamin D_3 (10.61 ± 0.97%) compared

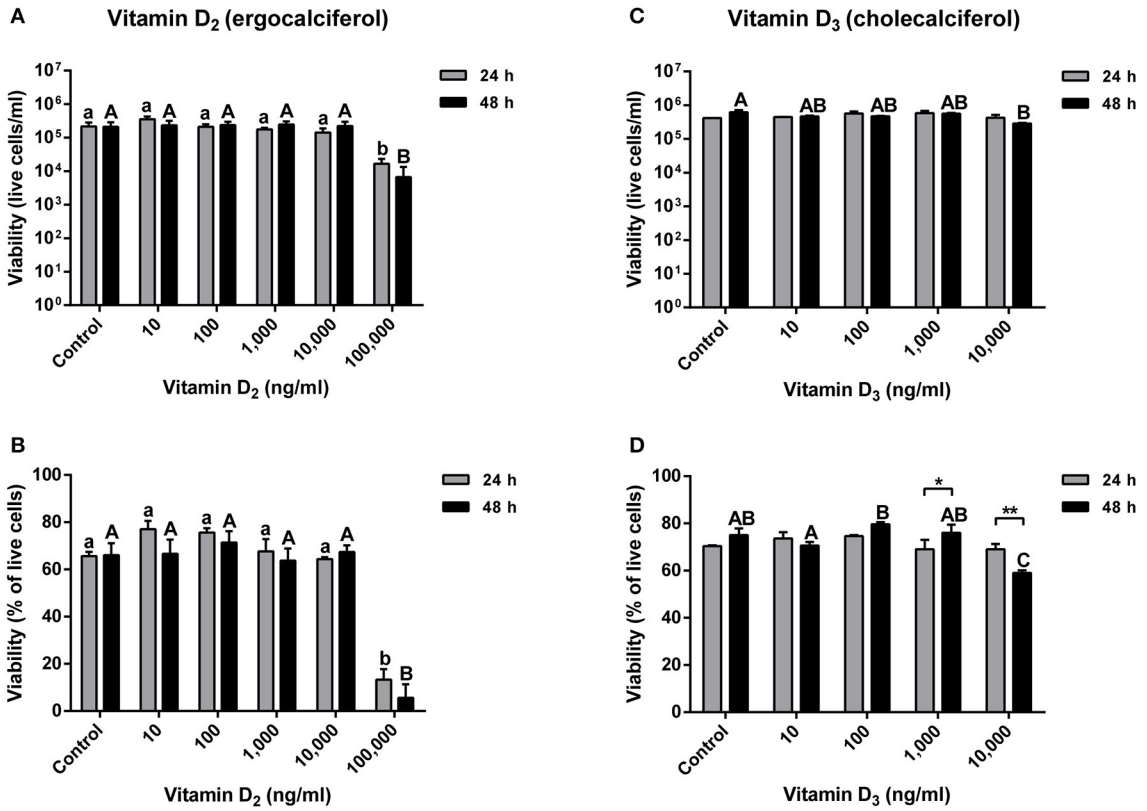

FIGURE 2 | Atlantic salmon primary macrophages treated with vitamin D_2 or D_3. **(A)** Live cells and **(B)** percentage of viability of primary macrophages treated with 10, 100, 1,000, 10,000, and 100,000 of vitamin D_2, were measured after 24 and 48 h of treatment. **(C)** Live cells and **(D)** percentage of viability of primary macrophages treated with 10, 100, 1,000, and 10,000 ng ml^{-1} of vitamin D_3 were measured after 24 and 48 h of treatment. Each value represents the mean ± S.E.M ($n = 6$). Lower case letters (a, b) show differences between treatments after 24 h. Upper case letters (A,B,C) show differences between treatments after 48 h. Asterisks (*) represent significant differences between treatments (*$p < 0.05$, **$p < 0.01$).

with the control group (51.56 ± 17.12%) (**Figure 3H**). In contrast, even when a tendency of lower invasion is observed, no significant differences were observed between the control group after 2, 3, and 4 h of infection compared with the fish cells pre-treated with vitamin D_3 (**Figure 3H**).

Atlantic Salmon Primary Macrophages Gene Expression

Transcript levels of innate immune response-related genes were evaluated by qPCR in Atlantic salmon primary macrophages after 3 h of the aforementioned treatments.

In the experiments conducted for both vitamin D_2 and D_3, a significant increase in the transcript expression of *il-1b* (**Figures 4A,F**), *il-8* (**Figures 4B,G**), *tnf-α* (**Figures 4C,H**), and s*tlr5* (**Figures 4E,J**) was observed in cells inoculated with live *A. salmonicida*, formalin-killed *A. salmonicida*, and in cells pre-treated with either vitamin D_2 or D_3 and then infected, compared to the PBS inoculated primary macrophages. In contrast, no differences in the expression of *il-1b*, *il-8*, *tnf-α*, and s*tlr5* were observed in Atlantic salmon cells inoculated only with 100 ng ml^{-1} or 1,000 ng ml^{-1} of each vitamin D form compared with the control (**Figures 4A–C,E–H,J**).

A different pattern was observed in the expression of *lect-2* transcript between both treatments. For instance, in cells pre-treated with vitamin D_2, no significant differences were observed in the expression of *lect-2* in any of the treatments compared with the PBS inoculated primary macrophages (**Figure 4D**). In contrast, *lect-2* was significantly up-regulated compared with the control in primary macrophages pre-treated with vitamin D_3 and then challenged with *A. salmonicida* (**Figure 4I**). The primary macrophages treated with live *A. salmonicida*, formalin-killed *A. salmonicida*, 100 ng ml^{-1} of vitamin D_3, and 1,000 ng ml^{-1} of vitamin D_3 did not show significant differences in the expression of *lect-2* compared with the control (**Figure 4I**).

Phagocytosis Assay

Atlantic salmon primary macrophages did not show significant differences in phagocytosis after 24 h of treatment with 100 ng ml^{-1} of vitamin D_2 (4.80 ± 1.62%) and vitamin D_3 (4.93 ± 1.56%), 1,000 ng ml^{-1} of vitamin D_2 (3.33 ± 0.67%) and vitamin D_3 (2.67 ± 0.41%), and 10,000 ng ml^{-1} of vitamin D_2 (0.97 ± 0.20%) and vitamin D_3 (0.87 ± 0.09%) compared with the control cells (4.80 ± 1.08%) (**Supplementary Figure 1**).

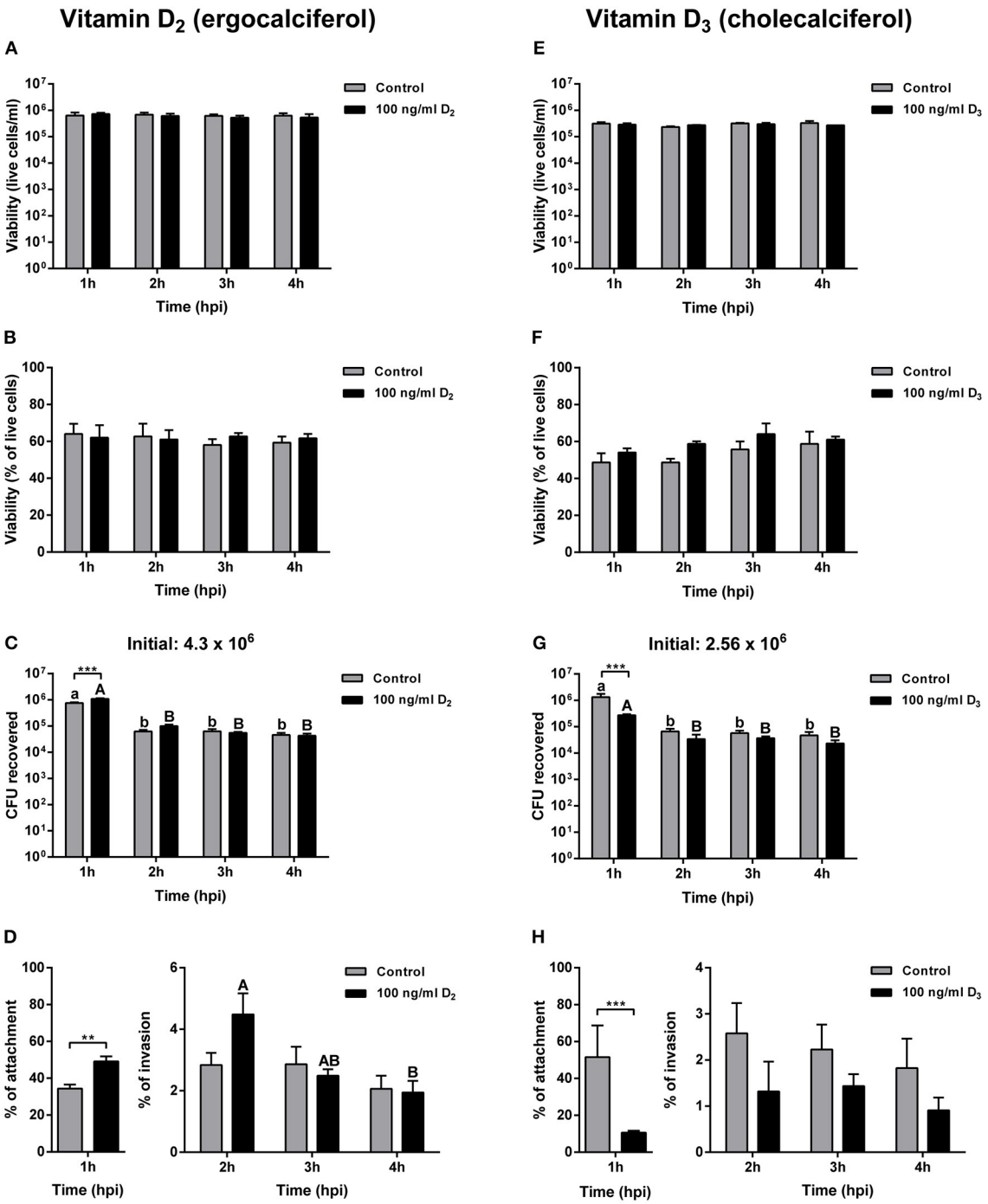

FIGURE 3 | Gentamicin exclusion assay in Atlantic salmon primary macrophages pre-treated for 24 h with either control or 100 ng ml^{-1} of vitamin D_2 or vitamin D_3, and then infected with *Aeromonas salmonicida* subsp. *salmonicida*. Live cells of primary macrophages pre-treated with vitamin D_2 **(A)**, or vitamin D_3 **(E)**; percentage of viability of primary macrophages pre-treated with vitamin D_2 **(B)**, or vitamin D_3 **(F)**, Colony forming unit (CFU) of *A. salmonicida* in Atlantic salmon primary macrophages pre-treated with vitamin D_2 **(C)**, or vitamin D_3 **(G)**; and percentage of attachment and invasion of *A. salmonicida* in Atlantic salmon primary macrophages pre-treated with vitamin D_2 **(D)**, or vitamin D_3 **(H)**, were measured 1, 2, 3, and 4 h post-infection. Initial *A. salmonicida* inoculum calculated in TSA Congo red plates are shown above the CFU figures. Each value represents the mean ± S.E.M ($n = 6$). Asterisks (*) represent significant differences between treatments on each time-point (**$p < 0.01$, ***$p < 0.001$). Lower case letters (a, b) show differences in the control at different time points post-infection. Upper case letters (A, B) show differences in vitamin D_2 or D_3 pre-treated cells in different time points post-infection.

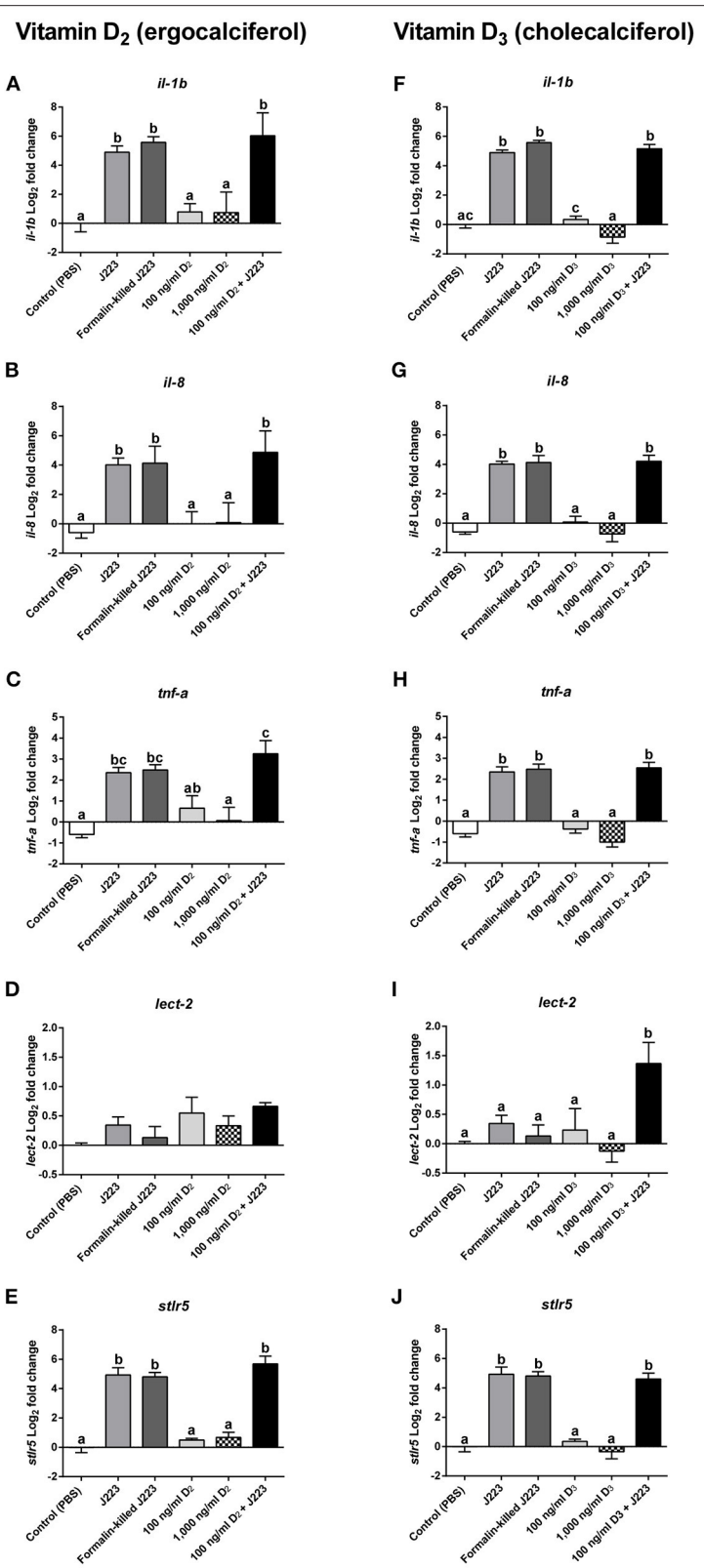

FIGURE 4 | Gene expression of **(A,F)** *Interleukin 1b* (*il-1b*), **(B,G)** *Interleukin 8* (*il-8*), **(C,H)** *Tumor necrosis factor alpha* (*tnf-α*), **(D,I)** *Leukocyte-derived chemotaxin 2* (*lect-2*), and **(E,J)** *soluble toll-like receptor 5* (*stlr5*) in Atlantic salmon primary macrophages isolated from head kidney pre-treated 24 h with either the control, vitamin

(Continued)

FIGURE 4 | D_2 (100 and 1,000 ng ml^{-1}) or vitamin D_3 (100 and 1,000 ng ml^{-1}), and then inoculated with PBS (control) or infected with live (J223) or exposed to formalin-killed *A. salmonicida* for 3 h. Relative expression was calculated using the $2^{(-\Delta\Delta Ct)}$ method and Log_2 converted using *β-actin* and *60S ribosomal protein L32* (*rpl32*) as internal reference genes. Each value is the mean ± S.E.M ($n = 6$). Different letters represent significant differences between treatments, $p < 0.05$.

DISCUSSION

Vitamin D is involved in important processes including mineral metabolism, cell growth, and cardiovascular physiology, among others (1–6). Moreover, it has been observed that vitamin D can stimulate the antibacterial immune response in mammals (7, 8). However, these effects and mechanisms have not been explored in fish cells. The two major sources of vitamin D in natural environments are vitamin D_2 and D_3, being obtained in fish after the ingestion of phytoplankton and zooplankton, respectively (9, 10). Different from terrestrial vertebrates that rely on the conversion of 7-dehydrocholesterol to vitamin D by using solar ultraviolet light (wavelength 380–500 nm) through the skin, fish seems to have alternative mechanims to obtaining vitamin D (4). For instance, it has been hypothesized that bony scales that are part of the fish skin are able to focus and convert the photons obtained from the blue light to breakdown the 7-dehydrocholesterol into vitamin D (53). This does not mean that fish lack of the mechanisms for photosynthesis of vitamin D through the skin. For instance, has been reported that rainbow trout (*Oncorhynchus mykiss*) and Mozambique tilapia (*Tilapia mossambicus*) have the mechanisms to convert 7-dehydrocholesterol into vitamin D, however, authors concluded that in natural environments photosynthesis of vitamin D does not play a significant role (4, 9, 54).

Initially it was thought that both vitamin D forms had the same impact on physiology (55), however, several studies have shown that vitamin D_3 is much more potent compared with vitamin D_2 (55, 56). This evidence suggests a differential modulation on the physiology of fish (i.e., innate immune system) in the presence of the specific vitamin D forms. Also, the effect that vitamin D forms can have on the growth of *A. salmonicida* has not yet been described.

To evaluate if *A. salmonicida* is able to grow in the presence of vitamin D_2 and D_3, a growth curve experiment was conducted in the presence of different concentrations of vitamin D_2 and vitamin D_3 for 48 h. Our results showed that only high concentrations of vitamin D_2 and D_3 reduced the growth of *A. salmonicida* after 48 h (**Figures 1A,B**). Normally, *A. salmonicida* is able to reach the stationary growth phase in ∼36 h (24, 57, 58). We observed a similar pattern of growth previously observed in *A. salmonicida* J223 strain (24) in culture media containing low concentrations of vitamin D_3 (100 and 1,000 ng ml^{-1}). Nevertheless, *A. salmonicida* seemed to tolerate higher concentrations of vitamin D_2 since only the highest concentration (100,000 ng ml^{-1}) reduced its growth rate. A previous study showed that high doses of vitamin C (128, 512, and 2048 mg/ml) can inhibit the growth of *Helicobacter pylori*, a risk factor for gastric carcinoma in mammals, during *in vitro* and *in vivo* experiments (59). Additionally, it has been reported that high concentrations of vitamin C (90 μM) can also inhibit the growth of *S. aureus* in *in vitro* conditions (60). High concentrations of vitamin D_2 and D_3 decreased the growth rate of *S. aureus* strain A1 after 24 h (14, 61). However, no significant differences were observed in the growth rate of *S. aureus* subsp. *aureus* (ATCC 27543) in the presence of different concentrations of vitamin D_3 after 48 h (8, 62). These results indicate that in the bacterial strains studied, vitamin D can inhibit growth when it is utilized in concentrations over 1,000 ng ml^{-1}, affecting both Gram negative and Gram positive bacteria.

The primary Atlantic salmon macrophage viability decreased after 24 and 48 h of exposure to 100,000 ng ml^{-1} of vitamin D_2, and a lower viability compared with the control was observed after 48 h with 10,000 ng ml^{-1} of vitamin D_3 (**Figure 2**). Similar to our results, it has been observed that low concentrations of vitamin D_3 (1, 10, and 50 nM) did not affect the viability of bovine mammary epithelial cells at 24 h (8). However, it has been reported that a decrease in the viability of bovine mammary epithelial cells in the presence of high concentrations of vitamin D_2 (6,000, 8,000, 10,000, 12,000, and 14,000 ng ml^{-1}) and D_3 (8,000, 10,000, 12,000, and 14,000 ng ml^{-1}) occurred after 24 h of exposure, suggesting that vitamin D can induce cell cycle arrest, apoptosis, or both (14, 63).

In Atlantic salmon, the estimated concentration of vitamin D in flesh varies between 2.9 μg to 18.5 μg per 100 g^{-1} (64). In our studies, the vitamin D concentrations utilized were similar to other studies conducted in mammalian cells used as a reference (8, 13, 14). The values obtained in the *A. salmonicida* growth curve and Atlantic salmon primary macrophages exposed to different concentrations of vitamin D_2 and D_3 (**Figures 1**, **2**), were utilized to determine the final non-toxic vitamin concentration (100 ng ml^{-1}) for further infection assays. The number of live cells and percentage of viability of Atlantic salmon primary macrophages after 1, 2, 3, and 4 h of infection did not show significant differences between the control and the vitamin D_2 or D_3 pre-treated cells (**Figures 2A,B,E,F**). Our findings agree with previous infection assays using *A. salmonicida* J223 in Atlantic cod primary macrophages, where no significant differences were observed in macrophage viability after 6 h of infection (42). This indicated that Atlantic salmon and Atlantic cod primary macrophages were not killed during this period by *A. salmonicida* J223. We previously suggested (42) that *A. salmonicida* controls the macrophages machinery to prevent cell apoptosis. As mentioned previously, vitamin D_3 in high concentration (8,000, 10,000, 12,000, and 14,000 ng ml^{-1}) could induce apoptosis (14, 63), perhaps in opposition to this suggested prevention of apoptosis produced by *A. salmonicida* (42). These results agree with the lower attachment and infection rates of *A. salmonicida* in cells pre-treated with D_3, where vitamin D_3 might interfere with the infection.

One of the most interesting findings of our results is related to the bacterial attachment and invasion. For instance, a significant

increase in *A. salmonicida* infection was observed at 1 h post-infection in primary macrophages pre-treated with vitamin D_2 compared with the control (**Figures 3C,D**). In contrast, a significant decrease in *A. salmonicida* attachment at 1 h was observed in cells pre-treated with vitamin D_3 compared with the control (**Figures 3G,H**). Previous studies indicated that vitamin D_3 has a stronger activity compared to vitamin D_2 in terrestrial mammals (55, 56). This agrees with our results where pre-treatment of primary macrophages with vitamin D_3 decreased *A. salmonicida* infection; while vitamin D_2 in contrast, seems to increase it infection. Our findings agree with the beneficial utilization of vitamin D_3 in aquafeeds (4, 65, 66) and with vitamin D_3 potentially having a broad positive effect in all vertebrates, including fish.

To complement our results described above, we explored part of the immune mechanism behind the beneficial effects of vitamin D by profiling the expression of specific innate immune genes using qPCR. An up-regulation of *il-1b*, *il-8*, *tnf-α*, and s*tlr5* occurred in primary macrophages inoculated with either live or formalin-killed *A. salmonicida* (**Figures 4A–C,E–H,J**). These results were expected, since cytokines and chemokines, such as *il-1b*, *il-8*, *tnf-α*, and the pattern recognition receptor (PRR) s*tlr5*, play essential roles controlling both acute and chronic inflammation in fish tissues mediated by macrophages (39). In Atlantic salmon, the evidence shows that this canonical macrophage innate immune response can be triggered rapidly by either a bacterial pathogen-associated molecular pattern (PAMP), such as lipopolysaccharide (LPS), or pathogens like *Yersinia ruckeri*, *Aeromonas salmonicida*, *Pseudomonas aeruginosa*, and *Flavobacterium psychrophilum*, among others (39, 67–70).

Some viruses, bacteria, and parasites can modify the expression of genes related with the host immune response as part of a mechanism of evading its defense mechanisms (71). In humans, three important infectious diseases (e.g., HIV, tuberculosis, and malaria) have developed highly effective mechanisms to subvert the immune response (71), making it difficult to control these diseases and develop effective vaccines. Further examples of this are *Yersinia pseudotuberculosis* and *Y. enterocolitica* which are able to control human macrophage immune response and induce apoptosis after the translocation of effector molecules through the type III secretion system (72–74).

In fish head kidney, a modulation of the expression of *il-1b* and the *major histocompatibility complex class 1* (*mhc-I*) has been observed in Atlantic salmon after being infested by the sea louse *Lepeophtheirus salmonis* (75). Moreover, Lewis et al. (76) showed in an Atlantic salmon head kidney (SHK-1) cell line that *L. salmonis* produces substances that modify the expression of genes encoding inflammatory mediators. Here, our results obtained during the infection with live *A. salmonicida* in Atlantic salmon primary macrophages showed no significant differences in the expression of *leukocyte-derived chemotaxin 2* (*lect-2)* compared with the control (**Figures 4D,I**). When the fish cells were pre-treated with vitamin D_2 and then infected with live bacteria, the gene expression also did not increase, suggesting that *lect-2* is not involved in the first line of defense against *A. salmonicida* in Atlantic salmon. However, the expression of *lect-2* in Atlantic salmon macrophages pre-treated with vitamin D_3 and challenged with live *A. salmonicida* was significantly up-regulated compared to the control (**Figure 4I**). *lect-2* is a chemotactic factor involved in the recruitment of neutrophils to the site of infection (39, 77). In the study conducted by Smith et al. (39), an up-regulation of *lect-2* was observed only in treatments with LPS, confirming that its role in the presence of external pathogenic agents is active in Atlantic salmon. Comparing the expression of *lect-2* in primary macrophages treated with live *A. salmonicida* and the samples pre-treated with vitamin D_3 and then inoculated with *A. salmonicida*, our results suggest that *A. salmonicida* prevent the transcriptional response of *lect-2*, perhaps to prevent neutrophil recruitment during infection. Our results suggest that pre-treatments with vitamin D_3 can counteract the effect of *A. salmonicida* on this particular gene, and up-regulate the expression of *lect-2* during *A. salmonicida* infection (**Figure 4I**).

To determine if vitamin D_2 and D_3 can also cause an effect on the phagocytosis of Atlantic salmon primary macrophages, the phagocytic activity was tested using fluorescent latex beads (**Supplementary Figure 1**). Phagocytosis is used by organisms to eliminate external agents such as bacteria in a highly efficient way (42, 52, 78, 79). The effect of vitamins on macrophages' phagocytic activity has been previously tested in Atlantic salmon, however, no significant variations were observed after treatments with vitamin C or vitamin E (80, 81). We found similar results in Atlantic salmon primary macrophages after 24 h pre-treatments with either vitamin D_2 or D_3, suggesting that, independent of the vitamin D used, the phagocytic activity of Atlantic salmon macrophages is not modulated by its action.

CONCLUSION

In this study we evaluated the effects of vitamin D_2 and D_3 on *A. salmonicida* growth, Atlantic salmon primary macrophage viability, and the fish cells' immune response. We determined that only high concentrations of vitamin D_2 (100,000 ng ml^{-1}) and vitamin D_3 (1,000 and 10,000 ng ml^{-1}) decreased the growth rate of *A. salmonicida*. Moreover, we determined that 100,000 ng $ml^{-1}$of vitamin D_2 and 10,000 ng ml^{-1} of vitamin D_3 decreased the viability of Atlantic salmon primary macrophages after 24 and 48 h. These results suggest that high doses of D_2 and D_3 are toxic for the bacterial and the eukaryotic cells.

Pre-treatment of primary macrophages with 100 ng $ml^{-1}$of either vitamin D_2 or D_3 did not have effects on cell viability. Nevertheless, one of the remarkable findings of our study was that pre-treatment with vitamin D_3 reduced *A. salmonicida* attachment, meanwhile, pre-treatment with vitamin D_2 increased attachment, and as a consequence also increased bacterial invasion.

Gene expression of *il-1b*, *il-8*, *tnf-α*, and s*tlr5* was up-regulated during *A. salmonicida* infection, agreeing with a canonical innate immune response. However, our results suggested that *A. salmonicida* was able to suppress the expression of *lect-2*, a gene involved in neutrophil recruitment, key in the fight against pathogen clearance. After the addition of vitamin D_2, no variation in the transcriptional expression of this gene was observed. However, cells pre-treated with vitamin D_3 and then

inoculated with live *A. salmonicida*, showed an up-regulation of *lect-2*, suggesting that vitamin D_3 can be useful to counteract the suppression triggered by the pathogen.

Altogether, our results show that vitamin D_3 seems to be a good candidate to be used as an immunostimulant in Atlantic salmon against *A. salmonicida* infection. The mechanisms on how vitamin D_3 modulates the *S. salar* macrophage immunity and its relation to specific receptors, like the vitamin D receptor, deserve future attention. In contrast, vitamin D_2 did not appear to have an effect on the modulation of the immune system of Atlantic salmon, suggesting that vitamin D_2 may not play an important role in the fish innate antibacterial immune response.

DATA AVAILABILITY STATEMENT

All datasets generated for this study are included in the article/**Supplementary Material**.

ETHICS STATEMENT

The animal study was reviewed and approved by the Memorial University Institutional Animal Care Committee.

AUTHOR CONTRIBUTIONS

MS-D and JS: conception and design of research, prepared figures, and drafted the manuscript. MS-D: macrophage isolation. JH: primer design. MS-D, KV, and SI: performed the experiments. MS-D, MR, and JS: interpreted the results of the experiments. MS-D, KV, SI, JH, MR, and JS: edited and revised the manuscript and approved the final version of the manuscript. MR and JS: funding support.

FUNDING

The authors are grateful to the support provided by Vitamin Initiative—Ocean Frontier Institute; Canada First—Ocean Frontier Institute (Module J.3); Memorial University Seed, Bridge and Multidisciplinary Funds; and NSERC-Discovery grants (2018-05942 to JS and 341304-2012 to MR).

ACKNOWLEDGMENTS

The authors thank the Dr. Joe Brown Aquatic Research Building (JBARB) staff for their assistance with the fish. We would like to thank Ma. Ignacia Diaz (Marine Microbial Pathogenesis and Vaccinology Laboratory) for her logistic support.

SUPPLEMENTARY MATERIAL

The Supplementary Material for this article can be found online at: https://www.frontiersin.org/articles/10.3389/fimmu.2019.03011/full#supplementary-material

REFERENCES

1. Zittermann A. Vitamin D in preventive medicine: are we ignoring the evidence? *Br J Nutr*. (2003) 89:552–72. doi: 10.1079/BJN2003837
2. Grant W. Epidemiology of disease risks in relation to vitamin D insufficiency. *Prog Biophys Mol Bio*. (2006) 92:65–79. doi: 10.1016/j.pbiomolbio.2006.02.013
3. Lips P. Vitamin D physiology. *Prog Biophys Mol Bio*. (2006) 92:4–8. doi: 10.1016/j.pbiomolbio.2006.02.016
4. Lock EJ, Waagbø R, Wendelaar-Bonga S, Flick G. The significance of vitamin D for fish: a review. *Aquac Nutr*. (2010) 16:100–16. doi: 10.1111/j.1365-2095.2009.00722.x
5. Borges M, Martini L, Rogero M. Current perspectives on vitamin D, immune system, and chronic diseases. *Nutrition*. (2011) 27:399–404. doi: 10.1016/j.nut.2010.07.022
6. Wang L, Xu H, Wang Y, Wang C, Li J, Zhao Z, et al. Effects of the supplementation of vitamin D_3 on the growth and vitamin D metabolites in juvenile Siberian sturgeon (*Acipenser baerii*). *Fish Physiol Biochem*. (2017) 43:901–9. doi: 10.1007/s10695-017-0344-5
7. Miller J, Gallo R. Vitamin D and innate immunity. *Dermatol Ther*. (2010) 23:13–22. doi: 10.1111/j.1529-8019.2009.01287.x
8. Téllez-Pérez A, Alva-Murillo N, Ochoa-Zarzosa A, López-Meza J. Cholecalciferol (vitamin D) differentially regulates antimicrobial peptide expression in bovine mammary epithelial cells: Implications during *Staphylococcus aureus* internalization. *Vet Microbiol*. (2012) 160:91–8. doi: 10.1016/j.vetmic.2012.05.007
9. Rao DS, Raghuramulu N. Food Chain as Origin of Vitamin D in Fish. *Comp Biochem Physiol A Mol Integr Physiol*. (1996) 114:15–9. doi: 10.1016/0300-9629(95)02024-1
10. Darias M, Mazurais D, Koumoundouros G, Cahu C, Zambonino-Infante J. Overview of vitamin D and C requirements in fish and their influence on the skeletal system. *Aquaculture*. (2011) 315:49–60. doi: 10.1016/j.aquaculture.2010.12.030
11. Mora JR, Iwata M, von Andrian U. Vitamin effects on the immune system: vitamins A and D take centre stage. *Nat Rev Immunol*. (2008) 8:685–98. doi: 10.1038/nri2378
12. Prentice A, Goldberg G, Schoenmakers I. Vitamin D across the lifecycle: physiology and biomarkers. *Am J Clin Nutr*. (2008) 88:500S−6. doi: 10.1093/ajcn/88.2.500S
13. Alva-Murillo N, Téllez-Pérez A, Medina-Estrada I, Álvarez-Aguilar C, Ochoa-Zarzosa A, López-Meza J. Modulation of the inflammatory response of bovine mammary epithelial cells by cholecalciferol (vitamin D) during *Staphylococcus aureus* internalization. *Microb Pathog*. (2014) 77:24–30. doi: 10.1016/j.micpath.2014.10.006
14. Yue Y, Hymøller L, Jensen S, Lauridsen C, Purup S. Effects of vitamin D and its metabolites on cell viability and *Staphylococcus aureus* invasion into bovine mammary epithelial cells. *Vet Microbiol*. (2017) 203:245–51. doi: 10.1016/j.vetmic.2017.03.008
15. Sadarangani S, Whitaker J, Poland G. "Let There Be Light": The role of Vitamin D in the immune response to vaccines. *Expert Rev Vaccines*. (2015) 14:1427–40. doi: 10.1586/14760584.2015.1082426
16. Asche F, Roll K, Sandvold, H. Sørvig A, Zhang D. Salmon aquaculture: Larger companies and increased production. *Aquacult Econ Manage*. (2013) 17:322–39. doi: 10.1080/13657305.2013.812156
17. Liu Y, Rosten T, Henriksen K, Hognes E, Summerfelt S, Vinci B. Comparative economic performance and carbon footprint of two farming models for producing Atlantic salmon (*Salmo salar*): Land-based closed containment system in freshwater and open net pen in seawater. *Aquacult Eng*. (2016) 71:1–12. doi: 10.1016/j.aquaeng.2016.01.001
18. FAO (2018). The State of World Fisheries and Aquaculture (SOFIA) - Meeting the Sustainable Development Goals, Food and Agriculture Organization, Rome, Italy.

19. Fryer J.L., and Sanders JE. Bacterial kidney disease of salmonid fish. *Ann. Rev. Microbiol*. (1981) 35, 273-298. doi: 10.1146/annurev.mi.35.100181.001421
20. Cvitanich JD, Gárate O, Smith CE. The isolation of a Rickettsia-like organism causing disease and mortality in Chilean salmonids and its confirmation by Koch's postulate. *J Fish Dis*. (1991) 14:121–45. doi: 10.1111/j.1365-2761.1991.tb00584.x
21. Toranzo AE, Magariños B, Romalde JL. A review of the main bacterial fish diseases in mariculture systems. *Aquaculture*. (2005) 246:37–61. doi: 10.1016/j.aquaculture.2005.01.002
22. Higuera G, Bastías R, Tsertsvadze G, Romero J, Espejo R. Recently discovered *Vibrio anguillarum* phages can protect against experimentally induced vibriosis in Atlantic salmon, *Salmo salar*. *Aquaculture*. (2013) 392–395:128–33. doi: 10.1016/j.aquaculture.2013.02.013
23. Maisey K, Montero R, Christodoulides M. Vaccines for Piscirickettsiosis (salmonid rickettsial septicaemia, SRS): The Chile perspective. *Expert Rev Vaccines*. (2016) 16:215–28. doi: 10.1080/14760584.2017.1244483
24. Valderrama K, Saravia M, Santander J. Phenotype of *Aeromonas salmonicida* sp. *salmonicida* cyclic adenosine 3',5'-monophosphate receptor protein (Crp) mutants and its virulence in rainbow trout (*Oncorhynchus mykiss*). *J Fish Dis*. (2017) 40:1849–56. doi: 10.1111/jfd.12658
25. Kaatari S, Tripp R. Cellular mechanisms of glucocorticoid immunosuppression in salmon. *J Fish Biol*. (1987) 31:129–32. doi: 10.1111/j.1095-8649.1987.tb05304.x
26. Robertson L, Thomas P, Arnold C, Trant J. Plasma cortisol and secondary stress responses of red drum to handling, transport, rearing density, and a disease outbreak. *Prog Fish Cult*. (1987) 49:1–12.
27. Siwicki AK, Anderson DP, Rumsey GL. Dietary intake of immunostimulants by rainbow trout affects non-specific immunity and protection against furunculosis. *Vet Immunol Immunopathol*. (1994) 41:125–39. doi: 10.1016/0165-2427(94)90062-0
28. Murray AL, Pascho RJ, Alcorn SW, Fairgrieve WT, Shearer KD, Roley D. Effects of various feed supplements containing fish protein hydrolysate or fish processing by-products on the innate immune functions of juvenile coho salmon (*Oncorhynchus kisutch*). *Aquaculture*. (2003) 220:643–53. doi: 10.1016/S0044-8486(02)00426-X
29. Dawood MA, Koshio S, Esteban MA. Beneficial roles of feed additives as immunostimulants in aquaculture: a review. *Rev Aquacult*. (2017) 10:950–74. doi: 10.1111/raq.12209
30. Sakai M. Current research status of fish immunostimulants. *Aquaculture*. (1999) 172:63–92. doi: 10.1016/S0044-8486(98)00436-0
31. Oliva-Teles A. Nutrition and health of aquaculture fish. *J Fish Dis*. (2012) 35:83–108. doi: 10.1111/j.1365-2761.2011.01333.x
32. Cook MT, Hayball PJ, Hutchinson W, Nowak BF, Hayball JD. Administration of a commercial immunostimulant preparation, EcoActiva^{TM} as a feed supplement enhances macrophage respiratory burst and the growth rate of snapper (*Pagrus auratus*, Sparidae (Bloch and Schneider)) in winter. *Fish Shellfish Immun*. (2003) 14:333–45. doi: 10.1006/fsim.2002.0441
33. Bridle A, Carter C, Morrison R, Nowak B. The effect of β-glucan administration on macrophage respiratory burst activity and Atlantic salmon, *Salmo salar* L., challenged with amoebic gill disease – evidence of inherent resistance. *J Fish Dis*. (2005) 28:347–56. doi: 10.1111/j.1365-2761.2005.00636.x
34. Song SK, Beck BR, Kim D, Park J, Kim J, Kim HD, et al. Prebiotics as immunostimulants in aquaculture: a review. *Fish Shellfish Immunol*. (2014) 40:40–8. doi: 10.1016/j.fsi.2014.06.016
35. Secombes CJ, Fletcher TC. The role of phagocytes in the protective mechanisms of fish. *Annu Rev Fish Dis*. (1992) 2:53–71. doi: 10.1016/0959-8030(92)90056-4
36. Esteban MA, Cuesta A, Chaves-Pozo E, Meseguer J. Phagocytosis in Teleosts. *Impl N Cells Involved Biol*. (2015) 4:907–22. doi: 10.3390/biology4040907
37. Torrecillas S, Makol A, Benítez-Santana T, Caballero MJ, Montero D, Sweetman J, et al. Reduced gut bacterial translocation in European sea bass (*Dicentrarchus labrax*) fed mannan oligosaccharides (MOS). *Fish Shellfish Immunol*. (2011) 30:674–81. doi: 10.1016/j.fsi.2010.12.020
38. Vogt L, Ramasamy U, Meyer D, Pullens G, Venema K, Faas MM, et al. Immune modulation by different types of β2→ 1-fructans is toll-like receptor dependent. *PLoS ONE*. (2013) 8:e68367. doi: 10.1371/journal.pone.0068367
39. Smith NC, Christian SL, Taylor RG, Santander J, Rise ML. Immune modulatory properties of 6-gingerol and resveratrol in Atlantic salmon macrophages. *Mol Immunol*. (2018) 95:10–9. doi: 10.1016/j.molimm.2018.01.004
40. Szodoray P, Nakken B, Gaal J, Jonsson R, Szegedi A, Zold E, et al. The complex role of vitamin D in autoimmune diseases. *Scand J Immunol*. (2008) 68:261–9. doi: 10.1111/j.1365-3083.2008.02127.x
41. Chagas C, Borges MC, Martini L, Rogero M. Focus on Vitamin D, Inflammation and Type 2 Diabetes. *Nutrients*. (2012) 4:52–67. doi: 10.3390/nu4010052
42. Soto-Dávila M, Hossain A, Chakraborty S, Rise ML, Santander J. *Aeromonas salmonicida* subsp. salmonicida early infection and immune response of Atlantic cod (*Gadus morhua* L) primary macrophages. *Front Immunol*. (2019) 10:1237. doi: 10.3389/fimmu.2019.01237
43. Sung K, Khan SA, Nawaz MS, Khan AA. A simple and efficient Triton X-100 boiling and chloroform extraction method of RNA isolation from Gram-positive and Gram-negative bacteria. *FEMS Microbiol Lett*. (2003) 229:97–101. doi: 10.1016/S0378-1097(03)00791-2
44. Santander J, Kilbourne J, Park JY, Martin T, Loh A, Diaz I, et al. Inflammatory effects of *Edwardsiella ictaluri* lipopolysaccharide modifications in catfish gut. *Infect Immun*. (2014) 82:3394–404. doi: 10.1128/IAI.01697-14
45. Sambrook J, Russell DW. *Molecular Cloning: A Laboratory Manual*. 3 rd ed. Cold Spring Harbor, NY: Cold Spring Harbor Laboratory (2001).
46. Xue X, Hixson SM, Hori TS, Booman M, Parrish CC, Anderson DM, et al. Atlantic salmon (*Salmo salar*) liver transcriptome response to diets containing *Camelina sativa* products. *Comp Biochem Physiol D Genomics Proteomics*. (2015) 14:1–15. doi: 10.1016/j.cbd.2015.01.005
47. Pontigo JP, Agüero MJ, Sanchez P, Oyarzún R, Vargas-Lagos C, Mancilla J, et al. Identification and expressional analysis of NLRC5 inflammasome gene in smolting Atlantic salmon (*Salmo salar*). *Fish Shellfish Immunol*. (2016) 58:259–65. doi: 10.1016/j.fsi.2016.09.031
48. Heidaru Z, Tinsley J, Bickerdike R, McLoughlin MF, Zou J, Martin SAM. Antiviral and metabolic gene expression responses to viral infection in Atlantic salmon (*Salmo salar*). *Fish Shellfish Immunol*. (2015) 42:297–305. doi: 10.1016/j.fsi.2014.11.003
49. Caballero-Solares A, Hall JR, Xue X, Eslamloo K, Taylor RG, Parrish CC, et al. The dietary replacement of marine ingredients by terrestrial animal and plant alternatives modulates the antiviral immune response of Atlantic salmon (*Salmo salar*). *Fish Shellfish Immunol*. (2017) 64:24–38. doi: 10.1016/j.fsi.2017.02.040
50. Pfaffl MW. A new mathematical model for relative quantification in real-time RT–PCR. *Nucleic Acids Res*. (2001) 29:e45. doi: 10.1093/nar/29.9.e45
51. Livak KJ, Schmittgen TD. Analysis of relative gene expression data using real-time quantitative PCR and the $2^{-\Delta\Delta CT}$ method. *Methods*. (2001) 25:402–8. doi: 10.1006/meth.2001.1262
52. Øverland H, Pettersen EF, Rønneseth A, Wergeland HI. Phagocytosis by B-cells and neutrophils in Atlantic salmon (*Salmo salar* L.) and Atlantic cod (*Gadus morhua* L.). *Fish Shellfish Immunol*. (2010) 28:193–204. doi: 10.1016/j.fsi.2009.10.021
53. Pierens SL, Fraser DR. The origin and metabolism of vitamin D in rainbow trout. *J Steroid Biochem Mol Biol*. (2015) 145:58–6. doi: 10.1016/j.jsbmb.2014.10.005
54. Holick MF, Holick SA, Guillard RL. On the origin and metabolism of vitamin D in the sea. In: Oguro C, Pang PKT, editors. *Comparative Endocrinology of Calcium Regulation*. Tokyo: Japan Scientific Societies Press (1982). p. 85–91.
55. Trang HM, Cole DE, Rubin LA, Pierratos A, Siu S, Vieth R. Evidence that vitamin D3 increases serum 25-hydroxyvitamin D more efficiently than does vitamin D2. *Am J Clin Nutr*. (1998) 68:854–8. doi: 10.1093/ajcn/68.4.854
56. Ostermeyer U, Schmidt T. Vitamin D and provitamin D in fish. *Eur Food Res Technol*. (2006) 222:403–13. doi: 10.1007/s00217-005-0086-y
57. Cipriano RC, Bullock G. *Furunculosis and other diseases caused by Aeromonas salmonicida*. Fish disease leaflet 66. Kearneysville, WV: USGS/Leetown Science Center Fish Health Branch (2001).
58. Connors E, Soto-Dávila M, Hossain A, Vasquez I, Gnanagobal H, Santander J. Identification and validation of reliable *Aeromonas salmonicida* subspecies salmonicida reference genes for differential gene expression analyses. *Infect Genet Evol*. (2019) 73:314–21. doi: 10.1016/j.meegid.2019.05.011

59. Zhang H, Wakisaka N, Maeda O, Yamamoto T. Vitamin C inhibits the growth of a bacterial risk factor for gastric carcinoma: *Helicobacter pylori*. Cancer. (1997) 80:1897–903
60. Kallio J, Jaakkola M, Mäki M, Kilpeläinen P, Virtanen V. Vitamin C inhibits *Staphylococcus aureus* growth and enhances the inhibitory effect of quercetin on growth of Escherichia coli *in vitro*. *Planta Med*. (2012) 78:1824–30. doi: 10.1055/s-0032-1315388
61. Aarestrup FM, Scott NL, Sordillo LM. Ability of Staphylococcus aureus coagulase genotypes to resist neutrophil bactericidal activity and phagocytosis. *Infect Immun*. (1994) 62:5679–82.
62. Gutiérrez-Barroso A, Anaya-Lopez JL, Lara-Zárate L, Loeza-Lara PD, López-Meza JE, Ochoa-Zarzosa A. Prolactin stimulates the internalization of *Staphylococcus aureus* and modulates the expression of inflammatory response genes in bovine mammary epithelial cells. *Vet Immunol Immunopathol*. (2008) 121:113–22. doi: 10.1016/j.vetimm.2007.09.007
63. Samuel S, Sitrin MD. Vitamin D's role in cell proliferation and differentiation. *Nutr Rev*. (2008) 66:116–24. doi: 10.1111/j.1753-4887.2008.00094.x
64. Jakobsen J, Smith C, Bysted A, Kevin D. Cashman 3 vitamin D in wild and farmed Atlantic salmon (*Salmo salar*) – What do we know? *Nutrients*. (2019) 11:982. doi: 10.3390/nu11050982
65. Barnett BJ, Cho CY, Slinger SJ. The essentiality of cholecalciferol in the diets of rainbow trout (*Salmo gairdneri*). *Comp Biochem Physiol*. (1979) 63:291–7. doi: 10.1016/0300-9629(79)90162-2
66. Barnett BJ, Cho CY, Slinger SJ. Relative biopotency of dietary ergocalciferol and cholecalciferol and the role of and requirement for vitamin D in rainbow trout (*Salmo gairdneri*). *J Nutr*. (1982) 112:2011–9.
67. Martin S, Blaney S, Houlihan D, Secombes CJ. Transcriptome response following administration of a live bacterial vaccine in Atlantic salmon (*Salmo salar*). *Mol Immunol*. (2006) 43:1900–11. doi: 10.1016/j.molimm.2005.10.007
68. Bridle A, Nosworthy E, Polinski M, Nowak B. Evidence of an antimicrobial-immunomodulatory role of Atlantic salmon cathelicidins during infection with *Yersinia ruckeri*. *PLoS ONE*. (2011) 6:e23417. doi: 10.1371/journal.pone.0023417
69. Santana A, Salinas N, Álvarez C, Mercado L, Guzmán F. Alpha-helical domain from IL-8 of salmonids: mechanism of action and identification of a novel antimicrobial function. *Biochem Biophys Res Commun*. (2018) 498:803–9. doi: 10.1016/j.bbrc.2018.03.061
70. Hoare R, Jung S, Ngo TPH, Bartie K, Bailey J, Thompson KD, Adams A. Efficacy and safety of a non-mineral oil adjuvanted injectable vaccine for the protection of Atlantic salmon (*Salmo salar* L.) against *Flavobacterium psychrophilum*. *Fish Shellfish Immun*. (2019) 85:44–51. doi: 10.1016/j.fsi.2017.10.005
71. Finlay B, McFadden G. Anti-immunology: evasion of the host immune system by bacterial and viral pathogens. *Cell*. (2006) 124:767–82. doi: 10.1016/j.cell.2006.01.034
72. Monack D, Mecsas J, Bouley D, Falkow S. Yersinia-induced apoptosis in vivo aids in the establishment of a systemic infection of mice. *J Exp Med*. (1998) 216:2127–37. doi: 10.1084/jem.188.11.2127
73. Schesser K, Splik A, Dukuzumuremyi J, Neurath M, Petterson S, Wolf-Watz H. The *yopJ* locus is required for *Yersinia*-mediated inhibition of NF-kB activation and cytokine expression: YopJ contains a eukaryotic SH2- like domain that is essential for its repressive activity. *Mol Microbiol*. (1998) 28:1067–79. doi: 10.1046/j.1365-2958.1998.00851.x
74. Gao LY, Kwaik YA. The modulation of host cell apoptosis by intracellular bacterial pathogens. *Trends Microbiol*. (2000) 8:306–13. doi: 10.1016/S0966-842X(00)01784-4
75. Fast MD, Muise DM, Easy RE, Ross NW, Johnson SC. The effects of *Lepeophtheirus salmonis* infections on the stress response and immunological status of Atlantic salmon (*Salmo salar*). *Fish Shellfish Immunol*. (2006) 21:228–41. doi: 10.1016/j.fsi.2005.11.010
76. Lewis DL, Barker DE, McKinley RS. Modulation of cellular innate immunity by *Lepeophtheirus salmonis* secretory products. *Fish Shellfish Immun*. (2014) 38:175–83. doi: 10.1016/j.fsi.2014.03.014
77. Yamagoe S, Yamakawa Y, Matsuo Y, Minowada J, Mizuno S, Suzuki K. Purification and primary amino acid sequence of a novel neutrophil chemotactic factor LECT2. *Immunol Lett*. (1996) 51:9–13. doi: 10.1016/0165-2478(96)02572-2
78. Rabinovitch M. Professional and non-professional phagocytes: an introduction. *Trends Cell Biol*. (1995) 5:85–7. doi: 10.1016/S0962-8924(00)88955-2
79. Neumann NF, Stafford JL, Barreda D, Ainsworth AJ, Belosevic M. Antimicrobial mechanisms of fish phagocytes and their role in host defence. *Dev Comp Immunol*. (2001) 25:807–25. doi: 10.1016/S0145-305X(01)00037-4
80. Hardie LJ, Fletcher TC, Secombes CJ. The effect of vitamin E on the immune response of the Atlantic Salmon (*Salmo salar* L.). *Aquaculture*. (1990) 87:1–13. doi: 10.1016/0044-8486(90)90206-3
81. Hardie LJ, Fletcher TC, Secombes CJ. The effect of dietary vitamin C on the immune response of the Atlantic salmon (*Salmo salar* L.). *Aquaculture*. (1991) 95:201–14. doi: 10.1016/0044-8486(91)90087-N

Conflict of Interest: The authors declare that the research was conducted in the absence of any commercial or financial relationships that could be construed as a potential conflict of interest.

frontiers in Immunology

ORIGINAL RESEARCH
published: 22 January 2020
doi: 10.3389/fimmu.2019.03015

Myelopoiesis of the Amphibian *Xenopus laevis* Is Segregated to the Bone Marrow, Away From Their Hematopoietic Peripheral Liver

Amulya Yaparla[1], *Phillip Reeves*[2†] *and Leon Grayfer*[1*]

[1] Department of Biological Sciences, George Washington University, Washington, DC, United States, [2] School Without Walls High School, Washington, DC, United States

Across vertebrates, hematopoiesis takes place within designated tissues, wherein committed myeloid progenitors further differentiate toward cells with megakaryocyte/erythroid potential (MEP) or those with granulocyte/macrophage potential (GMP). While the liver periphery (LP) of the *Xenopus laevis* amphibian functions as a principal site of hematopoiesis and contains MEPs, cells with GMP potential are instead segregated to the bone marrow (BM) of this animal. Presently, using gene expression and western blot analyses of blood cell lineage-specific transcription factors, we confirmed that while the *X. laevis* LP hosts hematopoietic stem cells and MEPs, their BM contains GMPs. In support of our hypothesis that cells bearing GMP potential originate from the frog LP and migrate through blood circulation to the BM in response to chemical cues; we demonstrated that medium conditioned by the *X. laevis* BM chemoattracts LP and peripheral blood cells. Compared to LP and by examining a comprehensive panel of chemokine genes, we showed that the *X. laevis* BM possessed greater expression of a single chemokine, CXCL12, the recombinant form of which was chemotactic to LP and peripheral blood cells and appeared to be a major chemotactic component within BM-conditioned medium. In confirmation of the hepatic origin of the cells that give rise to these frogs' GMPs, we also demonstrated that the *X. laevis* BM supported the growth of their LP-derived cells.

Keywords: hematopoiesis, myelopoiesis, peripheral liver, bone marrow, CXCL12

OPEN ACCESS

Edited by:
Xinjiang Lu,
Ningbo University, China

Reviewed by:
Katherine Buckley,
Auburn University, United States
Hai-peng Liu,
Xiamen University, China

****Correspondence:***
Leon Grayfer
leon_grayfer@gwu.edu

†Present address:
Phillip Reeves,
Department of Biology, University of Virginia, Charlottesville, VA, United States

Specialty section:
This article was submitted to Comparative Immunology, a section of the journal Frontiers in Immunology

Received: *23 August 2019*
Accepted: *09 December 2019*
Published: *22 January 2020*

Citation:
Yaparla A, Reeves P and Grayfer L (2020) Myelopoiesis of the Amphibian Xenopus laevis Is Segregated to the Bone Marrow, Away From Their Hematopoietic Peripheral Liver. Front. Immunol. 10:3015. doi: 10.3389/fimmu.2019.03015

INTRODUCTION

Across all vertebrates, pluripotent pre-committed and lineage-committed blood cell precursors reside within designated hematopoietic sites (1). During blood cell lineage commitment, the pluripotent stem cells give rise to common lymphoid (2) and common myeloid (3) progenitors (CLPs and CMPs, respectively). The CLPs further differentiate into B and T cell precursors, while the CMPs give rise to precursors of the megakaryocyte/erythroid (MEPs) or granulocyte/macrophage potential (GMPs) (3). Site(s) of adult animal hematopoiesis vary across vertebrata, from bone marrow in reptiles (4), birds (5, 6), and most mammalian species (7) to the head kidney in teleost fish (8, 9). In turn, the differentiation of GMPs toward the macrophage lineage depends on the activation of the colony stimulating factor-1 receptor (CSF-1R) (10) by its cognate ligand, colony stimulating factor-1 (CSF-1), which acts as a monopoietic growth

factor (11, 12). Similarly, the differentiation of MEPs toward the erythroid lineage depends on erythropoietin (EPO) (13, 14). Notably, while the peripheral (subcapsular) liver of the anuran amphibian *Xenopus laevis* is considered to be the principal site of hematopoiesis (14–16), we demonstrated that the cells responsive to CSF-1 reside in the *X. laevis* bone marrow and are absent from their peripheral liver (17, 18). Conversely, we (17) and others (14) showed that the *X. laevis* peripheral liver, but not their bone marrow, contains cells that respond to EPO to form erythroid-lineage cells. To date, the ontogeny of *X. laevis* bone marrow GMPs remains poorly understood.

The step-wise lineage commitment of pluripotent cells depends on external stimuli, including specific growth factors akin to CSF-1 and EPO, and progenitor cell-stromal cell interactions (19, 20). Concurrently, these commitment steps are marked by changes in gene expression of cell lineage-specific transcription factors, which are thus often used as markers to identifying the respective, lineage-committed cell populations (19–21). For example and pertinently to this work, as CMPs commit to MEPs or GMPs, they exhibit increased expression of *fli1*, *gata1*, and *nfe2* or *pu1*, *egr1*, *egr2*, and *gfi1,* respectively (19–21).

The retention of progenitors and certain committed blood cells within hematopoietic tissues, as well as the mobilization and homing of specific cell populations to disparate tissues within organisms, is mediated by designated chemokines (22). In general, chemokines are classified into four families based on the presence and positioning of conserved cysteine residues: C, CC, CXC, and CX3C (23). Chemokines typically act through cell-surface G-protein-coupled seven-transmembrane receptors and have been most thoroughly described in the context of leukocyte recruitment during immune responses (23). Conversely, the roles of chemokines in hematopoiesis first became evident from the analyses of the interaction between CXCL12 (also known as stem cell derived factor-1) and its receptor CXCR4 in mice, wherein the inactivation of the *cxcl12* and *cxcr4* genes resulted in defective hematopoiesis, cardiogenesis, and vascular development (24–26). The biological roles of CXCL12 have also been examined in other vertebrates such as fish and avian species, wherein studies have demonstrated the roles of CXCL12 in muscle formation, vascular development, and homing of hematopoietic stem cells (26–28). While the roles of the amphibian CXCL12 have not been extensively studied, the *X. laevis* CXCL12 has been shown to activate the frog CXCR4 (29).

Here we examine the *X. laevis* peripheral liver as a potential source of precursor cells to GMPs and assess the putative role of CXCL12 in homing of these cells to the myelopoietic bone marrow of this animal.

MATERIALS AND METHODS

Animals, Culture Media and Conditions

Outbred, ∼1- to 2-year-old adult *X. laevis* were purchased from Xenopus1 (Dexter, MI), housed, and handled under strict laboratory regulations of Animal Research Facility at the George Washington University (GWU) and as per the GWU Institutional Animal Care and Use Committee regulations (approval number 15-024).

All cell cultures were established in amphibian serum-free medium supplemented with 10% fetal bovine serum, 0.25% *X. laevis* serum, 10 μg/ml gentamycin (Thermo Fisher Scientific), 100 U/ml penicillin, and 100 μg/ml streptomycin (Gibco). Amphibian phosphate-buffered saline (APBS) that was used while isolating the cells has been previously described (18).

Production of Frog Recombinant Cytokines and Chemokines

X. laevis recombinant (r)CSF-1, rEPO, and rCXCL12 were produced using an Sf9 insect cell expression system by a previously described method (18). Briefly, PCR amplicons corresponding to the open reading frames of the respective signal peptide-cleaved proteins were ligated into the pMIB/V5 His A vector. Sf9 insect cells were transfected with the expression constructs (Cellfectin II, Invitrogen), and positive transfectants were selected using 10 μg/ml of blasticidin, their supernatants were screened for recombinant production by western blot against the V5 epitope on the proteins. The cultures expressing rCSF-1, rEPO, or rCXCL12 were scaled up and grown as 500-ml cultures for 5 days, and their supernatants were collected by centrifugation, concentrated against polyethylene glycol flakes (8 kDa) at 4°C, and dialyzed for 2 days against 150 mM sodium phosphate at 4°C. The recombinant proteins were isolated from these concentrated supernatants via Ni-NTA agarose columns (Qiagen), washed with 2 × 10 volumes of high-stringency wash buffer (0.5% tween 20, 20 mM sodium phosphate, 500 mM sodium chloride, and 100 mM imidazole), and 5 × 10 volumes of low-stringency wash buffer (as above, but with 40 mM imidazole). The recombinants were then eluted in 1-ml fractions with 250 mM imidazole. Western blot analysis was performed against the V5 epitopes on rCSF-1, rEPO, and rCXCL12 to confirm the presence of the recombinants. For each protein, the fractions expressing the recombinant were combined and further concentrated against polyethylene glycol flakes (8 KDa) and dialyzed overnight against APBS at 4°C. The protein concentrations were determined by Bradford protein assays (BioRad), and a protease inhibitor cocktail (Halt protease inhibitor cocktail; Thermo Scientific) was added to the purified proteins, which were then aliquoted and stored at −20°C until use. The composition of the recombinant proteins was tested by western blot against the V5 epitope on the protein (**Supplementary Figure 1**).

The recombinant control (r-ctrl) was produced by transfecting Sf9 cells with an empty pMIB/V5 His A insect expression vector (Invitrogen), collecting the resulting supernatants and processing these using the same methodology as described for rCSF-1/rEPO/rCXCL12.

Bone Marrow, Peripheral Liver, and Peripheral Blood Leukocyte Isolation and Culture

The liver periphery (LP) cells and bone marrow (BM) cells were isolated by a previously described method (30). Briefly, *X.*

laevis femurs and liver tissues were aseptically excised from five individual frogs ($N = 5$) that had been euthanized by tricaine mesylate overdose and cervical dislocation. Femurs were flushed with 10 ml of ice-cold APBS each, and the flushed cells were washed and re-suspended in culture medium.

The peripheral regions of the frog livers were aseptically peeled off using sterile tweezers and passed through 70-μm nylon mesh cell strainers (Fisher). The isolated cells were layered over 51% percoll (Sigma) (49% APBS) and centrifuged at 600 × *g* at 4°C for 20 min to separate out leukocytes from the red blood cells. The leukocytes containing interfaces were collected and washed with ice-cold APBS prior to culture.

Peripheral blood leukocyte (PBL) isolation was performed as follows. Blood was collected from euthanized animals ($N = 5$) by cardiac puncture into medium (containing 1 mg/ml heparin) and processed over 51% percoll, as described above for LP cells, to isolate PBLs.

All cells were enumerated using trypan blue (Invitrogen) live/dead exclusion method.

Toward the analyses of bone marrow chemokine gene expression, the frog femurs were flushed with APBS to remove non-stromal cells and were then repeatedly flushed with Trizol reagent (Invitrogen) to remove stromal/supporting cells. The RNA isolation and cDNA synthesis were carried out as described below.

To assess the effects of monopoietic and erythropoietic stimuli on LP and BM cells, five adult *X. laevis* ($N = 5$) were injected intraperitoneally (ip) with 5 μg of rCSF-1 or rEPO and euthanized 3 days later, and their LP and BM cells were isolated as described above.

Isolation of RNA and Quantitative Gene Expression Analyses

For all experiments, total RNA from *X. laevis* cells or tissues was isolated using Trizol reagent (Invitrogen) in accordance to the manufacturer's directions. The isolated RNAs (500 ng total) were reverse-transcribed into cDNAs using cDNA qscript supermix (Quanta), according to the manufacturer's instructions.

All quantitative gene expression analyses were performed using the CFX96 Real-Time System and iTaq Universal SYBR Green Supermix (Quanta). The BioRad CFX Manager software was employed for all expression analysis. All gene expression analyses were performed using the delta∧delta CT method, with expression examined relative to the *gapdh* endogenous control. For all experiments, the relative expression was normalized against the lowest observed expression within respective data set. All primers were validated prior to use, and the sequences of all employed primers are listed in **Supplementary Table 1**.

Western Blot Analyses of Cellular Transcription Factor Protein Levels

To examine transcription factor expression at the protein level, *X. laevis* LP and BM cells were isolated from three individual frogs ($N = 3$) and lysed in ice-cold radio-immunoprecipitation assay buffer (Thermo Fisher Scientific) in the presence of halt protease and phosphatase inhibitor cocktail (Thermo Fisher Scientific). Protein concentrations of the cell lysates were determined using Bradford protein assays (BioRad), and 30 μg of total protein per sample was resolved by SDS-PAGE and examined by western blot using mouse monoclonal antibodies against Tal1, Egr1, Gfi1, and actin (Santa Cruz) and a secondary goat anti-mouse HRP-conjugated antibody (Thermo Fisher Scientific). Densitometry was performed using ImageJ software. Prior to western blot analyses, protein sequence alignments of mammalian and *X. laevis* Tal1, Egr1, Gfi1, and actin proteins were performed to ensure that the respective epitopes targeted by each of the above antibodies were conserved in the respective *X. laevis* proteins.

Chemotaxis Assays

Chemotaxis assays were performed using blind well chemotaxis (Boyden) chambers (Neuro Probe), with 100-fold serial dilutions of rCXCL12, concentrations at 10–10^{-7} ng/ml (in culture medium), loaded into the bottom well of these chambers. The wells were overlaid with 13-mm chemotaxis filters (5 μm pore size; Neuro Probe), with addition of 10^4 LP cells or PBLs in 200-μl volumes of culture medium to the upper chambers. Chemotaxis assays were incubated at 27°C with 5% CO_2 for 3 h. Subsequently, the cells/medium was removed from the top chambers, and the upper sides of the filters were wiped with cotton swabs. The filters were then stained with Giemsa stain, and the numbers of migrating cells were determined by counting 10 random fields of view per lower side of each filter (×40 objective). For the chemokinesis experiments, both the lower and the upper wells of the chemotaxis chambers were loaded with the most potent chemoattractive concentrations of rCXCL12 (10^{-3} ng/ml), and the assays were performed as above.

For chemotaxis assays using supernatants derived from BM stroma, *X. laevis* femurs were isolated and gently flushed with 10 ml of APBS to remove any non-stromal cells, thus leaving the stroma intact. The femurs were then incubated overnight (16 h) in 1 ml of culture medium each, and the following day the femur-conditioned medium were centrifuged to remove any cells and debris and concentrated tenfold against polyethylene glycol flakes (8 KDa) at 4°C. These BM-conditioned media (BM-med) were serially diluted to 10^{-1} and 10^{-2} and used for chemotaxis assays as described above. Chemokinesis experiments were performed by adding tenfold concentrated BM-med to both upper and lower chemotaxis chambers.

Combined chemotaxis assays of rCXCL12 and BM-conditioned medium were performed by either loading rCXCL12 (10^{-3} ng/ml) into lower chemotaxis chambers and BM-med (tenfold concentrated) into upper chambers or vice-versa, with the target PBLs or LP cells (10^4) added to upper chambers. The enumerated chemotaxis was compared to cell migration toward the rCXCL12 (10^{-3} ng/ml) or BM-med alone (in lower chambers).

Cells derived from five individual animals ($N = 5$) were used for each and all chemotaxis assays and all assays performed as described above.

In vitro Culture of Peripheral Liver Cells Within Frog Bone Marrow

Frog femurs and LP cells were isolated as described above. The femurs were cut at the condyles on one side of each bone, thereby creating openings into individual femurs. For each animal, one femur bone was then gently flushed with

APBS, while the other was flushed with 10 ml of methanol to fix the BM stromal/supporting cells. The isolated LP cells (10^5) from respective animals were introduced into each of the two femurs from the corresponding animal by gently placing the opening side up into 10 ml of semi-solid culture medium (10% methyl cellulose) and incubating for 3 days at 27°C and 5% CO_2. Subsequent to this incubation, femurs were cut at the opposite condyles, and the cells were collected by flushing each bone with APBS and enumerated using trypan blue live/dead exclusion method. This experiment was repeated three times, each time using cells from six individual animals ($N = 6$) per experiment.

Statistical Analysis

For all gene expression and densitometry data, statistical analysis was conducted using paired Student's *T*-test. Chemotaxes data were examined using ANOVA and *post-hoc* Tukey tests via Graphpad Prism 7.0 software. Probability level of $P < 0.05$ was considered significant.

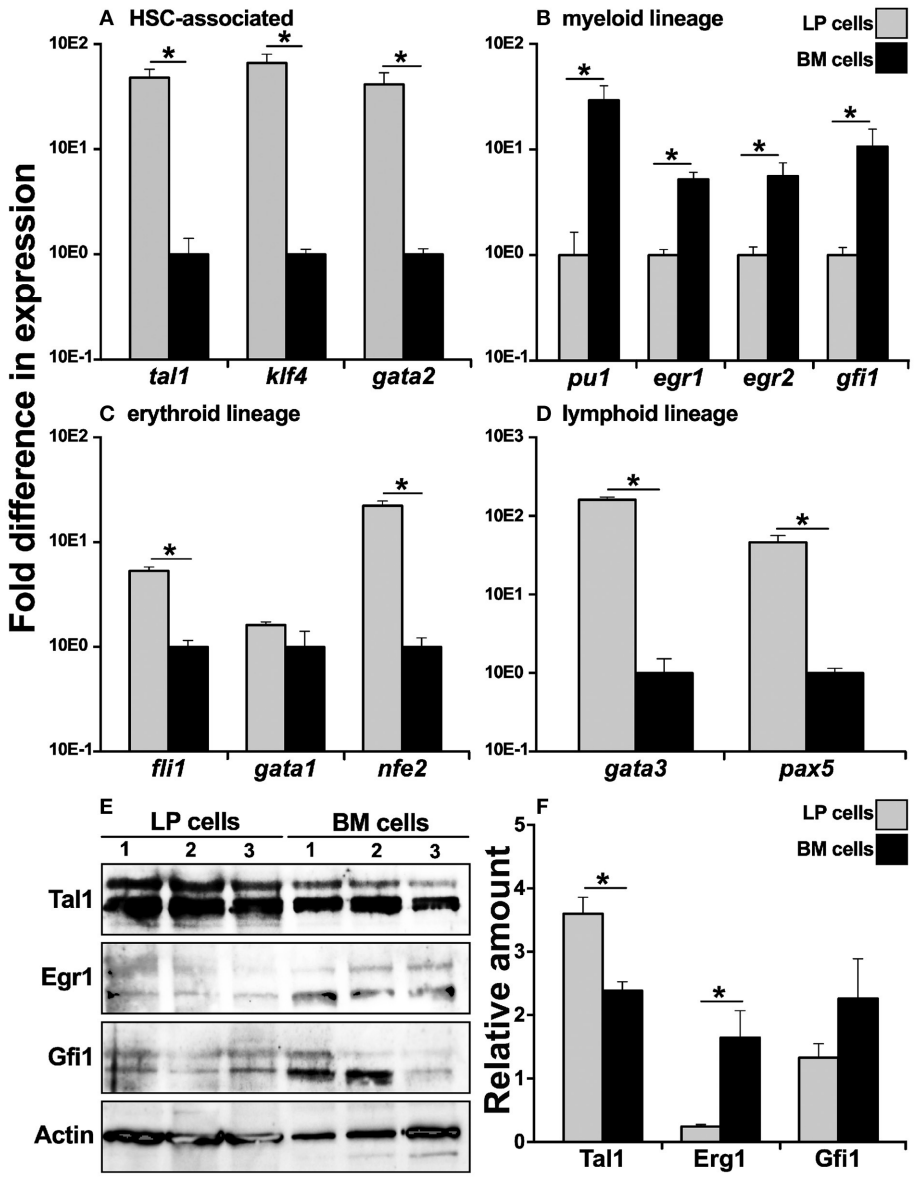

FIGURE 1 | Analysis of lineage-specific transcription factor gene expression in *X. laevis* liver periphery and bone marrow cells. *X. laevis* liver periphery and bone marrow cells were isolated and examined by qPCR for their expression of **(A)** HSC-associated, **(B)** myeloid lineage, **(C)** erythroid-lineage, and **(D)** lymphoid-lineage transcription factor genes. All gene expressions were quantified relative to the *gapdh* endogenous control and normalized against the lowest observed expression. 30 μg of total cell lysate proteins from LP and BM cells was used for western blot analysis to determine the protein levels of **(E)** Tal1, Egr1, and Gfi1 with beta actin as a loading control. The protein levels were quantified by **(F)** densitometry analyses using ImageJ software. Results are means ± SEM (**A–D**: $N = 5$; **E,F**: $N = 3$) and *asterisk* overhead of *horizontal lines* denotes statistical significance, $P < 0.05$.

RESULTS

X. laevis Peripheral Liver and Bone Marrow Cells Possess Distinct Expression Profiles of Lineage-Specific Transcription Factors

Since the *X. laevis* peripheral liver is host to most hematopoiesis in this animal (14–16), we examined whether this tissue is the source of cells that commit toward the bone marrow resident granulocyte macrophage precursors (GMPs). To this end, we compared cells from the *X. laevis* LP and BM for their respective gene expression of key transcription factors (TFs) associated with distinct blood cell lineage commitment. In comparison to BM cells, the LP-derived cells exhibited greater mRNA levels for TFs associated with hematopoietic stem cells (HSCs), including *tal1* (31), *klf4* (32), and *gata2* (33), thus corroborating that the peripheral liver is the principal hematopoietic site in *X. laevis* (**Figure 1A**). Interestingly, myeloid lineage-specific TFs, including *pu1* (34), *egr1* (35), *egr2* (36), and *gfi1* (37), were expressed at significantly greater levels by the BM cells compared to the LP cells (**Figure 1B**), supporting our previous finding that GMPs reside in the *X. laevis* bone marrow and are absent from their peripheral liver (17, 18). Furthermore, in comparison to BM cells, the LP cells displayed significantly greater gene expression for erythroid lineage TFs, including *fli1*(38) and *nfe2* (39), while *gata1* (40) was expressed at comparable levels in the both cell types (**Figure 1C**). The lymphoid lineage TFs *gata3* (41) and *pax5* (42) also displayed significantly greater mRNA levels in the LP cells compared to BM cells (**Figure 1D**). These findings supported our previous observations that the *X. laevis* peripheral liver hosts most blood cell development, excluding the bone marrow-mediated myelopoiesis (17).

To confirm the respective hematopoietic and myelopoietic nature of the *X. laevis* LP and BM cells, we assessed the two cell types for their relative protein levels of myeloid (Gfi1, Egr1) and HSC-associated (Tal1) transcription factors by western blot (**Figures 1E,F**). As expected, while LP cells possessed significantly greater protein levels of Tal1 (non-phosphorylated, lower bands; phosphorylated, upper bands), the *X. laevis* BM cells exhibited relatively more robust Gfi1 and Egr1 (non-phosphorylated, lower bands; phosphorylated, upper bands) protein levels (significantly so for Erg1) (**Figures 1E,F**).

X. laevis Bone Marrow and Liver Periphery Cells Respond to Monopoietic and Erythropoietic Stimuli, Respectively

Because we observed significantly greater myeloid TF expression by the BM cells, while the erythroid lineage TFs were more robustly expressed by the LP cells (**Figures 1B,C**, respectively), we next analyzed the expression of these respective lineage-specific markers in LP and BM cells isolated from animals that had been stimulated with recombinant forms of the principal mediators of monopoiesis and erythropoiesis, colony stimulating fator-1 (rCSF-1) or erythropoietin (rEPO), respectively. To this end, frogs were injected intraperitoneally (ip) with rCSF-1 or rEPO, and 3 days later, their LP and BM cells were examined for changes in TF gene expression. Neither LP cells nor BM cells from animals stimulated with either growth factor exhibited significant differences in their gene expression of the HSC-specific *tal1* and *klf4* TFs (**Figures 2A,B**). Interestingly, LP cells from rEPO-stimulated animals possessed significantly greater transcript levels for the erythroid TFs *gata1* and *nfe2* (**Figure 2B**). Conversely, BM cells, but not LP cells from rCSF-1-treated animals, exhibited a significantly elevated expression of the myeloid TFs *pu1* and *egr1* (**Figure 2A**). We did not observe changes in the expression of other examined myeloid lineage or HSC-specific TFs in the LP and BM cells from rCSF-1- and rEPO-stimulated frogs (**Figures 2A,B**).

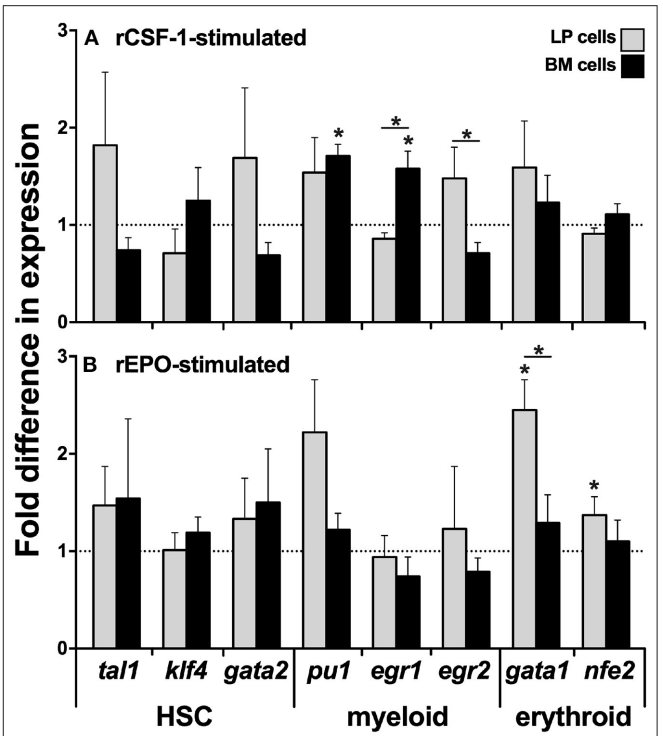

FIGURE 2 | Analysis of lineage-specific transcription factor gene expression in liver periphery and bone marrow cells from rCSF-1- and rEPO-stimulated *X. laevis*. Adult *X. laevis* frogs were injected intraperitoneally with 5 μg of rCSF-1, rEPO, or equal volumes of r-ctrl, and 3 days later their liver periphery and bone marrow cells were assessed for lineage-specific transcription factor gene expression in **(A)** rCSF-1-stimulated and **(B)** rEPO-stimulated cells. The examined genes included hematopoietic-associated TFs: *tal1*, *klf4*, *gata2*, *nfe2*; myeloid-lineage TFs: *pu1*, *egr1*, *egr2*; and erythroid lineage TFs: *gata1*, *nfe2*. All gene expressions was quantified relative to the *gapdh* endogenous control and the gene expression is presented relative to the respective gene expression in *r*-ctrl-treated animals; denoted by *dashed lines*. Results are means ± SEM ($N = 5$) and *asterisk* overhead of *horizontal lines* denote statistical significance between the two cell types and (*) denotes statistical differences between the r-ctrl and respective r-growth factor stimulation, within respective cell types, $P < 0.05$.

X. laevis Bone Marrow Produces Factors That Are Chemoattractive to Peripheral Liver Cells and Blood Leukocytes

We hypothesized that the *X. laevis* myeloid precursors originate in the LP and are traffick through blood circulation to the BM

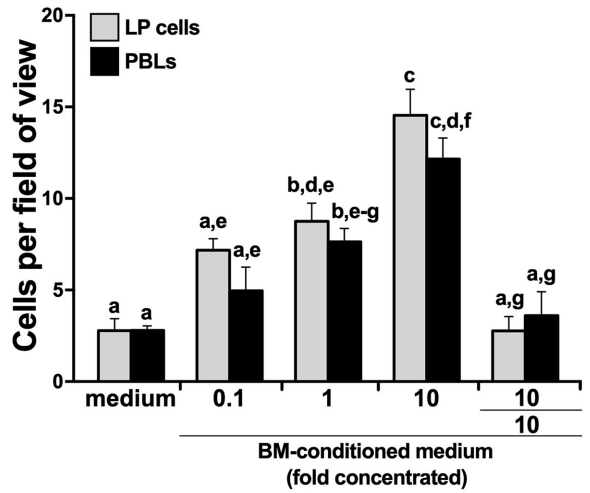

FIGURE 3 | *X. laevis* bone marrow-conditioned medium chemoattracts peripheral liver and blood leukocytes. Tenfold concentrated bone marrow-conditioned medium was serially diluted and examined for its ability to chemo-attract liver periphery (LP) cells and peripheral blood leukocytes (PBLs). Chemokinesis of LP cells and PBLs was measured by adding the tenfold concentrated BM-medium to both the upper and the lower chemotaxis chambers (denoted as 10/10). All chemotaxis/chemokinesis experiments were performed using cells from five individual animals ($N = 5$), enumerating 10 random fields of view per chemotaxis filter per animal. Results are means ± SEM. *Above-head letters* denote statistical designations: experimental groups described by distinct *letters* are statistically different ($P < 0.05$), while those marked by the same letters are not.

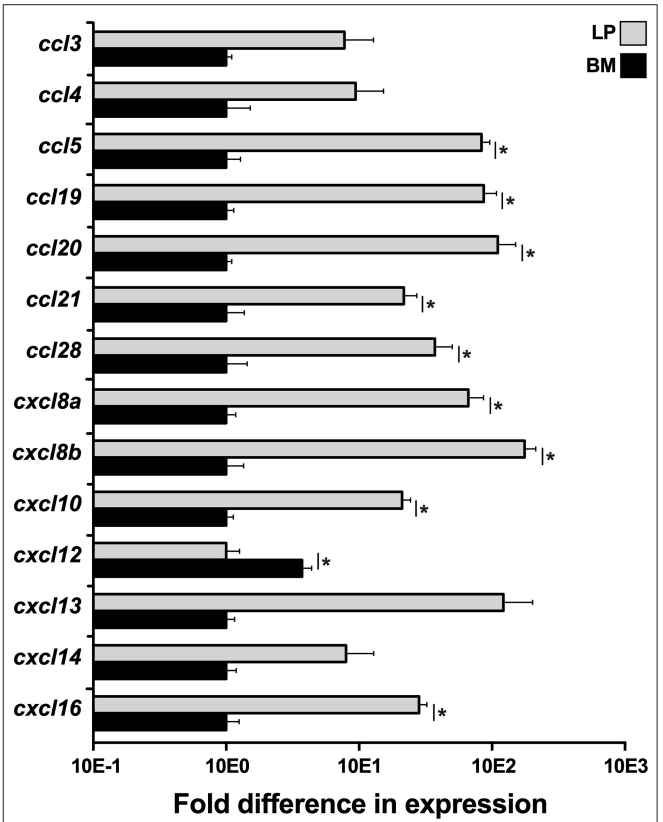

FIGURE 4 | Analysis of chemokine gene expression in *X. laevis* liver periphery and bone marrow. Frog liver periphery (LP) and bone marrow (BM) from five individual animals ($N = 5$) were examined for their expression of a panel of chemokine genes by qPCR. All gene expressions were quantified relative to the *gapdh* endogenous control and normalized against the lowest observed expression. Results are means ± SEM and (*) overhead of *horizontal lines* denote statistical significance, $P < 0.05$.

in response to specific BM-produced chemoattractive factors. To test this notion, we opened *X. laevis* femurs, flushed them to remove resident leukocytes, and incubated the resulting femur bones in medium, thereby conditioning the medium with any factors that would be produced by the BM stroma/supportive tissue. We then concentrated the conditioned medium tenfold and assessed the capacity of this conditioned medium to chemoattract LP cells and PBLs. As anticipated, both the LP cells and PBL populations displayed dose-dependent migration toward the BM-conditioned medium (**Figure 3**). The LP and peripheral blood cells migrating toward the BM-conditioned medium possessed somewhat mixed cytology, reminiscent of immature myeloid-lineage cells (**Supplementary Figure 2**).

To delineate whether this migration was gradient dependent (chemotaxis) or gradient independent (chemokinesis), we repeated the migration studies, this time adding BM stroma-condition medium (tenfold concentrated) to both upper and lower chemotaxis chambers, thereby disrupting any chemoattractant gradient. This resulted in significantly diminished migration of both LP cells and PBLs (**Figure 3**), indicating that the factors present in the conditioned medium were eliciting chemotaxis rather than chemokinesis.

X. laevis Peripheral Liver and Bone Marrow Stroma Possess Unique Chemokine Gene Expression Profiles

To elucidate what chemokines might be produced by the *X. laevis* BM stroma, we compared the LP and BM stromal cells for their gene expression of a panel of chemokines, including *ccl3*, *ccl4*, *ccl5*, *ccl19*, *ccl20*, *ccl21*, *ccl28*, *cxcl8a*, *cxcl8a*, *cxcl10*, *cxcl12*, *cxcl13*, *cxcl14*, and *cxcl16* (**Figure 4**). Most notably, the BM stromal cells possessed significantly greater transcript levels of a single chemokine, *cxcl12*, while the LP cells displayed greater mRNA levels of all other examined chemokines (**Figure 4**).

CXCL12 Is Chemotactic to *X. laevis* LP Cells and PBLs

To confirm the roles of the CXCL12 in the *X. laevis* homing of myeloid cells, we generated a recombinant form of the *X. laevis* CXCL12 (rCXCL12) and performed chemotaxis assays with LP cells and PBLs. As hypothesized, the rCXCL12 elicited concentration-dependent migration of both LP cells and PBLs (**Figure 5A**). Notably, at the lowest examined dose of 10^{-7} ng/ml, rCXCL12 resulted in significantly greater migration of LP cells compared to PBLs, whereas significantly greater numbers of PBLs than LP cells were recruited at 10^{-1} ng/ml of the chemokine (**Figure 5A**). Moreover, our chemokinesis studies indicated that rCXCL12 was eliciting chemotaxis rather than chemokinesis of both LP cells and PBLs (**Figure 5A**).

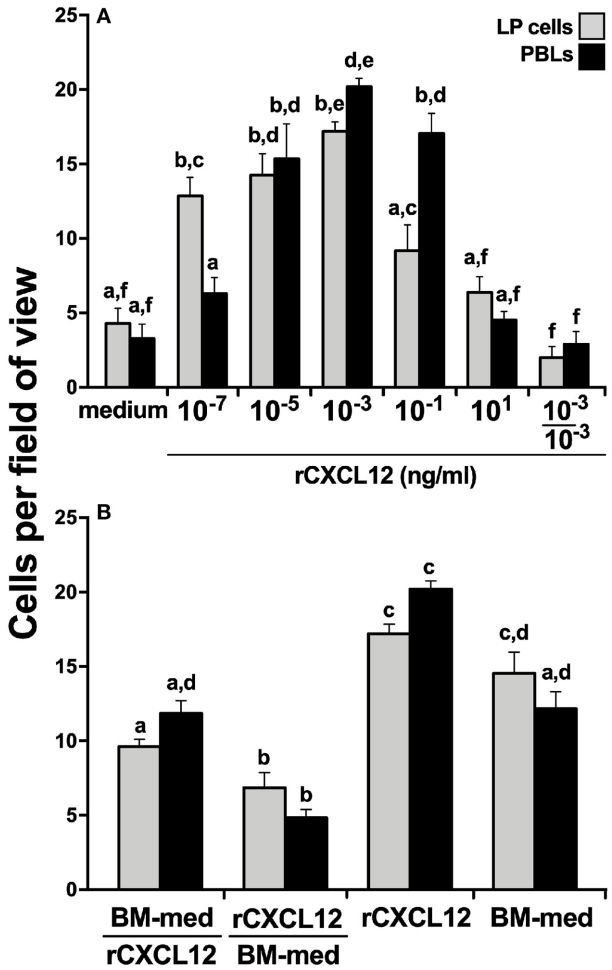

FIGURE 5 | *X. laevis* rCXCL12 is chemotactic to liver periphery and peripheral blood leucocytes. A recombinant *X. laevis* CXCL12 (rCXCL12, 10^{-7}-10^{1} ng/ml) was examined for its capacity to chemoattract **(A)** liver periphery (LP) cells or peripheral blood leucocytes (PBLs; 10^4 cells/well) with chemokinesis assessed by adding 10^{-3} ng/ml of rCXCL12 (optimal dose) to both the upper and the lower chemotaxis chambers. **(B)** The relative capacities of tenfold concentrated bone marrow conditioned medium (BM-med) and rCXCL12 (10^{-3} ng/ml) to chemoattract LP cells and PBLs (10^4 cells/well) were compared through chemokinesis experiments by adding either BM-med or rCXCL12 and rCXCL12 or BM-med to the upper and lower chemotaxis chambers, respectively (denoted as BM-med/rCXCL12; rCXCL12/BM-med) and compared to BM-med or rCXCL12 in only bottom wells. All chemotaxis/chemokinesis experiments were performed using cells from 5 individual animals ($N = 5$), enumerating 10 random fields of view per chemotaxis filter per animal. Results are means ± SEM. Above-head *letters* denote statistical designations: experimental groups described by distinct letters are statistically different ($P < 0.05$), while those marked by the same letters are not.

Because the *X. laevis* BM harbor GMPs and displayed robust *cxcl12* gene expression (**Figure 4**), while rCXCL12 was chemotactic to LP cells and PBLs (**Figure 5A**), we hypothesized that CXCL12 may be a major component of BM-conditioned medium. To address this notion, chemokinesis experiments were carried out using BM-conditioned medium (BM-med, obtained as described above and concentrated tenfold) and rCXCL12, with either rCXCL12 in the bottom chemotaxis chambers and with BM-med loaded into the upper wells, or vice-versa. LP cell and PBL chemotaxis was substantially reduced in either condition (**Figure 5B**) (significantly so when rCXCL12 was added to top wells), suggesting that indeed CXCL12 may be a major chemotactic component of BM-conditioned medium as it ablates the gradient-dependent chemotaxis elicited by BM-conditioned medium. Both LP cells and PBLs displayed a significantly greater migration toward rCXCL12 than toward the BM-med (**Figure 5B**), presumably owing to the greater concentration gradient established by the rCXCL12 than present in the BM-med.

The rCXCL12 Chemoattracts Myeloid-Lineage Cells

To define the lineage commitment of the rCXCL12-responsive LP cells and PBLs, we repeated the rCXCL12 chemotaxis experiment and isolated from the bottom chemotaxis chambers the LP cells and PBLs that migrated toward this chemokine. We then examined these cells for their gene expression of *cxcr4*, the cognate receptor for CXCL12 (43) as well as a panel of myeloid, hematopoietic, erythroid, and lymphoid cell lineage markers (**Figure 6**). Notably, both the LP cells and PBLs that chemotaxed toward rCXCL12 exhibited robust (compared to total input LP cells and PBLs, respectively) gene expression of CXCR4. While the LP cells chemotaxed toward rCXL12 possessed significantly lower gene expression of the macrophage *csf1r* (*c-fms*) compared to total LP cells; rCXCL12-recruited PBLs possessed significantly greater *csf1r* mRNA levels than total PBLs, and both rCXCL12-recuited LP cells and PBLs possessed significantly greater transcript levels for the granulocyte *csf3r* marker than total LP and PBL cells, respectively (**Figure 6**). Moreover, the PBLs but not LP cells recruited toward the rCXCL12 exhibited greater expression of myeloid lineage TFs, *pu1*, and *gfi1* than seen in total respective PBL and LP cells (**Figure 6**).

The rCXCL12-recruited LP cells and PBLs did not exhibit significantly greater levels of any of the examined HSC (*tal1*, *klf4*, *gata2*) or erythroid (*fli1*, *gata1*, *nfe2*)-lineage TF genes, compared to total respective cell subsets, while the rCXCL12-recruited LP cells possessed significantly lower expression of *klf4* (**Figure 6**). Compared to total LP cells and PBLs, the rCXCL12-recruited LP cells and PBLs exhibited significantly lower gene expression of *igm* [expressed by B cells; (44)], and while the recruited PBLs possessed greater *cd4* [expressed by T helper cells and some macrophages; (45, 46)] transcript levels, the chemotaxed LP cells exhibited greater mRNA levels of *cd8a* [expressed by cytotoxic T cells and some dendritic cells; (47, 48)] (**Figure 6**).

The *X. laevis* Bone Marrow Supports the Survival of Peripheral Liver-Derived Cells

In accordance to the above findings, we reasoned that if the LP is indeed the source of myeloid cell precursors that home to the BM, then the BM should be capable of supporting LP cell survival *in vitro*. To test this idea, we isolated LP cells and cultured them *in vitro* in semi-solid medium within flushed *X. laevis* femurs

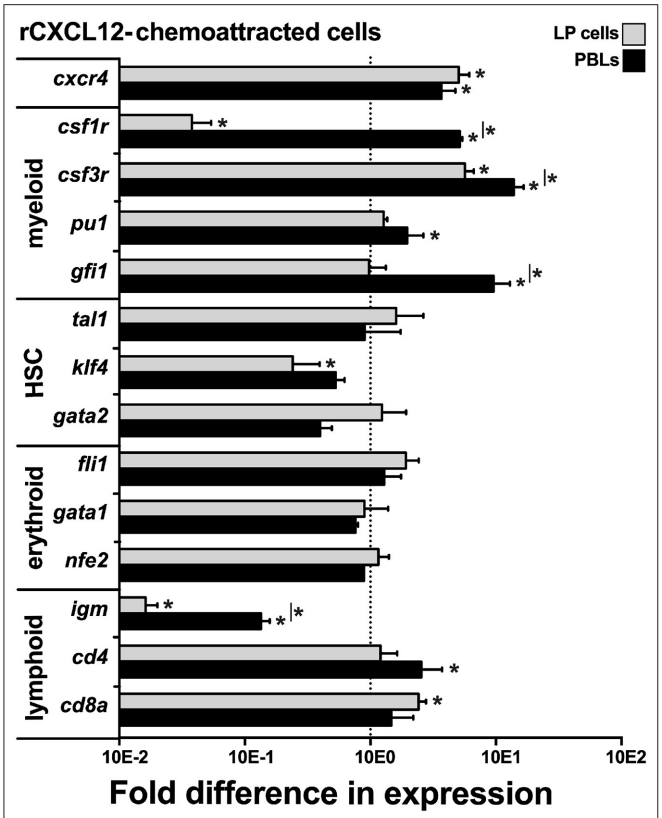

FIGURE 6 | *X. laevis* rCXCL12 chemoattracts myeloid-lineage cells. Chemotaxis assay using the optimal concentration of rCXCL12 (10^{-3} ng/ml) was performed on liver periphery (LP) cells and peripheral blood leucocytes (PBLs; 10^4 LP cells or PBLs/well, cell from five individual frogs, $N = 5$), and the chemoattracted cells were examined for their gene expression of *crcr4* (receptor for CXCL12); lineage specific markers for myeloid: *csf1r* (macrophage), *csf3r* (granulocyte), *pu1*, *gfi1*; HSC-associated: *tal1*, *klf4*, *gata2*; erythroid: *fli1*, *gata1*, *nfe2*, and lymphoid cell populations: *igm* (B cell); *cd4* (T helper cell); and *cd8* (cytotoxic T cell) by qPCR. All gene expressions was quantified relative to the *gapdh* endogenous control and normalized against the corresponding gene expression observed in the LP cells or PBLs (input, indicated by the *dashed line*) used in these chemotaxis experiments. Results are means ± SEM, (*) denotes statistical differences from the gene expression in total input LP or PBL population (indicated by the *dashed line*) and (*) above *horizontal bars* denote statistical differences between LP cells and PBLs, $P < 0.05$.

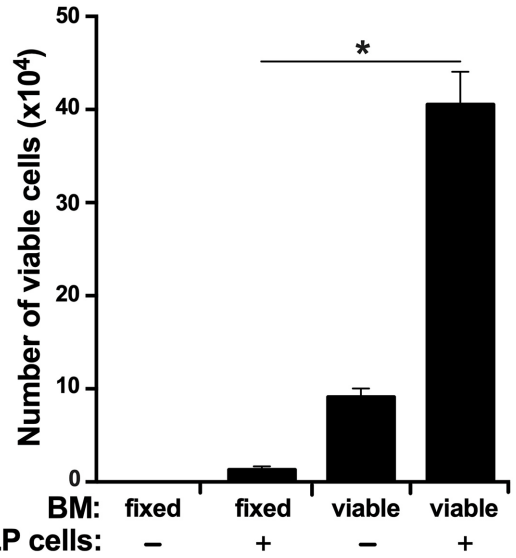

FIGURE 7 | The *X. laevis* bone marrow supports the survival of liver periphery cells. The frog femurs were isolated and cut at the condyles on one side of each bone to create an opening. One femur from each animal was flushed with saline and the other with methanol to fix the stromal/supportive cells. Liver periphery (LP) cells (10^5 cells per femur from the same respective animals) were introduced into each of the femurs and placed in semi-solid medium with the open-end facing up. After 3 days of incubation, the viable cells in these femurs were enumerated. Results represent combined data derived from three independent such experiments, each experiment assessing tissues/cells from six individual frogs ($N = 6$ per experiment; $N = 18$). Results are means ± SEM and (*) overhead of *horizontal lines* denote statistical significance, $P < 0.05$.

or femurs with methanol-fixed (and washed) stroma/supportive tissue. As expected, the LP cells displayed significantly greater survival when cultured within viable femur bones as compared to femurs that had been methanol-fixed, thus indicating that the BM is capable of supporting LP cells (**Figure 7**).

DISCUSSION

Mammalian hematopoiesis begins in the yolk sac, shifts to the aorta-gonad-mesonephros region of the developing embryo, then to the fetal liver followed by fetal spleen, and ultimately to the bone marrow (49). Similarly, during the early life of avian species, the liver acts as a hematopoietic site, with hematopoiesis later shifting to the avian bone marrow (5, 6). Interestingly, our previous findings indicate that hematopoiesis is segregated between different tissues in the adult *X. laevis*, with myelopoiesis occurring in the bone marrow and to our knowledge, the remaining blood cell development being facilitated by the peripheral liver (14–18). Notably, while the importance of transcription factors to hematopoiesis and lineage commitment has been well-established across vertebrates (19–21), our present transcription factor gene and protein expression analyses of the *X. laevis* peripheral liver and bone marrow cells corroborate our previous findings (17, 18) that while the peripheral liver hosts most hematopoiesis of this animal, the myelopoiesis and GMPs are segregated to the *X. laevis* bone marrow.

Numerous factors contribute to the specialized niche microenvironments within hematopoietic sites to facilitate blood cell development. These include specific cell populations that assist in the interactions between HSCs and the supportive tissues through anchoring/mobilization and production of cytokines/growth factors and chemokines, in addition to other instructive stimuli that may facilitate hematopoietic cell maintenance and regulation (19, 50, 51). Consistent with this, it is possible that one or several of such factors that are crucial for GMP homing, maintenance, and/or differentiation are present in the bone marrow and are absent from the peripheral liver, thus necessitating the segregation of hematopoiesis across these two sites within *X. laevis*. Interestingly, while the blood cell

development in adult aquatic anuran amphibian species occur in their peripheral liver tissues, as illustrated in *Xenopodinae* (14–16), this process occurs in the bone marrow of more terrestrial anuran species (52, 53), presumably exemplifying a step-wise evolutionary transition of hematopoiesis from hepatic tissues to bone marrow. Supporting this theory, more recently diverged terrestrial anuran amphibians, such as those of *Rana* genus, utilize their bone marrow as sites for erythropoiesis (54), while in the phylogenetically older aquatic anurans such as *Xenopodinae*, erythropoiesis occurs in the peripheral liver and is absent from their bone marrow (14, 17). Perhaps this suggests that from an evolutionary standpoint, the use of bone marrow as the principal hematopoietic site co-evolved with adaptation of vertebrate life from water to land. This notion is well-corroborated by the fact that most (relatively primordial) aquatic amphibians, such as those of *Gymnophiona* (legless caecilians and species more closely related to them) and *Urodela* (newts and salamanders) orders, are devoid of bone marrow hematopoiesis (52, 55), whereas terrestrial salamanders of the family *Plethodontidae* exclusively utilize their bone marrow toward granulopoiesis and lymphopoiesis (56).

The use of bone marrow as a site of hematopoiesis by amphibians appears to have co-evolved with progressively greater vascularization of this site and coincides with adaptation toward more terrestrial (rather than aquatic) life (57). For example, the bone marrow of the *Triturus pyrrhogaster* newt is composed predominantly of fat cells, with very poor vascular innervation and an apparent lack of any hematopoietic activity (57). Evolutionarily primordial aquatic anurans such as *Bombina* and *Xenopus* possess relatively rudimentary vascularization of their bone marrow compared to mammals and appear to host minimal bone marrow hematopoiesis, which appears to be limited to myelopoiesis in *Xenopus* (57). By contrast, more recently diverged terrestrial amphibians possess bone marrow with considerably more pronounced vascularization that is more akin to that seen within the mammalian bone marrow and coinciding with much greater hematopoiesis taking place within this site (57). As bone marrow-mediated hematopoiesis appears to have co-evolved with greater vascularization of this site, it is reasonable to speculate that this vascularization in turn would facilitate more efficient migration of HSCs to and from this site in response to chemotactic cues such as CXCL12.

Chemokines are not only critical to immune responses but also perform a plethora of functions such as mediating the migration, tissue homing, proliferation, mobilization, and survival of HSCs (22). In turn, during monopoiesis *csf1r* gene expression increases with myeloid lineage commitment (58, 59). Conversely, in addition to myeloid-lineage cells, *csf3r* (granulocyte colony-stimulating factor receptor, *gcsf*) is also expressed by mammalian HSCs, which facilitates CSF-3 (granulocyte colony stimulating factor, G-CSF)-mediated mobilization of HSCs out of the mammalian bone marrow into circulation (60, 61). Notably and compared to total LP cells, the rCXCL12-recruited LP cells possessed lower expression of *csf1r* but greater mRNA levels of *csf3r*. Conversely, the rCXCL12-recruited PBLs exhibited greater transcript levels for both myeloid receptor genes as compared to total PBLs. Concurrently, the CXCL12-recruited PBLs but not LP cells possessed significantly greater gene expression of transcription factors associated with myeloid-lineage commitment. Accordingly, we postulate that in *X. laevis*, CXCL12 (and very likely other factors) mobilizes cell population(s) with GMP potential out of the liver periphery into blood circulation, while the commitment to the GMP lineage occurs in circulation, presumably in response to myeloid growth factors. These GMP progenitor(s) is/are then recruited to the bone marrow by the bone marrow-produced CXCL12. The significantly lower transcript levels of *cxcl12* in the peripheral liver compared to that of the bone marrow presumably facilitates the egress of HSCs with GMP potential, resulting in their migration toward the bone marrow through blood circulation in a CXCL12 concentration gradient-dependent manner. We anticipate that the initial GMP lineage commitment occurs *en route* to the bone marrow and that further lineage-specific differentiation then ensues in the BM in response to local cues and growth factors, giving rise to myeloid cells such as macrophages and granulocytes (17, 18). Indeed the mammalian CXCL12 is essential to the homing of adult HSCs to the bone marrow and is crucial to the migration of HSCs from fetal liver to the bone marrow during development (24, 25). It is thus intriguing that a similar phenomenon appears to facilitate the GMP population of the adult *X. laevis* bone marrow toward myelopoiesis.

HSCs of adult mammals are known to migrate predominantly toward a CXCL12 concentration gradient (62), while the activation of the HSC cell surface-expressed CXCR4 by CXCL12 is indispensable to the regulation of HSC migration during adult life (24). In fact, targeted deletion of CXCR4 results in decreased HSC pools in the mammalian bone marrow (24). Although the *X. laevis* CXCL12 has been shown to signal through CXCR4 (23), the precise role(s) of this chemokine in *X. laevis* hematopoiesis in general and myelopoiesis in particular remain to be fully defined. Notably, our present results indicate that the *X. laevis* CXCL12 is more prominently expressed by their bone marrow than their hematopoietic peripheral liver and appears to be important to the migration/homing of some sort of GMP population(s) from the liver periphery to the bone marrow. It is interesting to consider that in *X. laevis*, CXCL12 has evolved to mediate the migration/homing of one or few hematopoietic progenitor subsets to the bone marrow, rather than functioning (as in mammals) as a more global regulator of HSCs within their peripheral liver, which serves as their principal hematopoietic tissue (14–16). Further studies of the roles of CXCL12 across phylogenetically disparate vertebrates possessing distinct hematopoiesis strategies may elucidate what aspects of the *X. laevis* (and mammalian) bone marrow physiology dictate the use of CXCL12 toward homing of progenitor cells toward this site.

In addition to CXCL12-mediated chemotaxes, the migration of mammalian fetal hepatic HSCs to the bone marrow is influenced by a number of other factors. For example, the role of CXCL12-CXCR4 in the migration of HSCs is

augmented by other soluble mediators including stem cell factor, whose chemotactic activity toward mouse fetal hepatic HSCs is synergistic with that of CXCL12 (63). Similarly, activation/signaling through the roundabout guidance receptor 4 (ROBO4) that is expressed by mammalian HSCs aids in the early migration of HSCs from fetal liver to fetal bone marrow and augments the CXCR4-mediated homing and population of HSCs into the adult bone marrow (64). Additionally, adhesion molecules such as cadherins, integrins, and selectins also play important roles in the movement of HSCs to distinct niches. For instance, N-cadherin and integrin β1 expressed on HSCs are involved in the homing and maintenance of these cells in the bone marrow (65, 66). Concurrently, P-selectins and E-selectins expressed by vascular endothelia in the bone marrow promote this HSC migration and homing (67). Furthermore, the migration of HSCs during development is also influenced by extracellular calcium concentration in the bone marrow, which are sensed by the HSC-expressed calcium-sensing receptors (CaRs) (68). Akin to mammals, the recruitment of *X. laevis* GMP into their bone marrow and retention therein undoubtedly depends on a plethora of other factors in addition to CXCL12. Our result showing that the *X. laevis* bone marrow promotes the survival of liver periphery-derived hematopoietic cells supports the notion that in addition to chemokine homing, other factors likely contribute to progenitor cell-bone marrow interactions.

Phylogenetically diverged vertebrate groups possess distinct hematopoiesis strategies, presumably reflecting the physiologies and habitats of those organisms. Despite these differences, vertebrates rely on many of the same soluble mediators, such as growth factors and chemokines, to facilitate their respective blood cell development. We believe that greater understanding of the biological roles of such evolutionarily conserved mediators in the contexts of disparate animal hematopoiesis strategies will grant much clearer understanding of the evolution of vertebrate hematopoiesis.

DATA AVAILABILITY STATEMENT

The datasets generated for this study are available on request to the corresponding author.

ETHICS STATEMENT

The animal study was reviewed and approved by the Institutional Animal Care and Use Committee (IACUC) (approval number 15-024).

AUTHOR CONTRIBUTIONS

AY and LG designed and planned the studies. AY and PR performed the experiments. AY analyzed the data, wrote the manuscript, and prepared the figures. LG contributed to investigation, review, and editing of the manuscript.

FUNDING

This work was funded by National Science Foundation CAREER Award (IOS: 1749427) to LG.

ACKNOWLEDGMENTS

AY thanks the GWU, Department of Biological Sciences for GTA support and support from the GWU Harlan Research program. PR thanks the Thomas Jefferson High School internship program. LG thanks the GWU Department of Biology. We thank the two reviewers whose helpful comments and insightful suggestions contributed to improving this manuscript.

SUPPLEMENTARY MATERIAL

The Supplementary Material for this article can be found online at: https://www.frontiersin.org/articles/10.3389/fimmu.2019.03015/full#supplementary-material

REFERENCES

1. Hough SR, Laslett AL, Grimmond SB, Kolle G, Pera MF. A continuum of cell states spans pluripotency and lineage commitment in human embryonic stem cells. *PLoS ONE.* (2009) 4:e7708. doi: 10.1371/journal.pone.0007708
2. Kondo M, Weissman IL, Akashi K. Identification of clonogenic common lymphoid progenitors in mouse bone marrow. *Cell.* (1997) 91:661–72. doi: 10.1016/S0092-8674(00)80453-5
3. Buza-Vidas N, Luc S, Jacobsen SEW. Delineation of the earliest lineage commitment steps of haematopoietic stem cells: new developments, controversies and major challenges. *Curr Opin Hematol.* (2007) 14:315–21. doi: 10.1097/MOH.0b013e3281de72bb
4. Zapata A, Leceta J, Villena A. Reptilian bone marrow. An ultrastructural study in the Spanish lizard, *Lacerta hispanica. J Morphol.* (1981) 168:137–49. doi: 10.1002/jmor.1051680203
5. Fellah JS, Jaffredo T, Nagy N, Dunon D. Development of the avian immune system. *Avian Immunol.* (2013) 23:45–63. doi: 10.1016/B978-0-12-396965-1.00003-0
6. Jaffredo T, Yvernogeau L. How the avian model has pioneered the field of hematopoietic development. *Exp Hematol.* (2014) 42:661–8. doi: 10.1016/j.exphem.2014.05.009
7. Dzierzak E, Speck NA. Of lineage and legacy: the development of mammalian hematopoietic stem cells. *Nat Immunol.* (2008) 9:129–36. doi: 10.1038/ni1560
8. Belosevic M, Hanington PC, Barreda DR. Development of goldfish macrophages *in vitro*. *Fish Shellfish Immunol.* (2006) 20:152–71. doi: 10.1016/j.fsi.2004.10.010
9. Neumann NF, Barreda DR, Belosevic M. Generation and functional analysis of distinct macrophage sub-populations from goldfish (*Carassius auratus L.*) kidney leukocyte cultures. *Fish Shellfish Immunol.* (2000) 10:1–20. doi: 10.1006/fsim.1999.0221
10. Tagoh H, Himes R, Clarke D, Leenen PJM, Riggs AD, Hume D, et al. Transcription factor complex formation and chromatin fine structure alterations at the murine c-fms (CSF-1 receptor) locus during maturation of myeloid precursor cells. *Genes Dev.* (2002) 16:1721–37. doi: 10.1101/gad.222002
11. Jones CV, Ricardo SD. Macrophages and CSF-1. *Organogenesis.* (2013) 9:249–60. doi: 10.4161/org.25676

12. Pixley FJ, Stanley ER. CSF-1 regulation of the wandering macrophage: complexity in action. *Trends Cell Biol.* (2004) 14:628–38. doi: 10.1016/j.tcb.2004.09.016
13. Fried W. Erythropoietin and erythropoiesis. *Exp Hematol.* (2009) 37:1007–15. doi: 10.1016/j.exphem.2009.05.010
14. Nogawa-Kosaka N, Sugai T, Nagasawa K, Tanizaki Y, Meguro M, Aizawa Y, et al. Identification of erythroid progenitors induced by erythropoietic activity in *Xenopus laevis*. *J Exp Biol.* (2011) 214:921–7. doi: 10.1242/jeb.050286
15. Hadji-Azimi I, Coosemans V, Canicatti C. B-lymphocyte populations in *Xenopus laevis*. *Dev Comp Immunol.* (1990) 14:69–84. doi: 10.1016/0145-305X(90)90009-4
16. Chen XD, Turpen JB. Intraembryonic origin of hepatic hematopoiesis in *Xenopus laevis*. *J Immunol Baltim Md.* (1995) 154:2557–67.
17. Yaparla A, Wendel ES, Grayfer L. The unique myelopoiesis strategy of the amphibian *Xenopus laevis*. *Dev Comp Immunol.* (2016) 63:136–43. doi: 10.1016/j.dci.2016.05.014
18. Grayfer L, Robert J. Colony-stimulating factor-1-responsive macrophage precursors reside in the amphibian (*Xenopus laevis*) bone marrow rather than the hematopoietic subcapsular liver. *J Innate Immun.* (2013) 5:531–42. doi: 10.1159/000346928
19. Zhu J, Emerson SG. Hematopoietic cytokines, transcription factors and lineage commitment. *Oncogene.* (2002) 21:3295–313. doi: 10.1038/sj.onc.1205318
20. Kehrl JH. Hematopoietic lineage commitment: role of transcription factors. *Stem Cells.* (1995) 13:223–41. doi: 10.1002/stem.5530130304
21. Orkin SH. Transcription factors and hematopoietic development. *J Biol Chem.* (1995) 270:4955–8. doi: 10.1074/jbc.270.10.4955
22. Broxmeyer HE. Regulation of hematopoiesis by chemokine family members. *Int J Hematol.* (2001) 74:9–17. doi: 10.1007/BF02982544
23. Hughes CE, Nibbs RJB. A guide to chemokines and their receptors. *FEBS J.* (2018) 285:2944–71. doi: 10.1111/febs.14466
24. Sugiyama T, Kohara H, Noda M, Nagasawa T. Maintenance of the hematopoietic stem cell pool by CXCL12-CXCR4 chemokine signaling in bone marrow stromal cell niches. *Immunity.* (2006) 25:977–88. doi: 10.1016/j.immuni.2006.10.016
25. Janssens R, Struyf S, Proost P. The unique structural and functional features of CXCL12. *Cell Mol Immunol.* (2018) 15:299. doi: 10.1038/cmi.2017.107
26. Stebler J, Spieler D, Slanchev K, Molyneaux KA, Richter U, Cojocaru V, et al. Primordial germ cell migration in the chick and mouse embryo: the role of the chemokine SDF-1/CXCL12. *Dev Biol.* (2004) 272:351–61. doi: 10.1016/j.ydbio.2004.05.009
27. David NB, Sapède D, Saint-Etienne L, Thisse C, Thisse B, Dambly-Chaudière C, et al. Molecular basis of cell migration in the fish lateral line: role of the chemokine receptor CXCR4 and of its ligand, SDF1. *Proc Natl Acad Sci USA.* (2002) 99:16297–302. doi: 10.1073/pnas.252339399
28. Chong SW, Nguyet LM, Jiang YJ, Korzh V. The chemokine Sdf-1 and its receptor Cxcr4 are required for formation of muscle in zebrafish. *BMC Dev Biol.* (2007) 22:7–54. doi: 10.1186/1471-213X-7-54
29. Braun M, Wunderlin M, Spieth K, Knöchel W, Gierschik P, Moepps B. *Xenopus laevis* stromal cell-derived factor 1: conservation of structure and function during vertebrate development. *J Immunol.* (2002) 168:2340–7. doi: 10.4049/jimmunol.168.5.2340
30. Yaparla A, Grayfer L. Isolation and culture of amphibian (*Xenopus laevis*) sub-capsular liver and bone marrow cells. *Methods Mol Biol.* (2018) 1865:275–81. doi: 10.1007/978-1-4939-8784-9_20
31. Vagapova ER, Spirin PV, Lebedev TD, Prassolov VS. The role of TAL1 in hematopoiesis and leukemogenesis. *Acta Nat.* (2018) 10:15–23. doi: 10.32607/20758251-2018-10-1-15-23
32. Ghaleb AM, Yang VW. Krüppel-like factor 4 (KLF4): what we currently know. *Gene.* (2017) 611:27–37. doi: 10.1016/j.gene.2017.02.025
33. Rodrigues NP, Tipping AJ, Wang Z, Enver T. GATA-2 mediated regulation of normal hematopoietic stem/progenitor cell function, myelodysplasia and myeloid leukemia. *Int J Biochem Cell Biol.* (2012) 44:457–60. doi: 10.1016/j.biocel.2011.12.004
34. Zhang DE, Hetherington CJ, Chen HM, Tenen DG. The macrophage transcription factor PU.1 directs tissue-specific expression of the macrophage colony-stimulating factor receptor. *Mol Cell Biol.* (1994) 14:373–81. doi: 10.1128/MCB.14.1.373
35. Krishnaraju K, Hoffman B, Liebermann DA. Early growth response gene 1 stimulates development of hematopoietic progenitor cells along the macrophage lineage at the expense of the granulocyte and erythroid lineages. *Blood.* (2001) 97:1298–305. doi: 10.1182/blood.V97.5.1298
36. Veremeyko T, Yung AWY, Anthony DC, Strekalova T, Ponomarev ED. Early growth response gene-2 is essential for M1 and M2 macrophage activation and plasticity by modulation of the transcription factor CEBPβ. *Front Immunol.* (2018) 9:2515. doi: 10.3389/fimmu.2018.02515
37. de la Luz Sierra M, Sakakibara S, Gasperini P, Salvucci O, Jiang K, McCormick PJ, et al. The transcription factor Gfi1 regulates G-CSF signaling and neutrophil development through the Ras activator RasGRP1. *Blood.* (2010) 115:3970–9. doi: 10.1182/blood-2009-10-246967
38. Tamir A, Howard J, Higgins RR, Li YJ, Berger L, Zacksenhaus E, et al. Fli-1, an Ets-related transcription factor, regulates erythropoietin-induced erythroid proliferation and differentiation: evidence for direct transcriptional repression of the Rb gene during differentiation. *Mol Cell Biol.* (1999) 19:4452–64. doi: 10.1128/MCB.19.6.4452
39. Andrews NC. Erythroid transcription factor NF-E2 coordinates hemoglobin synthesis. *Pediatr Res.* (1994) 36:419–23. doi: 10.1203/00006450-199410000-00001
40. Zheng J, Kitajima K, Sakai E, Kimura T, Minegishi N, Yamamoto M, et al. Differential effects of GATA-1 on proliferation and differentiation of erythroid lineage cells. *Blood.* (2006) 107:520–7. doi: 10.1182/blood-2005-04-1385
41. Hoyler T, Klose CSN, Souabni A, Turqueti-Neves A, Pfeifer D, Rawlins EL, et al. The transcription factor GATA-3 controls cell fate and maintenance of type 2 innate lymphoid cells. *Immunity.* (2012) 37:634–48. doi: 10.1016/j.immuni.2012.06.020
42. Medvedovic J, Ebert A, Tagoh H, Busslinger M. Pax5: a master regulator of B cell development and leukemogenesis. *Adv Immunol.* (2011) 111:179–206. doi: 10.1016/B978-0-12-385991-4.00005-2
43. Xu L, Li Y, Sun H, Li D, Hou T. Structural basis of the interactions between CXCR4 and CXCL12/SDF-1 revealed by theoretical approaches. *Mol Biosyst.* (2013) 9:2107–17. doi: 10.1039/c3mb70120d
44. Bleicher PA, Cohen N. Monoclonal anti-IgM can separate T cell from B cell proliferative responses in the frog, *Xenopus laevis*. *J Immunol.* (1981) 127:1549–55.
45. Jefferie WA, Green JR, Williams AF. Authentic T helper CD4 (W3/25) antigen on rat peritoneal macrophages. *J Exp Med.* (1985) 162:117–27. doi: 10.1084/jem.162.1.117
46. Zhu J, Paul WE. CD4 T cells: fates, functions, and faults. *Blood.* (2008) 112:1557–69. doi: 10.1182/blood-2008-05-078154
47. Leahy DJ, Axel R, Hendrickson WA. Crystal structure of a soluble form of the human T cell coreceptor CD8 at 2.6 A resolution. *Cell.* (1992) 68:1145–62. doi: 10.1016/0092-8674(92)90085-Q
48. Shortman K, Heath WR. The CD8+ dendritic cell subset. *Immunol Rev.* (2010) 234:18–31. doi: 10.1111/j.0105-2896.2009.00870.x
49. Lensch MW, Daley GQ. Origins of mammalian hematopoiesis: *in vivo* paradigms and *in vitro* models. *Curr Top Dev Biol.* (2004) 60:127–96. doi: 10.1016/S0070-2153(04)60005-6
50. Ciau-Uitz A, Monteiro R, Kirmizitas A, Patient R. Developmental hematopoiesis: ontogeny, genetic programming and conservation. *Exp Hematol.* (2014) 42:669–83. doi: 10.1016/j.exphem.2014.06.001
51. Schepers K, Campbell TB, Passegué E. Normal and leukemic stem cell niches: insights and therapeutic opportunities. *Cell Stem Cell.* (2015) 16:254–67. doi: 10.1016/j.stem.2015.02.014
52. Grayfer L, Robert J. Amphibian macrophage development and antiviral defenses. *Dev Comp Immunol.* (2016) 58:60–7. doi: 10.1016/j.dci.2015.12.008
53. Padial JM, Grant T, Frost DR. Molecular systematics of terraranas (Anura: *Brachycephaloidea*) with an assessment of the effects of alignment and optimality criteria. *Zootaxa.* (2014) 3825:1–132. doi: 10.11646/zootaxa.3825.1.1
54. Carver FJ, Meints RH. Studies of the development of frog hemopoietic tissue *in vitro*. I. Spleen culture assay of an erythropoietic factor in anemic frog blood. *J Exp Zool.* (1977) 201:37–46. doi: 10.1002/jez.1402010105
55. Bleyzac P, Cordier G, Exbrayat J-M. Morphological description of embryonic development of immune organs in *Typhlonectes compressicauda* (Amphibia, *Gymnophiona*). *J Herpetol.* (2005) 39:57–65. doi: 10.1670/0022-1511(2005)039[0057:MDOEDO]2.0.CO;2

56. Curtis SK, Cowden RR, Nagel JW. Ultrastructure of the bone marrow of the salamander *Plethodon glutinosus* (Caudata: *Plethodontidae*). *J Morphol.* (1979) 160:241–74. doi: 10.1002/jmor.1051600302
57. Tanaka Y. Architecture of the marrow vasculature in three amphibian species and its significance in hematopoietic development. *Am J Anat.* (1976) 145:485–97. doi: 10.1002/aja.1001450407
58. Stanley ER. Lineage commitment: cytokines instruct, at last! *Cell Stem Cell.* (2009) 5:234–6. doi: 10.1016/j.stem.2009.08.015
59. Mossadegh-Keller N, Sarrazin S, Kandalla PK, Espinosa L, Stanley ER, Nutt SL, et al. M-CSF instructs myeloid lineage fate in single haematopoietic stem cells. *Nature.* (2013) 497:239–43. doi: 10.1038/nature12026
60. Greenbaum AM, Link DC. Mechanisms of G-CSF-mediated hematopoietic stem and progenitor mobilization. *Leukemia.* (2011) 25:211–7. doi: 10.1038/leu.2010.248
61. Bernitz JM, Daniel MG, Fstkchyan YS, Moore K. Granulocyte colony-stimulating factor mobilizes dormant hematopoietic stem cells without proliferation in mice. *Blood.* (2017) 129:1901–12. doi: 10.1182/blood-2016-11-752923
62. Wright DE, Bowman EP, Wagers AJ, Butcher EC, Weissman IL. Hematopoietic stem cells are uniquely selective in their migratory response to chemokines. *J Exp Med.* (2002) 195:1145–54. doi: 10.1084/jem.20011284
63. Christensen JL, Wright DE, Wagers AJ, Weissman IL. Circulation and chemotaxis of fetal hematopoietic stem cells. *PLoS Biol.* (2004) 2:E75. doi: 10.1371/journal.pbio.0020075
64. Smith-Berdan S, Nguyen A, Hassanein D, Zimmer M, Ugarte F, Ciriza J, et al. Robo4 cooperates with Cxcr4 to specify hematopoietic stem cell localization to bone marrow niches. *Cell Stem Cell.* (2011) 8:72–83. doi: 10.1016/j.stem.2010.11.030
65. Ciriza J, Hall D, Lu A, Sena JRD, Al-Kuhlani M, García-Ojeda ME. Single-cell analysis of murine long-term hematopoietic stem cells reveals distinct patterns of gene expression during fetal migration. *PLoS ONE.* (2012) 7:e30542. doi: 10.1371/journal.pone.0030542
66. Potocnik AJ, Brakebusch C, Fässler R. Fetal and adult hematopoietic stem cells require beta1 integrin function for colonizing fetal liver, spleen, and bone marrow. *Immunity.* (2000) 12:653–63. doi: 10.1016/S1074-7613(00)80216-2
67. Ciriza J, García-Ojeda ME. Expression of migration-related genes is progressively upregulated in murine lineage-Sca-1+c-Kit+ population from the fetal to adult stages of development. *Stem Cell Res Ther.* (2010) 1:14. doi: 10.1186/scrt14
68. Lam BS, Cunningham C, Adams GB. Pharmacologic modulation of the calcium-sensing receptor enhances hematopoietic stem cell lodgment in the adult bone marrow. *Blood.* (2011) 117:1167–75. doi: 10.1182/blood-2010-05-286294

Conflict of Interest: The authors declare that the research was conducted in the absence of any commercial or financial relationships that could be construed as a potential conflict of interest.

frontiers in Immunology

METHODS
published: 18 February 2020
doi: 10.3389/fimmu.2020.00203

Imaging Flow Cytometry Protocols for Examining Phagocytosis of Microplastics and Bioparticles by Immune Cells of Aquatic Animals

*Youngjin Park[1], Isabel S. Abihssira-García[1], Sebastian Thalmann[2], Geert F. Wiegertjes[3], Daniel R. Barreda[4], Pål A. Olsvik[1] and Viswanath Kiron[1]**

[1] Faculty of Biosciences and Aquaculture, Nord University, Bodø, Norway, [2] Luminex B.V., 's-Hertogenbosch, Netherlands, [3] Aquaculture and Fisheries Group, Wageningen University & Research, Wageningen, Netherlands, [4] Department of Biological Sciences, University of Alberta, Edmonton, AB, Canada

Imaging flow cytometry (IFC) is a powerful tool which combines flow cytometry with digital microscopy to generate quantitative high-throughput imaging data. Despite various advantages of IFC over standard flow cytometry, widespread adoption of this technology for studies in aquatic sciences is limited, probably due to the relatively high equipment cost, complexity of image analysis-based data interpretation and lack of core facilities with trained personnel. Here, we describe the application of IFC to examine phagocytosis of particles including microplastics by cells from aquatic animals. For this purpose, we studied (1) live/dead cell assays and identification of cell types, (2) phagocytosis of degradable and non-degradable particles by Atlantic salmon head kidney cells and (3) the effect of incubation temperature on phagocytosis of degradable particles in three aquatic animals–Atlantic salmon, Nile tilapia, and blue mussel. The usefulness of the developed method was assessed by evaluating the effect of incubation temperature on phagocytosis. Our studies demonstrate that IFC provides significant benefits over standard flow cytometry in phagocytosis measurement by allowing integration of morphometric parameters, especially while identifying cell populations and distinguishing between different types of fluorescent particles and detecting their localization.

Keywords: ImageStream®^{X}, IFC, Atlantic salmon, Nile tilapia, blue mussel, phagocytosis

OPEN ACCESS

Edited by:
Kim Dawn Thompson, Moredun Research Institute, United Kingdom

Reviewed by:
Sebastian Reyes-Cerpa, Universidad Mayor, Chile
Caroline Fossum, Swedish University of Agricultural Sciences, Sweden

***Correspondence:**
Viswanath Kiron
kiron.viswanath@nord.no

Specialty section:
This article was submitted to Comparative Immunology, a section of the journal Frontiers in Immunology

Received: *20 October 2019*
Accepted: *27 January 2020*
Published: *18 February 2020*

Citation:
Park Y, Abihssira-García IS, Thalmann S, Wiegertjes GF, Barreda DR, Olsvik PA and Kiron V (2020) Imaging Flow Cytometry Protocols for Examining Phagocytosis of Microplastics and Bioparticles by Immune Cells of Aquatic Animals. Front. Immunol. 11:203. doi: 10.3389/fimmu.2020.00203

INTRODUCTION

Flow cytometry (FC) is widely employed for studying mammalian cells in particular and detecting biomarkers in clinical studies. FC systems quantify cell data within seconds and can provide information on cell phenotypes and functions. However, conventional FC is not designed to measure morphological and spatial information of single cells, and the technology is not able to efficiently detect dim and small particles (<300 nm) (1) as well as to distinguish aggregates of these small particles. Furthermore, although conventional FC can measure intra- and extra-cellular marker expressions, it does not provide information on marker localization. Another obstacle connected to conventional FC is auto-fluorescence. While the system cannot always precisely distinguish between false-positive and false-negative events (2), fine-tuning of instrument settings and protocol optimization can minimize the problem (3). Nevertheless, cell phenotype identification and functional analyses using conventional FC cannot be entirely objective as the equipment lacks image-capturing features. To overcome inaccuracies in acquiring cell data,

quantitative studies preferably rely on both conventional FC and fluorescent cell imaging.

Imaging flow cytometry (IFC), also called multispectral imaging flow cytometry, is a powerful tool that enables us to collect information from single cells, including those from fluorescent images. Major advantages of IFC are (1) high fluorescence sensitivity, (2) high image resolution capability, (3) high speed processing, (4) ability to analyse changes in cell or nuclear morphology, (5) rare cell detection ability, and (6) capacity to understand cell-cell interaction (2). Certain disciplines of biology, namely hematology (4), immunology (5), cell biology (6), and microbiology (7) have already benefited from IFC. However, application of IFC is still in its infancy when it comes to studies in aquatic sciences.

Researchers have reported IFC-based analyses of fish cells, using nucleus staining to understand cell morphology and employing fluorescent particles to determine phagocytic activity in goldfish (8, 9). Different particles such as fluorescent latex beads (10), zymosan-APC (8), and nanoparticles (11) have been used to analyse phagocytosis using IFC. These methods can be further optimized, depending on the characteristics of the particles, e.g., latex beads that are not degraded vis-à-vis pHrodo™ BioParticles® that emit fluorescent light upon acidification following ingestion by the target cells (10). Researchers have also improved the protocol for measuring particles' intensity in IFC (12). Overall, these studies provide the first information on the use of IFC to identify different cells and understand cell functions such as phagocytosis and the localization of markers of interest in cells from aquatic animals.

Though previous studies on aquatic animals have reported phagocytosis, here we present (1) basic, but optimized protocols for live/dead cell assay and identification of cell types (2), an improved protocol for examining phagocytosis of non-degradable (microplastic) and degradable (bioparticles) particles by immune cell types of fish, and (3) an optimized phagocytosis assay using cells harvested from three very different aquatic animals: cold water-adapted carnivorous marine fish (Atlantic salmon, *Salmo salar*), warm water-adapted omnivorous, freshwater fish (Nile tilapia, *Oreochromis niloticus*) and a cold water-adapted detritivorous/planktivorous marine mollusc (blue mussel, *Mytilus edulis*). Effect of incubation temperature was studied to verify the sensitivity and usefulness of the optimized phagocytosis assay.

METHODS

Ethics Statement

The studies were approved (Atlantic salmon: FOTS ID 10050, Nile tilapia: FOTS ID 1042) by the National Animal Research Authority in Norway (Mattilsynet). The fish rearing and handling procedures were according to the approved protocols of FDU.

Animals

Atlantic salmon (*S. salar*) in the weight range 700–900 g were used in this experiment. They were purchased from a commercial producer (Sundsfjord Smolt, Nygårdsjøen, Norway) and maintained at the Research Station of Nord University, Bodø, Norway. Fish were fed a commercial feed (Ewos AS, Bergen, Norway) and reared in a flow-through sea water system (temperature: 7–8°C, dissolved oxygen saturation: 87–92%, 24–h light cycle).

Nile tilapia (*O. niloticus*, 400–600 g) were bred and reared at the Research Station of Nord University in a freshwater recirculating aquaculture system (temperature: 28°C, pH: 7.6, dissolved oxygen saturation: 80% in outlet and 115% in inlet, 11 h dark/13 h light cycle). The fish were fed commercial feeds (Skretting, Stavanger, Norway) during the rearing period.

Adult blue mussels (*M. edulis*) were collected from a beach along the Saltenfjorden, Bodø, Norway (67°12′01″ N 14°37′56″ E) and transported to the Research Station, Nord University. Prior to isolation of hemocytes, they were kept for 2 days in running seawater at 7–8°C.

Cell Isolation

Cells from salmon and tilapia head kidney (HK) were grown in Leibovitz's L-15 Medium (L-15; Sigma-Aldrich, Oslo, Norway), supplemented with 100 μg/mL gentamicin sulfate (Sigma), 2 mM L-glutamine (Sigma) and 15 mM HEPES (Sigma). Osmolality of medium was adjusted by adding a solution consisting of 5% (v/v) 0.41 M NaCl, 0.33 M $NaHCO_3$, and 0.66 (w/v) D-glucose. Cell culture media were adjusted to 380 mOsm for salmon and 320 mOsm for tilapia. To culture the mussel hemocytes, filtered (through a 0.2 μm mesh) sea water was used as the medium.

Head kidney from salmon ($n = 6$) were sampled after the fish were killed with an overdose of MS-222 (Tricaine methane sulphonate; Argent Chemical Laboratories, Redmond, USA; 80 mg/L). Thereafter, the HK cells were isolated as described previously (13) with minor modifications. Briefly, HK was dissected out, and the tissues were transferred to 15 mL centrifuge tubes to make a total volume of 4 mL in ice-cold L-15+ (L-15 medium with 50 U/mL penicillin, 50 μg/mL streptomycin, 2% fetal bovine serum (FBS) and 10 U/mL heparin). The tissue was placed on a sterile 100 μM cell strainer (Falcon) and the cells were disrupted with the help of a syringe plunger. The harvested cells were washed twice in ice-cold L-15+. The cell suspension from salmon HK was then layered on 40/60% Percoll (Sigma) to separate HK leukocytes for magnetic-activated cell sorting (MACS) or layered on 34/51% Percoll to separate monocytes/macrophages for subsequent phagocytosis assays. After centrifugation (500 × g, 30 min, 4°C), the cells at the interface between the two Percoll gradients were collected and washed twice with ice-cold L-15-FBS free (L-15 medium with 50 U/mL penicillin, 50 μg/mL streptomycin) by centrifugation (500 × g, 5 min, 4°C). Cells were then kept in L-15+. HK phagocytic cells that were separated based on 34/51% Percoll gradient, were allowed to adhere on a petri dish for 3 days at 12°C. After removing the supernatant containing non-adherent cells, the petri dish with the adherent cells was placed on ice for 10 min, and the cells were collected by washing three times with 1.5 mL ice-cold PBS supplemented with 5 mM EDTA. Next, these collected cells were centrifuged (500 × g, 5 min, 4°C) and used for further analyses.

Head kidney from tilapia ($n = 6$) were collected after killing the fish with an overdose of clove oil (Sigma Aldrich, St. Louis,

MO, USA), and cells were harvested as described previously (14, 15), with minor modifications. Briefly, the HK tissues were transferred to 15 mL centrifuge tubes to make a total volume of 4 mL in ice-cold L-15+. The cells were harvested from the HK and washed twice as described for salmon. The cell suspension was layered on 34/51% Percoll to separate phagocytic cells, and then after centrifugation, cells at the interface were collected and washed twice in L-15-FBS free. The cells in the suspension were allowed to adhere on a petri dish containing L-15+ for 3 days at 25°C. After removing the supernatant containing non-adherent cells, the petri dish with the adherent cells was placed on ice for 10 min, and the cells were collected by washing three times with 1.5 mL ice-cold PBS supplemented with 5 mM EDTA. Next, the collected cells were centrifuged (500 × g, 5 min, 4°C) and used for further analyses.

In the fish experiments, the cells were counted using a portable cell counter (Scepter™ 2.0 cell counter, EMD Millipore, Darmstadt, Germany).

Hemocytes from adult mussels ($n = 6$) were isolated as described previously (16) with minor modifications. Briefly, hemolymph was drawn from the posterior adductor muscle using a 2 mL syringe equipped with a 23G-needle. The hemocytes from each mussel were counted using a Neubauer chamber, and 0.2×10^6 cells per sample were collected and re-suspended in 1 mL of filtered sea water to avoid formation of clumps.

Magnetic-Activated Cell Sorting (MACS) of Salmon IgM$^+$ Cells

The isolated salmon HK leukocytes (2×10^6 cells) were incubated with mouse anti-trout/salmon IgM (6.06 μg/mL; Aquatic Diagnostics Ltd, Sterling, UK) for 60 min at 4°C. After two washes with L-15+, the cells were incubated for 15 min at 4°C in a cocktail with a total volume of 100 μL, which contained L-15+, 1 μL of goat anti-mouse IgG-FITC (0.75 mg/mL; Thermo Fisher Scientific, Oslo, Norway) and 40 μL of goat anti-mouse IgG microbeads as per the instructions of the manufacturer (Miltenyi Biotec, Bergisch Gladbach, Germany). First, MACS LD columns (Miltenyi Biotec) that were placed in a magnetic separator of the multistand were washed using L-15+. The cell suspension was then transferred into the LD column. Following cell sorting, the positive cells were harvested and re-suspended in L-15+.

Live/Dead Cell Assay

In the studies on cells from salmon and tilapia, aliquots containing 1×10^6 cells in 50 μL PBS were transferred to 1.5 mL microcentrifuge tubes. Then 1 μL of propidium iodide (PI; 1 mg/mL, Sigma) was added to each sample to detect the dead cells in the cell suspension. In the case of mussel, aliquots containing 0.2×10^6 cells in 50 μL filtered sea water were transferred to 1.5 mL microcentrifuge tubes, and then 1 μL of DRAQ5™ (25 mM, Thermo Fisher Scientific) was added to each sample to detect the dead cells in the cell suspension. The tubes were gently mixed before the samples were run through the ImageStream®^{X} Mk II Imaging Flow Cytometer (Luminex Corporation, Austin, TX, USA). Cell analyses were performed on 10,000 cells acquired at a rate of 300 objects/second at low speed and a magnification of 40×. Dead cells were estimated as the percent of cells positive for either PI or DRAQ5™ (red fluorescent cells). After excluding the dead cells, viable cells were analyzed to generate brightfield (BF) area (size) vs. side scatter (SSC) intensity (complexity) dot plots. Instrument settings were kept identical throughout the study.

Phagocytosis Assay

In the first phagocytosis experiment, phagocytic cells from salmon HK were employed to study the uptake of two types of particles; non-degradable fluorescent polystyrene microplastic beads (2.1 μm; Magsphere Inc., California, USA) and degradable fluorescent bio-particles (>0.2 μm; pHrodo™ Red *Escherichia coli* Bioparticles, Thermo Fisher Scientific). In the second experiment, we used degradable fluorescent bio-particles only; to determine phagocytic ability and capacity of the cells from salmon, tilapia and mussel at two different incubation temperatures. Phagocytic ability was measured as the percent of phagocytic cells among the total macrophage-like cells or hemocytes. On the other hand, phagocytic capacity was measured as the mean number of particles per phagocytic cell. Phagocytic index (PI) or phagocytic activity was determined employing the equation (17, 18):

Phagocytic index (PI) = [% phagocytic cells containing at least one particle] × [mean particle count per phagocytic cell].

Briefly, fluorescent bio-particles were added at a cell:particle ratio of 1:5 per sample, both in the case of HK macrophages (0.5×10^6 cells) and hemocytes (0.2×10^6 cells). Cells suspensions and bio-particles were mixed and incubated for 2 h at different temperatures. Following incubation, cell suspensions were washed twice with 500 μL L-15+ by centrifugation (500 × g, 5 min, 4°C). The supernatant was discarded, and the resulting cell pellets were re-suspended in 50 μL PBS. The cell samples were run in an imaging flow cytometer (Luminex), equipped with a 10 mW 488 nm argon-ion laser, to detect the bio-particle fluorescence (577/35 nm bandpass; Channel 3). Thereafter, the images were analyzed using IDEAS 6.1.822.0 software (Luminex).

Data and Statistical Analyses

Statistical analysis was performed in RStudio version 1.1.463. Normality of the data was tested by Shapiro-Wilk Test, and the assumption of equal variance was checked by Bartlett's Test. Comparisons between the two groups were performed using unpaired Student's *t*-test. Statistically significant differences ($p < 0.05$) are reported for the phagocytosis data.

RESULTS

Live/Dead Cells and Leukocyte Populations From Salmon Head Kidney

To determine single cell area and to identify cell populations, we employed a basic gating strategy using the Brightfield Gradient Root Mean Square (RMS) feature of the imaging flow cytometer (see **Figure 1**). This strategy helped us to select the cells in best focus, i.e., this allowed us to obtain high quality images with RMS values >50 (**Figure 1A**). Next, we separated single cells from others (debris, doublets and aggregates; **Figure 1B**). Dead cells were excluded based on

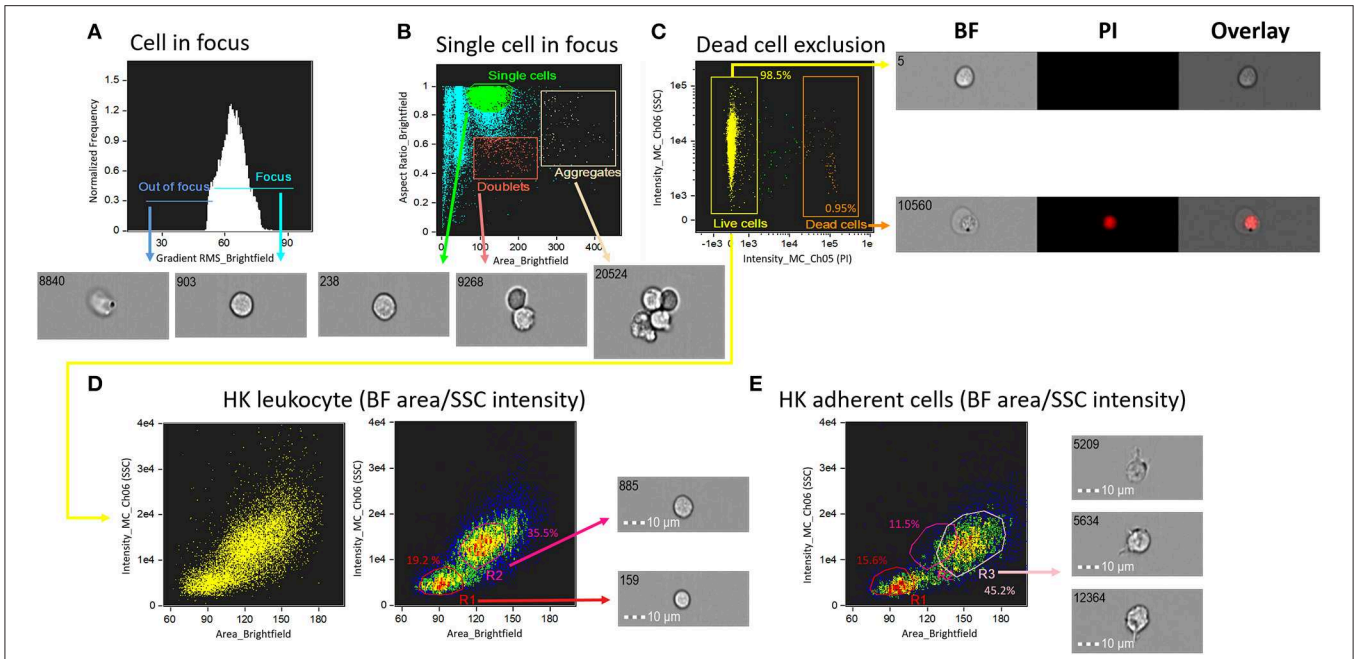

FIGURE 1 | Schematic of the gating strategy to determine areas and populations of head kidney cells from Atlantic salmon. **(A)** Focused cells were gated using IDEAS® gradient RMS feature which helps to select high-quality images with RMS values above 50. **(B)** Representative image showing the gated cells; single cells, doublets and aggregates are shown in a dot plot. Aspect ratio is a feature that evaluates an elliptical shape fitted around the detected object. The ratio is calculated as the minor axis divided by the major axis; a value close to 1 indicates that the cell has a circular shape, while a value in the range 0.4–0.8 signals the presence of doublets or aggregates if the individual cells are of oval morphology. **(C)** Orange dots are the dead cells that were excluded using propidium iodide, to separate the live cells (yellow dots). **(D)** HK leukocyte population is shown in a brightfield (BF) area (cell size) vs. side scatter (SSC) intensity (cell internal complexity) plot. **(E)** HK adherent cell (macrophage-like cell) population is shown in a BF area vs. SSC intensity plot. All cell images were captured with 40 × objective. Scale bar = 10 µm. BF, brightfield; PI, propidium iodide; R, region; R1, lymphocyte-like cells; R2, monocytes/macrophages-like cells; R3, macrophage-like cells.

positivity for PI (**Figure 1C**). The percentage of live cells were 98.5%. The brightfield (BF) area and side scatter (SSC) intensity of the live, single cells were assessed. We prepared a BF area vs. SSC intensity dot plot to show the salmon HK leukocyte populations (**Figure 1D**). Cells with smaller size (low BF area) and low SSC intensity were possibly lymphocyte-like cells (19.2%; R1 in **Figure 1D**) while those with larger size (BF area) and higher SSC intensity compared to lymphocyte-like cells were considered as monocytes/macrophages (35.5%; R2 in **Figure 1D**). **Figure 1E** shows salmon HK adherent cell populations in a BF area vs. SSC intensity dot plot; here, R3 is probably HK macrophage-like cells (45.2%). We conclude that using IFC, dead cells can be excluded, and different single cell populations can be better detected than in conventional FC.

Salmon Head Kidney IgM$^+$ Lymphocyte Identification

Salmon head kidney IgM$^+$ lymphocytes separated using MACS were used to ascertain their localization in a BF area vs. SSC intensity dot plot (**Figure 2**). For this purpose, cells were extracellularly stained with IgM-FITC, which enabled us to identify areas of negatively- and positively-stained B lymphocyte populations. Before MACS (**Figure 2A**), all cells were located in the IgM$^-$ area (right panel **Figure 2A**). After staining with IgM-FITC and performing MACS (**Figure 2B**), most cells were located in the IgM$^+$ area (89.8%; right panel **Figure 2B**). These data confirmed that the IgM$^+$ cells matched the location of the lymphocyte-like cells (R1 population in **Figure 1D**). Thus, we confirmed the localization of salmon IgM$^+$ cells using IFC.

Examining Phagocytosis Using Non-degradable Fluorescent Microplastic Beads

To determine the phagocytosis of microplastics by salmon HK cells, first, we plotted histograms of fluorescence intensity of non-degradable fluorescent polystyrene microplastic beads in live cells (**Figure 3A**). Because all the polystyrene beads were of similar size, we assumed that fluorescence intensity is proportional to the number of beads taken up by each phagocytic cell. Using IFC, we could exclude auto-fluorescence and could gate images with more pixels and higher intensity (phagocytic images with pixel value > 30 were considered to be of high quality) (**Figure 3B**). Caution was taken to exclude aggregates; addition of many microplastic beads can cause bead aggregation, leading to false identification of aggregates as phagocytic cells, especially in conventional FC. Next, we gated phagocytic cells that engulfed microplastic beads using an internalization score (**Figure 3C**). This score is the ratio of the particle intensity inside a cell to the intensity of the whole cell, and it is calculated after masking (which selects pixels

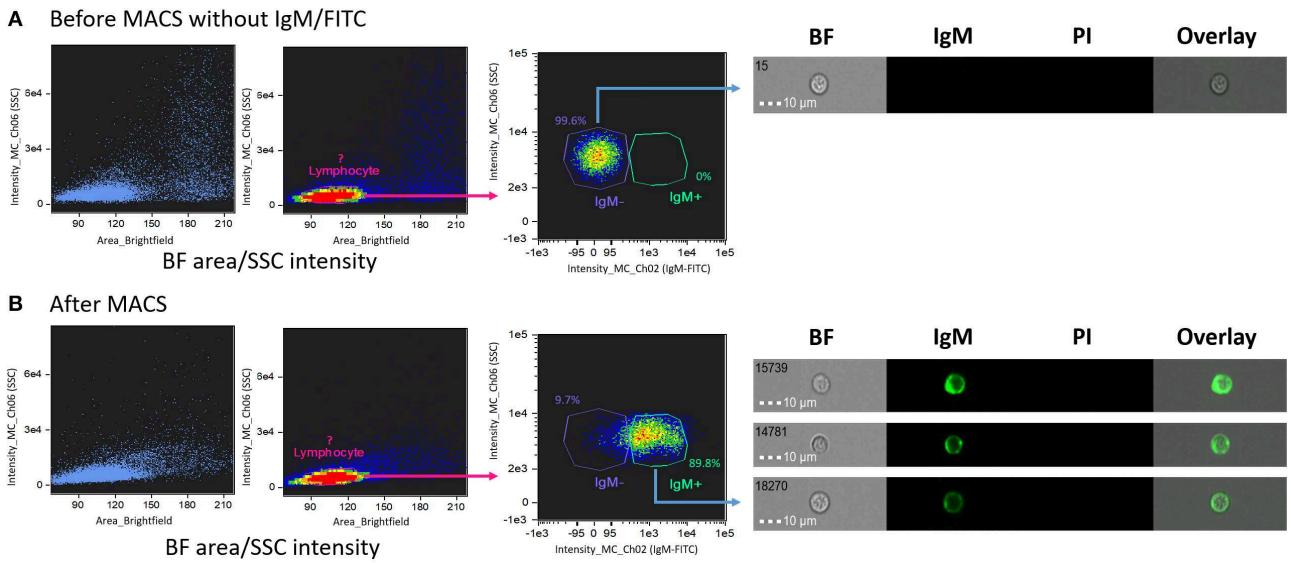

FIGURE 2 | Identification of salmon IgM$^+$ lymphocyte after magnetic-activated cell sorting (MACS). Dot plots of **(A)** HK leukocytes before and **(B)** after MACS separation. The left and middle plots in **(A,B)** show brightfield (BF) area vs. SSC intensity and the right plot in **(A,B)** shows the density of the target cells. Cells without IgM-FITC are shown in the IgM$^-$ gate (**A**, right panel) while IgM$^+$ cells after MACS are shown in the IgM$^+$ gate (**B**, right panel). All cell images were captured with 40 × objective. Scale bar = 10 μm. BF, brightfield; IgM, immunoglobulin M; PI, propidium iodide.

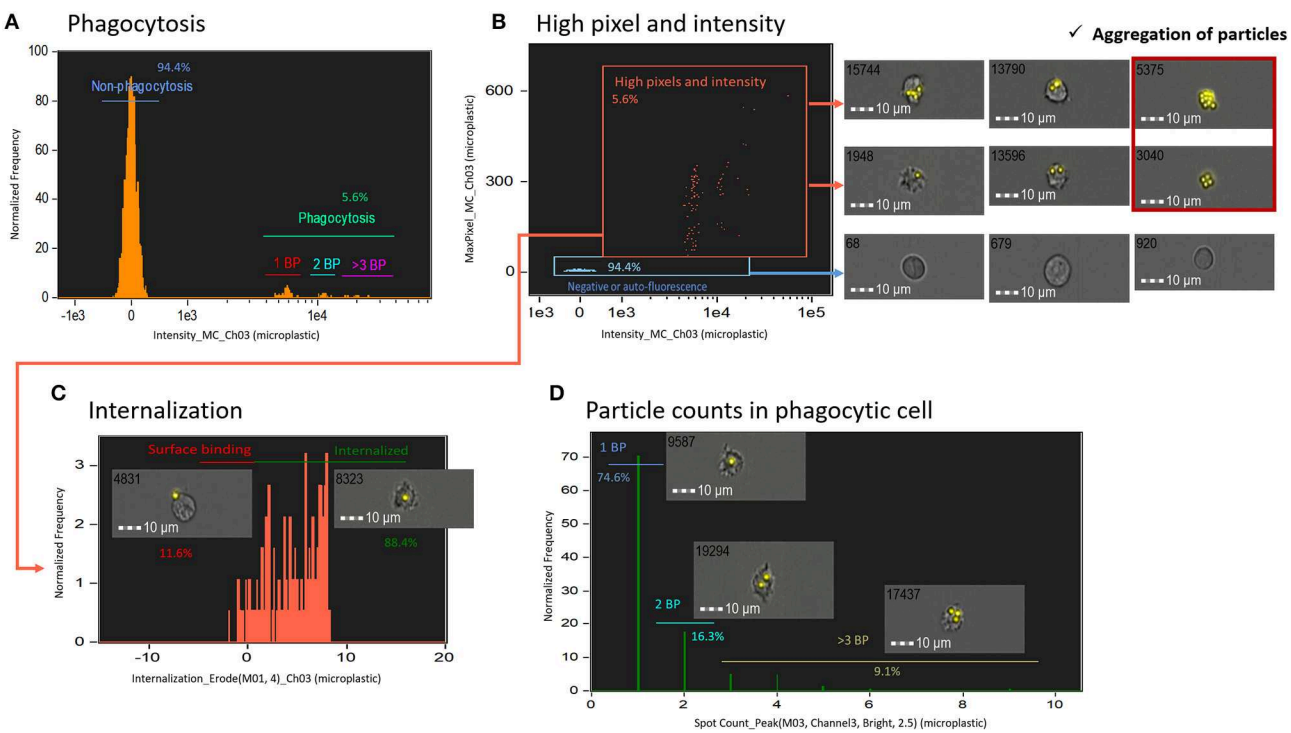

FIGURE 3 | Measurement of phagocytosis using non-degradable fluorescent particles (microplastics). **(A)** A histogram of fluorescent microplastic intensity in live cells. **(B)** To exclude auto-fluorescence and find the best images, images with more pixels and high intensity were gated. Errors may occur in conventional FC due to aggregation of microplastics. **(C)** Internalized cells were gated using internalization score. **(D)** Cells with internalized particles were plotted in a histogram of spot count, which shows the number of particles. All cell images were captured with 40 × objective. Scale bar = 10 μm. BP, bio-particle.

within an image based on their intensity and localization) with the following mask function [Erode (M01, 4)_Ch03]. The ratio indicated the proximity of microplastic to the center of the cell; cells with a score of > 0.3 were considered to have internalized particles and those with a score of < 0.3 were considered to have surface-bound particles (11). Finally, only cells with internalized particles were presented in a histogram of spot count feature, which is an ideal approach to quantify the masked spots in the cell (**Figure 3D**). Overall, IFC can be applied for detecting non-degradable microplastic beads inside the phagocytic cells and quantifying the number of beads. In addition, salmon HK phagocytic cells could recognize microplastics as foreign bodies although we observed only few phagocytosed particles.

Examining Phagocytosis Using Degradable Fluorescent Bio-particles

To determine phagocytosis of degradable bio-particles by salmon HK cells compared with non-degradable microplastics, first, we plotted histograms of fluorescence intensity of degradable bio-particles (**Figure 4A**). In comparison to the histogram of the non-degradable microplastic beads described above (**Figure 3**), it was more difficult to distinguish the number of bio-particles in this histogram. To exclude auto-fluorescence and obtain high-quality images, we adopted a gating strategy based on high pixel (pixel value > 30) and intensity of images (**Figure 4B**). We created two gates, one to include particles with high pixel and high intensity and the other one with negative or auto-fluorescence (histogram in **Figure 4B**). From the histogram, it is clear that overlapping particle intensity (orange) and auto-fluorescence (blue) curves can cause detection errors. Cells that had engulfed the bio-particles were gated using the internalization score as described in the previous section (**Figure 4C**). Finally, only cells with internalized particles are presented in a histogram of particle intensity to understand the number of particles in the phagocytic cells (**Figure 4D**). We found that to quantify the number of degradable particles, particle intensity-based protocol is a better strategy compared to the method employing spot count feature.

Optimizing IFC-Based Method for Phagocytosis Assay

To verify the validity of our IFC-based method, we used degradable fluorescent bio-particles from *E. coli* to assess the effect of incubation temperature on the phagocytic activity and capacity of phagocytic cells from three aquatic animals. The phagocytic ability of HK phagocytic cells from salmon (**Figure 5A**) and tilapia (**Figure 6A**) incubated at 12 and 25°C, respectively, was significantly higher compared to cells incubated at 4°C, but temperature did not significantly affect the phagocytic ability of hemocytes from blue mussel (**Figure 7A**). In contrast, the phagocytic capacity of none of the aquatic species tested

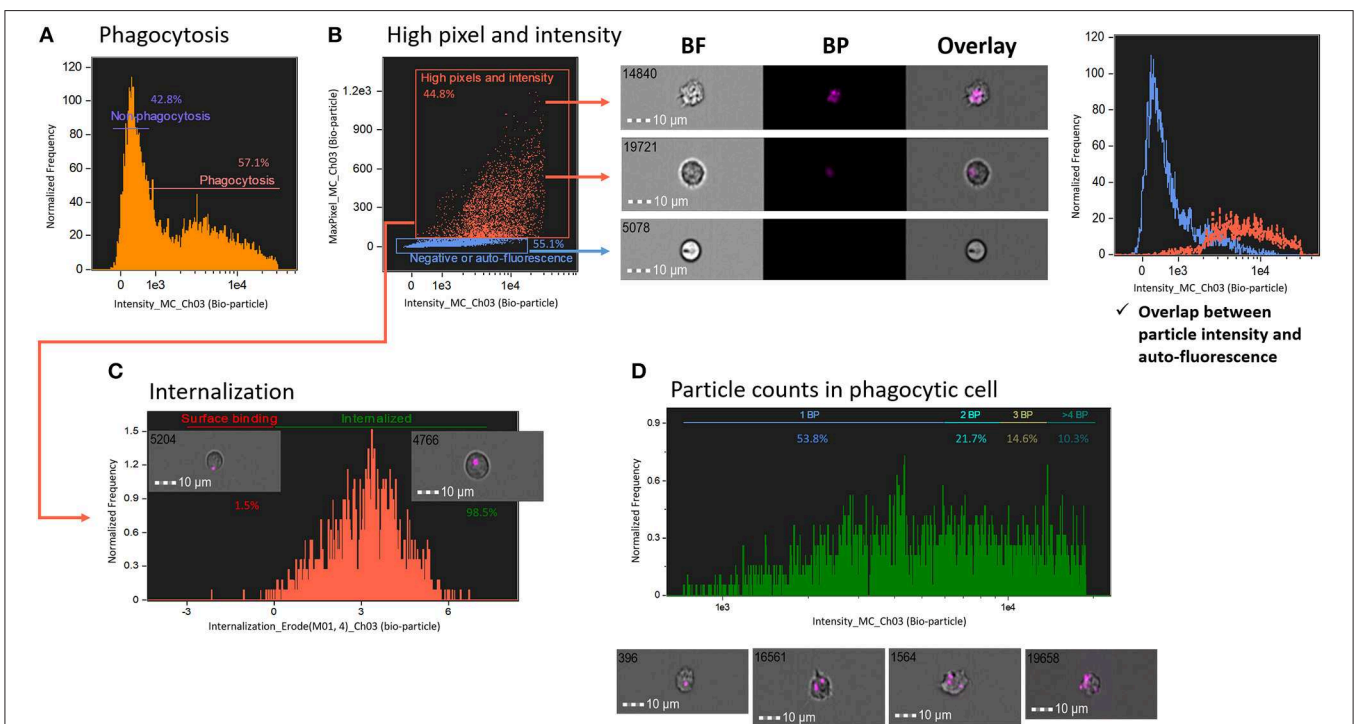

FIGURE 4 | Measurement of phagocytosis using degradable fluorescent particles (pHrodo™). **(A)** Live cells are plotted in a histogram of fluorescent bio-particle intensity. **(B)** To exclude auto-fluorescence and find the best image, images with more pixels and high intensity were gated. The histogram (right panel) points to the detection error caused by overlapping curves of particle intensity (orange) and auto-fluorescence (blue) in conventional flow cytometry. **(C)** Internalized cells were gated using internalization score. **(D)** Cells with internalized particles were plotted in a histogram of bio-particle intensity, which shows the number of particles. All cell images were captured with 40 × objective. Scale bar = 10 µm. BF, brightfield; BP, bio-particle.

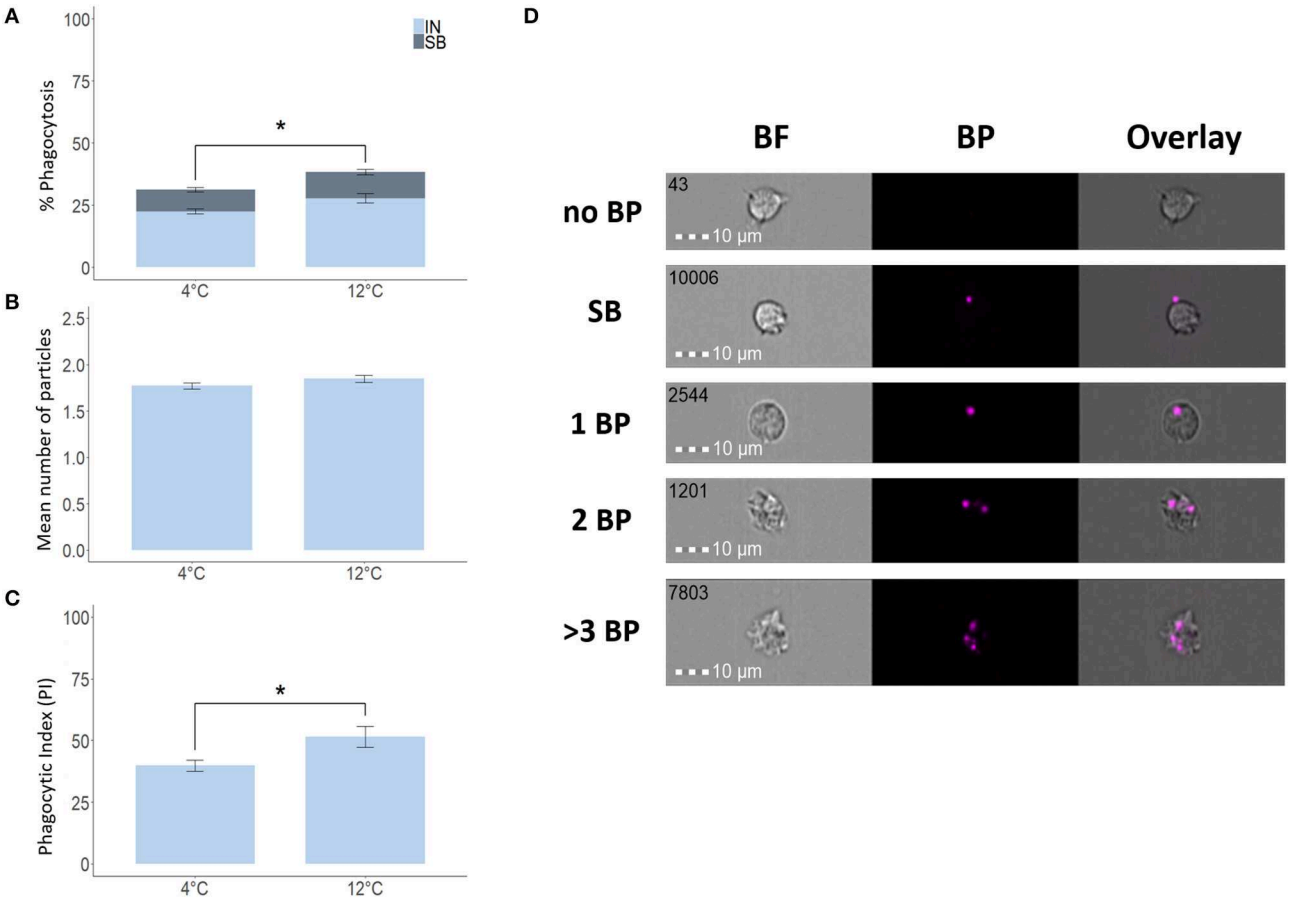

FIGURE 5 | Phagocytosis of Atlantic salmon head kidney macrophages incubated at different temperatures. Percent of phagocytic cells **(A)**, mean number of particles ingested per phagocytic cell **(B)** and phagocytic index, PI **(C)**. Representative cell images that show cells with no BP, SB, and 1BP, 2BP, and > 3BP **(D)**. Statistically significant differences ($p < 0.05$) are indicated using asterisks. Bar plots show the mean ± SD. Sample size = 6. All cell images were captured with 40 × objective. Scale bar = 10 µm. IN, internalization; SB, surface-binding particles; 1 BP, 2 BP, and > 3 BP, 1–3 internalized bio-particles; BF, brightfield.

was significantly affected by temperature (**Figures 5B,D**, **6B,D**, **7B,D**). The phagocytic index of only the salmon cells incubated at 12°C was significantly higher compared to cells incubated at 4°C (**Figure 5C**). This temperature effect could not be detected for the phagocytic index of tilapia HK cells (**Figure 6C**) and blue mussel hemocytes (**Figure 7C**) although the cells were incubated at higher values, i.e., 12 and 25°C, respectively. The optimized method for phagocytosis assay was well-applied to phagocytic cells from three aquatic animals. The results showed that unlike that of phagocytic cells from fishes, phagocytosis of the cells from mussel was not significantly affected by incubation temperature.

DISCUSSION

The major advantage of imaging flow cytometry (IFC) over conventional flow cytometry (FC) is its ability to distinguish between false-positive and false-negative events by considering additional features of the captured cellular images (2). The two systems share the basic principle (19). Although IFC has been widely adopted to study mammalian cell types, it is not yet commonly employed to investigate other organisms, including aquatic animals. There is a paucity of appropriate tools such as cell-specific markers, which hampers the wider adoption of new technologies like IFC. Furthermore, the associated protocols require thorough refining before IFC can be used to study cell types from aquatic animals. For example, as the weak and small fluorescence cannot be detected by the system, we employ masking and features within IDEAS software to accurately select the area of interest during image analysis (20). Our study describes procedures to accurately identify cellular phenotypes and quantify phagocytosis by cells from three very different aquatic animals.

In the present IFC study, we could successfully exclude dead cells and cell aggregates and could identify single leukocytes from Atlantic salmon HK based on bright field (BF) area and SSC intensity. We observed two distinct populations: cells located in the low BF area and low SSC intensity, and cells located in the high BF area and high SSC intensity. Our IFC results are in agreement with conventional FC data on HK leukocytes from salmon (21). A study on goldfish primary kidney macrophages

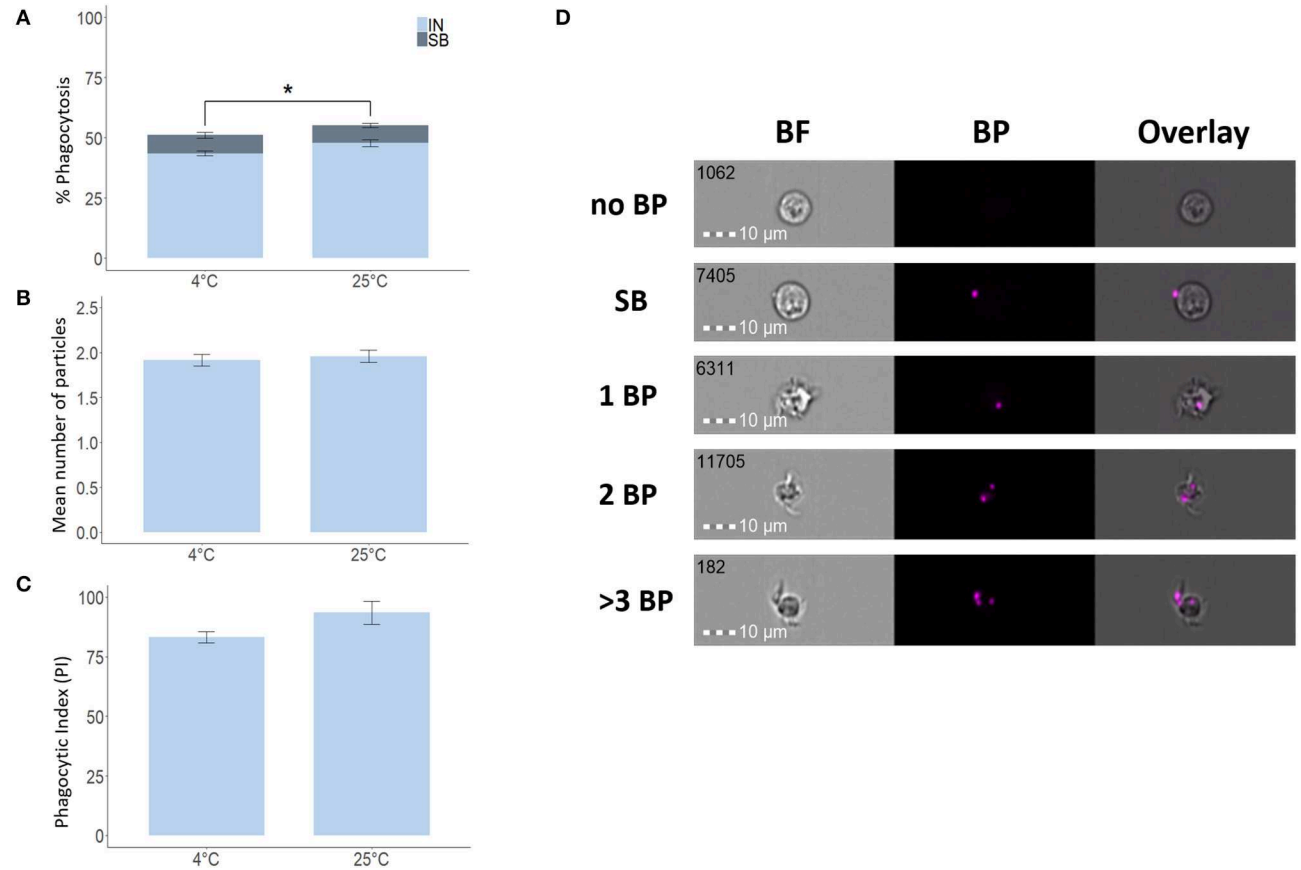

FIGURE 6 | Phagocytosis of Nile tilapia head kidney macrophages incubated at different temperatures. Percent of phagocytic cells **(A)**, mean number of particles ingested per phagocytic cell **(B)** and phagocytic index, PI **(C)**. Representative cell images that show cells with no BP, SB, and 1BP, 2BP, and > 3BP **(D)**. Statistically significant differences ($p < 0.05$) are indicated using asterisks. Bar plots show the mean ± SD. Sample size = 6. All cell images were captured with 40 × objective. Scale bar = 10 µm. IN, internalization; SB, surface-binding particles; 1 BP, 2 BP, and > 3 BP, 1–3 internalized bio-particles; BF, brightfield.

also compared IFC results with those from conventional FC data; both systems were used to identify cell sub-populations. Similar dot plots were generated for both flow cytometry systems, indicating that the replacement of forward scatter (FSC) which measures cell size in conventional FC by BF area in IFC (22) is a reliable approach, independent of fish species.

Interestingly, adherent cells from Atlantic salmon HK (R3, macrophage-like cells) were located in a higher BF area than R2 cells from the same organ (**Figures 1D,E**). The proportion of macrophage-like cells was approximately 45.2%. The macrophage-like cells in the R3 region displayed a similar morphology to that of the adherent TO cells, a cell line originating from salmon HK leukocytes (23). Furthermore, in another study that employed conventional FC, salmon macrophage-like cells were presented in an FSC vs. SSC plot (24). Similar to our gating, the author gated three regions in the plot and assumed that the two higher FSC regions contained macrophage-like cells which was ∼56% out of the total number of cells.

After optimizing the method to distinguish between lymphocytes from monocytes/macrophages, magnetic cell sorting (MACS) was performed to sort target lymphocytes using an IgM-specific antibody. The purity of IgM^+ cells after MACS was 89.8% which is similar to 92% in a salmon study (25). MACS enabled us to ascertain the area of lymphocyte-like cells as defined/interpreted from the BF area vs. SSC intensity plots. The sorted salmon IgM^+ cells were located in the low BF area and low SSC intensity gate, confirming a close area match to that of the lymphocyte-like cells. Similarly, a previous study on trout HK confirmed lymphocyte localization (low FSC and low SSC) using conventional FC, based on $CD4^+$T cell markers (26). In addition, employing conventional FC, percentage of IgM^+ and IgT^+ B cells in salmon HK cells were determined by gating the same area (25). The gate areas in **Figures 1**, **2** confirm the presence of lymphocytes.

After confirming the identity of the B lymphocytes in the low BF area vs. low SSC intensity gate, we explored the phagocytosis of the adherent monocytes/macrophages HK fraction. Phagocytosis is an important initial immune response with final entry of antigens into the phagosomes/lysosomes that stimulates the production of reactive oxygen species (27). Phagocytic activity is influenced by many factors such as cell

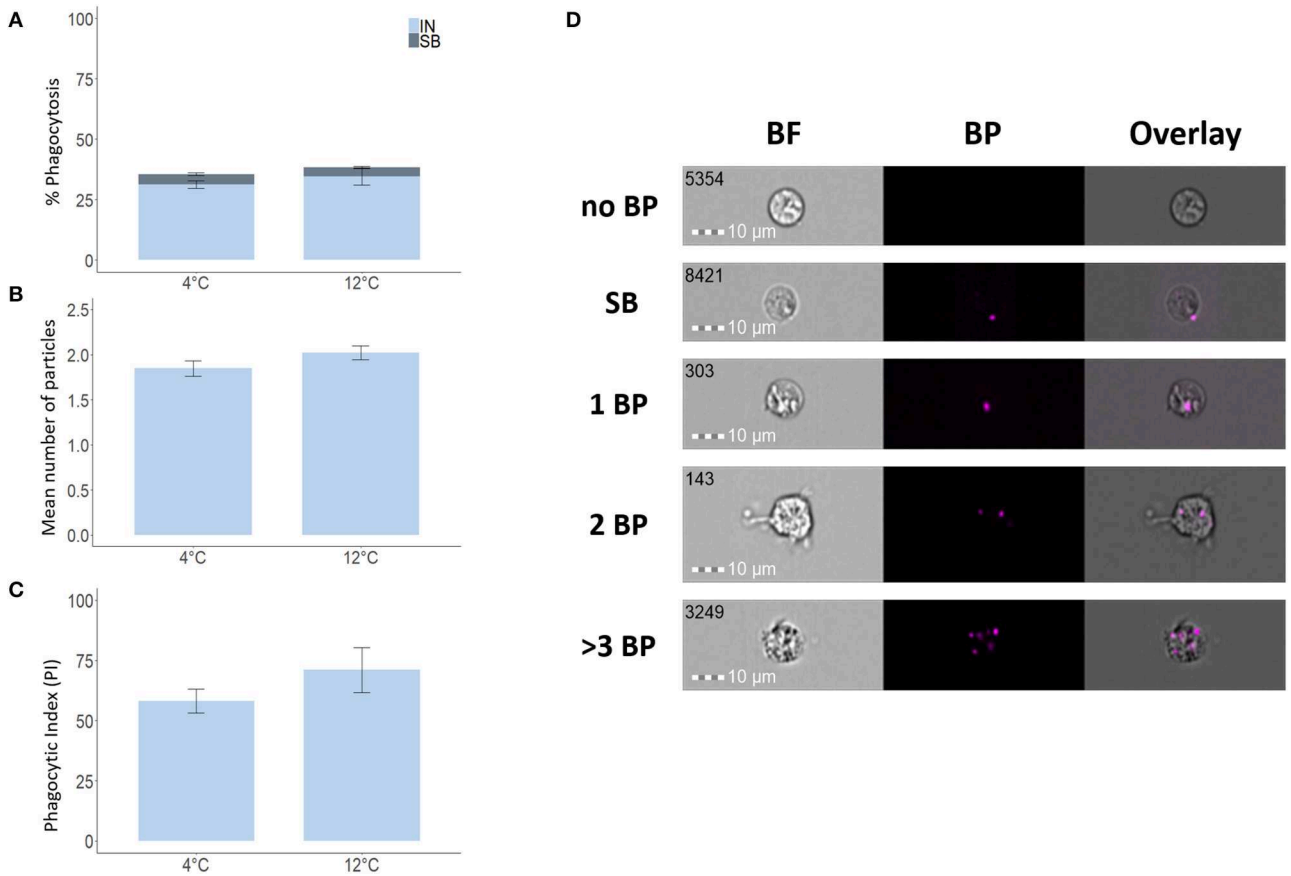

FIGURE 7 | Phagocytosis of blue mussel hemocytes incubated at different temperatures. Percent of phagocytic cells **(A)**, mean of number of particles ingested per phagocytic cell **(B),** and phagocytic index, PI **(C)**. Representative cell images that show cells with no BP, SB, and 1BP, 2BP, and > 3BP **(D)**. Statistically significant differences ($p < 0.05$) are indicated using asterisks. Bar plots show the mean ± SD. Sample size = 6. All cell images were captured with 40 × objective. Scale bar = 10 µm. IN, internalization; SB, surface-binding particles; 1 BP, 2 BP, and > 3 BP, 1–3 internalized bio-particles; BF, brightfield.

maturity, cytokine response, antigen presenting cell activation status (28) and the characteristics of phagocytosed antigens or particles (29). We explored the phagocytic activity of salmon HK cells using IFC, which allowed for not only quantification of the number of cells with internalized particles but also the localization of particles inside the cells. The IFC methods for assessing phagocytosis are complex, and researchers are yet to standardize them for different particle types. In the present study, we tested two different types of particles, non-degradable and degradable particles. This is the first IFC study that reports the use of microplastic as non-degradable particles and bio-particles from *E. coli* as degradable particles. Considering the growing debate on microplastic pollution of the marine ecosystem, studying phagocytosis of microplastics by immune cells from aquatic animals can be of particular interest from an environmental perspective. In our studies, with our sensitive IFC methodology, we could clearly detect microplastic particles engulfed by salmon macrophages, although only few particles were detected inside these cells. We, therefore, assume that these cell types can phagocytose microplastics as (foreign) particles. It should be pointed out that the salmon HK phagocytic cells were not able to uptake more microplastics; the reason could be that the cells can efficiently recognize microbe-derived particles (bio particle from *E. coli*) due to their natural antigenicity and phagocytose it more easily than an "unknown particle" such as the microplastic. Furthermore, the microplastic beads are not coated with any compound recognizable by the phagocytic cells, and they are larger compared to the bioparticles.

Compared to microplastic particles, the bio-particles are known to emit fluorescence within cells. However, this occurs only upon acidification, i.e., they emit fluorescence of a particular wavelength, depending on the pH level that the particle encounters. Hence, we suggest the use of fluorescent intensity feature rather than spot count feature to accurately assess the counts of degradable particles in phagocytes. Although a different feature was used to count the number of particles per phagocytic cell, a publication (12) has reported an IFC method for counting internalized fluorescent-labeled bacteria. The author succeeded in distinguishing between cells with high bright detail similarity score and those with low bright detail similarity score; the former one had internalized particles while other cells had external particles. Although the method of Smirnov et al. (12) gives

information on the overall degree of phagocytosis in phagocytic cells, it cannot accurately count the internalized particles. Thus, the bright detail similarity score and fluorescent intensity feature are effective in detecting and counting (as in this report) the mean number of internalized particles per phagocytic cell.

Although we did not perform a direct comparison between IFC and conventional FC, from our results we understand that false events such as auto-fluorescence and aggregated particles can be misinterpreted in the case of conventional FC. Pixel and intensity features were adjusted carefully in the present study to exclude the false-positive events. Caution should be exercised when gating phagocytic cells using these features because in IFC, cell size is measured based on pixels, and the sensitivity of the measurement is dependent on the cell size (19). Thus, in order to include the region of interest for analysis, the mask that identifies the intracellular compartment has to be adjusted for different types of cells and particles.

After standardizing the protocols for monocytes/macrophage phagocytosis, we optimized the methods for measuring phagocytosis, using degradable bio-particles, by cells from three very different aquatic animals—two fishes, Atlantic salmon and Nile tilapia and a mollusc, blue mussel—to evaluate the effect of incubation temperature on their phagocytic abilities and capacities. Our results indicated that phagocytosis of cells from the fishes can be affected by the incubation temperature. Although not directly comparable, phagocytosis of human leukocytes was reduced at higher and lower temperature compared to the normal host temperature range (30). Interestingly, the phagocytosis by hemocytes from blue mussel, a eurythermal species that can tolerate a broad temperature range from −1 to 20°C (31, 32), was not affected by incubation temperature.

In summary, IFC was used to study phagocytosis in fish and mussel cells. We were able to identify cell populations and determine the phagocytosis of different kinds of particles by quantifying the number of internalized particles and detecting the localization of particles in the phagocytes. This study provides important information about how IFC can be used in the field of fish immunology and ecotoxicology. Furthermore, the procedures described in this report may have wider application in aquatic sciences, to unravel the effects of microplastic-ingestion by living organisms in the oceans.

DATA AVAILABILITY STATEMENT

All datasets generated for this study are included in the article/supplementary material.

ETHICS STATEMENT

The animal study was reviewed and approved by National Animal Research Authority in Norway (Mattilsynet).

AUTHOR CONTRIBUTIONS

YP and VK conceived and designed the study. YP and IA-G performed the experiments. YP analyzed the data and wrote the first draft of the manuscript while IA-G wrote a section of it. ST, GW and DB provided suggestions to improve the IFC protocols. YP, IA-G, ST, GW, DB, PO, and VK read, revised, and approved the manuscript for submission.

FUNDING

This study was supported by the INFISH project (272004) funded by Regional Forskningsfond Nord-Norge (RFF Nord-Norge). YP was financially supported by Korean Government Scholarship—National Institute for International Education, South Korea.

ACKNOWLEDGMENTS

The support of the staff at the Research Station, Nord University, Norway is acknowledged. YP is grateful to the members of the Cell Biology and Immunology Group, Wageningen University, the Netherlands for teaching him the principles of flow cytometry. Bisa Saraswathy is thanked for her support in data analysis, helpful discussion, and manuscript preparation.

REFERENCES

1. Görgens A, Bremer M, Ferrer-Tur R, Murke F, Tertel T, Horn PA, et al. Optimisation of imaging flow cytometry for the analysis of single extracellular vesicles by using fluorescence-tagged vesicles as biological reference material. *J Extracell Vesicles.* (2019) 8:1587567. doi: 10.1080/20013078.2019.1587567
2. Barteneva NS, Fasler-Kan E, Vorobjev IA. Imaging flow cytometry: coping with heterogeneity in biological systems. *J Histochem Cytochem.* (2012) 60:723–33. doi: 10.1369/0022155412453052
3. Hulspas R, O'gorman MR, Wood BL, Gratama JW, Sutherland DR. Considerations for the control of background fluorescence in clinical flow cytometry. *Cytom B Clin Cytom.* (2009) 76:355–64. doi: 10.1002/cyto.b.20485
4. Van Beers EJ, Samsel L, Mendelsohn L, Saiyed R, Fertrin KY, Brantner CA, et al. Imaging flow cytometry for automated detection of hypoxia-induced erythrocyte shape change in sickle cell disease. *Am J Hematol.* (2014) 89:598–603. doi: 10.1002/ajh.23699
5. Ofir-Birin Y, Abou Karam P, Rudik A, Giladi T, Porat Z, Regev-Rudzki N. Monitoring extracellular vesicle cargo active uptake by imaging flow cytometry. *Front Immunol.* (2018) 9:1011. doi: 10.3389/fimmu.2018.01011
6. Piancone F, Saresella M, Marventano I, La Rosa F, Santangelo MA, Caputo D, et al. Monosodium urate crystals activate the inflammasome in primary progressive multiple sclerosis. *Front Immunol.* (2018) 9:983. doi: 10.3389/fimmu.2018.00983
7. Jenner D, Ducker C, Clark G, Prior J, Rowland CA. Using multispectral imaging flow cytometry to assess an *in vitro* intracellular *Burkholderia thailandensis* infection model. *Cytom A.* (2016) 89:328–37. doi: 10.1002/cyto.a.22809
8. Rieger AM, Konowalchuk JD, Grayfer L, Katzenback BA, Havixbeck JJ, Kiemele MD, et al. Fish and mammalian phagocytes differentially regulate pro-inflammatory and homeostatic responses *in vivo*. *PLoS ONE.* (2012) 7:e47070. doi: 10.1371/journal.pone.0047070
9. Rességuier J, Delaune E, Coolen A-L, Levraud J-P, Boudinot P, Le Guellec D, et al. Specific and efficient uptake of surfactant-free poly (lactic acid)

nanovaccine vehicles by mucosal dendritic cells in adult zebrafish after bath immersion. *Front Immunol.* (2017) 8:190. doi: 10.3389/fimmu.2017.00190
10. Parra D, Rieger AM, Li J, Zhang YA, Randall LM, Hunter CA, et al. Pivotal advance: peritoneal cavity B-1 B cells have phagocytic and microbicidal capacities and present phagocytosed antigen to CD4+ T cells. *J Leukocyte Biol.* (2012) 91:525–36. doi: 10.1189/jlb.0711372
11. Phanse Y, Ramer-Tait AE, Friend SL, Carrillo-Conde B, Lueth P, Oster CJ, et al. Analyzing cellular internalization of nanoparticles and bacteria by multi-spectral imaging flow cytometry. *J Visual Exp.* (2012) 64:e3884. doi: 10.3791/3884
12. Smirnov A, Solga MD, Lannigan J, Criss AK. An improved method for differentiating cell-bound from internalized particles by imaging flow cytometry. *J Immunol Methods.* (2015) 423:60–9. doi: 10.1016/j.jim.2015.04.028
13. Paulsen SM, Engstad RE, Robertsen B. Enhanced lysozyme production in Atlantic salmon (*Salmo salar* L.) macrophages treated with yeast β-glucan and bacterial lipopolysaccharide. *Fish Shellfish Immunol.* (2001) 11:23–37. doi: 10.1006/fsim.2000.0291
14. Pirarat N, Pinpimai K, Endo M, Katagiri T, Ponpornpisit A, Chansue N, et al. Modulation of intestinal morphology and immunity in Nile tilapia (*Oreochromis niloticus*) by *Lactobacillus rhamnosus* GG. *Res Vet Sci.* (2011) 91:e92–7. doi: 10.1016/j.rvsc.2011.02.014
15. Wen C-M. Development and characterization of a cell line from tilapia head kidney with melanomacrophage characteristics. *Fish Shellfish Immunol.* (2016) 49:442–9. doi: 10.1016/j.fsi.2016.01.013
16. Antoun SW. *Mussel (Mytilus edulis) hemocytes for in vitro testing* (dissertation/master's thesis). University of Oslo, Oslo, Norway (2011).
17. Barbuddhe SB, Malik SVS, Gupta LK. Effect of *in vitro* monocyte activation by *Listeria Monocytogenes* antigens on phagocytosis and production of reactive oxygen and nitrogen radicals in bovines. *Vet Immunol Immunopathol.* (1998) 64:149–59. doi: 10.1016/S0165-2427(98)00129-9
18. Fuentes A-L, Millis L, Vapenik J, Sigola L. Lipopolysaccharide-mediated enhancement of zymosan phagocytosis by RAW 264.7 macrophages is independent of opsonins, laminarin, mannan, and complement receptor 3. *J Surg Res.* (2014) 189:304–12. doi: 10.1016/j.jss.2014.03.024
19. Basiji DA. *Principles of Amnis Imaging Flow Cytometry in Imaging Flow Cytometry*. Berlin: Springer (2016) 13–21. doi: 10.1007/978-1-4939-3302-0_2
20. Grimwade LF, Fuller KA, Erber WN. Applications of imaging flow cytometry in the diagnostic assessment of acute leukaemia. *Methods.* (2017) 112:39–45. doi: 10.1016/j.ymeth.2016.06.023
21. Kalgraff CA, Wergeland HI, Pettersen EF. Flow cytometry assays of respiratory burst in Atlantic salmon (*Salmo salar* L.) and in Atlantic cod (*Gadus morhua* L.) leucocytes. *Fish Shellfish Immunol.* (2011)31:381–8. doi: 10.1016/j.fsi.2011.05.028
22. Rieger AM, Hall BE, Barreda DR. Macrophage activation differentially modulates particle binding, phagocytosis and downstream antimicrobial mechanisms. *Dev Compar Immunol.* (2010) 34:1144–59. doi: 10.1016/j.dci.2010.06.006
23. Pettersen EF, Ingerslev H-C, Stavang V, Egenberg M, Wergeland HI. A highly phagocytic cell line TO from Atlantic salmon is CD83 positive and M-CSFR negative, indicating a dendritic-like cell type. *Fish Shellfish Immunol.* (2008) 25:809–19. doi: 10.1016/j.fsi.2008.08.014
24. Ulvestad JS. *Studies on the stimulation of Atlantic salmon macrophage-like cells with emphasis on respiratory burst* (dissertation/master's thesis). UiT The Arctic University of Norway, Tromsø, Norway (2017).
25. Jenberie S, Thim HL, Sunyer JO, Skjødt K, Jensen I, Jørgensen JB. Profiling Atlantic salmon B cell populations: CpG-mediated TLR-ligation enhances IgM secretion and modulates immune gene expression. *Sci Rep.* (2018) 8:3565. doi: 10.1038/s41598-018-21895-9
26. Maisey K, Montero R, Corripio-Miyar Y, Toro-Ascuy D, Valenzuela B, Reyes-Cerpa S, et al. Isolation and characterization of salmonid CD4+ T cells. *J Immunol.* (2016) 196:4150–63. doi: 10.4049/jimmunol.1500439
27. Gartlan KH, Krashias G, Wegmann F, Hillson WR, Scherer EM, Greenberg PD, et al. Sterile inflammation induced by Carbopol elicits robust adaptive immune responses in the absence of pathogen-associated molecular patterns. *Vaccine.* (2016) 34:2188–96. doi: 10.1016/j.vaccine.2016.03.025
28. Gordon S. Phagocytosis: an immunobiologic process. *Immunity.* (2016) 44:463–75. doi: 10.1016/j.immuni.2016.02.026
29. Underhill DM, Goodridge HS. Information processing during phagocytosis. *Nat Rev Immunol.* (2012) 12:492. doi: 10.1038/nri3244
30. Peterson P, Verhoef J, Quie P. Influence of temperature on opsonization and phagocytosis of staphylococci. *Infect Immun.* (1977) 15:175–9. doi: 10.1128/IAI.15.1.175-179.1977
31. Hiscock K, Tyler-Walters H. Assessing the sensitivity of seabed species and biotopes–the Marine Life Information Network (MarLIN). *Hydrobiologia.* (2006) 555:309–20. doi: 10.1007/s10750-005-1127-z
32. Thyrring J, Rysgaard S, Blicher ME, Sejr MK. Metabolic cold adaptation and aerobic performance of blue mussels (*Mytilus edulis*) along a temperature gradient into the high Arctic region. *Marine Biol.* (2015) 162:235–43. doi: 10.1007/s00227-014-2575-7

Conflict of Interest: ST is an employee of Luminex B.V., which is a subsidiary of Luminex Corporation. Luminex Corporation is the manufacturer of the ImageStream$^{®X}$ Mk II Imaging Flow Cytometer.

The remaining authors declare that the research was conducted in the absence of any commercial or financial relationships that could be construed as a potential conflict of interest.

frontiers in Immunology

REVIEW
published: 25 February 2020
doi: 10.3389/fimmu.2020.00325

Chemokine Receptors and Phagocyte Biology in Zebrafish

*Frida Sommer, Vincenzo Torraca and Annemarie H. Meijer**

Institute of Biology Leiden, Leiden University, Leiden, Netherlands

Phagocytes are highly motile immune cells that ingest and clear microbial invaders, harmful substances, and dying cells. Their function is critically dependent on the expression of chemokine receptors, a class of G-protein-coupled receptors (GPCRs). Chemokine receptors coordinate the recruitment of phagocytes and other immune cells to sites of infection and damage, modulate inflammatory and wound healing responses, and direct cell differentiation, proliferation, and polarization. Besides, a structurally diverse group of atypical chemokine receptors (ACKRs) are unable to signal in G-protein-dependent fashion themselves but can shape chemokine gradients by fine-tuning the activity of conventional chemokine receptors. The optically transparent zebrafish embryos and larvae provide a powerful *in vivo* system to visualize phagocytes during development and study them as key elements of the immune response in real-time. In this review, we discuss how the zebrafish model has furthered our understanding of the role of two main classes of chemokine receptors, the CC and CXC subtypes, in phagocyte biology. We address the roles of the receptors in the migratory properties of phagocytes in zebrafish models for cancer, infectious disease, and inflammation. We illustrate how studies in zebrafish enable visualizing the contribution of chemokine receptors and ACKRs in shaping self-generated chemokine gradients of migrating cells. Taking the functional antagonism between two paralogs of the CXCR3 family as an example, we discuss how the duplication of chemokine receptor genes in zebrafish poses challenges, but also provides opportunities to study sub-functionalization or loss-of-function events. We emphasize how the zebrafish model has been instrumental to prove that the major determinant for the functional outcome of a chemokine receptor-ligand interaction is the cell-type expressing the receptor. Finally, we highlight relevant homologies and analogies between mammalian and zebrafish phagocyte function and discuss the potential of zebrafish models to further advance our understanding of chemokine receptors in innate immunity and disease.

Keywords: ***Mycobacterium marinum*, infection, wounding, zebrafish, cancer, inflammation, chemokine receptor, phagocytes**

OPEN ACCESS

Edited by:
Qing Deng,
Purdue University, United States

Reviewed by:
Yi Feng,
University of Edinburgh, United Kingdom
Milka Sarris,
University of Cambridge, United Kingdom

***Correspondence:**
Annemarie H. Meijer
a.h.meijer@biology.leidenuniv.nl

Specialty section:
This article was submitted to Comparative Immunology, a section of the journal Frontiers in Immunology

Received: *01 December 2019*
Accepted: *10 February 2020*
Published: *25 February 2020*

Citation:
Sommer F, Torraca V and Meijer AH (2020) Chemokine Receptors and Phagocyte Biology in Zebrafish. Front. Immunol. 11:325. doi: 10.3389/fimmu.2020.00325

INTRODUCTION

Phagocytosis refers to the recognition and internalization of particles larger than 0.5 μm into a plasma membrane-derived vesicle called the phagosome. Phagocytes are cells that can phagocytose harmful particles, pathogens, and dying cell debris. Phagocytes are broadly divided into professional and non-professional phagocytes (1). In non-professional phagocytes like

epithelial cells, endothelial cells, and fibroblasts, phagocytosis is a facultative function as these cells have other tissue-resident functions, although they can contribute to tissue homeostasis by phagocytosing apoptotic debris (2). In contrast, professional phagocytes efficiently identify, engulf, and clear invading pathogens, harmful substances, and dying cells. This group includes highly motile cells such as neutrophils, monocytes, macrophages, eosinophils, mast cells, and dendritic cells as well as tissue-resident cells like osteoclasts (3). Professional phagocytes express multiple specialized membrane-bound receptors that recognize target particles of different nature. Pattern recognition-receptors (PRRs) identify pathogen-associated molecular patterns (PAMPS) and damage-associated molecular patterns (DAMPS) and activate the immune response (1, 3). The phagocytosis process, itself is initiated by other surface receptors. Among these, scavenger receptors mediate the phagocytosis of endogenous ligands, like lipoproteins, as well as microbial invaders. Opsonic receptors recognize targets detected and bound by soluble host molecules, such as complement proteins and antibodies. Receptors for apoptotic cells recognize soluble cues secreted by dying cells (e.g., lysophosphatidylcholine and ATP) or characteristic molecules exposed on the surface of dying cells, such as phosphatidylserine (1, 2). Professional phagocytes play pivotal roles in immunomodulation, development, pathogen clearance and antigen presentation (2, 3).

In addition to pattern recognition and phagocytic receptors, phagocytes express various types of chemokine receptors that coordinate cell movement and confer certain functional properties to these cells (4, 5). Chemokine receptors belong to the G-protein-coupled receptor (GPCR) family and transiently activate GTP-binding proteins that remodel actin structures of the cytoskeleton to control the contractile machinery of the cell and direct cell migration [mm]. Dynamic actin rearrangements control the formation of pseudopodia during cell migration toward a target as well as the formation of protrusions that surround harmful particles and pathogens before internalization within the phagosome during phagocytosis (5–7). Chemokine receptors are essential for phagocyte function as they trigger the rearrangement of actin-containing structures required for cell motility, which is at the core of developmental and immunological processes and tissue maintenance and remodeling (8–10). Likewise, chemokine receptor signaling contributes to the differentiation, proliferation, and polarization of phagocytes, which are determining factors in host-pathogen interactions, inflammatory responses, inflammation resolution, and wound healing (4–6, 11, 12).

Zebrafish are increasingly used as a model species to study development and disease owing to the accessibility of the early life stages (embryos and larvae) for genetic analyses, chemical screens, and intravital imaging (6, 13–17). These useful features of the zebrafish have been exploited to study the roles of phagocytes in models of infectious and inflammatory diseases and cancer. In this review, we will illustrate how the zebrafish model contributed to our understanding of the role of chemokine signaling axes in phagocyte biology and highlight its main contributions to the understanding of chemokine signaling axes in phagocytes by addressing relevant homologies and analogies between mammalian and zebrafish phagocyte function. We will focus on the two major structural subfamilies of chemokine receptors, CC and CXC, and on the migratory properties of macrophages and neutrophils in the context of development and disease. We will discuss the regulatory role of atypical chemokine receptors (ACKRs), in shaping chemokine gradients and how duplication of chemokine receptor genes in zebrafish allows assessing sub-functionalization or loss/gain of function events and the challenges that gene duplication poses. Finally, we will discuss the potential of zebrafish models to further our understanding of chemokine receptors in innate immunity and immune-related disease.

FUNDAMENTALS OF CHEMOKINE SIGNALING AND REGULATION

Chemokines are small secretory and transmembrane cytokines that induce directed chemotaxis of macrophages and neutrophils through their specific receptors under pathological and homeostatic conditions (5, 7, 18). Chemokine receptors belong to the chordate-restricted class A of (rhodopsin-like) heptahelical G-protein coupled receptors (GPCRs), which is grouped into four subclasses according to the pattern of highly conserved cysteine residues they display near their N-terminus (CC, CXC, CX3C, and XC) (5, 19). The cysteine motif of a chemokine receptor is followed by an "R" for "receptor" or an "L" for ligands and a number indicating the chronological order in which the molecules were identified (5, 19, 20). A further subfamily containing the characteristic motif CX has been identified only in zebrafish at present (19). Following nomenclature conventions, human chemokine receptors are written in capital letters, while those of other species use the lowercase to simplify the distinction between species. The structure of chemokine receptors consists of an intracellular COOH terminus, an extracellular NH2 terminus, and seven transmembrane domains linked by three extracellular and three intracellular loops (5, 12) Chemokine receptors mediate leukocyte trafficking during cell migration processes such as infection, damage, development, cell proliferation and differentiation (21–24). GPCRs are the largest and most diverse family of membrane receptors in eukaryotes and the most common pharmaceutical target making chemokine receptors attractive targets to treat chronic inflammatory conditions (12, 25).

Inactive chemokine receptors are coupled to heterotrimeric G proteins. The Gα subunit is bound to GDP (guanosine diphosphate) in resting conditions and exchanges the GDP molecule for GTP (guanosine triphosphate) when the chemokine receptor binds a cognate ligand. The GTP-Gα subunit complex dissociates from the receptor and the Gβ-γ heterodimer, which triggers the canonical downstream signal pathways that ultimately result in the intracellular mobilization of Ca^{+2} and the rearrangement of cytoskeletal components required by the vesicle trafficking machinery and for cell migration (5, 26–28). Besides the conventional G protein-dependent signaling pathways, chemokine receptors can directly activate JAK/STAT (Janus kinase /Signal transducer and activator of transcription)

signaling, a pathway shown to induce chemotaxis of progenitor germ cells (PGCs) in zebrafish (6, 29–31). Furthermore, chemokine receptors can also signal through β-arrestin to mediate the internalization and intracellular degradation of chemokines and chemokine receptors (12, 30, 32, 33).

Chemokine networks are highly promiscuous and redundant and can result in antagonistic and synergistic interactions since different signaling pathways share signal transducing elements. Due to its complex nature, chemokine signaling axes build up tangled networks that need tight spatio-temporal regulation to evoke specific responses (34). Some regulatory mechanisms of chemokine signaling include biased signaling, allosteric modulation of receptor activation, receptor internalization, receptor dimerization, ligand sequestration and ligand processing (5, 28, 35, 36). Furthermore, the function of conventional chemokine receptors can be fine-tuned by ACKRs. These atypical chemokine receptors constitute a structurally diverse group unified by their shared function of shaping chemokine gradients. ACKRs cannot signal in the canonical G protein-mediated fashion, but most of them can signal through β-arrestins and mediate chemokine degradation (33, 37). Several studies demonstrate that the ligand-scavenging function of AKCRs provides an important regulatory mechanism during cell migration and phagocyte recruitment (33, 37–39).

ZEBRAFISH AS A WINDOW TO CHEMOKINE RECEPTOR FUNCTIONS

The zebrafish model has been successfully used to study how chemokine signaling networks determine macrophage and neutrophil functions and to ascribe these receptors a role in immunity, inflammation, and cancer models (4, 13, 16, 22, 40–42). It is a powerful vertebrate model well-suited for non-invasive *in-vivo* imaging given its optical transparency at early embryonic and larval stages. Transgenic lines specifically labeling neutrophils and macrophages by linking fluorescent proteins to the *mpx* and *lyz promoters* for the former, and the *mpeg1.1* and *mfap4* promoters for the latter, allow us to visualize and track these phagocytes at a whole organism level. A wide variety of gene-editing methods like CRISPR-Cas9 and transitory gene knockdown (morpholinos) or RNA-based gene overexpression can be delivered by microinjecting eggs at the single-cell stage (16, 43). The zebrafish model is ideal to assess developmental processes and since over 80% of all human disease genes identified so far have at least one functional homolog in zebrafish, it serves as a powerful animal model for human diseases too (22, 43).

Most human chemokine receptors and ACKRs have at least one (putative) zebrafish ortholog (6, 30, 44) as shown in **Table 1**. The last common ancestor of humans and zebrafish went through two rounds of whole-genome duplication during vertebrate evolution (19). Subsequently, a series of intrachromosomal duplication events occurred in the taxon that led to zebrafish (4, 19, 44, 46). These events resulted in the duplication of several chemokine receptor genes that either preserved their original function, lost their function, or acquired a new one (19, 44). While most of the human chemokine receptor genes can be found as single or multi-copy genes in the zebrafish genomes, some cases remain unresolved (**Figure 1**). For example, no homologs of CCR1, CCR3, and CCR5 are currently annotated in the Zebrafish Information Network (ZFIN) database. Moreover, there are zebrafish chemokine receptors annotated without a human counterpart, such as Ccr11 and Ccr12. Also, a CX family of chemokine receptors has been identified that is restricted to (zebra) fish (6, 19, 44).

This review will focus on the zebrafish homologs of human of CXCR1/2, CXCR3, CXCR4, ACKR3, and CCR2 (**Supplementary Table 1**) since these receptors have a known function in phagocyte function during development and inflammatory processes. Below we discuss how the genes encoding these receptors are conserved, and in some cases, duplicated in zebrafish. In the subsequent sections, we review how studies in zebrafish contributed to understanding the roles of these receptors in developmental and disease processes.

The Cxcr1/2-Cxcl8 Signaling Axis

The CXCR1/2-CXCL8 signaling axis is one of the primary chemotactic pathways in neutrophils and of major interest to assess inflammatory processes (45). Zebrafish chemokine receptors Cxcr1 (Il8ra) and Cxcr2 (Il8rb) are functionally homologous to their mammalian counterparts. Furthermore, chemokines of the CXCL8 (IL-8) family, which interact with these receptors, are conserved between humans and zebrafish, while not present in mice (75). Cxcr1 and 2 are highly expressed on zebrafish neutrophils and mediate their recruitment by binding to their shared ligands Cxcl8a, Cxcl8b1, Cxcl8b2, and Cxcl8b3 (Cxcl8L2.1, 0.2, and 0.3, respectively) (6, 19, 47, 52). Cxcl8a and the three Cxcl8b variants are all reported to act via Cxcr1 and Cxcr2 to induce neutrophil recruitment, whereby no specific binding patterns involving the three Cxcl8b variants have been reported so far (6, 47). The Cxcl18b chemokine found in zebrafish and other teleost fish also attracts neutrophils via Cxcr2 (56). Whether this chemokine activates Cxcr1 remains unknown.

The Cxcr3-Cxcl11 Signaling Axis

Human CXCR3 is predominantly expressed on T cells, but also multiple other leukocyte cell types, including macrophages (57, 58). The *cxcr3* gene is triplicated in zebrafish and the copies are referred to as *cxcr3.1, cxcr3.2,* and *cxcr3.3*. In humans, CXCR3 binds to CXCL9 (MIG: monokine induced by gamma interferon), CXCL10 (IP-10: interferon-gamma induced protein 10) and CXCL11 (I-TAC: inflammatory-inducible T-cell alpha chemoattractant) (19, 50). These chemokines are thought to be derived from a common *CXCL11*-like ancestral gene. In zebrafish seven *cxcl11*-like chemokine genes have been identified and are annotated as *cxcl11aa, ac, ad, ae, af,* and *ag* (57). The Cxcl11aa ligand has been functionally studied and was shown to mediate cell recruitment through Cxcr3.2 (48, 57, 58). Studies in zebrafish larvae have focused on *cxcr3.2* and *cxcr3.3*, which are expressed on macrophages and neutrophils while *cxcr3.1* is not detectable at this stage (57). While Cxcr3.2 appears to function as a conventional chemokine receptor, like human CXCR3, Cxcr3.3 has features of ACKRs such as a DCY motif instead of the highly conserved DRY motif that prevents classic G protein-mediated

TABLE 1 | Chemokine receptor genes, their ligands and their role in embryonic development, cancer progression, wound-induced inflammation and pathogen-driven inflammation.

Chemokine receptor	Human	Ligands	Zebrafish	Ligands	embryonic development	Cancer progression	Wound-induced inflammation	Pathogen-driven inflammation
CXCR1 (IL8RA)	CXCR1	CXCL6, 8 (IL-8)	Cxcr1 (Il8ra)	Cxcl8a (Cxcl8L1) Cxcl8b1, 3 (Cxcl8L2.1,0.3)		Neutrophil recruitment (15, 45). Sustained inflammation (15, 45–48). Tumor growth (45–47, 49). Tumor expansion (45, 47, 49).	Neutrophil recruitment, pro-inflammatory function (45, 47)	
CXCR2 (IL8RB)	CXCR2	CXCL1 (NAP3), 2 (MIP2 alpha), 3 (MIP2 beta), 5, 6, 7 (PPBP), 8 (IL-8)	Cxcr2 (Il8rb)	Cxcl8a (Cxcl8L1) Cxcl8b.1,0.2.3 (Cxcl8L2.1–0.3) Cxcl18b		Chronic inflammation (45, 47, 49).	Neutrophil reverse migration, anti-inflammatory function (45, 50, 51).	Neutrophil recruitment and bacterial clearance (51–55)
CXCR3	CXCR3A CXCR3B	CXCL4-B (PF4-B), 9-A/B (MIG-A/B), 10-A/B (IP-10A/B) 11A/B (I-TAC-A/B)	Cxcr3.1,2, 3	Cxcl11-like chemokines aa, ac, ad, ae, af and ag		Cell proliferation Cell survival Tumor expansion Angiostatic effect	Cxcr3.2 recruits macrophages and neutrophils to injury (47, 50, 56, 57). Cxcl11aa is a pro-inflammatory marker (M1) (58, 59).	**Cxcr3.2:** macrophage recruitment and motility (50, 56, 57), neutrophil recruitment (56, 57). **Cxcr3.3:** ligand scavenger, a regulator of Cxcr3.2 function (50).
CXCR4 (fusin)	CXCR4	CXCL12 (SDF1)	Cxcr4a Cxcr4b	Cxcl12b Cxcl12a	**Cxcr4a:** guidance of multicellular vessel growth and coordination of gastrulation movements (60, 61). **Cxcr4b:** progenitor germ cells (PGCs) (6, 31, 62–66).	Macrophage and neutrophil recruitment (45, 46, 67, 68). Tumor angiogenesis Tumor dissemination (67, 68).	Neutrophil recruitment and retention at the wounding site. Pro-inflammatory (69).	Neutrophil recruitment Bacterial clearance (55). Granuloma vascularization (52).
CCR2	CCR2	CCL2 (MCP1)	Ccr2	Ccl2 (mcp1)			Macrophage recruitment (53, 70). Ccr2 is an anti-inflammatory marker (M2) (71, 72).	Recruitment of permissive macrophages (71, 72).
ACKR3 (CXCR7)	ACKR3	CXCL11 (I-TAC) CXCL12 (SDF1)	Ackr3b (Cxcr7a/b)	Cxcl12a	Scavenges Cxcl12a to shape chemokine gradients (6, 36, 65, 66, 73).	Tumor angiogenesis Chemotaxis (74).		

signaling (12, 48). Supporting that Cxcr3.3 regulates Cxcr3.2 function, these paralogs have antagonistic effects on macrophage recruitment to sites of infection and injury in zebrafish (48, 57). The functional antagonism between the zebrafish paralogs *cxcr3.2* and *cxcr3.3* can be viewed as a regulatory mechanism analogous to the functional antagonism of human *CXCR3* splice variants *A* and *B* (50, 62, 76, 77).

The Cxcr4a/b-Ackr3/Cxcl12-Signaling Axis

CXCR4 signaling mediates functions of a variety of cell types, within and beyond the immune system (63, 78). The CXCR4-CXCL12 (SDF1: stromal cell-derived factor) axis is remarkably conserved between zebrafish and humans although both the receptor and ligand genes are duplicated in zebrafish and annotated as *cxcr4a/b* and *cxcl12a/b*, respectively (6, 30,

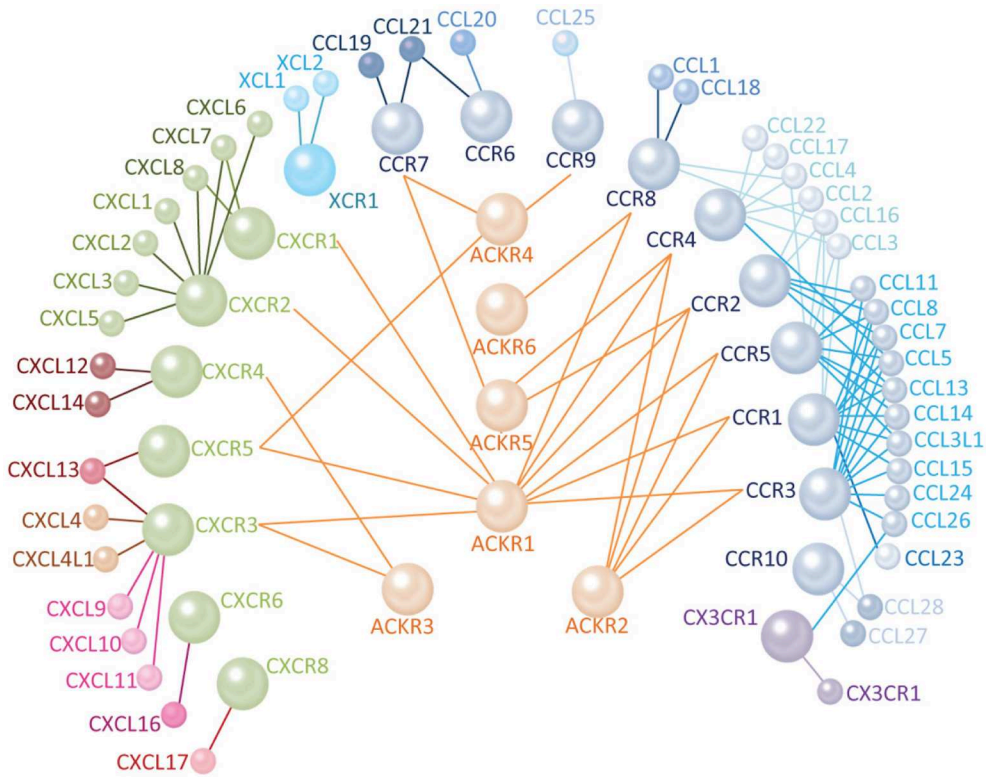

FIGURE 1 | Human chemokine signaling networks are highly promiscuous. There are 25 receptors and 45 ligands in the human chemokine signaling network including seven members of the CXCR family (green), 1 XCR (cyan), 10 CCR (blue), and 1 CX3CR (violet). The CXCL chemokines are shown in shades of pink, XCL in cyan, CCL in shades of blue, and CX3CL in violet. The color intensity of the lines connecting receptors and ligands indicates the binding specificity. Darker colors indicate a higher binding affinity. There are six characterized AKCRs (orange) that antagonize the function of conventional chemokine receptors (connected with lines) by binding one or more of their ligands.

64). Both Cxcr4 receptors can bind both ligands, although Cxcr4a preferentially binds to Cxcl12b and Cxcr4b binds Cxcl12a with a higher affinity (29). The duplication of the *cxcr4* gene in zebrafish is a representative example of gene sub-functionalization. Cxcr4a is primarily associated with cell proliferation and vessel extension, while Cxcr4b regulates neutrophil and macrophage interactions with other cell types and has been implicated in the modulation of inflammation, neutrophil and macrophage migration, metastatic and angiogenic events, and tissue regeneration (29, 64, 65, 79). In mammals, CXCR4-CXCL12 is subject to modulation by an atypical chemokine receptor ACKR3, which binds the CXCR4 ligand CXCL12 but also the CXCR3 ligand CXCL11 (63, 66). The zebrafish *ackr3b (cxcr7b)* gene is on the same chromosome as *cxcr4a/b* and it has been shown that the Ackr3b protein binds both Cxcl12 and Cxcl11 but cannot induce cell migration (79–82). By competing with Cxcr4b for the shared Cxcl12a ligand, Ackr3b helps to maintain chemokine gradients during chemotaxis (79, 80). The potential interaction between Ackr3b and Cxcr3.2-Cxcl11aa signaling has not been characterized yet (70). As discussed below, Ackr3b has been implicated in several pathological conditions as well as in zebrafish development (6, 66, 79, 80, 82).

The Ccr2-Ccl2 Signaling Axis

CCR2 is the receptor for monocyte chemoattractant protein −1 (MCP-1/CCL2) (53). Identifying zebrafish orthologs of human CC chemokine receptors has been challenging since multiple zebrafish *cc-* receptor genes have a remarkably high similarity to a single human *CC* chemokine receptor gene. However, a zebrafish *ccr2* orthologue could be identified in zebrafish, supported by functional evidence, as human CCL2 was shown to trigger macrophage recruitment in zebrafish embryos in a *ccr2*-dependent manner (53, 83).

The duplication of several chemokine receptor genes in zebrafish poses a challenge for the identification of homologies and at the same time, it provides an experimental platform to assess both loss of function and sub-functionalization events to further our understanding of chemokine signaling in phagocyte function as exemplified by the Cxcr4 and Cxcr3 paralogs (29, 48). In the following sections, we will illustrate how zebrafish embryonic development helped to unravel fundamental chemokine signaling mechanisms and discuss in detail the roles of zebrafish chemokine receptors Cxcr1/2, Cxcr3.2/3.3, Cxcr4b, Ackr3b, and Ccr2 in macrophage and neutrophil biology in the context of cancer and wound and pathogen-driven inflammation.

DISSECTING CHEMOKINE SIGNALING PRINCIPLES USING DEVELOPING ZEBRAFISH

The chemokine signaling axes involved in phagocyte biology are also functional in other cell types of the developing zebrafish embryo (84). This model brought fundamental new insight into the principles of chemokine signaling. It was a long-held idea that the membrane-spanning domains and the extracellular portions of a chemokine receptor conferred signal specificity (85). However, recent work on zebrafish showed that cell identity and chemokine receptor signal interpretation modules (CRIM) are the major determinants for the functional specificity of a chemokine receptor-ligand interaction (84, 85). The directed expression of chemokine receptors that were not naturally expressed by a cell through mRNA injections of zebrafish eggs showed that the foreign receptor could overtake the function of the original receptor in the presence of its ligand. Even receptors that do not share high sequence similarities, like CC and CXC receptors, were found to evoke the same response if expressed on the same cell-type showing that CRIM process a generic signal into a discrete response that is dictated by the cell type. Consistent with the fact that cell identity and CRIM determine the functional specificity of chemokine receptors, the same chemokine receptor can elicit very different biological responses depending on the cell that expresses it (84). For example, when Cxcr4a is expressed on hematopoietic progenitor cells, it modulates chemotaxis, yet in neuronal progenitor cells, it inhibits proliferation (86).

Studies in zebrafish embryos also contributed to elucidate regulatory mechanisms of chemokine signaling. One such process is the cleavage of certain chemokines (like Cxcl8) by matrix metalloproteinases (MMPs) to activate and confer them enhanced chemotactic properties. The use of a broad-spectrum MMP inhibitor showed reduced neutrophil and macrophage recruitment to sterile heart injury in zebrafish showing that MMPs are key mediators of inflammation and tissue regeneration (36). An outstanding example of ACKR-mediated regulation of chemotaxis comes from the characterization of the paralogs *cxcr4a* and *cxcr4b* and the interaction of the latter with Ackr3b to fine-tune single-cell migration during development. The Cxcl12b-scavenging function of Ackr3 is required for shaping a self-generated chemokine gradient that guides the migration of the lateral line cell primordium (6, 60, 79, 80). An analogous Cxcr4/Ackr3/Cxcl12 system indispensable to form an endogenous chemokine gradient within the mouse lymph node was described later, confirming the observation made in zebrafish (61). In fact, the identity of Ackr3b as a scavenger receptor that signals via β-arrestins was first described in zebrafish and later confirmed in human cells and mice (38). Similarly, Cxcr1/2-Cxcl8 driven migration of neutrophils along immobilized gradients within tissue was first described in zebrafish (73). During this process, tissue-bound chemokine gradients form through the binding of chemokine and heparan sulfate proteoglycans (HSPGs) resulting in a process called haptotaxis. This type of cell movement coordinates both directional guidance of cells (orthotaxis) and motility restriction in the proximity of the source of the chemotactic signal (73). Haptotaxis was later confirmed in murine dendritic cell recruitment via Ccl21 (87).

Among the chemokine receptors of phagocytes, it is especially the interacting Cxcr4/Ackr3 pair that has much broader roles in developmental processes. We briefly summarize the zebrafish studies that revealed these developmental roles below, which are important to take into account also when studying immune cell functions.

The Cxcr4a/b-Ackr3-Cxcl12 Axis in Development

Cxcr4a is mainly involved in guiding multicellular vessel growth (88) and in controlling proper gastrulation movements by ensuring adhesion between cell-matrix and endodermal cells (49). The Cxcr4b-Cxcl12a signaling axis regulates the migration of a wide range of cell types including neuronal cells, axons, neutrophils, neural crest cells, endothelial cells, and muscle cell precursors (6, 33, 49, 80, 88). Primordial germ cells express Cxcr4b and migrate toward Cxcl12a gradients tracing their migration route. These cells specifically respond to Cxcl12a and neglect the Cxcl12b ligand, involved in other developmental processes, which can be found along their migration path. Ackr3b, expressed mostly by somatic cells, plays a fundamental role in removing Cxcl12b from the extracellular space and clearing the path for PGC migration (31, 63, 65, 78). It scavenges chemokines to shape time and tissue-specific gradients to tightly regulate developmental processes involving cell migration (6, 79, 80). The Cxcr4a/b- Ackr3-Cxcl12 interaction was first observed *in vivo* during zebrafish PGCs migration (33). Ackr3 orchestrates the lysosomal degradation of Cxcl12a in a β-arrestin-dependent process while the receptor itself is recycled back to the plasma membrane (37). Moreover, the scavenging activity of Ackr3b is crucial for the maintenance of a self-generated chemokine gradient that directs the migration of the lateral line primordium during the development of the zebrafish posterior lateral line (PLL) (60, 79, 80).

CHEMOKINE RECEPTORS IN CANCER PROGRESSION

Cancer progression is strongly influenced by chemokine-dependent leukocyte recruitment and infiltration into primary tumors as well as by the subsequent dissemination of cancer cells from primary tumors into adjacent and distant tissues (15, 76, 89). Live visualization of fluorescently labeled tumor cells in zebrafish larvae enables early assessment of vascular remodeling events, tumor dissemination, and metastasis at the organismal level (24, 64). Zebrafish cancer models are also suitable to image early tumor-initiation events and the crucial interplay between the tumor cells and the microenvironment (45). In particular, xenotransplantation models, in which human invasive cells are systemically inoculated into zebrafish larvae, are useful to assess the interactions between human tumor cells and host leukocytes that underlie early metastatic onset (67). Additionally, the larval

zebrafish system offers a simple and robust screening platform for anti-tumor compounds targeting different stages (angiogenesis, metastasis, etc.), further emphasizing its translational value (24, 64).

The tumor environment is a highly inflammatory focus that attracts leukocytes through secretion of cytokines of different natures, including chemokines (45). Chemokine receptors CXCR1, 2, 3, 4, and 7 have been implicated in tumor angiogenesis, sustaining tumor growth and expansion both in zebrafish and humans, as discussed below. The role of CCR chemokine receptors in cancer using the zebrafish model has not been addressed yet.

The Cxcr1/Cxcr2-Cxcl8 Axis in Cancer

Neutrophils are the first responders to acute inflammation, infection, and damage. These cells exhibit remarkable phenotypic plasticity that is determined by the integration of extracellular cues (45). In zebrafish, cancer cells recruit neutrophils through chemokine receptors Cxcr1 and 2 and their Cxcl8 ligands (15, 75). Neutrophil populations have a dual role in the development of different cancers. Tumor-associated neutrophils (TANs) directly engage with tumor cells and are reported to support tumor growth, tissue invasion and angiogenesis mimicking sites of chronic inflammation. In contrast, anti-tumor neutrophils undergo apoptosis and reverse migration back into the vasculature, thereby favoring the resolution of inflammation (45, 75). Using the zebrafish model, it became clear that TANs are recruited to tumor-initiating sites through the Cxcr1-Cxcl8a pathway and that in this context, Cxcr2 is not required for efficient neutrophil recruitment. Fewer neutrophils are recruited to tumor-initiating foci in *cxcr1* mutant zebrafish larvae and proliferation of tumor cells is restricted, suggesting that TANs are critical for early stages of neoplasia and tumorigenesis (75). In agreement with these observations, Cxcr1 expression is lower in anti-tumor neutrophils that display a predominantly anti-inflammatory phenotype (52, 68).

The Cxcr4a/b-Ackr3–Cxcl12 Axis in Cancer

A vast body of literature associates the chemokine receptor CXCR4 with the development of cancer pathogenesis in humans, mice and zebrafish (6, 15, 24, 50, 74). Cxcr4b is highly expressed on zebrafish neutrophils and together with its ligand Cxcl2a, it facilitates tumor angiogenesis and dissemination into different tissues by attracting malignant Cxcr4-expressing cells into healthy organs and tissues where ligand can be found (63, 74, 76). Zebrafish larvae lacking *cxcr4b* (*ody* mutants) fail to induce micrometastases and to sustain human cancer cells after xenotransplantation. Basal neutrophil motility is attenuated and whole-body neutrophil counts are lower in *cxcr4b* mutants than in wild type (wt) larvae (67). Accordingly, tumors in *cxcl12a* mutant zebrafish cannot metastasize, further supporting that Cxcr4b signaling promotes tumor expansion (64).

While neutrophils are important cellular mediators of inflammation and play a central role in tumor initiation and expansion macrophages represent a significant amount of the leukocytes that infiltrate tumors. Macrophages phagocytose cancer cells and dying neutrophils whilst secreting immunomodulatory cytokines. Macrophages also express Cxcr4b and respond to Cxcl12a (11, 90). A study focused on glioblastoma progression used the zebrafish model to show that tumor cells secrete Cxcl12a to recruit macrophages to the tumor site (90). Cxcr4b-Cxcl12a signaling in macrophages is also linked to tumor-promoting functions by enhancing proliferation and invasiveness, modifying the extracellular matrix and favoring tumor neovascularization (15, 28, 65). Interestingly, live visualization of zebrafish macrophages and microglia showed dynamic interactions with cancer cells which did not result in phagocytosis of the malignant cells, thereby avoiding an anti-tumor function of macrophages (67). *cxcr4b* mutant larvae had a lower tumor burden in this context too and depletion of macrophages and microglia significantly reduced oncogenic cell proliferation, suggesting that Cxcr4b signaling promotes macrophage infiltration during initial stages of brain cancer (90).

As discussed above, Cxcr4b signaling can be fine-tuned through ligand scavenging by the atypical Ackr3b receptor. Human ACKR3is linked to tumor growth, invasion, and metastasis (11). Tumor cells and vascular endothelial cells of different tissues show an increased expression of Ackr3 and it has been suggested to include this receptor as a marker for cancer (63). A study by van Rechem et al. (91) found that Ackr3 is a direct target of the tumor suppressor HIC1 (Hypermethylated in Cancer 1) which is inactive in many human tumors. The role of Ackr3b in cancer pathogenesis is still unknown in zebrafish and as multiple studies found that Ackr3b depletion results in severe developmental abnormalities (6, 29, 30, 37), a gene knockout/down approach to assessing its role in cancer progression would require the development of cell-specific or conditional knockout systems.

CHEMOKINE RECEPTORS IN WOUND-INDUCED INFLAMMATION

The zebrafish model is well-suited to assess aseptic wound-induced inflammation and tissue regeneration either by amputating the ventral or tail fin or by pinching tissue with sterile needles (68, 69, 92). Recruitment of neutrophils first, and macrophages in a later phase, is key during the inflammatory response, which is broadly divided into three phases: early leukocyte recruitment, amplification or acute inflammation, and resolution (69). Neutrophils recruited shortly after damage secrete chemokines that activate tissue-resident cells and recruit more leukocytes to the injury, thereby amplifying inflammation. As described in the previous section, Cxcl8a is a strong neutrophil attractant and therefore, a central element at all stages of the inflammatory process (68, 69, 71). Neutrophils are known to be short-lived and to undergo apoptosis shortly after activation (40). However, a recently characterized subpopulation of neutrophils that returns to the circulation after activation has a longer lifespan and an anti-inflammatory effect (68, 69). The tail-amputation model using larval zebrafish is well-suited for tracking neutrophil reverse migration since it enables *in-vivo* tracking of these

cells at different stages of the inflammatory response (72, 92). It helped to establish that neutrophils recruited upon injury emerge from hematopoietic tissue in the proximity of the affected area, that they shuttle between the vasculature and the injury during acute inflammation and redistribute in a proximal direction to different sites of the body during the resolution phase (72). A detailed assessment of the transition from neutrophil recruitment and clustering during acute inflammation and neutrophil redistribution during the resolution phase showed to be regulated through Cxcl8a-induced trafficking and turnover of Cxcr1 and Cxcr2 on the membrane of neutrophils (71).

Two distinct subtypes of macrophages, pro-inflammatory and anti-inflammatory, drive the formation of a mass of highly proliferative stromal cells called blastema and subsequent tissue remodeling during epimorphic regeneration (51, 93). Using the zebrafish tail-amputation model with fluorescently labeled macrophages (mCherry) and Tnfa (GFP), Nguyen-Chi et al. showed that shortly after tail amputation both pro-inflammatory (GFP+) and ant-inflammatory macrophages (GFP-) accumulated in damaged tissue and that anti-inflammatory macrophages remained associated to the injury until regeneration was completed unlike pro-inflammatory macrophages, which retracted from the area. Chemical depletion of macrophages showed that the initial interaction between TNFa-expressing macrophages and the damaged area is required for blastema formation. Knockdown of the Tnfa receptor *tnfar1* confirmed that Tnfa is fundamental for fin regeneration as it primes blastema cells to undergo regeneration in zebrafish (93). This phenotypic polarization dynamics in macrophages had been reported in cell culture but it had not been confirmed in a live system. Below we discuss the chemokine receptors implicated in the wound-induced macrophage and neutrophil migration and polarization responses.

The Cxcr1/2-Cxcl8 Axis in Wound-Induced Inflammation

Both Cxcr1 and Cxcr2 are required for efficient recruitment of neutrophils to damaged areas at the initial stage of the inflammatory response (52). Cxcr2 and Cxcl8a (Cxcl8L1) and Cxcl8b (Cxcl8L2) are transcriptionally upregulated after tail amputation in zebrafish. However, Cxcl8a and Cxcl8b have differential roles in neutrophil migration during inflammatory responses. Cxcl8a mainly orchestrates neutrophil recruitment to sites on injury whereas Cxcl8b redirects neutrophils back into the bloodstream (94). Work in zebrafish also showed that the bidirectional movement of neutrophils between the injury and vasculature during acute inflammation is coordinated by distinct roles of Cxcr1 and Cxcr2 (75, 95). Neutrophils that undergo reverse migration express lower levels of Cxcr1 relative to Cxcr2, suggesting that Cxcr2 is involved in recruiting neutrophils back into the vasculature. Further research showed that the Cxcr1-Cxcl8a axis recruits neutrophils to the inflammatory focus while Cxcr2-Cxcl8a orchestrates reverse migration and resolution of inflammation (89). Recently, Coombs et al. showed that both Cxcr1 and Cxcr2 mediate the initial recruitment of neutrophils to damaged tissue but that these receptors exert different functions during the transition from acute inflammation to the resolution phase. Cxcr1 shows a strong initial response toward Cxcl8a but undergoes gradual desensitization followed by receptor internalization, whereas Cxcr2 remains stably expressed on the plasma membrane with sustained responsiveness toward Cxcl8b, and orchestrates neutrophil dispersal during the resolution phase (71).

Cxcr3 and Ccr2 Axes in Wound-Induced Inflammation

Macrophages are crucial players of the inflammatory response triggered by tissue damage and exhibit remarkable phenotypic plasticity (51, 54). Live tracking of fluorescently labeled macrophages in zebrafish showed that these cells are recruited to injury shortly after neutrophils at early stages [several papers]. Cxcr3.2, a functional CXCR3 ortholog in zebrafish, and Ccr2 both mediate the recruitment of macrophages to injury (48, 53, 57, 58, 83). Mutation of *cxcr3.2* and knockdown of *ccr2* result in attenuated recruitment of macrophages to the wound (57, 58). Cxcr3.2 depletion also reduced neutrophil recruitment, unlike Ccr2 knockdown which affected macrophages only (48, 58, 83). At the beginning of the inflammatory response, macrophages acquire a pro-inflammatory phenotype characterized by the secretion of inflammatory markers (M1) like Tnfa, Il1-b, and the Cxcr3.2 ligand Cxcl11aa. As the inflammatory process develops, they transit toward an anti-inflammatory phenotype (M2) characterized by the expression of chemokine receptor Ccr2 and Cxcr4b (51). Ccr2 is thought to mediate the transition from acute inflammation [M1] to tissue regeneration processes [M2] as phagocytosis of necrotic and apoptotic neutrophils by macrophages is associated with the beginning of tissue regeneration (69, 93).

The Cxcr4a/b-Ackr3-Cxcl12 Axis in Wound-Induced Inflammation

The chemokine signaling axis Cxcr4b-Cxcl12a is required for the proper development and distribution of neutrophils at early developmental stages and sustains inflammation by recruiting and retaining neutrophils at sites of injury (40, 96). CRISPR-Cas9-mediated knockdown of Cxcr4b and Cxcl12b significantly increased the clearance of apoptotic neutrophils by macrophages and enhanced reverse migration of neutrophils thereby ameliorating inflammation. Chemical inhibition of the Cxcr4b-Cxcl12a axis leads to a faster resolution of inflammation by hindering the retention of neutrophils at the inflammatory site (68, 97). Dominant gain-of-function truncations of CXCR4 are associated with warts, hypo-gammaglobulinemia, infections, and myelokathexis (WHIM) syndrome, a primary immunodeficiency disorder characterized by neutropenia (96). The expression of homologous Cxcr4 WHIM truncations in zebrafish showed that neutrophil release into the blood was impaired and recruitment

to injury after fin amputation was diminished. Larvae with the WHIM-truncated Cxcr4b displayed aberrant neutrophil development and distribution due to reduced chemotaxis, which could be reverted upon Cxcl12a depletion, suggesting that WHIM truncation increases Cxcr4b sensitivity toward Cxcl12a (96).

The possible interaction between Cxcr4b and Ackr3b during inflammation has not yet been addressed.

CHEMOKINE RECEPTORS IN PATHOGEN-INDUCED INFLAMMATION

Chemokine receptors play a fundamental role in the immune response against invading pathogens by mediating leukocyte trafficking to sites of infection (3, 4, 98). Bacterial infections can be followed from very early stages and with great detail using cell-specific fluorescent transgenic zebrafish lines and fluorescent bacteria. The optically clear larvae facilitate live visualization of complex host-pathogen interactions at the whole organism level and at the same time, it provides a reasonably simplified setting to assess chemokine signaling when used before adaptive immunity develops (55, 96, 98). Most of the studies on chemokine receptor function in the context of infection were performed with the zebrafish-*Mycobacterium marinum* (*Mm*) model for tuberculosis. This model provides a surrogate system that strongly resembles *Mycobacterium tuberculosis* (*Mtb*) pathogenesis in humans, including the formation of granulomas, the histological hallmark of tuberculosis. *Mm* is a natural pathogen of teleost fish and a close genetic relative of *Mtb* which permits assessing co-evolution between host and pathogen (55). Both *Mm* and *Mtb* can survive intracellularly in macrophages. Macrophages are the primary components of granulomas and play a dual role in mycobacterial pathogenesis. Macrophage recruitment to infection sites is crucial for neutralizing mycobacteria but it also provides them with a niche for replication and a vector for dissemination into host tissues (59).

The Cxcr2-Cxcl8 Axis in Pathogen-Induced Inflammation

Cxcr2 (but not Cxcr1) mediates infection-induced neutrophil mobilization from the caudal hematopoietic tissue (CHT) to infectious foci (99). Neutrophils are very efficient at killing pathogens through degranulation and the rapid release of reactive oxygen species (ROS) (100). Mycobacteria primarily infect macrophages to replicate and expand at initial stages of infection (83). At later stages, when the infection is well-established, neutrophils are recruited primarily through Cxcr2 and Cxcl8a secreted by macrophages and epithelial cells (101, 102). Unlike Cxcl8a, Cxcl18b is secreted by non-phagocytic cells of the stroma within granulomatous lesions during *Mm* infection (56). Neutrophils contribute to the phagocytosis and destruction of infected macrophages and are therefore crucial to control mycobacterial infection (101, 103).

The Cxcr3-Cxcl11 and Ccr2-Ccl2 Signaling Axis in Pathogen-Induced Inflammation

Chemokine receptors direct the course of mycobacterial infection by controlling leukocyte recruitment with distinctive microbicidal properties (51, 53, 93). *Mm* recruits macrophages at the early stages of infection through the Cxcr3.2 and Ccr2 chemokine receptors (48, 57, 83). Cambier et al. (83) proposed that phenolic glycolipid in the bacterial cell wall induces ccl2 transcription and recruits blood circulating monocytes via Ccr2 in a toll-like receptor-independent way. The monocytes recruited via Ccr2 are permissive to mycobacterial replication and are less efficient clearing the pathogen because they contain less inducible nitric oxide synthases (83). On the other hand, the authors suggest that toll-like receptor-mediated recruitment of tissue-resident macrophages primes cells to adopt a microbicidal phenotype and that mycobacteria evolved different mechanisms to evade detection by these cells. Once Ccr2-expressing monocytes are recruited, mycobacteria can transfer from the microbicidal tissue-resident macrophages to the Ccr2-expressing permissive monocytes. This permissive monocyte recruitment driven by mycobacteria will amplify the infection as infected macrophages that egress from the granuloma seed secondary granulomas away from the initial infection site (53). Interestingly, Cxcl11aa (the main ligand of Cxcr3.2) is induced in a manner dependent on the myeloid differentiation response gene 88 (myd88) (104). Myd88 serves as an adaptor molecule for the majority of toll-like receptors suggesting that macrophages recruited through Cxcr3.2 might have different microbicidal properties than those recruited through Ccr2 (104, 105).

The depletion of either Ccr2 or Cxcr3.2 results in a reduced recruitment of macrophages to sites of infection (53, 57, 58). However, *cxcr3.2* knockout limits *Mm* dissemination as fewer macrophages are recruited to sites of infection due to aberrant macrophage motility that prevents macrophage-mediated seeding of secondary infectious foci (57). Cxcr3.3 restricts Cxcr3.2 function in macrophages through its Cxcl11aa-scavenging function. Macrophages of *cxcr3.3* mutant zebrafish larvae are more mobile than wt controls, and recruitment to sites of infection and injury is, therefore, more efficient. Cxcr3.3 depleted larvae, show exacerbated Cxcr3.2 signaling due to higher ligand bioavailability and enhanced bacterial dissemination resulting from higher macrophage motility (48) (**Figure 2**).

The Cxcr4a/b-Ackr3-Cxcl12 Axis in Pathogen-Induced Inflammation

As mentioned in previous sections, neutrophils are recruited through Cxcr4b and the chemokine Cxcl12a (68, 97). The depletion of Cxcr4b in zebrafish led to a significant reduction in neutrophil recruitment to infectious foci and a higher bacterial burden further emphasizing the relevance of neutrophils in the control of mycobacterial infection (101). Macrophages expressing Cxcr4b have been implicated in the delivery proangiogenic signaling within the granulomatous structures although the mechanism is unknown. Granulomas in *cxcr4b*

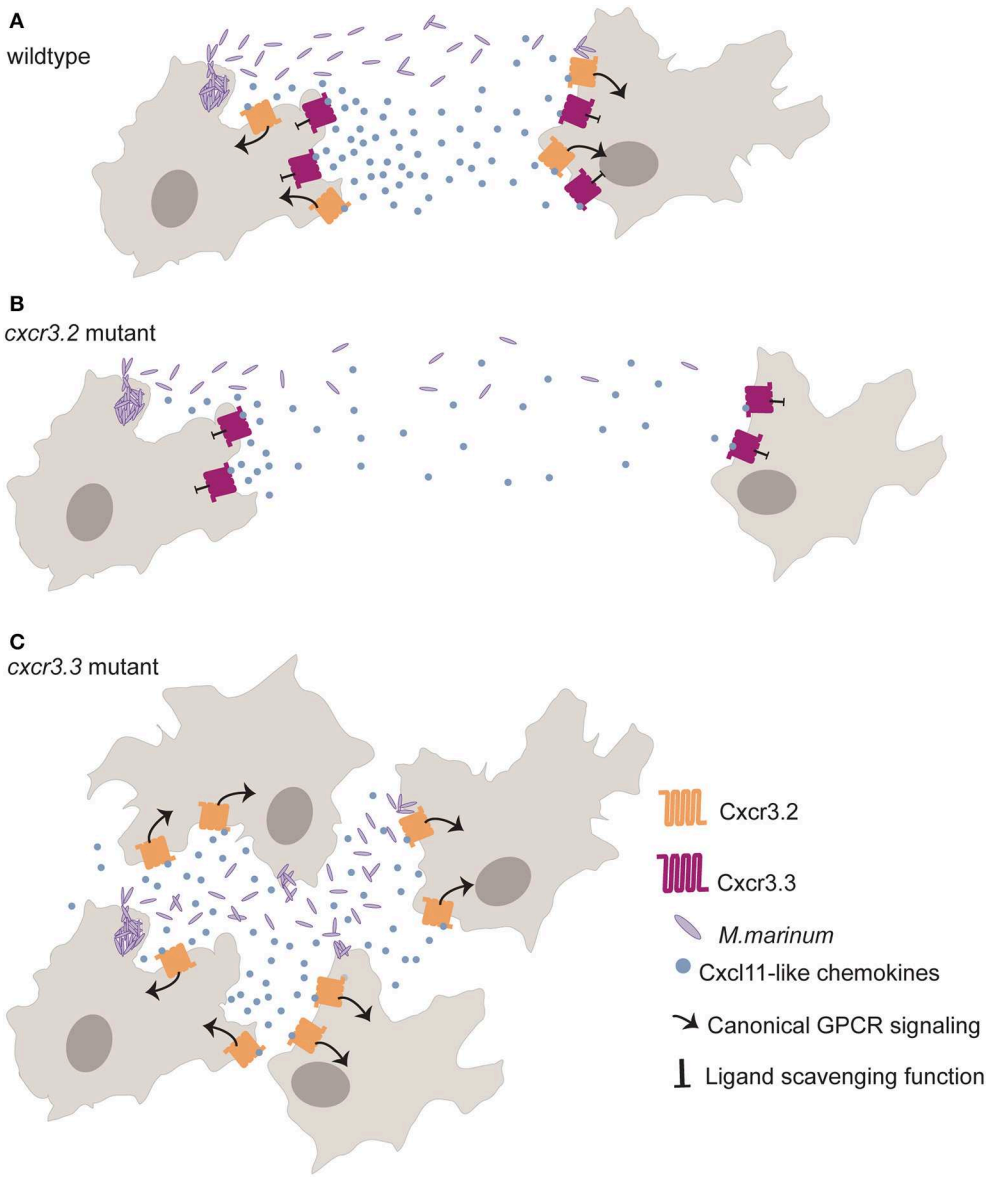

FIGURE 2 | The paralogs *cxcr3.2* and *cxcr3.3* have antagonistic functions that regulate macrophage recruitment to sites of infection. Cxcr3.2 (orange) is a functional homolog of human Cxcr3 required for macrophage recruitment to sites of infection and other inflammatory settings. Cxcr3.3 (dark red) displays the structural of Ackrs such as the substitution of the central Arginine (R) of the highly conserved E/DRY-motif for a Cysteine (DCY) that prevents canonical GPCR signaling (arrow). Cxcr3.3 regulates Cxcr3.2-mediated macrophage recruitment through its scavenging function (blunt arrow) of Cxcl11-like chemokines (blue dots). **(A)** Shows how macrophages infected with *M. marinum* (purple rods) recruit non-infected macrophages through the secretion of Cxcl11-like chemokines to contain the bacterial infection and to clear dying macrophages in wt zebrafish larvae. **(B)** shows how macrophage recruitment is reduced in *cxcr3.2* mutants (as an actively signaling chemokine is depleted) and how fewer macrophages become infected with *M. marinum* due to reduced macrophage motility, favoring the contention of mycobacterial infection. **(C)** shows enhanced recruitment of macrophages to sites of infection due to an exacerbated Cxcr3.2 signaling because of higher ligand availability in absence of the scavenging function of Cxcr3.3. The dissemination of mycobacteria into these newly recruited macrophages will later seed secondary granulomas, supporting the dissemination of the infection.

depleted zebrafish larvae were poorly vascularized, bacterial growth was restricted and dissemination reduced (106).

CONCLUDING REMARKS

The zebrafish model significantly contributed to the expansion of our knowledge on phagocyte behavior, function, and properties in the context of development, cancer progression, and sterile and pathogen-driven inflammation. Due to its genetic accessibility, zebrafish can be exploited to model congenital syndromes involving chemokine receptors implicated in leukocyte function, such as the WHIM syndrome (96). It has been of great value to unveil fundamental principles underlying chemokine signaling regulation, signal integration and to explore receptor

sub-functionalization events (6, 17, 98). Furthermore, the functional diversification of duplicated chemokine receptor genes in zebrafish might reveal core mechanisms of chemokine signaling, like the ligand processing function of MMPs and the Cxcr3.2-Cxcr3.3 functional antagonism, and expand our knowledge on the function and interaction of ACKRs as well as to identify and explore analogous regulatory systems in humans (36, 48).

The tight connection between chemokine receptors and macrophage and neutrophil recruitment posits them as interesting therapeutic targets to treat chronic inflammation, a condition that can be induced by persistent infections like mycobacterial infections and precedes pathologies like cancer, autoimmune diseases and tissue damage (68, 69). The development of antibodies targeting chemokine receptors or chemokines that mediate neutrophil recruitment like Cxcr1/2-Cxcl8 and Cxcr4/ Ackr3-Cxcl12 could be used as an alternative anti-inflammatory and anti-oncogenic treatment to modulate neutrophil recruitment to inflammatory foci and tumor-initiating niches, respectively (75). Promoting neutrophil reverse migration to accelerate the resolution of inflammation by pharmacologically inhibiting Cxcr1-Cxcl8a signaling presents another approach to counteract inflammation and to restrict tumor progression (45, 97). While pharmaceutical targeting of the Cxcr4/ Ackr3-Cxcl12 signaling axis to inflammatory conditions remains plausible, it should be noted that this pathway is central for embryonic development and therefore, a developing organism like zebrafish larvae, might not be an optimal model for screening compounds targeting these axes (6, 30).

CXCR3 signaling in cancer also presents a therapeutic target. Unlike the mutation of *ackr3b*, *cxcr3.2* and *cxcr3.3* mutant larvae showed no major effects on embryonic development. Therefore, in future work zebrafish larvae can be used to screen chemical inhibitors targeting the CXCR3 axis. Studies show that disrupting CXCR3 signaling using chemical antagonists results in lower tumor burden in human lung cancer due to reduced cell proliferation and survival as well as increased caspase-independent cell death (107). However, CXCR3 has also been ascribed an angiostatic effect that blocks tumor neovascularization and some of its platelet-derived ligands work as anti-tumor agents by inhibiting lymphangiogenesis (108). The role of Cxcr3 and Cxcr4 signaling axes and their interaction with Ackr3b in cancer progression have not been explored using the zebrafish model in the context of cancer, but it could contribute to clarify the discrepant observations made so far. Also, the disruption of Cxcr3.2 signaling in mycobacterial infection resulted in reduced granuloma formation in zebrafish, similar to CXCR3 knockout in mice (109). Fine-tuning CXCR3 signaling could, therefore, serve the development of host-directed antibacterial therapies to circumvent the treatment limitations imposed by the ever-growing multi-drug resistance of bacterial strains.

Considering that chemokine receptors mediate interactions between macrophages and their extracellular environment, it would be interesting to unravel the chemotactic cues underlying macrophage polarization and their localization during infectious, inflammatory and tissue regeneration processes. Therapies aimed at enhancing macrophage efferocytosis (clearance of apoptotic cells by phagocytes) of neutrophils during inflammation or biasing macrophage polarization toward an anti-inflammatory and regenerative phenotype could serve as novel targets of regenerative drugs (93). Zebrafish stands out as a powerful model to study macrophage functional plasticity during inflammation in real-time and within a whole organism mostly because of the availability of several M1 transgenic lines. The generation of fluorescent transgenic zebrafish lines for M2 markers, such as *cxcr4b* and *ccr2,* would be helpful to further dissect the role of chemokine receptor signaling in macrophage polarization (51, 93). Fine-tuning macrophage polarization could enable us to prime macrophages to adopt an inflammatory phenotype that favors pathogen clearance or a tissue-regenerative phenotype to reduce inflammation as a therapy against multiple pathogens and conditions.

Due to its accessibility and its many advantages, the zebrafish model keeps up with state-of-the-art technologies, such as genome editing techniques like CRISPR/Cas9, the application of cell/tissue-specific RNA-sequencing and proteomics analyses (16, 43, 98). Together with cutting-edge microscopy techniques like super-resolution microscopy and lattice light-sheet microscopy, which can provide information about dynamic intracellular processes, the identity of chemokine receptors' downstream effectors and signal integration events can be further investigated. The link between chemokine signaling and relevant intracellular processes, like autophagy, in several contexts, could be assessed in homeostasis and disease to reveal fundamental signaling and physiological mechanisms within phagocytes.

AUTHOR CONTRIBUTIONS

FS and AM wrote the manuscript. VT made **Figure 1** and reviewed the manuscript. All authors commented on the manuscript and approved the final version.

FUNDING

FS was supported by a fellowship from CONACYT (410804). VT was a Marie Curie fellow in the Initial Training Network FishForPharma (PITN-GA-2011-289209), funded by the 7th Framework Programme of the European Commission.

ACKNOWLEDGMENTS

We would like to thank Arwin Groenewoud for the critical reading of the cancer section and our funding bodies for supporting this project.

SUPPLEMENTARY MATERIAL

The Supplementary Material for this article can be found online at: https://www.frontiersin.org/articles/10.3389/fimmu.2020.00325/full#supplementary-material

REFERENCES

1. Rosales C, Uribe-Querol E. Phagocytosis: a fundamental process in immunity. *BioMed Res Int.* (2017) 2017:9042851. doi: 10.1155/2017/9042851
2. Serizier SB, McCall K. Scrambled eggs: apoptotic cell clearance by non-professional phagocytes in the drosophila ovary. *Front Immunol.* (2017) 8:1642. doi: 10.3389/fimmu.2017.01642
3. Dale DC, Boxer L, Liles WC. The phagocytes: neutrophils and monocytes. *Blood.* (2008) 112:935–45. doi: 10.1182/blood-2007-12-077917
4. Bajoghli B. Evolution and function of chemokine receptors in the immune system of lower vertebrates. *Eur J Immunol.* (2013) 43:1686–92. doi: 10.1002/eji.201343557
5. Bonecchi R, Galliera E, Borroni EM, Corsi MM, Locati M, Mantovani A. Chemokines and chemokine receptors: an overview. *Front Biosci.* (2009) 14:540–51. doi: 10.2741/3261
6. Bussmann J, Raz E. Chemokine-guided cell migration and motility in zebrafish development. *EMBO J.* (2015) 34:1309–18. doi: 10.15252/embj.201490105
7. Choi J, Selmi C, Leung PSC, Kenny TP, Roskams T, Gershwin ME. Chemokine and chemokine receptors in autoimmunity: the case of primary biliary cholangitis. *Expert Rev Clin Immunol.* (2016) 12:661–72. doi: 10.1586/1744666X.2016.1147956
8. Philips JA, Rubin EJ, Perrimon N. Drosophila RNAi screen reveals CD36 family member required for mycobacterial infection. *Science.* (2005) 309:1251–3. doi: 10.1126/science.1116006
9. Meyen D, Tarbashevich K, Banisch TU, Wittwer C, Reichman-Fried M, Maugis B, et al. Dynamic filopodia are required for chemokine-dependent intracellular polarization during guided cell migration *in vivo*. *Elife.* (2015) 4:e05279. doi: 10.7554/eLife.05279.041
10. Vázquez-Victorio G, González-Espinosa C, Espinosa-Riquer ZP, Macias-Silva M. GPCRs and actin—cytoskeleton dynamics. in *Methods Cell Biol.* (2016) 132:165–88. doi: 10.1016/bs.mcb.2015.10.003
11. Kulbe H, Levinson NR, Balkwill F, Wilson JL. The chemokine network in cancer-much more than directing cell movement. *Int J Dev Biol.* (2004) 48:489–96. doi: 10.1387/ijdb.041814hk
12. Stoy H, Gurevich VV. How genetic errors in GPCRs affect their function: possible therapeutic strategies. *Genes Dis.* (2015) 2:108–32. doi: 10.1016/j.gendis.2015.02.005
13. Cronan MR, Tobin DM. Fit for consumption: zebrafish as a model for tuberculosis. *Dis Models Mech.* (2014) 7:777–84. doi: 10.1242/dmm.016089
14. Flannagan RS, Grinstein S. Fly fishing with RNAi catches novel effectors of phagocytosis. *J Leukocyte Biol.* (2011) 89:643–5. doi: 10.1189/jlb.1210653
15. Freisinger CM, Huttenlocher A. Live imaging and gene expression analysis in zebrafish identifies a link between neutrophils and epithelial to mesenchymal transition. *PLoS ONE.* (2014) 9:e112183. doi: 10.1371/journal.pone.0112183
16. Gomes MC, Mostowy S. The case for modeling human infection in zebrafish. *Trends Microbiol.* (2019) 28:10–18. doi: 10.1016/j.tim.2019.08.005
17. Ramakrishnan L. The zebrafish guide to tuberculosis immunity and treatment. *Cold Spring Harb Symp Quant Biol.* (2013) 78:179–92. doi: 10.1101/sqb.2013.78.023283
18. DeVries ME, Kelvin AA, Xu L, Ran L, Robinson J, Kelvin DJ. Defining the origins and evolution of the chemokine/chemokine receptor system. *J Immunol.* (2006) 176:401–15. doi: 10.4049/jimmunol.176.1.401
19. Nomiyama H, Osada N, Yoshie O. Systematic classification of vertebrate chemokines based on conserved synteny and evolutionary history. *Genes Cells.* (2013) 18:1–16. doi: 10.1111/gtc.12013
20. Legler DF, Thelen M. New insights in chemokine signaling. *F1000Res.* (2018) 7:95. doi: 10.12688/f1000research.13130.1
21. Bernardini G, Antonangeli F, Bonanni V, Santoni A. Dysregulation of chemokine/chemokine receptor axes and NK cell tissue localization during diseases. *Front Immunol.* (2016) 7:402. doi: 10.3389/fimmu.2016.00402
22. Langheinrich U. Zebrafish: a new model on the pharmaceutical catwalk. *Bioessays.* (2003) 25:904–12. doi: 10.1002/bies.10326
23. Zabel BA, Rott A, Butcher EC. Leukocyte chemoattractant receptors in human disease pathogenesis. *Annu Rev Pathol.* (2015) 10:51–81. doi: 10.1146/annurev-pathol-012513-104640
24. Zhao S, Huang J, Ye J. A fresh look at zebrafish from the perspective of cancer research. *J Exp Clin Cancer Res.* (2015) 34:80. doi: 10.1186/s13046-015-0196-8
25. Bond RA, IJzerman AP. Recent developments in constitutive receptor activity and inverse agonism, and their potential for GPCR drug discovery. *Trends Pharmacol Sci.* (2006) 27:92–6. doi: 10.1016/j.tips.2005.12.007
26. Mortier A, Van Damme J, Proost P. Overview of the mechanisms regulating chemokine activity and availability. *Immunol Lett.* (2012) 145:2–9. doi: 10.1016/j.imlet.2012.04.015
27. Moser B, Wolf M, Walz A, Loetscher P. Chemokines: multiple levels of leukocyte migration control? *Trends Immunol.* (2004) 25:75–84. doi: 10.1016/j.it.2003.12.005
28. Rosanò L, Bagnato A. New insights into the regulation of the actin cytoskeleton dynamics by GPCR/β-arrestin in cancer invasion and metastasis. *Int Rev Cell Mol Biol.* (2019) 346:129–55. doi: 10.1016/bs.ircmb.2019.03.002
29. Boldajipour B, Doitsidou M, Tarbashevich K, Laguri C, Yu SR, Ries J, et al. Cxcl12 evolution–subfunctionalization of a ligand through altered interaction with the chemokine receptor. *Development.* (2011) 138:2909–14. doi: 10.1242/dev.068379
30. Raz E, Mahabaleshwar H. Chemokine signaling in embryonic cell migration: a fisheye view. *Development.* (2009) 136:1223–9. doi: 10.1242/dev.022418
31. Zhang XF, Wang JF, Matczak E, Proper JA, Groopman JE. Janus kinase 2 is involved in stromal cell–derived factor-1α-induced tyrosine phosphorylation of focal adhesion proteins and migration of hematopoietic progenitor cells. *Blood.* (2001) 97:3342–8. doi: 10.1182/blood.V97.11.3342
32. Venkatakrishnan AJ, Deupi X, Lebon G, Tate CG, Schertler GF, Babu MM. Molecular signatures of G-protein-coupled receptors. *Nature.* (2013) 494:185–94. doi: 10.1038/nature11896
33. Boldajipour B, Mahabaleshwar H, Kardash E, Reichman-Fried M, Blaser H, Minina S, et al. Control of chemokine-guided cell migration by ligand sequestration. *Cell.* (2008) 132:463–73. doi: 10.1016/j.cell.2007.12.034
34. Loetscher P, Clark-Lewis I. Agonistic and antagonistic activities of chemokines. *J Leukocyte Biol.* (2001) 69:881–4. doi: 10.1189/jlb.69.6.881
35. Zweemer AJM, Toraskar J, Heitman LH, IJzerman AP. Bias in chemokine receptor signalling. *Trends Immunol.* (2014) 35:243–52. doi: 10.1016/j.it.2014.02.004
36. Xu S, Webb SE, Lau TCK, Cheng SH. Matrix metalloproteinases (MMPs) mediate leukocyte recruitment during the inflammatory phase of zebrafish heart regeneration. *Sci Rep.* (2018) 8:1–14. doi: 10.1038/s41598-018-25490-w
37. Mahabaleshwar H, Tarbashevich K, Nowak M, Brand M, Raz E. β-arrestin control of late endosomal sorting facilitates decoy receptor function and chemokine gradient formation. *Development.* (2012) 139:2897–902. doi: 10.1242/dev.080408
38. Naumann U, Cameroni E, Pruenster M, Mahabaleshwar H, Raz E, Zerwes GH, et al. CXCR7 functions as a scavenger for CXCL12 and CXCL11. *PLoS ONE.* (2010) 5:e9175. doi: 10.1371/journal.pone.0009175
39. Vacchini A, Locati M, Borroni EM. Overview and potential unifying themes of the atypical chemokine receptor family. *J Leukocyte Biol.* (2016) 99:883–92. doi: 10.1189/jlb.2MR1015-477R
40. Henry KM, Loynes CA, Whyte MKB, Renshaw SA. Zebrafish as a model for the study of neutrophil biology. *J Leukocyte Biol.* (2013) 94:633–42. doi: 10.1189/jlb.1112594
41. Kochhan E, Siekmann AF. Zebrafish as a model to study chemokine function. *Methods Mol Biol.* (2013) 1013:145–59. doi: 10.1007/978-1-62703-426-5_9
42. Wittamer V, Bertrand JY, Gutschow PW, Traver D. Characterization of the mononuclear phagocyte system in zebrafish. *Blood.* (2011) 117:7126–35. doi: 10.1182/blood-2010-11-321448
43. Torraca V, Mostowy S. Zebrafish infection: from pathogenesis to cell biology. *Trends Cell Biol.* (2018) 28:143–56. doi: 10.1016/j.tcb.2017.10.002
44. Bird S, Tafalla C. Teleost chemokines and their receptors. *Biology.* (2015) 4:756–84. doi: 10.3390/biology4040756
45. Powell DR, Huttenlocher A. Neutrophils in the tumor microenvironment. *Trends Immunol.* (2016) 37:41–52. doi: 10.1016/j.it.2015.11.008
46. Chen J, Xu Q, Wang T, Collet B, Corripio-Miyar Y, Bird S, et al. Phylogenetic analysis of vertebrate CXC chemokines reveals novel lineage specific groups in teleost fish. *Dev Compar Immunol.* (2013) 41:137–52. doi: 10.1016/j.dci.2013.05.006

47. Boro M, Balaji KN. CXCL1 and CXCL2 Regulate NLRP3 inflammasome activation via G-protein–coupled receptor CXCR2. *J Immunol.* (2017) 199:1660–71. doi: 10.4049/jimmunol.1700129
48. Sommer F, Torraca V, Kamel SM, Lombardi A, Meijer AH. Frontline science: antagonism between regular and atypical Cxcr3 receptors regulates macrophage migration during infection and injury in zebrafish. *J Leukocyte Biol.* (2019) 107:185–203. doi: 10.1101/719526
49. Nair S, Schilling TF. Chemokine signaling controls endodermal migration during zebrafish gastrulation. *Science.* (2008) 322:89–92. doi: 10.1126/science.1160038
50. Billottet C, Quemener C, Bikfalvi A. CXCR3, a double-edged sword in tumor progression and angiogenesis. *Biochim Biophys Acta Rev Cancer.* (2013) 1836:287–95. doi: 10.1016/j.bbcan.2013.08.002
51. Nguyen-Chi M, Laplace-Builhe B, Travnickova J, Luz-Crawford P, Tejedor G, Phan QT, et al. Identification of polarized macrophage subsets in zebrafish. *Elife.* (2015) 4:e07288. doi: 10.7554/eLife.07288
52. Oliveira S, Rosowski EE, Huttenlocher A. Neutrophil migration in infection and wound repair: going forward in reverse. *Nat Rev Immunol.* (2016) 16:378. doi: 10.1038/nri.2016.49
53. Cambier CJ, O'Leary SM, O'Sullivan MP, Keane J, Ramakrishnan L. Phenolic glycolipid facilitates mycobacterial escape from microbicidal tissue-resident macrophages. *Immunity.* (2017) 47:552–65. doi: 10.1016/j.immuni.2017.08.003
54. Khan A, Singh VK, Hunter RL, Jagannath C. Macrophage heterogeneity and plasticity in tuberculosis. *J Leukocyte Biol.* (2019) 106:275–82. doi: 10.1002/JLB.MR0318-095RR
55. Lesley R, Ramakrishnan L. Insights into early mycobacterial pathogenesis from the zebrafish. *Cur Opin Microbiol.* (2008) 11:277–83. doi: 10.1016/j.mib.2008.05.013
56. Torraca V, Otto NA, Tavakoli-Tameh A, Meijer AH. The inflammatory chemokine Cxcl18b exerts neutrophil-specific chemotaxis via the promiscuous chemokine receptor Cxcr2 in zebrafish. *Dev Compar Immunol.* (2017) 67:57–65. doi: 10.1016/j.dci.2016.10.014
57. Torraca V, Cui C, Boland R, Bebelman PJ, Sar AM, Smit MJ, et al. The CXCR3-CXCL11 signaling axis mediates macrophage recruitment and dissemination of mycobacterial infection. *Dis Models Mech.* (2015) 8:253–69. doi: 10.1242/dmm.017756
58. Xie Y, Tolmeijer S, Oskam JM, Tonkens T, Meijer AH, Schaaf MMJ. Glucocorticoids inhibit macrophage differentiation towards a pro-inflammatory phenotype upon wounding without affecting their migration. *Dis Models Mech.* (2019) 12:dmm037887. doi: 10.1242/dmm.037887
59. Ramakrishnan L. Revisiting the role of the granuloma in tuberculosis. *Nat Rev Immunol.* (2012) 12:352. doi: 10.1038/nri3211
60. Venkiteswaran G, Lewellis SW, Wang J, Reynolds E, Nicholson C, Knaut H. Generation and dynamics of an endogenous, self-generated signaling gradient across a migrating tissue. *Cell.* (2013) 155:674–87. doi: 10.1016/j.cell.2013.09.046
61. Ulvmar MH, Werth K, Braun A, Kelay P, Hub E, Eller K, et al. The atypical chemokine receptor CCRL1 shapes functional CCL21 gradients in lymph nodes. *Nat Immunol.* (2014) 15:623–30. doi: 10.1038/ni.2889
62. Pradelli E, Karimdjee-Soilihi B, Michiels JF, Ricci JE, Millet MA, Vandenbos F, et al. Antagonism of chemokine receptor CXCR3 inhibits osteosarcoma metastasis to lungs. *Int J Cancer.* (2009) 125:2586–94. doi: 10.1002/ijc.24665
63. Sánchez-Martin L, Sánchez-Mateos P, Cabañas C. CXCR7 impact on CXCL12 biology and disease. *Trends Mol Med.* (2013) 19:12–22. doi: 10.1016/j.molmed.2012.10.004
64. Tulotta C, He S, van der Ent W, Chen L, Groenewoud A, Spaink HP, et al. Imaging cancer angiogenesis and metastasis in a zebrafish embryo model. *Adv Exp Med Biol.* (2016) 916:239–63. doi: 10.1007/978-3-319-30654-4_11
65. Balkwill F. The significance of cancer cell expression of the chemokine receptor CXCR4. *Semin Cancer Biol.* (2004) 14:171–9. doi: 10.1016/j.semcancer.2003.10.003
66. Li H, Liang R, Lu Y, Wang M, Li Z. Rtn3 regulates the expression level of chemokine receptor cxcr4 and is required for migration of primordial germ cells. *Int J Mol Sci.* (2016) 17:382. doi: 10.3390/ijms17040382
67. Tulotta C, Stefanescu C, Chen Q, Torraca V, Meijer AH, Snaar-Jagalska BE. CXCR4 signaling regulates metastatic onset by controlling neutrophil motility and response to malignant cells. *Sci Rep.* (2019) 9:2399. doi: 10.1038/s41598-019-38643-2
68. Ellett F, Elks PM, Robertson AL, Ogryzko NV, Renshaw SA. Defining the phenotype of neutrophils following reverse migration in zebrafish. *J Leukocyte Biol.* (2015) 98:975–81. doi: 10.1189/jlb.3MA0315-105R
69. Harvie EA, Huttenlocher A. Neutrophils in host defense: new insights from zebrafish. *J Leukocyte Biol.* (2015) 98:523–37. doi: 10.1189/jlb.4MR1114-524R
70. Singh AK, Arya RK, Trivedi AK, Sanyal S, Baral R, Dormond O, et al. Chemokine receptor trio: CXCR3, CXCR4 and CXCR7 crosstalk via CXCL11 and CXCL12. *Cytokine Growth Factor Rev.* (2013) 24:41–9. doi: 10.1016/j.cytogfr.2012.08.007
71. Coombs C, Georgantzoglou A, Walker HA, Patt J, Merten N, Poplimont H, et al. Chemokine receptor trafficking coordinates neutrophil clustering and dispersal at wounds in zebrafish. *Nat Commun.* (2019) 10:1–17. doi: 10.1038/s41467-019-13107-3
72. Yoo SK, Huttenlocher A. Spatiotemporal photolabeling of neutrophil trafficking during inflammation in live zebrafish. *J Leukocyte Biol.* (2011) 89:661–7. doi: 10.1189/jlb.1010567
73. Sarris M, Masson JB, Maurin D, Van der Aa LM, Boudinot P, Lortat-Jacob H, et al. Inflammatory chemokines direct and restrict leukocyte migration within live tissues as glycan-bound gradients. *Curr Biol.* (2012) 22:2375–82. doi: 10.1016/j.cub.2012.11.018
74. Chia K, Mazzolini J, Mione M, Sieger D. Tumor initiating cells induce Cxcr4-mediated infiltration of pro-tumoral macrophages into the brain. *Elife.* (2018) 7:e31918. doi: 10.7554/eLife.31918
75. Powell D, Lou M, Becker FB, Huttenlocher A. Cxcr1 mediates recruitment of neutrophils and supports proliferation of tumor-initiating astrocytes *in vivo*. *Sci Rep.* (2018) 8:13285. doi: 10.1038/s41598-018-31675-0
76. Cambien B, Karimdjee BF, Richard-Fiardo P, Bziouech H, Barthel R, Millet AM, et al. Organ-specific inhibition of metastatic colon carcinoma by CXCR3 antagonism. *Br J Cancer.* (2009) 100:1755. doi: 10.1038/sj.bjc.6605078
77. Groom JR, Luster AD. CXCR3 ligands: redundant, collaborative and antagonistic functions. *Immunol Cell Biol.* (2011) 89:207–15. doi: 10.1038/icb.2010.158
78. Thelen M, Thelen S. CXCR7, CXCR4 and CXCL12:an eccentric trio? *J Neuroimmunol.* (2008) 198:9–13. doi: 10.1016/j.jneuroim.2008.04.020
79. Dambly-Chaudière C, Cubedo N, Ghysen A. Control of cell migration in the development of the posterior lateral line: antagonistic interactions between the chemokine receptors CXCR4 and CXCR7/RDC1. *BMC Dev Biol.* (2007) 7:23. doi: 10.1186/1471-213X-7-23
80. Donà E, Barry JD, Valentin G, Quirin C, Khmelinskii A, Kunze A, et al. Directional tissue migration through a self-generated chemokine gradient. *Nature.* (2013) 503:285–9. doi: 10.1038/nature12635
81. Moissoglu K, Majumdar R, Parent CA. Cell migration: sinking in a gradient. *Curr Biol.* (2014) 24:R23–5. doi: 10.1016/j.cub.2013.10.075
82. Mahabaleshwar H, Boldajipour B, Raz E. Killing the messenger: The role of CXCR7 in regulating primordial germ cell migration. *Cell Adhesion Migrat.* (2008) 2:69–70. doi: 10.4161/cam.2.2.6027
83. Cambier CJ, Takaki KK, Larson RP, Hernandez RE, Tobin DM, Urdahl KB, et al. Mycobacteria manipulate macrophage recruitment through coordinated use of membrane lipids. *Nature.* (2014) 505:218–22. doi: 10.1038/nature12799
84. Malhotra D, Shin J, Solnica-Krezel L, Raz E. Spatio-temporal regulation of concurrent developmental processes by generic signaling downstream of chemokine receptors. *eLife.* (2018) 7:e33574. doi: 10.7554/eLife.33574
85. Xu Y, Hyun YM, Lim K, Lee H, Cummings RJ, Gerber SA, et al. Optogenetic control of chemokine receptor signal and T-cell migration. *Proc Natl Acad Sci USA.* (2014) 111:6371–6. doi: 10.1073/pnas.1319296111
86. Krathwohl MD, Kaiser JL. Chemokines promote quiescence and survival of human neural progenitor cells. *Stem Cells.* (2004) 22:109–18. doi: 10.1634/stemcells.22-1-109
87. Weber M, Hauschild R, Schwarz J, Moussion C, De Vries I, Legler DF, et al. Interstitial dendritic cell guidance by haptotactic chemokine gradients. *Science.* (2013) 339:328–32. doi: 10.1126/science.1228456

88. Siekmann AF, Standley C, Fogarty KE, Wolfe SA, Lawson ND. Chemokine signaling guides regional patterning of the first embryonic artery. *Genes Dev.* (2009) 23:2272–7. doi: 10.1101/gad.1813509
89. Powell D, Tauzin S, Hind LE, Deng Q, Beebe DJ, Huttenlocher A. Chemokine signaling and the regulation of bidirectional leukocyte migration in interstitial tissues. *Cell Rep.* (2017) 19:1572–85. doi: 10.1016/j.celrep.2017.04.078
90. Li Q, Barres BA. Microglia and macrophages in brain homeostasis and disease. *Nat Rev Immunol.* (2018) 18:225–42. doi: 10.1038/nri.2017.125
91. Van Rechem C, Rood BR, Touka M, Pinte S, Jenal M, Guérardel C, et al. Scavenger chemokine (CXC motif) receptor 7 (CXCR7) is a direct target gene of HIC1 (hypermethylated in cancer 1). *J Biol Chem.* (2009) 284:20927–35. doi: 10.1074/jbc.M109.022350
92. Yoo SK, Deng Q, Cavnar PJ, Wu YI, Hahn KM, Huttenlocher A. Differential regulation of protrusion and polarity by PI (3) K during neutrophil motility in live zebrafish. *Dev Cell.* (2010) 18:226–36. doi: 10.1016/j.devcel.2009.11.015
93. Nguyen-Chi M, Laplace-Builhé B, Travnickova J, Luz-Crawford P, Tejedor G, Lutfalla G, et al. TNF signaling and macrophages govern fin regeneration in zebrafish larvae. *Cell Death Dis.* (2017) 8:e2979. doi: 10.1038/cddis.2017.374
94. Zuñiga-Traslaviña C, Bravo K, Reyes AE, Feijóo CG. Cxcl8b and Cxcr2 regulate neutrophil migration through bloodstream in zebrafish. *J Immunol Res.* (2017) 2017:11. doi: 10.1155/2017/6530531
95. Oliveira S, Reyes-Aldasoro CC, Candel S, Renshaw SA, Mulero V, Calado Â. Cxcl8 (IL-8) mediates neutrophil recruitment and behavior in the zebrafish inflammatory response. *J Immunol.* (2013) 190:4349–59. doi: 10.4049/jimmunol.1203266
96. Walters KB, Green JM, Surfus JC, Yoo SK, Huttenlocher A. Live imaging of neutrophil motility in a zebrafish model of WHIM syndrome. *Blood.* (2010) 116:2803–11. doi: 10.1182/blood-2010-03-276972
97. Isles HM, Herman KD, Robertson AL, Loynes CA, Prince LR, Elks PM, et al. The CXCL12/CXCR4 signaling axis retains neutrophils at inflammatory sites in zebrafish. *Front Immunol.* (2019) 10:1784. doi: 10.3389/fimmu.2019.01784
98. Masud S, Torraca V, Meijer AH. Modeling infectious diseases in the context of a developing immune system. *Curr Topics Dev Biol.* (2017) 124:277–329. doi: 10.1016/bs.ctdb.2016.10.006
99. Deng Q, Sarris M, Bennin DA, Green JM, Herbomel P, Huttenlocher A. Localized bacterial infection induces systemic activation of neutrophils through Cxcr2 signaling in zebrafish. *J Leukocyte Biol.* (2013) 93:761–9. doi: 10.1189/jlb.1012534
100. Elks PM, Vaart M, Hensbergen V, Schutz E, Redd MJ, Murayama E, et al. Mycobacteria counteract a TLR-mediated nitrosative defense mechanism in a zebrafish infection model. *PLoS ONE.* (2014) 9:e100928. doi: 10.1371/journal.pone.0100928
101. Yang CT, Cambier CJ, Davis JM, Hall CJ, Crosier PS, Ramakrishnan L. Neutrophils exert protection in the early tuberculous granuloma by oxidative killing of mycobacteria phagocytosed from infected macrophages. *Cell Host Microbe.* (2012) 12:301–12. doi: 10.1016/j.chom.2012.07.009
102. Elks PM, Brizee S, Vaart M, Walmsley SR, Eeden FJ, Renshaw SA, et al. Hypoxia inducible factor signaling modulates susceptibility to mycobacterial infection via a nitric oxide dependent mechanism. *PLoS Pathog.* (2013) 9:e1003789. doi: 10.1371/journal.ppat.1003789
103. Lowe DM, Redford PS, Wilkinson RJ, O'Garra A, Martineau AR. Neutrophils in tuberculosis: friend or foe? *Trends Immunol.* (2012) 33:14–25. doi: 10.1016/j.it.2011.10.003
104. Rougeot J, Torraca V, Zakrzewska A, Kanwal Z, Jansen H, Spaink H, et al. RNAseq profiling of leukocyte populations in zebrafish larvae reveals a cxcl11 chemokine gene as a marker of macrophage polarization during mycobacterial infection. *Front Immunol.* (2019) 10:832. doi: 10.3389/fimmu.2019.00832
105. Hall C, Flores MV, Chien A, Davidson A, Crosier K, Crosier P. Transgenic zebrafish reporter lines reveal conserved toll-like receptor signaling potential in embryonic myeloid leukocytes and adult immune cell lineages. *J Leukocyte Biol.* (2009) 85:751–65. doi: 10.1189/jlb.0708405
106. Torraca V, Tulotta C, Snaar-Jagalska BE, Meijer AH. The chemokine receptor CXCR4 promotes granuloma formation by sustaining a mycobacteria-induced angiogenesis programme. *Sci Rep.* (2017) 7:45061. doi: 10.1038/srep45061
107. Aly S, Laskay T, Mages J, Malzan A, Lang R, Ehlers S. Interferon-gamma-dependent mechanisms of mycobacteria-induced pulmonary immunopathology: the role of angiostasis and CXCR3-targeted chemokines for granuloma necrosis. *J Pathol A J Pathol Soc Great Br Ireland.* (2007) 212:295–305. doi: 10.1002/path.2185
108. Luster AD, Greenberg SM, Leder P. The IP-10 chemokine binds to a specific cell surface heparan sulfate site shared with platelet factor 4 and inhibits endothelial cell proliferation. *J Exp Med.* (1995) 182:219–31. doi: 10.1084/jem.182.1.219
109. Chakravarty SD, Xu J, Lu B, Gerard C, Flynn J, Chan J. The chemokine receptor CXCR3 attenuates the control of chronic *Mycobacterium tuberculosis* infection in BALB/c mice. *J Immunol.* (2007) 178:1723–35. doi: 10.4049/jimmunol.178.3.1723

Conflict of Interest: The authors declare that the research was conducted in the absence of any commercial or financial relationships that could be construed as a potential conflict of interest.

The reviewer MS declared a past co-authorship with one of the authors, VT, to the handling editor.

frontiers in Immunology

ORIGINAL RESEARCH
published: 25 February 2020
doi: 10.3389/fimmu.2020.00152

Fish Macrophages Show Distinct Metabolic Signatures Upon Polarization

*Annelieke S. Wentzel[1], Joëlle J. E. Janssen[1,2], Vincent C. J. de Boer[2], Wouter G. van Veen[3], Maria Forlenza[1] and Geert F. Wiegertjes[4]**

[1] Cell Biology and Immunology Group, Wageningen University & Research, Wageningen, Netherlands, [2] Human and Animal Physiology Group, Wageningen University & Research, Wageningen, Netherlands, [3] Experimental Zoology Group, Wageningen University & Research, Wageningen, Netherlands, [4] Aquaculture and Fisheries Group, Wageningen University & Research, Wageningen, Netherlands

Macrophages play important roles in conditions ranging from host immune defense to tissue regeneration and polarize their functional phenotype accordingly. Next to differences in the use of L-arginine and the production of different cytokines, inflammatory M1 macrophages and anti-inflammatory M2 macrophages are also metabolically distinct. In mammals, M1 macrophages show metabolic reprogramming toward glycolysis, while M2 macrophages rely on oxidative phosphorylation to generate energy. The presence of polarized functional immune phenotypes conserved from mammals to fish led us to hypothesize that a similar metabolic reprogramming in polarized macrophages exists in carp. We studied mitochondrial function of M1 and M2 carp macrophages under basal and stressed conditions to determine oxidative capacity by real-time measurements of oxygen consumption and glycolytic capacity by measuring lactate-based acidification. In M1 macrophages, we found increased nitric oxide production and *irg1* expression in addition to altered oxidative phosphorylation and glycolysis. In M2 macrophages, we found increased arginase activity, and both oxidative phosphorylation and glycolysis were similar to control macrophages. These results indicate that M1 and M2 carp macrophages show distinct metabolic signatures and indicate that metabolic reprogramming may occur in carp M1 macrophages. This immunometabolic reprogramming likely supports the inflammatory phenotype of polarized macrophages in teleost fish such as carp, similar to what has been shown in mammals.

Keywords: M1 M2 macrophage polarization, metabolic reprogramming, teleost, glycolysis, oxidative phosphorylation (OXPHOS), oxidative metabolism, Seahorse, extracellular flux analysis

OPEN ACCESS

Edited by:
Xinjiang Lu,
Ningbo University, China

Reviewed by:
Jianguo Su,
Huazhong Agricultural University, China
Giuseppe Scapigliati,
Università Degli Studi della Tuscia, Italy

***Correspondence:**
Geert F. Wiegertjes
geert.wiegertjes@wur.nl

Specialty section:
This article was submitted to Comparative Immunology, a section of the journal Frontiers in Immunology

Received: *02 December 2019*
Accepted: *21 January 2020*
Published: *25 February 2020*

Citation:
Wentzel AS, Janssen JJE, de Boer VCJ, van Veen WG, Forlenza M and Wiegertjes GF (2020) Fish Macrophages Show Distinct Metabolic Signatures Upon Polarization. Front. Immunol. 11:152. doi: 10.3389/fimmu.2020.00152

INTRODUCTION

Macrophages are essential innate immune cells involved in host defense that play a role in initiating inflammation but also play a role in the resolution phase of inflammation and in tissue regeneration. These opposing conditions provide microenvironments that drive innate immune cells such as macrophages to display specific effector functions and tailor immune response to either combat pathogens or repair damage. In mammals, depending on the exact microenvironment, an array of different macrophage phenotypes can exist, with the most polarized phenotypes termed M1 and M2 (1). Inflammatory macrophages are commonly associated with T helper-1 responses (hence M1)

and produce pro-inflammatory cytokines, antimicrobial nitric oxide (NO), or other reactive oxygen radicals (ROS) (2–4). Anti-inflammatory macrophages are commonly associated with T helper-2 responses (hence M2), produce anti-inflammatory cytokines, and show increased arginase activity. Hence, M1 macrophages metabolize the amino acid L-arginine to produce NO, while M2 macrophages metabolize the same substrate to produce proline and polyamines (3). Thus, M1 and M2 macrophages show opposing metabolism of L-arginine.

In mammals, macrophages are also metabolically reprogrammed to enhance opposing pathways to generate energy upon polarization [reviewed by (5, 6)]. Most studies addressing macrophage immunometabolism have been performed in mice. IL-4–activated M2 macrophages rely primarily on oxidative phosphorylation (OXPHOS) for energy production, with the exact role of fatty acid oxidation still being debated (6). In contrast, upon activation with bacterial lipopolysaccharide (LPS) alone or in combination with IFN-γ, M1 macrophages show metabolic reprogramming from OXPHOS toward glycolysis. Reprogramming of M1 macrophages toward glycolysis is accompanied by two "breaks" in the tricarboxylic acid cycle (TCA cycle) and inhibition of parts of the electron transport chain (ETC) in the mitochondria (5) (**Figure 1**). The two breaks in the TCA cycle are due to lower activity and expression of isocitrate dehydrogenase and succinate dehydrogenase (SDH) and lead to an accumulation of citrate and succinate (**Figure 1**), which supports important pro-inflammatory immune functions of M1 macrophages. For example, accumulated citrate is shuttled out of the mitochondria, and subsequent accumulation in the cytosol contributes to the production of NO, ROS, and fatty acid synthesis for membrane and granule formation. Accumulated succinate contributes to ROS production and can stabilize hypoxia-inducible factor 1-alpha (HIF1α), which activates the glycolytic pathway and drives inflammation through increased expression of IL-1β (7). Released succinate acts as an alarmin in the extracellular microenvironment and is recycled to generate a feed-forward loop, further increasing IL-1β production (8). Last but not least, inhibition of the ETC is mediated both by NO and itaconate (**Figure 1**). Itaconate, produced from citrate with the enzyme encoded by *irg1*, is considered an important regulator of metabolic reprogramming, as it inhibits both the ETC and TCA cycle through SDH, but is also important to dampen inflammatory functions at later time points (6, 9). Therefore, metabolic reprogramming from oxidative metabolism to glycolysis supports several inflammatory immune functions in M1 macrophages.

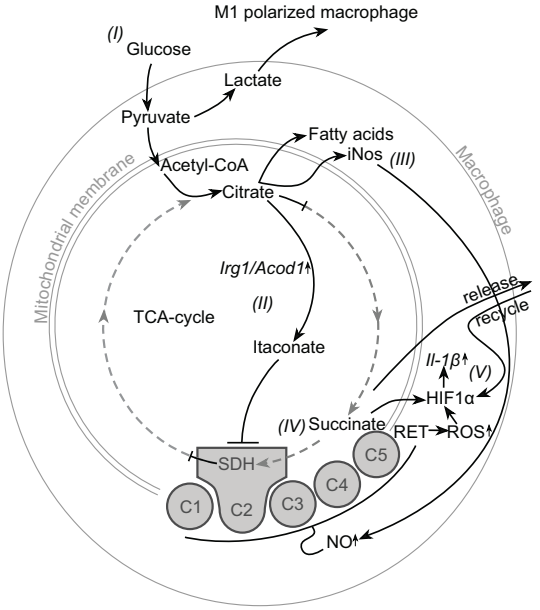

FIGURE 1 | Schematic representation of metabolic reprogramming toward glycolysis in M1 macrophages. Pathways indicated in black are retained or enhanced in M1, pathways indicated in (dashed) gray are reduced in M1. The uptake of glucose and glycolysis (I) is increased in M1, which results in excess pyruvate that is converted to lactate and released from the cell. In the mitochondria, two breaks in the TCA cycle result in the accumulation of citrate and succinate. Accumulation of citrate contributes to three important changes: (1) Citrate is converted to itaconate by the enzyme encoded by *Irg1* (II). Itaconate in turn can inhibit both the TCA cycle and the electron transport chain by blocking succinate dehydrogenase (SDH). (2) Citrate is also shuttled out of the mitochondria, where it promotes NO production and fatty acid synthesis (III). (3) Oxidative phosphorylation through the electron transport chain is inhibited, both by itaconate-mediated inhibition of SDH and by increased production of NO (IV). This causes increased levels of succinate, which stabilize hypoxia-inducible factor 1-alpha (HIF1α) and are also released and recycled by the cell. ROS generated by reverse electron transport (RET) over the hyperpolarized mitochondrial membrane also stabilize HIF1α, which in turn results in increased Il-1β expression (V). Figure based on (6).

Fish macrophages show several of the immune functions typically associated with M1 and M2 macrophages, and thus, macrophage polarization may be largely conserved (10–12). For example, M1 macrophages of carp show increased NO production after stimulation with LPS alone (13, 14) or in combination with Ifn-γ (15) and show increased expression of *il-1β* (10, 14). Zebrafish macrophages show stabilization of Hif1α and *il-1β* expression following mycobacterial infection (16, 17). M2 macrophages of carp and goldfish show increased arginase activity after stimulation with cAMP or Il-4 (10, 18). The apparent conservation of macrophage polarization led us to hypothesize a conservation of the underlying changes in energy metabolism and immunometabolic reprogramming in fish macrophages. We therefore studied mitochondrial function of M1 and M2 polarized carp macrophages under basal and stressed conditions. We determined oxidative capacity by real-time measurements of oxygen consumption, and we measured glycolytic capacity by measuring lactate-based acidification.

Abbreviations: ADP, adenosine diphosphate; ATP, adenosine triphosphate; BMDM, bone marrow–derived macrophage; cAMP, N^6,2′-O-dibutryladenosine 3′:5′-cyclic monophosphate sodium; ECAR, extracellular acidification rate; ETC, electron transport chain; FCCP, carbonyl cyanide-4 (trifluoromethoxy) phenylhydrazone; HIF1α, hypoxia-inducible factor 1-alpha; HKDM, head kidney–derived macrophage; IFN-γ, interferon-gamma; IL-1β, interleukin 1-beta; IL-4, interleukin 4; Irg1/Acod1, immune responsive gene 1/aconitate decarboxylase 1; LPS, lipopolysaccharide; NO, nitric oxide; OCR, oxygen consumption rate; OXPHOS, oxidative phosphorylation; PCS, pooled carp serum; RET, reverse electron transport; ROS, reactive oxygen species; SDH, succinate dehydrogenase; TCA cycle, tricarboxylic acid cycle.

Our data provide the first evidence that carp macrophages can use different pathways for energy metabolism associated with macrophage polarization in teleost fish. We discuss the implications of our findings for studying macrophage polarization in exothermic aquatic vertebrates.

MATERIALS AND METHODS

Animals

European common carp (*Cyprinus carpio carpio* L.) used for experiments were the offspring of a cross between the R3 strain of Polish origin and the R8 strain of Hungarian origin (19). Carp were bred and reared in the aquatic research facility of Wageningen University and Research at 20–23°C in recirculating UV-treated tap water and fed pelleted dry food (Skretting, Nutreco) twice daily. All experiments were performed with the approval of the Animal Experiments Committee of Wageningen University and Research (Ethical Committee documentation number 2017.W-0034).

In vitro Culture and Polarization of Head Kidney–Derived Carp Macrophages

The head kidney in teleost fish is a primary hematopoietic organ and can be considered the functional equivalent of bone marrow (20). Head kidney–derived macrophages (from hereon referred to as macrophages) were obtained as previously described (10). After 6 days of culture at 27°C, macrophages were polarized to M1 or M2 state. In short, macrophages were harvested by gentle scraping after incubation on ice for 15 min. Cells were pelleted at 450 × g for 10 min at 4°C before resuspension in cRPMI+ [RPMI 1640 culture medium with 25 mM HEPES and 2 mM L-glutamine (12-115F, Lonza), supplemented with L-glutamine (2 mM, Gibco), penicillin G (100 U/ml), streptomycin sulfate (100 μg/ml, Gibco) and heat-inactivated pooled carp serum (1.5% v/v)]. Cells were cultured at 27°C in the presence of 5% CO_2 in cRPMI+ unless indicated otherwise. Macrophages stimulated for 24 h with 20 or 50 μg/ml LPS (*Escherichia coli*, L2880, Sigma-Aldrich) were considered M1. Macrophages stimulated for 24 h with 0.5 mg/ml dibutyryl cAMP (N^6,2′-O-dibutryladenosine 3′:5′-cyclic monophosphate sodium D0627, Sigma Aldrich, abbreviated as cAMP) were considered M2.

NO Production

NO production for confirmation of functional polarization was determined in culture supernatants of polarized macrophages. In brief, 5×10^5 macrophages per well were seeded in 96-well plates (Corning) in 150 μl of cRPMI+. After polarization, NO production was determined as nitrite in 75 μl culture supernatant as described previously (21) and expressed in μM using a nitrite standard curve.

Arginase Activity

Arginase enzymatic activity for confirmation of functional polarization into M2 was measured in cell lysates and normalized using a ratio of the sample protein content compared to lysate of control cells. A total of 1.5×10^6 cells polarized for 24 h in 450 μl cRPMI+ were lysed in 100 μl of 0.1% Triton X-100. Protein content of the samples was determined using the Bradford protein dye reagent (Bio-Rad) according to the manufacturer's protocol. Arginase activity was measured in 25 μl lysate essentially as described previously for 50 μl lysate (10), but volumes were scaled down accordingly. Arginase activity was determined as the conversion of L-arginine to urea by arginase and expressed in nmol/min/10^6 cells.

Extracellular Lactate

The release of lactate into the culture supernatant was measured using a lactate colorimetric assay (Kit II K627, BioVision) in filtered samples (Amicon 10K spin column, Z677108-96EA, Sigma-Aldrich) according to the manufacturer's instructions. Briefly, 1.5×10^6 cells were polarized in 450 μl cRPMI+ before culture supernatants from triplicate wells were pooled and filtered. Fifty microliters of 25 × diluted culture supernatant was combined with 50 μl reaction mix in a 96-well plate and incubated for 30 min at room temperature. OD was measured at 450 nm, and the concentration of lactate present in culture supernatants was calculated based on a calibration curve supplied by the manufacturer.

Mito Stress Test

Extracellular flux analysis of polarized macrophages was performed by measuring oxygen consumption rate (OCR) and extracellular acidification rate (ECAR) using a Seahorse XFe96 extracellular flux analyzer (Agilent). We essentially applied the manufacturer's protocol and optimized culture conditions, cell density, and carbonyl cyanide-4 (trifluoromethoxy) phenylhydrazone (FCCP) concentrations to measure OCR and ECAR in carp macrophages and adjusted all incubation steps in the protocol to 27°C. For this, the XFe96 analyzer was kept at room temperature and set to 20°C, which would keep the analyzer at a stable 27°C ± 1°C during the complete assay.

To measure OCR and ECAR, culture medium of 1×10^5 macrophages/well-polarized for 24 h in XF96 V3 PS Cell Culture Microplates (Agilent) was replaced with 180 μl non-buffered Seahorse XF base medium supplemented with 10 mM D-glucose (Sigma) and 4 mM L-glutamine (Gibco) at pH 7.4. After incubation without CO_2 for 45 min at 27°C, OCR and ECAR were measured at basal level and after subsequent addition of 1.5 μM oligomycin, 0.2 μM FCCP, and 2.5 μM antimycin A/1.25 μM Rotenone/40 μM Hoechst DNA stain (all from Sigma). The standard 20 min equilibration cycle at the beginning of a Seahorse run was replaced by an incubation for 10 min without additional mixing before measurements were started. Measurement cycles consisted of 1 min mixing, 1 min waiting, and 3 min measuring. A minimum of four technical replicates were used for each condition.

To normalize OCR and ECAR measurements, we determined the area covered with Hoechst stained nuclei for each well according the manufacturer's instructions. We subsequently used the ratio for each well-compared to the average of all controls for normalization of the OCR and ECAR data. Images were taken with a Cytation 1 plate reader (BioTek) and analyzed using CellProfiler (Version 3.1.9).

Real-Time Activation of Macrophages

To track glycolysis and oxidative metabolism during activation of macrophages in real time, 1×10^5 macrophages/well were plated in XF96 V3 cell culture plates and cultured overnight. The cell culture medium was replaced with 180 µl Seahorse XF RPMI medium with 10 mM D-glucose and 4 mM L-glutamine (pH 7.4). After incubation without CO_2 for 45 min, OCR and ECAR were recorded at basal level and for at least 4 h after addition of 20 or 50 µg/ml LPS, 0.5 mg/ml cAMP, or medium for unstimulated controls as the first injection in the Seahorse run. The standard 20 min equilibration cycle at the beginning of a Seahorse run was replaced by an incubation for 10 min without additional mixing. Measurement cycles consist of 30 s mixing, 1.5 min waiting, and 3 min measuring. A minimum of four technical replicates were used for each condition.

Gene Expression Analysis of *irg1*

Transcriptome sequencing was performed as described previously (22, 23). After reads were aligned to the latest genome assembly of common carp (BioProject: PRJNA73579) (22), differential gene expression was analyzed using the bioinformatics package DESeq 2.0 (v1.22.2) and R statistical software (3.5.5) (24) as described before (23). Statistical analysis was performed using a paired design with unstimulated cells as control and performed for LPS-stimulated (30 µg/ml) and cAMP-stimulated (0.5 mg/ml) macrophages independently ($n = 3$ independent cultures for each stimulus).

Statistics

The mean of technical replicates was used for paired statistical analysis of $n = 6$ biological replicates (NO production, arginase activity, and Mito Stress test), $n = 5$ biological replicates (lactate assay), or $n = 3$ biological replicates (gene expression).

Analysis of NO, arginase assays, and lactate assays was performed with a repeated-measures ANOVA followed by Tukey's *post hoc* tests to determine significant differences between treatments. Normal distributions were confirmed (Shapiro–Wilk test), and in the absence of sphericity (Mauchly's test of sphericity), the Greenhouse–Geisser correction was applied. For Mito Stress test analysis, Friedman's two-way ANOVA by ranks was used followed by Dunn's *post hoc* tests for the non-normally distributed samples. Statistical analysis was performed using IBM SPSS statistics Version 26 and GraphPad Prism 5. Gene expression analysis was performed using DESeq2 as described above. Differences were considered significant when $p < 0.05$.

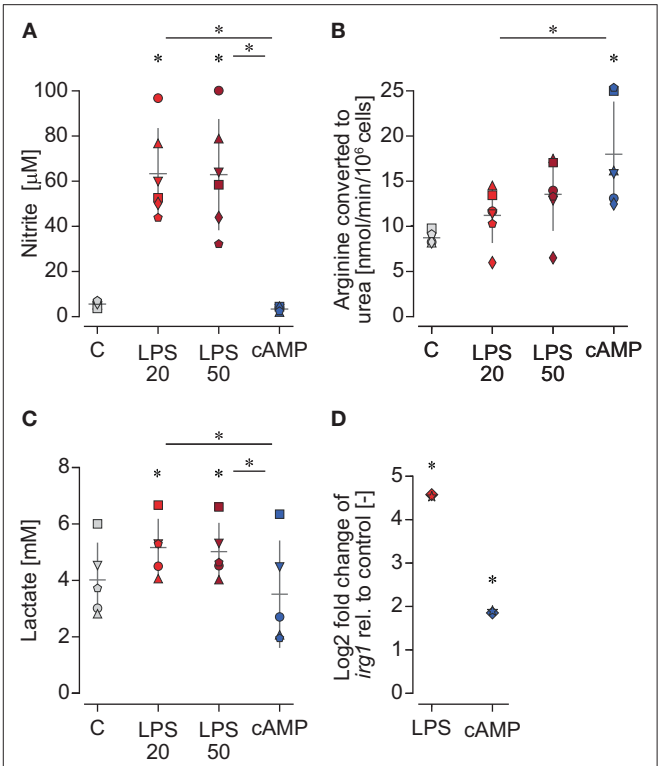

FIGURE 2 | Polarized macrophages of carp show indications of distinct metabolic profiles. Carp macrophages were left unstimulated (gray, control) or were polarized for 24 h with LPS (red; 20 or 50 µg/ml) or with cyclic AMP (blue; 0.5 mg/ml). **(A)** Nitric oxide production measured as nitrite concentration (µM). **(B)** Arginase activity measured as conversion of L-arginine to urea by arginase (nmol/min/10^6 cells). **(C)** Lactate concentration (mM). Shown are individual fish (each indicated by a unique symbol) and the mean and standard deviation of $n = 6$ **(A,B)** or $n = 5$ **(C)** biological replicates. **(D)** Gene expression of two carp *irg1* paralogs [cypCar_00026281 (star) and cypCar_00007903 (diamond)] stimulated for 6 h with 30 µg/ml LPS (red) or with 0.5 µg/ml cAMP (blue) analyzed by DEseq2 after transcriptome sequencing. Gene expression data are shown as log2 fold change compared to unstimulated controls ($n = 3$ biological replicates). Data **(A–C)** were analyzed using a repeated-measures ANOVA with Geisser–Greenhouse correction followed by Tukey's *post hoc* tests. Data **(D)** were analyzed by DEseq2 as part of a transcriptional study. Differences were considered significant when $p < 0.05$. Asterisks (*) indicate significant differences between stimulated and control groups or between groups (line with asterisk). Since there were no clear differences between the two concentrations of LPS, experiments were continued with 20 µg/ml LPS.

RESULTS

Metabolic Signatures of Polarized Carp Macrophages

Macrophages were confirmed as polarized prior to determining their metabolic pathways. LPS-stimulated M1 macrophages showed increased NO production compared to unstimulated macrophages, while cAMP-stimulated macrophages did not (**Figure 2A**). cAMP-stimulated M2 macrophages showed increased arginase activity compared to unstimulated macrophages, while LPS-stimulated macrophages did not (**Figure 2B**).

Metabolic signatures of polarized carp macrophages were examined by measuring extracellular lactate production, expression of *irg1*, and accumulation of intracellular citrate and succinate. All these parameters were shown to play a role in the metabolic reprogramming of murine M1 macrophages from OXPHOS toward glycolysis. In carp macrophages, increased lactate concentrations were measured in culture supernatants of M1 but not M2 macrophages compared to unstimulated macrophages (**Figure 2C**). Also, gene expression of *irg1* was increased to a much higher extent in M1 than M2 macrophages

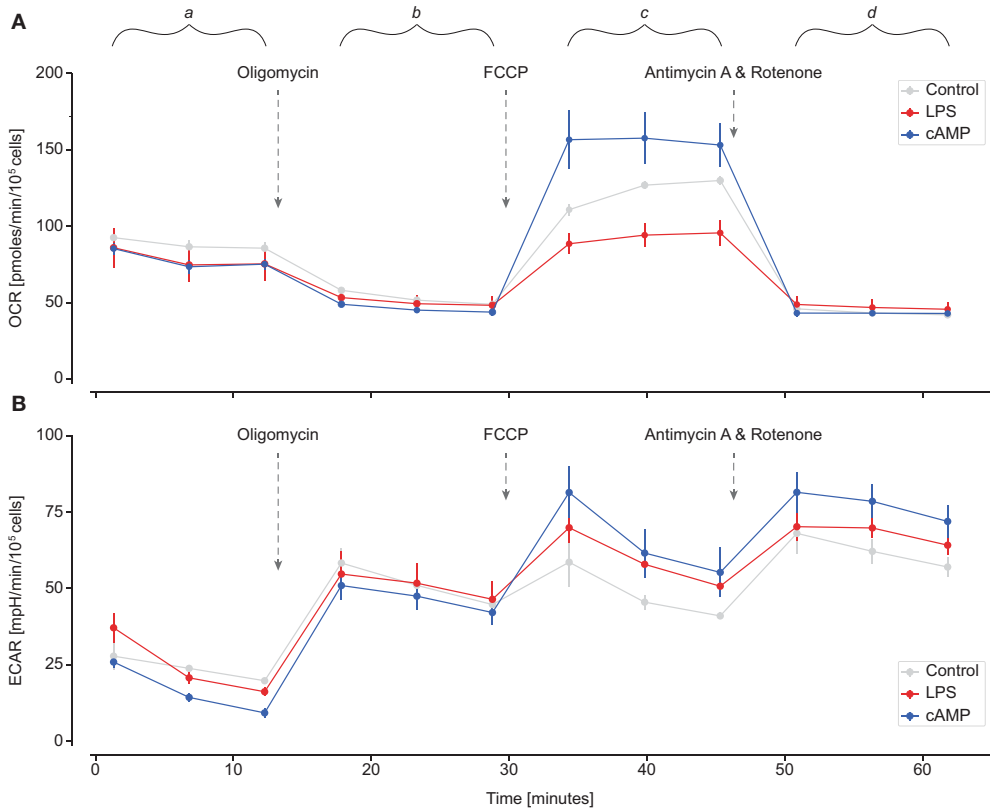

FIGURE 3 | Oxygen consumption rates (OCRs) and extracellular acidification rate (ECAR) of polarized carp macrophages. Carp macrophages were left unstimulated (gray, control) or were polarized for 24 h with LPS (red; 20 μg/ml) or with cyclic AMP (blue; 0.5 μg/ml). Graphs display Mito Stress test profiles of **(A)** OCR and **(B)** ECAR at basal level (time range a) and after subsequent addition of oligomycin (time range b), carbonyl cyanide-4 (trifluoromethoxy) phenylhydrazone (FCCP) (time range c), and antimycin/rotenone (time range d). Normalized rates are shown as mean and SEM of one representative experiment out of $n = 6$ biological replicates.

(**Figure 2D**). Accumulation of intracellular citrate did not show differences between M1 and M2 macrophages, whereas intracellular succinate could not be quantified because levels were below the detection limit (data not shown). Overall, the combination of increased lactate production and increased *irg1* expression indicated that carp M1 macrophages showed a metabolic reprogramming toward glycolysis.

OCR and ECAR of Polarized Carp Macrophages

To study in detail mitochondrial function and oxidative capacity in polarized carp macrophages, we first optimized the Seahorse Mito Stress test for use with carp macrophages at a lower (27°C) temperature. We optimized cell density to 1×10^5 cells/well and found carp macrophages to be particularly sensitive to FCCP with a relatively low optimum concentration of 0.2 μM (tested range 0.1–3 μM). Then, we determined OCR (**Figure 3A**) as a measure for oxidative metabolism and ECAR (**Figure 3B**) as a measure for glycolysis. M1 and M2 macrophages did not show clear differences in OCR or ECAR at basal level (time range *a*). Injection of oligomycin blocks complex V of the ETC and as such inhibits ATP production. Both M1 and M2 macrophages therefore decreased oxygen consumption while increasing extracellular acidification (time range *b*). Disruption of the mitochondrial membrane potential by injection of FCCP induces maximal oxygen consumption. Indeed, after FCCP injection, M1 and M2 macrophages both increased oxygen consumption, but M1 macrophages clearly showed much lower OCR than control or M2 macrophages (time range *c*). Finally, injection of antimycin A and rotenone inhibits complex IIV and complex I of the ETC, thereby completely blocking the ETC. M1 and M2 macrophages did not show differences in non-mitochondrial respiration after antimycin A and rotenone were injected (time range *d*).

Oxygen consumption and extracellular acidification data were used to quantify different metabolic parameters. Basal respiration and ATP-linked respiration (OCR used for ATP synthesis) were not significantly different between control and polarized carp macrophages. However, spare respiratory capacity after injection with FCCP (time range c) was significantly impaired in M1 carp macrophages, which reflected the impaired capacity of M1 macrophages to increase respiration and meet increased energy demands when stressed. Maximal respiration

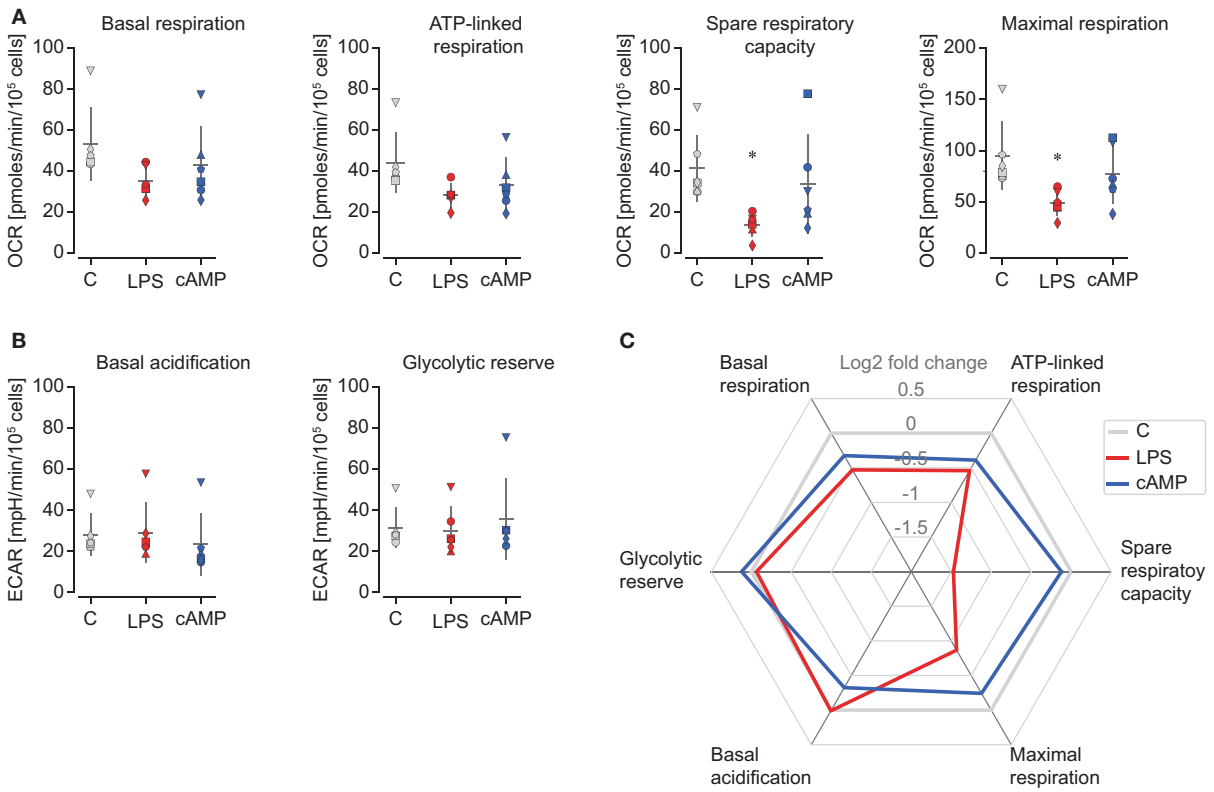

FIGURE 4 | Metabolic parameters underline differences in oxidative potential between polarized carp macrophages. Carp macrophages were left unstimulated (gray, control) or were polarized for 24 h with LPS (red; 20 μg/ml) or with cyclic AMP (blue; 0.5 mg/ml). **(A)** Oxidative parameters based on OCR include basal respiration (OCR_a–OCR_d), oxygen used for ATP synthesis (OCR_a–OCR_b), maximal respiration (OCR_c–OCR_d), and spare respiratory capacity (OCR_c–OCR_a). **(B)** Glycolytic parameters based on ECAR include basal acidification rate ($ECAR_a$) and glycolytic reserve ($ECAR_b$–$ECAR_a$). **(C)** Spider plot depicting both oxidative and glycolytic parameters of polarized carp macrophages (mean log2 fold change compared to respective controls). Metabolic parameters were calculated from normalized Mito Stress test profiles of polarized macrophages and based on the mean of three consecutive measurements as indicated in **Figure 3** with time periods a, b, c, or d. Normalized rates are shown for individual fish (each indicated by a unique icon) and the mean and SD of $n = 6$ biological replicates. Differences were considered significant when $p < 0.05$. Asterisks (*) indicate significant differences between stimulated and control groups.

was therefore also significantly reduced in M1 carp macrophages (**Figure 4A**). In contrast, basal acidification or glycolytic reserve did not change with polarization (**Figure 4B**), indicating that the above-discussed reduction in oxidative capacity of M1 was not mirrored by an increase in glycolysis. Taking all parameters together, polarized M1 macrophages of carp clearly show a different metabolic profile compared to control and M2 macrophages (**Figure 4C**).

Although lactate levels were increased in M1 macrophage culture supernatants (see **Figure 2C**), polarized carp macrophages did not show differences in basal ECAR or in glycolytic reserve after 24 h of polarization (see **Figures 3B**, **4B**). This could indicate that ECAR normalized after 24 h to control ECAR levels and that ECAR peaked at earlier time points than 24 h. We thus performed a preliminary real-time measurement of OCR and ECAR before, during, and immediately after activation of carp macrophages. We observed a rapid, dose-dependent increase in ECAR that remained high for the duration of the experiment, but only in M1 macrophages (LPS stimulation) (**Figure 5B**). In contrast, M2 macrophages (cAMP stimulation) showed a rapid but very short increase in ECAR which rapidly returned to values below controls. No differences in OCR were observed within this time frame (**Figure 5A**). These results suggest that M1 carp rapidly increase their basal glycolysis and that this increase is sustained up to 4 h but reverts to basal levels at 24 h.

DISCUSSION

Previous studies have shown a general conservation of carp macrophage immune function with respect to their ability to polarize toward a pro- or anti-inflammatory profile in response to conventional M1 or M2 stimuli. These observations led us to hypothesize the occurrence of metabolic reprogramming of polarized macrophages of carp. To study this hypothesis, we determined the oxidative and glycolytic capacity of M1 and M2 carp macrophages by measuring OCRs and ECARs under basal and stressed conditions in real time. Carp M1 macrophages show (i) reduced maximal respiration and (ii)

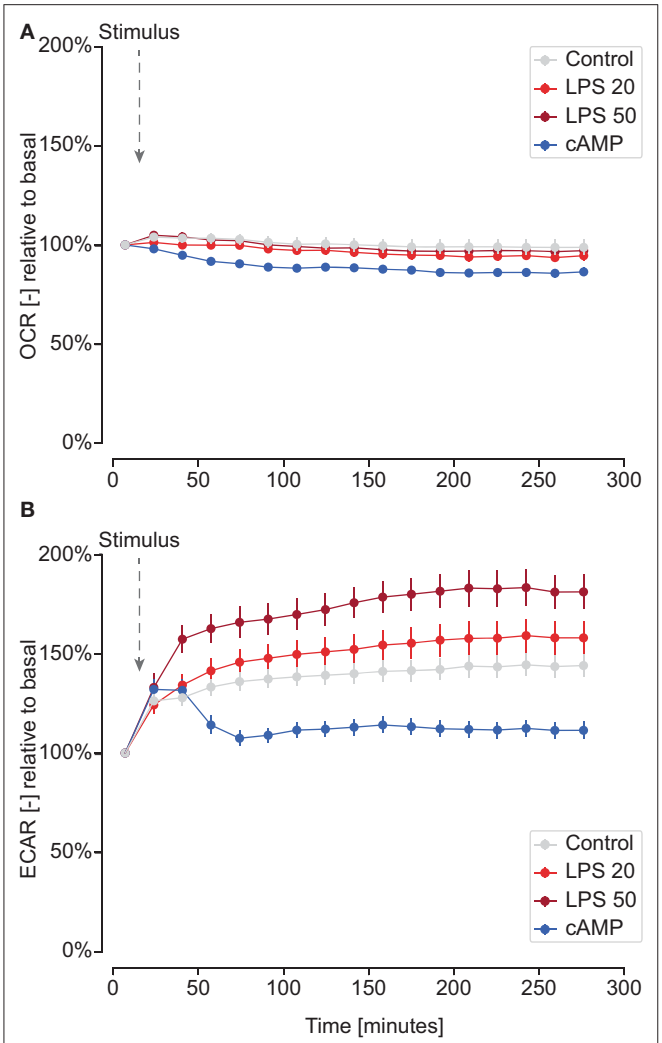

FIGURE 5 | Real-time measurements of ECAR after activation with LPS or cyclic AMP. Carp macrophages were left unstimulated (gray, control) or were stimulated with LPS (red; 20 μg/ml or 50 μg/ml) or with cyclic AMP (blue; 0.5 mg/ml) by injection after determining basal OCR and ECAR levels. Panels represent real-time measurements of OCR **(A)** and ECAR **(B)** for one representative fish out of two. Means of three consecutive OCR and ECAR measurements were normalized to basal level for each well using the mean of three basal measurements before injection of the stimulus. Markers represents the mean and SEM of technical replicates expressed relative to basal rates.

reduced spare respiratory capacity, both indicative of a reduction in oxidative capacity. Furthermore, carp M1 macrophages show (iii) increased lactate production after activation with LPS and a rapid increase in ECAR which is sustained up to 4 h but not 24 h. Finally, carp macrophages show (iv) increased production of NO and (v) increased gene expression of *irg1*, which encodes an enzyme that converts citrate to itaconate. Itaconate is a metabolite that can inhibit both the TCA cycle and the ETC, thus contributing to reduced oxidative capacity. Overall, carp M1 but not M2 macrophages show reduced oxidative metabolism and increased glycolysis.

To date, immunometabolic reprogramming of polarized macrophages has been demonstrated primarily in mice, where polarized macrophages show opposing pathways for energy metabolism: M2s rely on OXPHOS, whereas M1s are metabolically reprogrammed toward glycolysis. Our results indicate that carp M1 macrophages alter their energy metabolism in a manner similar to what has been described for murine M1 macrophages. On the other hand, carp M2 macrophages did not significantly alter their energy metabolism from control cells. Using real-time measurements similar to the ones applied in the present study for carp, M1 murine macrophages were shown to reprogram their energy metabolism toward glycolysis (25–27).

At basal level, murine M1 macrophages show increased glycolysis and reduced OXPHOS. When pushed toward maximal capacity, murine M1 macrophages show a drastic decrease in maximal respiration and spare respiratory capacity. This metabolic reprogramming appears to be responsible for their inability to repolarize from M1 to M2, as they do not regain their oxidative capacity upon repolarization, whereas M2 can repolarize into M1 macrophages without problems (26). At basal level, carp M1 macrophages did not show the increased glycolysis and reduced OXPHOS observed for murine M1 macrophages. This could be because the initial reprogramming of carp LPS-stimulated macrophages toward glycolysis had already been normalized at the start of our measurements. The absence of differences at basal level could be the result of several differences in experimental circumstances between the studies on macrophages of mouse and carp, among which are the exact origin of macrophages, stimuli, and temperature. However, the absence of a difference at basal level may also suggest that carp M1 macrophages were not terminally differentiated by LPS and could possibly still repolarize from M1 to M2, a hypothesis of interest for future studies. Overall, and similar to what has been observed for murine macrophages, carp M1 macrophages show reduced oxidative capacity when pushed to maximal respiration (**Figures 6A,B**). Although the absolute difference between polarized M1 and M2 macrophages appears smaller in carp than in mice, the energy metabolism of carp M1 macrophages appears similar to that of murine M1 macrophages.

In this study, we gained important insights into the metabolic pathways used by carp M1 macrophages and compared these to the metabolic pathways described for M1 polarized macrophages of mice (**Figure 6C**). Carp M1 macrophages increase lactate production and shift toward glycolysis immediately after stimulation with LPS, although the exact kinetics remain to be studied. Although we could not detect differences between M1 and M2 in citrate accumulation, we did detect an upregulation of *irg1* expression, which potentially leads to increased itaconate. In mice, both itaconate and NO can contribute to an inhibition of the ETC. Although we can detect increased *inos* gene expression and increased production of NO in carp M1 macrophages, the contribution of itaconate and/or NO to inhibition of the ETC in carp macrophages remains to be studied. Furthermore, although we previously reported an upregulation of *il-1β* in macrophages stimulated with LPS (10, 14) and although it is known that Hif1α is stabilized and linked to *il-1β* expression during mycobacterium infection of zebrafish (16, 17), it remains to be confirmed if Hif1α

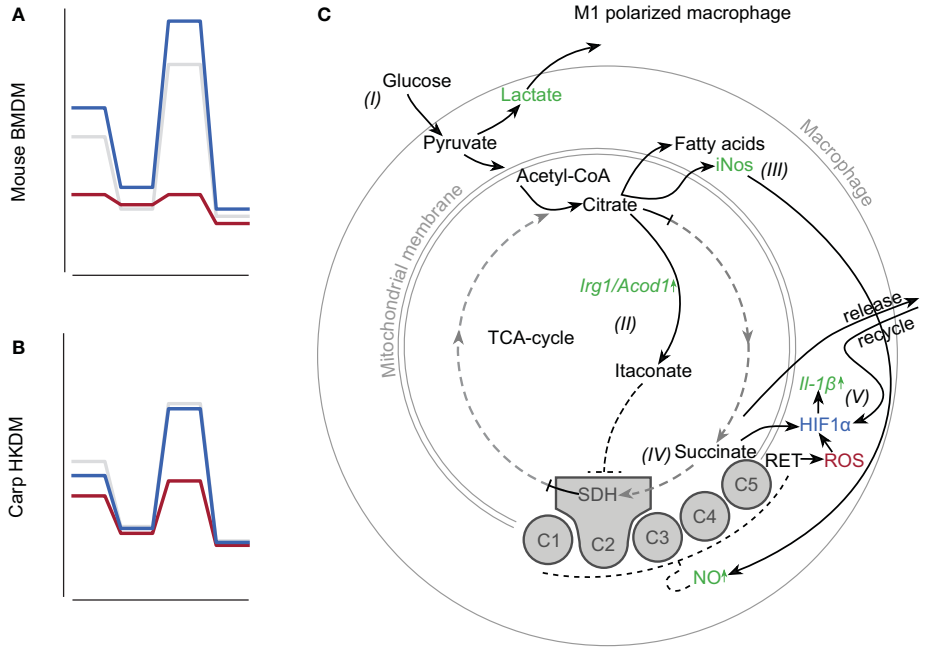

FIGURE 6 | Schematic representation of metabolic reprogramming of carp M1 macrophages upon stimulation with LPS. Schematics of OCRs for **(A)** murine bone marrow–derived macrophages [BMDMs; based on (25, 26)] and **(B)** carp head kidney–derived macrophages (HKDMs; this study). Colors represent control macrophages (gray), polarized M1 macrophages (red), or M2 macrophages (blue). **(C)** Schematic representation of metabolic reprogramming toward glycolysis in murine macrophages, but modified for carp M1 macrophages. Pathways in black are enhanced and pathways in gray with dashed lines are decreased in murine M1 macrophages. Text in green refers to intermediates with regulation in LPS-stimulated carp macrophages similar to regulation in mice. Text in blue refers to intermediates present in zebrafish but not yet studied in carp. Text in red refers to mechanisms present in carp M1 macrophages but not regulated similarly to those in mice. Figure based on (6). Description: (I) Increased lactate in culture supernatants suggests increased glycolysis. (II) LPS-stimulated macrophages show increased *irg1* expression and (III) increased *inos* gene expression and NO production. (IV) Reduced oxidative capacity suggests inhibition of the ETC to some degree, but the mechanism needs confirmation. Succinate accumulation could not be confirmed at this point. (V) Hif1α stabilization exists under inflammatory conditions and is linked to increased *il-1β* transcription in zebrafish (16, 17). Increased *il-1β* expression has been shown in carp (14), but causation has yet to be determined. ROS production occurs in carp macrophages but is low after LPS stimulation (28). Both succinate and ROS can theoretically stabilize Hif-1α, but the mechanisms need to be confirmed for carp.

stabilization is required for *il-1β* expression in carp. Since we do not generally observe ROS production by carp macrophages in response to LPS (28) and were not able to measure intracellular succinate, it remains to be determined which of the two would contribute to the stabilization of Hif1α. Overall, we provide evidence of clear similarities as well as differences between polarized macrophages of mouse and carp.

Carp M2 macrophages did not show a clear increase in maximal respiration compared to controls. Moreover, differences between basal and maximal capacity appeared to be relatively small when compared to those of mice (26). Again, differences in experimental conditions between the studies on macrophages of mouse and carp, among which are the exact origin of macrophages, stimuli, and temperature, can maybe help explain such differences. However, respiration in carp macrophages may also be regulated within more narrow boundaries than in mice: controlled use of oxygen may be particularly important in animals that breathe under water, where available oxygen levels can be more often critical than in air. Studies into the effect of oxygen availability on cellular energy metabolism, in particular, the metabolic reprogramming of innate immune cells, may therefore be of high interest for aquatic animals. Furthermore, oxygen availability is inversely related to temperature (29), and temperature can also directly influence mitochondrial function. For example, at lower temperatures, composition of the mitochondrial membrane changes to counteract reduced membrane fluidity, which in turn changes the ADP affinity of the mitochondria [reviewed by (30)]. Temperature may thus play an important role in metabolic reprogramming. Carp are ectothermic fish that can be acclimatized to a large temperature range and a large range of oxygen pressures, which makes our model adaptable to study mitochondrial functioning and metabolic reprogramming of innate immune cells under varying environmental conditions.

Our studies confirm the general conservation of carp macrophage immune function with respect to their ability to polarize toward a pro- or anti-inflammatory profile in response to conventional M1 or M2 stimuli, and further studies could refine the extent of this conservation. Our studies also help to improve the understanding of fundamental mechanisms underlying energy metabolism and metabolic reprogramming of immune cells in teleost fish and open a field of comparative immunometabolism for exothermics aquatic vertebrates.

DATA AVAILABILITY STATEMENT

The datasets generated for this study are available on request to the corresponding author.

ETHICS STATEMENT

The animal study was reviewed and approved by Animal Experiments Committee of Wageningen University and Research.

AUTHOR CONTRIBUTIONS

AW, JJ, VB, and GW contributed to the design of the experiments. AW performed experiments, and AW, WV, MF, and GW contributed to the analysis of data. GW acquired funding. AW drafted the manuscript, and GW, WV, MF, JJ, and VB critically reviewed the manuscript.

FUNDING

This research was funded by the European Commission under the 8th (H2020) Framework Program for Research and Technological Development of the European Union (PARAFISHCONTROL Grant No. 634429). JJ was funded by the NWO-WIAS Graduate Programme 2016 Grant [Wageningen Institute of Animal Sciences (WIAS) and Dutch Organization for Scientific Research (NWO)].

ACKNOWLEDGMENTS

Marleen Scheer is gratefully acknowledged for her assistance in obtaining head kidney leukocytes.

REFERENCES

1. Xue J, Schmidt SV, Sander J, Draffehn A, Krebs W, Quester I, et al. Transcriptome-based network analysis reveals a spectrum model of human macrophage activation. *Immunity*. (2014) 40:274–88. doi: 10.1016/j.immuni.2014.01.006
2. Nathan CF, Hibbs JB. Role of nitric oxide synthesis in macrophage antimicrobial activity. *Curr Opin Immunol.* (1991) 3:65–70. doi: 10.1016/0952-7915(91)90079-G
3. Mills CD, Kincaid K, Alt JM, Heilman MJ, Hill AM. M-1/M-2 Macrophages and the Th1/Th2 paradigm. *J Immunol.* (2000) 164:6166–73. doi: 10.4049/jimmunol.164.12.6166
4. Fang FC. Antimicrobial actions of reactive oxygen species. *MBio.* (2011) 2:e00141–11. doi: 10.1128/mBio.00141-11
5. O'Neill LAJ, Kishton RJ, Rathmell J. A guide to immunometabolism for immunologists. *Nat Rev Immunol.* (2016) 16:553–65. doi: 10.1038/nri.2016.70
6. Van den Bossche J, O'Neill LA, Menon D. Macrophage Immunometabolism: where are we (going)? *Trends Immunol.* (2017) 38:395–406. doi: 10.1016/j.it.2017.03.001
7. Tannahill GM, Curtis AM, Adamik J, Palsson-McDermott EM, McGettrick AF, Goel G, et al. Succinate is an inflammatory signal that induces IL-1β through HIF-1α. *Nature.* (2013) 496:238–42. doi: 10.1038/nature11986
8. Littlewood-Evans A, Sarret S, Apfel V, Loesle P, Dawson J, Zhang J, et al. GPR91 senses extracellular succinate released from inflammatory macrophages and exacerbates rheumatoid arthritis. *J Exp Med.* (2016) 213:1655–62. doi: 10.1084/jem.20160061
9. O'Neill LAJ, Artyomov MN. Itaconate: the poster child of metabolic reprogramming in macrophage function. *Nat Rev Immunol.* (2019) 19:273–81. doi: 10.1038/s41577-019-0128-5
10. Joerink M, Ribeiro CMS, Stet RJM, Hermsen T, Savelkoul HFJ, Wiegertjes GF. Head kidney-derived macrophages of common carp (*Cyprinus carpio* L.) show plasticity and functional polarization upon differential stimulation. *J Immunol.* (2006) 177:61–9. doi: 10.4049/jimmunol.177.1.61
11. Forlenza M, Fink IR, Raes G, Wiegertjes GF. Heterogeneity of macrophage activation in fish. *Dev Comp Immunol.* (2011) 35:1246–55. doi: 10.1016/j.dci.2011.03.008
12. Wiegertjes GF, Wentzel AS, Spaink HP, Elks PM, Fink IR. Polarization of immune responses in fish: The 'macrophages first' point of view. *Mol Immunol.* (2016) 69:146–56. doi: 10.1016/j.molimm.2015.09.026
13. Saeij JPJ, Stet RJM, Groeneveld A, Verburg-van Kemenade LBM, van Muiswinkel WB, Wiegertjes GF. Molecular and functional characterization of a fish inducible-type nitric oxide synthase. *Immunogenetics.* (2000) 51:339–46. doi: 10.1007/s002510050628
14. Piazzon MC, Savelkoul HFJ, Pietretti D, Wiegertjes GF, Forlenza M. Carp Il10 has anti-inflammatory activities on phagocytes, promotes proliferation of memory T cells, and regulates B cell differentiation and antibody secretion. *J Immunol.* (2015) 194:187–99. doi: 10.4049/jimmunol.1402093
15. Arts JAJ, Tijhaar EJ, Chadzinska M, Savelkoul HFJ, Verburg-van Kemenade BML. Functional analysis of carp interferon-gamma: evolutionary conservation of classical phagocyte activation. *Fish Shellfish Immunol.* (2010) 29:793–802. doi: 10.1016/j.fsi.2010.07.010
16. Elks PM, Brizee S, van der Vaart M, Walmsley SR, van Eeden FJ, Renshaw SA, et al. Hypoxia inducible factor signaling modulates susceptibility to mycobacterial infection via a nitric oxide dependent mechanism. *PLoS Pathog.* (2013) 9:e1003789. doi: 10.1371/journal.ppat.1003789
17. Ogryzko NV, Lewis A, Wilson HL, Meijer AH, Renshaw SA, Elks PM. Hif-1α-Induced Expression of Il-1β Protects against Mycobacterial Infection in Zebrafish. *J Immunol.* (2019) 202:494–502. doi: 10.4049/jimmunol.1801139
18. Hodgkinson JW, Fibke C, Belosevic M. Recombinant IL-4/13A and IL-4/13B induce arginase activity and down-regulate nitric oxide response of primary goldfish (Carassius auratus L.) macrophages. *Dev Comp Immunol.* (2017) 67:377–84. doi: 10.1016/j.dci.2016.08.014
19. Irnazarow I. Genetic variability of polish and hungarian carp lines. *Aquaculture.* (1995) 129:215. doi: 10.1016/0044-8486(95)91961-T
20. Zapata A, Amemiya CT. Phylogeny of lower vertebrates and their immunological structures BT. In: Du Pasquier L, Litman GW, editors. *Origin and Evolution of the Vertebrate Immune System*. Berlin; Heidelberg: Springer Berlin Heidelberg (2000). p. 67–107. doi: 10.1007/978-3-642-59674-2_5
21. Saeij JPJ, Van Muiswinkel WB, Groeneveld A, Wiegertjes GF. Immune modulation by fish kinetoplastid parasites: a role for nitric oxide. *Parasitology.* (2002) 124:77–86. doi: 10.1017/S0031182001008915
22. Kolder ICRM, van der Plas-Duivesteijn SJ, Tan G, Wiegertjes GF, Forlenza M, Guler AT, et al. A full-body transcriptome and proteome resource for the European common carp. *BMC Genomics.* (2016) 17:701. doi: 10.1186/s12864-016-3038-y
23. Petit J, Bailey EC, Wheeler RT, de Oliveira CAF, Forlenza M, Wiegertjes GF. Studies into β-Glucan recognition in fish suggests a key role for the C-type lectin pathway. *Front Immunol.* (2019) 10:280. doi: 10.3389/fimmu.2019.00280
24. Love MI, Huber W, Anders S. Moderated estimation of fold change and dispersion for RNA-seq data with DESeq2. *Genome Biol.* (2014) 15:550. doi: 10.1186/s13059-014-0550-8
25. Van den Bossche J, Baardman J, de Winther MPJ. Metabolic characterization of polarized M1 and M2 bone marrow-derived macrophages using real-time extracellular flux analysis. *J Vis Exp.* (2015) 28:53424. doi: 10.3791/53424
26. Van den Bossche J, Baardman J, Otto NA, van der Velden S, Neele AE, van den Berg SM, et al. Mitochondrial dysfunction prevents repolarization of inflammatory macrophages. *Cell Rep.* (2016) 17:684–96. doi: 10.1016/j.celrep.2016.09.008
27. Vijayan V, Pradhan P, Braud L, Fuchs HR, Gueler F, Motterlini R, et al. Human and murine macrophages exhibit differential metabolic responses

to lipopolysaccharide - A divergent role for glycolysis. *Redox Biol.* (2019) 22:101147. doi: 10.1016/j.redox.2019.101147
28. Pijanowski L, Scheer M, Verburg-van Kemenade BML, Chadzinska M. Production of inflammatory mediators and extracellular traps by carp macrophages and neutrophils in response to lipopolysaccharide and/or interferon-γ2. *Fish Shellfish Immunol.* (2015) 42:473–82. doi: 10.1016/j.fsi.2014.11.019
29. Wetzel RG. Oxygen. In: WETZEL RGBT, editor. *Limnology*. San Diego, CA: Academic Press (2001). p. 151–68. doi: 10.1016/B978-0-08-057439-4.50013-7
30. O'Brien KM. Mitochondrial biogenesis in cold-bodied fishes. *J Exp Biol.* (2011) 214:275–85. doi: 10.1242/jeb.046854

Conflict of Interest: The authors declare that the research was conducted in the absence of any commercial or financial relationships that could be construed as a potential conflict of interest.

frontiers in Immunology

REVIEW
published: 03 March 2020
doi: 10.3389/fimmu.2020.00268

Hemocyte-Mediated Phagocytosis in Crustaceans

Shan Liu[1†], *Shu-Cheng Zheng*[1†], *Yan-Lian Li*[3], *Jun Li*[4*] and *Hai-Peng Liu*[1,2*]

[1] State Key Laboratory of Marine Environmental Science, State-Province Joint Engineering Laboratory of Marine Bioproducts and Technology, Xiamen University, Xiamen, China, [2] Laboratory for Marine Biology and Biotechnology, Pilot National Laboratory for Marine Science and Technology, Qingdao, China, [3] Department of Life Science and Engineering, Jining University, Qufu, China, [4] School of Science and Medicine, Lake Superior State University, Sault Ste. Marie, MI, United States

Phagocytosis is an ancient, highly conserved process in all multicellular organisms, through which the host can protect itself against invading microorganisms and environmental particles, as well as remove self-apoptotic cells/cell debris to maintain tissue homeostasis. In crustacean, phagocytosis by hemocyte has also been well-recognized as a crucial defense mechanism for the host against infectious agents such as bacteria and viruses. In this review, we summarized the current knowledge of hemocyte-mediated phagocytosis, in particular focusing on the related receptors for recognition and internalization of pathogens as well as the downstream signal pathways and intracellular regulators involved in the process of hemocyte phagocytosis. We attempted to gain a deeper understanding of the phagocytic mechanism of different hemocytes and their contribution to the host defense immunity in crustaceans.

Keywords: phagocytosis, hemocyte, innate immunity, white spot syndrome virus, crustacean

OPEN ACCESS

Edited by:
Xinjiang Lu,
Ningbo University, China

Reviewed by:
Chenghua Li,
Ningbo University, China
Yueling Zhang,
Shantou University, China

***Correspondence:**
Jun Li
jli@lssu.edu
Hai-Peng Liu
haipengliu@xmu.edu.cn

[†] These authors have contributed equally to this work

Specialty section:
This article was submitted to Comparative Immunology, a section of the journal Frontiers in Immunology

Received: *29 December 2019*
Accepted: *03 February 2020*
Published: *03 March 2020*

Citation:
Liu S, Zheng S-C, Li Y-L, Li J and Liu H-P (2020) Hemocyte-Mediated Phagocytosis in Crustaceans. Front. Immunol. 11:268. doi: 10.3389/fimmu.2020.00268

INTRODUCTION

The fundamental theory of phagocytosis was first described by Élie Metchnikoff in 1882, which has been gradually established and well-understood over the past two centuries (1). Phagocytosis currently is described as an endocytic process that endogenous foreign particles or pathogens larger than 0.5 μm were first recognized by phagocyte surface receptor and then uptaken and engulfed into a plasma-membrane device, known as phagosome, following initiation of a signaling cascade to generate phagolysosome by fusion of phagosome with lysosomes. Finally, particles or pathogens within the phagolysosome will be degraded and cleared by the hydrolytic enzymes (2, 3). Phagocytosis has been considered as an essential defense mechanism of immune response to pathogens among eukaryotes, which are also implicated in diverse physiological processes, including development, apoptotic, tissue repair, and host defense (4). Owing to its importance and contributions to the innate and adaptive immune function in relation to human and animal health, phagocytosis still remains of great interests to many scientists.

Nowadays, aquaculture industry has become one of the most important resources for providing the people of the premium animal proteins, and employments over the world, especially in China and many Southeast Asian countries (5). However, the rapid expansion and development of aquaculture industries has been significantly inhibited due to infectious diseases, the key challenge imposed to sustainable aquaculture in China. Particularly, *Vibrio* bacteria and white spot syndrome virus (WSSV) have been recognized as the main threats among these pathogens in crustacean (6, 7). However, no effective strategies are available so far to control the outbreak of infectious diseases in crustacean aquaculture due to lack of knowledge about host–pathogen interaction, in particular the poor understanding of the host defensing immune function in crustaceans.

During the past few decades, hemocyte-mediated phagocytosis, as one of the most important innate cellular immune function, has also received great attention in crustacean, and a good progress in elucidating the involvement of hemocyte-mediated phagocytosis, as well as its protective roles and mechanisms, against bacterial and viral infections has been achieved. In this review, we summarized the recent progress about phagocytosis of pathogens by hemocyte in crustaceans, in particular focusing on the novel findings about related receptors for recognition and internalization of pathogens as well as the downstream signal pathways and intracellular regulators involved in the process of hemocyte phagocytosis. We attempted to gain a deeper understanding of the phagocytic mechanism of different hemocytes and their contribution to the host defense immunity in crustaceans, which will be beneficial for the establishment of potential effective strategies to control diseases caused by viruses and bacteria in crustacean industries.

BIOLOGICAL CHARACTERISTICS OF HEMOCYTE

Phagocytes occur in many species, with extreme variations in abundance, evolving from the most primitive unicellular organisms, such as amoeba *Dictyostelium discoideum*, to higher multicellular vertebrates. Phagocytes in higher vertebrates, like mammalian species, have been highly specified into multifarious phagocytic cells, including neutrophils, eosinophils, monocytes/macrophages, dendritic cells, and osteoclasts, and termed as professional phagocytes, whereas others, so-called non-professional phagocytes, mainly include epithelial cells (8). However, regarding invertebrates, such as insects and crustaceans, phagocytes are kindly equivalent to hemocytes, which not only are involved in encapsulation, coagulation, and melanization but also exhibit phagocytic activities (9). Based on limited knowledge on crustacean hemocytes, three distinct types of hemocytes, named as hyaline cells, semigranular cells, and granular cells, have been classified and identified in most of crustaceans mainly based on cell size, nuclear/cytoplasmic (N/C) ratio, and the number of intracellular granules (10, 11). Hyaline cells have been characterized by their smallest cell size, having none or very few cytoplasmic granules, and the highest N/C ratios, while granular cells are the biggest cells with lowest N/C ratios and filled with larger cytoplasmic granules within hemocytes. As for semigranular cells, they are featured as their middle cell size between granular and hyaline cells, with smaller N/C ratios, and contain more cytoplasmic granules, but the number of granules is less than that of granular cells. Further molecular markers have also been proposed in a previous study for distinguishing different hemocytes of signal crayfish *Pacifastacus leniusculus*, and their results showed the potential application of superoxide dismutase (SOD) and two-domain Kazal proteinase inhibitor (KPI) to differentiate the granular and semigranular cells, respectively; however, more detailed molecular evidences are still required to further confirm their specificity in hemocyte classification (12).

Given its essential role in innate immune system, hemocyte homeostasis is of great importance for the health of crustaceans. Actually, the crustacean hematopoiesis has been well-investigated and described in several species since it was first reported in the early 1800s, such as shore crab *Carcinus maenas*, the lobster *Homarus americanus*, and signal crayfish *P. leniusculus* [an extensive review is made available by Lin and Söderhäll (13)]. For example, a study on signal crayfish *P. leniusculus* indicated that their hematopoietic tissue (Hpt) contain at least five different cell types corresponding to various developmental stages of granular and semigranular cells (11). Type 1 cells may be the precursor stem cells for the different cell lineages, and type 2 cells may be the precursor of granular and semigranular cells, both of which are the main cell types in Hpt. Types 3 and 4 may be the precursors of granular cells, whereas type 5 cells may lead to differentiating to semigranular cells (13). For the phagocytic capacity of different subpopulation of hemocytes in insects, previous studies demonstrated that plasmatocytes are the main phagocytic hemocytes in *Drosophila*, while granular cell and plasmatocyte are the main phagocytic hemocytes in Lepidoptera (14). Similarly, different subpopulation of hemocytes in diverse species or even in the same species of crustaceans also exhibited variable phagocytic activities. For instance, the higher phagocytic capacity has been observed in the hyaline cells rather than granular and semigranular cells of *C. maenas*, *Carcinus aestuarii* (15), and *Eriocheir sinensis* (16, 17), while main phagocytic capabilities of granular and semigranular cells were observed in *Macrobrachium rosenbergii*, *Penaeus monodon*, and *Cherax quadricarinatus* (17–20). Higher phagocytic activities were also demonstrated in the semigranular cells of signal crayfish *P. leniusculus*. In contrast, the phagocytic activity of semigranular cells was weaker than that of granular cells in *Scylla paramamosain* (15). However, it is noteworthy to mention that different subpopulations of hemocytes seem to exhibit specific preferences in phagocytosis of different bacteria or viruses. For instance, *Escherichia coli* was mainly ingested and cleared by semigranular and granular cells, whereas WSSV was mostly ingested by semigranular cells in red claw crayfish *C. quadricarinatus* (20). Although phagocytosis has been found in different subpopulation of hemocytes in distinct species, thus far, it is still very difficult to clearly classify the high amounts of evolutionary diversity of crustaceans. Meanwhile, the differentiating and developmental mechanisms of different subpopulations of hemocytes are also unclear. Therefore, more researches especially focused on fundamental theories still need to better characterize the characteristics of subpopulations of hemocytes and their corresponding phagocytosis in crustaceans.

RECEPTOR OR OPSONIN-MEDIATED PATHOGEN RECOGNITION

In mammals, microorganisms are initially recognized by phagocyte receptors, including Fcγ receptor, complement receptor, fibronectin receptor (α5β1 integrin) and launch phagocytosis (3). Furthermore, the process of phagocytosis can be facilitated once pathogens were coated with opsonins (known

as opsonization) because both opsonins and pathogen-associated molecular patterns (PAMPs) on the surface of pathogens are in turn easily recognized by phagocyte receptors. Phagocytosis mediated by hemocytes has been a great contribution to the defense in crustaceans against various pathogens, including *Vibrio parahaemolyticus*, *Vibrio harveyi*, *Staphylococcus aureus*, *Aeromonas hydrophila*, and WSSV. The receptors on the surface of hemocytes, such as lectins, scavenger receptors, immunoglobulin-related protein, and fibrinogen-related protein, have been reported in relation to phagocytosis for fighting pathogens (21–24). In the following, we summarized and discussed the recent advances on the involvement of related receptors or opsonin of hemocytes and their mediating recognition of pathogens in crustaceans.

Lectins

Lectins are featured by carbohydrate recognition domain (CRD) that consists of ∼110–130 amino acids and binds to carbohydrates. So far, many groups of lectins, including C-type, F-type, I-type, L-type, M-type, P-type, R-type, chitinase-like lectins, ficolins, calnexin, galectins, and intelectins, have been identified in crustaceans (21). It has been reported that lectins can act as opsonin or receptors in crustaceans to participate in the phagocytosis of foreign pathogens, including several bacteria and WSSV (21).

The C-type lectins (CTLs) were well-characterized among these lectins and highly conserved in crustaceans, which also acted as receptors to bind and agglutinate bacteria or served as opsonins to promote the phagocytosis of bacteria and viruses. Until now, various CTLs have been found to be implicated in phagocytosis in shrimp, crayfish, and crab, including *P. monodon*, *Litopenaeus vannamei*, *S. paramamosain*, *Fenneropenaeus chinensis*, and *Procambarus clarkii* (**Table 1**). In *P. monodon*, *Pm*Lec was found not only to act as a pattern recognition receptor (PRR) to recognize *E. coli* through binding with lipopolysaccharide (LPS) but also to function as an opsonin to enhance hemocyte phagocytosis (25). Since then, several lectins have also been identified in *L. vannamei*, which exhibited distinct levels on phagocytic activity against bacteria (27). For instance, the phagocytic rates against *V. parahaemolyticus* were decreased to 8.3, 4.5, and 2.5% after silencing the genes of *Lv*CTL5, *Lv*CTLU, and *Lv*LdlrCTL, respectively, in comparison with control groups. It is obvious that the phagocytic activity mediated by *Lv*CTL5 was significantly higher than the other two CTLs. Similarly, both *Pc*Lec3 from *P. clarkii* and *Sp*CTL-B from *S. paramamosain* could also promote the phagocytic activity of hemocytes against *Vibrio anguillarum* and *V. parahemolyticus*, respectively (31, 32). Meanwhile, the expression of phagocytosis-related genes, like *Sp*Myosin, *Sp*Rab5, and *Sp*LAMP [lysosomal-associated membrane protein 1-like protein (LAMP)], could be enhanced by *Sp*CTL-B.

Apart from C-type lectins, L-type lectins and galectins, another type of lectin, were also identified as important opsonins to promote phagocytosis against bacteria and viruses in crustaceans. Both *Mj*LTL1 and galectin were found to be able to enhance agglutination activity for bacterial clearance and hemocytes phagocytosis against *V. anguillarum* in *Marsupenaeus japonicus* and *L. vannamei*, respectively (34, 35). However, more types of lectins from various crustacean species and the molecular mechanisms involved in phagocytosis are extremely lacking, which need to be further elucidated for better understanding of lectin-mediated phagocytosis in innate immunity in crustaceans.

Scavenger Receptors

Scavenger receptors (SRs) are transmembrane proteins that can bind to modified low-density lipoproteins (LDLs), a broad range of polyanionic ligands and cell wall components, which play an essential role in physiological or pathological processes, such as intracellular cargo transport and clearance of pathogen and apoptotic cell (43). SRs occur on the surface of professional phagocytes in both mammalian species and invertebrates, which can be divided into nine heterogeneous classes (A–I) on the basis of their structural diversities (22, 39). SRs generally mediate phagocytosis of non-opsonic pathogens through recognizing PAMPs, including LPS and lipoteichoic acid (LTA). More recently, one of the class B scavenger receptors (SR-Bs), designated as *Sp*SR-B, was found to a be functional phagocytic receptor in the mud crab *S. paramamosain*. The *Sp*SR-B recombinant protein could bind onto the surface of *S. cerevisiae*, *V. parahaemolyticus*, *V. alginolyticus*, *A. hydrophila*, *E. coli*, *S. aureus*, and β streptococcus. Moreover, *Sp*SR-B-mediated phagocytosis could promote the clearance of *V. parahaemolyticus* and *S. aureus*. Meanwhile, the expression of phagocytosis-related genes *SpLamp*, *SpRab5*, *SpArp*, and *SpMyosin* were significantly downregulated when the *Sp*SR-B gene was knocked down in hemocytes (36). Other studies also proved that class B scavenger receptors (SRBs) could bind to *S. aureus* and enhance the phagocytotic rate to facilitate subsequent microbial clearance in *M. japonicus* and *E. sinensis* (39, 40). In *E. sinensis*, the phagocytic rate for *V. parahaemolyticus* was decreased from approximately 21 to 15% after silencing of the *EsSR-B1* gene, while the phagocytic rate for *S. aureus* was decreased from ∼15 to −7%. All the findings indicated that SRB-mediated phagocytosis of *S. aureus*, *V. anguillarum*, or *V. parahaemolyticus* was very variable with regard to various host species (36, 39).

In addition, the class C scavenger receptors (SR-Cs), similar to that of mammalian class A scavenger receptors (SR-As), specifically recognized LPS of Gram-negative bacteria (22). *Mj*SRC, a class C scavenger receptor characterized from *M. japonicus*, was found to be able to mediate phagocytosis of WSSV by binding the viral envelope protein VP19 and then restrict viral replication (37). Meanwhile, *Mj*SRC could also act as a phagocytotic receptor for enhancing phagocytosis and restricting bacterial proliferation through recognizing *V. anguillarum* and *S. aureus* using its extracellular domains to bind bacterial polysaccharides, such as LPS and LTA (38). Owing to abundant heterogeneous classes of the SRs, it is worthy to further prove whether any other classes of SRs, besides SR-Bs and SR-Cs, are participating in hemocyte phagocytosis in crustaceans against bacterial or viral infection.

Down Syndrome Cell Adhesion Molecule

Owing to the lack of adaptive immune system for invertebrates, it is commonly accepted that the crustaceans are solely dependent

TABLE 1 | Phagocytic receptors, ligands, and hemocyte-mediated phagocytosis of pathogens in crustaceans in previous studies.

Receptors	Isoforms	Domains	Ligands	Hemocyte-mediated phagocytosis of pathogens	Species	References
C-type lectin	*Pm*Lec	CRD, QPD	LPS	*E. coli*	*P. monodon*	(25)
	*Lv*Lec	CRD	–	*V. alginolyticus*	*L. vannamei*	(26)
	*Lv*CTL5	CRD	–	*V. parahaemolyticus*	*L. vannamei*	(27)
	*Lv*CTLU	CRD	–	*V. parahaemolyticus*	*L. vannamei*	(28)
	*Lv*LdlrCTL	CRD, LDLR	–	*V. parahaemolyticus*	*L. vannamei*	(29)
	*Fc*Lec4	QPD	–	*V. anguillarum*	*F. chinensis*	(30)
	*Sp*CTL-B	CRD	–	*V. parahaemolyticus*	*S. paramamosain*	(31)
	*Pc*Lec3	CRD, Ig	LPS, PGN, LTA	*V. anguillarum*	*P. clarkii*	(32)
	*Pc*LT	CRD	Envelope protein VP28, VP19	*V. alginolyticus*	*P. clarkii*	(33)
L-type lectin	*Mj*LTL1	CRD	LPS, PGN, LTA	*V. anguillarum*	*M. japonicus*	(34)
Galectins	*Lv*Gal	CRD	–	*V. anguillarum*	*L. vannamei*	(35)
Scavenger receptors	*Sp*SRB	CD36	–	*V. parahaemolyticus and S. aureus*	*S. paramamosain*	(36)
	*Mj*SRC	MAM, CCP	LPS, LTA, Envelope protein VP19	WSSV, *V. anguillarum* and *S. aureus*	*M. japonicus*	(37, 38)
	*Mj*SRB1	CD36	LPS, LTA	*V. anguillarum* and *S. aureus*	*M. japonicus*	(39)
	*Es*SRB1	CD36	–	*V. parahaemolyticus* and *S. aureus*	*E. sinensis*	(40)
Immunoglobulin-related proteins	*Es*Dscam	Ig, FN	–	*V. parahaemolyticus* and *S. aureus*	*E. sinensis*	(41)
Fibrinogen-related proteins	*Mj*FREP2	FReD	LPS, PGN, envelope protein VP28	*V. anguillarum* and *S. aureus*	*M. japonicus*	(42)

CRD, carbohydrate recognition domain; QPD, Gln-Pro-Asp domain; LDLR, low-density lipoprotein receptor; Ig, immunoglobulin; SRC, class C scavenger receptor; SRB, class B scavenger receptor; MAM, domain in meprin; CCP, complement control protein domains; WSSV, white spot syndrome virus; Dscam, Down syndrome cell adhesion molecule; FN, fibronectin; FReD, fibrinogen-related domain; LPS, lipopolysaccharide; PGN, peptidoglycan; LTA, lipoteichoic acid; CD36, cluster of differentiation 36; –, not available.

on innate immunity for the organisms against microbial infections. However, a highly variable immunoglobulin-related protein, named as Down syndrome cell adhesion molecule (Dscam), has been identified in both insects and crustaceans (24). As an immunoglobulin super family (IgSF) member, Dscam is composed of a cluster of immunoglobulin (Ig) and fibronectin (FN) domains (37). The first arthropod Dscam, which mostly presents in the neural system, fat body cells, hemocytes, and hemolymph serum in *D. melanogaster* (*Dm*Dscam), has been demonstrated as a phagocytic receptor (44). The *Drosophila* Dscam can generate more than 38,000 distinct extracellular domains by mutually exclusive alternative splicing of exons and potentially act as phagocytic receptors and/or opsonin for the recognition of various pathogens. In addition, the phagocytic activity of hemocytes was significantly decreased if the *Dm*Dscam gene expression was silenced in hemocytes (44). Similar to *Dm*Dscam, Dscams identified in *Anopheles gambiae* and *Daphnia pulex* can generate 31,920 and 13,312 alternatives splicing forms, respectively. After silencing of their Dscam gene in *A. gambiae* (*AgDscam*), the phagocytic capacity of the Sua5B cells was suppressed against *E. coli* and *S. aureus*. In crustacean, significantly high diversities of Dscam, generated by a variety of alternative splicing form repertoires with combination of three highly hypervariable Ig domain 2, 3, and 7, have been reported in *L. vannamei*, *P. mondon*, *C. quadricarinatus*, and *E. sinensis* (41, 45–47). For instance, the variable regions of *Lv*Dscam located in the Ig2, Ig3, and Ig7 domain could potentially encode at least 8,970 unique isoforms, which are speculated to play active roles in response to a spectrum of pathogens (47).

More recently, the *Es*Dscam identified from Chinese mitten crab (*E. sinensis*) could potentially produce over 30,600 isoforms, and certain *Es*Dscam isoforms were found to specifically bind with *S. aureus*, *Bacillus subtilis*, *A. hydrophila*, and *V. parahaemolyticus*, respectively, and then could facilitate efficient clearance of the bacteria through phagocytosis. Further investigations revealed that *Es*Dscam contains two forms: soluble Dscam (*Es*-sDscam) and membrane-bound Dscam (*Es*-mDscam). Like an opsonin, coating of *Es*-sDscam onto specific bacteria, such as *S. aureus* and *V. parahemolyticus*, could enhance the phagocytic ingesting of these bacteria, while such promoting phagocytic function was abolished for the truncated recombinant *Es*-sDscam. With respect to *Es*-mDscam, it served as a phagocytic receptor for *Es*-sDscam through interacting with the same isoform of *Es*-sDscam. In addition, studies have been

demonstrated that higher expression level of *Es*Dscam is in parallel to stronger and longer lasting phagocytic capacity of hemocytes in the immune priming *E. sinensis* with exposure to *A. hydrophila* (48). However, the underlying molecular mechanism of Dscam-mediated phagocytosis as well as its functioning regulation in response to bacterial and viral infections remain insufficient at present. Importantly, whether arthropod Dscam can serve as an antibody analog during the innate immune response against pathogenic infection, especially when we considered about the biological and functional specificity of a pathogen, if there is, remained to be further studied.

Fibrinogen-Related Proteins

Fibrinogen-related proteins (FREPs, also known as FBNs), containing a highly conserved fibrinogen-related domain (FReD), are one family of the pattern recognition receptors (PRRs) that consist of 53 putative members in *A. gambiae*, while only 20 known FREP members in *D. melanogaster* (49). The *A. gambiae* FREPs family has been proven to play a crucial role in mosquito against bacteria and malaria parasites, in which FREPs could bind with *E. coli*, *Pseudomonas veronii*, and *Beauveria bassiana*. FBN9 can form dimers for binding to the bacterial surfaces with different affinities (23). FREPs have also been reported to play an important role in the innate immunity of crustaceans. For instance, fibrinogen-related proteins were identified from *M. japonicus* (*Mj*FREP1 and *Mj*FREP2) (19, 42), which exhibited different expression levels in different tissues. Both *Mj*FREP1 and *Mj*FREP2 could bind to *V. anguillarum* and *S. aureus* through interaction with LPS and peptidoglycan (PGN). Furthermore, *Mj*FREP2 could recognize the invading bacteria and facilitate bacterial clearance by promoting the phagocytosis of hemocytes. However, the molecular mechanism underlying hemocyte phagocytosis mediated by FREPs still needs further investigations, in consideration to their key roles in innate immunity.

SIGNALING CASCADES INVOLVED IN PHAGOSOME FORMATION AND MATURATION

After coating with opsonin and recognition of the pathogens by related phagocytic receptors, a series of signaling events for initiating phagocytosis will be thereby triggered, and will result in remodeling of the actin cytoskeleton to produce membrane pseudopods for internalizing the pathogen to form phagosome (50). Then, phagosomes gradually fuse with early and late endosomes and eventually fuse with lysosome to generate phagolysosome. Importantly, small GTPases of the Rab family represent a key cluster of molecules that closely related to phagosome formation and maturation by modulating the remodeling of cytoskeleton. Although no direct evidence about phagosome formation and maturation for engulfing and ingesting microorganism was demonstrated in crustacean, to our best knowledge, several important components, mainly small GTPases members such as Rab6, Rab7, RhoA, and Ran, have been reported in some species of shrimp for their involvement in the signaling cascades of the highly conserved processes (51–54). Most of them have also been proven previously to play essential roles in regulating the actin polymerization and dynamic remodeling to form phagosome in vertebrates (51).

Rab7 is a well-known key protein that localizes on the membrane of late endosome and plays a critical role in the phagosome maturation, which has also been found to promote the phagocytosis against *S. aureus* and *V. parahaemolyticus* in hemocytes of *E. sinensis* (55). However, the role of Rab7, as well as the conversion of Rab5 to Rab7, is still poorly understood in crustaceans. Another Rab family member termed as *Pj*Rab6, was found to directly interact with β-actin, tropomyosin, and the WSSV envelope protein VP466 for generating a complex to regulate hemocytic phagocytosis in *P. japonicus* (56). Interestingly, a further study found that viral envelope protein VP466 was employed by the host cell to increase the GTPase activity of PjRab6 to induce rearrangements of the actin cytoskeleton for the formation of actin stress fibers and subsequently promote the phagocytosis against WSSV (57). All findings indicated that phagocytosis is a complicated process, in particular, phagosome formation and maturation, which not only require host factors but also is associated with the utilization of pathogens components. Moreover, as an important member in phagosome formation and maturation, it is not surprising that *Pj*Rab6 could also increase the hemocytic phagocytosis against bacteria, such as *V. parahaemolyticus*, although the regulatory molecular events involved in the phagocytosis of bacteria are still unclear [**Figure 1**; (54)].

Besides, as one of the Ras GTPase superfamily members, *Mj*RhoA has also been identified in *M. japonicus* to be able to induce the expression level of phagocytosis-related genes ROCK2 and Arp2/3 as well as to promote the phagocytosis rate against *V. anguillarum* in hemocytes (51). Both ROCK2 and Arp2/3 were reported to be implicated in the integrin-mediated phagocytosis pathway (51). Previously, a C-type lectin receptor, *Fc*Lec4, was found to be able to facilitate phagocytosis and bacterial clearance through binding to its receptor β-integrin in *F. chinensis* (30). Further study showed that *Mj*RhoA participated in hemocytes phagocytosis against *V. anguillarum* infection via β-integrin-dependent signaling pathway, which was the downstream factor for β-integrin (51). Ran GTPases, another family of the small G protein superfamily, has also been found to be involved in phagosome formation and maturation in crustacean hemocytes. For example, *Pj*Ran, a Ran GTPase identified from *P. japonicus*, has been proven to modulate hemocytic phagocytosis against WSSV via interaction with the cytoskeleton protein myosin (58). Given the importance and contribution to modulate phagocytosis, researches on exploring more members of the small GTPases family are necessary for understanding the molecular mechanism underlying phagosome formation and maturation against pathogens. Beyond that, the development of phagolysosome also needs to recruit more host components, such as the vacuolar ATPase and NADPH oxidase complex, while various organelles including mitochondria, the endoplasmic reticulum, and Golgi-derived vesicles are also required to make contributions to this complicated physiological process (50). However, extremely poor knowledge is available

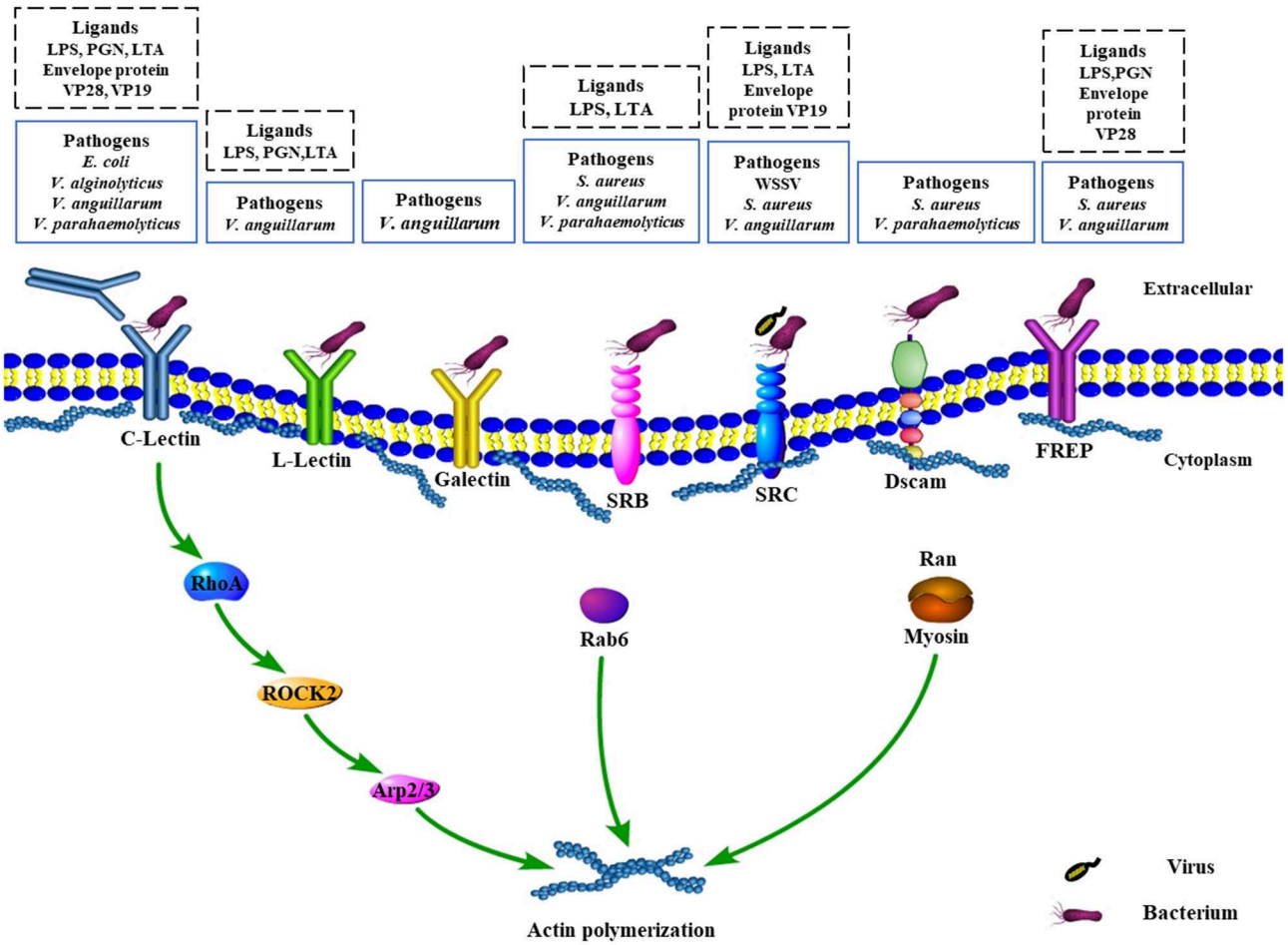

FIGURE 1 | Schematic representation of recognition of pathogens by surface receptors and signaling pathways involved in phagocytosis in crustaceans. C-Lectin, L-Lectin, galectin, SRB, SRC, Dscam, and FREP are selected and modified from previous publications. For more details of all the molecules, please refer to the related references. C-Lectin serves as opsonin or receptor to recognize the invading bacteria and regulate the expression of downstream factor RhoA, which further stimulates the activity of the ROCK2 and Arp2/3 to participate in actin polymerization (51). In addition, Rab6 participates in actin polymerization. Meanwhile, Ran interacts with myosin to participate in actin polymerization. ROCK2, serine/threonine kinase Rho kinase 2; SRC, class C scavenger receptor; SRB, class B scavenger receptor; Dscam, Down syndrome cell adhesion molecule; FREP, fibrinogen-related proteins.

about that due to limited studies conducted in this field in crustaceans.

OTHER FACTORS INVOLVED IN PHAGOCYTOSIS

Although lots of molecular mechanisms in phagosome formation and maturation have not been well-investigated in crustacean, however, increasing evidence showed that some other factors could also modulate phagocytosis against bacteria. Among them, antimicrobial peptides (AMPs) have been reported as one of the most important components to participate in phagocytosis in crustaceans.

AMPs have been well-characterized as important effectors in the innate immune system in both insect and crustacean, which are mainly expressed in hemocytes and then released into the hemolymph for defensing against a broad spectrum of microorganisms (59). Until now, several types of AMPs, such as penaeidins, antilipopolysaccharide factors, and crustins, have been discovered in crustaceans. Interestingly, in addition to their antimicrobial activity, some AMPs also seem to participate in the phagocytosis of pathogens during microbial infection in shrimp.

Penaeidins are one family of antimicrobial peptides that consist of proline-rich N-terminals and a C-terminal cysteine-rich region (60). To date, ∼40 penaeidins have been identified in shrimp, which belong to five types based on their similarity of amino acid sequences. Recently, a penaeidin with an additional serine-rich region (*Mj*Pen-II) from *M. japonicus* showed not only antimicrobial but also phagocytic activity (61). The rate of phagocytosis was significantly decreased after the *Mj*Pen-II gene was silenced, while compensation with injection of *Mj*Pen-II recombinant protein *in vivo* could increase the phagocytic activity. Further study showed that *Mj*Pen-II could eliminate

bacteria through directly inhibiting bacterial growth as well as promoting phagocytosis.

Crustins are another type of antibacterial peptides that contain a single whey acidic protein domain at the C-terminus. In shrimp, two isoforms of crustins, including *Mj*Cru I-1 and crustin-like peptide, have been characterized to be associated with phagocytosis, which were increased in hemocytes after challenge with bacteria (62). Meanwhile, both of them exhibited binding activity to bacteria followed by the increased phagocytosis of hemocyte. In addition, the phagocytic rate of WSSV was significantly decreased when the crustin-like gene was knocked down in shrimp hemocytes, whereas the phagocytic rate of *V. alginolyticus* was increased in hemocytes, exhibiting different biological effect against microorganisms (62). However, the underlying regulatory molecular mechanism of AMP-mediated phagocytosis is still extremely limited, which is worthy of further investigations.

Except AMPs, some other molecules have also been reported to regulate phagocytosis of invading pathogens in crustaceans. For instance, the recombinant phagocytosis-activating protein (PAP) was shown to significantly promote the phagocytic activity of hemocytes in *P. monodon* (63). Two neuroendocrine factors, crustacean hyperglycemic hormone (CHH) and dopamine, were also found to participate in phagocytosis in *L. vannamei* hemocytes. CHH exhibited regulating capacity on phagocytosis through activating nuclear factor kappa B (NF-κB) signaling pathway family members and phagocytosis-related proteins, while dopamine acted as a phagocytosis-related factor to inhibit phagocytosis (64, 65). Except for proteins, some microRNAs (miRNAs) have also been found to play critical roles in regulating phagocytosis process in crustaceans. In hemocytes of *M. japonicus*, miR-1 has been found to negatively regulate the phagocytic activity through interaction with the 3′ untranslated region (UTR) of clathrin heavy chain 1 (CLTC1) gene (66). Moreover, miR-12 and miR-965 were also found to be able to enhance the phagocytosis of WSSV via direct targeting phosphatase and tensin homolog (PTEN) and viral gene wsv240, respectively (67, 68), while another miR-100 could promote the antibacterial and antiviral immune response but through regulating the total hemocyte count and phagocytosis in *M. japonicus* (69). In addition, the shrimp-specific miR-S5 acted as a regulator on hemocyte phagocytic progress via negatively regulating myosin expression (70). Taken together, miRNAs act as regulator involved in antibacterial or antiviral immune responses through direct targeting viral genes or cytoskeleton-related genes accordingly. However, the specific regulatory mechanism of miRNA involved in phagocytosis against pathogens needs to be further studied.

CONCLUSION AND FUTURE PERSPECTIVE

Although several cellular surface receptors/opsonin and intracellular regulator for mediating phagocytosis against bacteria and viruses have been reported in hemocytes from multiple species of crustaceans, limited studies make it extremely unclear until now about the molecular mechanism of recognition of pathogens and the downstream signaling events, in particular those in relation to phagosome formation and maturation, as well as microbe destruction in crustaceans. Future research will be focused on the following fundamental questions in relation to the above concerns. For instance, besides the three described types of hemocytes involved in the phagocytosis in crustaceans, are there any other phagocytic cells types present in crustaceans and additional surface receptors involved in pathogen recognition? What are the regulatory mechanisms for various phagocytic receptors located on hemocytes to cooperate with each other during phagocytosis of different microorganisms? More importantly, are the processes of phagosome formation and maturation in crustaceans similar to that in vertebrates? Last but not least, how does the cooperation occur among various intracellular regulators to mediate phagocytosis, and are there other novel signaling pathways involved in the regulation on hemocyte-mediated phagocytosis? Successfully addressing these important questions will pave avenues to deeper understanding of phagocytosis against microbial infection in crustaceans, in which the fundamental mechanism of phagocytosis in crustacean will benefit the establishment of more efficient control strategies against disease in crustacean farming.

AUTHOR CONTRIBUTIONS

SL and S-CZ wrote the manuscript. Y-LL contributed to suggestion and discussion. JL and H-PL designed and finally polished the manuscript.

FUNDING

This work was funded by the National Key Research and Development Program of China (2018YFD0900502), the Natural Science Foundation of China (U1605214, 41676135), and the Fundamental Research Funds for the Central Universities (20720180123).

REFERENCES

1. Vaughan RB. The romantic rationalist: a study of Elie Metchnikoff. *Med Hist.* (1965) 9:201–15. doi: 10.1017/S0025727300030702
2. Flannagan RS, Jaumouillé V, Grinstein S. The cell biology of phagocytosis. *Annu Rev Pathol.* (2012) 7:61–98. doi: 10.1146/annurev-pathol-011811-132445
3. Underhill DM, Goodridge HS. Information processing during phagocytosis. *Nat Rev Immunol.* (2012) 12:492–502. doi: 10.1038/nri3244
4. Freeman SA, Sergio S. Phagocytosis: receptors, signal integration, and the cytoskeleton. *Immunol Rev.* (2015) 262:193–215. doi: 10.1111/imr.12212
5. Oakey J, Smith C, Underwood D, Afsharnasab M, Alday-Sanz V, Dhar A, et al. Global distribution of white spot syndrome virus genotypes

determined using a novel genotyping assay. *Arch Virol.* (2019) 164:2061–82. doi: 10.1007/s00705-019-04265-2
6. Zheng SC, Xu JY, Liu HP. Cellular entry of white spot syndrome virus and antiviral immunity mediated by cellular receptors in crustaceans. *Fish Shellfish Immunol.* (2019) 93:580–8. doi: 10.1016/j.fsi.2019.08.011
7. Xiong J, Dai W, Li C. Advances, challenges, and directions in shrimp disease control: the guidelines from an ecological perspective. *Appl Microbiol Biotechnol.* (2016) 100:6947–54. doi: 10.1007/s00253-016-7679-1
8. Gordon S. Phagocytosis: an immunobiologic process. *Immunity.* (2016) 44:463–75. doi: 10.1016/j.immuni.2016.02.026
9. Johansson MW, Keyser P, Sritunyalucksana K, Söderhäll K. Crustacean haemocytes and haematopoiesis. *Aquaculture.* (2000) 191:45–52. doi: 10.1016/S0044-8486(00)00418-X
10. Battison A, Cawthorn R, Horney B. Classification of *Homarus americanus* hemocytes and the use of differential hemocyte counts in lobsters infected with *Aerococcus viridans var. homari* (Gaffkemia). *J Invertebr Pathol.* (2003) 84:177–97. doi: 10.1016/j.jip.2003.11.005
11. Söderhäll I. Crustacean hematopoiesis. *Dev Comp Immunol.* (2016) 58:129–41. doi: 10.1016/j.dci.2015.12.009
12. Wu L, Söderhäll I, Kim YA, Liu HP, Söderhäll K. Hemocyte-lineage marker proteins in a crustacean, the freshwater crayfish, *Pacifastacus leniusculus*. *Proteomics.* (2008) 8:4226–35. doi: 10.1002/pmic.200800177
13. Lin X, Söderhäll I. Crustacean hematopoiesis and the astakine cytokines. *Blood.* (2011) 117:6417–24. doi: 10.1182/blood-2010-11-320614
14. Lavine MD, Strand MR. Insect hemocytes and their role in immunity. *Insect Biochem Mol Biol.* (2002) 32:1295–309. doi: 10.1016/S0965-1748(02)00092-9
15. Zhou YL, Gu WB, Tu DD, Zhu QH, Zhou ZK, Chen YY, et al. Hemocytes of the mud crab *Scylla paramamosain*: Cytometric, morphological characterization and involvement in immune responses. *Fish Shellfish Immunol.* (2017) 72:459–69. doi: 10.1016/j.fsi.2017.10.055
16. Lv S, Xu J, Zhao J, Yin N, Lu B, Li S, et al. Classification and phagocytosis of circulating haemocytes in Chinese mitten crab (*Eriocheir sinensis*) and the effect of extrinsic stimulation on circulating haemocytes *in vivo*. *Fish Shellfish Immunol.* (2014) 39:415–22. doi: 10.1016/j.fsi.2014.05.036
17. Sang HM, Fotedar R. Effects of mannan oligosaccharide dietary supplementation on performances of the tropical spiny lobsters juvenile (*Panulirus ornatus*, Fabricius 1798). *Fish Shellfish Immunol.* (2010) 28:483–9. doi: 10.1016/j.fsi.2009.12.011
18. Sung HH, Hwang SF, Tasi FM. Responses of giant freshwater prawn (*Macrobrachium rosenbergii*) to challenge by two strains of *Aeromonas spp*. *J Invertebr Pathol.* (2000) 76:278–84. doi: 10.1006/jipa.2000.4981
19. Chai YM, Zhu Q, Yu SS, Zhao XF, Wang JX. A novel protein with a fibrinogen-like domain involved in the innate immune response of *Marsupenaeus japonicus*. *Fish Shellfish Immunol.* (2012) 32:307–15. doi: 10.1016/j.fsi.2011.11.020
20. Li F, Chang X, Xu L, Yang F. Different roles of crayfish hemocytes in the uptake of foreign particles. *Fish Shellfish Immunol.* (2018) 77:112–9. doi: 10.1016/j.fsi.2018.03.029
21. Wang XW, Wang JX. Diversity and multiple functions of lectins in shrimp immunity. *Dev Comp Immunol.* (2013) 39:27–38. doi: 10.1016/j.dci.2012.04.009
22. Canton J, Neculai D, Grinstein S. Scavenger receptors in homeostasis and immunity. *Nat Rev Immunol.* (2013) 13:621–34. doi: 10.1038/nri3515
23. Dong Y, Dimopoulos G. Anopheles fibrinogen-related proteins provide expanded pattern recognition capacity against bacteria and malaria parasites. *J Biol Chem.* (2009) 284:9835–44. doi: 10.1074/jbc.M807084200
24. Dong Y, Taylor HE, Dimopoulos G. *AgDscam*, a hypervariable immunoglobulin domain-containing receptor of the *Anopheles gambiae* innate immune system. *PLoS Biol.* (2006) 4:e229. doi: 10.1371/journal.pbio.0040229
25. Luo T, Yang HF, Zhang X, Xu X. Purification, characterization and cDNA cloning of a novel lipopolysaccharide-binding lectin from the shrimp *Penaeus monodon*. *Dev Comp Immunol.* (2006) 30:607–17. doi: 10.1016/j.dci.2005.10.004
26. Zhang X, Pan L, Yu J, Huang H. One recombinant C-type lectin (*Lv*Lec) from white shrimp *Litopenaeus vannamei* affected the haemocyte immune response *in vitro*. *Fish Shellfish Immunol.* (2019) 89:35–42. doi: 10.1016/j.fsi.2019.03.029
27. Luo M, Yang L, Wang ZA, Zuo H, Weng S, He J, et al. A novel C-type lectin with microbiostatic and immune regulatory functions from *Litopenaeus vannamei*. *Fish Shellfish Immunol.* (2019) 93:361–8. doi: 10.1016/j.fsi.2019.07.047
28. Song F, Chen GL, Lu KC, Fan JQ, Yan MT, He HH, et al. Identification and functional characterization of a C-type lectin gene from *Litopenaeus vannamei* that is associated with ER-stress response. *Fish Shellfish Immunol.* (2019) 93:977–85. doi: 10.1016/j.fsi.2019.08.056
29. Liang ZW, Yang LW, Zheng JF, Zuo HL, Weng SP, He JG, et al. A low-density lipoprotein receptor (LDLR) class a domain-containing C-type lectin from *Litopenaeus vannamei* plays opposite roles in antibacterial and antiviral responses. *Dev Comp Immunol.* (2019) 92:29–34. doi: 10.1016/j.dci.2018.11.002
30. Wang XW, Zhao XF, Wang JX. C-type lectin binds to beta integrin to promote hemocytic phagocytosis in shrimp. *J Biol Chem.* (2014) 289:2405–14. doi: 10.1074/jbc.M113.528885
31. Wei X, Wang L, Sun W, Zhang M, Ma H, Zhang Y, et al. C-type lectin B (*Sp*CTL-B) regulates the expression of antimicrobial peptides and promotes phagocytosis in mud crab *Scylla paramamosain*. *Dev Comp Immunol.* (2018) 84:213–29. doi: 10.1016/j.dci.2018.02.016
32. Zhang XW, Wang Y, Wang XW, Wang L, Mu Y, Wang JX. A C-type lectin with an immunoglobulin-like domain promotes phagocytosis of hemocytes in crayfish *Procambarus clarkii*. *Sci Rep.* (2016) 6:29924. doi: 10.1038/srep29924
33. Chen DD, Meng XL, Xu JP, Yu JY, Meng MX, Wang J. *Pc*LT, a novel C-type lectin from *Procambarus clarkii*, is involved in the innate defense against *Vibrio alginolyticus* and WSSV. *Dev Comp Immunol.* (2013) 39:255–64. doi: 10.1016/j.dci.2012.10.003
34. Sen X, Lei W, Xian-Wei W, Yan-Ran Z, Wen-Jie B, Xiao-Fan Z, et al. L-Type lectin from the kuruma shrimp *Marsupenaeus japonicus* promotes hemocyte phagocytosis. *Dev Comp Immunol.* (2014) 44:397–405. doi: 10.1016/j.dci.2014.01.016
35. Hou FJ, Liu YJ, He SL, Wang XZ, Mao AT, Liu ZG, et al. A galectin from shrimp *Litopenaeus vannamei* is involved in immune recognition and bacteria phagocytosis. *Fish Shellfish Immunol.* (2015) 44:584–91. doi: 10.1016/j.fsi.2015.03.017
36. Kong T, Gong Y, Liu Y, Wen X, Tran NT, Aweya JJ, et al. Scavenger receptor B promotes bacteria clearance by enhancing phagocytosis and attenuates white spot syndrome virus proliferation in *Scylla paramamosian*. *Fish Shellfish Immunol.* (2018) 78:79–90. doi: 10.1016/j.fsi.2018.04.027
37. Yang MC, Shi XZ, Yang HT, Sun JJ, Xu L, Wang XW, et al. Wang. Scavenger receptor C mediates phagocytosis of white spot syndrome virus and restricts virus proliferation in shrimp. *PLoS Pathog.* (2016) 12:e1006127. doi: 10.1371/journal.ppat.1006127
38. Yang MC, Yang HT, Li J, Sun JJ, Bi WJ, Niu GJ, et al. Scavenger receptor C promotes bacterial clearance in kuruma shrimp *Marsupenaeus japonicus* by enhancing hemocyte phagocytosis and AMP expression. *Fish Shellfish Immunol.* (2017) 67:254–62. doi: 10.1016/j.fsi.2017.06.003
39. Bi WJ, Li DX, Xu YH, Xu S, Li J, Zhao XF, et al. Scavenger receptor B protects shrimp from bacteria by enhancing phagocytosis and regulating expression of antimicrobial peptides. *Dev Comp Immunol.* (2015) 51:10–21. doi: 10.1016/j.dci.2015.02.001
40. Wu YM, Yang L, Li XJ, Li L, Wang Q, Li WW. A class B scavenger receptor from *Eriocheir sinensis* (*Es*SR-B1) restricts bacteria proliferation by promoting phagocytosis. *Fish Shellfish Immunol.* (2017) 70:426–36. doi: 10.1016/j.fsi.2017.09.034
41. Li XJ, Yang L, Li D, Zhu YT, Wang Q, Li WW. Pathogen-specific binding soluble down syndrome cell adhesion molecule (Dscam) regulates phagocytosis via membrane-bound Dscam in crab. *Front Immunol.* (2018) 9:801. doi: 10.3389/fimmu.2018.00801
42. Sun JJ, Lan JF, Shi XZ, Yang MC, Yang HT, Zhao XF, et al. A fibrinogen-related protein (FREP) is involved in the antibacterial immunity of *Marsupenaeus japonicus*. *Fish Shellfish Immunol.* (2014) 39:296–304. doi: 10.1016/j.fsi.2014.05.005
43. Lu Y, Su F, Li Q, Zhang J, Li Y, Tang T, et al. Pattern recognition receptors in *Drosophila* immune responses. *Dev Comp Immunol.* (2020) 102:103468. doi: 10.1016/j.dci.2019.103468

44. Watson FL, Puttmann-Holgado R, Thomas F, Lamar DL, Hughes M, Kondo M, et al. Extensive diversity of Ig-superfamily proteins in the immune system of insects. *Science.* (2005) 309:1874–78. doi: 10.1126/science.1116887
45. Li D, Yu AQ, Li XJ, Zhu YT, Jin XK, Li WW, et al. Antimicrobial activity of a novel hypervariable immunoglobulin domain-containing receptor Dscam in *Cherax quadricarinatus*. *Fish Shellfish Immunol.* (2015) 47:766–76. doi: 10.1016/j.fsi.2015.10.025
46. Chou PH, Chang HS, Chen IT, Lee CW, Hung HY, Han-Ching Wang KC. *Penaeus monodon* Dscam (*Pm*Dscam) has a highly diverse cytoplasmic tail and is the first membrane-bound shrimp Dscam to be reported. *Fish Shellfish Immunol.* (2011) 30:1109–23. doi: 10.1016/j.fsi.2011.02.009
47. Chou PH, Chang HS, Chen IT, Lin HY, Chen YM, Yang HL, et al. The putative invertebrate adaptive immune protein *Litopenaeus vannamei* Dscam (*Lv*Dscam) is the first reported Dscam to lack a transmembrane domain and cytoplasmic tail. *Dev Comp Immunol.* (2009) 33:1258–67. doi: 10.1016/j.dci.2009.07.006
48. Wang J, Yang B, Wang W, Song X, Jiang Q, Qiu L, et al. The enhanced immune protection in Chinese mitten crab *Eriocheir sinensis* against the second exposure to bacteria *Aeromonas hydrophila*. *Front Immunol.* (2019) 10:2041. doi: 10.3389/fimmu.2019.02041
49. Wang X, Zhao Q, Christensen BM. Identification and characterization of the fibrinogen-like domain of fibrinogen-related proteins in the mosquito, *Anopheles gambiae*, and the fruitfly, *Drosophila melanogaster*, genomes. *BMC Genomics.* (2005) 6:114. doi: 10.1186/1471-2164-6-114
50. Pauwels M, Trost M, Beyaert R, Hoffmann E. Patterns, receptors, and signals: regulation of phagosome maturation. *Trends Immunol.* (2017) 38:407–22. doi: 10.1016/j.it.2017.03.006
51. Xu JD, Diao MQ, Niu GJ, Wang XW, Zhao XF, Wang JX. A small GTPase, RhoA, inhibits bacterial infection through integrin mediated phagocytosis in invertebrates. *Front Immunol.* (2018) 9:1928. doi: 10.3389/fimmu.2018.01928
52. Sayedyahossein S, Dagnino L. Integrins and small GTPases as modulators of phagocytosis. *Int Rev Cel Mol Biol.* (2013) 302:321–54. doi: 10.1016/B978-0-12-407699-0.00006-6
53. Zhao Z, Jiang CX, Zhang XB. Effects of immunostimulants targeting Ran GTPase on phagocytosis against virus infection in shrimp. *Fish Shellfish Immunol.* (2011) 31:1013–8. doi: 10.1016/j.fsi.2011.08.022
54. Zong RR, Wu WL, Xu JY, Zhang XB. Regulation of phagocytosis against bacterium by Rab GTPase in shrimp *Marsupenaeus japonicus*. *Fish Shellfish Immunol.* (2008) 25:258–63. doi: 10.1016/j.fsi.2008.05.006
55. Wang Q, Li H, Zhou K, Qin X, Wang Q, Li W. Rab7 controls innate immunity by regulating phagocytosis and antimicrobial peptide expression in Chinese mitten crab. *Fish Shellfish Immunol.* (2019) 95:259–67. doi: 10.1016/j.fsi.2019.10.037
56. Wu WL, Zong RR, Xu JY, Zhang XB. Antiviral phagocytosis is regulated by a novel rab-dependent complex in shrimp *Penaeus japonicus*. *J Proteome Res.* (2008) 7:424–31. doi: 10.1021/pr700639t
57. Ye T, Zong R, Zhang X. The role of white spot syndrome virus (WSSV) VP466 protein in shrimp antiviral phagocytosis. *Fish Shellfish Immunol.* (2012) 33:350–8. doi: 10.1016/j.fsi.2012.05.017
58. Liu WF, Han F, Zhang XB. Ran GTPase regulates hemocytic phagocytosis of shrimp by interaction with myosin. *J Proteome Res.* (2009) 8:1198–206. doi: 10.1021/pr800840x
59. Tassanakajon A, Amparyup P, Somboonwiwat K, Supungul P. Cationic antimicrobial peptides in *penaeid* shrimp. *Mar Biotechnol.* (2011) 13:639–57. doi: 10.1007/s10126-011-9381-8
60. Vaseeharan B, Shanthi S, Chen JC, Espineira M. Molecular cloning, sequence analysis and expression of Fein-Penaeidin from the haemocytes of Indian white shrimp *Fenneropenaeus indicus*. *Results Immunol.* (2012) 2:35–43. doi: 10.1016/j.rinim.2012.02.001
61. An MY, Gao J, Zhao XF, Wang JX. A new subfamily of penaeidin with an additional serine-rich region from kuruma shrimp (*Marsupenaeus japonicus*) contributes to antimicrobial and phagocytic activities. *Dev Comp Immunol.* (2016) 59:186–98. doi: 10.1016/j.dci.2016.02.001
62. Sun B, Wang Z, Zhu F. The crustin-like peptide plays opposite role in shrimp immune response to *Vibrio alginolyticus* and white spot syndrome virus (WSSV) infection. *Fish Shellfish Immunol.* (2017) 66:487–96. doi: 10.1016/j.fsi.2017.05.055
63. Deachamag P, Intaraphad U, Phongdara A, Chotigeat W. Expression of a phagocytosis activating protein (PAP) gene in immunized black tiger shrimp. *Aquaculture.* (2006) 255:165–72. doi: 10.1016/j.aquaculture.2006.01.010
64. Xu L, Pan L, Zhang X, Wei C. Effects of crustacean hyperglycemic hormone (CHH) on regulation of hemocyte intracellular signaling pathways and phagocytosis in white shrimp *Litopenaeus vannamei*. *Fish Shellfish Immunol.* (2019) 93:559–66. doi: 10.1016/j.fsi.2019.07.051
65. Tong R, Wei C, Pan L, Zhang X. Effects of dopamine on immune signaling pathway factors, phagocytosis and exocytosis in hemocytes of *Litopenaeus vannamei*. *Dev Comp Immunol.* (2019) 102:103473. doi: 10.1016/j.dci.2019.103473
66. Liu C, Wang J, Zhang X. The involvement of MiR-1-clathrin pathway in the regulation of phagocytosis. *PLoS ONE.* (2014) 9:e98747. doi: 10.1371/journal.pone.0098747
67. Shu L, Zhang X. Shrimp miR-12 suppresses white spot syndrome virus infection by synchronously triggering antiviral phagocytosis and apoptosis pathways. *Front Immunol.* (2017) 8:855. doi: 10.3389/fimmu.2017.00855
68. Shu L, Li CR, Zhang XB. The role of shrimp miR-965 in virus infection. *Fish Shellfish Immunol.* (2016) 54:427–34. doi: 10.1016/j.fsi.2016.04.129
69. Wang Z, Zhu F. MicroRNA-100 is involved in shrimp immune response to white spot syndrome virus (WSSV) and *Vibrio alginolyticus* infection. *Sci Rep.* (2017) 7:42334. doi: 10.1038/srep42334
70. Wang Z, Zhu F. Different roles of a novel shrimp microRNA in white spot syndrome virus (WSSV) and *Vibrio alginolyticus* infection. *Dev Comp Immunol.* (2018) 79:21–30. doi: 10.1016/j.dci.2017.10.002

Conflict of Interest: The authors declare that the research was conducted in the absence of any commercial or financial relationships that could be construed as a potential conflict of interest.

frontiers in Immunology

ORIGINAL RESEARCH
published: 20 March 2020
doi: 10.3389/fimmu.2020.00416

Phagocyte Transcriptomic Analysis Reveals Focal Adhesion Kinase (FAK) and Heparan Sulfate Proteoglycans (HSPGs) as Major Regulators in Anti-bacterial Defense of *Crassostrea hongkongensis*

Yue Lin[1,2], *Fan Mao*[1,3,4], *Nai-Kei Wong*[5], *Xiangyu Zhang*[1,2], *Kunna Liu*[1,2], *Minwei Huang*[1,3,4], *Haitao Ma*[1,3,4], *Zhiming Xiang*[1,3,4], *Jun Li*[1,3,4], *Shu Xiao*[1,3,4], *Yang Zhang*[1,3,4]* and *Ziniu Yu*[1,3,4]*

[1] CAS Key Laboratory of Tropical Marine Bio-resources and Ecology, Guangdong Provincial Key Laboratory of Applied Marine Biology, South China Sea Institute of Oceanology, Chinese Academy of Science, Guangzhou, China, [2] University of Chinese Academy of Sciences, Beijing, China, [3] Innovation Academy of South China Sea Ecology and Environmental Engineering (ISEE), Chinese Academy of Sciences, Guangzhou, China, [4] Southern Marine Science and Engineering Guangdong Laboratory, Guangzhou, China, [5] National Clinical Research Center for Infectious Diseases, Shenzhen Third People's Hospital, The Second Hospital Affiliated to Southern University of Science and Technology, Shenzhen, China

OPEN ACCESS

Edited by:
Xinjiang Lu,
Ningbo University, China

Reviewed by:
James L. Stafford,
University of Alberta, Canada
Linlin Zhang,
Institute of Oceanology (CAS), China
George N. Tzanakakis,
University of Crete, Greece

***Correspondence:**
Yang Zhang
yzhang@scsio.ac.cn
Ziniu Yu
carlzyu@scsio.ac.cn

Specialty section:
This article was submitted to Comparative Immunology, a section of the journal Frontiers in Immunology

Received: 02 December 2019
Accepted: 24 February 2020
Published: 20 March 2020

Citation:
Lin Y, Mao F, Wong N-K, Zhang X, Liu K, Huang M, Ma H, Xiang Z, Li J, Xiao S, Zhang Y and Yu Z (2020) Phagocyte Transcriptomic Analysis Reveals Focal Adhesion Kinase (FAK) and Heparan Sulfate Proteoglycans (HSPGs) as Major Regulators in Anti-bacterial Defense of Crassostrea hongkongensis. Front. Immunol. 11:416. doi: 10.3389/fimmu.2020.00416

Invertebrates generally lack adaptive immunity and compensate for this with highly efficient innate immune machineries such as phagocytosis by hemocytes to eradicate invading pathogens. However, how extrinsically cued hemocytes marshal internal signals to accomplish phagocytosis is not yet fully understood. To this end, we established a facile magnetic cell sorting method to enrich professional phagocytes from hemocytes of the Hong Kong oyster (*Crassostrea hongkongensis*), an ecologically and commercially valuable marine invertebrate. Transcriptomic analysis on presorted cells shows that phagocytes maintain a remarkable array of differentially expressed genes that distinguish them from non-phagocytes, including 352 significantly upregulated genes and 479 downregulated genes. Pathway annotations reveal that focal adhesion and extracellular matrix–receptor interactions were the most conspicuously enriched pathways in phagocytes. Phagocytosis rate dramatically declined in the presence of an FAK inhibitor, confirming importance of the focal adhesion pathway in regulating phagocytosis. In addition, we also found that heparan sulfate proteoglycan (HSPG) families were lineage-specifically expanded in *C. hongkongensis* and abundantly expressed in phagocytes. Efficiency of phagocytosis and hemocytes aggregation was markedly reduced upon blockage of endogenous synthesis of HSPGs, thus implicating these proteins as key surface receptors in pathogen recognition and initiation of phagocytosis.

Keywords: phagocytes, heparan sulfate proteoglycans (HSPGs), focal adhesion kinase (FAK), transcriptome, *Crassostrea hongkongensis*

INTRODUCTION

Phagocytes are crucial executors in innate host defense against invading microbial pathogens, including bacteria and fungi (1, 2). In mammals, neutrophils and macrophage constitute the bulk of these frontline defenders mediating diverse immunological processes including recognition, engulfment, and elimination of microbes (3–5). Impairment of phagocytic functions is often associated with microbial infections and could bring adverse consequences to pathogen replication, immune evasion, and host mortality (6). In teleosts, B lymphocytes were demonstrated to possess potent phagocytic and bactericidal capacities, implying incomplete hemocytopoiesis in the lower vertebrates (7, 8). In contrast, invertebrates have a simple but robust innate immune system to cope with dynamically evolving immune challenges (9, 10). Emerging evidences suggest that circulating hemocytes are indispensable to innate immune response, nutrition, wound healing, detoxification, and even shell mineralization (11, 12). Essentially, surveillance and elimination of pathogens depend heavily on phagocytic capacities of hemocytes, whose efficiency in containing and killing pathogens is intimately tied to disease resistance of individual hosts (13).

Over the past decade, substantial progress has been made on the molecular mechanisms underlying aspects of phagocyte immunity, such as pathogen recognition, phagocytic degradation, and immune evasion in mammals (14, 15). To illustrate, phagocytes can migrate toward infection sites through chemotaxis. Several chemokine receptors, such as C-X-C chemokine receptors and G protein–coupled receptors, are involved in sensing chemotactic ligands and initiating signaling transduction in host cells (16, 17). Consequently, pathogen-recognition receptors (PRRs) on phagocyte membranes recognize specific pathogen-associated molecular patterns and trigger off events leading to phagocytosis, phagosome maturation, and degradation of pathogen components (18). Generally, the Toll-like receptor, C-type lectin receptor, and NOD-like receptor are engaged as the principal phagocyte PRRs involved in initiation of an immune response (19–22). Furthermore, phagosome maturation is mediated by Rab GTPases, which drive the formation of phagolysosomes and lysosomal fusion to enable antimicrobial activities via toxic oxidants and proteolytic enzymes (23). However, despite extensive investigation on the molecular basis of mammalian phagocytic functions, systematic and comprehensive studies on immune processes in invertebrate phagocytes are still wanting.

Recent evidence shows that efficiency of phagocytosis is varied in different lineages (24, 25). Among them, filter-feeding species such as bivalves have the most efficient phagocytes (26, 27), providing an excellent model for investigating phagocyte immunity in lower invertebrates. Notably, the Hong Kong oyster (*Crassostrea hongkongensis*) is an edible bivalve species endemic to estuarine and coastal regions of the South China Sea, with an aquacultural history of more than 700 years (28). As a sessile bivalve species, *C. hongkongensis* lives by filtering seawater and is prone to pathogenic infections due to prevalence of microbes in the estuarine regions (29). Therefore, the oyster has evolved an efficient host defense system with high phagocytic activities to safeguard its survival within ecologically dynamic environments (30). Recently, advances in omics studies on the evolutionarily close *Crassostrea gigas* have demonstrated that lysosomal protease cathepsin L is one of the key contributors to pathogen killing in hemocytes (31). However, the other important events including pathogen recognition and activation of signaling pathways in phagocytes remain underexamined in oysters. In this study, *C. hongkongensis* phagocytes were systematically isolated by means of magnetic latex beads for cell sorting, and subsequent transcriptomic analysis provided a fuller picture on the molecular basis of phagocyte-dependent host defense. To highlight, the heparan sulfate proteoglycans (HSPGs) family was lineage-specifically expanded and enriched in expression in *C. hongkongensis* phagocytes, implying a crucial role for such surface receptors in bacterial recognition and phagocytosis initiation. In addition, we also found that focal adhesion kinase (FAK) signaling is a highly active process subserving key phagocytic functions including productive phagocytosis in oysters.

MATERIALS AND METHODS

Animal Culture and Hemocyte Preparation

Crassostrea hongkongensis specimens consisted of 2-year-old healthy individuals with an average weight of 100 g and a shell height of 10.00 ± 0.05 cm. All samples were collected from a local breeding farm in Zhanjiang, China. Oysters were cultivated in aerated sand-filtered seawater for at least 1 week before experiments, and the culture was maintained at 22°C. Oysters were fed with *Tetraselmis suecica* and *Isochrysis galbana* every other day for 1 week prior to use. All experimental manipulations were performed in accordance with local guidelines on care and use of laboratory animals. Oyster hemolymph was extracted from cardiocoelom of the oysters by using a medical-grade syringe (0.45 × 15.5 mm) and hemolymph from each individual counted toward one sample. Samples were stored on ice and added to an equal volume of marine anticoagulant (MAC1; 0.1 M glucose, 15 mM trisodium citrate, 13 mM citric acid, 10 mM EDTA, 0.45 M NaCl, pH 7.0) to prevent coagulation. Physiological status of hemocytes was assessed under a light microscope (EVOS FL) to determine their suitability for subsequent experiments.

Cell Sorting Assay With Magnetic Beads

Thirty-six oysters were randomly divided into groups in triplicates. Hemocytes in suspension were gathered as ∼1 mL hemolymph per oyster into a 15 mL centrifuge tube (Corning, New York, USA). Cells were incubated with glucan coated magnetic beads (Micromod, Rostock, Germany), which are made of an iron oxide core with a diameter of 1.5 μm, at a ratio of 50 (i.e., 50 beads per cell). After 30 min of incubation, cells were resuspended in 20 mM HEPES solution (Sangon Biotech, Shanghai, China). Cells that had engulfed magnetic beads were absorbed to the tube wall by a magnetic grate, whereas other cells remained in the liquid phase. Cells from the liquid phase were transferred into a separate tube for analysis of phagocytosis. Then, magnetically retained cells were washed three times with HEPES solution. Cells exhibiting phagocytic

properties toward magnetic beads were collected as a sample of phagocytes. Subsequently, all hemocytes were harvested as a pellet by centrifugation at 300 g at 4°C for 10 min.

Library Construction and RNA-seq

Total RNA was extracted from hemocytes without lymph by using TriZol reagent (Invitrogen, California, America) according to manufacturer's instructions. Cells were ground in liquid nitrogen in a 2-mL tube, followed by homogenization for 2 min. The homogenate was centrifuged for 5 min, at 12,000 g at 4°C. Then, the supernatant was mixed with 0.3 mL chloroform/isoamyl alcohol (24:1), which was equilibrated with gentle shaking for 15 s, followed by centrifugation at 12,000 g at 4°C for 10 min. After centrifugation, RNA retained in the upper aqueous phase was recovered and transferred into a new tube with as the supernatant to which was added an equal volume of isopropyl alcohol, followed by centrifugation at 12,000 g for 10 min at 4°C. Upon removal of the supernatant, RNA pellet was washed twice with 1 mL prechilled 75% ethanol. The mix was centrifuged at 12,000 g at 4°C for 5 min. Residual ethanol was discarded, followed by air drying of the pellet for 5 to 10 min in a biosafety cabinet. Finally, 25 to 100 μL of DEPC-treated water was added to dissolve RNA. Total RNA was assessed for quality and quantified by using NanoDrop 2000 and Agilent Technologies 2100 bioanalyzer (Thermo Fisher Scientific, Massachusetts, USA). For reverse transcription into cDNA, oligo(dT)-attached magnetic beads were used to purify mRNA and deplete rRNA. Purified mRNA was fragmented into small pieces with fragment buffer. First-strand cDNA was generated by using random N6 primer and hexamer-primed reverse transcription, followed by second-strand cDNA synthesis. Subsequently, cDNA fragments obtained from previous steps were amplified by polymerase chain reaction (PCR), and products were purified by Ampure XP beads (Beckman Coulter, California, USA) and eluted in EB solution. The final products were validated in an Agilent Technologies 2100 bioanalyzer for quality control. Double-stranded PCR products from previous steps were heated for denaturing and circularized by a splint oligo sequence to accomplish the final library. Single-strand circle DNA was formatted as the final library, which was amplified to make DNA nanoballs comprising more than 300 copies of one molecule. DNA nanoballs were loaded into the patterned nanoarray, and single-end 50 bases reads were generated on a BGI seq500 platform (BGI, Shenzhen, China). All raw data were submitted to the NCBI database with the accession number SRR10531303–SRR10531311.

Bioinformatics Analysis

Based on algorithms of the software SOAPnuke, clean reads were isolated from raw data and saved in FASTQ format in preparation for quantitative analysis. These clean reads were mapped onto a *C. hongkongensis* transcriptome database by using Bowtie2 (32), and mapped reads subsequently were summarized and normalized to RPKM by means of the RESM software (33). In addition, R cor was used to calculate the Pearson correlation coefficients of the samples. Principal components analysis was performed by using princomp. Differentially expressed genes (DEGs) were tested for statistical significance by DEseq2 methods, based on negative binomial distribution with the following threshold settings: fold change $\geq$2.00 and adjusted $p < 0.05$ (34). Further, the genes were subjected to analyses with Gene Ontology (35) and KEGG Orthology (36). Gene Ontology functional enrichment was also performed by utilizing phyper of R and *p*-value. Finally, false discovery rate (FDR) was calculated for each *p*-value, and we defined FDR <0.01 as significantly enriched (37). Amino acid sequences of HSPGs orthologs in the target species were obtained by homologous Blast with the NCBI database. The GenBank accession numbers corresponding to the HSPG sequences analyzed are as listed in **Supplementary Table 4**. A phylogenetic tree was constructed with Clustal Omega (https://www.ebi.ac.uk/Tools/msa/) by the neighbor-joining method and analyzed with Interactive Tree of Life program, iTOL (http://itol.embl.de/). Protein domains and signal peptides were predicted with Simple Modular Architecture Research Tool (SMART), version 4.0 (http://smart.embl-heidelberg.de/).

Flow Cytometric Analysis

Approximately 10^5 hemocytes were plated to six-well plates and supplemented with an equal volume of lymph and left for further culture for 20 min. Then, live *Escherichia coli* with a green fluorescent protein (GFP) plasmid was added into the wells to achieve an MOI (multiplicity of infection) of 50. After 30 min, the antibiotic gentamicin (50 μg/mL) was added to kill off non-engulfed bacteria outside host cells, for incubation for 10 min (38). Cells were then washed three times with 20 mM HEPES solution (Sangon Biotech, Shanghai, China). Finally, cells were resuspended to detect the GFP fluorescence intensity by Guava easyCyte 5HT flow cytometer (Guava Technologies, California, USA). Cells were selected from the cyclized gate to remove cell debris. And all the conditions were adjusted to the proper level. Following step collected 10,000 hemocytes and was analyzed by FlowJo-V10 software (New Jersey, USA), in which three biological repeats were guaranteed for each group, and one group of hemocytes without any treatment was set as negative control.

Validation of Biological Effects via Pharmacological Inhibition of Proteins

The inhibitors served as the specific blocker to suppress the function of HSPGs and FAK. Heparin (MedChemExpress, New Jersey, USA) and chlorate (J&K Scientific, Beijing, China) were the common inhibitors for decreasing expression of HSPG, and PF-573228 (Selleck Chemicals, Houston, USA) did that for FAK. Experiment set three kinds of concentration gradients to treat the hemocytes; each group was disposed with the same amount of time. Focal adhesion kinase inhibitor solution (concentration: 0, 1, 5, 10 μM) was dissolved in 20 mM HEPES solution and incubated with hemocytes for 30 min. Chlorate as an HSPG specific inhibitor could work after 2-h treatment in hemocytes. Its concentration gradient was set for four groups, 0, 1, 5, and 10 mM, respectively. But heparin was diluted by HEPES solution for final concentrations, 0, 10, 20, and 40 μM, incubating with cells for 30 min. Following that the hemocyte was stimulated by the GFP fluorescent bacteria for 30 min, the data of fluorescent

intensity from cells was acquired by flow cytometry to figure out the proper concentration and the effect of these three factors, when the experimental group was compared to the control.

Confocal Microscopy

Prior to phagocytic experiment, hemocytes were cultured in Petri dish for 20 min. Afterward, the hemocytes were subject to different treatment with the three kinds of inhibitors at the proper concentrations, respectively, of which sodium chlorate is a metabolic inhibitor to prevent proper sulfation of HSPGs, whereas heparin is a glycosaminoglycan (GAG) competitively inhibiting tau binding to HSPGs. Then, removing the drug, the GFP fluorescence bacteria (the proportion with the cells 50:1) were added into the dish to stimulate the hemocytes starting phagocytosis. Half an hour later, the gentamicin solution was used to kill bacteria that were outside of cells; further washing buffer removed the extra bacteria. Then, the hemocytes were fixed for 20 min in 4% paraformaldehyde dissolved in phosphate-buffered saline. HEPES solution was used to wash the cells before the cell nucleus of hemocyte was stained by DAPI (Sigma, California, USA) excited by the violet (405 nm) laser line; the cytomembrane was fluorescent red by Dil (Beyotime, Shanghai, China) excited by the violet (549 nm) laser line. Confocal microscopy was performed to image the difference of these two groups compared to the control. After hemocytes were incubated with red fluorescent beads, confocal microscopy captured the pictures to illustrate the cellular morphology, and ImageJ (Maryland, USA) calculated the fluorescent intensity. For aggregation test, hemocytes were transferred into Petri dishes for 20 min. Then, heparin and chlorate made the HSPG loss activity after treatment; the cell nucleus was fluorescent blue by DAPI, and the cytomembrane was fluorescent red by Dil. Confocal microscopy took the images for analyzing the significant difference of aggregation among these data. The software ImageJ assisted in analyzing the image data.

Statistical Analysis

Statistical analysis was performed with GraphPad Prism 8 (GraphPad Software Inc., San Diego, California, USA), and values were expressed as mean ± SD. Statistical significance of differences between the control and treated groups was determined by Student *t*-test or one-way analysis of variance. Differences determined at $^{*}p < 0.05$, $^{**}p < 0.01$ or $^{***}p < 0.001$ were considered significant.

RESULTS

Isolation of Oyster Phagocytes by Magnetic Bead Sorting

A cell sorting assay based on magnetic beads was used to separate phagocytes and non-phagocytes from total hemocytes, in which magnetic-enriched cells were considered as phagocytes, and non-enriched cells were non-phagocytes (**Figure 1**). Our results showed that 87.6 to 91.7% of magnetically sorted phagocytes engulfed at least one magnetic beads, whereas only no more than 5% of non-phagocytes contained them (**Supplementary Figure 1**). Meanwhile, we also observed that the majority of the phagocytes were composed of granulocytes (82.8%) with hyalinocytes as a minority, which suggests that a small proportion of hyalinocytes could participate in phagocytic defense.

Transcriptomic Analysis of Regulatory DEGs in Phagocytes

A series of RNA-seq libraries were constructed from phagocytes, non-phagocytes, and hemocytes, each group consisting of three biological replicates. Further sequencing and low-quality filtration, each one obtained about 23.8 million clean reads, which were mapped onto a Hong Kong oyster genome (unpublished data) as the reference. Percentages of total mapped reads approached 76.18–80.19%, whereas percentages of unique mapped reads were about 71.34–74.53% (**Supplementary Materials**). Pearson correlation analysis of total expression profiles reveals that there is a high correlation within each group, supporting the reliability of biological replicates (**Figure 2A**). Principal component analysis further reveals that phagocytes had distinct expression profiles vs. that of non-phagocytes (**Figure 2B**). Next, we pinpointed DEGs of phagocytes through comparisons with non-phagocytes. A total of 831 DEGs comprising 352 upregulated genes and 479 downregulated genes were found (**Figure 2C**, **Supplementary Table 2**). Remarkably, several signaling pathways, in particular, focal adhesion (48 genes, rich factor 3.38, $p = 1.19 \times 10^{-13}$), extracellular matrix (ECM)–receptor interaction (29 genes, rich factor 3.94, $p = 2.93 \times 10^{-10}$), PI3K-Akt signaling pathway (33 genes, rich factor 2.54, $p = 8.86 \times 10^{-7}$), and tumor necrosis factor signaling pathway (19 genes, rich factor 3.38, $p = 3.67 \times 10^{-6}$) were significantly enriched in professional phagocytes, suggesting the coordinated nature of these regulatory genes in oyster phagocytes (**Figure 2D**, **Supplementary Table 3**).

Focal Adhesion Signaling Pathway Is Active in Phagocytes and Regulates Phagocytic Capacity

Focal adhesion is one of significantly enriched signaling pathways with highest confidence values as mentioned previously. Indeed, 25 of DEGs were included, and 21 of them were significantly high expression in phagocytes, highlighting the active focal adhesion signaling pathway in oyster phagocytes (**Figure 3A**). Specifically, two of FAKs, one of P130Cas, and eight of filamins (seven of filamin A and one of filamin C) were identified, and they constituted the key components of this pathway (**Figure 3A**). Within this pathway, FAK is an indispensable member that orchestrates exogenous signaling to instruct cell behaviors. To validate whether FAK controls phagocytic capacities of oyster hemocytes, the FAK-specific inhibitor PF-573228 was used to block activation of FAK signaling. Results show that PF-573228 suppressed the phagocytic abilities of hemocytes in a dose-dependent manner, with a 0.34- and 0.44-fold change in phagocytic ability being elicited by the inhibitor at 5 and 10 μM, respectively (**Figure 3B**), implying a crucial role of FAK in phagocyte activation.

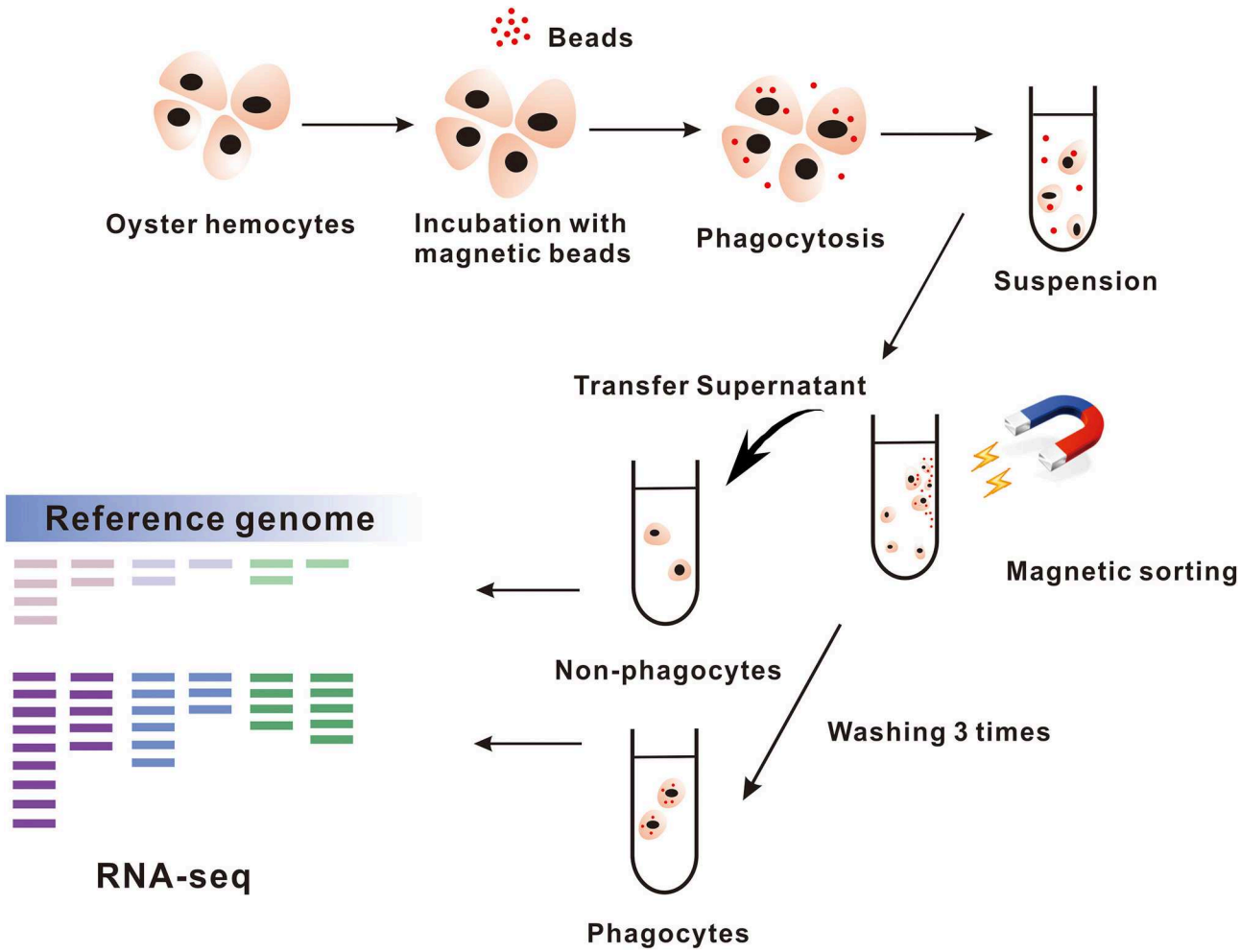

FIGURE 1 | The process of magnetic beads sorting phagocytes. The hemocytes in *Crassostrea hongkongensis* are gathered for incubating with magnetic beads and then sorted by magnetic grate. The cells remaining in supernatant are the non-phagocytes. Transcriptome analyzes the samples of phagocytes and non-phagocytes.

HSPGs Are Lineage-Specifically Expanded and Abundantly Expressed in Phagocytes

Another significantly enriched pathway is an ECM–receptor interaction pathway with secondary high confidence value (2.93E-10). Heatmap showed that a total of 29 DEGs were involved in ECM–receptor interaction, and 75.86% (22/29) were dominantly expressed in the phagocytes, among which three main matrix proteins were found to be eight of HSPGs, two of integrins, and four of collagens (**Figure 4A**). Strikingly, the structure organization showed that HSPG contains massive tandem IG domain, suggesting its possible function in bacterial recognition and immune regulation (**Figure 4B**). Moreover, phylogenetical analysis indicated that members of HSPG family are clustered into lineage-specific clades, strongly implying lineage-specific expansion of HSPGs in mollusks (**Figure 4C**). Additionally, eight of HSPGs in *C. hongkongensis*, seven of HSPGs in *Crassostrea virginica*, and seven of HSPGs in *C. giags* were also clustered into species-specific clades except for *Ch*HSPGX5, suggesting that the HSPG family was recently expanded after oyster speciation (**Figure 4C**). Taken together, specific expansion and dominant expression of HSPGs in oyster phagocytes highlight its essential role in innate defense.

Blockade of Phagocytosis and Aggregation by HSPG Inhibitors in Hemocytes

To examine the exact roles of HSPGs in oyster hemocytes, two chemical inhibitors, chlorate and heparin, were utilized to assess the effects of HSPGs on hemocyte function. Flow cytometry analysis shows that chlorate, an inhibitor for prevention of HSPGs sulfation, significantly decreased by 0.55- and 0.76-fold of phagocytic activities at concentrations of 1 to 10 mM (**Figure 5A**). Similarly, the other competitive inhibitor of HSPG, heparin, also demonstrated strongly suppressive effect on phagocytic ability of hemocytes, which obviously reduced 0.66- and 0.85-fold when treated at 10 to 40 μM (**Figure 5B**). Meanwhile, the inhibitory effects of chlorate and heparin on the phagocytic activities were confirmed by observations in confocal microscopy, where the concentrations used for chlorate

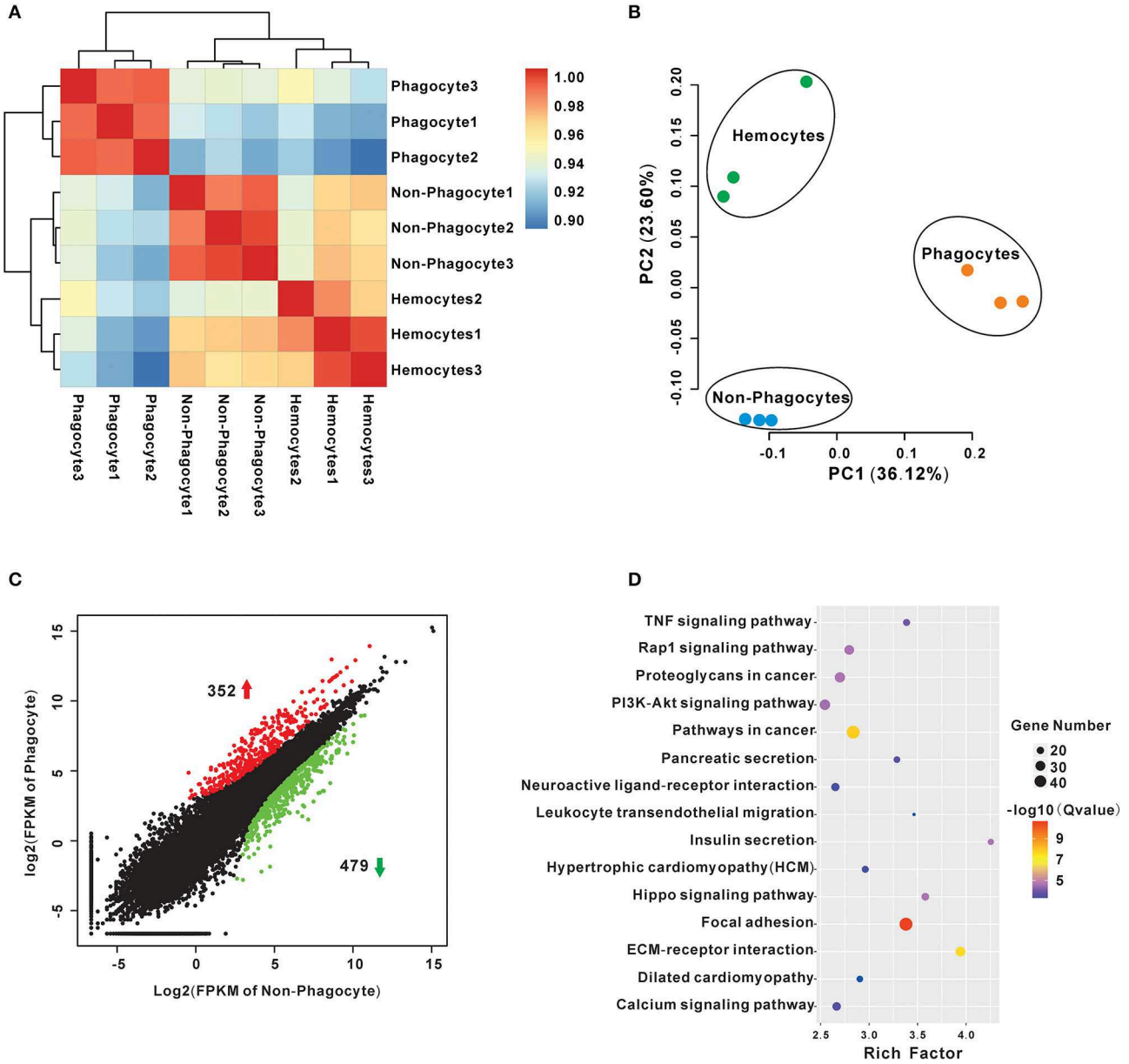

FIGURE 2 | Transcriptome analysis of differences between *Crassostrea hongkongensis* phagocytes and non-phagocytes. **(A)** Transcript expression profiles of hemocytes were analyzed by means of RNA-seq quantification. The heatmap shows the square of correlation among phagocyte, non-phagocyte, and hemocyte group. Each sample contains three independent biological replicates. **(B)** Principal components analysis plots of gene expression for the three groups of hemocytes using the normalized transcriptome expression. Each group was represented by different-color dots: green for hemocytes, orange for phagocytes, and blue for non-phagocytes. **(C)** Identification of DEGs between phagocytes and non-phagocytes. The red dots show genes were significantly upregulated in phagocytes, whereas the green dots denote downregulated genes. **(D)** KEGG enrichment analysis of DEGs between phagocytes and non-phagocytes. The scatterplots illustrate the DEGs enriched in many functional pathways. The enrichment factor of this figure is the ratio of the DEGs number to that of total sample; the dot size denotes the number of DEGs with different colors that are according to the *q*-value range.

and heparin were 1 mM and 10 μM, respectively (**Figure 5C**). Additionally, HSPG inhibitors also had clear effects on the aggregation of hemocytes. Compared to resting hemocytes, treatment with either chlorate (1 mM) or heparin (10 μM) resulted in a decrease of 55.6 and 84.2% aggregation of hemocytes, respectively (**Figure 6**).

DISCUSSION

Phagocytes in vertebrate or invertebrates are uniquely endowed with a powerful antimicrobial apparatus, which is characterized by efficient engulfment and subsequent destruction of invading pathogens during phagocytosis (39). In bivalves including *C.*

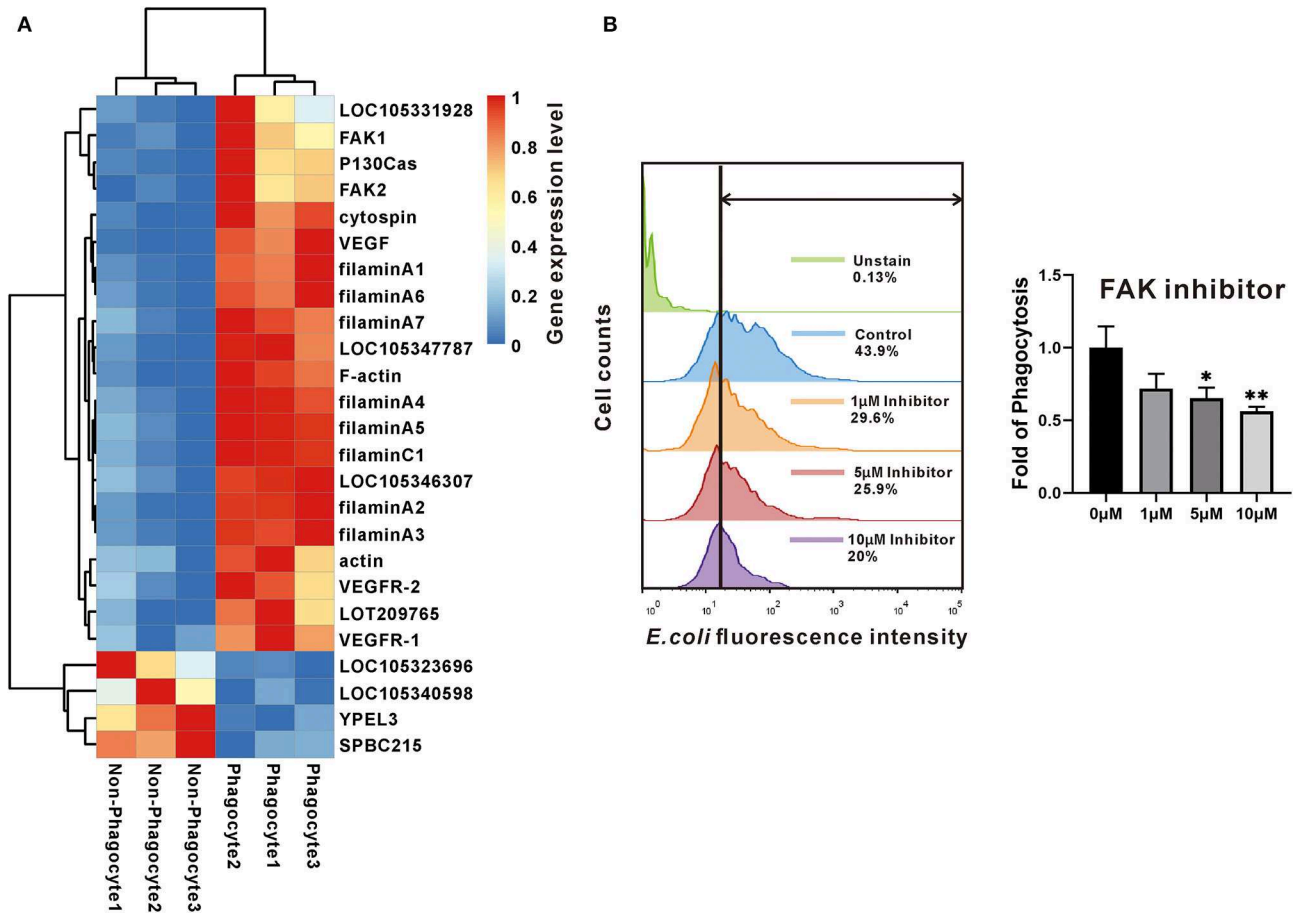

FIGURE 3 | The expression and effect of FAK in phagocytes. **(A)** The heatmap chart used the changes in colors to show differences of the gene expression level between phagocytes and non-phagocytes. **(B)** The effect of FAK in phagocytosis. Flow cytometry determined the fluorescence intensity that hemocytes contained. Green shows the data of negative control; blue is the normal control; orange, red, and purple show the experimental samples that were treated with different concentrations of inhibitor. While the bar chart compares the fold of phagocytotic ability among the four groups that were under concentration gradient of FAK inhibitor. The bars indicated the fold of phagocytosis. The amount relative to the internal control is expressed as mean ± SD ($n = 3$). Significant differences relative to control were indicated (*P <0.05 and **P < 0.01).

hongkongensis, hemocytes populating the circulatory system make up an expert cell population dedicated to innate immune defense. Conventionally, these have been classified into at least two hemocyte subtypes, granulocytes and hyalinocytes, on grounds of morphology and function (40, 41). Although granulocytes are typically more active in phagocytic activities and reactive oxygen species production compared with hyalinocytes (42), growing evidence suggests that fractions of hyalinocytes also possess capacities for phagocytosis and clearing foreign particles or pathogens (43, 44). In all cases, elucidating the exact mechanisms of phagocytic defense necessitates reliable isolation of phagocytes from a complex mélange of hemocytes having an apparent continuum of differentiation status. To set out for this task, we first successfully isolated the phagocytes from oyster hemocytes by means of cell sorting with magnetic latex beads, which is an efficient and convenient isolation approach widely used in studies on neuronal and megakaryocytic cells (45, 46).

In transcriptomic analysis on phagocyte activation, two significantly enriched and functionally related major pathways, focal adhesion and ECM–receptor interaction, emerged with the highest statistical confidence. Characteristically, the ECM consists in part of secreted extracellular macromolecules, including collagen fibers, proteoglycans, and adhesive matrix proteins (47, 48). Consequently, ECM forms an essential microenvironment to provide a structurally and biochemically dynamic scaffold for surrounding cells, with vital regulatory roles such as cellular communication, cell migration, growth, and differentiation (49). Moreover, accumulating evidence shows that ECM function is instrumental to many facets of host immunity such as phagocytosis, aggregation, and endocytosis in both vertebrates and invertebrates (50–53). For instance, integrin-dependent phagocytosis has been identified in many invertebrate species, including shrimp (54), phylum Cnidaria (55), *Geodia cydonium* (56), *Mytilus trossulus* (57), and *C. gigas* (58). As a molecular pattern recognition receptor, integrin has

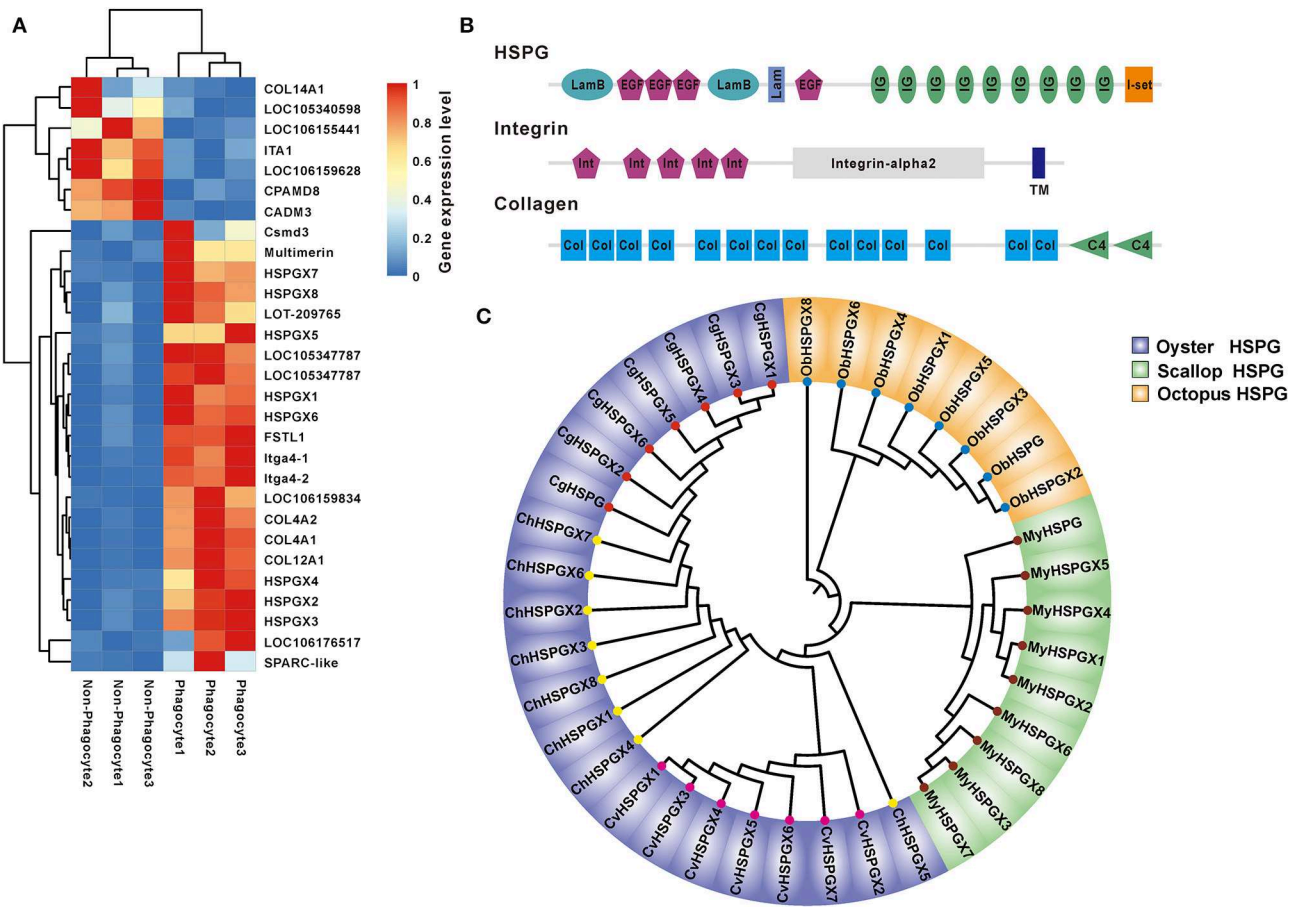

FIGURE 4 | The expression and bioinformatics analysis of HSPGs. **(A)** The heatmap presents the expression level of ECM–receptor interaction in phagocytes and non-phagocytes. **(B)** The domain architecture of HSPG, integrin, and collagen. **(C)** Phylogenetic analysis of mollusk HSPGs, which include *Crassostrea gigas*, *Crassostrea virginica*, *Crassostrea hongkongensis*, *Mizuhopecten yessoensis*, and *Octopus bimaculoides*. The neighbor-joining phylogenetic tree was constructed with 1,000 replications of bootstrap.

been reported to mediate invasion of *Vibrio splendidus* LGP32 into hemocytes of *C. gigas*, illustrating the multilayered function of integrin in phagocyte promotion or pathogen invasion (38, 59). Indeed, high abundance of integrin was invariably observed in oyster phagocytes, consistent with its functional importance.

Moreover, FAK, another significantly enriched pathway in phagocytes, has been recognized as a regulator centrally linking integrin signaling to cell response, including cytoskeleton remodeling, cell migration, and phagocytosis (60, 61). Two orthologs of FAKs are present in the transcriptomics of *C. hongkongensis*, both of which showed significantly high transcriptional expression in activated phagocytes. Functional validation demonstrates that phagocytic rate dramatically declined upon treatment with an FAK inhibitor, confirming the engagement of FAK in the regulation of phagocytosis in oyster hemocytes. According to the focal adhesion pathway, not only FAK was upregulated, but also its partners, integrin, filamin A, and P130cas, have high expression in phagocytes. Focal adhesion kinase as a cytoplasmic tyrosine kinase is typically activated by interaction with integrins at sites of focal contact, leading to reorganization of cytoskeleton with downstream factors, such as p130Cas and filamin A, to promote phagocytosis (62–64) (**Figure 7**). Interestingly, high FAK expression was also observed during the late-stage tumorigenesis in human, which implicates critical role of FAK in cancer progression and metastasis (65). Given that cancer cells and phagocytes share some common capacities such as high motility and infiltration, FAK signaling may be mechanistically exploited as a conserved pathway in those distinct cell models.

Quite strikingly, eight members of HSPGs are found to be lineage-specifically expanded and predominantly expressed in phagocytes, strongly supporting an important role of HSPG in activated phagocytes. Heparan sulfate proteoglycans are a family of typical proteoglycans with one or more covalently attached heparan sulfate (HS) chains (66, 67). Substantial studies show that HSPGs can act as versatile regulators in diverse signaling pathways, including Wnt, Hedgehog, and transforming growth factor β, thus impacting cell functions in development, cell migration, and autophagy (68–70). Moreover, HSPGs have been found to operate as cell surface receptors to mediate endocytosis

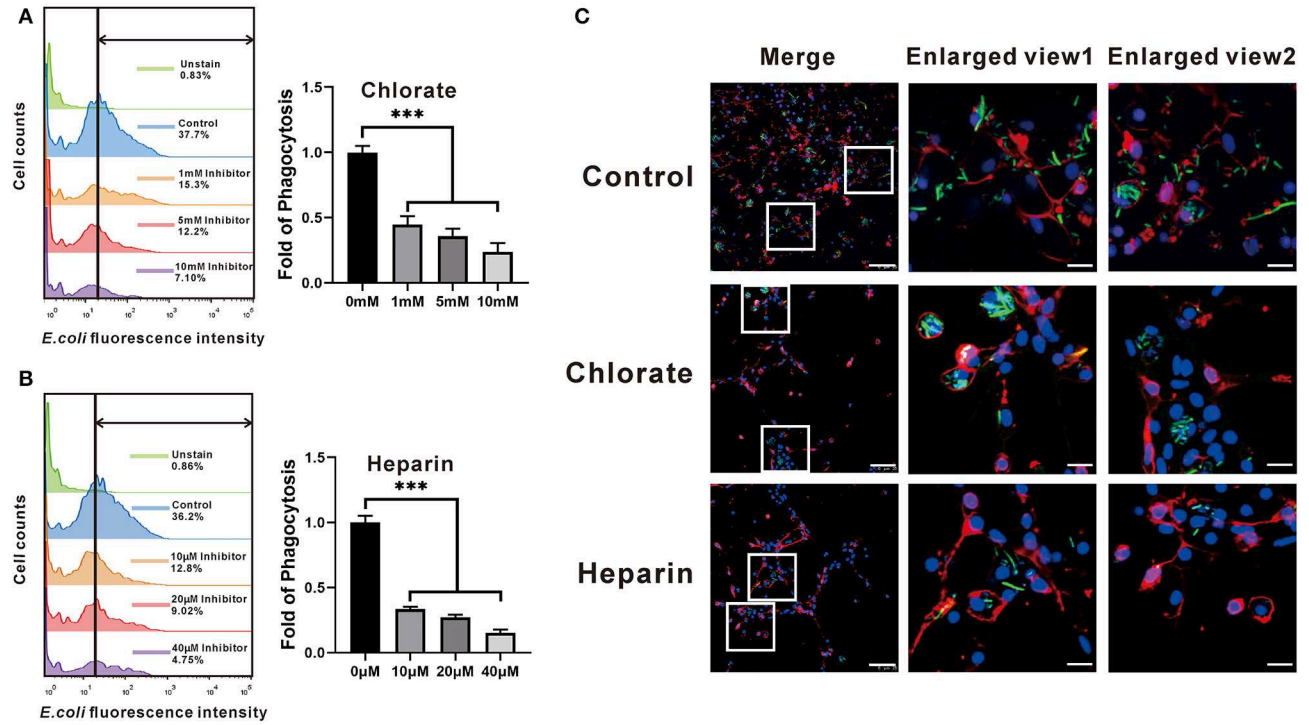

FIGURE 5 | Comparison of the phagocytotic ability among the four groups that had different expressions of HSPG. The expression of HSPG was reduced by the specific inhibitors, chlorate **(A)** and heparin **(B)**. The changes of fluorescence intensity that hemocytes contained were detected by flow cytometry. And the bar charts compare the phagocytotic ability of different groups in fold. The bars indicate the fold of phagocytosis. The amount relative to the internal control is expressed as mean ± SD ($n = 3$). Significant differences relative to control were indicated (***$P < 0.001$). **(C)** The phagocytotic function of HSPG on the phagocytes. The figures show the phagocytotic changes of hemocytes that were captured by confocal microscopy. The DAPI represents the nuclear; the dye of Dil shows the position of cell membrane; the green fluorescence is on behalf of bacteria. The scale bar of enlarged views is 5 μM; the others are 25 μM.

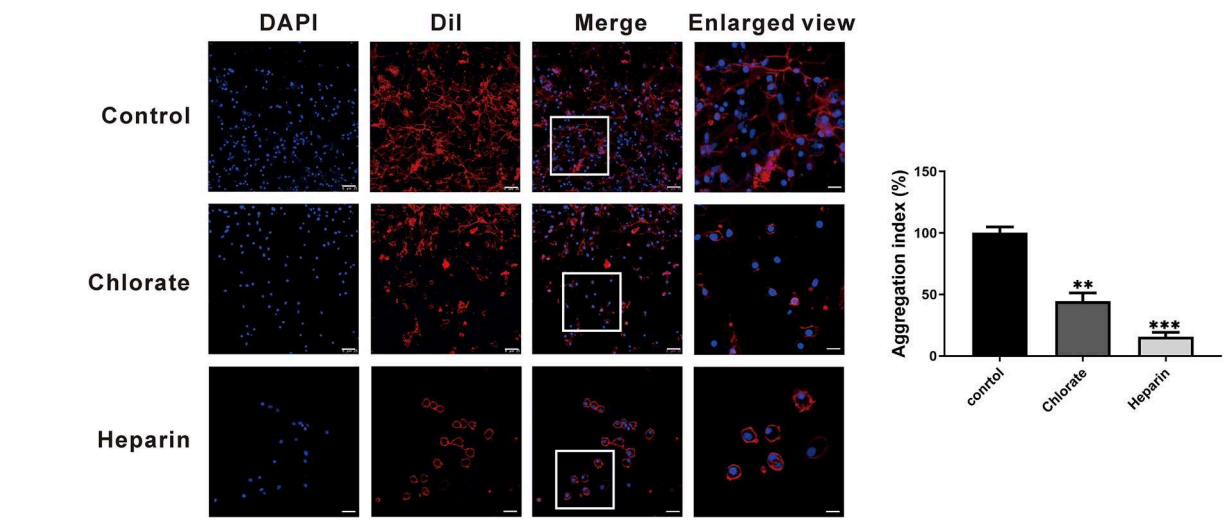

FIGURE 6 | The agglutinative effect of HSPG on the phagocytes. The hemocytes were stained with DAPI and Dil to show the distribution of cells. The control group compares with other experimental groups that were treated with two kinds of specific HSPG inhibitors, chlorate and heparin. The concentrations used for chlorate and heparin were 1 mM and 10 μM. The scale bar of enlarged views is 5 μM; the others are 25 μM. The bar chart indicated the aggregation index. The amount relative to the internal control is expressed as mean ± SD ($n = 3$). Significant differences relative to control were indicated (**$p < 0.001$ and ***$p < 0.001$).

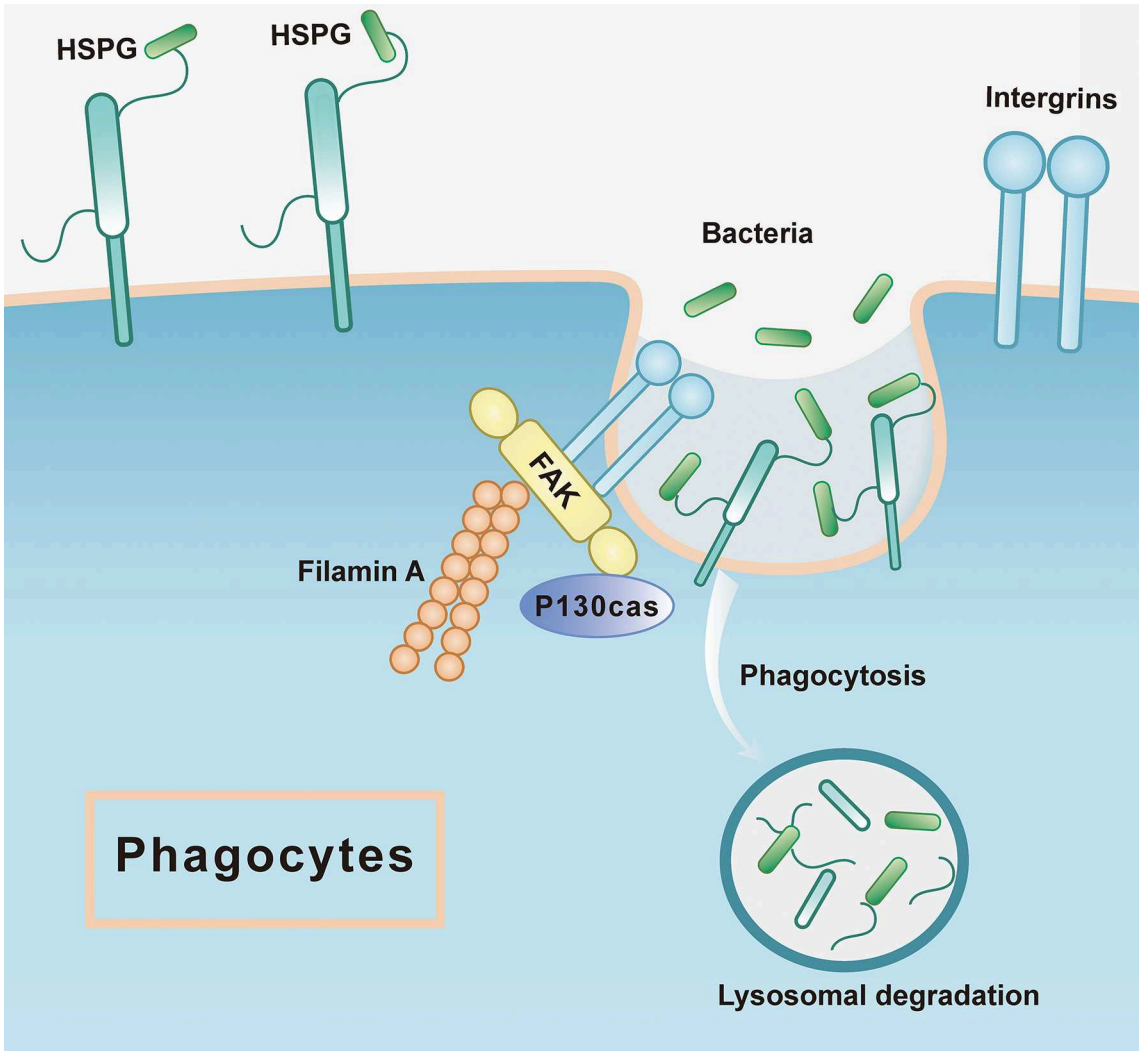

FIGURE 7 | The mode pattern of FAK and HSPG in phagocytes. The HSPG works as the receptor that is located at the cell membrane to recognize the microorganism such as bacteria, which is the first step of phagocytosis, while the integrin could stimulate the downstream pathways where FAK is active to associate the other proteins such as filamin A, P130cas. Subsequently, the bacteria would be sent to lysosomal degradation.

or internalization (71, 72). As phagocytosis is one specific form of endocytosis, it is reasonable to speculate that HSPG may take part in the regulation of phagocytic function in oysters. Two chemical agents, chlorate and heparin, were used to verify the function of HSPGs in our study. Chlorate is a potent inhibitor of sulfation reactions in the biosynthesis of GAGs, which include HSs, an indispensable component for decoration of HSPGs (73, 74). Treatment of chlorate can effectively suppress the phagocytic activity in oyster hemocytes, corroborating the crucial roles of HSPGs as mentioned previously. Because chlorate can indiscriminately modulate sulfation of GAGs including HSs, chondroitin sulfate (CS), and dermatan sulfate (DS), we can't preclude the possibility that CS/DS proteoglycans may also be involved in chlorate-mediated phagocytic suppression (75). However, the use of heparin helps to establish the importance of HS in phagocytosis, as it can block the interactions of HS with its binding partners (76). Therefore, dose-dependent repressive effects of chlorate and heparin on the phagocytic activity in oyster hemocytes constitute evidence supporting the notion that HSPGs can function as cell surface receptors to mediate phagocytosis in invertebrates.

In mammals, it has been shown that infections by human papillomavirus type 16 depend on HSPG binding with viral particles and integrin-induced FAK activation (77). Moreover, an orthologous protein of HSPG (syndecan 4) was found to be necessary for focal adhesion formation and related downstream signal transduction (78). Taken together, these findings have shed light on the molecular details of phagocytic activation in oyster hemocytes (**Figure 7**). Elaborate matrices of HSPGs exist in high abundance in these phagocytes as cell surface receptors to capture invading bacteria and subsequently transduce danger signals by activating FAK signaling with the aid of integrins. Eventually,

FAK signaling cascades trigger cytoskeletal remodeling to promote phagocytosis and other aspects of antibacterial defense. In addition, it has been reported that signaling pathways for cell aggregation are conserved and indispensable to phagocytosis in bivalve hemocytes (79). In this study, we observed that phagocytes manifested a higher aggregation rate compared to non-phagocytes. Pharmacological blockage of HSPGs synthesis strikingly changed the morphology of hemocytes and halted their aggregation in oysters, again shedding light on distinct aspects of HSPG function in regulating phagocyte behaviors.

In conclusion, an ingenious yet practically facile method was proposed to separate phagocytes and non-phagocytes efficiently. Transcriptomic analysis yielded fresh insights into the fundamental molecular differences between these groups. According to existing databases, there were ample DEGs contributing to their phenotypic disparity, of which we examined in detail two key factors, FAK and HSPGs. We then proceeded to experimentally verify their roles in phagocytic function. Both FAK and HSPGs showed significant effects on phagocytosis in hemocytes. Moreover, HSPG apparently also played a crucial role in hemocyte aggregation. Phagocytosis is an integral part of invertebrate innate immunity, requiring the cooperation of numerous sophisticated biomolecules, engineered to protect host cells. Based on our current transcriptomic analysis, a large number of such active biomolecules have been revealed, whose exact biological roles warrant further exploration or validation.

DATA AVAILABILITY STATEMENT

The datasets generated for this study can be found in the SRR10531303- SRR10531311.

AUTHOR CONTRIBUTIONS

YL implemented phagocyte sorting, flow cytometry detecting phagocytotic ability, and confocal microscopy imaging the phenomenon. YL, XZ, and KL analyzed the data of flow cytometry, while the fluorescence of pictures were calculated by ZX, JL, and SX. HM and MH performed RNA extraction for transcriptome. YZ and FM carried out bioinformatics analyses of transcriptomic data. YZ and ZY designed the research. YZ, YL, and N-KW wrote the manuscript and language proof.

FUNDING

This work was supported by the National Key R&D Program of China (2018YFC1406505), the National Science Foundation of China (Nos. 31572640 and 31572661), Science and Technology Program of Guangzhou, China (No. 201804020073), the Guangdong Special Support Program of Youth Scientific and Technological Innovation (No. 2015TQ01N139), the Program of the Pearl River Young Talents of Science and Technology in Guangzhou of China (201806010003), Institution of South China Sea Ecology and Environmental Engineering, Chinese Academy of Sciences (ISEE2018PY01, ISEE2018PY03, ISEE2018ZD01), Science and Technology Planning Project of Guangdong Province, China (2017B030314052, 201707010177).

SUPPLEMENTARY MATERIAL

The Supplementary Material for this article can be found online at: https://www.frontiersin.org/articles/10.3389/fimmu.2020.00416/full#supplementary-material

Supplementary Figure 1 | The pictures of Phagocytes and Non-Phagocytes.

REFERENCES

1. Erwig LP, Gow NA. Interactions of fungal pathogens with phagocytes. *Nat Rev Microbiol*. (2016) 14:163–76. doi: 10.1038/nrmicro.2015.21
2. Kaufmann SHE, Dorhoi A. Molecular determinants in phagocyte-bacteria interactions. *Immunity*. (2016) 44:476–91. doi: 10.1016/j.immuni.2016.02.014
3. Hellebrekers P, Hietbrink F, Vrisekoop N, Leenen LPH, Koenderman L. Neutrophil functional heterogeneity: identification of competitive phagocytosis. *Front Immunol*. (2017) 8:1498. doi: 10.3389/fimmu.2017.01498
4. Arango Duque G, Descoteaux A. Macrophage cytokines: involvement in immunity and infectious diseases. *Front Immunol*. (2014) 5:491. doi: 10.3389/fimmu.2014.00491
5. Silva MT, Correia-Neves M. Neutrophils and macrophages: the main partners of phagocyte cell systems. *Front Immunol*. (2012) 3:174. doi: 10.3389/fimmu.2012.00174
6. Murray PJ, Wynn TA. Protective and pathogenic functions of macrophage subsets. *Nat Rev Immunol*. (2011) 11:723–37. doi: 10.1038/nri3073
7. Esteban MA, Cuesta A, Chaves-Pozo E, Meseguer J. Phagocytosis in teleosts. Implications of the new cells involved. *Biology*. (2015) 4:907–22. doi: 10.3390/biology4040907
8. Nagasawa T, Nakayasu C, Rieger AM, Barreda DR, Somamoto T, Nakao M. Phagocytosis by thrombocytes is a conserved innate immune mechanism in lower vertebrates. *Front Immunol*. (2014) 5:445. doi: 10.3389/fimmu.2014.00445
9. Venier P, Varotto L, Rosani U, Millino C, Celegato B, Bernante F, et al. Insights into the innate immunity of the Mediterranean mussel *Mytilus galloprovincialis*. *BMC Genomics*. (2011) 12:69. doi: 10.1186/1471-2164-12-69
10. Akira S, Uematsu S, Takeuchi O. Pathogen recognition and innate immunity. *Cell*. (2006) 124:783–801. doi: 10.1016/j.cell.2006.02.015
11. Huang J, Li S, Liu Y, Liu C, Xie L, Zhang R. Hemocytes in the extrapallial space of *Pinctada fucata* are involved in immunity and biomineralization. *Sci Rep*. (2018) 8:4657. doi: 10.1038/s41598-018-22961-y
12. Wood W, Faria C, Jacinto A. Distinct mechanisms regulate hemocyte chemotaxis during development and wound healing in *Drosophila Melanogaster*. *J Cell Biol*. (2006) 173:405–16. doi: 10.1083/jcb.200508161
13. Hillyer JF, Schmidt SL, Christensen BM. Hemocyte-mediated phagocytosis and melanization in the mosquito armigeres subalbatus following immune challenge by bacteria. *Cell Tissue Res*. (2003) 313:117–27. doi: 10.1007/s00441-003-0744-y
14. Gordon S. Phagocytosis: an immunobiologic process. *Immunity*. (2016) 44:463–75. doi: 10.1016/j.immuni.2016.02.026
15. Aderem A. Phagocytosis and the inflammatory response. *J Infect Dis*. (2003) 187(Suppl. 2):S340–5. doi: 10.1086/374747
16. Laan M, Cui ZH, Hoshino H, Lotvall J, Sjostrand M, Gruenert DC, et al. Neutrophil recruitment by human IL-17 via C-X-C chemokine release in the airways. *J Immunol*. (1999) 162:2347–52.
17. Vassilatis DK, Hohmann JG, Zeng H, Li F, Ranchalis JE, Mortrud MT, et al. The G protein-coupled receptor repertoires of human and mouse. *Proc Natl Acad Sci USA*. (2003) 100:4903–8. doi: 10.1073/pnas.0230374100

18. O'Neill L. Specificity in the innate response: pathogen recognition by toll-like receptor combinations. *Trends Immunol*. (2001) 22:70. doi: 10.1016/S1471-4906(00)01842-1
19. Medzhitov R. Toll-like receptors and innate immunity. *Nat Rev Immunol*. (2001) 1:135–45. doi: 10.1038/35100529
20. Gulden E, Wen L. Toll-like receptor activation in immunity vs. tolerance in autoimmune diabetes. *Front Immunol*. (2014) 5:119. doi: 10.3389/fimmu.2014.00119
21. Ostrop J, Lang R. Contact, collaboration, and conflict: signal integration of Syk-coupled C-type lectin receptors. *J Immunol*. (2017) 198:1403–14. doi: 10.4049/jimmunol.1601665
22. Fritz JH, Ferrero RL, Philpott DJ, Girardin SE. Nod-like proteins in immunity, inflammation and disease. *Nat Immunol*. (2006) 7:1250–7. doi: 10.1038/ni1412
23. Seto S, Tsujimura K, Koide Y. Rab GTPases regulating phagosome maturation are differentially recruited to mycobacterial phagosomes. *Traffic*. (2011) 12:407–20. doi: 10.1111/j.1600-0854.2011.01165.x
24. Villena JA, Cousin B, Penicaud L, Casteilla L. Adipose tissues display differential phagocytic and microbicidal activities depending on their localization. *Int J Obes Relat Metab Disord*. (2001) 25:1275–80. doi: 10.1038/sj.ijo.0801680
25. Rangaraju S, Raza SA, Li NX, Betarbet R, Dammer EB, Duong D, et al. Differential phagocytic properties of CD45(low) microglia and CD45(high) brain mononuclear phagocytes-activation and age-related effects. *Front Immunol*. (2018) 9:405. doi: 10.3389/fimmu.2018.00405
26. Takahashi KG, Izumi-Nakajima N, Mori K. Unique phagocytic properties of hemocytes of Pacific oyster crassostrea gigas against yeast and yeast cell-wall derivatives. *Fish Shellfish Immunol*. (2017) 70:575–82. doi: 10.1016/j.fsi.2017.09.027
27. Canesi L, Gallo G, Gavioli M, Pruzzo C. Bacteria-hemocyte interactions and phagocytosis in marine bivalves. *Microsc Res Tech*. (2002) 57:469–76. doi: 10.1002/jemt.10100
28. Lam K, Morton B. Mitochondrial DNA and morphological identification of a new species of crassostrea (bivalvia: ostreidae) cultured for centuries in the Pearl river Delta, Hong Kong, China. *Aquaculture*. (2003) 228:1–13. doi: 10.1016/S0044-8486(03)00215-1
29. Chen X, Wei W, Wang J, Li H, Sun J, Ma R, et al. Tide driven microbial dynamics through virus-host interactions in the estuarine ecosystem. *Water Res*. (2019) 160:118–29. doi: 10.1016/j.watres.2019.05.051
30. Carballal MJ, Lopez C, Azevedo C, Villalba A. *In vitro* study of phagocytic ability of mytilus galloprovincialis Lmk haemocytes. *Fish Shellfish Immunol*. (1997) 7:403–16. doi: 10.1006/fsim.1997.0094
31. Jiang S, Qiu L, Wang L, Jia Z, Lv Z, Wang M, et al. Transcriptomic and quantitative proteomic analyses provide insights into the phagocytic killing of hemocytes in the oyster crassostrea gigas. *Front Immunol*. (2018) 9:1280. doi: 10.3389/fimmu.2018.01280
32. Langmead B, Salzberg SL. Fast gapped-read alignment with bowtie 2. *Nat Methods*. (2012) 9:357–9. doi: 10.1038/nmeth.1923
33. Li B, Dewey CN. RSEM: accurate transcript quantification from RNA-Seq data with or without a reference genome. *BMC Bioinform*. (2011) 12:323. doi: 10.1186/1471-2105-12-323
34. Love MI, Huber W, Anders S. Moderated estimation of fold change and dispersion for RNA-seq data with DESeq2. *Genome Biol*. (2014) 15:550. doi: 10.1186/s13059-014-0550-8
35. Ye J, Zhang Y, Cui H, Liu J, Wu Y, Cheng Y, et al. WEGO 2.0: a web tool for analyzing and plotting go annotations, 2018 update. *Nucleic Acids Res*. (2018) 46:W71–5. doi: 10.1093/nar/gky400
36. Kanehisa M, Sato Y, Furumichi M, Morishima K, Tanabe M. New approach for understanding genome variations in KEGG. *Nucleic Acids Res*. (2019) 47:D590–5. doi: 10.1093/nar/gky962
37. Kanehisa M, Araki M, Goto S, Hattori M, Hirakawa M, Itoh M, et al. KEGG for linking genomes to life and the environment. *Nucleic Acids Res*. (2008) 36:D480–4. doi: 10.1093/nar/gkm882
38. Duperthuy M, Schmitt P, Garzon E, Caro A, Rosa RD, Le Roux F, et al. Use of OmpU porins for attachment and invasion of crassostrea gigas immune cells by the oyster pathogen vibrio splendidus. *Proc Natl Acad Sci USA*. (2011) 108:2993–8. doi: 10.1073/pnas.1015326108
39. Roberts RE, Hallett MB. Neutrophil cell shape change: mechanism and signalling during cell spreading and phagocytosis. *Int J Mol Sci*. (2019) 20:1383. doi: 10.3390/ijms20061383
40. Donaghy L, Hong HK, Lambert C, Park HS, Shim WJ, Choi KS. First characterisation of the populations and immune-related activities of hemocytes from two edible gastropod species, the disk abalone, *Haliotis* discus discuss and the spiny top shell, turbo cornutus. *Fish Shellfish Immunol*. (2010) 28:87–97. doi: 10.1016/j.fsi.2009.10.006
41. Donaghy L, Lambert C, Choi KS, Soudant P. Hemocytes of the carpet shell clam (*Ruditapes decussatus*) and the manila clam (*Ruditapes philippinarum*): current knowledge and future prospects. *Aquaculture*. (2009) 297:10–24. doi: 10.1016/j.aquaculture.2009.09.003
42. Li J, Zhang Y, Mao F, Lin Y, Xiao S, Xiang Z, et al. The first morphologic and functional characterization of hemocytes in Hong Kong oyster, crassostrea hongkongensis. *Fish Shellfish Immunol*. (2018) 81:423–9. doi: 10.1016/j.fsi.2018.05.062
43. Hine PM. The inter-relationships of bivalve haemocytes. *Fish Shellfish Immunol*. (1999) 9:367–85. doi: 10.1006/fsim.1998.0205
44. Goedken M, De Guise S. Flow cytometry as a tool to quantify oyster defence mechanisms. *Fish Shellfish Immunol*. (2004) 16:539–52. doi: 10.1016/j.fsi.2003.09.009
45. Welzel G, Seitz D, Schuster S. Magnetic-activated cell sorting (MACS) can be used as a large-scale method for establishing zebrafish neuronal cell cultures. *Sci Rep*. (2015) 5:7959. doi: 10.1038/srep07959
46. Schmitz B, Radbruch A, Kummel T, Wickenhauser C, Korb H, Hansmann ML, et al. Magnetic activated cell sorting (Macs) - a new immunomagnetic method for megakaryocytic cell isolation - comparison of different separation techniques. *Eur J Haematol*. (1994) 52:267–75. doi: 10.1111/j.1600-0609.1994.tb00095.x
47. Theocharis AD, Skandalis SS, Gialeli C, Karamanos NK. Extracellular matrix structure. *Adv Drug Deliv Rev*. (2016) 97:4–27. doi: 10.1016/j.addr.2015.11.001
48. Yanagishita M. Function of proteoglycans in the extracellular matrix. *Acta Pathol Jpn*. (1993) 43:283–93. doi: 10.1111/j.1440-1827.1993.tb02569.x
49. Bosman FT, Stamenkovic I. Functional structure and composition of the extracellular matrix. *J Pathol*. (2003) 200:423–8. doi: 10.1002/path.1437
50. Edens WA, Sharling L, Cheng G, Shapira R, Kinkade JM, Lee T, et al. Tyrosine cross-linking of extracellular matrix is catalyzed by duox, a multidomain oxidase/peroxidase with homology to the phagocyte oxidase subunit gp91phox. *J Cell Biol*. (2001) 154:879–91. doi: 10.1083/jcb.200103132
51. Silva LM, Munoz-Caro T, Burgos RA, Hidalgo MA, Taubert A, Hermosilla C. Far beyond phagocytosis: phagocyte-derived extracellular traps act efficiently against protozoan parasites *in vitro* and *in vivo*. *Media Inflamm*. (2016) 2016:5898074. doi: 10.1155/2016/5898074
52. Young TH, Tu HR, Chan CC, Huang YC, Yen MH, Cheng NC, et al. The enhancement of dermal papilla cell aggregation by extracellular matrix proteins through effects on cell-substratum adhesivity and cell motility. *Biomaterials*. (2009) 30:5031–40. doi: 10.1016/j.biomaterials.2009.05.065
53. Johansson MW. Cell adhesion molecules in invertebrate immunity. *Dev Comp Immunol*. (1999) 23:303–15. doi: 10.1016/S0145-305X(99)00013-0
54. Wang XW, Zhao XF, Wang JX. C-type lectin binds to beta-integrin to promote hemocytic phagocytosis in an invertebrate. *J Biol Chem*. (2014) 289:2405–14. doi: 10.1074/jbc.M113.528885
55. Brower DL, Brower SM, Hayward DC, Ball EE. Molecular evolution of integrins: genes encoding integrin beta subunits from a coral and a sponge. *Proc Natl Acad Sci USA*. (1997) 94:9182–7. doi: 10.1073/pnas.94.17.9182
56. Pancer Z, Kruse M, Muller I, Muller WE. On the origin of metazoan adhesion receptors: cloning of integrin alpha subunit from the sponge geodia cydonium. *Mol Biol Evol*. (1997) 14:391–8. doi: 10.1093/oxfordjournals.molbev.a025775
57. Maiorova MA, Odintsova NA. β Integrin-like protein-mediated adhesion and its disturbances during cell cultivation of the mussel *Mytilus trossulus*. *Cell Tissue Res*. (2015) 361:581–92. doi: 10.1007/s00441-015-2122-y
58. Lv Z, Qiu L, Jia Z, Wang W, Liu Z, Wang L, et al. The activated β-integrin (CgβV) enhances RGD-binding and phagocytic capabilities of hemocytes in crassostrea gigas. *Fish Shellfish Immunol*. (2019) 87:638–49. doi: 10.1016/j.fsi.2019.01.047
59. Jia Z, Zhang T, Jiang S, Wang M, Cheng Q, Sun M, et al. An integrin from oyster crassostrea gigas mediates the phagocytosis toward *Vibrio*

splendidus through LPS binding activity. *Dev Comp Immunol*. (2015) 53:253–64. doi: 10.1016/j.dci.2015.07.014
60. Ilic D, Furuta Y, Kanazawa S, Takeda N, Sobue K, Nakatsuji N, et al. Reduced cell motility and enhanced focal adhesion contact formation in cells from FAK-deficient mice. *Nature*. (1995) 377:539–44. doi: 10.1038/377539a0
61. Sieg DJ, Hauck CR, Schlaepfer DD. Required role of focal adhesion kinase (FAK) for integrin-stimulated cell migration. *J Cell Sci*. (1999) 112:2677–91.
62. Finnemann SC. Focal adhesion kinase signaling promotes phagocytosis of integrin-bound photoreceptors. *EMBO J*. (2003) 22:4143–54. doi: 10.1093/emboj/cdg416
63. Vuori K, Hirai H, Aizawa S, Ruoslahti E. Introduction of p130cas signaling complex formation upon integrin-mediated cell adhesion: a role for Src family kinases. *Mol Cell Biol*. (1996) 16:2606–13. doi: 10.1128/MCB.16.6.2606
64. Wieczorek K, Wiktorska M, Sacewicz-Hofman I, Boncela J, Lewinski A, Kowalska MA, et al. Filamin a upregulation correlates with snail-induced epithelial to mesenchymal transition (EMT) and cell adhesion but its inhibition increases the migration of colon adenocarcinoma HT29 cells. *Exp Cell Res*. (2017) 359:163–70. doi: 10.1016/j.yexcr.2017.07.035
65. Parsons JT, Slack-Davis J, Tilghman R, Roberts WG. Focal adhesion kinase: targeting adhesion signaling pathways for therapeutic intervention. *Clin Cancer Res*. (2008) 14:627–32. doi: 10.1158/1078-0432.CCR-07-2220
66. Esko JD, Lindahl U. Molecular diversity of heparan sulfate. *J Clin Invest*. (2001) 108:169–73. doi: 10.1172/JCI200113530
67. Esko JD, Selleck SB. Order out of chaos: assembly of ligand binding sites in heparan sulfate. *Annu Rev Biochem*. (2002) 71:435–71. doi: 10.1146/annurev.biochem.71.110601.135458
68. Reynolds-Peterson CE, Zhao N, Xu J, Serman TM, Xu J, Selleck SB. Heparan sulfate proteoglycans regulate autophagy in drosophila. *Autophagy*. (2017) 13:1262–79. doi: 10.1080/15548627.2017.1304867
69. Park H, Kim M, Kim HJ, Lee Y, Seo Y, Pham CD, et al. Heparan sulfate proteoglycans (HSPGs) and chondroitin sulfate proteoglycans (CSPGs) function as endocytic receptors for an internalizing anti-nucleic acid antibody. *Sci Rep*. (2017) 7:14373. doi: 10.1038/s41598-017-14793-z
70. Kinnunen T, Huang Z, Townsend J, Gatdula MM, Brown JR, Esko JD, et al. Heparan 2-O-sulfotransferase, hst-2, is essential for normal cell migration in *Caenorhabditis elegans*. *Proc Natl Acad Sci USA*. (2005) 102:1507–12. doi: 10.1073/pnas.0401591102
71. Christianson HC, Belting M. Heparan sulfate proteoglycan as a cell-surface endocytosis receptor. *Matrix Biol*. (2014) 35:51–5. doi: 10.1016/j.matbio.2013.10.004
72. Holmes BB, DeVos SL, Kfoury N, Li M, Jacks R, Yanamandra K, et al. Heparan sulfate proteoglycans mediate internalization and propagation of specific proteopathic seeds. *Proc Natl Acad Sci USA*. (2013) 110:E3138–47. doi: 10.1073/pnas.1301440110
73. Safaiyan F, Kolset SO, Prydz K, Gottfridsson E, Lindahl U, Salmivirta M. Selective effects of sodium chlorate treatment on the sulfation of heparan sulfate. *J Biol Chem*. (1999) 274:36267–73. doi: 10.1074/jbc.274.51.36267
74. Sarrazin S, Lamanna WC, Esko JD. Heparan sulfate proteoglycans. *Cold Spring Harb Perspect Biol*. (2011) 3:a004952. doi: 10.1101/cshperspect.a004952
75. Ramachandra R, Namburi RB, Dupont ST, Ortega-Martinez O, van Kuppevelt TH, Lindahl U, et al. A potential role for chondroitin sulfate/dermatan sulfate in arm regeneration in *Amphiura filiformis*. *Glycobiology*. (2017) 27:438–49. doi: 10.1093/glycob/cwx010
76. Meneghetti MC, Hughes AJ, Rudd TR, Nader HB, Powell AK, Yates EA, et al. Heparan sulfate and heparin interactions with proteins. *J R Soc Interface*. (2015) 12:0589. doi: 10.1098/rsif.2015.0589
77. Abban CY, Meneses PI. Usage of heparan sulfate, integrins, and FAK in HPV16 infection. *Virology*. (2010) 403:1–16. doi: 10.1016/j.virol.2010.04.007
78. Woods A, Couchman JR. Syndecan-4 and focal adhesion function. *Curr Opin Cell Biol*. (2001) 13:578–83. doi: 10.1016/S0955-0674(00)00254-4
79. Hegaret H, Wikfors GH, Soudant P. Flow cytometric analysis of haemocytes from eastern oysters, crassostrea virginica, subjected to a sudden temperature elevation II. Haemocyte functions: aggregation, viability, phagocytosis, and respiratory burst. *J Exp Mar Biol Ecol*. (2003) 293:249–65. doi: 10.1016/S0022-0981(03)00235-1

Conflict of Interest: The authors declare that the research was conducted in the absence of any commercial or financial relationships that could be construed as a potential conflict of interest.

frontiers in Immunology

ORIGINAL RESEARCH
published: 31 March 2020
doi: 10.3389/fimmu.2020.00500

Dynamic Interplay of Host and Pathogens in an Avian Whole-Blood Model

Sravya Sreekantapuram[1†], *Teresa Lehnert*[2†], *Maria T. E. Praße*[2,3], *Angela Berndt*[4], *Christian Berens*[4], *Marc Thilo Figge*[2,3*†] *and Ilse D. Jacobsen*[1,3*†]

[1] *Research Group Microbial Immunology, Leibniz Institute for Natural Product Research and Infection Biology, Hans Knöll Institut, Jena, Germany,* [2] *Research Group Applied Systems Biology, Leibniz Institute for Natural Product Research and Infection Biology, Hans Knöll Institut, Jena, Germany,* [3] *Faculty of Biological Sciences, Institute of Microbiology, Friedrich Schiller University Jena, Jena, Germany,* [4] *Institute of Molecular Pathogenesis, Friedrich-Loeffler-Institut, Jena, Germany*

Microbial survival in blood is an essential step toward the development of disseminated diseases and blood stream infections. For poultry, however, little is known about the interactions of host cells and pathogens in blood. We established an *ex vivo* chicken whole-blood infection assay as a tool to analyze interactions between host cells and three model pathogens, *Escherichia coli*, *Staphylococcus aureus*, and *Candida albicans*. Following a systems biology approach, we complemented the experimental measurements with functional and quantitative immune characteristics by virtual infection modeling. All three pathogens were killed in whole blood, but each to a different extent and with different kinetics. Monocytes, and to a lesser extent heterophils, associated with pathogens. Both association with host cells and transcriptional activation of genes encoding immune-associated functions differed depending on both the pathogen and the genetic background of the chickens. Our results provide first insights into quantitative interactions of three model pathogens with different immune cell populations in avian blood, demonstrating a broad spectrum of different characteristics during the immune response that depends on the pathogen and the chicken line.

Keywords: chicken whole blood, avian immune response, *Escherichia coli*, *Staphylococcus aureus*, *Candida albicans*

OPEN ACCESS

Edited by:
Xinjiang Lu,
Ningbo University, China

Reviewed by:
Javier Santander,
Memorial University of Newfoundland, Canada
Kenneth James Genovese,
Agricultural Research Service (USDA), United States

***Correspondence:**
Marc Thilo Figge
thilo.figge@leibniz-hki.de
Ilse D. Jacobsen
ilse.jacobsen@leibniz-hki.de

†These authors have contributed equally to this work

Specialty section:
This article was submitted to Comparative Immunology, a section of the journal Frontiers in Immunology

Received: *09 December 2019*
Accepted: *04 March 2020*
Published: *31 March 2020*

Citation:
Sreekantapuram S, Lehnert T, Praße MTE, Berndt A, Berens C, Figge MT and Jacobsen ID (2020) Dynamic Interplay of Host and Pathogens in an Avian Whole-Blood Model. Front. Immunol. 11:500. doi: 10.3389/fimmu.2020.00500

INTRODUCTION

Bacterial infections in chicken affect not only animal health and welfare, but also have significant economic impact (1), due to the increasing restrictions in the use of antimicrobials in order to prevent the increase of antibiotic resistance in zoonotic bacteria. Since the emergence of resistant bacteria might impair the efficacy of antibiotic treatment, alternative approaches to combating bacterial infections in poultry are necessary. One possibility is the development of vaccines (2), another selective breeding aimed at higher intrinsic resistance (3). For a rational approach to either of the strategies, it is however necessary to understand the host response to the infection. While the avian response to zoonotic *Salmonella* and *Campylobacter* has been studied in detail, the knowledge on the response of the avian immune system to other bacterial pathogens is very limited (4).

This applies for example to colibacillosis, an infection caused by pathogenic strains of the Gram-negative bacterium *Escherichia coli*. Colibacillosis often initially manifests in the respiratory tract, but the bacteria can spread into the blood stream leading to colisepticaemia and infection

of distal body sites and organs (5, 6). Survival in the blood stream is an essential feature of *E. coli* strains to be able to cause disseminated colibacillosis, as exemplified by the correlation of serum resistance and the ability to survive in the blood stream and infect internal organs in chickens (7, 8). While the recruitment of immune cells to solid organs (9), and the transcriptional response of internal organs and peripheral blood leukocytes to colibacillosis has been studied (10, 11), to our knowledge, it remains unknown which immune cells interact with *E. coli* within avian blood.

Another common agent causing infections in poultry is *Staphylococcus aureus*, a Gram-positive bacterium (12, 13). *S. aureus* infections can affect various organ systems, including skin, mucosal membranes, and, via hematogenous spread, also tendon sheaths, joints, and bones (12, 14, 15). In severe cases, septicemia occurs (13). As for infections with *E. coli*, the immune response of chickens to *S. aureus* has not been studied in detail and it remains unclear which immune cells interact with these bacteria in blood during dissemination or septicemia. In order to investigate the interactions with immune cells and the fate of the pathogens in avian blood, we adapted a human whole-blood infection assay previously described for analyzing interactions between blood components and the facultative fungal pathogen *Candida albicans* (16, 17) and the host response to bacterial infection (18). *C. albicans* was also included in this study; it is a common colonizer of mucosal surfaces of a variety of birds, including chickens, but also one of the most frequent causes of fungal infection (19, 20). Infections predominantly affect the mucosa of the crop, esophagus and intestine, but hematogenous dissemination can occur, leading to retarded growth, hepatic and renal congestion, and neural disturbance (19, 21, 22).

Because it had previously been shown that host genetics can have a significant influence on infections in chickens (23, 24), two different White Leghorn chicken lines were used. These lines (WLA and R11) differ in their egg laying performance (25), susceptibility to lipopolysaccharide (LPS) challenge (26), and response to avian influenza virus (27).

In line with our previous studies on whole-blood infections in humans (17, 28–30), the experimental whole-blood infection assay was complemented by virtual infection modeling. By calibrating the virtual infection model to experimental data, the functional characteristics of the immune response in avian whole blood were quantified. Moreover, representing the complexity of whole-blood by a mechanistic mathematical model enabled us to identify essential and novel immune processes during the immune response in avian whole blood. To this end, we implemented several state-based virtual infection models that differ by the presence of potential immune response mechanisms, like the killing of pathogens in extracellular space or by immune cells.

MATERIALS AND METHODS

Animals and Ethics Statement

Two White Leghorn chicken lines differing in their egg laying performances were used in this study: WLA as a high producing line and R11, a low producer (25, 26, 31). WLA originates from a breeding line of Lohmann Tierzucht GmbH, Cuxhaven. The White Leghorn line R11 has been managed as conservation flock at the institute since 1965, originally derived from the Cornell Line K (32). Chicks were hatched from the eggs (kindly provided by Prof. Steffen Weigend; ING) and housed at the facilities of Friedrich-Loeffler-Institut, Jena, Germany under pathogen free conditions. Animal housing was performed in accordance with the guidelines for animal welfare set by the European Community. Throughout the study, the chickens were reared and kept under standardized conditions at 18–20°C and a relative humidity of 50–60%. Commercial feed in powder form (without antibiotics or other additives) and drinking water were both available *ad libitum*. The study was carried out in strict accordance with the German Animal Welfare Act under supervision of the authorized institutional Agent for Animal Protection. Six animals, aged 16–19 months, from each chicken line were used for each experiment conducted in this study.

Whole-Blood *ex-vivo* Infection Assay

Blood samples (total amount: four ml per animal and sampling) were collected by jugular venipuncture into commercial hirudin-coated syringes (S-Monovette®, 2.7 ml Hirudin, Sarstedt, Germany). Hirudin was chosen as anti-coagulant as it was previously shown to have no effect on complement activation (33). After addition of 10^6 microbial cells per ml, the blood was incubated at 40°C, 5% CO_2 under constant rotation for 240 min. Samples were collected every 30 min for flow cytometry, microscopy, determination of colony forming units (CFU), and PCR.

Pathogens Used in This Study

GFP-expressing strains of *Candida albicans* [CaGFP (17)], *Staphylococcus aureus* [6850/pALC1743 (34, 35)] and *Escherichia coli* ATCC 25922 (36) were used for *ex vivo* infection of avian blood. To generate the GFP-expressing *E. coli*, a plasmid constitutively expressing the GFP-variant GFP+ (37) was constructed by first fusing the promoter of the *cat* gene from pACYC184 (38) to the coding sequence of the *gfp*+ gene via overlap extension PCR (39) using a thermostable high-fidelity DNA polymerase and the following oligonucleotides: PcatXbaI-F: 5′-CATGAATCTAGAACGGAAGATCACTTCGCAG-3′; CatSDGFP-R: 5′-CTTCTCCTTTGCTAGCCATTTTAGCTCC TCCTCGATAACTCAAAAAATACGCC-3′; CatSDGFP-F: 5′-GGCGTATTTTTTGAGTTATCGAGGAGGAGCTAAAATG GCTAGCAAAGGAGAAG-3′.

GFP+EcoRI-R: 5′-ACCAACTGGTAATGGTAGC-3′. The resulting 923 bp PCR fragment was restricted with EcoRI and XbaI (New England Biolabs, Frankfurt, Germany) and ligated with likewise-restricted pUC19 (40) yielding the plasmid pUC19Pcatgfp+. Chemically competent cells of *E. coli* ATCC 25922 (36) were then transformed with the plasmid pUC19Pcatgfp+.

C. albicans was cultivated overnight in yeast extract peptone dextrose (YPD) medium (20 g/l peptone, Otto Nordwald, Hamburg, Germany; 10 g/l yeast extract, Serva, Heidelberg,

Germany; 20 g/l dextrose, Carl Roth, Karlsruhe, Germany; pH adjusted to 7.0 with NaOH) at 30°C, 180 rpm. The overnight culture was inoculated 1:50 into fresh YPD medium and incubated at 30°C, 180 rpm until OD_{600} 1.0 was reached. *S. aureus* and *E. coli* were cultivated overnight at 37°C, 180 rpm in lysogeny broth (LB medium: tryptone 10 g/l, Carl Roth; yeast extract 5 g/l, Serva; sodium chloride 10 g/l, Carl Roth; pH adjusted to 7.0 with NaOH). The overnight culture was inoculated 1:100 into fresh LB medium and incubated at 37°C, 180 rpm until OD_{600} 0.6–0.7 was reached. The cultures were then washed thrice in phosphate buffered saline (PBS). The number of *C. albicans* cells was determined by counting using a Neubauer chamber. The number of bacterial cells was calculated based on the OD_{600} - CFU correlation. Cultures were diluted to the desired concentrations with PBS before inoculation of whole blood.

Quantification of Pathogen Survival

To determine the survival of pathogens in avian whole blood, serial dilutions of the samples collected at different time points were plated on blood agar plates in 2–4 technical replicates. CFU counts were determined after overnight incubation at 30°C (for *C. albicans*) and 37°C (for *S. aureus* and *E. coli*).

Flow Cytometry

To determine both the number of immune cells and which immune cells interacted with the pathogens, cells were incubated with monoclonal antibodies (mAB) targeting the monocyte/macrophage marker KULO1-RPE (41), the macrophage/thrombocyte marker K1-RPE (42), the leucocyte marker CD45-APC (43), the B-cell marker BU1-APC-Cy7, and the T-cell marker CD3-SPRD (PE-Cy5) (44, 45). All antibodies were obtained from Southern biotechnology associates (Eching, Germany). Conjugation of mAb K1 to R-PE and BU1 to APC-Cy7 was performed using the respective Abcam conjugation kits according to the manufacturer's instructions. For staining, 50 µl of blood diluted 1:50 with PBS was mixed with 20 µl of an antibody mixture containing the directly conjugated K1, KULO1, CD45, BU1, and CD3 in the end concentrations of 0.2 µg in a Trucount tube containing beads for absolute quantification (BD Biosciences; Heidelberg, Germany) and incubated at room temperature for 45 min in the dark. 300 µl of PBS was then added to the sample, which was kept in the dark until measurement. The measurements were performed on a FACSCanto II (BD Biosciences; Heidelberg, Germany) and analyzed using the software FACSDiva (Version 6.1.3, BD Biosciences). Up to 20,000 trucount beads were recorded together with immune cells in each sample, for absolute quantification of the cell populations. Absolute cell numbers were then calculated using the following formula (46):

$$\frac{Absolute\ cell\ count}{\mu l\ of\ blood} = \frac{cells\ counted}{beads\ counted} \times \frac{total\ content\ of\ beads\ per\ tube}{blood\ volume\ per\ tube}. \quad (1)$$

Numbers of monocytes and thrombocytes were calculated from the dot plot K1/KULO1 against CD45. Single populations of T and B cells were obtained from the $CD45^+$ but $K1^-/KUL01^-$ leucocyte population shown in the dot plot of CD3 against BU1. Heterophils were identified within the $CD45^+$ cell population plotted against SSC. All single populations were back-gated against FSC/SSC for their absolute number calculations. Prior to analysis of immune cell populations, doublets were excluded by means of the FSC-H and FSC-A dot pot. The GFP-expressing pathogens were identified and recorded using the FITC channel and were sub-gated against immune cell specific markers to obtain the percentage of pathogens interacting with the different immune cells.

RNA Extraction and Quantitative Real-Time Reverse Transcription (RT)-PCR

To analyze the transcription of immune-related genes, total RNA was extracted from 100 µl of blood using the RNeasy Mini Kit for blood (Qiagen) according to the manufacturer's protocol. The QuantiTect SYBR Green real-time one-step RT-PCR kit (Qiagen) and avian-specific primers for IFN-γ, IL-1β, IL-6, IL-8, iNOS, K60, LITAF and MIP-1β (47–49) were used to determine mRNA expression levels. The expression was normalized to the house keeping gene glycerinaldehyde-3-phosphat (GAPDH) and expressed as fold change compared to non-infected samples using the threshold method for quantification ($2^{(-\Delta\Delta C_T)}$) (50). Additional information on primer efficacy and *Ct* values for the housekeeping gene are provided in the **Supplementary Material**.

Statistical Analyses

Six independent biological replicates derived from different animals were used for all experiments. Data is represented as arithmetic mean ± SD. Normality distribution was assessed using the Kolmogorov Smirnov test in GraphPad Prism 7. Data was analyzed by 2-way ANOVA followed by Tukey's multiple comparison test (GraphPad Prism 7) to compare infected and non-infected samples, different time points, different pathogens and different chicken lines. *P*-values ≤ 0.05 were considered significant.

Mathematical Modeling

We adapted our human whole-blood model (17, 28–30) and generated state-based models (SBMs) that simulate the immune reactions during infection in avian whole-blood samples. In order to cope with known differences between fungal and bacterial infection scenarios in avian blood, we implemented slightly different models for bacteria and fungi. Both models comprise states that represent the various cell types, which take part in the immune response, i.e., heterophils (*He*), monocytes (*M*), and the pathogens (P). Furthermore, the SBMs contain states for different subpopulations of the pathogens, which are pathogens in extracellular space that are alive (P_{AE}) or killed (P_{KE}), and living or killed pathogens that are within the monocytes (P_{AM}, P_{KM}) or within the heterophils (P_{AHe}, P_{KHe}). Please note that living pathogens were termed "alive" and dead pathogens "killed" within the mathematical model, and that these phrases are used throughout this manuscript in this context. The number of alive and killed pathogens within in an immune cell is counted by the indizes *i* and *j*, respectively, so that monocytes and heterophils are represented by $M_{i,j}$ and $He_{i,j}$. **Figure 1** depicts all states and possible state transitions of the SBMs for bacterial

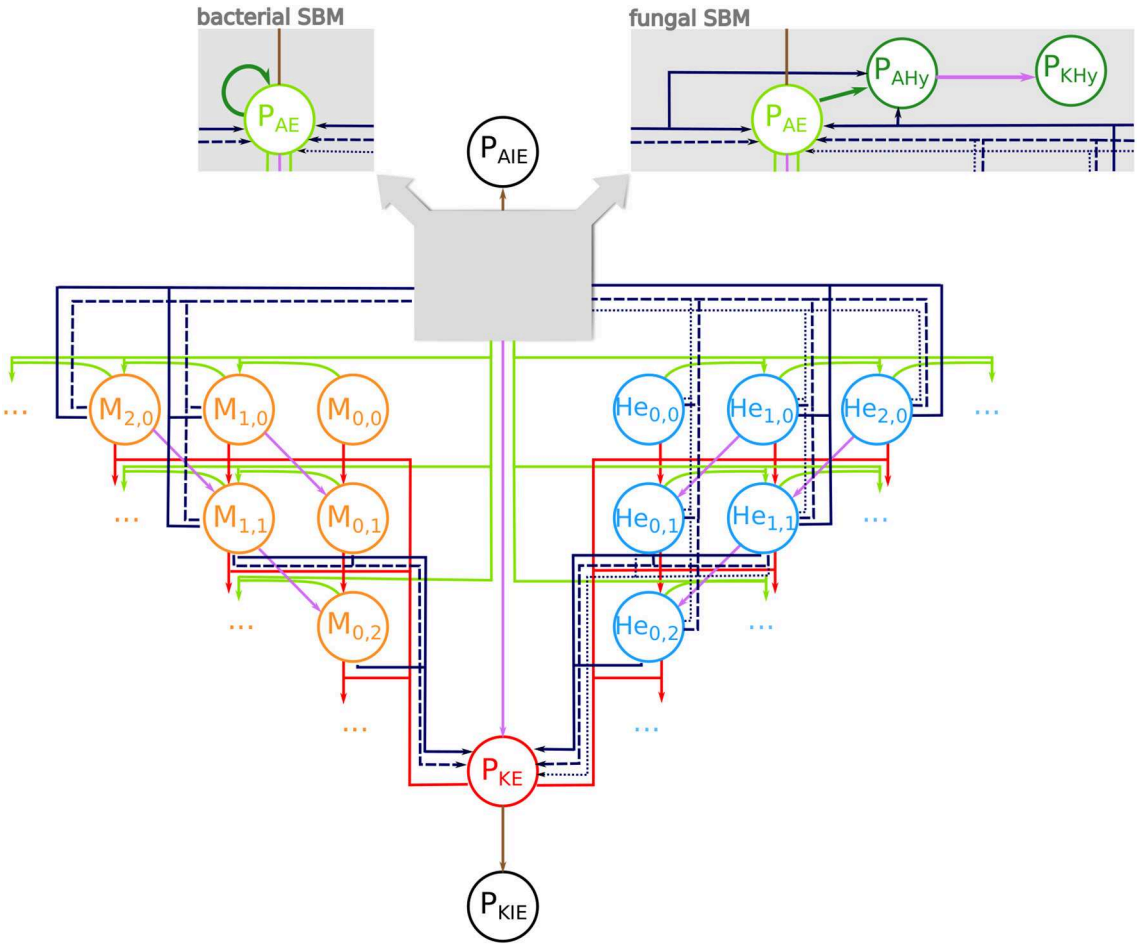

FIGURE 1 | State-based model of avian whole-blood infection. Schematic picture of the state-based model (SBM) for the immune response in avian whole blood upon infection with either of the three pathogens *S. aureus* and *E. coli* or *C. albicans*. The states (circles) represent the different cell populations of pathogens (P) and the two immune cell types of monocytes ($M_{i,j}$) and heterophils ($He_{i,j}$) with *i* alive and *j* killed pathogens. The model contains respective states for extracellular pathogens that are alive (P_{AE}) or killed (P_{KE}) as well as immune evasive pathogens that are alive (P_{AIE}) or have been killed (P_{KIE}). The SBM for fungal infection additionally contains states for alive pathogens in hyphal form (P_{AHy}) that can be killed by extracellular factors (P_{KHy}) (see right gray box). In the bacterial SBM, alive extracellular pathogens can proliferate (dark green arrow) (see left gray box). Connections between the states refer to possible state transitions that represent biological reactions during infection. Alive and killed extracellular pathogens can be phagocytosed (green and red arrows). The purple connections indicate killing of pathogens either in extracellular space or within immune cells. The dark blue connections represent the different mechanisms of immune cell killing. These are heterophil killing by stress factors with rate κ^{He}_{stress} (dotted lines), immune cell killing by extracellular peptides (dashed lines) and immune cell killing by lysis induced by alive intracellular pathogens (solid lines).

and fungal infection scenarios. The state transitions represent the immune reactions during infection with the pathogens. Since the knowledge about these reactions is very limited, we started with the human SBM as a basis and added reactions that are either known or mandatory to reconcile simulations with the experimental measurements.

This SBM contains nine transition rates that characterize the nine different reactions. In analogy to the human SBM, these include phagocytosis by monocytes (Φ_M) and heterophils (Φ_{He}), extracellular killing of pathogens ($\kappa^P_{EK}(t)$), intracellular killing of the pathogens in monocytes (κ^P_M) and in heterophils (κ^P_{He}) as well as a process where pathogens become immune evasive and can evade killing and/or phagocytosis (ρ). Furthermore, we added the killing of heterophils by stress factors that are independent of infection and induced by the experimental set up (κ^{He}_{stress}). Additionally, we assumed that in avian blood the monocytes and heterophils can be killed by a process caused by factors released by pathogens into the extracellular space (κ^M_{EM}, κ^{He}_{EM}). As previously indicated we implemented bacterial proliferation (o) and the hyphae formation of fungi (Ψ) as pathogen specific reactions. A complete list of the transition rates with the respective state transitions and a concise description is given in **Table 1**.

In order to take the morphological switch of *C. albicans* cells from yeast to hyphal form into account, the fungal SBM additionally contains states for alive pathogens in hyphal form

TABLE 1 | Transition rates of the avian SBM. For details see Materials and Methods section and Hünniger et al. (17) and Lehnert et al. (28).

Transition rate	Description	State transition
ϕ_M	Phagocytosis by monocytes	$M_{i,j} + P_{AE} \rightarrow M_{i+1,j}$
ϕ_{He}	Phagocytosis by heterophils	$He_{i,j} + P_{AE} \rightarrow He_{i+1,j}$
κ^P_M	Intracellular killing of pathogens by monocytes	$M_{i,j} \rightarrow M_{i-1,j+1}$
κ^P_{He}	Intracellular killing of pathogens by heterophils	$He_{i,j} \rightarrow He_{i-1,j+1}$
$\kappa^P_{EK}(t)$	Extrallular killing by antimicrobial proteins that were released by first-time phagocytosis by heterophils. The rate depends on the activity of antimicrobial proteins ($\overline{\kappa_{EK}}$) and the decay of their activity (γ) as defined in Hünniger et al. (17) and Lehnert et al. (28)	$P_{AE} \rightarrow P_{KE}$ $P_{AHy} \rightarrow P_{KHy}$
ρ	Acquire immune evasion against phagocytosis and/ or extracellular killing	$P_{AE} \rightarrow P_{AIE}$ $P_{KE} \rightarrow P_{KIE}$
κ^{He}_{stress}	Killing of heterophils by stress	$He_{i,j} \rightarrow iP_{AE} + jP_{KE}$
κ^M_{EM}	Killing of monocytes by extracellular mechanisms that are pathogen dependent	$M_{i,j} \rightarrow iP_{AE} + jP_{KE}$
κ^{He}_{EM}	Killing of heterophils by mechanisms that are not cellularly induced but pathogen dependent	$He_{i,j} \rightarrow iP_{AE} + jP_{KE}$
o	Proliferation rate of bacteria	$P_{AE} \rightarrow 2P_{AE}$ $M_{i,j} \rightarrow M_{i+1,j}$ $He_{i,j} \rightarrow He_{i+1,j}$
Ψ	Formation of fungal hyphae in extracellular space	$P_{AE} \rightarrow P_{Hy}$
κ^P_{EK}	Extracellular killing by constant concentration of antimicrobials	$P_{AE} \rightarrow P_{KE}$ $P_{AHy} \rightarrow P_{KHy}$
κ^M_{lysis}	Killing of monocytes by pathogen-induced lysis	Fungal SBM: $M_{i,j} \rightarrow P_{Hy} + (i-1)P_{AE} + jP_{KE}$ Bacterial SBM: $M_{i,j} \rightarrow iP_{AE} + jP_{KE}$
κ^{He}_{lysis}	Killing of heterophils by pathogen-induced lysis	$He_{i,j} \rightarrow P_{Hy} + (i-1)P_{AE} + jP_{KE}$ $He_{i,j} \rightarrow iP_{AE} + jP_{KE}$

(P_{AHy}) and killed pathogens in hyphal form (P_{KHy}). Furthermore, the fungal SBM comprises additional transitions that represent the switch to the hyphal form in extracellular space ($P_{AE} \rightarrow P_{AHy}$) with rate Ψ. Similar to alive extracellular *C. albicans* yeast cells (P_{AE}), extracellular hyphae (P_{AHy}) can also be killed ($P_{AHy} \rightarrow P_{KHy}$) by the same extracellular killing mechanisms as yeast. The SBM for the infection scenario with either of the bacteria *S. aureus* and *E. coli*, contains bacterial proliferation which takes place either within immune cells or in extracellular space with rate.

As mentioned before, the described SBMs for fungal and bacterial infection contain a single mechanism for killing of pathogens in extracellular space and, therefore, we refer to these models as SEK-SBMs (Single Extracellular Killing mechanism-SBMs). These SEK-SBMs differ only with respect to hyphae formation and proliferation in order to represent the differences between fungal and bacterial infection scenarios. In addition to the SEK-SBMs, we implemented the MEK-SBMs (Multiple Extracellular Killing mechanism-SBMs), where extracellular killing is not only caused by effectors released by immune cells upon first phagocytosis (with rate $\kappa^P_{EK}(t)$), but also caused by effectors present immediately upon infection. We assume that these effectors are present in high concentration so that their effect is temporally constant and does not decrease during the time of the infection. Therefore, we defined the constant rate κ^P_{EK} for this transition in the MEK-SBMs (see **Table 1**).

In addition to immune cell killing by extracellular microbial factors with rate κ^M_{EM} for monocytes and κ^{He}_{EM} for heterophils, we considered the possibility that immune cells can be killed by intracellular pathogens. Here, we assumed that pathogens can escape phagocytosis by actively breaking through the immune cell membrane. Thereby, the immune cell membrane will be destroyed and alive and killed internalized pathogens will be released into the extracellular space. This lysis by pathogens takes place in monocytes with rate κ^M_{lysis} and in heterophils with rate κ^{He}_{lysis}. The corresponding transitions are given in **Table 1** for bacterial infections and for C. *albicans* infection, where this lytic escape is initiated by intracellular hyphae formation.

The SBMs were simulated by applying a random selection simulation algorithm (51), where the simulation time is divided into equidistant time intervals (Δt) and at each discrete time step, each cell can perform a transition from state S to state S' with probability $P_{S\rightarrow S'}$ that is defined by $P_{S\rightarrow S'} = r_{S\rightarrow S'} \times \Delta t$. We used the simulation algorithm as described in form of a flow chart in (28). In order to compare the model simulation with the kinetics observed from experimental whole-blood infection assays, we defined so called combined units, which are composed of specific model states, in order to form the counterparts of the five experimental measurements. The survival assays yield the kinetics of alive and killed pathogens. In both models, the alive pathogens are combined in

$$P_A \equiv P_{AE} + P_{AIE} + \sum\nolimits_{i\geq 0} \sum\nolimits_{j\geq 0} \left(M_{i,j} + He_{i,j}\right) i \qquad (2)$$

In the SBM of the fungal infection scenario, the combined unit P_A additionally involves the alive pathogens in hyphal form P_{AHy}. The killed pathogens in the models are summarized in

$$P_K \equiv P_{KE} + P_{KIE} + \sum\nolimits_{i\geq 0} \sum\nolimits_{j\geq 0} \left(M_{i,j} + He_{i,j}\right) j \qquad (3)$$

where again, the SBM of fungal infection scenario additionally involves P_{KHy}, the killed pathogens in hyphal form. The measurements of the Flow Cytometry analysis, i.e., the association either to monocytes or heterophils, or to none of them were compared, respectively with the combined units

$$P_M \equiv \sum\nolimits_{i\geq 0} \sum\nolimits_{j\geq 0} \left(i + j\right) M_{i,j} \qquad (4)$$

$$P_{He} \equiv \sum\nolimits_{i\geq 0} \sum\nolimits_{j\geq 0} \left(i + j\right) He_{i,j} \qquad (5)$$

and

$$P_E \equiv P_{AE} + P_{KE} + P_{AIE} + P_{KIE} \qquad (6)$$

Note that the combined unit of pathogens in extracellular space, P_E, also incorporates the alive and killed pathogens in hyphal form (P_{AHy}, P_{KHy}) in the fungal SBM, in comparison to the bacterial SBM. The total number of pathogens is given by $P \equiv P_E+P_N+P_M$ and $P \equiv P_A+P_K$ in the fungal SBMs. In the bacterial SBMs $P \neq P_A + P_K$, because the number of alive pathogens can increase by bacterial proliferation.

Since additionally the number of heterophils and monocytes could be quantified in the whole-blood assays, we defined combined units that, respectively, record the number of heterophils

$$He \equiv \sum_{i\geq 0} \sum_{j\geq 0} He_{i,j} \tag{7}$$

and monocytes

$$M \equiv \sum_{i\geq 0} \sum_{j\geq 0} M_{i,j} \tag{8}$$

Details on the parameter estimation procedure as well as on the comparison of various models by the Akaike information criterion are provided in the **Supplementary Material**.

RESULTS

Chicken-Line Specific Decrease of Monocytes and Heterophils in Whole Blood

As the aim of this study was to analyze the interaction of pathogens with avian immune cells in an *ex vivo* whole-blood model, we first determined if the different leukocyte populations remained stable using flow cytometry. The absolute numbers of monocytes and T cells declined within the first 30–60 min for both chicken lines, but remained stable thereafter (**Supplementary Figure 1**, **Supplementary Table 1**). The number of B cells did not change over time. Thrombocytes moderately decreased within the first 60 min in blood from R11 chickens only, and heterophil numbers showed a slow steady decrease over time in WLA chickens (**Supplementary Figure 1**, **Supplementary Table 1**).

Next, we determined whether infection with *C. albicans*, *S. aureus*, or *E. coli* affected the number of immune cells. In WLA chickens, a time dependent decrease in monocytes and heterophils was observed during the course of infection (**Figures 2A,B**). For the *E. coli* infection, the monocyte numbers were significantly lower at 210 and 240 min after infection compared to the non-infected samples ($p = 0.005$ and 0.049, respectively, two-sided unpaired *t*-test). The numbers of other leukocytes and thrombocytes in infected WLA blood remained stable (**Figures 2C–E**). Infection did not significantly affect leukocyte and thrombocyte numbers in the blood samples of R11 chickens (**Figures 2F–J**), but a moderate non-significant decrease of monocytes and heterophils in blood infected with *E. coli* was observed (**Figures 2F,G**). Thus, line-specific and pathogen-specific differences in the viability of monocytes and heterophils following infection were observed.

Pathogens Are Killed in Avian Blood

Next, we determined to which extent the different pathogens survived in avian blood. The number of viable pathogens determined by CFU declined over time in both chicken lines and for all pathogens used (**Figures 3A,B**). The highest and fastest killing rate was observed for *C. albicans*, which was significantly reduced within the first 30 min and killed more efficiently than both *S. aureus* and *E. coli* during the early phase of infection (**Supplementary Table 2**). After the initial drop in *C. albicans* CFU 30 min after infection, CFU slowly declined until 120 min (WLA) or 150 min (R11) after infection, followed by a more pronounced decline toward the next time point, suggesting biphasic killing kinetics.

Similar biphasic pathogen survival was observed for *S. aureus*: CFU remained relatively stable until 90 min after infection followed by a steep decline to 120 min, which was more pronounced in WLA blood. Following this decline, CFU remained stable until the end of the experiment in blood from R11 chickens, but increased again in WLA blood, resulting in similar numbers of *S. aureus* in the blood of both chicken lines at the end of the experiment (**Figures 3A,B**, **Supplementary Table 2**). In contrast, the number of viable *E. coli* cells showed a steadier decline starting 60 min after infection in both chicken lines. Thus, while all pathogens were killed to a certain extent in avian blood, the killing rates and dynamics differed significantly depending on the pathogen, without differences between the chicken lines.

Association of Pathogens With the Different Types of Leukocytes Is Pathogen and Chicken Line Dependent

One possible explanation for the different survival rates of the different pathogens in avian blood could be differences in the interaction with leukocytes, which was assessed by flow cytometry.

Clear differences between WLA and R11 chickens were observed for *E. coli* and *S. aureus*: While both bacterial pathogens were predominantly found in association with monocytes in blood of WLA chickens (**Figures 4A,B**), a substantial proportion associated with heterophils in the blood of R11 chickens (**Figures 4D,E**). The relative number of *E. coli* cells detected as being associated with heterophils in R11 blood decreased over time, which could have been caused by either disassociation or killing-mediated loss of the fluorescence signal. In the blood of both WLA and R11 chickens, the overall number of *S. aureus* associated with monocytes increased moderately over time, but remained more stable for *E. coli*. For *C. albicans*, a similar association pattern was observed in both chicken lines: Fungal cells were found to be associated to a slightly higher extent with monocytes than with heterophils (**Figures 4C,F**). The fraction of fungal cells associated to immune cells was stable after 30 min until the end of the experiment. All pathogens also interacted with thrombocytes, but this interaction was more prominent for the bacterial species than for *C. albicans*. Association with thrombocytes at early time points was more profound in R11

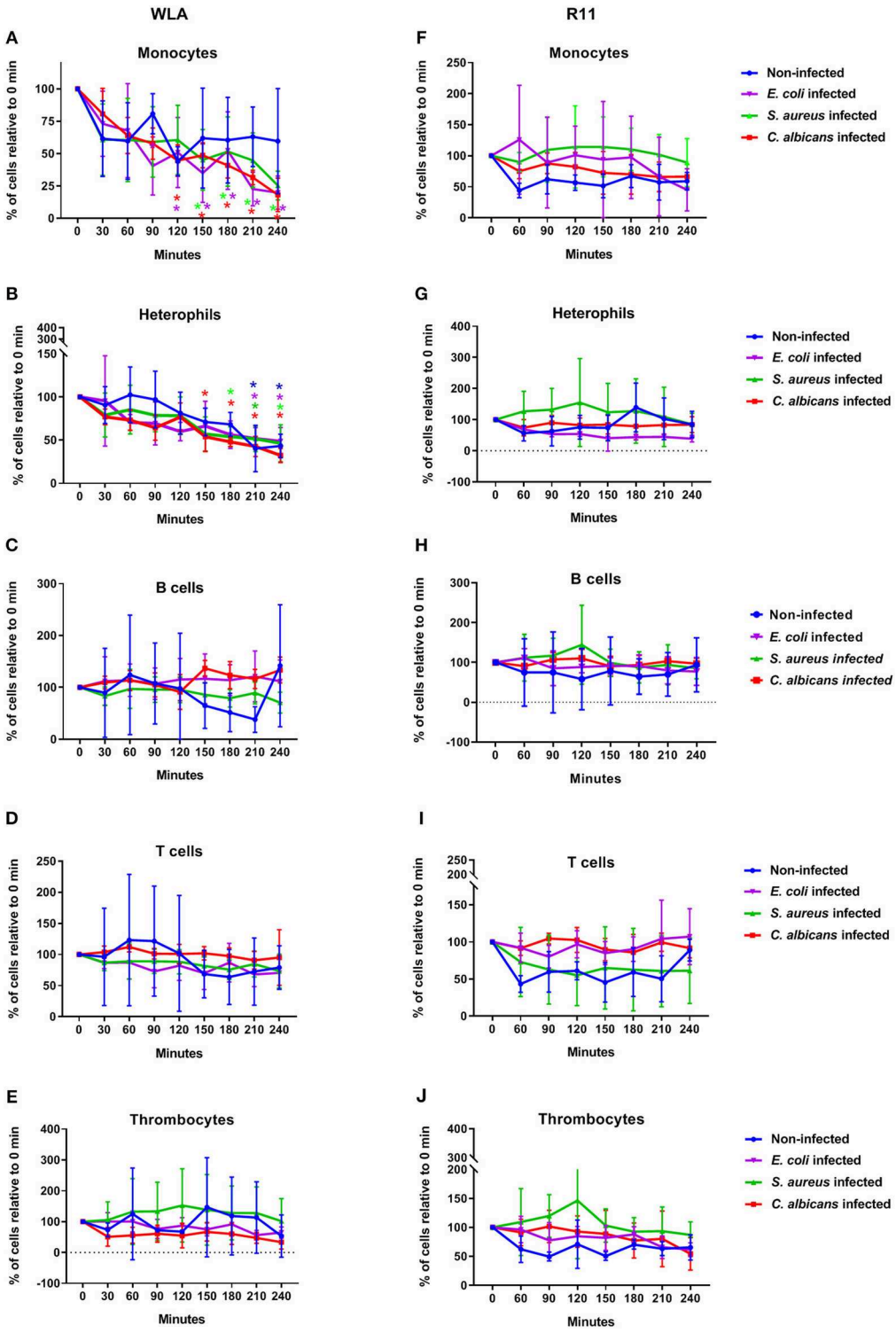

FIGURE 2 | Immune cell numbers in avian whole blood over the course of infection. Avian whole blood from the chicken lines WLA (left) and R11 (right) was infected *ex-vivo* with *C. albicans, S. aureus*, or *E. coli* for 240 min. Absolute numbers were determined for the different immune cell populations using flow cytometry and are depicted in percentage of the numbers at 0 min: Monocytes **(A,F)**, heterophils **(B,G)**, B cells **(C,H)**, T cells **(D,I)**, and thrombocytes **(E,J)**. Data of six independent experiments using blood from different donors is presented as mean and SD. *indicates significant difference compared to 0 min ($p < 0.05$) with the color representing the respective condition: Blue: non-infected blood, purple: *E. coli,* green: *S. aureus*, red: *C. albicans*.

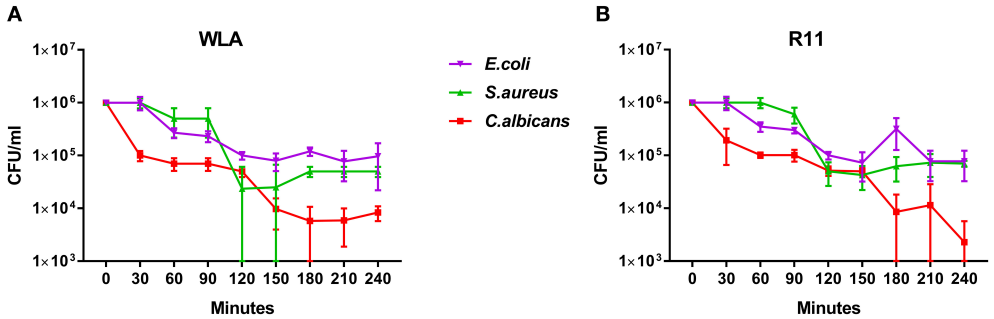

FIGURE 3 | Survival of different pathogens in avian blood. Colony forming units of the different pathogens were determined in the inoculum (0 min) and from samples taken every 30 min to 240 min after infection of whole blood from WLA chickens **(A)** and R11 chickens **(B)**. Data of six independent experiments using blood from different donors is presented as mean and SD.

blood. None of the three pathogens was found to be associated with T or B cells in the blood of either of the chicken lines.

Taken together, the data showed that all pathogens associated with monocytes, while the rate of interaction with heterophils was chicken line and pathogen-dependent. Association occurred rapidly and became relatively stable after reaching a certain time point.

Mathematical Modeling Revealed Relevant Immune Reactions

Based on the measurements conducted in the experimental whole-blood infection assay, we developed different virtual infection models (see Materials and Methods section). We defined different state-based models (SBMs) for fungal infection, involving the switch to hyphal form with rate Ψ, as this morphological transition was observed in blood smears (**Supplementary Figure 2**). For bacterial infection, bacterial proliferation with rate was included. Furthermore, we defined models that differ in their killing mechanisms of pathogens in extracellular space. We implemented the SEK-SBMs, containing a single extracellular killing mechanism for pathogens, and the MEK-SBMs with multiple extracellular killing mechanisms for pathogens (see Materials and Methods section). Since a decrease in immune cells counts in the non-infected samples was only observed for heterophils in WLA chickens (see **Figure 2B**), we calibrated the SBM to heterophil kinetics of uninfected samples of WLA chickens and could predict the value of this killing rate of heterophils caused by stress (κ^{He}_{stress}). Therefore, we set the value of $\kappa^{He}_{stress} = 2.6 \times 10^{-2}\ s^{-1}$ for infection scenarios with WLA chickens. For infection of samples from R11 chicken we set this rate to zero ($\kappa^{He}_{stress} = 0\ s^{-1}$), because the immune cell numbers remain fairly constant over time in the non-infected samples (see **Figures 2F,G**). A complete list of the resulting transition rate values for all models is provided in **Supplementary Tables 3–7**.

Multiple Extracellular Killing Mechanisms Essential to Resemble Survival of Pathogens

The experimental measurements on survival of pathogens revealed that for all infection scenarios the number of pathogens decreased during the length of the infection assay (see **Figures 3**, **5**). We calibrated the SEK-SBMs and the MEK-SBMs to the experimental measurements and found that simulations of both models were qualitatively in line with the experimental data (see **Figure 5**). Both SBMs predicted not only a decrease of viable pathogens but also that for both chicken lines *C. albicans* cells were killed faster and to a larger amount than bacterial cells. The values for the extracellular killing rates were also higher for fungal than for bacterial infection, as shown in **Figure 6A** for SEK-SBM and in **Figures 6B**, **C** for MEK-SBM. Note that for the *C. albicans* infection in the MEK-SBMs, the value of κ^{P}_{EM} was largest, but not the values of $\kappa^{P}_{EM}(t)$. Despite these similar qualitative predictions for *C. albicans* infection, data simulated by the SEK-SBMs caused larger least squares error (LSE) in the combined unit of alive pathogens P_A (**Supplementary Figures 3A,B**) and also a larger total LSE (**Supplementary Figure 4A**) in comparison to the MEK-SBMs. This is caused by a larger deviation of the simulated data from SEK-SBM to the experimental data from 0 to 60 min after infection (**Figures 5A,B**) in comparison with the MEK-SBM (**Figures 5C,D**). Moreover, for this infection scenario, the MEK-SBM showed a smaller AIC_C than the SEK-SBM (**Supplementary Figure 4D**) indicating that the improvement in terms of the LSE by the MEK-SBM can compensate for the increase in model complexity in comparison to the SEK-SBM. For a direct comparison of simulations of both SBMs we refer to **Supplementary Figure 5**. Further differences between the simulations by the two SBMs are visible for the number of alive *E. coli* during infection of WLA chicken (**Supplementary Figure 5C**). Simulations by the SEK-SBM caused a larger AIC_C and larger LSE values for the combined unit P_A (**Supplementary Figure 3**) and the sum (**Supplementary Figure 4**), which was mainly caused by increasing deviations to the experimental data starting 120 min after infection (**Figure 5A**) in comparison to the MEK-SBM (**Figure 5C**). Even though the values of the extracellular killing rate $\kappa^{P}_{EM}(t)$ are predicted to be higher in the SEK-SBM than in the MEK-SBM (**Supplementary Figure 6**), the MEK-SBM simulations showed a more rapid decrease of alive *C. albicans* cells and *E. coli* cells because of the additional extracellular killing rate κ^{P}_{EM}, which enables pathogen killing immediately upon infection without any temporal shift. Both SBMs predict a

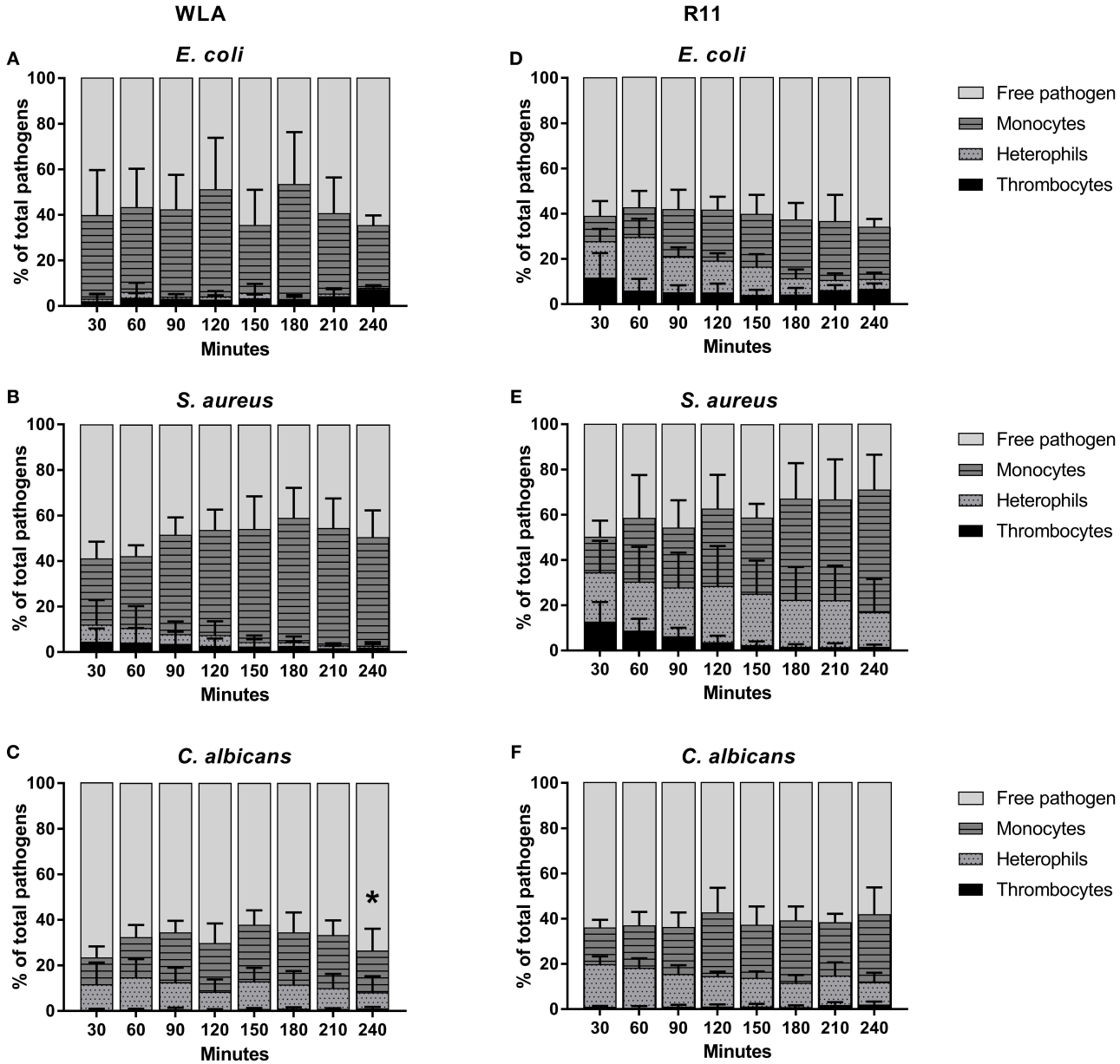

FIGURE 4 | Association of pathogens with host cells in whole blood. Association of *E. coli* **(A,D)**, *S. aureus* **(B,E)** and *C. albicans* **(C,F)** with host cells in whole blood of WLA (left) and R11 chickens (right) was determined by flow cytometry and is presented as percentage of pathogens associated with the host cell type relative to the total pathogen population in blood. Data of six independent experiments using blood from different donors is presented as mean and SD. * indicates significance of monocytes compared to R11 chickens ($p < 0.05$).

similar decrease of alive *S. aureus* cells during infection (**Figure 5**, **Supplementary Figure 5**). Of note, none of the SBMs could simulate the biphasic course of *S. aureus* killing that was observed for infection of samples from both chicken lines.

Phagocytosis Rates of Immune Cells Are Pathogen-Specific and Differ Quantitatively

As shown in **Figure 7**, the SEK-SBMs and the MEK-SBMs can be calibrated to the experimental data of pathogen association to immune cells so that the respective simulations are in qualitative agreement with the experimental data. However, we observed quantitative differences for the infection of samples from both chicken lines with *C. albicans*. In comparison to the MEK-SBM, the SEK-SBM simulated larger fractions of fungal cells that were associated to heterophils (**Figures 7A,B**, **Supplementary Figures 7A,B**), causing larger deviations from the experimental data as reflected by a larger LSE for the combined unit P_{HE} (**Supplementary Figures 3A,B**). The larger fraction of pathogens phagocytosed by heterophils is caused by higher phagocytosis rates in the SEK-SBM in comparison to

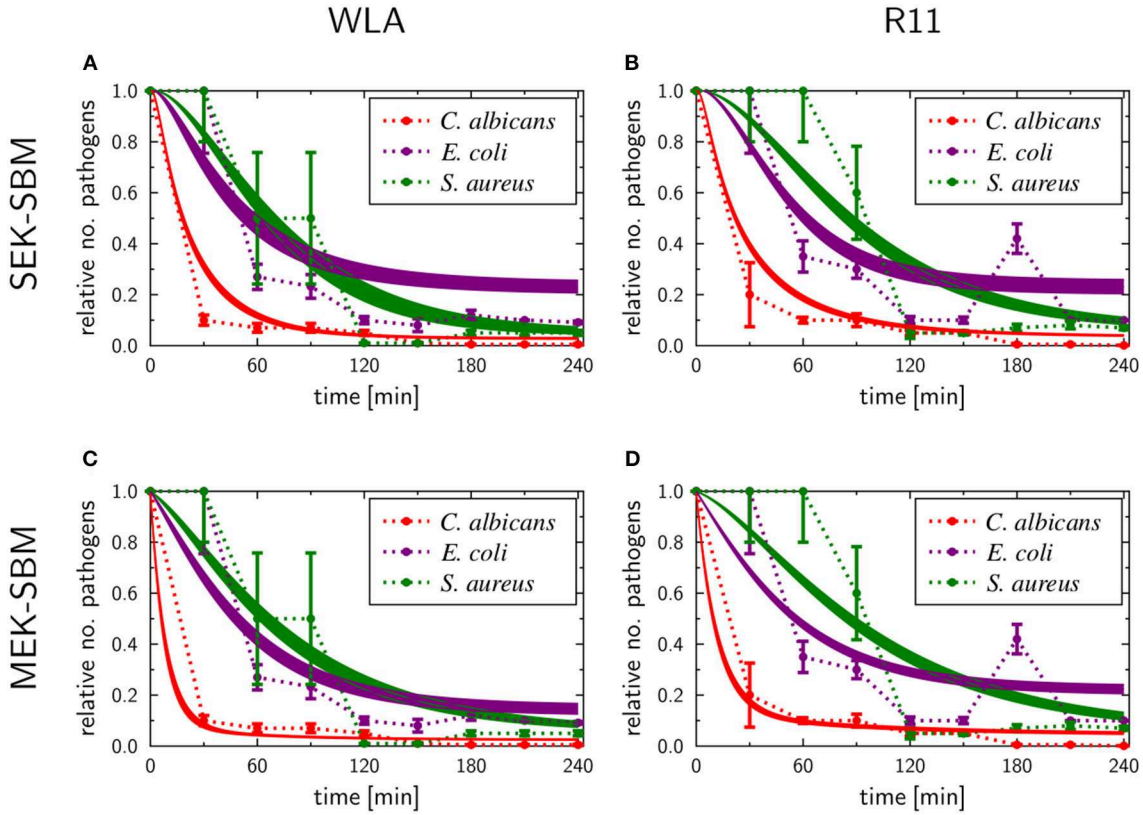

FIGURE 5 | SBM simulations for survival of different pathogens. Time courses of living pathogens resulting from the simulations with the SEK-SBM (single extracellular killing mechanism of pathogens) **(A,B)** and the MEK-SBM (multiple extracellular killing mechanisms of pathogens) **(C,D)**. Solid lines represent SBM simulations that were calibrated to experimentally measured data on pathogen survival (data points that were connected by dashed lines as guide for the eye). The thickness of the solid lines represents the mean ± standard deviation of simulation results observed from 50 simulations for normally distributed transition rates. The models were calibrated to measurements of either *C. albicans* (red lines), *E. coli* (purple lines) or *S. aureus* (green lines) that were injected into samples from WLA chickens (left column) and R11 chickens (right column).

the MEK-SBM (**Figures 8A,B**, **Supplementary Figures 9A,D**). This is also applicable to phagocytosis by heterophils during *E. coli* infection of samples from R11 chicken (**Figure 7D**, **Supplementary Figures 7D**, **8E**) and phagocytosis by monocytes during *E. coli* infection of samples from WLA chicken (**Figure 7C**, **Supplementary Figure 9**, **Figures 8A,B**, **Supplementary Figure 8B**). However, both models, the SEK-SBMs and the MEK-SBMs, predicted that not only the fraction of phagocytosed pathogens was larger for monocytes than for heterophils (**Figure 7**), but also the corresponding functional parameters, i.e., the phagocytosis rates, were larger for monocytes (Φ_M) in comparison to heterophils (Φ_{He}) for all infection scenarios (**Figures 8A,B**). The SEK-SBMs predicted that Φ_M is larger than Φ_{He} with at least a factor of $\Phi_M/\Phi_{He} = 2.6$ for WLA infection with *C. albicans* and up to a factor of $\Phi_M/\Phi_{He} = 89.8$ for WLA infection with *E. coli* (see **Supplementary Table 8** for all other infection scenarios). The MEK-SBMs predicted even larger differences between the phagocytosis rates, with at least $\Phi_M/\Phi_{He} = 5.4$ for infection with *E. coli* in R11 blood and up to $\Phi_M/\Phi_{He} = 101.7$ for WLA blood infection with *E. coli*. Furthermore, both models predicted that the phagocytosis rates of heterophils (Φ_{He}) were higher for bacterial infection of R11 blood compared to WLA (**Figures 8A,B**, **Supplementary Table 9**). For fungal infection, the SEK-SBM predicted that Φ_{He} is larger in WLA chickens than in R11 chickens (**Figure 8A**). In contrast, the MEK-SBM predicted the opposite relation of Φ_{He} between the chicken-lines.

Taken together, the mathematical models predicted that the experimentally observed chicken-line specific association to heterophils was caused by chicken-line specific phagocytosis rates and not by differences in the immune cell numbers.

Immune Cell Killing Mechanism Is Essential to Simulate Immune Response in Avian Whole-Blood Infection

As measured using flow cytometry, we observed chicken line-specific and pathogen-specific characteristics in the kinetics of immune cell counts during whole-blood infection (see section "3.1 Impact of infection on leukocyte numbers"). For infection with any of the three pathogens, the number of monocytes and heterophils decreased faster in WLA blood than in samples from R11 chickens (**Figure 2**, **Figure 9**,

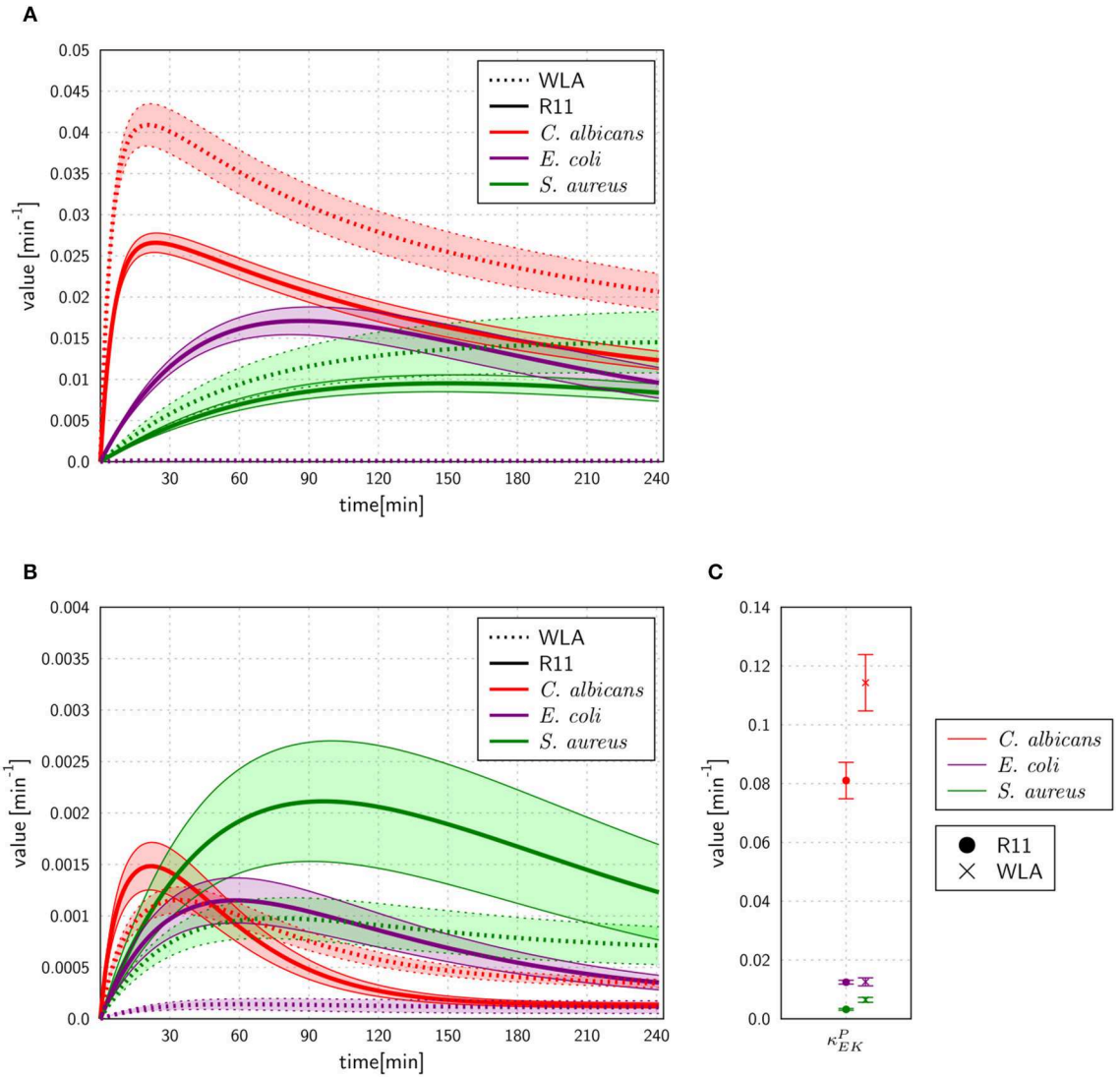

FIGURE 6 | Rates for extracellular killing of pathogens predicted by the SEK-SBM **(A)** and the MEK-SBM **(B,C)**. The time course of extracellular killing caused by antimicrobial peptides that were released upon initial phagocytosis by heterophils [with rate $\kappa^P_{EK}(t)$] is depicted in **(A)** for the SEK-SBM and in **(B)** for the MEK-SBM. The latter SBM additionally contains the mechanism of extracellular killing by peptides that were present immediately upon infection. The predicted values of the respective rate κ^P_{EM} are shown for the different infection scenarios in **(C)**.

Supplementary Figures 10, 11). The predicted monocyte killing rates (κ^M_{EM}) of both SBMs were higher in infection scenarios with samples from WLA chickens than in samples from R11 chickens (**Figures 8C,D**, **Supplementary Table 10**). This relation was not found for the killing rates of heterophils (κ^{He}_{EM}). Here, higher killing rates were observed in WLA than in R11 blood only for the *S. aureus* infection. Furthermore, we observed that in *E. coli* infected R11 blood the number of both immune cell types decreased faster compared to both *S. aureus* and *C. albicans* cells (**Figure 1**). As shown in **Figure 8** and **Supplementary Table 11**, these pathogen-specific characteristics are likely due to higher immune cell killing rates during *E. coli* infection.

In order to test whether the mechanism of immune cell killing is essential for avian whole-blood infection, we excluded this mechanism from the fungal and bacterial MEK-SBMs and calibrated the adapted model to the experimental time-series data. However, we observed that in this case the simulations resemble neither the kinetics of heterophil (**Supplementary Figure 12**) nor monocyte counts (**Supplementary Figure 13**).

Furthermore, we considered whether the decrease of immune cells can be caused by intracellular pathogens. In case of *C. albicans* cells, we assumed that intracellular hyphae formation can cause immune cell lysis. We adapted the MEK-SBMs by implementing immune cell lysis that is caused by viable,

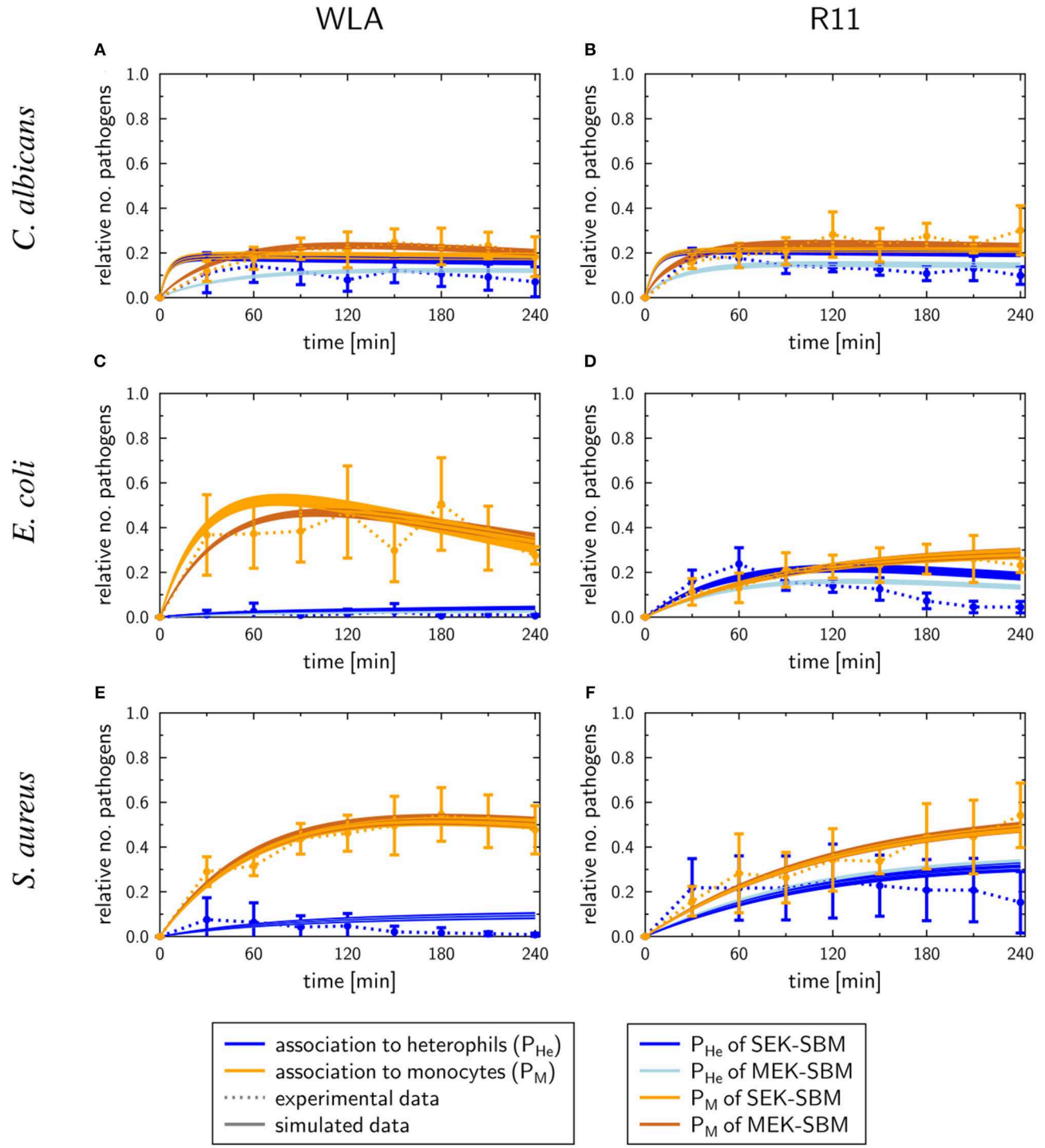

FIGURE 7 | SBM simulations for pathogen association to immune cells. Time courses of the combined units for pathogens in heterophils (P_{He}) and pathogens in monocytes (P_M) resulting from the simulations with the SEK-SBM (single extracellular killing mechanism of pathogens) and the MEK-SBM (multiple extracellular killing mechanisms of pathogens). Solid lines represent SBM simulations that were calibrated to experimentally measured data (data points connected by dashed lines as guide for the eye). The thickness of the solid lines represents the mean ± standard deviation of simulation results observed from 50 simulations for normally distributed transition rates. The models were calibrated to measurements of either *C. albicans* **(A,B)**, *E. coli* **(C,D)** or *S. aureus* **(E,F)** that were injected into samples from WLA chickens (left) and R11 chickens (right).

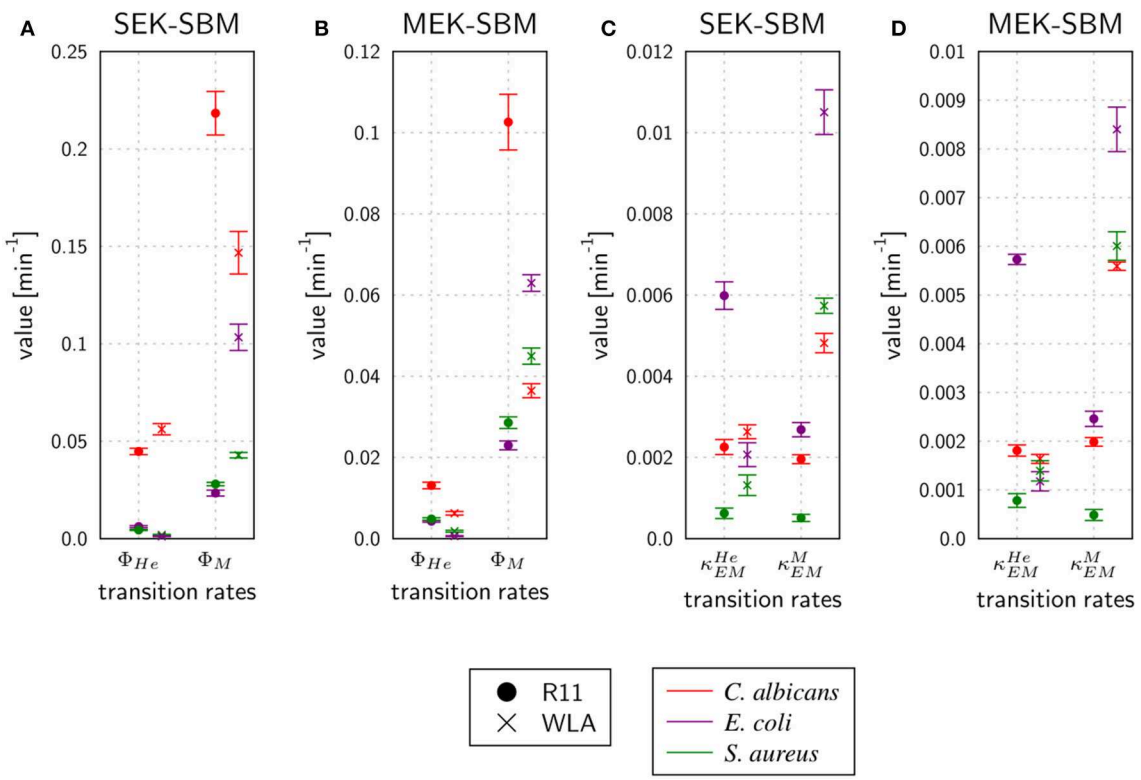

FIGURE 8 | Rates for phagocytosis of pathogens and immune cell killing by extracellular mechanisms predicted by the SEK-SBM **(A,C)** and the MEK-SBM **(B,D)**. Predicted mean values and standard deviations (error bars) of phagocytosis rates of heterophils (Φ_{He}) and monocytes (Φ_M) **(A,B)** and the rate of heterophil killing (κ_{EM}^{He}) and monocyte killing (κ_{EM}^{M}) by extracellular mechanisms that are stimulated in the presence of pathogens **(C,D)**.

intracellular pathogens and calibrated this model to the experimental measurements. We found that this model does not notably increase the agreement with the experimental data in terms of LSE and moreover showed a larger AIC_C in comparison to the MEK-SBM (**Supplementary Figure 14**) due to the larger number of model parameters. We also tested whether immune cell lysis only can explain the immune cell kinetics. This was realized by deleting the mechanism of immune cell killing by extracellular factors with rates κ_{EM}^{M} and κ_{EM}^{He}. However, as shown in **Supplementary Figures 15, 16**, this model does not resemble the immune cell kinetics during bacterial and fungal infection.

Expression of Genes Encoding Immune-Related Effectors

To determine whether the association of pathogens with immune cells induced inflammatory responses in whole blood, the transcription of the pro-inflammatory cytokines IFNγ, IL-1β, IL-6, the chemokines IL-8 (CXCLi2), K60 (CXCLi1), and MIP-1β, the effector iNOS, and the central transcription factor LITAF (the avian TNF homolog) was analyzed by quantitative RT-PCR (**Figure 10**, **Supplementary Figure 17**). Both chicken lines responded to pathogen challenge with increased gene expression, which was generally more pronounced in the blood of R11 chickens. A notable exception was iNOS, which was upregulated to a lower extent in R11 blood cells. Following *S. aureus* infection, the kinetics of gene induction were also comparable between both cell lines, but differences were observed in blood challenged with *E. coli* or *C. albicans*, respectively: In response to *E. coli*, increased expression of IFNγ, IL-1β, IL-6, IL-8, K60, and MIP1β was observed in R11 blood cells already at early time points, whereas a more gradual increase was observed in WLA blood. Infection with *C. albicans* led to early upregulation of all factors analyzed in WLA blood, with the exception of IL-1β and IL-6, which were not induced by infection (**Figure 10**). The level of induction was comparable to or higher than those observed post infection with *E. coli* or *S. aureus*. In contrast, IL-1β and IL-6 were induced by *C. albicans* in blood cells of R11 chickens, but the induction of these and all other genes analyzed was less pronounced in response to *C. albicans* compared to both bacterial species. Thus, while both chicken lines responded to all pathogens by increased expression of genes associated with immune reactions, both pathogen- and chicken-line dependent differences were observed.

DISCUSSION

The aim of this study was to better understand the interaction of model pathogens with avian blood as an important step in the pathogenesis of disseminated infections and during bacteremia. Therefore we employed an *ex vivo* whole-blood infection assay in combination with mathematical infection modeling. The

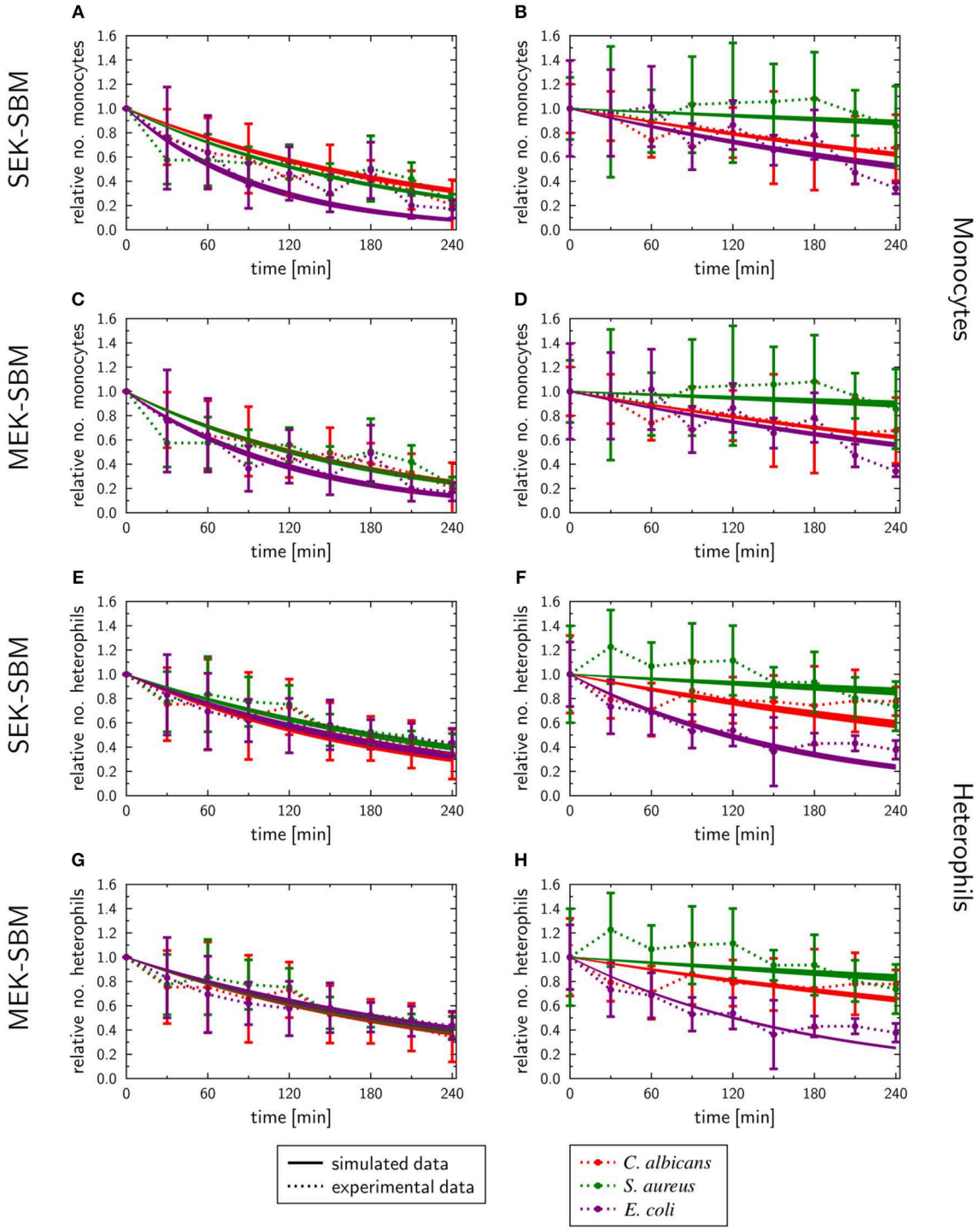

FIGURE 9 | SBM simulations of the immune cell numbers during infection. Time course of the monocytes **(A–D)** and heterophils **(E–H)** predicted units for pathogens in heterophils (P_{He}) and pathogens in monocytes (P_M) that were simulated by the SEK-SBM (single extracellular killing mechanism of pathogens) and the MEK-SBM (multiple extracellular killing mechanisms of pathogens). Solid lines represent SBM simulations that were calibrated to experimentally measured data (data points connected by dashed lines as guide for the eye). The thickness of the solid lines represents the mean ± standard deviation of simulation results observed from 50 simulations for normally distributed transition rates. The models were calibrated to measurements of either *C. albicans* cells (red lines), *E. coli* cells (purple lines) or *S. aureus* cells (green lines) that were injected into samples from WLA chickens (left column) and R11 chickens (right column).

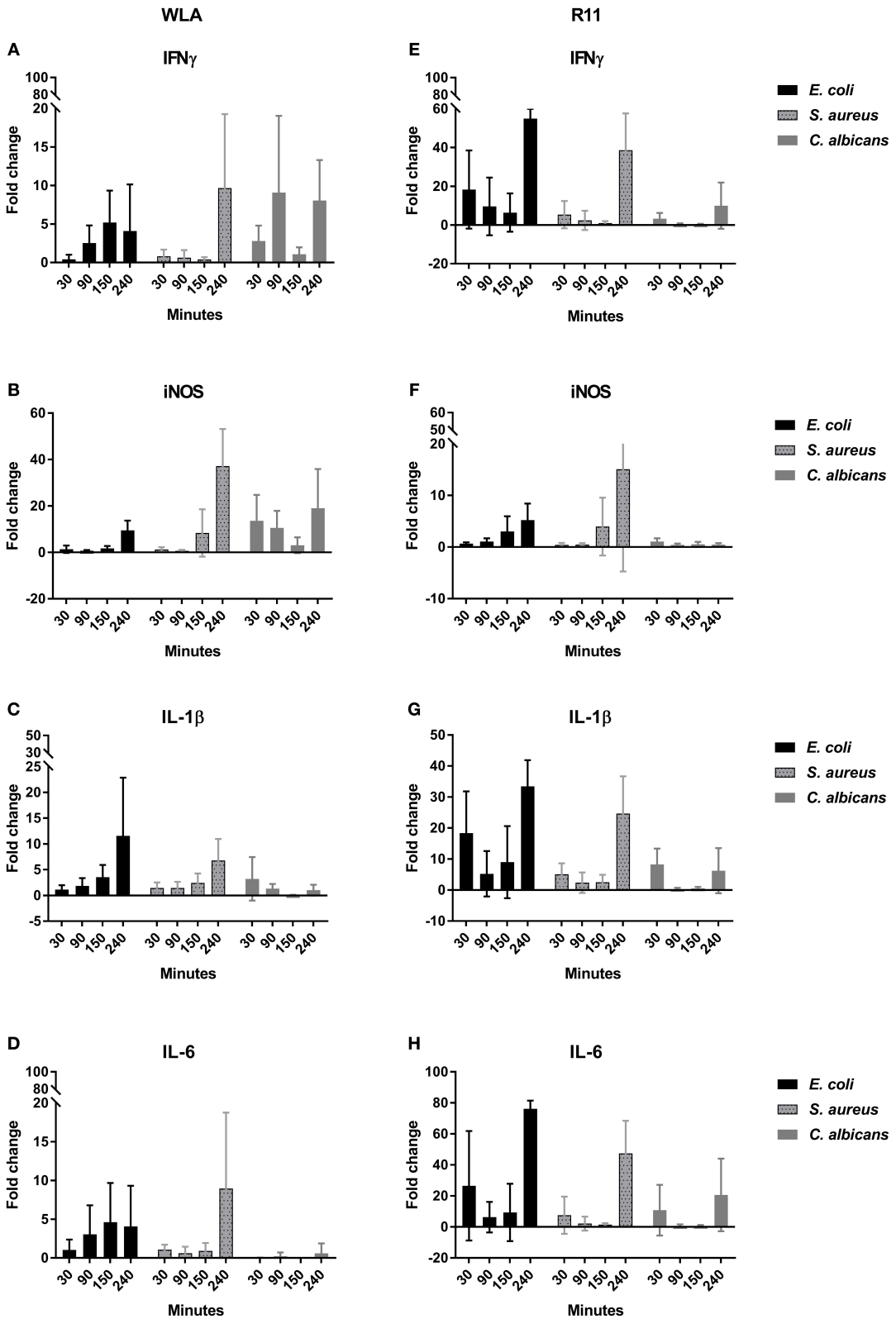

FIGURE 10 | Expression of the genes encoding IFNγ **(A,E)**, iNOS **(B,F)**, IL-1β **(C,G)**, and IL-6 **(D,H)** in infected chicken blood. Left: WLA chickens; right: R11 chickens. Gene expression was normalized to GAPDH and expressed as fold change compared to non-infected samples. The graphs represent the fold change of gene expression in infected avian whole blood relative to non-infected blood samples at the respective time points. Data of six independent experiments using blood from different donors is presented as mean and SD.

advantage of the experimental whole-blood assay is that it enables identification of the immune cells that interact with a pathogen in a complex setting allowing for cross talk of immune cells. Furthermore, the absence of isolation and purification steps prevents accidental pre-activation of immune cells that could occur in the use of primary cells isolated from blood (52). Our set up was similar to a recently published approach for measuring phagocytic activity of chicken leukocytes (53), with the differences that we (i) discriminated between various immune cell populations, and (ii) performed a time course analysis. It should be noted that neither our method nor the approach by Nagahizadeh et al. (53) can clearly distinguish between attachment of pathogens to and phagocytosis by immune cells. We therefore refer to the biological interactions observed as association rather than phagocytosis. However, it has been shown that association of *C. albicans* with innate immune cells in human blood usually indicates phagocytosis (17), and it appears likely that this is also the case in chicken blood not only for *C. albicans* but also for the bacterial pathogens. In this context, it should also be noted that the overall association of microbes with immune cells in our model appeared to be relatively stable over time. However, this does not indicate stable interactions on a cell-to-cell basis, as (i) degradation of the fluorescence signal in killed pathogens would lead to a loss of association of the corresponding immune cell in flow cytometry analysis, (ii) microbes might escape from immune cells, and (iii) free microbes might be taken up by other immune cells.

These possibilities, and the assumption that association is indicative of or leading to phagocytosis, were incorporated into the mathematical model. By mapping the complex biological system of *ex vivo* whole-blood infection into a mechanistic mathematical model, we could not only quantify functional characteristics of the immune response but also identify novel immune mechanisms. Since the knowledge concerning immune mechanisms in avian blood is limited, we started with our established human virtual infection model (17, 28) and stepwise added known as well as potential immune mechanisms. By calibrating these models to experimental measurements and subsequently scoring the models by their agreement with experimental data, using the least squares error (LSE) and the Akaike information criteria confirmed that the immune reactions included in the model were justified and necessary to be able to model the experimental data.

A possible technical concern of the *ex-vivo* whole-blood infection assay is the stability of this model system over time. As a decline in absolute cell numbers was only observed for heterophils, and to a lesser extent monocytes, in WLA chickens over the observation period of 240 min, we can assume that this system is reasonably stable within this time frame, similar to the human *ex vivo* whole-blood model previously described (17). We however accounted for the heterophil decrease by implementing the mechanism of heterophil death caused by stress factors of the experimental setting into the mathematical models. By calibrating the model to heterophil kinetics of non-infected WLA samples we could quantify the corresponding reaction rate and distinguish this rate from immune cell killing caused by infection. Upon infection, a decrease in cell numbers was observed for monocytes and heterophils from WLA chickens, while the immune cell decrease was less pronounced in R11 chickens, except for infection by *E. coli*. Since the virtual infection models differentiated between immune cell killing caused by stress and caused by infection, we could quantify the relative contribution of each pathogen to immune cell killing and the differences between the immune cell types and the chicken lines. We found that in WLA blood, the killing rate of monocytes is higher than that of heterophils; also, more monocytes are killed in WLA than in R11 blood. Moreover, in R11 blood the immune cell killing rate is highest for an *E. coli* infection. Both bacterial pathogens tested also displayed a significantly more pronounced interaction with monocytes in WLA blood compared to R11. Thus, increased interaction with monocytes coincided with a stronger decrease in monocyte numbers, suggesting killing of monocytes by *E. coli* and *S. aureus*. This explanation would contrast results from *in vitro* experiments in which *E. coli* did not lead to detectable chicken macrophage killing within the first 4 h (54). Similarly, the viability of mammalian macrophages is not substantially impaired by infection with *S. aureus* within the first 4 h, even though killing occurs at later time points (55). To our knowledge the fate of avian macrophages challenged with *S. aureus* has not been investigated so far, but assuming that interactions would be similar to those reported for mammalian macrophages, our data could indicate significant differences in the outcome of bacteria-macrophage interactions *in vitro* compared to the *ex vivo* whole-blood model. This could be due to differences between circulating monocytes and the macrophage cell line used for the *in vitro* studies, the bacterial strain used, or immune cell responses might be influenced by the more complex environment in whole blood compared to tissue culture.

However, by adding and removing potential reactions within the mathematical model, we found that immune cell killing is likely not exclusively caused by viable, intracellular pathogens that perform lysis. In addition, immune cell killing caused by extracellular factors that originate from pathogens independent of their viability, was essential to calibrate the model to the experimental data. While we deemed it to be beyond the scope of this study to test these hypotheses experimentally, it highlights how bioinformatical modeling can generate novel hypotheses from complex experimental data that could be tested in future studies.

An unexpected observation was the clear drop of *S. aureus* CFU numbers from 90 to 120 min after infection in both chicken lines. This could have been mediated by intracellular killing of bacteria by immune cells, possibly monocytes, which showed higher association to *S. aureus* in the blood of WLA chickens, which correlates also with the more pronounced reduction in the bacterial CFU counts at this time point. After this reduction, the CFU counts, however, remained stable (R11) or even increased (WLA). Although macrophages can kill *S. aureus*, *in vitro* experiments using mammalian cells demonstrated that a subpopulation is able to survive in macrophages, before it escapes and replicates extracellularly (55). A similar mechanism would explain the observed kinetics of *S. aureus* CFU in avian blood. So far, the mathematical models could not simulate

the biphasic kinetics of viable *S. aureus* cells in avian whole-blood, because the killing and proliferation mechanisms were implemented as reactions with rates that are constant in time. In future studies, these mechanisms could be characterized by time-dependent rates. However, one should keep in mind that this would imply an increase in model complexity. Furthermore, the Next-Reaction simulation algorithm (56), an improved implementation of the original algorithm by Gillespie (57, 58), must be applied to simulate the model dynamics, since the Random Selection method does not accurately simulate systems with time-dependent rates (51).

In comparison to bacterial killing, we found that fungal cells were killed faster and to a larger extent than bacterial cells in both chicken lines. Even taking into account that bacterial cells can proliferate during infection, the predicted killing rates were lower compared to those for fungal infections. Furthermore, we found that multiple extracellular killing mechanisms of pathogens were necessary to calibrate the model to the experimentally measured numbers of viable pathogens. Only the MEK-SBM with multiple extracellular killing mechanisms could accurately simulate the kinetics of alive *E. coli* cells in R11 chicken and alive *C. albicans* cells in R11 and WLA chicken, as also justified by the smallest LSE and the best information criterion AIC_C for these infection scenarios. A likely biological explanation is the release of antimicrobial peptides by activated host cells (59).

As similar/identical characteristics among all infection scenarios, we observed that the degree of pathogen association and the phagocytosis rate is higher for monocytes in comparison to heterophils. This observation clearly reveals differences to the immune responses observed in human whole blood, where monocytes show less association to pathogens and lower phagocytosis rates in comparison to neutrophils (17). However, we also observed chicken-line specific heterophil association and phagocytosis for bacterial infection. Infection with either of the two bacterial species induced a stronger response by heterophils in R11 blood in comparison to WLA blood. Both monocytes/macrophages and heterophils are recruited during bacterial infections *in vivo* and are thought to contribute to pathogen clearance (4). Our results would thus warrant future comparative analyses addressing both the relative contribution of either type of innate immune cells to pathogen killing and the potential differences depending on the genetic background. Future studies could also address whether different types of immune cells respond to a different degree to bacterial vs. fungal pathogens as we observed a higher degree of association of bacterial pathogens with monocytes than heterophils.

Heterophil interaction might be essential for reducing fungal burden, as *C. albicans* differs from both *S. aureus* and *E. coli* in its *in vitro* interaction with macrophages: *C. albicans* kills 20-50% of macrophages within the first hours of interaction *in vitro* (60, 61). This early macrophage killing by *C. albicans* is mediated by pyroptosis, a type of programmed cell death. Whether this process can also occur in avian macrophages is unclear (62), but it would explain the reduction of monocytes upon *Candida* infection in WLA blood. The declining number of monocytes however does not exclude contribution of these cells to fungal killing in our model; rapid phagocytosis by monocytes/macrophages (63) and macrophage efficacy against *Candida* species have been demonstrated previously (64), making it likely that avian monocytes/macrophages contribute to fungal clearance.

Due to the limited capacity of macrophages to control *C. albicans*, neutrophils are considered to be the main effector cells during candidiasis in mammals (17, 65, 66). They are also by far the dominating cell type associated with *C. albicans* in human blood, where monocytes comprise only a minor fraction of the cells interacting with the fungus (17). Avian heterophils can rapidly phagocytose and inactivate *C. albicans* (67, 68), and, additionally, antimicrobial peptides of heterophils have been shown to be effective against *C. albicans* (69). Chicken serum alone, in contrast, does not inhibit *Candida* (68). Thus, release of antimicrobial peptides following degranulation of heterophils could explain the significant killing of *C. albicans* cells. It should also be noted, that all microbes used in this study were cultured in standard media under standard conditions, and that the pathogens have to adapt to the altered environment when inoculated into the blood. Clinical blood stream infections with these pathogens in contrast usually originate from mucosal sites, such as the gut or the respiratory tract. Adaptation to these niches might better prepare the microorganisms for the interactions with immune cells once they enter the blood stream (70–73).

The nucleated thrombocytes of avian species also contribute to the overall immune response in blood by phagocytosis of pathogens and upregulation of proinflammatory cytokines (4, 74). We did, however, only observe low association rates of pathogens with thrombocytes in our model, making it unlikely that these cells make a significant direct contribution to microbial clearance. Nonetheless, thrombocytes might be important for the overall host response by influencing other immune cells, for example, by the release of stimulating cytokines. Expression of cytokine genes and genes encoding other immune-related factors was increased in whole blood following infection, consistent with the previously reported induction of proinflammatory cytokines in human whole blood infected with *C. albicans* (17). As our data was based on mRNA analysis of whole blood, it however remains unknown which cells in the model are responsible for the observed upregulation. Without cell type-based analysis, it is furthermore not possible to determine the reason for the observed differences between the chicken lines; these might be due to the differences in association of pathogens with the different types of immune cells, leading to differences in the number of cells of a given subset being activated by physical contact to microbes. Also, heterophils and monocytes can be expected to differ in their transcriptional responses both qualitatively and quantitatively, so that differences in the extent of association could affect the overall transcriptional response. It is however also conceivable that distinct types of immune cells in the two chicken lines used in this study differ in their response to pathogens, as has previously been demonstrated for other chicken lines (75–77).

This possibility would have to be tested using isolated subsets of immune cells.

In summary, we describe here an *ex vivo* avian whole-blood infection assay analyzed by flow cytometry in combination with biomathematical modeling. Our results provide first insights into the interaction of three model pathogens with different immune cell populations in chicken blood, demonstrating differences depending not only on the pathogen but also on the chicken line. Furthermore, microbial clearance rates differed between the pathogens. The application of mechanistic virtual infection modeling predicted essential and novel immune mechanisms. It should be noted that our study focused only on a few factors (physical interaction with immune cells and expression of selected cytokines) that affect the outcome of host-pathogen interaction in this complex model. The contribution of important immune effector mechanisms such as complement or the release of antimicrobial peptides (e.g., lysozyme) were not addressed. Analyzing complement activation and antimicrobial peptides will likely provide important further insights in the activation and relevance of these host defense mechanisms. Furthermore, analysis of the global transcriptional changes, for example by using sequencing approaches, would provide a more comprehensive overview on the reaction of cells in whole blood during infection. To elucidate the functional importance of the associations observed as well as the underlying molecular mechanisms, it would be helpful to selectively deplete distinct types of immune cells and/or to functionally analyze immune cells isolated from naïve and infected blood.

DATA AVAILABILITY STATEMENT

All datasets generated for this study are included in the article/**Supplementary Material**.

ETHICS STATEMENT

The protocol was approved by the Committee on the Ethics of Animal Experiments and the Protection of Animals of the State of Thuringia, Germany (permit number 04-001-14).

AUTHOR CONTRIBUTIONS

IJ, AB, and MF conceived the study. SS, TL, MP, and CB performed the experiments. SS, TL, MP, IJ, AB, and MF analyzed the data. IJ and TL drafted the manuscript. SS, TL, MP, AB, CB, MF, and IJ revised and approved the manuscript.

FUNDING

This project was funded by the funding line Strategic Networking in the Leibniz Association within the framework of the Leibniz Science Campus InfectoOptics (Project BLOODi) in Jena. Funders had no role in study design, analyses and interpretation of data, in the writing of the report, and in the decision to submit the article for publication.

ACKNOWLEDGMENTS

We thank Katrin Schlehahn for excellent technical support especially with the RT-PCR experiments. SS is a member of the Jena School for Microbial Communication (JSMC).

SUPPLEMENTARY MATERIAL

The Supplementary Material for this article can be found online at: https://www.frontiersin.org/articles/10.3389/fimmu.2020.00500/full#supplementary-material

Datasheet 1 | Tables.

Datasheet 2 | Supplementary methods and figures.

REFERENCES

1. Chai SJ, Cole D, Nisler A, Mahon BE. Poultry: the most common food in outbreaks with known pathogens, United States, 1998–2012. *Epidemiol Infect.* (2016) 145:316–25. doi: 10.1017/S0950268816002375
2. Desin TS, Köster W, Potter AA. Salmonella vaccines in poultry: past, present and future. *Expert Rev Vaccines.* (2013) 12:87–96. doi: 10.1586/erv.12.138
3. Berghof TVL, Matthijs MGR, Arts JAJ, Bovenhuis H, Dwars RM, van der Poel JJ, et al. Selective breeding for high natural antibody level increases resistance to avian pathogenic *Escherichia coli* (APEC) in chickens. *Dev Comp Immunol.* (2019) 93:45–57. doi: 10.1016/j.dci.2018.12.007
4. Wigley P. Immunity to bacterial infection in the chicken. *Dev Comp Immunol.* (2013) 41:413–7. doi: 10.1016/j.dci.2013.04.008
5. Guabiraba R, Schouler C. Avian colibacillosis: still many black holes. *FEMS Microbiol Lett.* (2015) 362:fnv118. doi: 10.1093/femsle/fnv118
6. Dziva F, Stevens MP. Colibacillosis in poultry: unravelling the molecular basis of virulence of avian pathogenic *Escherichia coli* in their natural hosts. *Avian Pathol.* (2008) 37:355–66. doi: 10.1080/03079450802216652
7. Mellata M, Dho-Moulin M, Dozois CM, Curtiss R 3rd, Brown PK, Arne P, et al. Role of virulence factors in resistance of avian pathogenic *Escherichia coli* to serum and in pathogenicity. *Infect Immun.* (2003) 71:536–40. doi: 10.1128/IAI.71.1.536-540.2003
8. Nolan LK, Horne SM, Giddings CW, Foley SL, Johnson TJ, Lynne AM, et al. Resistance to serum complement, iss, and virulence of avian *Escherichia coli*. *Vet Res Commun.* (2003) 27:101–10. doi: 10.1023/A:1022854902700
9. Antao EM, Glodde S, Li G, Sharifi R, Homeier T, Laturnus C, et al. The chicken as a natural model for extraintestinal infections caused by avian pathogenic *Escherichia coli* (APEC). *Microb Pathog.* (2008) 45:361–9. doi: 10.1016/j.micpath.2008.08.005
10. Nie Q, Sandford EE, Zhang X, Nolan LK, Lamont SJ. Deep sequencing-based transcriptome analysis of chicken spleen in response to avian pathogenic *Escherichia coli* (APEC) infection. *PLoS ONE.* (2012) 7:e41645. doi: 10.1371/journal.pone.0041645
11. Sandford EE, Orr M, Shelby M, Li X, Zhou H, Johnson TJ, et al. Leukocyte transcriptome from chickens infected with avian pathogenic *Escherichia coli* identifies pathways associated with resistance. *Results Immunol.* (2012) 2:44–53. doi: 10.1016/j.rinim.2012.02.003
12. Awan MA, Matsumoto M. Heterogeneity of staphylococci and other bacteria isolated from six-week-old broiler chickens. *Poult Sci.* (1998) 77:944–9. doi: 10.1093/ps/77.7.944
13. Smyth JA, McNamee PT. Staphylococci, Streptococci and Enterococci. In: Jordan F, Pattison M, Alexander D, Faraghe T, editors. *Poultry Diseases, 5th Edn.* London: W.B. Sauders (2001). p. 163–9.

14. Kibenge FS, Robertson MD, Wilcox GE, Pass DA. Bacterial and viral agents associated with tenosynovitis in broiler breeders in Western Australia. *Avian Pathol.* (1982) 11:351–9. doi: 10.1080/03079458208436110
15. Mutalib A, Riddell C, Osborne AD. Studies on the pathogenesis of staphylococcal osteomyelitis in chickens. I. Effect of stress on experimentally induced osteomyelitis. *Avian Dis.* (1983) 27:141–56. doi: 10.2307/1590379
16. Hünniger K, Bieber K, Martin R, Lehnert T, Figge MT, Löffler J, et al. A second stimulus required for enhanced antifungal activity of human neutrophils in blood is provided by anaphylatoxin C5a. *J Immunol.* (2015) 194:1199–210. doi: 10.4049/jimmunol.1401845
17. Hünniger K, Lehnert T, Bieber K, Martin R, Figge MT, Kurzai O. A virtual infection model quantifies innate effector mechanisms and *Candida albicans* immune escape in human blood. *PLoS Comput Biol.* (2014) 10:e1003479. doi: 10.1371/journal.pcbi.1003479
18. Dix A, Hünniger K, Weber M, Guthke R, Kurzai O, Linde J. Biomarker-based classification of bacterial and fungal whole-blood infections in a genome-wide expression study. *Front Microbiol.* (2015) 6:171. doi: 10.3389/fmicb.2015.00171
19. Dhama K, Chakraborty S, Verma AK, Tiwari R, Barathidasan R, Kumar A, et al. Fungal/mycotic diseases of poultry-diagnosis, treatment and control: a review. *Pak J Biol Sci.* (2013) 16:1626–40. doi: 10.3923/pjbs.2013.1626.1640
20. Curtis Velasco M. Candidiasis and cryptococcosis in birds. *Semin Avian Exot Pet Med.* (2000) 9:75–81. doi: 10.1053/AX.2000.4620
21. Tsai SS, Park JH, Hirai K, Itakura C. Aspergillosis and candidiasis in psittacine and passeriforme birds with particular reference to nasal lesions. *Avian Pathol.* (1992) 21:699–709. doi: 10.1080/03079459208418892
22. Wyatt RD, Simmons DG, Hamilton PB. Induced systemic candidiasis in young broiler chickens. *Avian Dis.* (1975) 19:533–43. doi: 10.2307/1589079
23. Swaggerty CL, Pevzner IY, Lowry VK, Farnell MB, Kogut MH. Functional comparison of heterophils isolated from commercial broiler chickens. *Avian Pathol.* (2003) 32:95–102. doi: 10.1080/0307945021000070769
24. Redmond SB, Chuammitri P, Andreasen CB, Palic D, Lamont SJ. Genetic control of chicken heterophil function in advanced intercross lines: associations with novel and with known *Salmonella* resistance loci and a likely mechanism for cell death in extracellular trap production. *Immunogenetics.* (2011) 63:449–58. doi: 10.1007/s00251-011-0523-y
25. Lieboldt M-A, Halle I, Frahm J, Schrader L, Baulain U, Henning M, et al. Phylogenic versus selection effects on growth development, egg laying and egg quality in purebred laying hens. *Europ Poult Sci.* (2015) 79:1–16. doi: 10.1399/eps.2015.89
26. Lieboldt MA, Frahm J, Halle I, Gors S, Schrader L, Weigend S, et al. Metabolic and clinical response to *Escherichia coli* lipopolysaccharide in layer pullets of different genetic backgrounds supplied with graded dietary L-arginine. *Poult Sci.* (2016) 95:595–611. doi: 10.3382/ps/pev359
27. Blohm U, Weigend S, Preisinger R, Beer M, Hoffmann D. Immunological competence of different domestic chicken breeds against avian influenza infection. *Avian Dis.* (2016) 60(1 Suppl.):262–8. doi: 10.1637/11159-051615-RegR
28. Lehnert T, Timme S, Pollmacher J, Hünniger K, Kurzai O, Figge MT. Bottom-up modeling approach for the quantitative estimation of parameters in pathogen-host interactions. *Front Microbiol.* (2015) 6:608. doi: 10.3389/fmicb.2015.00608
29. Prausse MTE, Lehnert T, Timme S, Hünniger K, Leonhardt I, Kurzai O, et al. Predictive virtual infection modeling of fungal immune evasion in human whole blood. *Front Immunol.* (2018) 9:560. doi: 10.3389/fimmu.2018.00560
30. Timme S, Lehnert T, Prausse MTE, Hünniger K, Leonhardt I, Kurzai O, et al. Quantitative simulations predict treatment strategies against fungal infections in virtual neutropenic patients. *Front Immunol.* (2018) 9:667. doi: 10.3389/fimmu.2018.00667
31. Polasky C, Weigend S, Schrader L, Berndt A. Non-specific activation of CD8alpha-characterised gammadelta T cells in PBL cultures of different chicken lines. *Vet Immunol Immunopathol.* (2016) 179:1–7. doi: 10.1016/j.vetimm.2016.07.008
32. Hartmann W. Evaluation of major genes affecting resistance to disease in poultry. *Worlds Poult Sci J.* (1997) 53:231–52. doi: 10.1079/WPS19970019
33. Mollnes TE, Brekke OL, Fung M, Fure H, Christiansen D, Bergseth G, et al. Essential role of the C5a receptor in E coli-induced oxidative burst and phagocytosis revealed by a novel lepirudin-based human whole blood model of inflammation. *Blood.* (2002) 100:1869–77.
34. Balwit JM, van Langevelde P, Vann JM, Proctor RA. Gentamicin-resistant menadione and hemin auxotrophic staphylococcus aureus persist within cultured endothelial cells. *J Infect Dis.* (1994) 170:1033–7. doi: 10.1093/infdis/170.4.1033
35. Kahl BC, Goulian M, van Wamel W, Herrmann M, Simon SM, Kaplan G, et al. Staphylococcus aureus RN6390 replicates and induces apoptosis in a pulmonary epithelial cell line. *Infect Immun.* (2000) 68:5385–92. doi: 10.1128/IAI.68.9.5385-5392.2000
36. Minogue TD, Daligault HA, Davenport KW, Bishop-Lilly KA, Broomall SM, Bruce DC, et al. Complete genome assembly of *Escherichia coli* ATCC 25922, a serotype O6 reference strain. *Genome Announc.* (2014) 2:e00969–14. doi: 10.1128/genomeA.00969-14
37. Scholz O, Thiel A, Hillen W, Niederweis M. Quantitative analysis of gene expression with an improved green fluorescent protein. p6. *Eur J Biochem.* (2000) 267:1565–70. doi: 10.1046/j.1432-1327.2000.01170.x
38. Chang AC, Cohen SN. Construction and characterization of amplifiable multicopy DNA cloning vehicles derived from the P15A cryptic miniplasmid. *J Bacteriol.* (1978) 134:1141–56. doi: 10.1128/JB.134.3.1141-1156.1978
39. Ho SN, Hunt HD, Horton RM, Pullen JK, Pease LR. Site-directed mutagenesis by overlap extension using the polymerase chain reaction. *Gene.* (1989) 77:51–9. doi: 10.1016/0378-1119(89)90358-2
40. Yanisch-Perron C, Vieira J, Messing J. Improved M13 phage cloning vectors and host strains: nucleotide sequences of the M13mp18 and pUC19 vectors. *Gene.* (1985) 33:103–19. doi: 10.1016/0378-1119(85)90120-9
41. Mast J, Goddeeris BM, Peeters K, Vandesande F, Berghman LR. Characterisation of chicken monocytes, macrophages and interdigitating cells by the monoclonal antibody KUL01. *Vet Immunol Immunopathol.* (1998) 61:343–57. doi: 10.1016/S0165-2427(97)00152-9
42. Kaspers B, Lillehoj HS, Lillehoj EP. Chicken macrophages and thrombocytes share a common cell surface antigen defined by a monoclonal antibody. *Vet Immunol Immunopathol.* (1993) 36:333–46. doi: 10.1016/0165-2427(93)90029-4
43. Viertlboeck BC, Gobel TW. Chicken thrombocytes express the CD51/CD61 integrin. *Vet Immunol Immunopathol.* (2007) 119:137–41. doi: 10.1016/j.vetimm.2007.06.017
44. Chen CL, Ager LL, Gartland GL, Cooper MD. Identification of a T3/T cell receptor complex in chickens. *J Exp Med.* (1986) 164:375–80. doi: 10.1084/jem.164.1.375
45. Rothwell CJ, Vervelde L, Davison TF. Identification of chicken Bu-1 alloantigens using the monoclonal antibody AV20. *Vet Immunol Immunopathol.* (1996) 55:225–34. doi: 10.1016/S0165-2427(96)05635-8
46. Seliger C, Schaerer B, Kohn M, Pendl H, Weigend S, Kaspers B, et al. A rapid high-precision flow cytometry based technique for total white blood cell counting in chickens. *Vet Immunol Immunopathol.* (2012) 145:86–99. doi: 10.1016/j.vetimm.2011.10.010
47. Berndt A, Wilhelm A, Jugert C, Pieper J, Sachse K, Methner U. Chicken cecum immune response to *Salmonella enterica* serovars of different levels of invasiveness. *Infect. Immunity.* (2007) 75:5993–6007. doi: 10.1128/IAI.00695-07
48. Carvajal BG, Methner U, Pieper J, Berndt A. Effects of *Salmonella enterica* serovar Enteritidis on cellular recruitment and cytokine gene expression in caecum of vaccinated chickens. *Vaccine.* (2008) 26:5423–33. doi: 10.1016/j.vaccine.2008.07.088
49. Wang J, Adelson DL, Yilmaz A, Sze S-H, Jin Y, Zhu JJ. Genomic organization, annotation, and ligand-receptor inferences of chicken chemokines and chemokine receptor genes based on comparative genomics. *BMC Genomics.* (2005) 6:45. doi: 10.1186/1471-2164-6-45
50. Pfaffl MW. A new mathematical model for relative quantification in real-time RT-PCR. *Nucleic Acids Res.* (2001) 29:e45. doi: 10.1093/nar/29.9.e45
51. Figge MT. Stochastic discrete event simulation of germinal center reactions. *Phys Rev E Stat Nonlin Soft Matter Phys.* (2005) 71(5 Pt 1):051907. doi: 10.1103/PhysRevE.71.051907

52. Greve B, Beller C, Cassens U, Sibrowski W, Severin E, Göhde W. High-grade loss of leukocytes and hematopoietic progenitor cells caused by erythrocyte-lysing procedures for flow cytometric analyses. *J Hematother Stem Cell Res.* (2003) 12:321–30. doi: 10.1089/152581603322023052
53. Naghizadeh M, Larsen FT, Wattrang E, Norup LR, Dalgaard TS. Rapid whole blood assay using flow cytometry for measuring phagocytic activity of chicken leukocytes. *Vet Immunol Immunopathol.* (2019) 207:53–61. doi: 10.1016/j.vetimm.2018.11.014
54. Peng L, Matthijs MGR, Haagsman HP, Veldhuizen EJA. Avian pathogenic *Escherichia coli*-induced activation of chicken macrophage HD11cells. *Dev Comp Immunol.* (2018) 87:75–83. doi: 10.1016/j.dci.2018.05.019
55. Flannagan RS, Heit B, Heinrichs DE. Intracellular replication of *Staphylococcus aureus* in mature phagolysosomes in macrophages precedes host cell death, and bacterial escape and dissemination. *Cell Microbiol.* (2016) 18:514–35. doi: 10.1111/cmi.12527
56. Gibson MA, Bruck J. Efficient exact stochastic simulation of chemical systems with many species and many channels. *J Phys Chem A.* (2000) 104:1876–89. doi: 10.1021/jp993732q
57. Gillespie D. Exact stochastic simulation of coupled chemical-reactions. *J Phys Chem.* (1977) 81:2340–61. doi: 10.1021/j100540a008
58. Gillespie D. A general method of numerically simulating the stochastic time evolution of coupled chemical reactions. *J Comput Phys.* (1976) 22:403–34. doi: 10.1016/0021-9991(76)90041-3
59. Genovese KJ, He H, Swaggerty CL, Kogut MH. The avian heterophil. *Dev Comp Immunol.* (2013) 41:334–40. doi: 10.1016/j.dci.2013.03.021
60. Uwamahoro N, Verma-Gaur J, Shen HH, Qu Y, Lewis R, Lu J, et al. The pathogen *Candida albicans* hijacks pyroptosis for escape from macrophages. *mBio.* (2014) 5:e00003–14. doi: 10.1128/mBio.00003-14
61. Vylkova S, Lorenz MC. Phagosomal neutralization by the fungal pathogen *candida albicans* induces macrophage pyroptosis. *Infect Immun.* (2017) 85:e00832–16. doi: 10.1128/IAI.00832-16
62. Vrentas CE, Schaut RG, Boggiatto PM, Olsen SC, Sutterwala FS, Moayeri M. Inflammasomes in livestock and wildlife: Insights into the intersection of pathogens and natural host species. *Vet Immunol Immunopathol.* (2018) 201:49–56. doi: 10.1016/j.vetimm.2018.05.008
63. Passantino L, Massaro MA, Jirillo F, Di Modugno D, Ribaud MR, Modugno GD, et al. Antigenically activated avian erythrocytes release cytokine-like factors: a conserved phylogenetic function discovered in fish. *Immunopharmacol Immunotoxicol.* (2007) 29:141–52. doi: 10.1080/08923970701284664
64. Harmon BG, Glisson JR. *In vitro* microbicidal activity of avian peritoneal macrophages. *Avian Dis.* (1989) 33:177–81. doi: 10.2307/1591085
65. Duggan S, Leonhardt I, Hunniger K, Kurzai O. Host response to *Candida albicans* bloodstream infection and sepsis. *Virulence.* (2015) 6:316–26. doi: 10.4161/21505594.2014.988096
66. Fradin C, de Groot P, MacCallum D, Schaller M, Klis F, Odds FC, et al. Granulocytes govern the transcriptional response, morphology and proliferation of *Candida albicans* in human blood. *Mol Microbiol.* (2005) 56:397–415. doi: 10.1111/j.1365-2958.2005.04557.x
67. Terron MP, Cubero J, Barriga C, Ortega E, Rodriguez AB. Phagocytosis of *Candida albicans* and superoxide anion levels in ring dove (*Streptopelia risoria*) heterophils: effect of melatonin. *J Neuroendocrinol.* (2003) 15:1111–5. doi: 10.1111/j.1365-2826.2003.01103.x
68. Brune K, Leffell MS, Spitznagel JK. Microbicidal activity of peroxidaseless chicken heterophile leukocytes. *Infect Immunity.* (1972) 5:283–7. doi: 10.1128/IAI.5.3.283-287.1972
69. Evans EW, Beach FG, Moore KM, Jackwood MW, Glisson JR, Harmon BG. Antimicrobial activity of chicken and turkey heterophil peptides CHP1, CHP2, THP1, and THP3. *Vet Microbiol.* (1995) 47:295–303. doi: 10.1016/0378-1135(95)00126-3
70. Alteri CJ, Mobley HLT. *Escherichia coli* physiology and metabolism dictates adaptation to diverse host microenvironments. *Curr Opin Microbiol.* (2012) 15:3–9. doi: 10.1016/j.mib.2011.12.004
71. Njoroge JW, Nguyen Y, Curtis MM, Moreira CG, Sperandio V. Virulence meets metabolism: Cra and KdpE gene regulation in enterohemorrhagic *Escherichia coli*. *mBio.* (2012) 3:e00280. doi: 10.1128/mBio.00280-12
72. Ene IV, Adya AK, Wehmeier S, Brand AC, MacCallum DM, Gow NA, et al. Host carbon sources modulate cell wall architecture, drug resistance and virulence in a fungal pathogen. *Cell Microbiol.* (2012) 14:1319–35. doi: 10.1111/j.1462-5822.2012.01813.x
73. Brown SA, Palmer KL, Whiteley M. Revisiting the host as a growth medium. *Nat Rev Microbiol.* (2008) 6:657–66. doi: 10.1038/nrmicro1955
74. Ferdous F, Saski C, Bridges W, Burns M, Dunn H, Elliott K, et al. Transcriptome profile of the chicken thrombocyte: new implications as an advanced immune effector cell. *PLoS ONE.* (2016) 11:e0163890. doi: 10.1371/journal.pone.0163890
75. Swaggerty CL, Kogut MH, Ferro PJ, Rothwell L, Pevzner IY, Kaiser P. Differential cytokine mRNA expression in heterophils isolated from *Salmonella*-resistant and -susceptible chickens. *Immunology.* (2004) 113:139–48. doi: 10.1111/j.1365-2567.2004.01939.x
76. Chausse AM, Grepinet O, Bottreau E, Le Vern Y, Menanteau P, Trotereau J, et al. Expression of Toll-like receptor 4 and downstream effectors in selected cecal cell subpopulations of chicks resistant or susceptible to *Salmonella* carrier state. *Infect Immun.* (2011) 79:3445–54. doi: 10.1128/IAI.00025-11
77. Swaggerty CL, Kaiser P, Rothwell L, Pevzner IY, Kogut MH. Heterophil cytokine mRNA profiles from genetically distinct lines of chickens with differential heterophil-mediated innate immune responses. *Avian Pathol.* (2006) 35:102–8. doi: 10.1080/03079450600597535

Conflict of Interest: The authors declare that the research was conducted in the absence of any commercial or financial relationships that could be construed as a potential conflict of interest.

frontiers in Immunology

ORIGINAL RESEARCH
published: 07 April 2020
doi: 10.3389/fimmu.2020.00584

Differential Effects of Drinking Water Quality on Phagocyte Responses of Broiler Chickens Against Fungal and Bacterial Challenges

Juan A. More-Bayona[1], *Débora Torrealba*[1], *Caitlin Thomson*[1], *Jeremy Wakaruk*[2] *and Daniel R. Barreda*[1,2]*

[1] *Laboratory of Immunology and Animal Health, Department of Biological Sciences, University of Alberta, Edmonton, AB, Canada,* [2] *Department of Agricultural, Food and Nutritional Sciences, University of Alberta, Edmonton, AB, Canada*

Combinatorial effects of xenobiotics in water on health may occur even at levels within current acceptable guidelines for individual chemicals. Herein, we took advantage of the sensitivity of the immune system and an avian animal model to examine the impact of xenobiotic mixtures on animal health. Water was derived from an underground well in Alberta, Canada and met guidelines for consumption, but contained a number of contaminants. Changes to chicken immunity were evaluated following acute (7d) exposure to contaminated water under basal and immune challenged conditions. An increase in resident macrophages and a decrease in CD8+ lymphocytes were identified in the abdominal cavity, which served as a relevant site where immune leukocytes could be examined. Subsequent intra-abdominal immune stimulation detected differential *in vivo* acute inflammatory responses to fungal and bacterial challenges. Leukocyte recruitment into the challenge site and activation of phagocyte antimicrobial responses were affected. These functional responses paralleled molecular changes in the expression for pro-inflammatory and regulatory genes. In all, this study primarily highlights dysregulation of phagocyte responses following acute (7d) exposure of poultry to contaminated water. Given that production food animals hold a unique position at the interface of animal, environmental and human health, this emphasizes the need to consider the impact of xenobiotic mixtures in our assessments of water quality.

Keywords: drinking water quality, phagocyte function, acute inflammation, fungal and bacterial challenges, comparative immunology

OPEN ACCESS

Edited by:
Xinjiang Lu,
Ningbo University, China

Reviewed by:
Antonio J. Piantino Ferreira,
University of São Paulo, Brazil
Adenilda Cristina Honorio-França,
Universidade Federal de Mato Grosso, Brazil

***Correspondence:**
Daniel R. Barreda
d.barreda@ualberta.ca

Specialty section:
This article was submitted to Comparative Immunology, a section of the journal Frontiers in Immunology

Received: *07 December 2019*
Accepted: *13 March 2020*
Published: *07 April 2020*

Citation:
More-Bayona JA, Torrealba D, Thomson C, Wakaruk J and Barreda DR (2020) Differential Effects of Drinking Water Quality on Phagocyte Responses of Broiler Chickens Against Fungal and Bacterial Challenges. Front. Immunol. 11:584. doi: 10.3389/fimmu.2020.00584

INTRODUCTION

Water is the most important element for any living organism (1, 2), essential to immune function and the maintenance of homeostasis. This translates into meaningful implications for animal health and performance. To date, most studies on water contamination have focused on the effects of individual contaminants, and concentration values that exceed recommended levels. Given the abundance of different contaminants in the environment, we and others believe that added emphasis should be placed on the combinatorial biological effects of chemicals in these mixtures and their by-products (3–6). This, however, requires a focus on functional read-outs rather than conventional examination for the presence of a growing list of individual contaminants using

chemical analyses. Further, it requires added availability of reagents to capture the impact of these mixtures on a range of terrestrial and aquatic organisms.

Production food animals hold a unique position at the interface of animal, environmental and human health (7–9). Among others, they serve as important sentinels for pathogens and xenobiotics. In the present study, we identified multiple contaminants present in underground water and assessed their combinatorial effects on chicken immunity following acute 7-day exposure. We focused on phagocyte responses, first measuring pre-challenge numbers for resident macrophages and their activation state, as indicators of changes to basal immunity. We then paired these with evaluation of molecular and cellular responses following *in vivo* intra-abdominal challenges with two well-defined fungal and bacterial models. Our fungal model, zymosan, has been widely used in comparative systems and has provided important insights into mechanisms governing the induction and control of acute inflammation (10–15). Our bacterial model, Salmonella enterica serovar Typhimurium (ST), is among the most common and relevant enteric pathogens for the food production industry and public health (16–18). ST is well established to engage phagocyte subsets, inducing marked heterophil and macrophage recruitment and activation in infected chickens (17, 19). Evaluation of these early changes in phagocyte numbers and function showed that contaminants in underground raw water, even within acceptable concentrations, induce marked effects on bird immunity.

MATERIALS AND METHODS

Chickens

Three-week-old Ross 708 broiler chickens (*Gallus gallus*) were used. All animals were housed in the Poultry Research Facility of the Agriculture, Food and Nutritional Sciences at the University of Alberta. Animals were grouped into two experimental treatments: raw underground well water (raw well water) and tap water control group (tap water). Animals were maintained according to guidelines specified by the Canadian Council on Animal Care, and protocols approved by the University of Alberta Animal Care and Use Committee. Maximum efforts were made to minimize animal stress and chickens terminated by cervical dislocation and exsanguination.

Treatment

Drinking water was administrated for 7 days. Following water treatment, chickens were abdominally challenged using zymosan (2.5 mg, Sigma Aldrich), resuspended in 500 μl of 1x $PBS^{-/-}$ (no calcium, no magnesium). Zymosan is a well-established pathogen mimic obtained from *Saccharomyces cerevisae*, which promotes immune cell activation and function through mannose and β-glucans receptors. Previous *in vitro* and *in vivo* studies have shown that zymosan phagocytosis results in activation of pro-inflammatory responses that include induction of pro-inflammatory cytokines, production of reactive oxygen and nitrogen intermediates and increased infiltration of leukocytes, predominantly neutrophils (20–26). The zymosan dose was selected because it allowed for natural transition to resolution of acute inflammatory processes, thus providing a self-resolving peritonitis model for *in vivo* examination of the impact of water quality on bird immunity (10, 27–30). For bacterial challenges, we focused on a *Salmonella enterica* serovar typhimurium X4232 strain (ST). This is a nalidixic-acid resistant strain that have been broadly used to examine inflammation in multiple animal models. In our experimental design, ST was cultured on xylose lysine deoxycolate agar (XLD) for 24 hours at 37°C followed by culture in LB broth at 37°C at 150 rpm for 20 h to obtain 10^9 CFU/ml of culture broth. ST was heat-killed at 80°C in a water bath for 1 h an d resuspended in 1x $PBS^{-/-}$. The goal was to provide a bacterially induced self-resolving immune challenge that would not suffer from confounding factors associated with microbial growth. Heat-killed ST (HKST; 10^9 CFU) was resuspended in 500 μl and keep at −4°C until injection.

Abdominal Lavage

Chickens were euthanized via cervical dislocation and animals were bled to minimize potential blood contamination into the abdominal cavity, as previously described (13, 14). Leukocytes were recovered by injecting 20 ml of incomplete RPMI media into the lower left quadrant at the abdominal site. Harvested leukocytes were kept at 4°C. Non-injected chickens were used as negative controls.

Definition of Phagocyte Populations

Phagocytes were identified using imaging flow cytometry along with modified Wright-Giemsa staining (Hema3). For Hema3 (Fischer Scientific), leukocyte cytospins were stained according to the manufacturer's specifications and analyzed through light microscopy. For imaging flow cytometry, a dot plot of events using area (size, x-axis) vs intensity channel 6 (internal complexity, y-axis) was created to define the different subpopulations using leukocyte morphology and nuclear staining (Draq5). Monoclonal antibodies further helped to define specific leukocyte subpopulations. Monocyte/macrophage labeling was performed using the KUL01 antibody marker (Abcam). This antibody recognizes a homolog of the mammalian mannose receptor C-type, MRC1 (also called CD206) (31, 32). The KUL01 antibody was added to a final concentration of 1:1000, followed by 30 min incubation at 41°C. Cells were washed in $PBS^{-/-}$ and fixed in 1% of formaldehyde. PE anti-chicken $CD4^+$ and Cy5 anti-chicken $CD8^+$ (Abcam) were used for $CD4^+$ and $CD8^+$ T lymphocytes staining, respectively. Anti $CD4^+$ antibody was added at 1:1000 dilution and anti $CD8^+$ T lymphocytes antibody at 1:2000 dilution. Leukocytes were incubated at −4°C for 30 min and followed by 20 min at room temperature. Hoechst 33342 was added as nuclear staining.

Analysis of Phagocyte Function

ROS production was measured using CellROX (Molecular probes), as previously described (13, 14). NO production was determined using DAF-FM diacetate (Molecular Probes) oxidation staining. DAF-FM diacetate reagent was diluted 1:25 in 1x $PBS^{-/-}$ and 4 μl was added for incubation for 30 min at 41°C. Phagocytes were washed with 1x $PBS^{-/-}$ and fixed in 1% formaldehyde.

TABLE 1 | Primers used for qPCR analysis.

Gene	Primer name	Sense	Sequence	Accession number
Interleukin 2	**IL-2**	Fw	ACCGGAAGTGAATGCAAGAT	AF000631
		Rv	AGTGGTCCCAGAATGGACAG	AF000631
Interleukin 8	**IL-8**	Fw	GGCTTGCTAGGGGAAATGA	AJ009800
		Rv	AGCTGACTCTGACTAGGAAACTGT	AJ009800
Tumoral necrosis factor alpha	**TNF-α**	Fw	GTTGACTTGGCTGTCGTGTG	AY765397.1
		Rv	TCAGAGCATCAACGCAAAAG	AY765397.1
Interleukin 1 beta	**IL-1β**	Fw	AGGTCAACATCGCCACCTAC	NM_204524.1
		Rv	ACGAGATGGAAACCAGCAAC	NM_204524.1
Transforming growth factor beta	**TGF-β**	Fw	CGACCTCGACACCGACTACT	NM_001318456.1
		Rv	CCACTTCCACTGCAGATCCT	NM_001318456.1
Inducible nitric oxide synthase	**i-NOS**	Fw	CTCTCACAGGCCTTGACATATT	D85422.1
		Rv	CAGTCTCTGTTTGTCTCCTTCC	D85422.1
Ribosomal 28 subunit	**r28S**	Fw	GGCGAAGCCAGAGGAAACT	FM165415
		Rv	GACGACCGATTTGCACGTC	FM165415
Actin beta	**ACTB**	Fw	CCAGACATCAGGGTGTGATGG	AJ719605
		Rv	CTCCATATCATCCCAGTTGGTGA	AJ719605

Gene Expression

Abdominal leukocytes were kept in Trizol (Thermo Fisher Scientific), stored in liquid nitrogen and total RNA was extracted following manufacturer's specifications. RNA concentration and quality were evaluated using Nanodrop ND-1000 (Thermo Fisher Scientific) and Bioanalyser-2100 with the RNA 6000 Nano Kit (Agilent Technologies), respectively. Samples had a RIN higher than 7.5. cDNA was synthesized with 650 ng of total RNA in a final volume of 20 μl using iScript Kit (BioRad). Transcripts of r28s and ACTB were used as reference genes for quantification purposes. qPCR was carried out using SYBR Green (prepared by Molecular Biology Services Unit staff at the University of Alberta), 500 nM of primers and 2.5 μl of cDNA previously diluted in 10 μl of final volume; and evaluated using the QuantStudio 6 Flex Real-Time PCR System (Applied Biosystems). Primers for qPCR are described in **Table 1**. Relative quantification was performed according to Livak's method (33). Samples were run in triplicates and results were statistically analyzed using Two-way ANOVA followed by Sidak's multiple comparison test to estimate differences between treatments.

Statistical Analysis

GraphPad Prism software was used to assess statistical differences and significance between groups using two-way ANOVA and Sidak's multiple comparison tests. Statistics with $p < 0.05$ were considered significant.

RESULTS

Raw Water Source Selection and Analysis

Raw well water was obtained from a poultry producer in south eastern Alberta, Canada located in an area of high chemical and high fertilizer expense (20, 34), and in close proximity to point source contamination from a natural gas extraction well (located approximately 500 m from water source). The local producer uses this well water as the water source for one chicken coup. Unique to this producer is another nearby coup under his operation, which uses municipal tap water as its water source. We considered this an excellent opportunity to examine source effects as both cohorts were managed by the same producer using equivalent procedures, with only the water being a variable. There were also anecdotal accounts of animal health and performance effects, and the producer had noted a significant difference in the quality of litter across both locations. The litter of the coup where well water is consumed was said to contain higher levels of moisture likely due to a laxative effect. This required the facility have greater ventilation to maintain suitable humidity.

Water was analyzed according to CALA (Canadian Association for Laboratory Accreditation) and ISO17025 standards. Parameters selected for analysis are known to have detrimental effects on human and animal health (21). Higher levels of ammonia, phosphates or potassium for the area pointed to a presence of contaminants stemming from agricultural activities. A summary of the results found in the raw water source used and comparisons to tap water are provided in **Table 2**. From more than 150 elements tested in the well water used, some were found to be near but above acceptable guidelines, including calcium carbonate and bicarbonate, sulfates and sodium. We also found trace concentrations of total penta chloro-dibenzo-p-dioxin and octa chloro-dibenzo-p-dioxin, members of a group known as dioxins. Additional parameters were significantly lower than maximum acceptable levels and, thus, not included in the table.

Raw Well Water Increases Basal Numbers of Abdominal Resident Macrophages While Decreasing $CD8^+$ T Lymphocytes in Chickens

We first evaluated whether acute exposure to raw well water resulted in changes to basal chicken immunity and used the abdominal cavity as a relevant site where immune leukocytes

TABLE 2 | Summary of xenobiotics found in raw and tap water.

Parameter name	Units	Results (raw)	Results (tap)	Max. acceptable concentration
Total dissolved solids	ppm	970	230	1000
Chloride	ppm	23	6.5	200
Ph	pH	8.40	8.03	7.0–10.5
Alkalinity (CaCO3, Bicarb)	ppm	570	170	300
Nitrates	ppm	<0.01	0.32	25
Sulfates	ppm	220	77	200
Iron	ppm	0.06	<0.06	0.3
Calcium	ppm	6.6	46	60
Copper	ppm	0.0034	0.42	0.6
Magnesium	ppm	0.93	13	125
Manganese	ppm	0.015	<0.0040	0.05
Sodium	ppm	390	17	150
Zinc	ppm	0.0061	0.034	1.5
Total Penta CCD*	pg/L	1.54	N/A	2**-2.3***pg/Kg/day
Octa CDD*	pg/L	5.7	N/A	2**-2.3***pg/Kg/day
Fecal coliforms	CFU	0	0	0

*chloro-dibenzo-p-dioxin.
**World health organization (35).
***European Commisision's Scientific Committee on Food (36).

could be examined. We identified a higher proportion of abdominal macrophages in animals that consumed raw well water for 7d compared to animals which were provided with normal tap water, even though the former still met stringent Canadian drinking water guidelines for consumption (**Figure 1**, $p = 0.012$). In contrast, we observed a reduced proportion of CD8+ T lymphocytes in the raw well water group compared to the tap water control group (**Figure 1**, $p = 0.023$). No changes were observed in the proportions of CD4+ leukocytes between control and raw well water exposed groups under non-immune challenged conditions (data not shown).

Drinking Water Quality Affects Leukocyte Recruitment During Acute Inflammation

Results above showed that drinking water quality affected resident leukocyte numbers even when exposure was limited to 7 days. We then evaluated the impact under immune challenged conditions. Birds were injected intra-abdominally with zymosan or heat killed Salmonella enterica serovar Typhimurium (HKST) following this same 7d water exposure. Leukocyte recruitment was assessed 4, 12 and 48 h after *in vivo* challenge (**Figure 2A**). Values were not significantly different across raw well water and tap water (control) treatments when total leukocyte migration numbers were considered. Higher resolution analyses, however, showed extended heterophil retention within the abdominal cavity for birds in the raw well water group following *in vivo* bacterial challenge (**Figure 2B**, 48 h post-challenge, $p = 0.019$). Concurrently, the proportion of monocyte/macrophages remained lower in the raw well water group at this 48 h time point (**Figure 2B**, $p = 0.004$). Although our fungal challenge showed similar kinetics of leukocyte recruitment, dominated by heterophil infiltration, the effect on heterophil retention was limited to the bacterial challenge (**Figure 2B**).

Drinking Water Quality Affects Phagocyte Function at the Immune Challenge Site

ROS and NO production were selected as highly conserved antimicrobial mechanisms of immune defense. Fungal stimulation led to a higher proportion of ROS producing leukocytes in chickens that consumed raw well water (60% compared to 30% ROS producing leukocytes in control tap water group; **Figure 3**, $p= 0.0009$). In contrast, no difference was observed between tap (control) and raw well water groups following heat-killed Salmonella stimulation. Chicken NO production was also affected by drinking water quality. However, unlike ROS this was not evident when total leukocyte population was considered. Higher resolution analysis at the single cell level using imaging flow cytometry showed that levels of heterophil NO production were downregulated by 12 h post zymosan challenge in animals exposed to raw well water, compared to the control group which remained high at this time point (**Figure 3**, $p = 0.041$). As with production of reactive oxygen intermediates, the impact on NO production was limited to our fungal challenge.

Raw Well Water Promoted Expression of Pro-inflammatory Leukocyte Genes During Acute Inflammation

The impact of raw well water on leukocyte recruitment and function highlighted above paralleled changes observed at the molecular level. Effects were most pronounced in the zymosan-challenged group and impacted both kinetics and absolute levels of pro-inflammatory gene expression. Differences were evident as early as (4 h), where leukocytes derived from birds supplied with raw well water showed significantly higher levels of gene expression for TNFα, IL-1β, IL-8, and iNOS (**Figure 4**; TNFα $p < 0.001$; IL-1β $p = 0.0013$; IL-8 $p < 0.0001$; iNOS $p < 0.0001$). Notably, anti-inflammatory cytokine gene expression (TGF-β) was also upregulated early in the acute inflammatory response among leukocytes derived from the raw well water group, consistent with dysregulation of the immune response (**Figure 4**, $p < 0.0001$). Parallel experiments using our heat killed Salmonella enterica serovar Typhimurium *in vivo* challenge also displayed a dysregulated phenotype with upregulation of IL-8 and downregulation of IL-2 in the raw well water group. However, the effect was less marked than with the fungal *in vivo* challenge model shown above.

DISCUSSION

Assessment of water quality has become more challenging given the number and variety of xenobiotics that can enter the water supply from various sources. For pesticides and fertilizers, monitoring studies have shown that they are reaching Canada's water resources (22–25). While concentrations of these chemicals

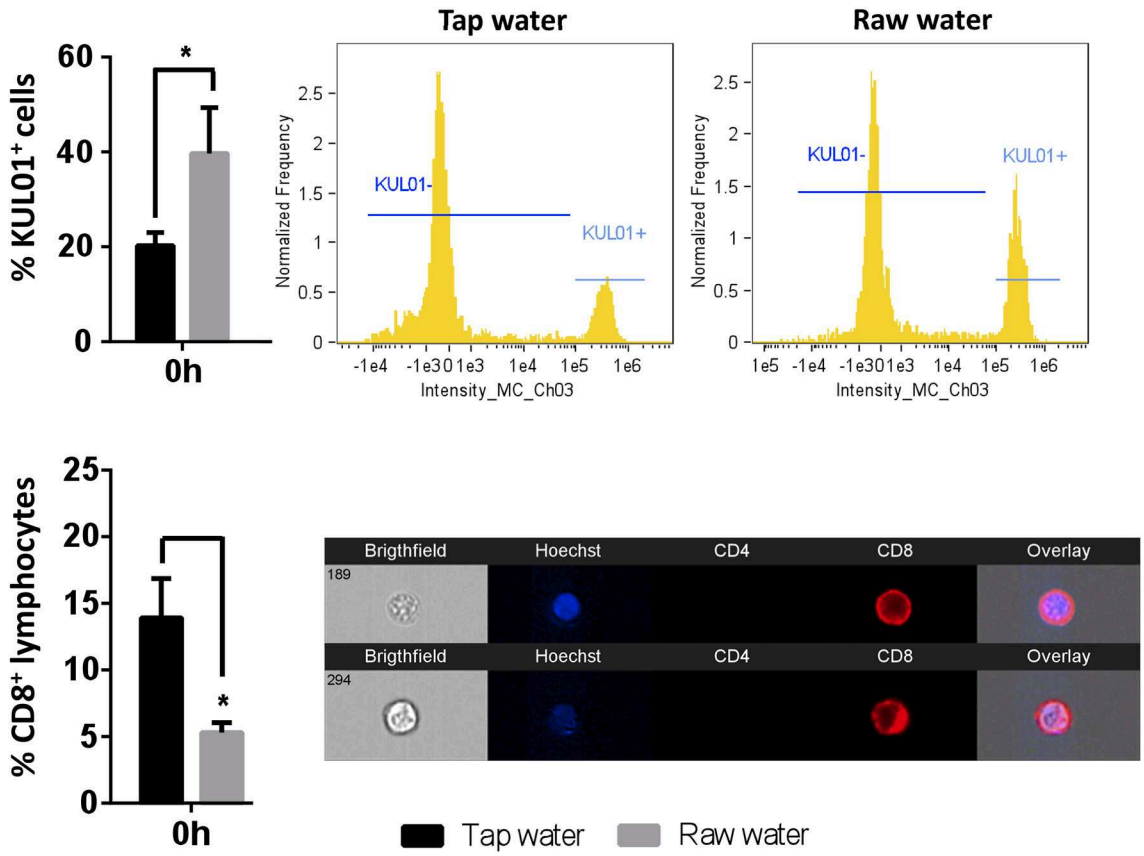

FIGURE 1 | Short-term exposure to raw well drinking water impacts resident macrophage and lymphocyte numbers in broiler chickens. Birds were exposed to well water as drinking source for 7d. Leukocytes were isolated through abdominal lavage and incubated with anti-PE-KUL01 antibody, to determine the proportions of resident macrophages. CD8 T lymphocytes were identified using a Cy5 anti-chicken CD8 antibody. Data represents mean ± SEM ($n = 6$). Differences were assessed using two-way ANOVA and Sidak's multiple comparison test. *$p < 0.05$.

in water are generally low, they are commonly detected, particularly in regions of significant urban or agricultural development. Overall, farmland applications of pesticides and fertilizers have almost tripled in Alberta over the last 25 years (23). For pesticides, Alberta shows the second-highest amount of pesticide utilization in Canada, and although the relatively dry climate reduces the potential risk for water contamination throughout the year, significant risk still exists during episodes of surface water runoff (26). Unfortunately, the River Pesticide Index from which these values are derived from does not measure the risk to aquatic life, irrigated crop production, or drinking water sources (25). At the same time that agriculture operations continue to expand in this province, both the number and size of smaller communities near agricultural centers in the North and South Saskatchewan River Basins continue to increase (37, 38). These smaller communities display the highest vulnerability to water contamination episodes because of the proximity to the sources of contamination, their reliance of the water resources for drinking water, recreation, and irrigation of field crops, and because personnel and infrastructure for water treatment is often limited compared to larger population centers (39–41). As such, the convergence between expanding agricultural operations and local rural populations creates added risk for occurrence of acute and chronic diseases associated with exposure to pathogens and/or chemicals. In one example, the high levels of mixed animal agriculture in the Oldman river region have already been linked to one of the highest incidences of gastroenteritis in Canada (42, 43). These issues are not limited to Canada, but increasingly relevant globally (44–48).

Production animals fill a central position at the interface environment, animal and human health. They serve as sentinels for multiple infections and environmental contaminants, and impacts to their health status can facilitate the spread of infectious agents to consumers and the environment. Given the broad use of water resources for production animal rearing both geographically and throughout an animal's development, drinking water can play a significant and sustained role in the health of these animals. In this study, we identified no instances of morbidity or mortality in any of the treatment groups. However, we identified multiple effects of drinking water on bird immunity, even though this well water met stringent Canadian drinking water guidelines for consumption. Short-term (7d) exposure

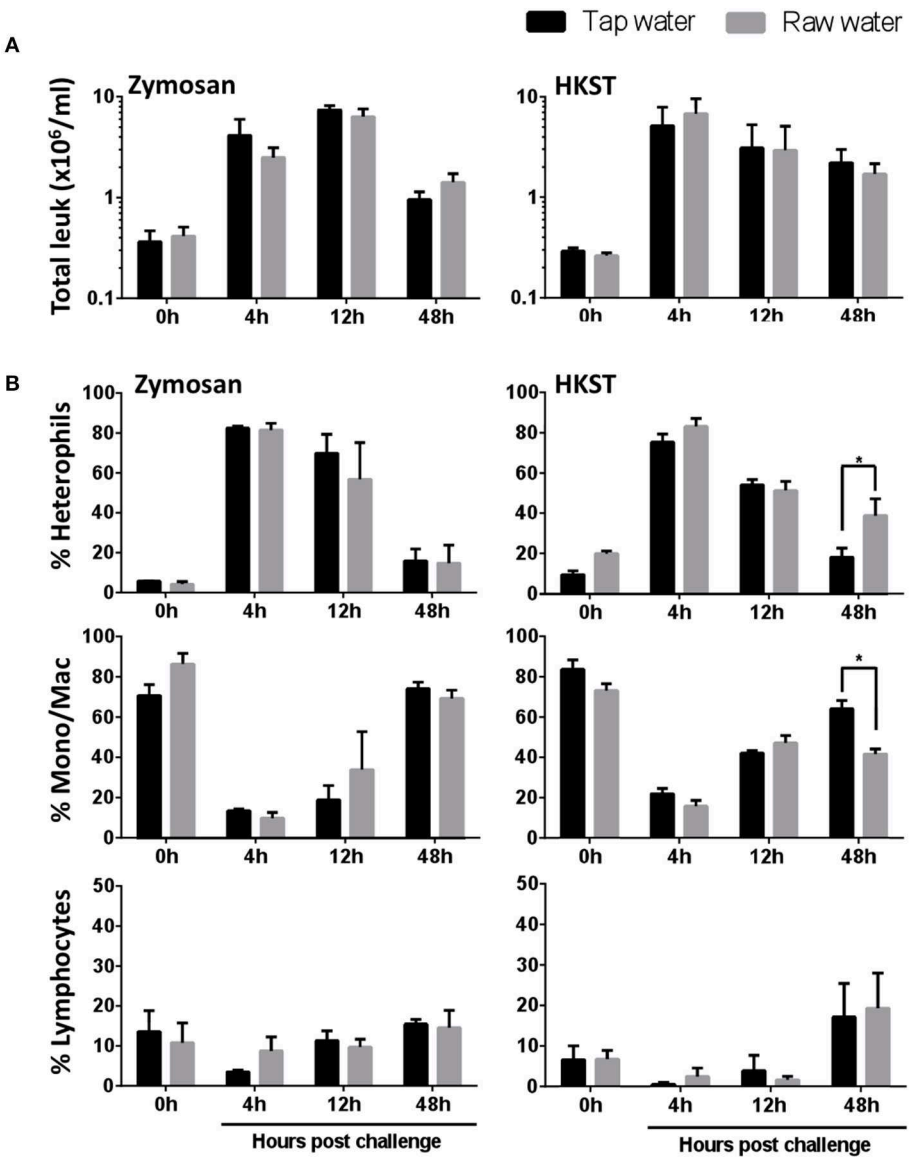

FIGURE 2 | Raw well water differentially affects leukocyte recruitment following fungal and bacterial *in vivo* stimulation. Following 7d raw well water consumption, birds were challenged *in vivo* via intra-abdominal route using zymosan (fungal) or heat killed Salmonella enterica serovar Typhimurium (HKST; bacterial). Abdominal lavages were performed at 0, 4, 12, and 48 h post intra-abdominal challenge. **(A)** Total leukocytes were counted using a hemocytometer and light microscopy. **(B)** The proportions of heterophils, monocyte/macrophages and lymphocytes were determined using Imaging flow cytometry along with conventional Wright Giemsa staining. Data represents mean ± SEM ($n = 7$). Differences were evaluated using two-way ANOVA and Sidak's multiple comparison test. $^*p < 0.05$.

to xenobiotic mixtures through drinking water changed the resident leukocyte profile of test birds, with greater numbers of macrophages and lower numbers of CD8+ lymphocytes in the chicken abdominal cavity. We expect that these basal changes are associated with changes in the capacity of these birds to recognize and respond to pathogen infiltration. This is consistent with previous reports using murine models, where tissue macrophage numbers were shown to change following chemical exposure (49, 50). Notably, this is the first report of changes in the abundance of $CD8^+$ T lymphocytes after xenobiotic exposure. Our understanding of leukocyte subsets in chickens, and reagents to examine them, continues to expand. It will be interesting to take advantage of these in the coming years as we look to gain added resolution into the impact of xenobiotics on subset composition for the leukocyte pool under basal and immune challenged conditions.

The contributions of immune defenses to host integrity are tightly linked to the effective induction and resolution of inflammatory processes (51–53). Deviations in efficient leukocyte recruitment to infection sites can severely impact host health, disease transmission and performance (52, 53). Our results showed extended heterophil retention within the abdominal

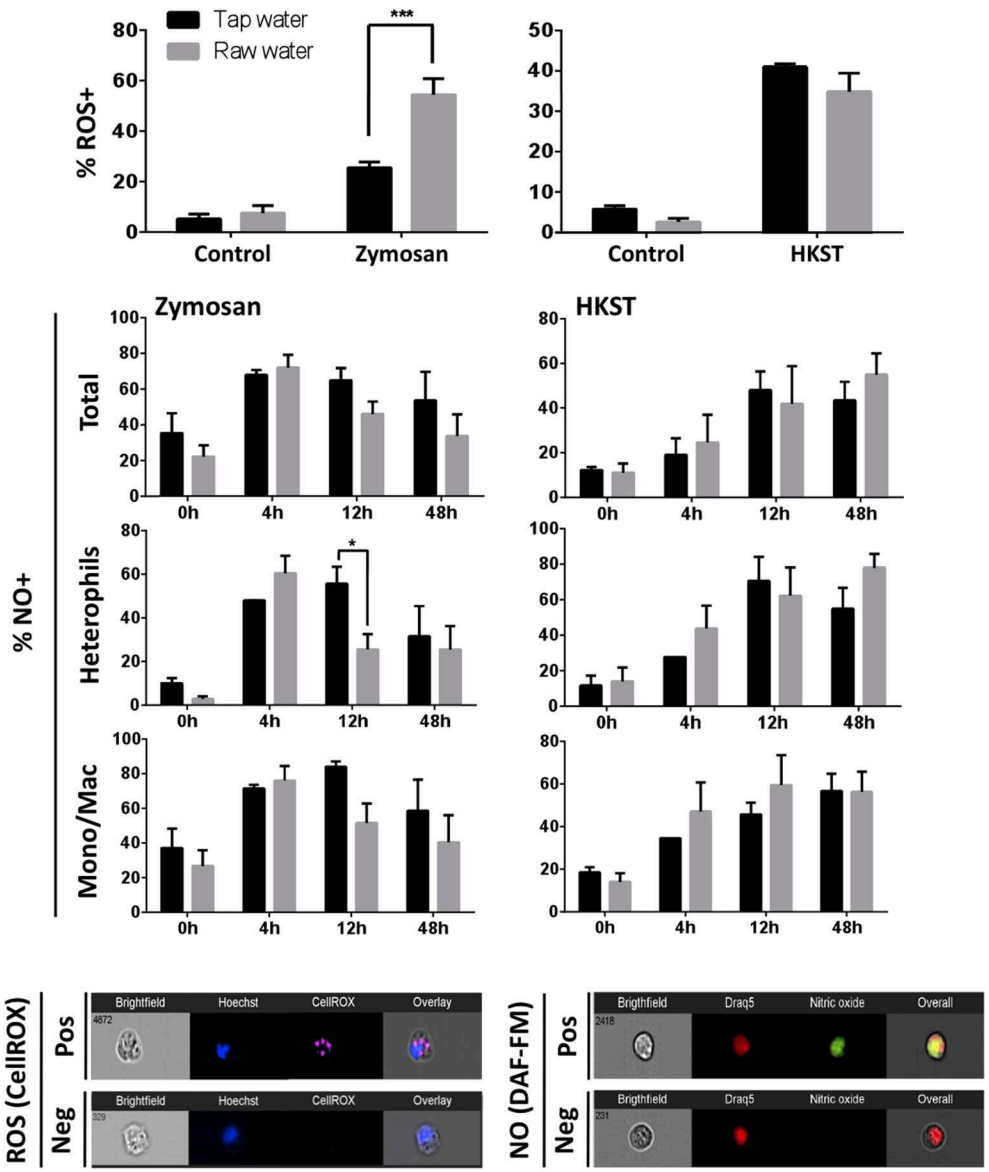

FIGURE 3 | Raw well water treatment differentially impacts phagocyte antimicrobial responses. Birds were exposed to well water as drinking source for 7d and subsequently exposed to fungal or bacterial *in vivo* stimulation. Respiratory burst (ROS production) capacity in isolated leukocytes was assessed using CellROX. Nitric oxide (NO) production was determined using DAF-FM diacetate. Data represents mean ± SEM ($n = 5$). Significant differences were identified using two-way ANOVA and Sidak's multiple comparison test (***$p < 0.001$; *$p < 0.05$). Representative images from an ImageStream MKII flow cytometer show positive (pos) and negative (neg) cells following staining with CellROX and DAF-FM diacetate.

cavity for birds in the raw well water group following *in vivo* bacterial challenge (**Figure 5**). These higher heterophil levels in late phases of acute inflammation coupled to maintenance of ROS and NO production capacity, suggests an extended pro-inflammatory phenotype following bacterial challenge. The concurrent lower proportion of monocyte/macrophages late in the acute inflammation process further suggests a lower capacity and/or slower transition toward activation of tissue repair mechanisms at the infection site. This has broad implications for resolution of inflammatory responses, energy expenditure and the efficient activation of downstream adaptive mechanisms of immunity upon bacterial infection. Interestingly, differential effects were detected in leukocyte recruitment and retention between the fungal and bacterial *in vivo* challenges used in this study. Characterization of phagocyte ROS and NO production also highlighted differential effects among fungal and bacterial challenges. Among the potential implications of these effects, is a differential impact of xenobiotics to the susceptibility of these animals to various infectious challenges.

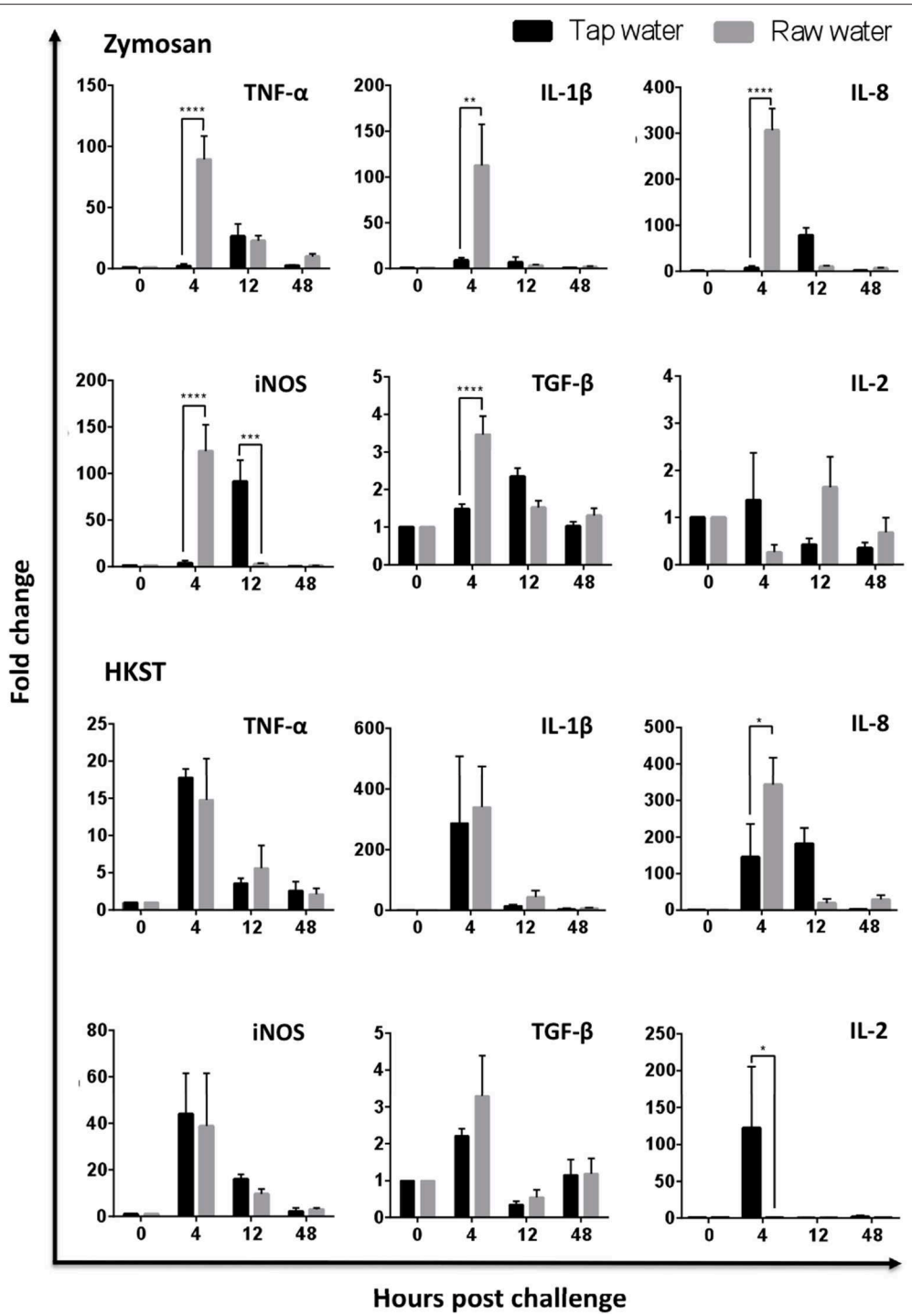

FIGURE 4 | Raw well water treatment induces changes in leukocyte expression of pro-inflammatory and regulatory genes. Birds were exposed to well water as drinking source for 7d and subsequently exposed to fungal or bacterial *in vivo* stimulation. Abdominal leukocytes were harvested at 0, 4, 12, and 48 h post challenge. Gene expression was analyzed by qPCR. Data represents mean ± SEM ($n = 4$). Significant differences were analyzed using two-way ANOVA and Sidak's multiple comparison test. *$p < 0.05$, **$p < 0.01$, ***$p < 0.001$, ****$p < 0.0001$.

The impact of raw well water on leukocyte recruitment and function highlighted above paralleled changes observed at the molecular level. The kinetics and absolute levels of gene expression changed for multiple pro-inflammatory mediators, particularly among zymosan challenged birds. Importantly, gene expression of the anti-inflammatory

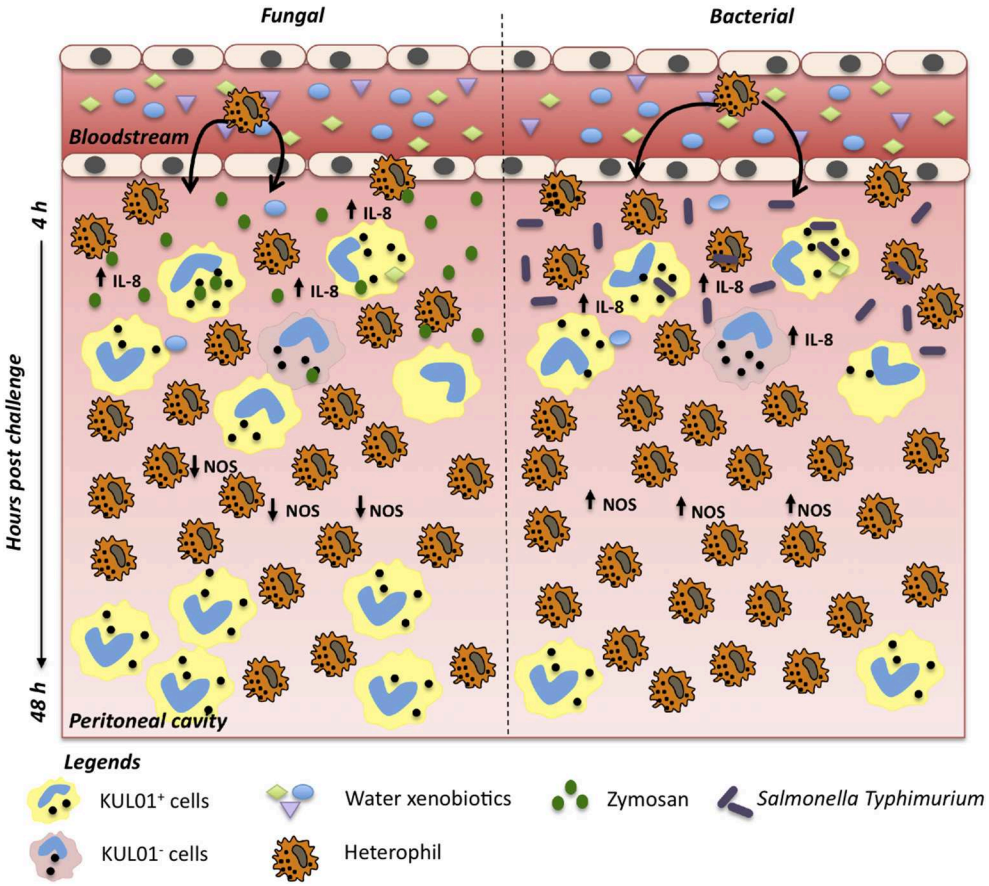

FIGURE 5 | Differential effect of raw water in chicken acute inflammation against fungi and bacterial challenges. After intra-abdominal challenge, following acute exposure to raw water, promotes differential effect on inflammatory process. In a fungi model, we observed marked heterophil infiltration a few hours after *in vivo* challenge, likely driven by a more prominent resident macrophage pool along with an upregulated IL-8, TNF-α, and IL-1β expression. At 12 h post challenge, NO levels and iNOS gene expression were downregulated. Acute inflammatory process is largely complete by 48 h post challenge, allowing a return to homeostasis. In a bacterial model, we also observed marked heterophil infiltration which paralleled up-regulation of IL-8 gene expression. No down-regulation effect was observed in the cellular and molecular levels of NO at 12 h post-challenge. However, 48 h post challenge, heterophil proportions remained higher, while monocyte/macrophage pool remained lower, consistent with a longer acute pro-inflammatory response.

cytokine TGF-β was also upregulated early in the acute inflammatory response among leukocytes derived from the raw well water group. This is consistent with molecular changes observed in other models with individual chemicals, where exposure was shown to promote higher expression in genes including IL-1β, TGF β, and others (50, 54, 55). Together, this suggests dysregulation of the acute inflammatory response following exposure to xenobiotics in drinking water. It will be important to determine if these alterations further compromise the engagement of adaptive mechanisms of immunity and potentially impact the development of long-term protection against pathogens.

Altogether, this work provides added depth in our understanding of the impact of drinking water quality on immune function. Among the greatest advantages of this strategy, is the temporal integration of individual and interactive effects of exposure to multiple contaminants into a few measurable parameters. Our work also demonstrates that these functional platforms can be setup in non-classical animal models to target discrete effects on animal populations that sit at the interface between animal, public and environmental health. As others have already noted, unfortunately, current maximum acceptable levels for individual contaminants in water do not account for the synergistic biological effects of related chemicals and their breakdown products (3, 4, 56, 57). Further, comprehensive screens for individual contaminants are cost prohibitive and thus can only focus on a discrete number of representative compounds. Thus, it is critical that combinatorial effects of chemicals that act through the same or parallel pathways complement existing assessments of water quality. Where possible, performance metrics should also be used as added relevant indicators for the impact of water quality on bird health.

DATA AVAILABILITY STATEMENT

The raw data supporting the conclusions of this article will be made available by the authors, without undue reservation, to any qualified researcher.

ETHICS STATEMENT

The animal study was reviewed and approved by the University of Alberta Animal Care and Use Committee.

AUTHOR CONTRIBUTIONS

JM-B and DB jointly conceived the experimental design. JM-B conducted experiments, analyzed, and interpreted the data. DT conducted qPCR experiments and edited parts of the manuscript. CT contributed with part of *ex vivo* experiments. JW edited part of the manuscript and provided logistic support. JM-B and DB wrote the manuscript. All authors approved this final version.

FUNDING

This work was supported by Natural Sciences and Engineering Council of Canada (NSERC grant number RGPIN-2018-05768) and Alberta Livestock and Meat Agency (ALMA grant number 2015R036R) grants to DB. JM-B was supported by a National Fund for Innovation in Science and Technology (FINCyT/Innovate-Peru) scholarship and a Graduate Teaching Assistantship by the Department of Biological Sciences at the University of Alberta. DT was supported by a CONICYT-Chile postdoctoral fellowship (Becas Chile N: 74170029).

ACKNOWLEDGMENTS

We would also like to offer special thanks to the Poultry Research Facility staff of the Department of Agricultural, Food and Nutritional Science at the University of Alberta for their contributions during this study.

REFERENCES

1. Ball P. Water is an active matrix of life for cell and molecular biology. *Proc Natl Acad Sci USA*. (2017) 114:13327–35. doi: 10.1073/pnas.1703781114
2. Wiggins PM. Role of Water in Some Biological Processes. *Microbiol Rev*. (1990) 54:432–49. doi: 10.1128/MMBR.54.4.432-449.1990
3. Alexander J, Hetland R, Vikse R, Dybing E, Eriksen G, Farstad W, et al. Combined toxic effects of multiple chemical exposures. *Nor Sci Comm Food Saf*. (2008) 1–105.
4. Escher BI, Fenner K. Recent advances in environmental risk assessment of transformation products. *Environ Sci Technol*. (2011) 45:3835–47. doi: 10.1021/es1030799
5. Robert J, McGuire CC, Kim F, Nagel SC, Price SJ, Lawrence BP, et al. Water contaminants associated with unconventional oil and gas extraction cause immunotoxicity to amphibian tadpoles. *Toxicol Sci*. (2018) 166:39–50. doi: 10.1093/toxsci/kfy179
6. Robert J, McGuire CC, Nagel S, Lawrence BP, Andino FJ. Developmental exposure to chemicals associated with unconventional oil and gas extraction alters immune homeostasis and viral immunity of the amphibian Xenopus. *Sci Total Environ*. (2019) 671:644–54. doi: 10.1016/j.scitotenv.2019.03.395
7. Goossens KE, Ward AC, Lowenthal JW, Bean AGD. Chicken interferons, their receptors and interferon-stimulated genes. *Dev Comp Immunol*. (2013) 41:370–6. doi: 10.1016/j.dci.2013.05.020
8. Magor KE, Miranzo Navarro D, Barber MRW, Petkau K, Fleming-Canepa X, Blyth GAD, et al. Defense genes missing from the flight division. *Dev Comp Immunol*. (2013) 41:377–88. doi: 10.1016/j.dci.2013.04.010
9. Stewart CR, Keyburn AL, Deffrasnes C, Tompkins SM. Potential directions for chicken immunology research. *Dev Comp Immunol*. (2013) 41:463–8. doi: 10.1016/j.dci.2013.05.011
10. Cash JL, White GE, Greaves DR. Zymosan-induced peritonitis as a simple experimental system for the study of inflammation. *Methods Enzymol*. (2009) 461:379–96. doi: 10.1016/S0076-6879(09)05417-2
11. Kolaczkowska E, Barteczko M, Plytycz B, Arnold B. Role of lymphocytes in the course of murine zymosan-induced peritonitis. *Inflamm Res*. (2008) 57:272–8. doi: 10.1007/s00011-007-7131-1
12. Leypoldt JK, Kamerath CD, Gilson JF. Acute peritonitis in a C57BL/6 mouse model of peritoneal dialysis. *Adv Perit Dial*. (2007) 23:66–70.
13. More-Bayona JA, Karuppannan AK, Trites MJ, Barreda DR. Application of imaging flow cytometry for characterization of acute inflammation in non-classical animal model systems. *Methods*. (2017) 112:167–74. doi: 10.1016/j.ymeth.2016.06.013
14. More-Bayona JA, Kumar A, Barreda DR. Contribution of leukocytes to the induction and resolution of the acute in flammatory response in chickens. *Dev Comp Immunol*. (2017) 74:167–77. doi: 10.1016/j.dci.2017.04.018
15. Rao TS, Currie JL, Shaffer AF, Isakson PC. *In vivo* characterization of zymosan-induced mouse peritoneal inflammation. *J Pharmacol Exp Ther*. (1994) 269:917–25.
16. Ipinza F, Collao B, Monsalva D, Bustamante VH, Luraschi R, Alegría-Arcos M, et al. Participation of the salmonella OmpD porin in the infection of RAW264.7 macrophages and BALB/c mice. *PLoS ONE*. (2014) 9:e111062. doi: 10.1371/journal.pone.0111062
17. Kaiser P, Rothwell L, Galyov EE, Barrow PA, Burnside J, Wigley P. Differential cytokine expression in avian cells in response to invasion by *Salmonella typhimurium*, *Salmonella enteritidis* and *Salmonella gallinarum*. *Microbiology*. (2000) 146:3217–26. doi: 10.1099/00221287-146-12-3217
18. Riber U, Lind P. Interaction between *Salmonella typhimurium* and phagocytic cells in pigs Phagocytosis, oxidative burst and killing in polymorphonuclear leukocytes and monocytes. *Vet Immunol Immunopathol*. (1999) 67:259–70. doi: 10.1016/S0165-2427(98)00233-5
19. Kogut MH, McGruder E, Hargis B, Corrier D, Deloach J. Characterization of the Pattern of Inflammatory Cell Influ in Chicks Following the Intraperitoneal Administration of Live *Salmonella enteritidis* and Salmonella enteritidis-immune Lymphokines. *Poult Sci*. (1995) 74:8–17. doi: 10.3382/ps.0740008
20. Agricultural and Agri-Food Canada. *Fertilizer Expense Index for the Agricultural Area of Alberta*. (2001). Agricultural and Agri-Food Canada.
21. MacDonald D, Caux P, Fan G, Walker S, Bonnell M. Canadian water quality guidelines for the protection of agricultural water uses - protocols. *Can Counc Minist Environ*. (1999) 1–21.
22. Alberta Environment and Sustainable Resource Development. *Pesticide Index*. (2011). Alberta Environment and Sustainable Resource Development.
23. Alberta Environment and Sustainable Resource Development. *Impact of Land Use on Water*. (2013).
24. Anderson A-M, Saffran KA, Byrtus G. *Pesticides in Alberta Surface Waters. Water Sciences Branch and Pesticide Management Branch, Alberta Environmental Protection*. (1997).
25. Phelan C. Pesticides in Alberta's Agricultural *Watersheds*: A Synthesis. *Alberta Agriculture and Rural Development*. (2012).
26. Eilers W, MacKay R, Graham L, Lefebvre A. Environmental Sustainability of Canadian Agriculture: Report #3. *In Agri-Environmental Indicator Report Series*. Agriculture and Agri-Food Canada. (2010).
27. Brown GD, Taylor PR, Reid DM, Willment JA, Williams DL, Martinez-Pomares L, et al. Dectin-1 is a major beta-glucan receptor on macrophages. *J Exp Med*. (2002) 196:407–12. doi: 10.1084/jem.20020470

28. Chadzinska M, Leon-Kloosterziel KM, Plytycz B, Lidy Verburg-van Kemenade BM. *In vivo* kinetics of cytokine expression during peritonitis in carp: evidence for innate and alternative macrophage polarization. *Dev Comp Immunol*. (2008) 32:509–18. doi: 10.1016/j.dci.2007.08.008
29. Cuzzocrea S, Zingarelli B, Sautebin L, Rizzo A, Crisafulli C, Campo GM, et al. Multiple organ failure following zymosan-induced peritonitis is mediated by nitric oxide. *Shock*. (1997) 8:268–75. doi: 10.1097/00024382-199710000-00006
30. Rieger AM, Konowalchuk JD, Grayfer L, Katzenback BA, Havixbeck JJ, Kiemele MD, et al. Fish and mammalian phagocytes differentially regulate pro-inflammatory and homeostatic responses *in vivo*. *PLoS ONE*. (2012) 7:e47070. doi: 10.1371/journal.pone.0047070
31. Mast J. Characterisation of chicken monocytes, macrophages and interdigitating cells by the monoclonal antibody KUL01. *Vet Immunol Immunopathol*. (1998) 61:343–57. doi: 10.1016/S0165-2427(97)00152-9
32. Staines K, Hunt LG, Young JR, Butter C. Evolution of an expanded mannose receptor gene family. *PLoS ONE*. (2014) 9:e110330. doi: 10.1371/journal.pone.0110330
33. Livak KJ, Schmittgen TD. Analysis of relative gene expression data using real-time quantitative PCR and the 2∧delta delta CT method. *Methods*. (2001) 25:402–8. doi: 10.1006/meth.2001.1262
34. Agricultural and Agri-Food Canada. *Chemical Expense Index for the Agricultural Area of Alberta*. (2001). Agricultural and Agri-Food Canada.
35. WHO. Polychlorinated dibenzodioxins, polychlorinated dibenzofurans, and coplanar polychlorinated biphenyls. In: *Safety Evaluation of Certain Food Additives and Contaminants*. WHO Food Additives Series, No. 48. Geneva: World Health Organization (2002). Available online at: http://www.inchem.org/documents/jecfa/jecmono/v48je20.htm
36. EC. *Fact Sheet on Dioxin in Feed and Food: Opinion of the Scientific Committee on Food on the Risk Assessment of Dioxins and Dioxin-Like PCBS in Food*. Brussel: European Commisision's Scientific Committee on Food (2001). Available online at:https://ec.europa.eu/food/sites/food/files/safety/docs/cs_contaminants_catalogue_dioxins_report-20001117.pdf
37. Alberta Municipal Affairs. *Municipal Census & Population Lists*. (2012).
38. Alberta Treasury Board and Finance. *Economy & Statistics*. (2013). Available online at: http://www.finance.alberta.ca/aboutalberta/index.html (accessed November 01, 2019).
39. Hrudey SE, Hebert PC, Stanbrook MB, Sibbald B, Flegel K, MacDonald N, et al. Safe water? Depends on where you live! *Can Med Assoc J*. (2008) 178:975:7. doi: 10.1503/cmaj.080374
40. Koning CW, Saffran KA, Little JL, et al. Water quality monitoring: the basis for watershed management in the Oldman River Basin, Canada. *Water Sci Technol*. (2006) 53:153–61. doi: 10.2166/wst.2006.308
41. Peterson H, Torchia M. Safe drinking water for rural Canadians. *Can Med Assoc J*. (2008) 179:55. doi: 10.1503/cmaj.1080061
42. Jokinen CC, Edge TA, Koning W, Laing CR, Lapen DR, Miller J, Mutschall S, et al. Spatial and temporal drivers of zoonotic pathogen contamination of an agricultural watershed. *J Environ Qual*. (2012) 41:242–52. doi: 10.2134/jeq2011.0203
43. Khakhria R, Woodward D, Johnson W. *Salmonella, Shigellae, pathogenic E. coli, Campylobacter and Aeromonas identified in Canada: Annual Summary (1994)*. National Laboratory for Enteric Pathogens, LCDC, Health Canada. (1996).
44. Carr RM, Blumenthal UJ, Mara DD. Guidelines for the safe use of wastewater in agriculture: revisiting WHO guidelines. *Water Sci Technol*. (2004) 50:31–8. doi: 10.2166/wst.2004.0081
45. Frisbie SH, Mitchell EJ, Sarkar B. Urgent need to reevaluate the latest World Health Organization guidelines for toxic inorganic substances in drinking water. *Environ Health*. (2015) 14:63. doi: 10.1186/s12940-015-0050-7
46. Sobsey MD, Bartram S. Water quality and health in the new millennium: the role of the World Health Organization Guidelines for Drinking-Water Quality. *Forum Nutr*. (2003) 56:396–405.
47. Moe CL, Rheingans RD. Global challenges in water, sanitation and health. *J Water Health*. (2006) 4(Suppl. 1):41–57. doi: 10.2166/wh.2006.0043
48. Sousa JCG, Ribeiro AR, Barbosa MO, Pereira MFR, Silva AMT. A review on environmental monitoring of water organic pollutants identified by EU guidelines. *J Hazard Mater*. (2018) 344:146–62. doi: 10.1016/j.jhazmat.2017.09.058
49. Vogel A, Nishimura N, Sciullo E, Wong P, Li W, Matsumura F. Modulation of the chemokines KC and MCP-1 by 2, 3, 7, 8-tetrachlorodibenzo-p -dioxin (TCDD) in mice. *Arch Biochem Biophys*. (2007) 461:169–75. doi: 10.1016/j.abb.2007.01.015
50. Vogel C, Donat S, Do O. Effect of subchronic 2,3,7,8-tetrachlorodibenzo-p-dioxin exposure on immune system and target gene responses in mice: calculation of benchmark doses for CYP1A1 and CYP1A2 related enzyme activities. *Arch Toxicol*. (1997) 71:372–82. doi: 10.1007/s002040050401
51. Freire M, Van Dyke T. Natural resolution of inflammation. *Periodontology (2000)*. (2013). 63:149–64. doi: 10.1111/prd.12034
52. Gilroy D, De Maeyer R. New insights into the resolution of inflammation. *Semin Immunol*. (2015) 27:161–8. doi: 10.1016/j.smim.2015.05.003
53. Sansbury BE, Spite M. Resolution of acute inflammation and the role of resolvins in immunity, thrombosis, and vascular biology. *Circ Res*. (2016) 119:113–31. doi: 10.1161/CIRCRESAHA.116.307308
54. Lamb CL, Cholico GN, Perkins DE, Fewkes MT, Oxford JT, Lujan TJ, et al. Aryl Hydrocarbon receptor activation by TCDD modulates expression of extracellular matrix remodeling genes during experimental liver fibrosis. *Biomed Res Int*. (2016). 2016:5309328. doi: 10.1155/2016/5309328
55. Moos AB, Baecher-Steppan L, Kerkvlietbt NI. Acute inflammatory response to SRBC in mice treated with TCDD. *Toxicol Appl Pharmacol*. (1994) 127:331–5. doi: 10.1006/taap.1994.1169
56. Klecka G, Persoon C, Currie R. Chemicals of emerging concern in the Great Lakes Basin: an analysis of environmental exposures. *Rev Environ Contam Toxicol*. (2010) 207:1–93. doi: 10.1007/978-1-4419-6406-9_1
57. Vanderslice RR, Orme J, Ohanian EV, Sonich-Mullin C. Problems in assessing the risks of mixtures of contaminants in drinking water. *Toxicol Ind Health*. (1989) 5:747–55. doi: 10.1177/074823378900500512

Conflict of Interest: The authors declare that the research was conducted in the absence of any commercial or financial relationships that could be construed as a potential conflict of interest.

frontiers in Immunology

ORIGINAL RESEARCH
published: 27 May 2020
doi: 10.3389/fimmu.2020.00911

Transcriptomic Evidence Reveals the Molecular Basis for Functional Differentiation of Hemocytes in a Marine Invertebrate, *Crassostrea gigas*

Fan Mao [1,2,3†], Nai-Kei Wong [4†], Yue Lin [1,2,3], Xiangyu Zhang [1,2,3], Kunna Liu [1,2,3], Minwei Huang [1,2,3], Duo Xu [1,2,3], Zhiming Xiang [1,2,3], Jun Li [1,2,3], Yang Zhang [1,2,3] and Ziniu Yu [1,2,3*]*

[1] CAS Key Laboratory of Tropical Marine Bio-resources and Ecology and Guangdong Provincial Key Laboratory of Applied Marine Biology, South China Sea Institute of Oceanology, Chinese Academy of Science, Guangzhou, China, [2] Southern Marine Science and Engineering Guangdong Laboratory (Guangzhou), Guangzhou, China, [3] Innovation Academy of South China Sea Ecology and Environmental Engineering, Chinese Academy of Sciences, Guangzhou, China, [4] Department of Infectious Diseases, Shenzhen Third People's Hospital, The Second Hospital Affiliated to Southern University of Science and Technology, Shenzhen, China

Hemocytes play unequivocally central roles in host immune defense of bivalve mollusks, though the exact mechanisms underlying their functional differentiation are only partially understood. To this end, granulocytes and hyalinocytes were sorted via flow cytometry from hemocytes of the Pacific oyster *Crassostrea gigas*, and consequently quantitative transcriptomic analysis revealed a striking array of differentially expressed genes (DEGs), which were globally upregulated in granulocytes, dedicating to functional differentiation among oyster hemocytes. Our network of DEGs illustrated actively engaged signaling pathways, with Cdc42/Cdc42l being a core regulator of pathway network, which was validated by a dramatically reduced capacity for hemocyte phagocytosis in the presence of Cdc42 inhibitors. Additionally, a number of transcription factors were identified among DEGs, including ELK, HELT, and Fos, which were predominantly expressed in granulocytes. The AP-1 transcription factor Fos was confirmed to facilitate functional differentiation of hemocytes in an assay on binding to target genes by the AP-1 binding site, consistent with downstream phagocytosis and ROS production. Importantly, Cdc42/Cdc42l were also regulated by the expression of Fos, providing a possible regulatory mechanism-guided hemocyte functional differentiation. Findings in this study have bridged a knowledge gap on the mechanistic underpinnings of functional differentiation of hemocytes in a marine invertebrate *C. gigas*, which promise to facilitate research on the evolution of immune defense and functional differentiation of phagocyte in higher-order and more recent phyla.

Keywords: oyster, functional differentiation, granulocytes, Cdc42, Fos

OPEN ACCESS

Edited by:
Xinjiang Lu,
Ningbo University, China

Reviewed by:
Xiaotong Wang,
Ludong University, China
Li Li,
University of Texas Southwestern Medical Center, United States

***Correspondence:**
Yang Zhang
yzhang@scsio.ac.cn
Ziniu Yu
carlzyu@scsio.ac.cn

[†] These authors have contributed equally to this work

Specialty section:
This article was submitted to Comparative Immunology, a section of the journal Frontiers in Immunology

Received: *01 December 2019*
Accepted: *20 April 2020*
Published: *27 May 2020*

Citation:
Mao F, Wong N-K, Lin Y, Zhang X, Liu K, Huang M, Xu D, Xiang Z, Li J, Zhang Y and Yu Z (2020) Transcriptomic Evidence Reveals the Molecular Basis for Functional Differentiation of Hemocytes in a Marine Invertebrate, Crassostrea gigas. Front. Immunol. 11:911. doi: 10.3389/fimmu.2020.00911

INTRODUCTION

Marine invertebrates are intrinsically useful reductionist models for investigating host defense primarily based on innate immunity. In bivalve mollusks, an open circulatory system is populated by hemocytes, which patrols between hemal sinus and soft tissues. These immunologically plastic cells excel at performing a diverse range of cellular functions including phagocytosis of invading pathogens, encapsulation of bulky invaders, enzymatic digestion and transport of nutrients, and biosynthesis and secretion of humoral factors (1–3). Hemocytes have been variously classified in terms of their morphology, cytochemistry, and function. Other methods such as flow cytometry (4, 5), density-gradient centrifugation (6), and immunostaining of cell surface proteins (7, 8) have also been proposed to characterize hemocyte subtypes. Despite some controversies, it is generally agreed that hemocyte subtypes in mollusks consist of two principal cell types in the hemolymph: granulocytes and hyalinocytes (also known as agranulocytes) (9, 10). However, hemocyte subtypes have been further divided into three, four, and even more different populations based on different parameters applied by researchers for various bivalve species (5, 11–13). Consequently, it is often difficult to compare or generalize findings between studies. In mollusks, as is true in many other invertebrates, the presence of a hemopoietic organ is not the norm; hemocytes may instead be formed in various ways. For example, spontaneous mitosis of hemocytes increases during circulation in hemolymph vessels, sinuses, and soft tissues (14–16). This raises the possibility of observing plasticity during various stages of hemocyte maturation, rather than simply categorizing cells into distinct subtypes (17–19).

Conventionally, the presence or absence of cytoplasmic granules as an intuitive criterion has inspired the classification of hemocytes into granulocytes and hyalinocytes, as mentioned above. These two cell types have been reported in many species, including *Mytilus edulis* (20), *Tapes philippinarum* (21), *Biomphalaria glabrata* (22), *Ruditapes decussatus* (23), and *Crassostrea gigas* (24). Of the two, hyalinocytes are cells that are smaller and harbor few or no cytoplasmic granules. They can be morphologically further divided into two subclasses: small hyalinocytes with large nuclei and large hyalinocytes with small nuclei and large cytoplasm (14). Granulocytes are characterized by their ability to efficiently phagocytize microorganisms, generate reactive oxygen species (ROS) and express hydrolytic enzymes that contribute to intracellular killing (25–28). In general, granulocytes have a greater phagocytic capacity than hyalinocytes. To this date, however, the molecular mechanisms underlying the functional differentiation of hemocytes remain largely enigmatic.

The granulocytes are evolutionary analogous of macrophage and neutrophil in mammals, which could be functionally differentiated from circulating monocytes in the bloodstream after infection or vaccination circulate (29). Combined action of critical transcription factors can determine the expression of myeloid-specific genes and the generation of macrophages (30). Moreover, transcription factors are anticipated to play pivotal roles in marshalling proliferative and differentiated signals into genetic programs, determining the cell fate, growth stimulation, functional activation, and lineage-specific evolution (31–33). It has been proposed that specific transcription factor activity is mandatory for multiple lymphoid lineages, such as *Nfil3* and *Tcf1* for innate lymphoid cell (ILC) development (34) and *Ets* family transcription factors for NK cell development (35, 36). It is also known that PI3K/AKT signaling cascade plays a vital role in the synthesis of granules during stressful stimulation (37).

Previous studies in oyster have shown that granules in granulocytes react for acid phosphatase, which is a typical characteristic of lysosomes and participates in intracellular digestion of particles, widely accepted as markers of functional differentiation of hemocytes (38). However, how granules and proteolytic enzymes arise to generate functional hemocytes is at best incompletely understood in oyster. The Pacific oyster, *C. gigas*, one of the most prominent aquacultural mullosk species with global distribution, depends on innate immunity for anti-infective defense. A wide range of microorganisms can be phagocytized and cleared by *C. gigas* hemocytes. With the advent of technological improvements, flow cytometry (FACS) has been applied to analyze cellular properties in hemocytes including cell types and their frequency (4, 5, 39). In this study, we attempted to investigate the potential determinants of plasticity leading to the functional differentiation between hyalinocytes and granulocytes. *C. gigas* hemocytes were isolated and analyzed by FACS coupled to quantitative transcriptomics analysis, which provided a new modality for comparing differential genes in the two hemocytes subtypes. A panel of differentially expressed genes (DEGs) of high interest including key transcriptional factors was identified in this study. A network on the basis of DEGs was constructed to illustrate the relationship between actively engaged signaling pathways and core components implicated in functional differentiation of hemocytes. Additionally, the potential significance of transcriptional factors regulating functional activity of hemocytes was further scrutinized via knocking down expression of the specific genes *in vivo*.

MATERIALS AND METHODS

Animal Collection and Maintenance

The Pacific oysters, *C. gigas* (2 years old with an average shell length of 100 mm), were obtained from Qingdao, Shandong Province, China, and maintained at 22–25°C in tanks with re-circulating seawater before experiments. Treatment-naïve and pathogen-free oysters were chosen for experiments, independently of their genetic background. Oysters were fed twice daily on *Tetraselmis suecica* and *Isochrysis galbana*. They were held for 2 weeks prior to experimentation.

Hemocyte Preparation

To collect hemocytes, the oyster shell was carefully opened and all mantle fluid was drained. Approximately 1 ml of hemolymph per oyster was sampled from adult *C. gigas* individuals by using a 1-ml syringe with a 25-mm needle inserted into the pericardial cavity. Immediately, hemolymph was placed on ice to prevent hemocyte aggregation, followed by centrifugation at 1,500 × *g* at 10°C for 10 min. Cell pellets containing hemocytes were

removed and suspended in 1 ml of cell protection medium, as previously reported (32). Samples were kept on ice until used for experiments.

Sorting of Granulocytes and Hyalinocytes

Hemolymph samples were analyzed and sorted by using a BD Biosciences FACSCanto II flow cytometer (Becton Dickinson, USA). For each group, 10 oysters were randomly grouped for hemocyte preparation and cell sorting. A total of four groups of hemocytes (R1, R2, R3, and R4) were used in sorting granulocytes and hyalinocytes. After preparation as mentioned above, hemocytes were sorted on the basis of their cellular granularity and cell sizes in flow cytometry by using CellQuest program. For each sample, 20,000 cells were sorted.

Imaging of Granulocytes and Hyalinocytes

Sorted cell subpopulations were imaged by light microscopy and transmission electron microscopy (TEM). Briefly, granulocytes and hyalinocytes were placed onto glass slides, and their observations were carried out under a light microscope (Nikon E100). Additionally, hemocytes were also prepared for examination under a transmission electron microscope. Briefly, sorted granulocytes and hyalinocytes were mixed with 5% glutaraldehyde fixative solution, followed by centrifugation to remove supernatant. Then, cells were prefixed again with 2.5% glutaraldehyde fixative solution at 4°C, followed by mixing in 1% osmium tetroxide and dehydration in ethanol. Subsequently, cells were embedded in Epon epoxy resin, and left to harden at 60°C. Ultrathin sections were prepared on a Leica EMuC7 and post-stained with 0.5% aqueous uranyl acetate, and then exposed to lead citrate. Finally, electron micrographs of the sections were acquired under a Hitachi HT7700 transmission electron microscope.

Flow Cytometry Analysis

To compare phagocytic abilities of granulocytes and hyalinocytes, FITC-labeled bacteria (*Vibrio parahaemolyticus* E151) were added to hemocytes (2.5×10^5 cells) cultured in a 24-well plate for 15 min, in a 50:1 ratio (hemocytes/bacteria). Trypan blue (1.2 mg/ml) was used to quench surface-bound FITC-labeled bacteria. Then, hemocytes were washed three times with Tris buffer (50 mM at pH 8.0) and re-suspended in PBS supplemented with 15% EDTA. Subsequently, flow cytometry analysis was performed to quantify hemocyte subpopulations. Granulocytes and hyalinocytes were gated by using at least 10,000 events per sample based on cellular granularity and cell sizes. To compare capacities for ROS generation in granulocytes and hyalinocytes, hemocytes were collected and stained with 5 μM dichlorodihydrofluorescein diacetate (DCFH, prepared with PBS buffer) in plasma at room temperature for 60 min. Then, hemocytes were washed with pre-warmed PBS to remove excess probe, followed by data acquisition by flow cytometry. At least 10,000 events per sample were collected for comparison on ROS production between granulocytes and hyalinocytes. Flow cytometry data were analyzed using FlowJo software, and statistical difference was calculated by Student's *t* test for triplicated data of granulocytes and hyalinocytes.

Library Preparation and RNA Sequencing

RNA library was prepared using the REPLI-g WTA single cell kit (150063, Qiagen, German). Briefly, a single cell sample (containing 1,000 cells) is lysed efficiently within 5 min. Following cell lysis, gDNA was removed prior to WTA process. Poly-adenylated transcripts were amplified by using oligo dT primers. Synthesized cDNA was ligated using a high-efficiency ligation mix. Ligated cDNA was amplified utilizing MDA technology, with novel REPLI-g SensiPhi DNA polymerase, in an isothermal reaction lasting 2 h. Consequently, amplified cDNA was examined for its suitability for RNA sequencing. After construction of a cDNA library, Qubit 2.0 and Agilent 2100 were used to detect concentrations of the library. Q-PCR method was used to accurately quantify effective concentrations of the library to ensure quality of the library. Subsequently, high-throughput sequencing was performed with HiSeq2500, and sequencing reading length was SE50. Original image data files obtained from Illumina HiSeq2500 high-throughput sequencing platforms were transformed into raw data or raw reads by the base calling. Results were stored in FASTQ file format, which contained information of sequenced transcripts and their corresponding sequencing quality information. Four biological replicates of transcriptomic sequencing were obtained in each case, and all raw data were deposited in the NCBI Sequence Read Archive database under the accession number PRJNA591303. Information on sequencing data is as presented in **Table S1**.

Bioinformatics in Transcriptomic Analysis

Sequence alignment and subsequent analysis were performed using the designated *C. gigas* genome as a reference genome using TopHat2 software (40). Information of alignment efficiency statistics is as presented in **Table S2**. Bowtie (41) was used for comparison and transcript expression levels were estimated according to comparison results in conjunction with information from Cufflinks/RSEM (42). Finally, RPKM (41) values were used to gauge the expression abundance of corresponding Unigenes, for calculating and comparing gene expression differences between individual samples. Absolute values of $\log_2$ (fold change) > 1 and FDR (false discovery rate) value < 0.01 were set as threshold parameters to determine DEGs in granulocytes and hyalinocytes in each group (**Table S3**). Then, differential combinatorial analysis on DEGs in each group was performed to determine common DEGs. BLAST software was used to sequence the DEGs with NR, Swiss-Prot, GO, COG, and KEGG to obtain annotation information on DEGs as shown in **Table S4**. Results from KEGG analysis are as presented in **Figure S1**. Factoextra R Package was applied in principal component analysis (PCA). RNA expression levels of DEGs in different *C. gigas* tissues were analyzed based on *C. gigas* transcriptomic data (43).

Protein Network Mapping

STRING server (http://string.embl.de) was used to predict interacting partners in protein—protein interactions. We compared protein—protein interactions using the protein databases of *Danio rerio* and *Drosophila melanogaster*, which are species considered evolutionarily relevant to oysters. Further, the *D. rerio* protein database was found to be more suitable

for constructing protein interactomes of oyster hemocytes DEGs, based on the number and similarity of aligned proteins. Networks were constructed based on proteins predicted from DEGs ($p < 0.05$) between granulocytes and hyalinocytes. Disconnected nodes were hidden. The entire networks are available for interactive visualization of protein interactions in Cytoscape session file.

Inhibition Assay on Cdc42 Protein

In addition, flow cytometry was also conducted to explore the functional roles of Cdc42 protein in granulocytes and hyalinocytes using inhibitors of Cdc42 (MLS-573151: Cat. no. C4738; Casin, Cat. no. B6103. APExBIO, USA). The dosage of the inhibitors were determined on the basis of published literatures (44–46). First, oyster hemocytes were harvested from the pericardial cavity and seeded into a 24-well plate for 15 min. This was followed by addition of inhibitors at appropriate concentrations (Casin at 10 μM and MLS-573151 at 50 μM) for 15 min. Ten microliters of FITC-labeled beads (Sigma, USA, 90305) and FITC-labeled bacteria (*V. parahaemolyticus* E151) were added to hemocytes (2.5×10^5 cells) in a 50:1 ratio (hemocytes/bacteria), which were incubated at room temperature for 15 min. Upon establishment of phagocytosis (15 min), all samples were incubated with Trypan blue (1.2 mg/ml) to quench surface-bound FITC-labeled beads or bacteria, and further washed twice with PBS buffer supplemented with 15% EDTA to remove non-phagocytic beads or bacteria. Finally, flow cytometry analysis was performed to quantify phagocytosis-related fluorescence in oyster hemocytes. Gates were applied to define granulocytes and hyalinocytes. Cell phagocytosis was monitored using at least 10,000 event per sample. Data was analyzed with FlowJo software, and statistical difference was determined by one-way ANOVA for triplicated data of granulocytes and hyalinocytes. Moreover, the suppressive effect of the Cdc42 inhibitors in oyster was validated by test the expression level of Wiskott–Aldrich Syndrome Protein (WASP), which is considered as the core effector of Cdc42.

In vivo RNAi Assay

To clarify the roles of ELK, HELT, and Fos in generation of functional granulocytes, the genes were knocked down *in vivo via* dsRNA-mediated RNA interference. The primers used to synthesize dsRNA are as shown in **Table 1**. ELK, HELT, Fos, and a GFP cDNA fragment (negative control) were amplified with primer pairs of T7 promoter overhangs in the Promega RiboMAX™ Express RNAi System. PCR products were used as templates to synthesize dsRNA according to the manufacturer's instructions. For this experiment, oysters were randomly divided into four groups: ELK-interference group (iELK), HELT-interference group (iHELT), Fos-interference group (iFos), and control group (iGFP). Each oyster was injected with 50 μg dsRNA and individuals from each group were randomly selected for collection of hemocytes. iGFP indicated the control group that was injected with equal amount of GFP dsRNA. All the experimental groups were compared with the iGFP group to calculate the transcriptional effects of these transcription factors on target genes. RNAi efficiency was ascertained by two independent quantitative real-time PCR. In each independent experiment, three samples were applied to detect the gene mRNA expression profile. Genes related to phagocytosis and ROS production were determined by qRT-PCR (quantitative real-time PCR) after knockdown of ELK, HELT, and Fos.

TABLE 1 | Primers used in this study.

Name of Primers	Sequence (5′-3′)
dsHELT-F	GGATCCTAATACGACTCACTATAGGTAGTGAATGGTTTTC TTCGGAC
dsHELT-R	GGATCCTAATACGACTCACTATAGGAGAATAAGCCGGT GAAAGGA
dsTranF-F	GGATCCTAATACGACTCACTATAGGCAAACCGCCTTATTA TTGAAAC
dsTranF-R	GGATCCTAATACGACTCACTATAGGAAGAGGAGGGTCCG TTAGTG
dsElk3-F	GGATCCTAATACGACTCACTATAGGGGACACCAATGTGA CGCTAT
dsElk3-R	GGATCCTAATACGACTCACTATAGGAGGGCAGATGCTT CAGTTTT
β-actin F	AAGATATTGCAGCTTTAGTCGT
β-actin R	TTCTGTCCCATACCAACCAT
qHELT-F	GAGCAGACTTCACACAAGATCA
qHELT-R	CTATTTTCAAAGCGTAAACCAA
qElk3-F	AATGCCATCGCCTCCTCTTC
qElk3-R	ATGGAGACTTTCGGACTTGGA
qTranF-F	ACCCGCACCACCATCCTC
qTranF-R	AGATTTGTGGGCACCGACTG
qRab11-F	GGAAACAGGCAAAGGCAAGA
qRab11-R	AATGACGAGTCCAGCAAGGG
qCD63-F	TTAGAAATCTCGGCGGGAATA
qCD63-R	GACACTCCACAACATTTGAACTCTT
qRho1-F	GGAACCAGTCAAATCGCAAGA
Rho1-R	GAGCTGCCCTAGTGGCTGTT
qLAMP-F	TCTAGAACTGATATTATGTA
qLAMP-R	AATGTTTTCATTGTGCATTA
qSOD-F	TACGAAAACTCCATGCATT
qSOD-R	TTCATTATGGTACAGTT
qFerritin1-F	AACGGGAACATGCTGAA
qFerritin1-R	TTGCTCCTCCAAGTAGT
qFerritin2-F	AGTTGATGAAATACCAGA
qFerritin2-R	TCAGAAATCTCCTTGAT
qNd5-F	CAATAAAGACGTAACTTTT
qNd5-R	TGGATGGGATAGTTACAAAT
qCdc42-F	GACACGGCTGGAAAGGAGG
qCdc42-R	TAAATGGCGTGTTTGGCACA
qCdc42l-F	GTGGAGAAGTTCTGGGTCAATGA
qCdc42l-R	CTATCCCGTCGCCCGTTTT
qCYTB-F	AGGGCTTAGCCTAGCTCACGT
qCYTB-R	CGCCAACAGCAATGCAAAC

Expression Profile Analysis by qRT-PCR

qRT-PCR was conducted using a LightCycler 480 (Roche) with a reaction volume of 10 μl containing 1 μl of template cDNA, 5

μl of 2×SYBR Green Mix, 0.5 μl of each primer (10 pmol/μl), and 3 μl of PCR-grade water. The qRT-PCR cycle program consisted of one cycle of 95°C for 1 min, followed by 40 cycles of amplification at 95°C for 15 s, 55°C for 15 s, 72°C for 20 s, and 85°C for 20 s. The relative expression of the genes was calculated using the $2^{-\Delta\Delta CT}$ method. All experiments were performed in triplicate using β-actin mRNA as an internal control. All data are represented in terms of relative mRNA levels.

Prediction of Transcription Factor Binding Sites

PROMO prediction software (http://alggen.lsi.upc.es/) was used to identify the transcription factor binding sites of some transcription factors (ELK, HELT, and Fos), phagocytosis-related genes (LAMP, Rab11, CD63, Cdc42, Cdc42l, and Rho), and ROS production-related genes (SOD, ferritin1, ferritin2, Nd5, and CytB1).

Dual-Luciferase Reporter Assay

Subsequently, promoter sequence of Cdc42 [−485, −1] bp and Cdc42l [−349, −1] bp were cloned into pGL3 basic plasmid for dual luciferase reporter assay. For DNA transfection, cells were seeded and allowed to grow to about 70% confluence, followed by plasmid transfection with Viafect reagent (Promega, USA) according to the manufacturer's recommendations. For dual-luciferase reporter assays, HEK293T cells were transiently co-transfected with pRL-TK vector (20 ng/μl), luciferase reporter vectors (AP-1 reporter Luc, Cdc42-promoter Luc, and Cdc42l-promoter Luc, 300 ng/well), and recombinant plasmid pcDNA (0, 150, and 300 ng/well). Cdc42-promoter and Cdc42l-promoter reporter vectors were constructed by cloning the promoter sequence of Cdc42 and Cdc42l to pGL3-basic plasmid. AP-1 reporter vectors used in this study were previously constructed in our laboratory. A pRL-TK vector (Promega, USA) was used as an internal control. Cells were transfected in serum-free culture medium for 4–6 h, followed by replacement of culture medium with fresh complete MEM.

At 48 h post-transfection, HEK293T cells in 48-well plates were washed with PBS twice and lysed. Firefly and Renilla luciferase activity was measured in a luciferase reporter assay system (Promega, USA) according to the manufacturer's instructions. Relative luciferase activity was calculated by normalization to Renilla luciferase values. Experimental results are expressed as fold changes relative to the empty vector control. All results are represented as the mean ± SEM. Statistical significance was analyzed with GraphPad software.

Electrophoretic Mobility Shift Assay (EMSA)

A biotin-labeled AP-1 probe was designed (GeneWiz, USA) and used to perform EMSA. Detection of biotin-labeled DNA by chemiluminescence was performed based on an established protocol (Thermo Fisher, USA, 20148). Briefly, biotin-labeled double-stranded DNA was incubated with hemocyte extract proteins, and then non-denatured gel electrophoresis was performed. The DNA was then transferred rapidly (30 min) to a positively charged nylon membrane for purple diplomatic conjugation, which then proceeded directly to detection.

RESULTS

Cell Typing and Morphological and Functional Characterization of Hemocyte Subtypes

Crassostrea gigas hemocytes are professional immune effector cells adept at phagocytosis and killing of bacteria. For cell sorting, hemolymph from 10 oysters was analyzed by flow cytometry, in which two cell populations with distinguishable complexity (slide scatter, SSC) and continuous size (forward scatter, FSC) were found (**Figure 1A**). A representative section with low SSC constituted an agranular population, corresponding to hyalinocytes. Another representative section with high SSC was a high-granularity population, corresponding to granulocytes. Then, these two subpopulations of oyster hemocytes were sorted for RNA extraction and transcriptomic analysis, which were also confirmed based on morphological features under a light microscopy (**Figure 1B**). Ultrastructural analysis by TEM revealed detailed morphological traits (as shown in **Figure 1B**). Evidently, *C. gigas* hyalinocytes were characterized by few or no granules in the cytoplasm, which were packed with vacuoles. In contrast, *C. gigas* granulocytes were characterized by an eccentric nucleus and numerous cytoplasmic granules.

Phagocytic activities of different hemocyte subpopulations were examined by flow cytometry analysis, as shown in **Figure 1C** (*left panel*). After incubation with FITC-labeled bacteria, phagocytic indices of granulocytes and hyalinocytes were quantified. Higher fluorescence intensities were detected in granulocytes, which could ingest more bacteria to emit stronger fluorescence. The hyalinocyte population reported weaker fluorescence intensities and low phagocytosis rates. Furthermore, the phagocytic index was ∼58 ± 8.6% in granulocytes and 12 ± 2.4% in hyalinocytes. Phagocytic capacity of granulocytes was significantly higher than that of hyalinocytes ($p < 0.01$) as shown in **Figure 1D** (*blue panel*). Spontaneous production of ROS during oxidative bursts was also examined with the probe DCFH in oyster hemocytes by flow cytometry, as shown in **Figure 1C** (*right panel*). For oysters under resting condition, basal levels of ROS production of granulocytes were significantly higher than those in hyalinocytes ($p < 0.05$), as shown in **Figure 1D** (*red panel*).

Transcriptomic Analysis on DEGs in Granulocytes and Hyalinocytes

To enable analysis on the molecular determinants of functional differentiation, cell subpopulations were first sorted based on cell size and granularity, given a lack of granulocyte-specific or hyalinocyte-specific antibodies. A wide range of granulocyte and hyalinocyte transcriptome libraries were constructed from four groups mentioned above and sequenced by using a high-throughput RNA-seq platform. Next, PCA was conducted for whole datasets. PCA results for all surveyed genes in granulocytes and hyalinocytes suggested that genes in datasets obtained

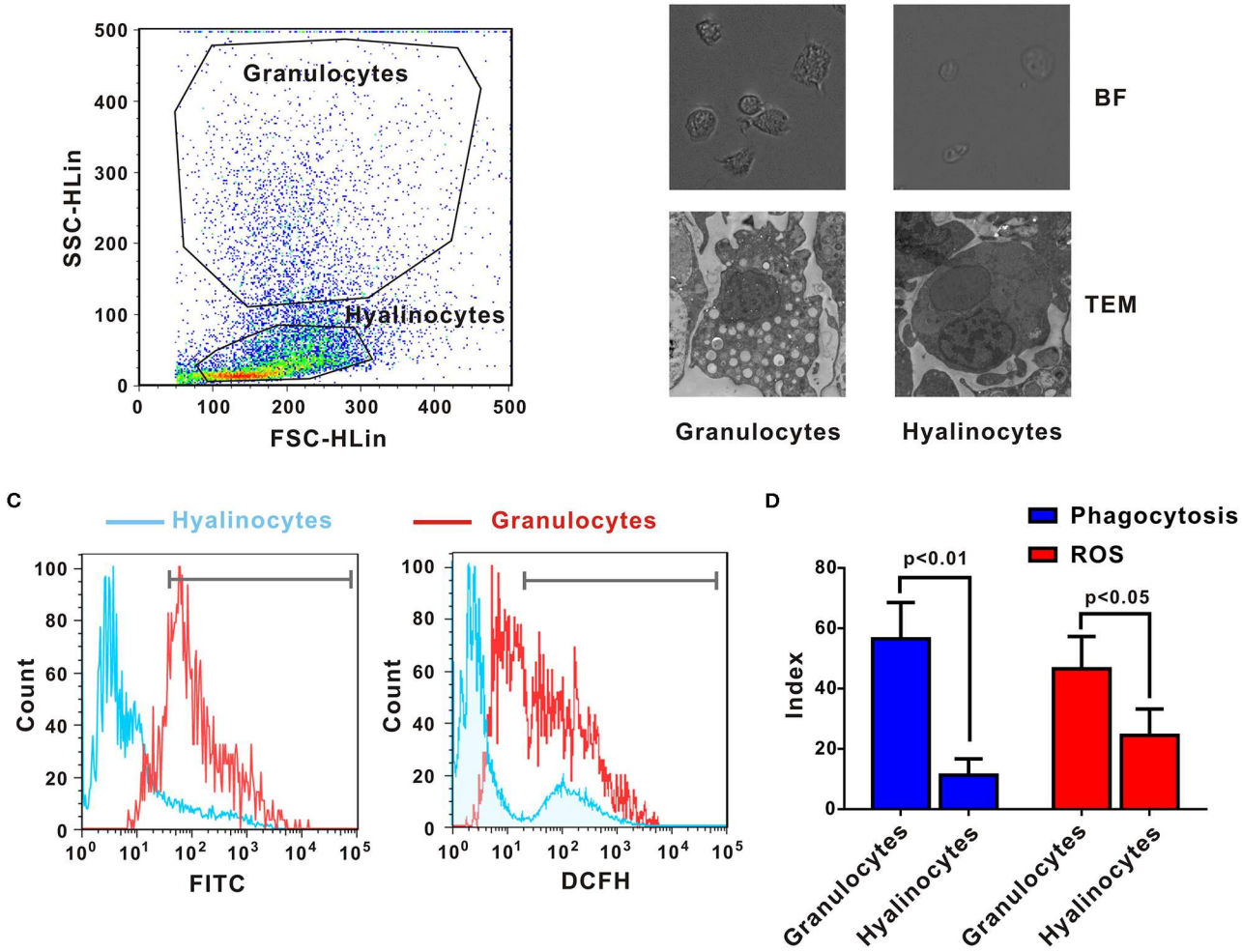

FIGURE 1 | Morphological and functional characterization of *C. gigas* granulocytes and hyalinocytes. **(A)** Flow cytometry analysis was conducted to define hemocyte subpopulations. Granulocytes and hyalinocytes were gated, respectively. **(B)** Granulocytes and hyalinocytes were imaged by light microscopy and TEM. **(C)** Flow cytometry analysis on the differences between granulocytes and hyalinocytes in terms of phagocytosis (*left panel*) and ROS production (*right panel*). The blue line here represents the functional parameters of hyalinocytes, and the red line represents those of granulocytes. **(D)** Data analysis was performed by using GraphPad 5 software and vertical bars represent mean ± SEM ($n = 3$). Phagocytosis index was represented in the left panel and ROS production was represented in the right panel.

from the same cell subpopulations clustered tightly; different cell subpopulations were discriminated at different groups, indicating that there is a high degree of homogeneity in gene expression pattern in each hemocyte type (**Figure 2A**). The profiles revealed disparity in gene expression between oyster granulocytes and hyalinocytes.

In order to further clarify the differences between granulocytes and hyalinocytes at the transcriptomic level, analysis was performed to screen for DEGs under different biological conditions. Biological replicates (R1, R2, R3, and R4) were established as described in Materials and Methods. We first screened for DEGs of granulocytes and hyalinocytes in the biological replicates. In between-group comparisons, genes having a FDR value < 0.01 and fold change (FC) ≥ 2 found by DESeq were assigned as DEGs. Then, we screened for common DEGs among R1, R2, R3, and R4, after determining that 175 genes were expressed at significantly different levels (**Figure 2B**). We also validated the expression level of key DEGs via QPCR, and the result was displayed in **Figure S1**. In addition, we analyzed the mRNA expression level of DEGs in different tissues including hemocytes, outer mantle, inner mantle, digestive grand, female gonad, gill, adductor muscle, labial palps, mixture of adult tissues, and male gonad (**Figure 2C**), based on the published *C. gigas* transcriptomic data (43). Predominant transcript expression patterns in hemocytes were established. Subsequently, a heatmap of DEG expression levels in granulocytes and hyalinocytes was constructed (**Figure 2D**). The correlation

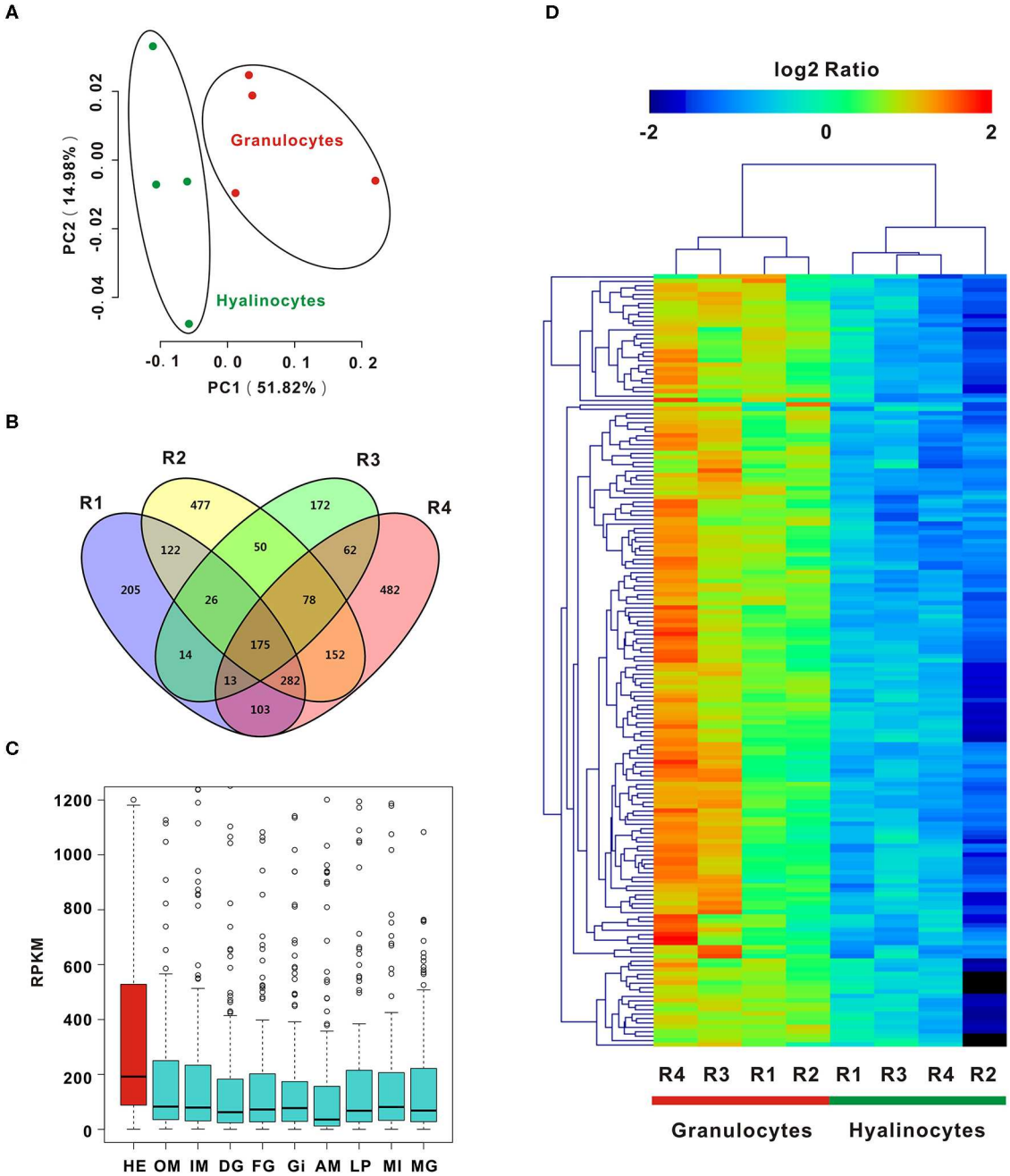

FIGURE 2 | PCA and DEGs analysis of *C. gigas* granulocytes and hyalinocytes. **(A)** Scores plot of principal components analysis on *C. gigas* hemocyte subpopulations (granulocytes and hyalinocytes). PC1 and PC2: principal component 1 and principal component 2. Each point represents a metabolite profile of a biological replicate. **(B)** DEGs were first explored in each group for comparison between granulocytes and hyalinocytes. Venn diagram was constructed to determine common DEGs in the four groups (R1, R2, R3, and R4). **(C)** Tissue distribution of DEGs in *C. gigas*. Red box represents the high expression of DEGs in hemocytes. HE, hemocytes; OM, outer mantle; IM, inner mantle; DG, digestive grand; FG, female gonad; GI, gill; AM, adductor muscle; LP, labial palps; MI, mixture of adult tissues; MG, male gonad. **(D)** Data for relative expression levels of genes were obtained by DEGs data. Colors from red to blue indicate range of $\log_2$ ratio values (in descending order); red color indicates high expression level and blue color indicates low expression level.

distance of DEGs were analyzed and presented in **Figure S3**, in which stronger heterogeneity was observed in granulocytes rather than hyalinocytes. Surprisingly, all common DEGs in the biological replicates were upregulated in granulocytes, suggesting more complex regulation network in the granulocytes than hyalinocytes.

Cdc42 Regulatory Network Revealed by Analysis on DEG Pathway Networks

As an attempt to shed light on the possible functions of significantly expressed genes identified in transcriptomic analysis, KEGG pathway analysis was performed to pinpoint pathways that contributed importantly to functional differentiation of hemocytes (**Figure S2**). In this aspect, our results implicated 10 overrepresented pathways (Q value < 0.05), among which "regulation of actin cytoskeleton," "Fc gamma R-mediated phagocytosis," "leukocyte transendothelial migration," and "pathogenic *Escherichia coli* infection" are generally related to granulocytes formation. Furthermore, to delineate the dynamic details of oyster hemocytes during functional differentiation, we mapped out a DEG pathway network based on predicted proteins corresponding to all 175 DEGs in the transcriptomic analysis. Essentially, these genes could primarily be organized into several categories, namely, "regulation of actin cytoskeleton," "phagosome and endocytosis," "MAPK signaling pathway," "mitochondrial respiratory chainm" "ribosome and translation," "lysosome," and "metabolism," Meanwhile, these genes formed a regulatory network resolving around Cdc42 (cell division control protein 42) as a core member (**Figure 3A**). Cdc42 is a central protein implicated in the regulation of cell cycle and is known to critically impact a variety of signaling events and cellular processes in many organisms (47).

In order to verify what extent Cdc42 was involved in regulating hemocyte function, two Cdc42 inhibitors, MLS-573151 and Casin, were used to scrutinize the process (46). The dosage of these inhibitors was also validated by observing significantly suppressive expression on WASP, the downstream molecular of Cdc42, which was displayed in **Figure S4**. As expected, the fluorescence intensities of phagocytosed beads (**Figure 3B**) or bacteria (**Figure 3C**) in hemocytes, taken as a measure of phagocytosis efficiency, were markedly reduced in granulocytes treated with MLS-573151 or casin compared to that in the control group (one-way ANOVA; statistical significance determined at $p < 0.05$). Specifically, the phagocytosis index of MLS-573151-treated groups was about 3.0-fold lower than that of the control, for either case of internalized FITC-labeled beads or FITC-labeled bacteria. In the case of casin, the inhibition of phagocytosis index dropped from 62 to 35% for internalized FITC-labeled beads and 69 to 35% for internalized FITC-labeled bacteria. Nevertheless, the Cdc42 inhibitors harbored little effect on phagocytosis index of hyalinocytes. These results show that both Cdc42 inhibitors (casin and MLS-573151) could effectively inhibit the phagocytic ability of granulocytes, thereby confirming the important role of Cdc42 in regulating granulocytes function.

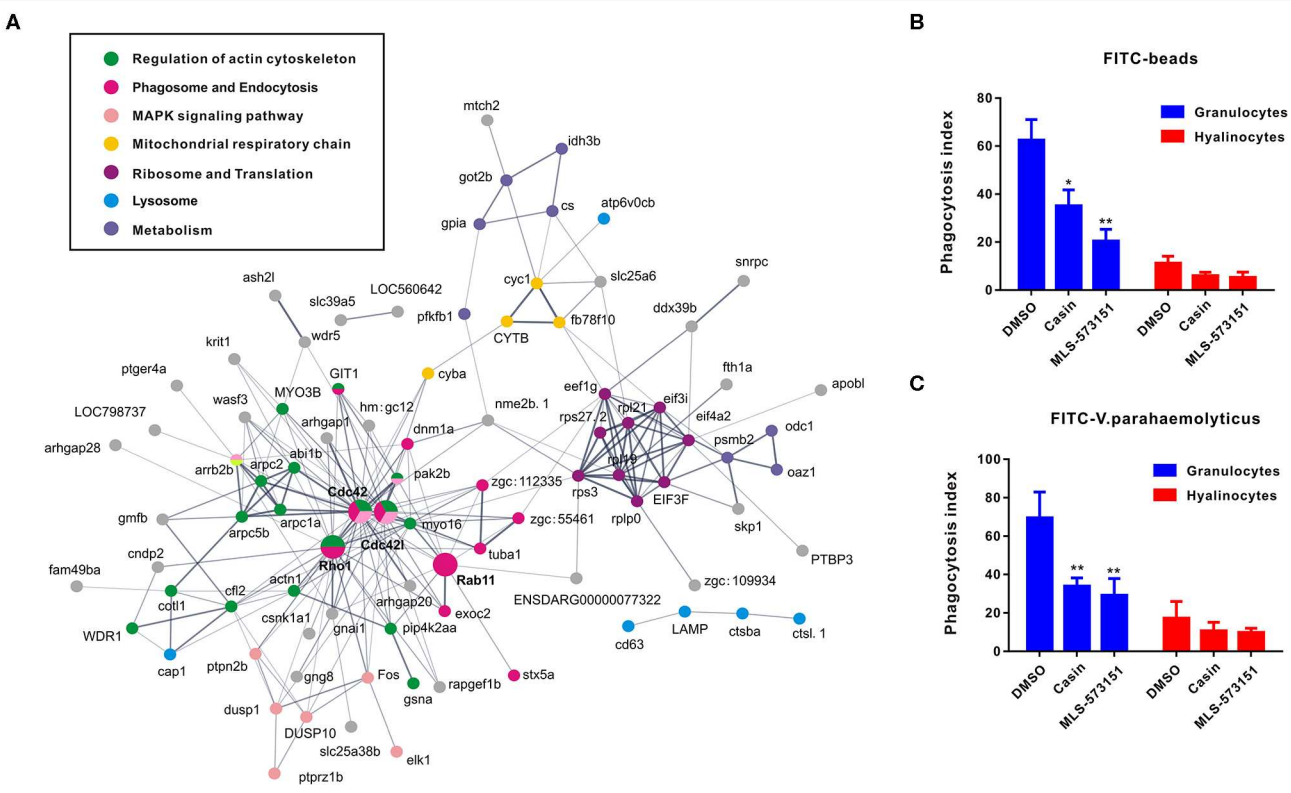

FIGURE 3 | Networks based on DEGs implicating central roles of Cdc42 in granulocyte phagocytosis. **(A)** Networks are represented here schematically. Nodes represent proteins. Edges represent interactions between proteins. Different colors represent different pathways and proteins. **(B,C)** Phagocytosis index of FITC beads **(B)** or FITC-labeled bacteria (*V. pa*) **(C)** by *C. gigas* granulocytes and hyalinocytes in the presence of Cdc42 inhibitors (casin and MLS-573151). Blue panel represents granulocytes and red panel represents hyalinocytes. $^{*}p < 0.05$; $^{**}p < 0.01$.

Regulatory Roles of Transcription Factor FOS in Transcriptional Activation of Granulocyte-Specific Genes

Transcription factor network has long been considered to orchestrate hematopoiesis or cell differentiation, guiding gene expression to become a more specific type of cell. To further elucidate the regulatory functional mechanisms of granulocyte-specific genes, several important and predominantly expressed transcription factors in granulocytes, including *ELK*, *HELT*, and Fos, were identified and knocked down by RNAi to explore their potential function in hemocytes (**Figure 4A**). Interference of single transcription factors had been successfully achieved by RNAi techniques, and qPCR analysis of gene mRNA expression after RNAi showed that knockdown of Fos could effectively reduce the expression of essential phagocytosis related genes, such as LAMP, Rab11, CD63, Cdc42, etc. (required for phagocytosis) and reduce the expression of ferritin1 and ferritin2 (implicated in ROS production). However, knockdown of other transcription factors had no apparent impact on the expression of these genes (**Figure 4B**). Subsequently, we obtained the promoter sequences of these Fos target genes and established a common transcription factor binding site, the AP1 binding site TGANTCA (**Figure 4C**), which further validated the regulatory role of Fos in these target genes, suggesting the regulatory role of Fos in phagocytosis and ROS production.

Furthermore, *in silico* prediction showed that multiple AP-1 binding sites located in the proximal promoters of Cdc42 and Cdc42l (**Figures S5**, **S6**). To assess whether Fos could direct transcriptional activation of Cdc42, the AP-1 reporter (*blue panel*), Cdc42-promoter reporter (*red panel*), Cdc42-like (Cdc42l)-promoter reporter (*green panel*), and two negative control vectors (pGL3 vector, *black panel*, and ISRE reporter, *gray panel*) were used to detect Fos transcriptional activity. In this study, we observed that Fos could enhance activation of the AP-1 reporter by 7.5-fold with a transfection dose of 300 ng, and this activation was found to be dose-dependent (**Figure 4D**, *blue panel*). No obviously activated effect was observed in two negative control groups, indicating the specifically transcriptional activity of Fos on Cdc42 promoter and AP-1 site. Moreover, Fos also produced enhancing effects on the Cdc42-promoter with an increase of more than 10-fold (**Figure 4D**, *red panel*) and also activated ∼6.0-fold on activity of Cdc42l-promoter reporters (**Figure 4D**, *green panel*), suggesting that Fos participated in the Cdc42 and Cdc42l regulatory signaling networks. These results suggest that activation of Fos strongly facilitated the gene expression involving the AP1 gene, Cdc42, and Cdc42-like promoter sequences.

To validate functional specificity of AP-1 binding site in hemocytes, EMSA was performed to probe interactions between extracted hemocyte proteins and transcription factor binding sites and AP1 binding site. As shown in **Figure 4E**, a clear shift band became observable upon incubation of the biotin-labeled AP-1 probe with extracted hemocyte proteins (Lane 2), with respect to a negative control (Lane 1). Meanwhile, high concentrations of a competitive probe (unlabeled AP-1 probe) resulted in abolition of binding of extracted hemocyte proteins to the probe (lane 3), whereas addition of excess mutant probe (T**A**ANT**T**A) had no effect on the binding of extracted hemocyte protein to the AP-1 probe (lane 4). Collectively, these results lend strong support to the establishment of Fos as a pivotal regulator in functional differentiation of hemocytes, via the AP-1 binding site.

DISCUSSION

Hemocytes have been long recognized for their vital roles in host immune response, which encompass precisely regulated processes such as recognizing, locating, ingesting, transporting, and digesting foreign particles (48). Traditionally, mollusk hemocytes are broadly classified into granulocytes and hyalinocytes on the basis of their morphological heterogeneity in invertebrates (13, 14, 28). Our observations via light microscopy and TEM also suggest this in *C. gigas*. Granulocytes are distinguished from other hemocytes by a defining anatomical feature, their large and ample cytoplasmic granules, while hyalinocytes have hyaline cytoplasm and silky appearance. Cytoplasmic granules in granulocytes are loaded with a variety of hydrolases designed to destroy phagocytosed foreign particles (38, 49, 50). The capacities for phagocytosis and ROS production of granulocytes in *C. gigas* are evidently greater than those of hyalinocytes, as demonstrated in this study, in agreement with previous reports (26). Although the molecular mechanisms underlying hemocyte phagocytosis and bacteria clearance have been extensively studied (51), the molecular determinants governing functional differentiation of hemocytes remain largely unknown. Sorting of hemocyte subpopulations coupled to transcriptomic analysis is ideal for advancing a more comprehensive view on functional differentiation between granulocytes and hyalinocytes in *C. gigas*. In our study, two hemocyte subpopulations profiled through four groups analyzed (50 samples per group) could be distinguished on the basis of granule content (SSC), while cell size (FSC) varied continuously over a wide range (19). Cells of different size classes were sorted and subsequently subjected to transcriptomic analysis for global identification of DEGs in granulocytes. This proposed strategy is advantageous for exploring the molecular driving functional heterogeneity and diversity in granulocytes, in conjunction with morphological and functional observations.

Granulocytes of *C. gigas* exhibit a number of important morphological and functional characteristics (48, 52, 53) and employ distinct molecular components and related signaling pathways, which make them stand out from hyalinocytes. Transcriptomic analysis here highlights a large array of DEGs, nearly all of which were prominently upregulated in granulocytes. These high expressed genes are themselves predominantly found in hemocytes in comparison with other tissues and are functionally involved in at least seven signaling pathways. Among these pathways, regulation of actin cytoskeleton, phagosome, and endocytosis, and lysosome were most relevant to phagocytosis (54, 55), corroborating the strong capacity of granulocytes for engulfing microbes. Extensive works have previously established that the mitogen-activated

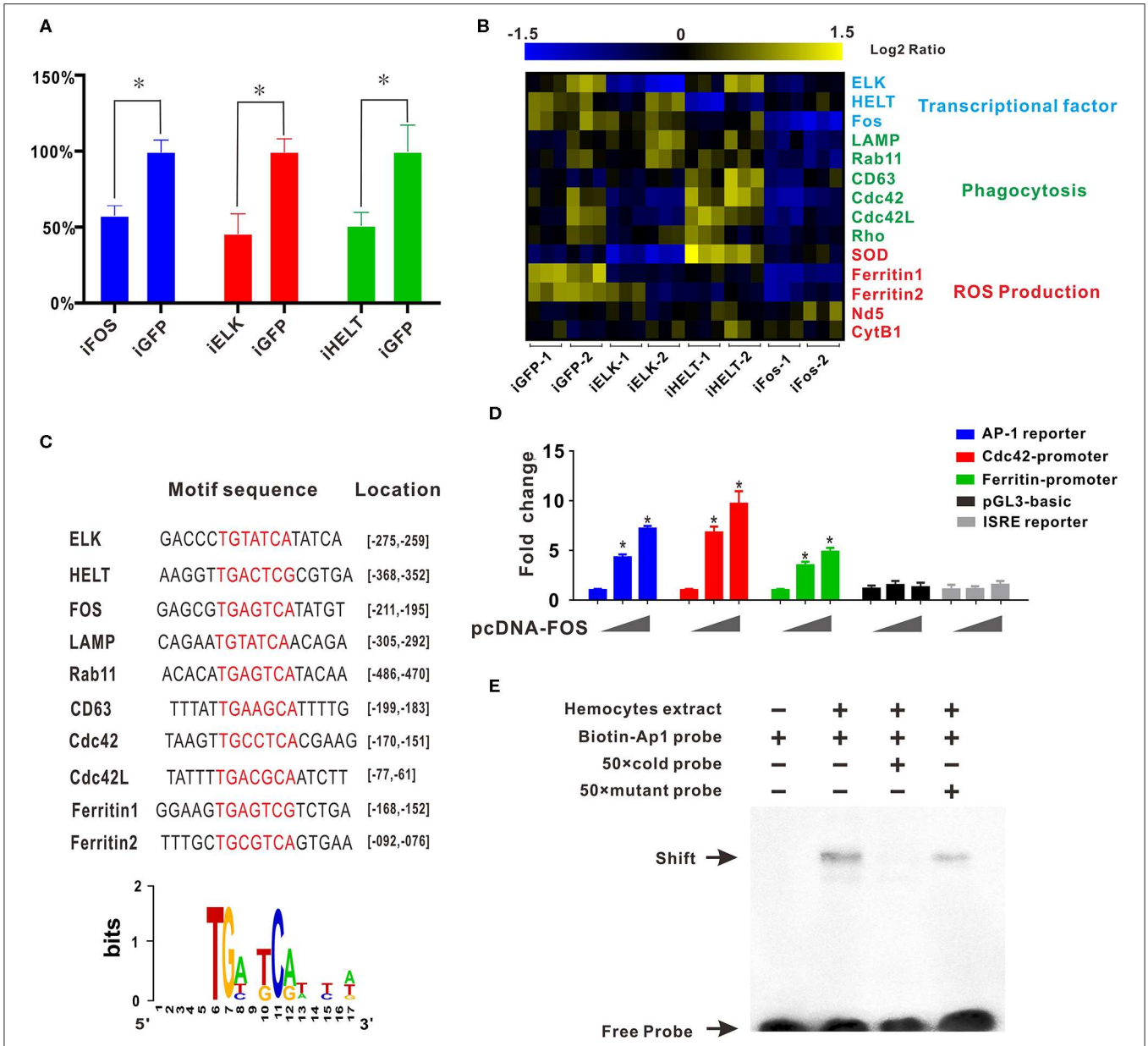

FIGURE 4 | Transcription factor Fos regulates transcriptional activation of granulocyte-specific genes. **(A)** Inhibition rate of RNA interference of three transcription factors (Fos, ELK, and HELT) *in vivo*. *Blue panel*, interference of Fos; *red panel*, interference of ELK; *green panel*, interference of HELT. **(B)** mRNA expression levels of immunity-related genes after knockdown of three transcription factors (ELK, HELT, and Fos). Detected genes were classified into three groups based on their potential functions: transcription factors, phagocytosis, and ROS production. Colors from yellow to blue indicate range of $\log_2$ ratio values (in descending order); yellow color indicates high expression level and blue color indicates low expression level. **(C)** Transcription factor binding site prediction software identified an AP-1 site that was highlighted in promoter element sequence of some immunity-related genes. Specific nucleotides were marked with red color. **(D)** Relative luciferase activity by expression of Fos plasmid for the luciferase reporter genes, AP-1 reporter Luc (*blue panel*), Cdc42 promoter reporter Luc (*red panel*), Cdc42l promoter reporter Luc (*green panel*), pGL3-basic vector (*black panel*), and ISRE-luc reporter (*gray panel*) in HEK293T cells. Plasmid pcDNA-Fos were added in gradient concentration (0, 150, and 300 ng). $^*p < 0.05$. **(E)** AP-1 probe was labeled with biotin and incubated with *C. gigas*-extracted hemocyte proteins. Unlabeled specific competitor sequences (cold probe) were used in a 50-fold surplus over labeled target.

protein kinase (MAPK) pathway plays critical roles in the regulation of a wide range of cellular processes including cell proliferation, differentiation, migration, senescence, and apoptosis (56). Of note, MAPK activity has been shown to respond to hematopoietic cytokines and growth factors, promoting the regulation of hematopoiesis (57). Furthermore, MAPK in mollusks was reported to be activated by various forms of extracellular stimulation and operate as a key regulator in immunity (58, 59). Our DEG analysis reveals that MAPK participated in granulocyte activities to regulate functional

activities, prior to the hyalinocytes, suggesting its involvement in *C. gigas* functional differentiation of hemocytes.

Notably, the DEGs in granulocytes formed a regulatory network with Cdc42 as a core member, which orchestrates the regulation of actin cytoskeleton, phagosome and endocytosis, and MAPK signaling pathway. Our results strongly support the notion that the phagocytosis capacity of granulocytes was dampened in the presence of Cdc42 inhibitors. Cdc42 is a small GTP-binding protein of the Rho family, which act as molecular switches between inactive GDP and active GTP-bound states to regulate actin remodeling (60, 61). In addition, another GTP-binding protein, Rho, was found to be closely connected with Cdc42 and Cdc42l in our pathway networks. Rho was the first Rho family protein to be implicated in the regulation of actin remodeling in response to extracellular signals (60). Thus, phagocytosis in granulocytes appears to be driven by Cdc42 as a regulatory switch in actin-dependent events. In this context, it is noteworthy that Cdc42-dependent actin dynamics has been suggested to control cell maturation, secretory activity (62), endocytosis (63), and cell adhesion to the extracellular matrix (64). Previously, dendritic cell maturation was reportedly accompanied by substantial rearrangements of actin cytoskeleton, leading to an enhanced transport of vesicle to the cell surface (65). In this current study, we provided fresh evidence on the significance of Cdc42 as a regulator to give rise to functional granulocytes in *C. gigas*, although the precise mechanistic details with which Cdc42 acts to regulate granulocyte phagocytosis remain to be elaborated.

Clearly, functional differentiation is regulated by various endogenous and exogenous factors, among which, transcriptional regulators play a pivotal role in modulating cell development, leading to functional heterogeneity and diversity between cells (66). Indeed, four transcription factors were identified in granulocyte-specific genes, including HELT, ELK, Fos, and microphthalmia-associated transcription factor (MITF). However, literature-based evidences supported that HELT, ELK, and Fos have strong potentials in regulation of hematopoiesis (67–69). Furthermore, AP-1 (activator protein 1, Fos/Jun) transcription factors have been shown to be versatile regulators in the functional development of hematopoietic cell lineages, including monocytes/macrophages (70), granulocytes (71, 72), megakaryocytes (73), mastocytes (74), and erythroid lineages (75). AP-1 computes extracellular signals into expression programs of specific target genes that have AP-1 binding sites in their promoter or enhancer regions (76). In agreement with this idea, knockdown of expression of the AP-1 transcription factor Fos in *C. gigas* diminished the expression levels of genes involved in phagocytosis (LAMP, Rab11, CD63, Cdc42, Cdc42l, and Rho) and ROS production (SOD, ferritin1, ferritin2, Nd5, and CytB1). Evidence from our promoter analysis indicates that all of these downstream genes harbor the AP-1 binding site (TGTATCA). AP-1 binding site is commonly identified in the genes required for phagocytosis and ROS production. Additionally, a network of DEGs illustrated actively engaged signaling pathways, with Cdc42 and Cdc42l being a core regulator of pathway network in functional differentiation of hemocytes. By means of a dual-luciferase reporter assay, it was demonstrated that *C. gigas* Cdc42 and Cdc42l are, in turn, also tightly regulated by the expression of Fos. These observations thus offer compelling evidence for the functional significance of transcription factor Fos in transcriptional activation of granulocyte-specific genes and then consequently promote the functional differentiation of hemocytes in *C. gigas*. However, due to the lack of powerful transgene techniques or available oyster hemocytes cell lines so far, it is still difficult to perform the rescue experiment by reactivation of Cdc42 with Fos knockdown in oyster hemocyte, which limited us to obtain directive evidence of Fos/Cdc42 guiding the functional differentiation of granulocytes.

Hemocytes constitute a crucial cellular component of *C. gigas* immunity, though the processes underpinning their formation (or hematopoiesis) in mollusks are far from completely understood. It has been generally agreed that invertebrate granulocytes are more phagocytic than agranulocytes (28, 77) and show similarities to the human granulocyte–monocyte macrophage lineage, particularly vertebrate monocytes/macrophages. The mononuclear phagocyte lineage undergoes a multistep process toward maturation from bone marrow precursors to tissue macrophages (MAC) via circulating blood monocytes (MO) (30, 78, 79). In this study, it is established that an intricate assembly of molecular switches is at work to control several hallmarks of granulocyte biology and regulate functional differentiation of hemocytes in a marine invertebrate, *C. gigas*. For simplicity, we propose

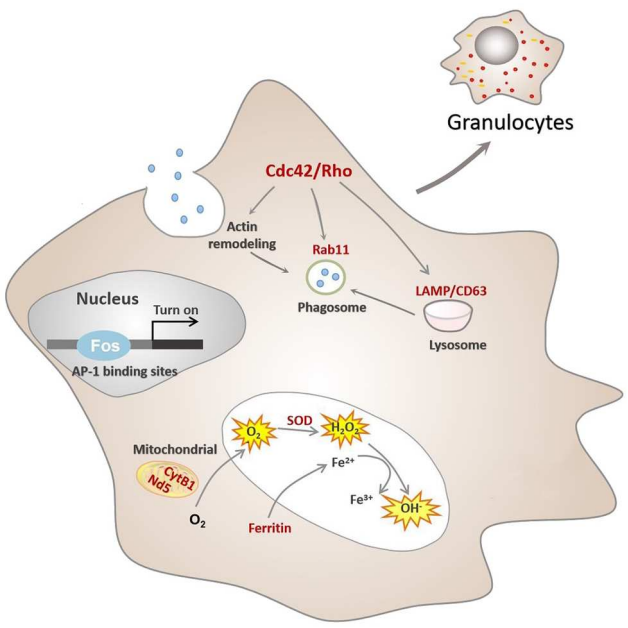

FIGURE 5 | Conceptualization of functional differentiation of hemocytes in *C. gigas*. During functional differentiation, expression of the transcription factor Fos rises, which turns on transcription by binding to the AP-1 binding site of target genes, marked in red color. These target genes contribute to functional activities of granulocytes, including ROS production and phagocytosis. Cdc42/Cdc42l, the core regulators of granulocytes pathway network, were also transcriptionally controlled by Fos to promote actin rearrangement during phagosome formation in granulocytes, ultimately facilitating phagocytosis.

a developmental sequence of *C. gigas* hemocytes, as shown in **Figure 5**. Although hematopoiesis is common to all animals with circulatory systems, the precise mechanisms and outcomes of hematopoietic events are quite different due to genetic complexity and interactions across different species. Hence, this study has put forward a novel molecular picture on functional differentiation of hemocytes in *C. gigas*, which may ultimately facilitate our understanding of how immune defense systems evolve and operate in higher-order and more recent phyla.

DATA AVAILABILITY STATEMENT

The datasets generated for this study can be found in the NCBI Sequence Read Archive database under the accession number PRJNA591303.

ETHICS STATEMENT

Experiments in this study were conducted with approval from Experimental Animal Ethics Committee, South China Sea Institute of Oceanology, Chinese Academy of Sciences, China.

AUTHOR'S NOTE

Experiments in this study followed standard biosecurity and institutional safety procedures.

AUTHOR CONTRIBUTIONS

FM conceived the study, analyzed the transcriptome data, performed flow cytometry, RNAi, imaging and EMSA experiments, and prepared the manuscript. YL performed the transcriptomic analysis and protein annotation. XZ performed the inhibition experiment. MH and DX performed the motif analysis and dual-luciferase reporter assay. ZX and JL prepared the hemocytes. YZ, N-KW, and ZY conceived and interpreted the data, and prepared the manuscript. All authors drafted the work, revised it critically for important intellectual content, and approved the final version.

FUNDING

This work was supported by the National Science Foundation of China (No. 31902404), the Key Special Project for Introduced Talents Team of Southern Marine Science and Engineering Guangdong Laboratory (Guangzhou) (GML2019ZD0407), the China Agricultural Research System (No. CARS-49), the Science and Technology Program of Guangzhou, China (No.201804020073), the Program of the Pearl River Young Talents of Science and Technology in Guangzhou of China (201806010003), the Institution of South China Sea Ecology and Environmental Engineering, Chinese Academy of Sciences (ISEE2018PY01, ISEE2018PY03, and ISEE2018ZD01), and the Science and Technology Planning Project of Guangdong Province, China (2017B030314052 and 201707010177).

ACKNOWLEDGMENTS

We are deeply grateful to the support of lab members and collaborators, who have provided us with able assistance or valuable advice at every stage of this study.

SUPPLEMENTARY MATERIAL

The Supplementary Material for this article can be found online at: https://www.frontiersin.org/articles/10.3389/fimmu.2020.00911/full#supplementary-material

Figure S1 | (A,B) KEGG pathway analysis.

Figure S2 | Q-PCR validation of key DEGs.

Figure S3 | Correlation plot of DEGs.

Figure S4 | Relative expression level of WASP after Cdc42 inhibition.

Figure S5 | Cdc42 promoter.

Figure S6 | Cdc42L promoter.

Table S1 | Sequencing data.

Table S2 | Alignment efficiency statistics.

Table S3 | DEG analysis.

Table S4 | DEGs in common.

REFERENCES

1. Canesi L, Gallo G, Gavioli M, Pruzzo C. Bacteria-hemocyte interactions and phagocytosis in marine bivalves. *Microsc Res Tech*. (2002) 57:469–76. doi: 10.1002/jemt.10100
2. Allam B, Pales Espinosa E. Bivalve immunity and response to infections: are we looking at the right place? *Fish Shellfish Immunol*. (2016) 53:4–12. doi: 10.1016/j.fsi.2016.03.037
3. Song L, Wang L, Qiu L, Zhang H. Bivalve immunity. *Invertebr Immunity*. (2010) 708:44–65. doi: 10.1007/978-1-4419-8059-5_3
4. Xue QG, Renault T, Chilmonczyk S. Flow cytometric assessment of haemocyte sub-populations in the European flat oyster, ostrea edulis, haemolymph. *Fish Shellfish Immunol*. (2001) 11:557–67. doi: 10.1006/fsim.2001.0335
5. Allam B, Ashton-Alcox KA, Ford SE. Flow cytometric comparison of haemocytes from three species of bivalve molluscs. *Fish Shellf Immunol*. (2002) 13:141–58. doi: 10.1006/fsim.2001.0389
6. Xue Q, Renault T, Cochennec N, Gerard A. Separation of European flat oyster, istrea edulis, haemocytes by density gradient centrifugation and SDS-PAGE characterisation of separated haemocyte sub-populations. *Fish Shellf Immunol*. (2000) 10:155–65. doi: 10.1006/fsim.1999.0234
7. Jing X, Wenbin Z. Comparison of antigenicity among haemocytes of seven bivalve species by monoclonal antibodies against haemocytes of scallop (Chlamys farreri). *Fish Shellfish Immunol*. (2006) 20:528–35. doi: 10.1016/j.fsi.2005.07.001
8. Xue Q, Renault T. Monoclonal antibodies to European flat oyster ostrea edulis hemocytes: characterization and tissue distribution of granulocytes in adult and developing animals. *Dev Comparative Immunol*. (2001) 25:187–94. doi: 10.1016/S0145-305X(00)00058-6
9. Cheng TC, Foley DA. Hemolymph cells of the bivalve mollusc mercenaria mercenaria: an electron microscopical study. *J Invert Pathol*. (1975) 26:341–51. doi: 10.1016/0022-2011(75)90232-3

10. Suresh K, Mohandas A. Number and types of hemocytes in sunetta scripta and villorita cyprinoides var. cochinensis (bivalvia), and leukocytosis subsequent to bacterial challenge. *J Invert Pathol*. (1990) 55:312–8. doi: 10.1016/0022-2011(90)90072-E
11. Söderhäll K, Smith VJ. Separation of the haemocyte populations of carcinusmaenas and other marine decapods, and prophenoloxidase distribution. *Dev Comparative Immunol*. (1983) 7:229–39. doi: 10.1016/0145-305X(83)90004-6
12. Ray M, Bhunia NS, Bhunia AS, Ray S. A comparative analyses of morphological variations, phagocytosis and generation of cytotoxic agents in flow cytometrically isolated hemocytes of Indian molluscs. *Fish Shellf Immunol*. (2013) 34:244–53. doi: 10.1016/j.fsi.2012.11.006
13. Cheng TC. A classification of molluscan hemocytes based on functional evidences. *Comparative Pathobiol*. (1984) 6:111–46. doi: 10.1007/978-1-4684-4766-8_5
14. Cheng TC. Bivalves. In: Ratcliffe NA, Rowley AF, editors. *Invertebrate Blood Cells*. New York, NY: Academic Press (1981). p. 233–300.
15. King JG, Hillyer JF. Spatial and temporal *in vivo* analysis of circulating and sessile immune cells in mosquitoes: hemocyte mitosis following infection. *BMC Biol*. (2013) 11:55. doi: 10.1186/1741-7007-11-55
16. Pila EA, Sullivan JT, Wu XZ, Fang J, Rudko SP, Gordy MA, et al. Haematopoiesis in molluscs: a review of haemocyte development and function in gastropods, cephalopods and bivalves. *Dev Comparative Immunol*. (2016) 58:119–28. doi: 10.1016/j.dci.2015.11.010
17. Ottaviani E, Franchini A, Barbieri D, Kletsas D. Comparative and morphofunctional studies on mytilus galloprovincialis hemocytes: presence of two aging-related hemocyte stages. *Ital J Zool*. (1998) 65:349–54. doi: 10.1080/11250009809386772
18. Mix MC. A general model for leukocyte cell renewal in bivalve mollusks. *Marine Fish*. (1976) 38:37–41.
19. Rebelo Mde F, Figueiredo Ede S, Mariante RM, Nobrega A, de Barros CM, Allodi S. New insights from the oyster crassostrea rhizophorae on bivalve circulating hemocytes. *PLoS ONE*. (2013) 8:e57384. doi: 10.1371/journal.pone.0057384
20. Pipe RK, Farley SR, Coles JA. The separation and characterisation of haemocytes from the mussel mytilus edulis. *Cell Tissue Res*. (1997) 289:537–45. doi: 10.1007/s004410050899
21. Cima F, Matozzo V, Marin MG, Ballarin L. Haemocytes of the clam rapes philippinarum (Adams & Reeve, 1850): morphofunctional characterisation. *Fish Shellfish Immunol*. (2000) 10:677–93. doi: 10.1006/fsim.2000.0282
22. Cheng TC, Auld KR. Hemocytes of the pulmonate gastropod biomphalaria glabrata. *J Invert Pathol*. (1977) 30:119–22. doi: 10.1016/0022-2011(77)90052-0
23. Lopez C, Carballal MJ, Azevedo C, Villalba A. Morphological characterization of the hemocytes of the clam, ruditapes decussatus (mollusca: bivalvia). *J Invert Pathol*. (1997) 69:51–7. doi: 10.1006/jipa.1996.4639
24. Chang SJ, Tseng SM, Chou HY. Morphological characterization via light and electron microscopy of the hemocytes of two cultured bivalves: a comparison study between the hard clam (*Meretrix lusoria*) and pacific oyster (*Crassostrea gigas*). *Zool Stud*. (2005) 44:144–52. doi: 10.1016/j.micron.2016.03.003
25. Cheng TC, Huang JW, Karadogan H, Renwrantz LR, Yoshino TP. Separation of oyster hemocytes by density gradient centrifugation and identification of their surface-receptors. *J Invert Pathol*. (1980) 36:35–40. doi: 10.1016/0022-2011(80)90132-9
26. Wang W, Li M, Wang L, Chen H, Liu Z, Jia Z, et al. The granulocytes are the main immunocompetent hemocytes in *Crassostrea gigas*. *Dev Compar Immunol*. (2017) 67:221–8. doi: 10.1016/j.dci.2016.09.017
27. Kuchel RP, Raftos DA, Birch D, Vella N. Haemocyte morphology and function in the akoya pearl oyster, pinctada imbricata. *J Invert Pathol*. (2010) 105:36–48. doi: 10.1016/j.jip.2010.04.011
28. Hine PM. The inter-relationships of bivalve haemocytes. *Fish Shellfish Immunol*. (1999) 9:367–85. doi: 10.1006/fsim.1998.0205
29. Saeed S, Quintin J, Kerstens HH, Rao NA, Aghajanirefah A, Matarese F, et al. Epigenetic programming of monocyte-to-macrophage differentiation and trained innate immunity. *Science*. (2014) 345:1251086. doi: 10.1126/science.1251086
30. Valledor AF, Borras FE, Cullell-Young M, Celada A. Transcription factors that regulate monocyte/macrophage differentiation. *J Leukocyte Biol*. (1998) 63:405–17. doi: 10.1002/jlb.63.4.405
31. Liebermann DA, Hoffman-Liebermann B. Genetic programs of myeloid cell differentiation. *Curr Opin Hematol*. (1994) 1:24–32.
32. Robb L, Elefanty AG, Begley CG. Transcriptional control of hematopoiesis. *Blood*. (1999) 87:4025-39. doi: 10.1016/b978-012624960-6/50003-0
33. Medzhitov R, Horng T. Transcriptional control of the inflammatory response. *Nat Rev Immunol*. (2009) 9:692–703. doi: 10.1038/nri2634
34. Zook EC, Kee BL. Development of innate lymphoid cells. *Nat Immunol*. (2016) 17:775–82. doi: 10.1038/ni.3481
35. Barton K, Muthusamy N, Fischer C, Ting C-N, Walunas TL, Lanier LL, et al. The Ets-1 transcription factor is required for the development of natural killer cells in mice. *Immunity*. (1998) 9:555–63. doi: 10.1016/S1074-7613(00)80638-X
36. Geiger TL, Sun JC. Development and maturation of natural killer cells. *Curr Opin Immunol*. (2016) 39:82–9. doi: 10.1016/j.coi.2016.01.007
37. Zhdanov VV, Miroshnichenko LA, Udut EV, Polyakova TY, Zyuz'kov GN, Simanina EV, et al. Role of signaling molecules in the regulation of granulocytopoiesis during stress-inducing stimulation. *Bull Exp Biol Med*. (2019) 166:344–7. doi: 10.1007/s10517-019-04347-w
38. Cheng TC, Downs JC. Intracellular acid phosphatase and lysozyme levels in subpopulations of oyster, *Crassostrea virginica*, hemocytes. *J Invert Pathol*. (1988) 52:163–7. doi: 10.1016/0022-2011(88)90116-4
39. Li J, Zhang Y, Mao F, Lin Y, Xiao S, Xiang Z, et al. The first morphologic and functional characterization of hemocytes in Hong Kong oyster, crassostrea hongkongensis. *Fish Shellf Immunol*. (2018) 81:423–9. doi: 10.1016/j.fsi.2018.05.062
40. Kim D, Pertea G, Trapnell C, Pimentel H, Kelley R, Salzberg SL. TopHat2: accurate alignment of transcriptomes in the presence of insertions, deletions and gene fusions. *Genome Biol*. (2013) 14:R36. doi: 10.1186/gb-2013-14-4-r36
41. Langmead B, Trapnell C, Pop M, Salzberg SL. Ultrafast and memory-efficient alignment of short DNA sequences to the human genome. *Genome Biol*. (2009) 10:R25. doi: 10.1186/gb-2009-10-3-r25
42. Mortazavi A, Williams BA, McCue K, Schaeffer L, Wold B. Mapping and quantifying mammalian transcriptomes by RNA-Seq. *Nat Methods*. (2008) 5:621–8. doi: 10.1038/nmeth.1226
43. Zhang G, Fang X, Guo X, Li L, Luo R, Xu F, et al. The oyster genome reveals stress adaptation and complexity of shell formation. *Nature*. (2012) 490:49–54. doi: 10.1038/nature11413
44. Florian MC, Dorr K, Niebel A, Daria D, Schrezenmeier H, Rojewski M, et al. Cdc42 activity regulates hematopoietic stem cell aging and rejuvenation. *Cell Stem Cell*. (2012) 10:520–30. doi: 10.1016/j.stem.2012.04.007
45. Sakamori R, Das S, Yu S, Feng S, Stypulkowski E, Guan Y, et al. Cdc42 and Rab8a are critical for intestinal stem cell division, survival, and differentiation in mice. *J Clin Invest*. (2012) 122:1052–65. doi: 10.1172/JCI60282
46. Surviladze Z, Waller A, Wu Y, Romero E, Edwards BS, Wandinger-Ness A, et al. Identification of a small GTPase inhibitor using a high-throughput flow cytometry bead-based multiplex assay. *J Biomol Screen*. (2010) 15:10–20. doi: 10.1177/1087057109352240
47. Gerasimcik N, He M, Dahlberg CIM, Kuznetsov NV, Severinson E, Westerberg LS. The small Rho GTPases Rac1 and Rac2 are Important for T-Cell independent antigen responses and for suppressing switching to IgG2b in mice. *Front Immunol*. (2017) 8:1264. doi: 10.3389/fimmu.2017.01264
48. Fisher WS. Structure and Functions of Oyster Hemocytes. In: Brehélin M. editors. *Immunity in Invertebrates. Proceedings in Life Sciences*. Berlin, Heidelberg: Springer (1986). p. 25–35. doi: 10.1007/978-3-642-70768-1_3
49. Carballal MJ, Lopez C, Azevedo C, Villalba A. *In vitro* study of phagocytic ability of mytilus galloprovincialis Lmk haemocytes. *Fish Shellfish Immunol*. (1997) 7:403–16. doi: 10.1006/fsim.1997.0094
50. Carballal MJ, Lopez C, Azevedo C, Villalba A. Enzymes involved in defense functions of hemocytes of mussel mytilus galloprovincialis. *J Invert Bathol*. (1997) 70:96–105. doi: 10.1006/jipa.1997.4670
51. Jiang S, Qiu LM, Wang LL, Jia ZH, Lv Z, Wang MQ, et al. Transcriptomic and quantitative proteomic analyses provide insights into the phagocytic killing of hemocytes in the oyster crassostrea gigas. *Front Immunol*. (2018) 9:1280. doi: 10.3389/fimmu.2018.01280

52. Lambert C, Soudant P, Choquet G, Paillard C. Measurement of crassostrea gigas hemocyte oxidative metabolism by flow cytometry and the inhibiting capacity of pathogenic vibrios. *Fish Shellfish Immunol.* (2003) 15:225–40. doi: 10.1016/S1050-4648(02)00160-2
53. Bachere E, Chagot D, Grizel H. Separation of Crassostrea gigas hemocytes by density gradient centrifugation and counterflow centrifugal elutriation. *Dev comparative Immunol.* (1988) 12:549–59. doi: 10.1016/0145-305X(88)90071-7
54. Underhill DM, Ozinsky A. Phagocytosis of microbes: complexity in action. *Ann Rev Immunol.* (2002) 20:825–52. doi: 10.1146/annurev.immunol.20.103001.114744
55. Aderem A, Underhill DM. Mechanisms of phagocytosis in macrophages. *Ann Rev Immunol.* (1999) 17:593–623. doi: 10.1146/annurev.immunol.17.1.593
56. Sun Y, Liu WZ, Liu T, Feng X, Yang N, Zhou HF. Signaling pathway of MAPK/ERK in cell proliferation, differentiation, migration, senescence and apoptosis. *J Recep Signal Transd Res.* (2015) 35:600–4. doi: 10.3109/10799893.2015.1030412
57. Geest CR, Coffer PJ. MAPK signaling pathways in the regulation of hematopoiesis. *J Leukoc Biol.* (2009) 86:237–50. doi: 10.1189/jlb.0209097
58. Qu F, Xiang Z, Zhang Y, Li J, Xiao S, Zhang Y, et al. A novel p38 MAPK indentified from crassostrea hongkongensis and its involvement in host response to immune challenges. *Mol Immunol.* (2016) 79:113–24. doi: 10.1016/j.molimm.2016.10.001
59. Wang Z, Wang B, Chen G, Jian J, Lu Y, Xu Y, et al. Transcriptome analysis of the pearl oyster (Pinctada fucata) hemocytes in response to vibrio alginolyticus infection. *Gene.* (2016) 575:421–8. doi: 10.1016/j.gene.2015.09.014
60. Hall A. Small GTP-binding proteins and the regulation of the actin cytoskeleton. *Ann Rev Cell Biol.* (1994) 10:31–54. doi: 10.1146/annurev.cb.10.110194.000335
61. Tybulewicz VLJ, Henderson RB. Rho family GTPases and their regulators in lymphocytes. *Nat Rev Immunol.* (2009) 9:630–44. doi: 10.1038/nri2606
62. Schulz AM, Stutte S, Hogl S, Luckashenak N, Dudziak D, Leroy C, et al. Cdc42-dependent actin dynamics controls maturation and secretory activity of dendritic cells. *J Cell Biol.* (2015) 211:553–67. doi: 10.1083/jcb.201503128
63. Garrett WS, Chen LM, Kroschewski R, Ebersold M, Turley S, Trombetta S, et al. Developmental control of endocytosis in dendritic cells by Cdc42. *Cell.* (2000) 102:325–34. doi: 10.1016/S0092-8674(00)00038-6
64. Allen WE, Jones GE, Pollard JW, Ridley AJ. Rho, Rac and Cdc42 regulate actin organization and cell adhesion in macrophages. *J Cell Sci.* (1997) 110:707–20.
65. West MA, Wallin RP, Matthews SP, Svensson HG, Zaru R, Ljunggren HG, et al. Enhanced dendritic cell antigen capture via toll-like receptor-induced actin remodeling. *Science.* (2004) 305:1153–7. doi: 10.1126/science.1099153
66. Hasan S, Naqvi AR, Rizvi A. Transcriptional regulation of emergency granulopoiesis in leukemia. *Front Immunol.* (2018) 9:481. doi: 10.3389/fimmu.2018.00481
67. Sharrocks AD. The ETS-domain transcription factor family. *Nat Rev Mol Cell Biol.* (2001) 2:827–37. doi: 10.1038/35099076
68. Alvarez Y, Municio C, Hugo E, Zhu J, Alonso S, Hu X, et al. Notch- and transducin-like enhancer of split (TLE)-dependent histone deacetylation explain interleukin 12 (IL-12) p70 inhibition by zymosan. *J Biol Chem.* (2011) 286:16583–95. doi: 10.1074/jbc.M111.222158
69. Lee SY, Yoon J, Lee MH, Jung SK, Kim DJ, Bode AM, et al. The role of heterodimeric AP-1 protein comprised of JunD and c-Fos proteins in hematopoiesis. *J Biol Chem.* (2012) 287:31342–8. doi: 10.1074/jbc.M112.387266
70. Auwerx J. The human leukemia cell line, THP-1: a multifacetted model for the study of monocyte-macrophage differentiation. *Experientia.* (1991) 47:22–31. doi: 10.1007/BF02041244
71. Liebermann DA, Gregory B, Hoffman B. AP-1 (Fos/Jun) transcription factors in hematopoietic differentiation and apoptosis. *Int J Oncol.* (1998) 12:685–700. doi: 10.3892/ijo.12.3.685
72. Friedman AD. Transcriptional control of granulocyte and monocyte development. *Oncogene.* (2007) 26:6816–28. doi: 10.1038/sj.onc.1210764
73. Limb JK, Yoon S, Lee KE, Kim BH, Lee S, Bae YS, et al. Regulation of megakaryocytic differentiation of K562 cells by FosB, a member of the fos family of AP-1 transcription factors. *Cell Mol Life Sci.* (2009) 66:1962–73. doi: 10.1007/s00018-009-8775-5
74. Tshori S, Nechushtan H. Mast cell transcription factors–regulators of cell fate and phenotype. *Biochim Biophys Acta.* (2012) 1822:42–8. doi: 10.1016/j.bbadis.2010.12.024
75. Rosson D, O'Brien TG. AP-1 activity affects the levels of induced erythroid and megakaryocytic differentiation of K562 cells. *Arch Biochem Biophys.* (1998) 352:298–305. doi: 10.1006/abbi.1998.0597
76. Jochum W, Passegue E, Wagner EF. AP-1 in mouse development and tumorigenesis. *Oncogene.* (2001) 20:2401–12. doi: 10.1038/sj.onc.1204389
77. Goedken M, De Guise S. Flow cytometry as a tool to quantify oyster defence mechanisms. *Fish Shellfish Immunol.* (2004) 16:539–52. doi: 10.1016/j.fsi.2003.09.009
78. Andreesen R, Brugger W, Scheibenbogen C, Kreutz M, Leser HG, Rehm A, et al. Surface phenotype analysis of human monocyte to macrophage maturation. *J Leukoc Biol.* (1990) 47:490–7. doi: 10.1002/jlb.47.6.490
79. Krause SW, Rehli M, Kreutz M, Schwarzfischer L, Paulauskis JD, Andreesen R. Differential screening identifies genetic markers of monocyte to macrophage maturation. *J Leukoc Biol.* (1996) 60:540–5. doi: 10.1002/jlb.60.4.540

Conflict of Interest: The authors declare that the research was conducted in the absence of any commercial or financial relationships that could be construed as a potential conflict of interest.

frontiers in Immunology

REVIEW
published: 27 May 2020
doi: 10.3389/fimmu.2020.00824

Recent Advances on Phagocytic B Cells in Teleost Fish

Liting Wu[1†], *Zhendong Qin*[2†], *Haipeng Liu*[3,4], *Li Lin*[2,4], *Jianmin Ye*[1,4*] *and Jun Li*[2,4,5*]

[1] *Guangdong Provincial Key Laboratory for Healthy and Safe Aquaculture, Institute of Modern Aquaculture Science and Engineering, School of Life Sciences, South China Normal University, Guangzhou, China,* [2] *Guangzhou Key Laboratory of Aquatic Animal Diseases and Waterfowl Breeding, Guangdong Provincial Water Environment and Aquatic Products Security Engineering Technology Research Center, College of Animal Sciences and Technology, Zhongkai University of Agriculture and Engineering, Guangzhou, China,* [3] *State Key Laboratory of Marine Environmental Science, State-Province Joint Engineering Laboratory of Marine Bioproducts and Technology, Xiamen University, Xiamen, China,* [4] *Laboratory for Marine Fisheries Science and Food Production Processes, Laboratory for Marine Biology and Biotechnology, Pilot National Laboratory for Marine Science and Technology, Qingdao, China,* [5] *School of Science and Medicine, Lake Superior State University, Sault Ste. Marie, MI, United States*

The momentous discovery of phagocytic activity in teleost B cells has caused a dramatic paradigm shift from the belief that phagocytosis is performed mainly by professional phagocytes derived from common myeloid progenitor cells, such as macrophages/monocytes, neutrophils, and dendritic cells. Recent advances on phagocytic B cells and their microbicidal ability in teleost fish position B cells at the crossroads, bridging innate with adaptive immunity. Most importantly, an increasing body of experimental evidence demonstrates that, in both teleosts and mammals, phagocytic B cells can recognize, take up, and destroy particulate antigens and then present those processed antigens to $CD4^+$ T cells to elicit adaptive immune responses and that the phagocytosis is mediated by pattern recognition receptors and involves multiple cytokines. Thus, current findings collectively indicate that teleost phagocytic B cells, as well as their counterpart mammalian B1-B cells, can be considered one kind of professional phagocyte. The aim of this review is to summarize recent advances regarding teleost phagocytic B cells, with a particular focus on the recognizing receptors and modulating mechanisms of phagocytic B cells and the process of antigen presentation for T-cell activation. We also attempt to provide new insights into the adaptive evolution of the teleost fish phagocytic B cell on the basis of its innate and adaptive roles.

Keywords: teleost fish, B cells, phagocytosis, cytokines, antigen presentation

OPEN ACCESS

Edited by:
Xinjiang Lu,
Ningbo University, China

Reviewed by:
Yishan Lu,
Guangdong Ocean University, China
Yong-An Zhang,
Huazhong Agricultural University, China

***Correspondence:**
Jianmin Ye
jmye@m.scnu.edu.cn
Jun Li
jli@lssu.edu

[†]*These authors have contributed equally to this work*

Specialty section:
This article was submitted to Comparative Immunology, a section of the journal Frontiers in Immunology

Received: *16 February 2020*
Accepted: *14 April 2020*
Published: *27 May 2020*

Citation:
Wu L, Qin Z, Liu H, Lin L, Ye J and Li J (2020) Recent Advances on Phagocytic B Cells in Teleost Fish. Front. Immunol. 11:824. doi: 10.3389/fimmu.2020.00824

INTRODUCTION

It has become well-accepted that B cells in all vertebrates are functional antibody-secreting cells (ASCs) for the production of specific antibodies in response to certain invading foreign antigens and that they play vital roles in adaptive immunity (1). Phagocytosis is a specific form of endocytosis of phagocytes by which solid particles (including microbial pathogens) are internalized to form phagosomes and phagolysosomes, followed by antigen degradation to destroy the invaders or continued processing of antigenic information, eventually initiating adaptive immunity in vertebrates (2–4). Phagocytosis plays an essential role of linking the innate

and adaptive immune responses in vertebrates. Classical phagocytosis is mainly accomplished by "professional" phagocytes, including macrophages/monocytes, neutrophils, and dendritic cells, but some "amateur" phagocytes (such as epithelial cells and fibroblasts) are able to engulf particulate antigens to a much lower degree in comparison to professional phagocytes (5). Although B cells are considered to be one of the three major professional antigen-presenting cells (APCs), it is well-recognized that they have the main responsibility of binding specific soluble antigenic peptides through B-cell receptors (BCRs) but do not phagocytose and present large non-specific particulate antigens. Therefore, the long-held paradigm is that B cells are non-phagocytic cells, even though evidence has been reported that $CD5^+$ B-cell lymphoma was able to differentiate to macrophage-like cells (6). However, in 2006, Li et al. showed direct evidence for the first time in vertebrates that B cells derived from teleost fish and frog are capable of phagocytic and bactericidal activity through the formation of phagolysosome, a unique innate immunity that was previously only identified in professional phagocytes (7). Besides teleost fish, this novel phagocytic capability of B cells has also been extended into other vertebrates like reptiles (8), mice, and human (B1 subset) (9–13). Since then, numerous studies have been carried out in an attempt to elucidate the involvement of phagocytic B cells and their related novel aspects in both innate and adaptive immune responses, especially their evolutionary origins and the functional relationships between different B-cell subsets and macrophages. Details regarding those recent findings have been summarized and discussed in several excellent reviews (14, 15).

It is well-known that fish have both an innate and an adaptive immune system. Thus far, most of the elements of the innate immune system of higher vertebrates, as well as the counterpart molecules/receptors related to the mammalian adaptive immune system, including immunoglobulins, B-cell receptor (BCR), major histocompatibility complex class I and II (MHC I and MHC II), CD4, CD8, T cell receptor (TCR), etc., have also been identified in teleost fish (16). A variety of novel findings originally from studies on the fish immune system have led to major groundbreaking discoveries of previously unknown molecules and biochemical pathways involved in mammalian immunity (17–20). Due to the unique place of this fish on the evolutional timeline of life, the teleost fish has become an excellent non-classical animal model for exploring the evolutionary history of defense immune reactions in mammals (16, 21). As a vital facet of innate immunity, phagocytosis plays essential roles in bridging the innate and adaptive immune reactions in both teleost fish and mammalian species (22). The newly uncovered phagocytic and bactericidal capabilities of B cells not only lead to a paradigm shift for the fish immune system (7) but also open a new door for us to rethink the evolutionary structure and functional network as well as the underlying regulatory mechanisms of the current mammalian immune system. Increasing studies on phagocytic B cells indicated that the phagocytosis is mediated by a series of molecules related to innate and adaptive immunity (19). However, due to the limited availability of specific reagents for fish, the study on teleost phagocytic B cells is still at a very early stage, and more efforts are urgently required for further exploration of detailed immune functions in teleosts and in mammals as well.

In this review, we try to summarize the most recent advances in the following areas in relation to the phagocytosis of teleost B cells: (1) phagocytic B-cell subsets in teleost fish; (2) phagocytic receptors and related pathways involved in B-cell phagocytosis; (3) modulating cytokines in B-cell phagocytosis; (4) involvement of phagocytic B cells in antigen presentation; (5) effects of B-cell adaptive functioning (differentiation) on B-cell phagocytic capacity. We aim to better understand the innate roles of fish phagocytic B cells in interacting and activating their adaptive immune functions in the primitive vertebrate and hopefully to provide novel evolutionary insights for further elucidation of the interaction mechanisms of the innate and adaptive immune system in mammalian species.

PHAGOCYTIC B-CELL SUBSETS IN TELEOST FISH

Until now, three different immunoglobulin isotypes (IgM, IgD, and IgT/Z), which are accordingly secreted by three major B-cell subsets (IgM^+/IgD^+, IgM^-/IgD^+, and IgM^-/IgT^+, or IgM^-/IgZ^+), have been identified and described in teleosts (23–26). IgM^+ B cells (IgM^+/IgD^+ lineage), as well as the IgM, have been found as the major B cells and the most abundant immunoglobulin present in the serum of teleost fish, and these play crucial roles in fish systemic adaptive immunity (27–31). IgT/Z, secreted by the previously unknown IgT^+ B cell (IgM^-/IgZ^+ lineage), which is a functional equivalent to IgA in mammals and birds, has also been demonstrated as a major player specialized in the teleost mucosa-associated lymphoid tissues (MALT), like intestine, skin, and gill, as well as in nasal-associated lymphoid tissue (NALT), pharyngeal mucosa, and buccal mucosa (32–36). The structural and functional specificity of IgT and IgT^+ B cells, their important roles in mucosal immunity in teleost fish, as well as the potentially applicable aspects in aquaculture for developing novel strategies to prevent infectious diseases, have been reviewed elsewhere (26, 37). IgD has long been recognized as a co-expressed molecule maker with IgM on the surface of matured naïve IgM^+/IgD^+ B cells. More interestingly, a novel IgM^-/IgD^+ B-cell subset and two different types of secreted IgD have recently been characterized in two teleost species, catfish and trout, respectively; however, very little is known about the function of IgD and the two types of IgD^+ B cells in teleost fish (38–40).

The phagocytic and bacteria-killing abilities of IgM^+ B cells were originally discovered and characterized by Li et al. in rainbow trout (*Oncorhynchus mykiss*) and catfish (*Ictalurus punctatus*) (7). In their subsequent study, a previously unknown IgM^-/IgT^+ B-cell subset, which uniquely secretes IgT, was identified in rainbow trout, and it is also capable of phagocytic and microbicidal activity (41). With regard to IgD^+ B cells, the involvement of surface IgD in the phagocytic activity of IgM^+/IgD^+ B cells is still unclear, and thus far, no reports are available that address the phagocytic ability of the newly identified IgM^-/IgD^+ B cells in catfish and trout. However,

the evidence that IgD^+/IgM^- plasmablasts constitute a major lymphocyte population in the teleost intestine and gills implies that the IgD^+ cells may play potential roles in MALT (42).

The unavailability of specific monoclonal antibodies (mAbs) or B-cell markers is a major barrier that has slowed down the exploration of the phagocytic activities of teleost fish B cells (16). In recent years, the number of reports on the phagocytic B cells of teleost fish has been rapidly increasing. In addition to rainbow trout and catfish, as shown in **Table 1**, phagocytic B cells from about 10 different teleost fish species have been identified. It needs to be pointed out that most of these studies were only focused on IgM^+ B-cell subsets due to the shortage of specific mAbs against IgT or IgD in these fish species. In these investigations, different functions of the teleost fish B cells were revealed in adaptive immunity or innate immunity. Although the IgM^+ B cells are capable of phagocytosis, their phagocytic capabilities differ significantly in different fish species (15, 43). For example, Overland et al. demonstrated very varied phagocytic activities by incubating fluorescent beads with IgM^+ B cells derived from either head kidney (HKL) or peripheral blood (PBL) of Atlantic salmon (*Salmo salar* L.) and cod (*Gadus morhua* L.), respectively (43). Similarly, highly variable phagocytic abilities for the IgM^+ B cells to ingest microbeads or different microbial particles were also observed in zebrafish (*Danio rerio*), lumpfish (*Cyclopterus lumpus* L.), half-smooth tongue sole (*Cynoglossus semilaevis*), large yellow croaker (*Larimichthys crocea*), turbot (*Scophthalmus maximus*), and Japanese flounder (*Paralichthys olivaceus*) (46, 52, 61). It is worth noting that various factors, as well as those mentioned above such as fish species and different immune organs/tissues, should also be seriously considered during phagocytic activity assay, for example, the physiological status of the fish, the size and nature of target particles, and the methods applied to incubate phagocytic B cells with various particles (mainly including the ratio of B cells to target particles, the opportunity for targets to interact with B cells, and the duration of incubation) (7, 53). In addition, the phagocytic process in both mammals and teleost B cells can be inhibited in a dose-dependent manner by cytochalasin B and colchicine, which indicates the involvement of cellular microtubules and microfilaments in B cells to internalize particles and bacteria (7, 10, 12, 41).

PHAGOCYTIC RECEPTORS TO INITIATE B-CELL PHAGOCYTOSIS

Similar to professional phagocytes, it has been clearly evidenced that both IgM^+ and IgT^+ B cells of rainbow trout phagocytose and kill bacteria through engulfment of target particles into phagosome and subsequent formation of maturated phagolysosome (**Figure 1**), and a similar actin polarization internalizing process has also been demonstrated in phagocytic B cells (7, 45). However, the involvement of functional receptors on the surface of phagocytic B cells for initial recognition of and interaction with certain molecules of target particles, as well as the difference from professional phagocytes, is not yet well-understood. Li and his colleagues demonstrated that the phagocytic activity of IgM^+ and IgT^+ B cells could be significantly enhanced once the target bacteria had been opsonized with antiserum or complement, which indicated a similar involvement of Fc receptor and complement receptors in the phagocytosis of both B cells and professional phagocytes (7, 45). Moreover, solid evidence has also confirmed the presence of C3a and C5a receptors on the surface of trout IgM^+ B cells and also on granulocytes (62–64). In addition, significant enhancement of C3d-linked target particles being phagocytosed by trout IgM^+ B cells indicated the presence of a mammalian CR2-like receptor (C3d receptor) on the surface of fish B cell (65). Similar phenomena that up-regulated phagocytosis were discovered in mouse IgM^+ B cells after incubation with complement-opsonized target particles (11). The cooperation of complement and phagocytic B cells both in teleost and mammalian species indicates the essential importance of B cells in the linkage of innate and adaptive immunity (**Figure 1**).

Their obvious difference from macrophages is that teleost B cells express B-cell-specific markers, including mIgM, CD79a, and CD79b, which constitute the BCR complex (66). BCR is crucial not only for specific binding of foreign antigens but also for signal transduction and the downstream regulation of B-cell activation and differentiation. Primary human B cells have shown the ability to uptake live *Salmonella* but not dead ones through BCR (67), but it remains to be clarified whether the internalizing process is a BCR-mediated or bacteria-mediated mechanism on this occasion. It has been demonstrated that phagocytosis of murine B1-a and B1-b B cells derived from the peritoneal cavity is BCR-independent (12). However, there was a report that *bcr*-transgenic mice whose B cells expressed more BCR exhibited 3-fold higher phagocytic activity than littermate control mice, which suggested that the transgenic BCR might promote B-cell phagocytosis (10). Regarding teleost B cells, we recently identified a co-stimulatory signal molecule that is equivalent to mammalian B cell-associated receptor (CD22) in Japanese flounder (54). The CD22-like molecule can not only provide a co-stimulatory signal for activation of IgM^+ B cells but also play essential regulatory roles in the macropinocytosis-dependent pathway principally relied upon by turbot and Japanese flounder IgM^+ B cells to internalize large particles (53, 54). This finding implies that teleost BCR, associated with its co-receptors, might be a crucial mediator in relation to B-cell phagocytosis as shown in mammals. Although the macropinocytosis-dependent pathway of turbot and Japanese flounder IgM^+ B cells likely implies the existence of another non-receptor-mediated endocytosis pathway in teleost IgM^+ B cells (53, 54), the regulation of CD22 in macropinocytosis-dependent endocytosis seems to indicate that macropinocytosis is regulated by other receptors instead of BCR. Thus, further studies are necessarily required to figure out the contribution of BCR as well as other co-receptors to B cells in ingesting large particulate antigens.

Due to being responsible for pattern recognition receptors (PRRs) that recognize a wide variety of pathogen-associated molecular patterns (PAMPs) to initiate phagocytosis (68), besides the abovementioned receptors, other cell surface molecules (receptors) especially the common PRRs identified on professional phagocytes, such as Toll-like receptors (TLRs),

TABLE 1 | Studies of phagocytic B cells in teleost fish from 2006 until now.

Time	Species	B-cell subsets	Phagocytic ability	Microbicidal ability	Antigen-presenting ability	References
2006	*Oncorhynchus mykiss*	IgM^+	YES	YES	NA	(7)
	Ictalurus punctatus	IgM^+	YES	YES	NA	
2010	*Oncorhynchus mykiss*	IgM^+ and IgT^+	YES	YES	NA	(41)
	Salmo salar L.	IgM^+	YES	NA	NA	(43)
	Gadus morhua L.	IgM^+	YES	NA	NA	(43)
2013	*Danio rerio*	IgM^+	Little	Little	NA	(44)
2014	*Danio rerio*	IgM^+	YES	YES	YES	(45)
2015	*Cyclopterus lumpus* L.	IgM^+	YES	NA	NA	(46)
2016	*Oncorhynchus mykiss*	IgM^+	YES	NA	YES	(47)
2017	*Oncorhynchus mykiss*	IgM^+	YES	YES	NA	(48)
	Oncorhynchus mykiss	IgM^+	YES	NA	YES	(49)
	Oncorhynchus mykiss	IgM^+ and IgT^+	YES	YES	NA	(50)
	Oncorhynchus mykiss	IgM^+	YES	NA	NA	(51)
	Cynoglossus semilaevis	IgM^+	YES	NA	NA	(52)
2018	*Scophthalmus maximus*	IgM^+	YSE	NA	NA	(53)
	Paralichthys olivaceus	IgM^+	YES	YES	NA	(54)
	Oncorhynchus mykiss	IgM^+	NA	NA	YES	(55)
2019	*Oreochromis niloticus*	IgM^{lo} and IgM^{hi}	YES	YES	NA	(56)
	Oncorhynchus mykiss	IgM^+	YES	YES	YES	(57)
	Oncorhynchus mykiss	IgM^+	YES	YES	YES	(58)
	Paralichthys olivaceus	IgM^+	YES	YES	NA	(59)
	Paralichthys olivaceus	IgM^+	YES	YES	YES	(60)
	Larimichthys crocea	IgM^+	YES	NA	NA	(61)

"NA" indicates no data; "YES" indicates that the cells have the function; "Little" indicates there is little phagocytosis of B cells.

Retinoic acid-inducible gene (RIG)-I-like receptors (RLRs), NOD-like receptors (NLRs), and C-type lectin receptors (CLRs), may also be involved in B-cell phagocytosis (69). Thus, far, few studies of PRRs are available in relation to the phagocytosis of teleost B cells.

TLRs, a family of single, non-catalytic, membrane-spanning PRRs, are responsible for pathogen sensing by recognizing specific PAMPs and then activating signaling cascades to trigger innate immunity (70). In rainbow trout, multiple TLR genes were analyzed in IgM^+ B cells, which suggested an important role for B cells in triggering the innate immune function (71). Particularly, a CpG oligodeoxynucleotides (ODN)-mediated TLR9 ligation has been described for the up-regulation effect on phagocytic capacities of splenic IgM^+ B cells in Atlantic salmon and rainbow trout (57, 72). In addition, RLRs, NLRs, and CLRs have been identified in teleost fish with similar antiviral or antibacterial immune functions as in mammals (73–78); however, there is not yet any direct evidence to show their regulatory effects on teleost B-cell phagocytosis (**Figure 1**).

FISH CYTOKINES MODULATING B-CELL PHAGOCYTOSIS

Cytokines are produced by various immune cells, including professional phagocytes, and can be classified as interleukins, chemokines, interferons, tumor necrosis factors (TNFs), and growth factors on the basis of their structure and function (79). To date, all of the major cytokine families existing in mammals have been found in teleost fish, and they play important roles in regulating hematopoiesis, inflammation, and adaptive immunity (80). Numerous investigations have been carried out in an attempt to elucidate the regulation mechanisms of fish cytokines in both innate and adaptive immune responses; here, we only review the regulating roles of certain cytokines in the phagocytosis of teleost B cells (**Figure 1**).

Interleukins are intercellular cytokines, and, to date, the regulatory mechanisms of interleukin-6 and−10 (IL-6 and IL-10) in the phagocytic activity of teleost IgM^+ B cells have been recognized (47, 59). Studies have indicated that IL-6 has no effect on the phagocytic activity of rainbow trout IgM^+ B cells (47), whereas IL-10 could enhance the phagocytosis of IgM^+ B cells in flounder (59). Moreover, IL-10R and STAT3 have been found to be involved in the regulation of IL-10-stimulated phagocytosis (59). The positive effect of IL-2 on phagocytosis has been explored in myeloid-origin cells in rainbow trout; however, a divergent effect was observed on PBL lymphoid cells, even though its effect on B lymphocytes was not separately investigated (81). Other interleukins have been cloned and characterized in teleost fish, but the effects on teleost B-cell phagocytosis have not yet been explored (18).

Chemokines consist of a superfamily of small proteins (8–10 kDa) that are involved in a variety of immune and inflammatory

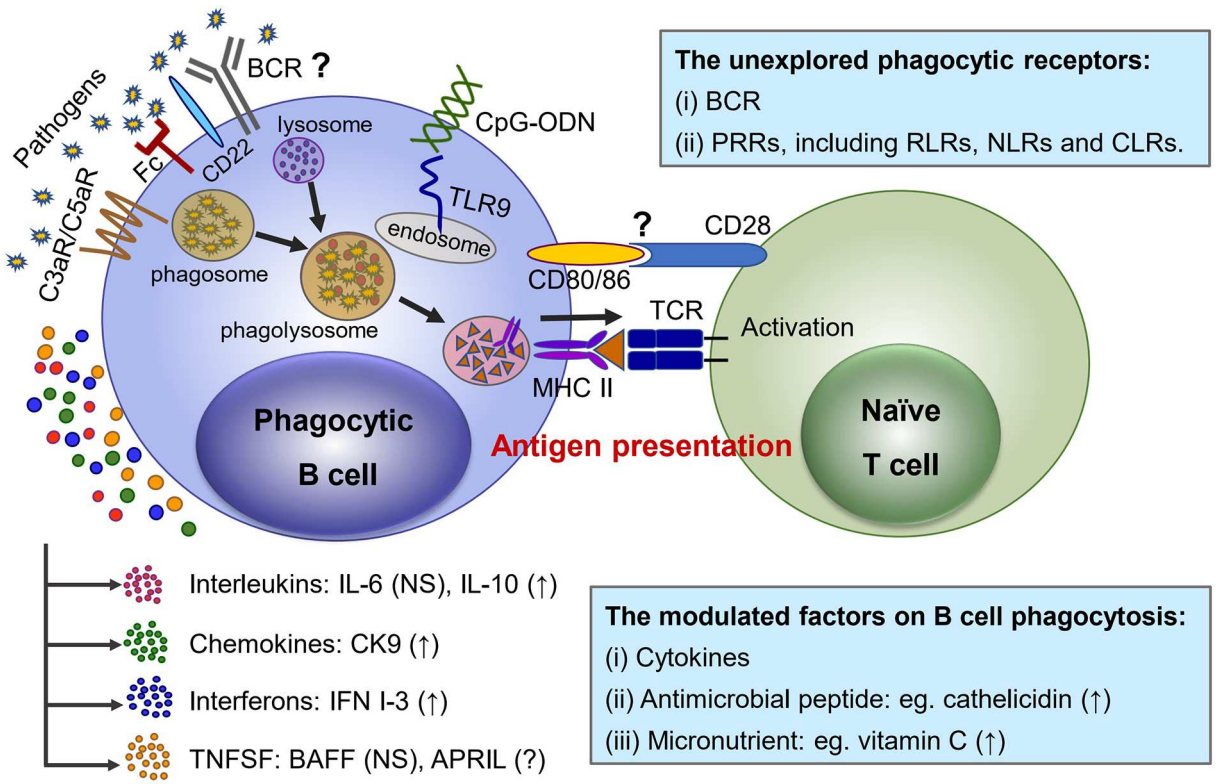

FIGURE 1 | Phagocytic receptors and modulating factors functioning in the phagocytosis as well as the antigen-presenting effect to naïve T cells in teleost phagocytic B cells. (1) Fc, C3a, and C5a receptors presenting at the surface of teleost B cells are involved in phagocytosis. CD22 plays regulatory roles in the micropinocytosis-dependent pathway to internalize large particles by turbot and Japanese flounder IgM^+ B cells, but the contribution of BCR remains to be further studied. The PRRs recognize a wide variety of PAMPs to initiate phagocytosis, and TLR9 ligation is mediated by CpG ODN, resulting in the phagocytic capacities of splenic IgM^+ B cells being up-regulated. Other PRRs, including RLRs, NLRs, and CLRs, remain to be explored. (2) Some cytokines are involved in the phagocytosis regulation of teleost B cells; specifically, IL-10, CK9, and IFN I-3 up-regulate phagocytosis, while IL-6 and BAFF have no significant effect. Other factors, such as antimicrobial peptide (cathelicidin) or micronutrients (vitamin C), have been proved to have an up-regulation function on teleost B-cell phagocytosis. (3) Pathogens (such as bacteria and viruses) are recognized by teleost B cells and engulfed into a vesicle as phagosome, with subsequent formation of maturated phagolysosome with a lysosome. The phagocytic B cells digest the internalized contents into component parts and proceed to antigen presentation with MHC II, which activates naïve T cells. However, no direct evidence has yet clarified how CD80/86 interact with CD28 in naïve T cells when B cells proceed to antigen presentation. "?" means as yet unknown; "NS" indicates no significant effect; "↑" means up-regulation.

responses. In general, they act primarily as chemoattractants and activators for recruiting specific types of leukocytes (82). CK9, a CC chemokine in rainbow trout (resembling mammalian CCL25), has been shown to have a strong chemotactic capacity and to up-regulate phagocytic capacity for both IgM^+ B cells and macrophages (83). Though many chemokines have been identified in rainbow trout, functional study of B-cell phagocytosis is still limited. For example, for CK11, its antimicrobial activity rather than its phagocytic activity has been recovered (84).

Interferons (IFNs) are a group of proteins that are made and released by host cells in response to intracellular pathogens (such as viruses, bacteria, or parasites) (85). A recent study indicated that type I interferon-3 (IFN I-3) significantly enhanced phagocytosis of IgM^+ B cells for *Lactococcus lactis* and *Edwardsiella tarda* (60). However, no other interferons have been explored for their roles in the phagocytosis of teleost B cells.

The TNF ligand superfamily (TNFSF) represents a multifunctional proinflammatory cytokine that activates signaling pathways for cell survival, apoptosis, inflammatory responses, and cellular differentiation (86). More recently, B cell-activating factor (BAFF), a proliferation-inducing ligand (APRIL), and BAFF-APRIL-like molecule (BALM), as well as the BAFF receptor (BAFF-R) and other related molecules, were identified in rainbow trout (49, 55, 87, 88). However, a recent study indicated that BAFF did not alter the phagocytic activity of IgM^+ B cells (49). In regard to APRIL or BALM, their function in B-cell phagocytosis in teleosts remains to be further investigated.

Interestingly, cathelicidin, a kind of antimicrobial peptide, was found to be able to significantly facilitate the phagocytic, intracellular bactericidal, and reactive oxygen species activities in trout IgM^+ and IgT^+ B cells (50), a phenomenon that has been well-characterized previously in macrophages.

These findings provide new evidence in support of the close relationship between B cells and macrophages in vertebrates. Additionally, vitamin C, an essential micronutrient, has also been reported to significantly increase the phagocytosis activity of teleost IgM^+ B cells from head kidney when pre-incubated, while co-incubation has no obvious effect (51). Although Vitamin C does not affect cytokine expression (including IL-1β, IL-8, COX-2B, TNF-α, cathelicidin 2, and hepcidin) of head kidney leukocytes, the impact on IgM^+ B cells remains unknown. Whether vitamin C acts via modulating the transcriptome of cytokines to regulate IgM^+ B-cell phagocytic activity, like cathelicidin, which improves the phagocytosis of IgM^+ B cells (50), needs to be explored further.

INVOLVEMENT OF PHAGOCYTIC B CELLS IN ANTIGEN PRESENTATION

Phagocytosis not only provides a critical first line of defense against invading pathogens but is also a very efficient mechanism for antigen presentation in order to link innate with adaptive immune processes. Professional phagocytes (macrophages and dendritic cells) and B cells have long been recognized in higher vertebrates as professional APCs that provide antigenic ligands to activate T cells (22). Among them, professional phagocytes are generally characterized as having high efficiency in ingesting and destroying internalized pathogens, followed by effective presentation of antigens to both $CD4^+$ and $CD8^+$ T cells (2, 4), whereas B cells mainly process soluble antigens and are restricted to loading antigens onto MHC II and eventually presenting antigens to $CD4^+$ T cells (89). Currently, phagocytosis and bactericidal abilities have been identified in teleost B cells as well as in mammalian B1-B cells (7, 10–12), and the next to be expected is that a previously unrecognized function of presenting internalized particulate antigens to elicit T cells will be revealed. It was first demonstrated in mammals that the phagocytic B1-B cells derived from the murine peritoneal cavity, liver, or spleen have the ability to present antigen to $CD4^+$ T cells, which indicated that B1-B cells are a kind of APC and are able not only to present soluble antigens but also to effectively present ingested large particulate antigens (**Figure 1**) (10–12, 67). Similarly, the phagocytic IgM^+ B cells in zebrafish have also been proved to act as pivotal initiating APCs (similar to dendritic cells) that prime adaptive immunity when presenting both soluble antigens and bacterial particles to prime naïve $CD4^+$ T cell proliferation, which was mediated by MHC II and costimulatory molecules (CD80/CD86 and CD83) (45). In addition, indirect evidence of significant up-regulation of antigen-presenting-capacity related genes, including MHC II, as well as CD83 and CD80/86, in phagocytic IgM^+ B cells have been described in a number of teleost species in response to various pathogenic bacteria or viruses, which indicates that teleost IgM^+ cells act as APCs during the course of a pathogenic infection (56, 90, 91). However, the ability of phagocytic B cells to cross-present particulate antigens to $CD8^+$ T cells is unknown and needs to be investigated in the future in both mammals and teleost fish.

In addition, it needs to be pointed out that the strikingly high number of B cells in teleost fish blood combined with their significantly high phagocytic and intracellular killing abilities implies that fish phagocytic B cells may play more important roles in effective antigen presentation than mammalian B cells (7, 12).

B-CELL DIFFERENTIATION AND PHAGOCYTIC CAPACITY

Apart from the different B-cell subsets, which variously express IgM, IgD, or IgT/Z, in teleost fish, attention has also been paid to the phagocytic activity of teleost B cells at different developmental and differentiation stages (44, 92). Unlike for mammals, there are no specific antibodies available to distinguish teleost B cells precisely on their developmental/differentiation status, which hinders further exploration of the effects on their phagocytic function. However, examining the expression levels of B-cell-specific transcription factors can provide a comparative approach for studying teleost B-cell development (93). Thus, far, Paired box-5 (Pax5), Early B cell Factor-1 (EBF1), B lymphocyte-induced protein-1 (Blimp1), and X-box protein I (XbpI) have been identified in rainbow trout and applied to differentiate resting B cells, activated B cells, plasmablasts, and plasma cells (94–96). Pax5 is expressed from pre-B cells to mature B cells, while Blimp1 is a master regulator of terminal B cells by down-regulating the expression of Pax5 and leading to the maturation of plasmablasts to plasma cells (92). Significantly higher expressions of Pax5 and Blimp1 have been demonstrated in resting IgM^+ B cells than in IgM^- cells (71, 97, 98). However, Pax5 is usually suppressed by its repressor, Blimp1, in activating B cells, leading to shifts in the expression of immunoglobulin from membrane to secreted forms (99). In rainbow trout, the IgM^+ B cells from the peritoneal cavity have been proposed to be classifiable as IgM^{hi} or IgM^{lo} B cells on the basis of membrane IgM (mIgM) concentration, respectively (92). Moreover, they can also be distinguished as either a naïve B-cell subset or an antibody-secreting subset depending on the expression levels of Pax5 and Blimp1 genes (58). Similarly, in our recent study, IgM^{hi} and IgM^{lo} B cells, which resemble naïve/mature B cells and plasma-like cells, respectively, have also been described in the peripheral blood of Nile tilapia (*Oreochromis niloticus*) (56, 100). We demonstrated that B-cell differentiation may cause a decrease in phagocytic capacity but not in phagocytic ability of phagocytic IgM^+ B cells in Nile tilapia (56). Moreover, MHC II expression was significantly higher in the phagocytic IgM^{hi} B cells than in the IgM^{lo} B cells, implying that a variable antigen-presentation capacity exists in IgM^+ B cells under different differentiation status (56). The change in the phagocytic activity in teleost B cells following the differentiation process seems in line with the shift in their specialized function of secreting antibody in humoral immunity. It is well known that mammalian B2-B cells comprise the major portion of peripheral blood B cells and are specialized as antibody-secreting B cells; whether similar functional B-cell subsets exist in teleost fish remains to be investigated.

CONCLUDING REMARKS AND PROSPECTIVE DIRECTIONS

Phagocytosis is the first line of defense of the immune system to eliminate most invading pathogenic microorganisms and is an essential part of tissue homeostasis and remodeling, which offers protective defense to bodies. Phagocytic B cells are capable of taking up distinct microbial pathogens by interacting with different receptors through related regulatory pathways, subsequently presenting the antigen to prime naïve T cells, and finally initiating B cell differentiation to secret specific antibodies. Comparative studies on such phagocytic activity of B cells from different species have also dug deeper to understand their origin and the evolutionary and functional relationships of mammalian B cells and macrophages. However, current studies also raise concerns that may be addressed by future prospective studies on teleost phagocytic B cells, such as: (1) whether there are any different receptors required by phagocytic B cells as opposed to professional phagocytes (macrophages, neutrophils, and dendritic cells) in responding to different microorganisms (species, and/or virulence); (2) whether any different regulating mechanisms and pathways are involved in the phagocytic and antigen-presenting process in B cells as opposed to the professional phagocytes; (3) how the phagocytic B cells modulate and deal with differently sized, specific and non-specific, particulate and soluble antigens with/without BCR to generate the specificity of the finally produced antibodies? Further investigations to address the above concerns will not only provide new insights into the immune defense regulations of phagocytic B cells in teleost fish but will also enable a better understanding of the evolution and origin of the mammalian immune system. Particularly, it is of great interest to explore teleost phagocytic B cells and their regulatory mechanisms so as to facilitate the development of novel and more effective strategies to prevent infectious diseases in the aquaculture industry.

AUTHOR CONTRIBUTIONS

JL, LW, and ZQ wrote the manuscript. LL, HL, and JY contributed with suggestions, discussions, and critical reading of the manuscript. JY and JL designed the contents of this paper.

FUNDING

This study was supported by the National Natural Science Foundation of China (31972818, 31528019). JL was partially supported by the Taishan Scholarship and Pearl River Scholarship from Shandong Province and Guangdong Province, respectively.

REFERENCES

1. Parra D, Takizawa F, Sunyer JO. Evolution of B cell immunity. *Annu Rev Anim Biosci.* (2013) 1:65–97. doi: 10.1146/annurev-animal-031412-103651
2. Stuart LM, Ezekowitz RA. Phagocytosis: elegant complexity. *Immunity*. (2005) 22:539–50. doi: 10.1016/j.immuni.2005.05.002
3. Tauber AI. Metchnikoff and the phagocytosis theory. *Nat Rev Mol Cell Biol.* (2003) 4:897–901. doi: 10.1038/nrm1244
4. Watts C, Amigorena S. Phagocytosis and antigen presentation. *Semin Immunol*. (2001) 13:373–9. doi: 10.1006/smim.2001.0334
5. Rabinovitch M. Professional and non-professional phagocytes: an introduction. *Trends Cell Biol*. (1995) 5:85–7. doi: 10.1016/S0962-8924(00)88955-2
6. Borrello MA, Phipps RP. The B/macrophage cell: an elusive link between CD5(+) B lymphocytes and macrophages. *Immunol Today*. (1996) 17:471–5.
7. Li J, Barreda DR, Zhang Y, Boshra H, Gelman AE, LaPatra S, et al. B lymphocytes from early vertebrates have potent phagocytic and microbicidal abilities. *Nat Immunol*. (2006) 7:1116–24. doi: 10.1038/ni1389
8. Zimmerman LM, Vogel LA, Edwards KA, Bowden RM. Phagocytic B cells in a reptile. *Biol Lett*. (2010) 6:270–3. doi: 10.1098/rsbl.2009.0692
9. Eckl-Dorna J and Batista FD: BCR-mediated uptake of antigen linked to TLR9 ligand stimulates B-cell proliferation and antigen-specific plasma cell formation. *Blood*. (2009) 113:3969–77. doi: 10.1182/blood-2008-10-185421
10. Gao J, Ma X, Gu W, Fu M, An J, Xing Y, et al. Novel functions of murine B1 cells: Active phagocytic and microbicidal abilities. *Eur J Immunol*. (2012) 42:982–92. doi: 10.1002/eji.201141519
11. Nakashima M, Kinoshita M, Nakashima H, Habu Y, Miyazaki H, Shono S, et al. Pivotal advance: characterization of mouse liver phagocytic B cells in innate immunity. *J Leukocyte Biol*. (2012) 91:537–46. doi: 10.1189/jlb.0411214
12. Parra D, Rieger AM, Li J, Zhang Y, Randall LM, Hunter CA, et al. Pivotal advance: peritoneal cavity B-1 B cells have phagocytic and microbicidal capacities and present phagocytosed antigen to CD4+ T cells. *J Leukocyte Biol*. (2012) 91:525–36. doi: 10.1189/jlb.0711372
13. Zhu Q, Zhang M, Shi M, Liu Y, Zhao Q, Wang W, et al. Human B cells have an active phagocytic capability and undergo immune activation upon phagocytosis of mycobacterium tuberculosis. *Immunobiology*. (2016) 221:558–67. doi: 10.1016/j.imbio.2015.12.003
14. Cancro MP. Editorial: phagocytic B cells: deja vu all over again? *J Leukocyte Biol*. (2012) 91:519–21. doi: 10.1189/jlb.1111540
15. Zhu L, Shao T, Nie L, Zhu L, Xiang L, Shao J. Evolutionary implication of B-1 lineage cells from innate to adaptive immunity. *Mol Immunol*. (2016) 69:123–30. doi: 10.1016/j.molimm.2015.10.014
16. Sunyer JO. Evolutionary and functional relationships of B cells from fish and mammals: insights into their novel roles in phagocytosis and presentation of particulate antigen. *Infect Disord Drug Targets*. (2012) 12:200–12. doi: 10.2174/187152612800564419
17. Palti Y. Toll-like receptors in bony fish: From genomics to function. *Dev Comp Immunol*. (2011) 35:1263–72. doi: 10.1016/j.dci.2011.03.006
18. Secombes CJ, Wang T, Bird S. The interleukins of fish. *Dev Comp Immunol*. (2011) 35:1336–45. doi: 10.1016/j.dci.2011.05.001
19. Zhu L, Nie L, Zhu G, Xiang L, Shao J. Advances in research of fish immune-relevant genes: a comparative overview of innate and adaptive immunity in teleosts. *Dev Comp Immunol*. (2013) 39:39–62. doi: 10.1016/j.dci.2012.04.001
20. Zou J, Redmond AK, Qi Z, Dooley H, Secombes CJ. The CXC chemokine receptors of fish: insights into CXCR evolution in the vertebrates. *Gen Comp Endocrinol*. (2015) 215:117–31. doi: 10.1016/j.ygcen.2015.01.004
21. Sunyer JO. Fishing for mammalian paradigms in the teleost immune system. *Nat Immunol*. (2013) 14:320–26. doi: 10.1038/ni.2549
22. Flannagan RS, Cosio G, Grinstein S. Antimicrobial mechanisms of phagocytes and bacterial evasion strategies. *Nat Rev Microbiol*. (2009) 7:355–66. doi: 10.1038/nrmicro2128
23. Hansen JD, Landis ED, Phillips RB. Discovery of a unique Ig heavy-chain isotype (IgT) in rainbow trout: implications for a distinctive B cell developmental pathway in teleost fish. *Proc Natl Acad Sci USA*. (2005) 102:6919–24. doi: 10.1073/pnas.0500027102
24. Danilova N, Bussmann J, Jekosch K, Steiner LA. The immunoglobulin heavy-chain locus in zebrafish: identification expression of a previously

unknown isotype, immunoglobulin Z. *Nat Immunol*. (2005) 6:295–302. doi: 10.1038/ni1166
25. Wilson M, Bengten E, Miller NW, Clem LW, DuPasquier L, Warr GW. A novel chimeric Ig heavy chain from a teleost fish shares similarities to IgD. *Proc Natl Acad Sci USA*. (1997) 94:4593–7. doi: 10.1073/pnas.94.9.4593
26. Parra D, Korytar T, Takizawa F, Sunyer JO. B cells and their role in the teleost gut. *Dev Comp Immunol*. (2016) 64:150–66. doi: 10.1016/j.dci.2016.03.013
27. Bromage ES, Kaattari IM, Zwollo P, Kaattari SL. Plasmablast and plasma cell production and distribution in trout immune tissues. *J Immunol*. (2004) 173:7317–23. doi: 10.4049/jimmunol.173.12.7317
28. Zwollo P, Cole S, Bromage E, Kaattari S. B cell heterogeneity in the teleost kidney: Evidence for a maturation gradient from anterior to posterior kidney. *J Immunol*. (2005) 174:6608–16. doi: 10.4049/jimmunol.174.11.6608
29. Ye J, Bromage ES, Kaattari SL. The strength of B cell interaction with antigen determines the degree of IgM polymerization. *J Immunol*. (2010) 184:844–50. doi: 10.4049/jimmunol.0902364
30. Ye J, Kaattari IM, Kaattari SL. The differential dynamics of antibody subpopulation expression during affinity maturation in a teleost. *Fish Shellfish Immunol*. (2011) 30:372–7. doi: 10.1016/j.fsi.2010.11.013
31. Ye J, Kaattari IM, Kaattari SL. Plasmablasts and plasma cells: reconsidering teleost immune system organization. *Dev Comp Immunol*. (2011) 35:1273–81. doi: 10.1016/j.dci.2011.03.005
32. Xu Z, Parra D, Gomez D, Salinas I, Zhang Y, Jorgensen LV, et al. Teleost skin, an ancient mucosal surface that elicits gut-like immune responses. *Proc Natl Acad Sci USA*. (2013) 110:13097–102. doi: 10.1073/pnas.1304319110
33. Xu Z, Takizawa F, Parra D, Gomez D, Jorgensen LV, LaPatra SE, et al. Mucosal immunoglobulins at respiratory surfaces mark an ancient association that predates the emergence of tetrapods. *Nat Commun*. (2016) 7:10728. doi: 10.1038/ncomms10728
34. Yu Y, Kong W, Yin Y, Dong F, Huang Z, Yin G, et al. Mucosal immunoglobulins protect the olfactory organ of teleost fish against parasitic infection. *PLoS Pathog*. (2018) 14:e1007251. doi: 10.1371/journal.ppat.1007251
35. Kong W, Yu Y, Dong S, Huang Z, Ding L, Cao J, et al. Pharyngeal immunity in early vertebrates provides functional and evolutionary insight into mucosal homeostasis. *J Immunol*. (2019) 203:3054–67. doi: 10.4049/jimmunol.1900863
36. Yu Y, Kong W, Xu H, Huang Z, Zhang X, Ding L, et al. Convergent evolution of mucosal immune responses at the buccal cavity of teleost fish. *Iscience*. (2019) 19:821–35. doi: 10.1016/j.isci.2019.08.034
37. Salinas I, Zhang Y, Sunyer JO. Mucosal immunoglobulins and B cells of teleost fish. *Dev Comp Immunol*. (2011) 35:1346–65. doi: 10.1016/j.dci.2011.11.009
38. Edholm ES, Bengten E, Stafford JL, Sahoo M, Taylor EB, Miller NW, et al. Identification of two IgD(+) B cell populations in channel catfish, *Ictalurus punctatus*. *J Immunol*. (2010) 185:4082–94. doi: 10.4049/jimmunol.1000631
39. Edholm ES, Bengten E, Wilson M. Insights into the function of IgD. *Dev Comp Immunol*. (2011) 35:1309–16. doi: 10.1016/j.dci.2011.03.002
40. Ramirez-Gomez F, Greene W, Rego K, Hansen JD, Costa G, Kataria P, et al. Discovery and characterization of secretory IgD in rainbow trout: secretory IgD is produced through a novel splicing mechanism. *J Immunol*. (2012) 188:1341–9. doi: 10.4049/jimmunol.1101938
41. Zhang Y, Salinas I, Li J, Parra D, Bjork S, Xu Z, et al. IgT, a primitive immunoglobulin class specialized in mucosal immunity. *Nat Immunol*. (2010) 11:827–82. doi: 10.1038/ni.1913
42. Perdiguero P, Martin-Martin A, Benedicenti O, Diaz-Rosales P, Morel E, Munoz-Atienza E, et al. Teleost IgD(+)IgM(-) B cells mount clonally expanded and mildly mutated intestinal IgD responses in the absence of lymphoid follicles. *Cell Rep*. (2019) 29:4223–35.e4225. doi: 10.1016/j.celrep.2019.11.101
43. Overland HS, Pettersen EF, Ronneseth A, Wergeland HI. Phagocytosis by B-cells and neutrophils in Atlantic salmon (*Salmo salar* L.) and Atlantic cod (*Gadus morhua* L.). *Fish Shellfish Immunol*. (2010) 28:193–204. doi: 10.1016/j.fsi.2009.10.021
44. Page DM, Wittamer V, Bertrand JY, Lewis KL, Pratt DN, Delgado N, et al. An evolutionarily conserved program of B-cell development and activation in zebrafish. *Blood*. (2013) 122:e1-11. doi: 10.1182/blood-2012-12-471029
45. Zhu L, Lin A, Shao T, Nie L, Dong W, Xiang L, et al. B cells in teleost fish act as pivotal initiating APCs in priming adaptive immunity: an evolutionary perspective on the origin of the B-1 cell subset and B7 molecules. *J Immunol*. (2014) 192:2699–714. doi: 10.4049/jimmunol.1301312
46. Ronneseth A, Ghebretnsae DB, Wergeland HI, Haugland GT. Functional characterization of IgM(+) B cells and adaptive immunity in lumpfish (*Cyclopterus lumpus* L.). *Dev Comp Immunol*. (2015) 52:132–43. doi: 10.1016/j.dci.2015.05.010
47. Abos B, Wang T, Castro R, Granja AG, Leal E, Havixbeck J, et al. Distinct differentiation programs triggered by IL-6 and LPS in teleost IgM(+) B cells in the absence of germinal centers. *Sci Rep*. (2016) 6:30004. doi: 10.1038/srep30004
48. Castro R, Abos B, Gonzalez L, Granja AG, Tafalla C. Expansion and differentiation of IgM(+) B cells in the rainbow trout peritoneal cavity in response to different antigens. *Dev Comp Immunol*. (2017) 70:119–27. doi: 10.1016/j.dci.2017.01.012
49. Tafalla C, Gonzalez L, Castro R, Granja AG. B cell-activating factor regulates different aspects of B cell functionality and is produced by a subset of splenic B cells in teleost fish. *Front Immunol*. (2017) 8:295. doi: 10.3389/fimmu.2017.00295
50. Zhang X, Wang P, Zhang N, Chen D, Nie P, Li J, et al. B cell functions can be modulated by antimicrobial peptides in rainbow trout *Oncorhynchus mykiss*: novel insights into the innate nature of B cells in fish. *Front Immunol*. (2017) 8:388. doi: 10.3389/fimmu.2017.00388
51. Leal E, Zarza C and Tafalla C: Effect of vitamin C on innate immune responses of rainbow trout (*Oncorhynchus mykiss*) leukocytes. *Fish Shellfish Immunol*. (2017) 67:179–88. doi: 10.1016/j.fsi.2017.06.021
52. Yang S, Tang X, Sheng X, Xing J, Zhan W. Development of monoclonal antibodies against IgM of half-smooth tongue sole (*Cynoglossus semilaevis*) and analysis of phagocytosis of fluorescence microspheres by mIgM plus lymphocytes. *Fish Shellfish Immunol*. (2017) 66:280–8. doi: 10.1016/j.fsi.2017.05.019
53. Li Y, Sun L, Li J. Internalization of large particles by turbot (*Scophthalmus maximus*) IgM(+) B cells mainly depends on macropinocytosis. *Dev Comp Immunol*. (2018) 82:31–8. doi: 10.1016/j.dci.2017.12.028
54. Li Y, Sun L, Li J. Macropinocytosis-dependent endocytosis of Japanese flounder IgM(+) B cells and its regulation by CD22. *Fish Shellfish Immunol*. (2019) 84:138–47. doi: 10.1016/j.fsi.2018.09.068
55. Soleto I, Morel E, Martin D, Granja AG, Tafalla C. Regulation of IgM(+) B cell activities by rainbow trout APRIL reveals specific effects of this cytokine in lower vertebrates. *Front Immunol*. (2018) 9:1880. doi: 10.3389/fimmu.2018.01880
56. Wu L, Kong L, Yang Y, Bian X, Wu S, Li B, et al. Effects of cell differentiation on the phagocytic activities of IgM(+) B cells in a teleost fish. *Front Immunol*. (2019) 10:2225. doi: 10.3389/fimmu.2019.02225
57. Simon R, Diaz-Rosales P, Morel E, Martin D, Granja AG, Tafalla C. CpG oligodeoxynucleotides modulate innate and adaptive functions of IgM(+) B cells in rainbow trout. *Front Immunol*. (2019) 10:584. doi: 10.3389/fimmu.2019.00584
58. Granja AG, Tafalla C. Different IgM(+) B cell subpopulations residing within the peritoneal cavity of vaccinated rainbow trout are differently regulated by BAFF. *Fish Shellfish Immunol*. (2019) 85:9–17. doi: 10.1016/j.fsi.2017.10.003
59. Yang S, Tang X, Sheng X, Xing J, Zhan W. Analysis of the role of IL-10 in the phagocytosis of mIgM(+) B lymphocytes in flounder (*Paralichthys olivaceus*). *Fish Shellfish Immunol*. (2019) 92:813–20. doi: 10.1016/j.fsi.2019.06.059
60. Tang X, Yang S, Sheng X, Xing J, Zhan W. Transcriptome analysis of immune response of mIgM(+) B lymphocytes in Japanese flounder (*Paralichthys olivaceus*) to *Lactococcus lactis in vitro* revealed that IFN I-3 could enhance their phagocytosis. *Front Immunol*. (2019) 10:1622. doi: 10.3389/fimmu.2019.01622
61. Huang Y, Yuan X, Mu P, Li Q, Ao J, Chen X. Development of monoclonal antibody against IgM of large yellow croaker (*Larimichthys crocea*) and characterization of IgM(+) B cells. *Fish Shellfish Immunol*. (2019) 91:216–22. doi: 10.1016/j.fsi.2019.05.035
62. Boshra H, Li J, Peters R, Hansen J, Matlapudi A, Sunyer JO. Cloning, expression, cellular distribution, and role in chemotaxis of a C5a receptor in

rainbow trout: the first identification of a C5a receptor in a nonmammalian species. *J Immunol.* (2004) 172:4381–90. doi: 10.4049/jimmunol.172.7.4381
63. Boshra H, Wang T, Hove-Madsen L, Hansen J, Li J, Matlapudi A, et al. Characterization of a C3a receptor in rainbow trout and Xenopus: the first identification of C3a receptors in nonmammalian species. *J Immunol.* (2005) 175:2427–37. doi: 10.4049/jimmunol.175.4.2427
64. Li J, Barreda DR, Zhang Y, Boshra H, Gelman AE, LaPatra S, et al. Complement and B cell cooperation in teleost fish: Role in phagocytosis and inflammation. *Mol Immunol.* (2007) 44:205. doi: 10.1016/j.molimm.2006.07.136
65. Li J, Zhang Y, Sunyer JO. Identification of a phagocytic complement C3d receptor in rainbow trout. *J Immunol.* (2007) 178(Suppl. 1):S106.
66. Wu L, Bian X, Kong L, Yin X, Mu L, Wu S, et al. B cell receptor accessory molecule CD79 gets involved in response against *Streptococcus agalactiae* infection and BCR signaling in Nile tilapia (*Oreochromis niloticus*). *Fish Shellfish Immunol.* (2019) 87:212–19. doi: 10.1016/j.fsi.2019.01.012
67. Souwer Y, Griekspoor A, Jorritsma T, de Wit J, Janssen H, Neefjes J, et al. B cell receptor-mediated internalization of *Salmonella*: a novel pathway for autonomous B cell activation and antibody production. *J Immunol.* (2009) 182:7473–81. doi: 10.4049/jimmunol.0802831
68. Desjardins M, Houde M, Gagnon E. Phagocytosis: the convoluted way from nutrition to adaptive immunity. *Immunol Rev.* (2005) 207:158–65. doi: 10.1111/j.0105-2896.2005.00319.x
69. Takeuchi O, Akira S. Pattern recognition receptors and inflammation. *Cell.* (2010) 140:805–20. doi: 10.1016/j.cell.2010.01.022
70. Rauta PR, Samanta M, Dash HR, Nayak B, Das S. Toll-like receptors (TLRs) in aquatic animals: signaling pathways, expressions and immune responses *Immunol Lett.* (2014) 158:14–24. doi: 10.1016/j.imlet.2013.11.013
71. Abos B, Castro R, Pignatelli J, Luque A, Gonzalez L, Tafalla C. Transcriptional heterogeneity of IgM(+) cells in rainbow trout (*Oncorhynchus mykiss*) tissues. *PLoS ONE.* (2013) 8:e82737. doi: 10.1371/journal.pone.0082737
72. Jenberie S, Thim HL, Sunyer JO, Skjodt K, Jensen I, Jorgensen JB. Profiling atlantic salmon B cell populations: CpG-mediated TLR-ligation enhances IgM secretion and modulates immune gene expression. *Sci Rep.* (2018) 8:3565. doi: 10.1038/s41598-018-21895-9
73. Zhang J, Zhang Y, Wu M, Wang B, Chen C, Gui J. Fish MAVs is involved in RLR pathway-mediated IFN response. *Fish Shellfish Immunol.* (2014) 41:222–30. doi: 10.1016/j.fsi.2014.09.002
74. Wang W, Asim M, Yi L, Hegazy AM, Hu X, Zhou Y, et al. Abortive infection of snakehead fish vesiculovirus in ZF4 cells was associated with the RLRs pathway activation by viral replicative intermediates. *Int J Mol Sci.* (2015) 16:6235–50. doi: 10.3390/ijms16036235
75. Nie L, Xu X, Xiang L, Shao J and Chen J: Mutual regulation of NOD2 and RIG-I in zebrafish provides insights into the coordination between innate antibacterial and antiviral signaling pathways. *Int J Mol Sci.* (2017) 18:1147. doi: 10.3390/ijms18061147
76. Motta V, Soares F, Sun T, Philpott DJ. Nod-like receptors: versatile cytosolic sentinels. *Physiol Rev.* (2015) 95:149–78. doi: 10.1152/physrev.00009.2014
77. Zou P, Chang M, Li Y, Xue N, Li J, Chen S, et al. NOD2 in zebrafish functions in antibacterial also antiviral responses via NF-kappa B, also MDA5, RIG-I MAVS. *Fish Shellfish Immunol.* (2016) 55:173–85. doi: 10.1016/j.fsi.2016.05.031
78. Bi D, Wang Y, Gao Y, Li X, Chu Q, Cui J, et al. Recognition of lipopolysaccharide and activation of NF-kappaB by cytosolic sensor NOD1 in teleost fish. *Front Immunol.* (2018) 9:1413. doi: 10.3389/fimmu.2018.01413
79. Bixler SL, Goff AJ. The role of cytokines and chemokines in filovirus infection. *Viruses-Basel.* (2015) 7:5489–507. doi: 10.3390/v7102892
80. Zou J, Secombes CJ. The function of fish cytokines. *Biology.* (2016) 5:23. doi: 10.3390/biology5020023
81. Wang T, Hu Y, Wangkahart E, Liu F, Wang A, Zahran E, et al. Interleukin (IL)-2 is a key regulator of T helper 1 and T helper 2 cytokine expression in fish: Functional characterization of two divergent IL2 paralogs in salmonids. *Front Immunol.* (2018) 9:1638. doi: 10.3389/fimmu.2018.01683
82. Alejo A, Tafalla C. Chemokines in teleost fish species. *Dev Comp Immunol.* (2011) 35:1215–22. doi: 10.1016/j.dci.2011.03.011
83. Aquilino C, Granja AG, Castro R, Wang T, Abos B, Parra D, et al. Rainbow trout CK9, a CCL25-like ancient chemokine that attracts and regulates B cells and macrophages, the main antigen presenting cells in fish. *Oncotarget.* (2016) 7:17547–64. doi: 10.18632/oncotarget.8163
84. Munoz-Atienza E, Aquilino C, Syahputra K, Al-Jubury A, Araujo C, Skov J, et al. CK11, a teleost chemokine with a potent antimicrobial activity. *J Immunol.* (2019) 202:857–70. doi: 10.4049/jimmunol.1800568
85. Zou J, Secombes CJ. Teleost fish interferons and their role in immunity. *Dev Comp Immunol.* (2011) 35:1376–87. doi: 10.1016/j.dci.2011.07.001
86. Tafalla C, Granja AG. Novel insights on the regulation of B cell functionality by members of the tumor necrosis factor superfamily in jawed fish. *Front Immunol.* (2018) 9:1285. doi: 10.3389/fimmu.2018.01285
87. Granja AG, Holland JW, Pignatelli J, Secombes CJ, Tafalla C. Characterization of BAFF and APRIL subfamily receptors in rainbow trout (*Oncorhynchus mykiss*). Potential role of the BAFF / APRIL axis in the pathogenesis of proliferative kidney disease. *PLoS ONE.* (2017) 12:e0174249. doi: 10.1371/journal.pone.0174249
88. Soleto I, Abos B, Castro R, Gonzalez L, Tafalla C, Granja AG. The BAFF / APRIL axis plays an important role in virus-induced peritoneal responses in rainbow trout. *Fish Shellfish Immunol.* (2017) 64:210–17. doi: 10.1016/j.fsi.2017.03.023
89. Wilson AB: MHC and adaptive immunity in teleost fishes. *Immunogenetics.* (2017) 69:521–8. doi: 10.1007/s00251-017-1009-3
90. Diaz-Rosales P, Munoz-Atienza E, Tafalla C. Role of teleost B cells in viral immunity. *Fish Shellfish Immunol.* (2019) 86:135–42. doi: 10.1016/j.fsi.2018.11.039
91. Abos B, Castro R, Gonzalez Granja A, Havixbeck JJ, Barreda DR, Tafalla C. Early activation of teleost B cells in response to rhabdovirus infection. *J Virol.* (2015) 89:1768–80. doi: 10.1128/JVI.03080-14
92. Zwollo P. Dissecting teleost B cell differentiation using transcription factors. *Dev Comp Immunol.* (2011) 35:898–905. doi: 10.1016/j.dci.2011.01.009
93. Northrup DL, Allman D. Transcriptional regulation of early B cell development. *Immunol Res.* (2008) 42:106–17. doi: 10.1007/s12026-008-8043-z
94. Barr M, Mott K, Zwollo P. Defining terminally differentiating B cell populations in rainbow trout immune tissues using the transcription factor XbpI. *Fish Shellfish Immunol.* (2011) 31:727–35. doi: 10.1016/j.fsi.2011.06.018
95. Zwollo P, Haines A, Rosato P, Gumulak-Smith J. Molecular and cellular analysis of B-cell populations in the rainbow trout using Pax5 and immunoglobulin markers. *Dev Comp Immunol.* (2008) 32:1482–496. doi: 10.1016/j.dci.2008.06.008
96. Zwollo P, Ray JC, Sestito M, Kiernan E, Wiens GD, Kaattari S, et al. B cell signatures of BCWD-resistant and susceptible lines of rainbow trout: a shift towards more EBF-expressing progenitors and fewer mature B cells in resistant animals. *Dev Comp Immunol.* (2015) 48:1–12. doi: 10.1016/j.dci.2014.07.018
97. Wu L, Gao A, Kong L, Wu S, Yang Y, Bian X, et al. Molecular characterization and transcriptional expression of a B cell transcription factor Pax5 in Nile tilapia (*Oreochromis niloticus*). *Fish Shellfish Immunol.* (2019) 90:165–72. doi: 10.1016/j.fsi.2019.04.059
98. Wu L, Zhou E, Gao A, Kong L, Wu S, Bian X, et al. Blimp-1 is involved in B cell activation and maturation in Nile tilapia (*Oreochromis niloticus*). *Dev Comp Immunol.* (2019) 98:137–47. doi: 10.1016/j.dci.2019.05.002
99. Kallies A, Nutt SL. Terminal differentiation of lymphocytes depends on Blimp-1. *Curr Opin Immunol.* (2007) 19:156–62. doi: 10.1016/j.coi.2007.01.003
100. Wu L, Yang Y, Kong L, Bian X, Guo Z, Fu S, et al. Comparative transcriptome analysis of the transcriptional heterogeneity in different IgM(+) cell subsets from peripheral blood of Nile tilapia (*Oreochromis niloticus*). *Fish Shellfish Immunol.* (2019) 93:612–22. doi: 10.1016/j.fsi.2019.08.023

Conflict of Interest: The authors declare that the research was conducted in the absence of any commercial or financial relationships that could be construed as a potential conflict of interest.

frontiers in Immunology

REVIEW
published: 05 June 2020
doi: 10.3389/fimmu.2020.01094

The Diverse Roles of Phagocytes During Bacterial and Fungal Infections and Sterile Inflammation: Lessons From Zebrafish

*Tanja Linnerz and Christopher J. Hall**

Department of Molecular Medicine and Pathology, Faculty of Medical and Health Sciences, University of Auckland, Auckland, New Zealand

The immediate and natural reaction to both infectious challenges and sterile insults (wounds, tissue trauma or crystal deposition) is an acute inflammatory response. This inflammatory response is mediated by activation of the innate immune system largely comprising professional phagocytes (neutrophils and macrophages). Zebrafish (*danio rerio*) larvae possess many advantages as a model organism, including their genetic tractability and highly conserved innate immune system. Exploiting these attributes and the live imaging potential of optically transparent zebrafish larvae has greatly contributed to our understanding of how neutrophils and macrophages orchestrate the initiation and resolution phases of inflammatory responses. Numerous bacterial and fungal infection models have been successfully established using zebrafish as an animal model and studies investigating neutrophil and macrophage behavior to sterile insults have also provided unique insights. In this review we highlight how examining the larval zebrafish response to specific bacterial and fungal pathogens has uncovered cellular and molecular mechanisms behind a variety of phagocyte responses, from those that protect the host to those that are detrimental. We also describe how modeling sterile inflammation in larval zebrafish has provided an opportunity to dissect signaling pathways that control the recruitment, and fate, of phagocytes at inflammatory sites. Finally, we briefly discuss some current limitations, and opportunities to improve, the zebrafish model system for studying phagocyte biology.

Keywords: zebrafish, phagocytes, macrophages, neutrophils, infection, sterile inflammation, innate immunity

OPEN ACCESS

Edited by:
Xinjiang Lu,
Ningbo University, China

Reviewed by:
Annemarie H. Meijer,
Leiden University, Netherlands
Robert T. Wheeler,
University of Maine, United States

****Correspondence:***
Christopher J. Hall
c.hall@auckland.ac.nz

Specialty section:
This article was submitted to Comparative Immunology, a section of the journal Frontiers in Immunology

Received: *23 February 2020*
Accepted: *06 May 2020*
Published: *05 June 2020*

Citation:
Linnerz T and Hall CJ (2020) The Diverse Roles of Phagocytes During Bacterial and Fungal Infections and Sterile Inflammation: Lessons From Zebrafish. Front. Immunol. 11:1094. doi: 10.3389/fimmu.2020.01094

INTRODUCTION

The zebrafish (*danio rerio*) is a well-established model organism used to study a variety of biological and pathological processes. These studies range from developmental biology, genetics (1), cancer (2, 3), neurobiological diseases/neurodegeneration (4), cardiovascular diseases (5), to metabolic (6) and infectious diseases (7–9). Zebrafish embryos and larvae offer unique properties, as they are externally fertilized, thus allowing easy access to the developing embryo throughout its rapid life cycle. Moreover, adult zebrafish can generate a large number of offspring on a weekly basis, and the larvae are optically transparent, a physical trait that can be exploited using transgenic reporter lines for non-invasive live imaging. With respect to live imaging immune responses, transgenic lines that label different types of phagocytes (**Table 1**), enable the observation of the inflammatory response to

TABLE 1 | Examples of transgenic lines routinely used to visualize phagocytes in larval zebrafish.

	Transgenic line(s)	Experimental use	References
Myeloid-progenitors	*Tg(spi1:EGFP)*^{pA301}	Cell labeling (whole cell)	(10)
	Tg(zpu.1:EGFP)^{df5}		(11)
Neutrophils	*Tg(mpx:EGFP)*^{i114}	Cell labeling (whole cell)	(12)
	Tg(zMPO:GFP)		(13)
	Tg(mpx:Dendra2)	Cell tracking (photoconversion)	(14)
	Tg(mpx:Gal4)^{j222}*;UAS-E1b:Kaede)*^{s1999t}		(15)
	Tg(lyz:GAL4.VP16)^{j252}*; (UAS-E1b:Kaede)*^{s1999t}		(16)
	Tg(mpx:EGFPCAAX)^{gl27}	Cell labeling (cell membrane)	(17)
	Tg(lyz:EGFP)^{nz115}*; Tg(lyz:DsRED2)*^{nz50}	Cell labeling (whole cell)	(18)
Macrophages	*Tg(mpeg1:EGFP)*^{gl22}	Cell labeling (whole cell)	(19)
	Tg(mpeg1:mCherry)^{gl23}		
	Tg(mpeg1: mCherryCAAX)^{sh378}	Cell labeling (cell membrane)	(20)
	Tg(mpeg1: mCherry-F)^{ump2}	Cell labeling (cell membrane)	(21)
	Tg(mpeg1:Dendra2)	Cell tracking (photoconversion)	(14)
	Tg(csf1ra:GFP)^{sh377}	Cell labeling (whole cell)	(22)
	Tg(mpeg1:tdTomato-CAAX)^{xt3}	Cell labeling (cell membrane)	(23)
	Tg(mfap4:mTurquoise2)^{xt27}	Cell labeling (whole cell)	(24)
	Tg(mfap4:tdTomato)^{xt12}		
	Tg(mfap4:tdTomato-CAAX)^{xt6}	Cell labeling (cell membrane)	
	Tg(mfap4:dLanYFP:CAAX)^{xt11}		
Eosinophils	*Tg(gata2*^{high}*:eGFP)*	Cell labeling (whole cell)	(25)

injuries and infections in a living animal. Furthermore, the concurrent use of fluorescently-labeled pathogens in infection studies allows the real-time observation of host-pathogen interactions *in vivo*. Besides the imaging potential and genetic amenability, the zebrafish model offers the capacity for high-throughput drug screening to facilitate antimicrobial discovery and in-depth studies of virulence factors.

Another major advantage lies in the fact that the human and zebrafish genomes share high homology and the immune system is highly conserved. Even though the developmental origin of the zebrafish immune system differs to some extent from their mammalian counterparts, all major relevant immune cell types have been described in the fish including phagocytic myeloid cells of the innate immune system (26, 27). The innate immune system provides the first line of defense against invading pathogens and is comprised of physical barriers, biochemical effector molecules such as complement factors, antimicrobial peptides, cytokines (chemokines, interferons, and interleukins) and phagocytes. A major effector function of the complement system is to opsonize pathogens and to recruit professional phagocytic cells, such as macrophages and neutrophils (28).

Macrophages and neutrophils are highly migratory cells, which are both capable of phagocytosis and subsequent killing of pathogens. Phagocytosis plays a central role in the defense against invading pathogens and in tissue inflammation and the successive process of healing, where macrophages and neutrophils remove cell debris and restore tissue homeostasis (29, 30). Besides the recognition of opsonins, phagocytosis can also be triggered by the direct binding of pathogen-associated molecular patterns (PAMPs) to pattern recognition receptors (PRRs) on macrophages and neutrophils (29, 30). Once pathogens are internalized, they reside in an intracellular vacuole, the phagosome, which further matures to the phagolysosome where effective killing mechanisms are initiated (31). Additionally, membrane-bound or intracellular-residing Toll-like receptors (TLRs), which belong to the group of PRRs, contribute to the effective recognition of pathogens and the activation of phagocytes (32). The activation of TLRs activates downstream signaling pathways such as nuclear factor kappa-light-chain-enhancer of activated B cells NF-κB, which results in the production and release of pro-inflammatory cytokines by professional phagocytes (33). Transgenic zebrafish reporter lines have been generated utilizing NF-κB recognition sequences and promoters of immune-response genes (including pro-inflammatory cytokines) enabling the differentiation of neutrophil and macrophage activation states (**Table 2**). These lines have been instrumental in beginning to reveal that the functional heterogeneity of larval zebrafish phagocytes is similar to that of their mammalian counterparts (42).

The roles of neutrophils and macrophages are often complementary to each other during inflammatory responses, however, the kinetics of their recruitment can be variable, depending on the source of the insult. Neutrophils are usually the first responders after tissue injury and invasion of pathogens, except if patrolling tissue-resident macrophages encounter the microbes first (43). Regardless of the source of the insult, the second professional phagocyte population is commonly recruited shortly thereafter. Both phagocytes react to tissue damage and infection primarily by phagocytosis of foreign particles or tissue debris. Whereas, neutrophils have a higher

TABLE 2 | Examples of transgenic lines routinely used to visualize and differentiate phagocyte activation states.

Activation marker	Transgenic line(s)	Expression confirmed in	References
il1b expression	*TgBAC(il1b:egfp)*^{sh445}	Neutrophils and macrophages	(34)
	Tg(il1b:EGFP-F)^{ump3}	Neutrophils and macrophages	(35)
	TgBAC(il1b:NTR-EGFP)^{tyt205}	Defined as myeloid cells*	(36)
irg1 expression	*Tg(irg1:EGFP)*^{nz26}	Macrophages only	(37)
nfkb expression	*Tg(Nf-kB:EGFP)*^{nc1}	Macrophages	(38, 39)
	Tg(8xHs.NFκB:GFP,Luciferase)^{hdb5}	Defined as immune cells*	(40)
tnfa expression	*TgBAC(tnfa:GFP)*^{pd1028}	Macrophages	(41)
	Tg(tnfa:eGFP-F)^{ump5}	Macrophages	(42)

**Yet to be confirmed as neutrophils or macrophages.*

TABLE 3 | Examples of transgenic lines routinely used to manipulate phagocyte numbers.

Cell type ablated	Transgenic line(s)	References
Macrophages	*Tg(mpeg1:Gal4FF*^{gl25}*;UAS-E1b:nfsB-mCherry*^{c264}*)*	(19, 48)
	Tg(cfms:Gal4.VP16)^{jl86}*;UAS:nfsB.mCherry)*^{j149}	(49)
Neutrophils	*Tg(lyz:ntr-p2A-LanYFP)*^{xt14}	(23)
	Tg(-8.mpx:KalTA4 ^{gl28}*; UAS-E1b:nfsB-mCherry)*^{c264}	(50)

microbicidal activity through degranulation, the production of reactive oxygen species (ROS), and are capable of neutrophil extracellular trap formation (44, 45); macrophages destroy pathogens and debris intracellularly in the phagolysosome for antigen-presentation, and additionally release cytotoxic factors and initiate chemokine and cytokine production (31, 46). All of the described pathways and the downstream components related to the innate immune response against pathogens or injuries are remarkably conserved between zebrafish and mammals. One interesting property of the zebrafish larval immune system is that the adaptive arm of the immune system takes ∼3–4 weeks to develop (47). This creates the exclusive opportunity to study the innate response without interference of adaptive immunity in the early embryonic and larval stages. Furthermore, pharmacologic and genetic techniques exist to specifically deplete phagocyte subsets in larval zebrafish, including the use of liposomal clodronate for macrophage ablation (21) and transgenic lines for nitroreductase-mediated ablation of neutrophils or macrophages (**Table 3**). Using these ablation techniques, the specific contribution of neutrophils and macrophages to inflammatory responses can be dissected.

Over the last 20 years, the zebrafish has evolved as a model organism for many infectious diseases, including bacterial [reviewed in Neely (7)], fungal [reviewed in Rosowski et al., (9)], viral [reviewed in Varela et al., (8)] and parasitic infections (51). Here we focus on studies examining the phagocyte responses to specific bacterial and fungal infections that have revealed fundamental insights into a spectrum of phagocyte responses, from those that are host protective to those that are detrimental. We also discuss how modeling sterile inflammation in larval zebrafish has enabled a deeper understanding of the signaling systems that regulate the directed movement of phagocytes druing inflammation.

PHAGOCYTE RESPONSES DURING BACTERIAL AND FUNGAL INFECTION

There is a constant need to study infectious diseases and develop novel treatment strategies, especially in the context of growing antibiotic resistance, nosocomial infections, superinfections, and (re-)emerging new pathogens. In many cases, patients rely on a proper innate immune response as a first line of defense, particularly immunocompromised patients. This qualifies the zebrafish as a suitable model due to temporal segregation in the development of innate and adaptive immunity. In addition, infectious challenges can be readily delivered to different anatomical sites within larval zebrafish depending on the microorganism being used and the particular innate immune cell response under investigation (**Figure 1A**). Many significant studies have utilized the zebrafish model to further our understanding of the host response to important viral [reviewed in Varela et al., (8)] and parasitic infections (51). For the purpose of this review, we have chosen to focus on examples of bacterial and fungal infections that illustrate the heterogenous nature of phagocyte responses. These include host protective phagocyte functions and those that are detrimental, such as facilitating the dissemination of infection or promoting tissue damage.

Bacterial Infections

Modeling bacterial infections in zebrafish has contributed significantly to our understanding of the early innate immune response toward numerous bacterial infections in humans [reviewed in Neely (7)]. Professional phagocytes play an essential role in limiting bacterial growth and eradicating infection. However, bacteria have evolved different strategies to delay or avoid efficient killing mechanisms in phagocytes. In the following section, we focus on the zebrafish response to *Mycobacterium marinum* (*M. marinum*), as well as studies using *Mycobacterium leprae* (*M. leprae*), *Burkholderia cenocepacia* (*B. cenocepacia*), and

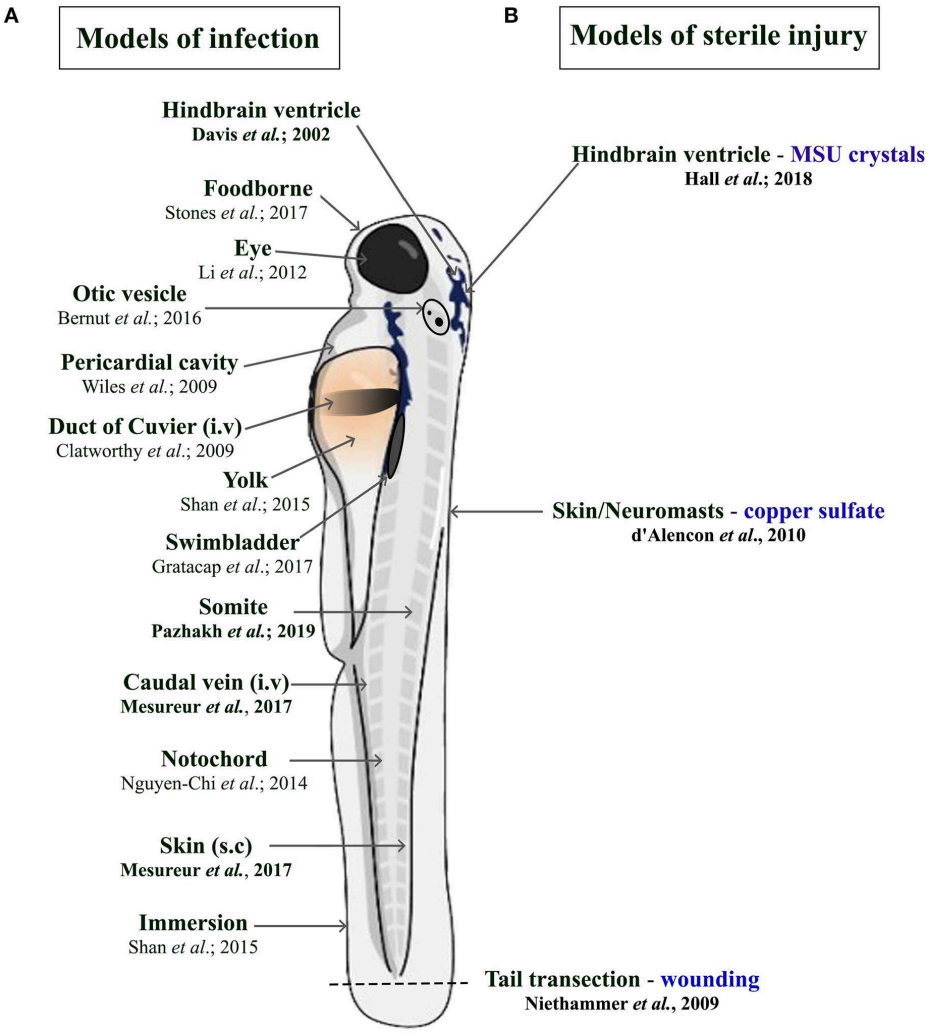

FIGURE 1 | Schematic illustration of the different delivery routes in larval zebrafish for pathogens. (**A**, left side) and to model sterile inflammation (**B**, right side). In the sterile injury section, the stimulus is specified by blue writing. All delivery routes show an exemplary reference, with the ones covered in this review highlighted in bold.

Staphylococcus aureus (*S. aureus*) that show different ways in which the phagocyte response can be host protective or harmful.

The Macrophage Response to *Mycobacterium marinum* Is Largely Host Protective

A classic example of how phagocytes, particularly macrophages, provide a host protective function has been shown in the tuberculosis-like zebrafish disease model using the closely related natural fish pathogen *M. marinum*. Tuberculosis, which is caused by *Mycobacterium tuberculosis* (*M. tuberculosis*), is a persistent major health threat worldwide and remains astonishingly successful in infecting millions of people every year (52). Long-existing conventional views on human tuberculosis pathogenesis have been challenged in the last decade using the closely related pathogen *M. marinum*, to model a tuberculosis-like disease in zebrafish.

Granulomas are clinical hallmark features of tuberculosis and are highly organized structures consisting of infected macrophages at their cores surrounded by lymphocytes, necrotic cell debris (the caseum) and a fibrotic cell layer (53). The granuloma has been generally viewed as a compact barrier and static structure, which restricts bacterial growth and thereby limits their spread (54, 55). Elegant studies in *M. marinum*-infected larval zebrafish have revealed that early granuloma-like structures can form independent of an adaptive immune response, where mycobacteria are predominantly engulfed by macrophages. This initiates the expansion of the granuloma-like structure through the recruitment of uninfected macrophages (56, 57). The recruitment of macrophages is thereby dependent on the bacterial secreted protein ESAT6 (encoded by the RD1 virulence locus) that drives *matrix metallopeptidase 9* expression in epithelial cells neighboring infected macrophages (58, 59). Infected macrophages then quickly undergo cell death and are

engulfed by newly arriving uninfected macrophages resulting in accelerated *M. marinum* proliferation and cellular expansion of the granuloma (60). Tracking of individual macrophage responses has also revealed that some infected macrophages leave the granuloma to disseminate the infection by establishing secondary granulomas (60). A more recent study has also shown that when macrophage supply becomes limiting there is a transition from a granuloma that supports mycobacterial growth within macrophages to one favoring macrophage necrosis and the discharge of mycobacteria into the extracellular granuloma milieu (61).

Studies in zebrafish have also revealed several cues that contribute to the onset of macrophage necrosis, including alterations in levels of the pro-inflammatory cytokine tumor necrosis factor (TNF). Transient knockdown experiments using Morpholinos against the TNF-receptor were able to dissect the pleiotropic role of TNF during *M. marinum* pathogenesis (62). In this study, decreased TNF levels induced a hypo-inflammatory state accompanied by augmented mycobacterial growth and accelerated granuloma formation, which ultimately led to enhanced necrosis of macrophages, granuloma breakdown and extracellular proliferation of *M. marinum* (62). Surprisingly, a similar outcome was achieved when excessive TNF levels were present (63). While co-injected recombinant TNF in *M. marinum*-infected zebrafish larvae initially reduced mycobacterial burden, macrophages underwent necroptosis (programmed necrosis) induced by a RIPK1-RIPK3-dependent mechanism, which in turn enhanced mitochondrial ROS production (64). Exploiting the relative ease of exposing larval zebrafish to chemical inhibitors, it was shown that two pathways cooperate to induce this ROS-dependent macrophage necrosis via an inter-organellar circuit (65). Initially, mitochondrial ROS activates ceramide production via the lysosomal enzyme acid sphingomyelinase (aSM). Ceramide, in turn, activates the cytosolic protein BAX, which promotes calcium flow through ryanodine receptors (RyR) from the endoplasmatic reticulum back into the mitochondria. The influx of calcium overloads the macrophage mitochondria, ultimately leading to the activation of the mitochondrial matrix protein cyclophilin D, which induces necrosis (65). This TNF-mediated necrosis mechanism was shown to be conserved for *M. marinum* and *M. tuberculosis*-infected human macrophages (65). The detailed molecular dissection of these TNF-responsive pathways offers a wide array of potential new druggable targets, which have already been applied and validated in the zebrafish tuberculosis model. Promising novel treatments involve inhibitors for cyclophilin D (such as Alisporivir), aSM-blocking drugs (the tricyclic antidepressant Desipramine), calcium channel-blocking drugs (LTCC inhibitors such as Verapamil), RyR-blockers (Dantrolene), or ROS scavengers (64, 65). Many of those drugs are currently in clinical trials or have been approved for the treatment of other diseases. Besides balancing adequate TNF levels in tuberculosis progression, new potential routes for treatment could furthermore include maintaining stable macrophage numbers (61) and specifically targeting macrophages with drug-loaded nanoparticles or liposomes, such as Rifampicin, in the early course of the disease (66, 67).

The role of neutrophils in tuberculosis infection is less clear. While mammalian *in vivo* studies investigating the role of neutrophils during tuberculosis are conflicting (68, 69), zebrafish studies have shown that neutrophils appear to be less important in controlling infection. Although mycobacteria can evade direct phagocytosis by larval zebrafish neutrophils, caspase-mediated cell death of infected macrophages within the granuloma attracts neutrophils, which phagocytose dying macrophages. After this indirect uptake of mycobacteria, neutrophils can directly kill the bacteria by NADPH oxidase-mediated ROS production (70). Even though neutrophils do not appear to be essential to control tuberculosis infection, higher bacterial burdens in later stages of infection have been shown to be accompanied by neutropenia (71). Moreover, forced production of reactive nitrogen species in neutrophils through manipulation of hypoxia-inducible factor 1 (Hif-1α) signaling prior to mycobacteria infection, can induce protection in the host (72). Manipulating either mycobacterial neutrophil evasion strategies or the HIF-1 pathway offer interesting new routes for potential therapeutic interventions. Collectively, these studies investigating the larval zebrafish innate immune response to *M. marinum* have greatly enhanced our understanding of *M. tuberculosis* pathogenesis (**Figure 2A**) and uncovered new mechanistic insights that may allow for the development of promising new treatments.

The Macrophage Response to *Mycobacterium leprae* and *Burkholderia cenocepacia* Damages the Host

A close relative to *M. marinum* and *M. tuberculosis* is *M. leprae*, a non-motile bacterium that causes leprosy in humans. This bacterium grows at 30°C, which makes it difficult to study in mammalian animal models adequately. However, it renders the poikilothermic zebrafish an excellent model organism, which develops clinical symptoms comparable to the human disease (73). A distinct feature of *M. leprae* infection is a widespread demyelinating neuropathy, which manifests as a disorganization and decompaction of myelin sheaths and subsequent axonal damage (74). As with other Mycobacteria species, initial infection and replication occurs in macrophages. Surprisingly, the neurological disease is not directly caused by the pathogen *per se*, but by patrolling infected macrophages. This was demonstrated using a combination of confocal and transmission electron microscopy techniques in larval zebrafish (73). Macrophages were shown to interact with an *M. leprae*-specific component of the outer cell membrane, a triglycosylated phenolic glycolipid 1 (PGL-1), which led to inducible nitric oxide synthase (iNOS)-driven production of neurotoxic nitric oxide. This macrophage source of reactive nitrogen species then caused mitochondrial damage in adjacent axons (**Figure 2B**). There are currently two hypotheses for how infected macrophages can reach the nerves: one possibility is through an overlying skin lesion that allows for direct seeding of macrophages from a granuloma into a nearby peripheral nerve (75). The second suggests that infected macrophages, which are not enclosed in a granulomatous structure, extravasate from the blood vessels, to patrol axons, similar to their behavior under homeostatic conditions (73, 76).

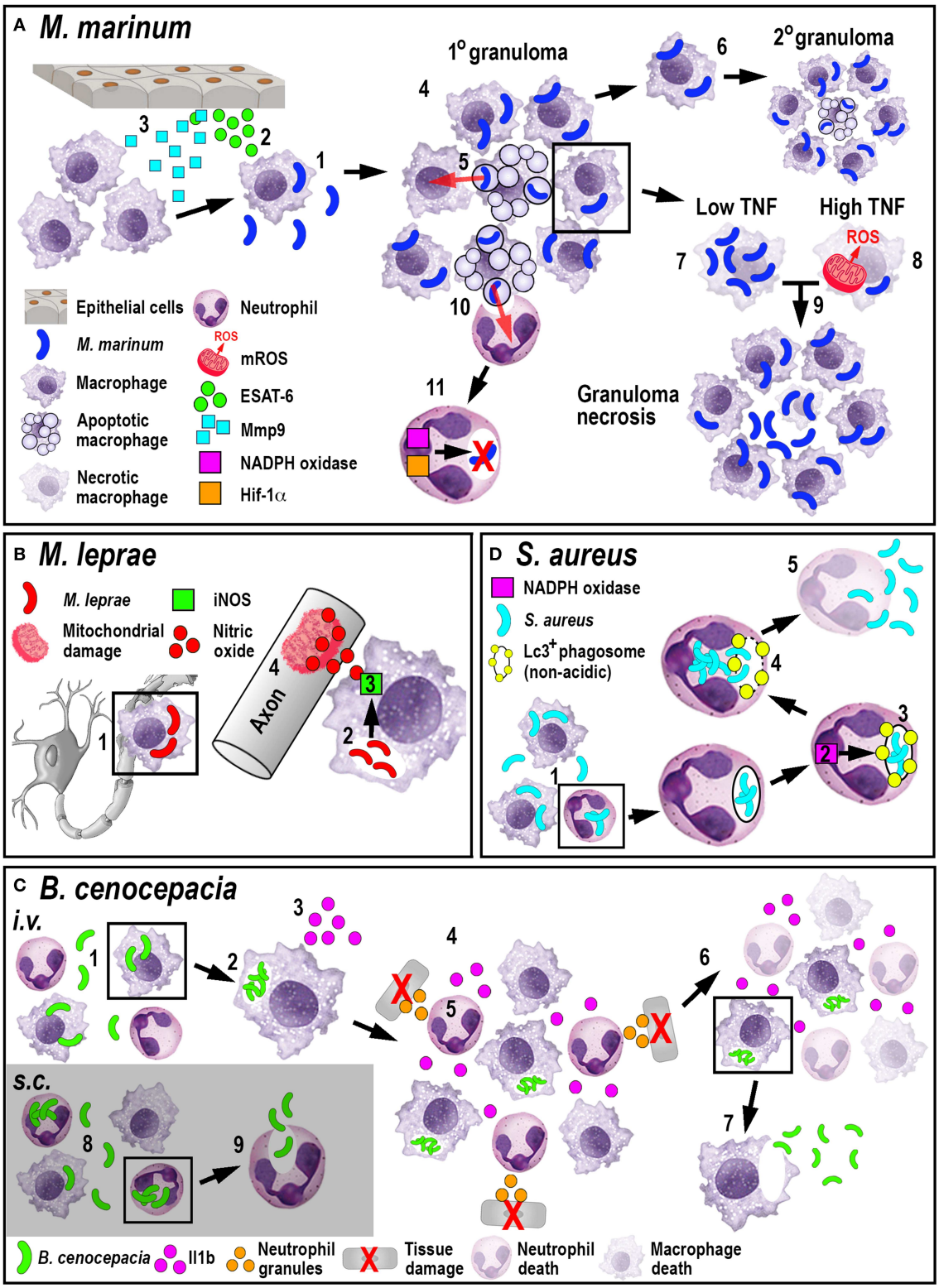

FIGURE 2 | Schematic illustration of the phagocyte responses to the bacterial pathogens *M. marinum* **(A)**, *M. leprae* **(B)**, *B. cenocepacia* **(C),** and *S. aureus* **(D)**. **(A)** Macrophages phagocytose *M. marinum* (1) and release ESAT-6 (2). ESAT-6-driven Mmp9 production by epithelial cells leads to macrophage recruitment (3) and granuloma formation (4). Newly-arriving macrophages become infected by engulfing dying infected macrophages (5). Infected macrophages can establish secondary

(Continued)

FIGURE 2 | granulomas (6). Low TNF levels promote intracellular bacterial growth and macrophage necrosis (7). High TNF levels promote mROS production within infected macrophages that, although initially bactericidal, also leads to necrosis (8). Necrosis results in the release of bacteria into the extracellular milieu (9). Neutrophils can phagocytose infected macrophage debris (10) and kill *M. marinum* by NADPH oxidase-mediated ROS production and Hif-1α-dependent reactive nitrogen species production (11). **(B)** *M. leprae*-infected macrophages migrate along nerve axons (1), where PGL-1 (2) stimulates iNOS-driven nitric oxide production in macrophages (3) that damages mitochondria in adjacent axons (4). **(C)** Following *i.v.* delivery, macrophages phagocytose *B. cenocepacia* (1) providing a replication niche (2). Infected macrophages produce Il1b (3) that attracts neutrophils and macrophages (4), leading to tissue damage resulting from degranulating neutrophils (5). The inflammatory response also leads to myeloid cell ablation that favors the survival of infected macrophages (6). *B. cenocepacia* can disseminate through non-lytic escape from infected macrophages (7). Following *s.c.* infection, neutrophils phagocytose *B. cenocepacia* (8) but are inefficient in killing the bacteria and instead release the bacteria into the extracellular milieu (9). **(D)** Following phagocytosis of *S. aureus* by neutrophils (1), NADPH oxidase activity (2) contributes to the formation of non-acidic Lc3-positive phagosomes (3) that provide a replication niche. Phagosome membrane damage results in the release of bacteria into the cytosol (4), neutrophil death and bacterial dissemination (5).

The latter hypothesis would support how leprosy manifests as such a widespread neuropathy in comparison to other mycobacterial diseases.

Similar to *M. leprae* infection, the macrophage response to another opportunistic pathogen *B. cenocepacia* can be detrimental to the host. *B. cenocepacia* belongs to the *Burkholderia cepacia complex* (*Bcc*) and can emerge as an opportunistic pathogen, particularly in cystic fibrosis patients and immunocompromised individuals (77). *B. cenocepacia* is extremely virulent in the zebrafish model, and macrophages were shown to be vital for initial infection and replication (78). Depending on the infection route, intravenously (*i.v.*) or subcutaneously (*s.c.*), live imaging experiments within infected larvae revealed that phagocytes engaged with *B. cenocepacia* in different ways. If *B. cenocepacia* was administered *i.v.*, neutrophils and macrophages were both recruited to the infection site. However, only few bacteria were phagocytosed by neutrophils triggering degranulation that resulted in tissue damage and increased bacterial burden. Following *s.c.* infection, neutrophils predominantly phagocytosed *B. cenocepacia* but failed to kill the bacteria. Instead infected neutrophils adopted a circular morphology and ejected the bacteria back into the extracellular space, suggesting non-lytic exocytosis or a NET-based mechanism that was unable to destroy *B. cenocepacia* effectively (79).

In contrast, macrophages predominantly phagocytosed bacteria following *i.v.* delivery and engaged with *B. cenocepacia* at later stages following *s.c.* infection. Regardless of the administration route, *B. cenocepacia* failed to efficiently replicate within macrophage-depleted hosts, resulting in enhanced survival (79). This effect on survival was partially dependent on macrophage-derived Il1b, which induced both host-protective and fatal pro-inflammatory consequences. Additionally, expression analysis showed a global downregulation of the macrophage- and neutrophil-marking genes *mpeg1* and *mpx* after infection, suggesting systemic myeloid cell death through massive inflammation, bestowing a survival advantage specifically to infected macrophages through an unknown mechanism. After intracellular replication in macrophages, *B. cenocepacia* was shown to utilize a non-lytic escape mechanism to infect neighboring cells after leaving the macrophage vacuole, which resulted in a systemic and fatal infection (78). *B. cenocepacia* infection provides an excellent example of how phagocytes demonstrate diverse responses during infections (**Figure 2C**), where macrophages exacerbate disease outcome instead of protecting the host.

Neutrophils Provide an Intraphagocytic Niche for *Staphylococcus aureus*

S. aureus is a gram-positive opportunistic pathogen, usually residing on the skin and in nasal cavities of healthy carriers. In immunocompromised individuals, especially in hospitals, *S. aureus* is one of the leading causes of fatal bacteremia/sepsis, skin infections, pneumonia, endocarditis, and osteomyelitis (80). Another serious complication is the growing emergence of antibiotic-resistant strains, such as the methicillin-resistant (MRSA), and vancomycin-resistant (VRSA) *S. aureus* strains, which additionally complicate effective and life-saving treatments. The control of systemic *S. aureus* infection in larval zebrafish was strongly dependent on phagocytes, as neutrophil and macrophage ablation caused exponential growth of GFP-tagged *S. aureus* in the circulation and rapid death of infected larvae (81). Chemical ablation of either neutrophils or macrophages revealed that both cell populations were indispensable for controlling infection, however, macrophages seemed to be more important for this process as they predominantly phagocytosed the bacteria (82). Furthermore, *S. aureus* uses neutrophils as an intraphagocytic niche for host immune evasion (82, 83). Once *S. aureus* is phagocytosed by neutrophils, the bacteria utilize the host autophagy machinery to successfully evade intracellular killing mechanisms. After internalization, the neutrophil-intrinsic NADPH oxidase prompts Lc3-associated phagosome formation, which contains the bacteria and provides a protective niche as these phagosomes do not acidify. *S. aureus* subsequently damage the Lc3-associated phagosomal membrane, resulting in bacterial proliferation and dissemination (**Figure 2D**) (83).

This host immune evasion strategy is particularly important in the context of mixed-strain infections, where a drug-resistant mutant can be present in a bacteria population. It had been demonstrated in previous experiments that the injection of an equal ratio of two differentially labeled *S. aureus* strains, resulted in one of the injected strains dominating the infected larvae, despite identical initial proliferation (82). This preferential expansion was the result of a few individual bacteria that exclusively survived within neutrophils (82, 83). Furthermore, this behavior correlates with antibiotic resistance. It has been demonstrated that if multiple *S. aureus* strains were present in a host with differential antibiotic resistances (drug-resistant vs. drug-sensitive), the drug-resistant strain predominated even if only sub-curative amounts of the antibiotic were present (84). This effect was not observed in phagocyte-depleted larvae, suggesting that drug-resistant *S. aureus* strains are

more likely to use the autophagy-mediated immune evasion strategy. Understanding the diverse mechanisms through which phagocytes engage with pathogens and how different bacteria can avoid or exploit host innate immune responses, promises to reveal new anti-microbial strategies that are of clinical need in the age of increasing antibiotic resistance.

Fungal Infections

Modeling fungal infections in zebrafish has gained increasing attention within the last decade. Two significant reasons have contributed to this popularity. Firstly, many fungal pathogens prefer lower incubation temperatures (33°C), which resemble the lungs, outer limbs and skin temperature of humans (85), which is easily practicable with zebrafish embryos. Secondly, zebrafish embryos and larvae resemble late-stage HIV-infected patients, as they do not possess a functional adaptive immune system, rendering this model ideal to study opportunistic fungi (86). Comprehensive reviews describing the modeling of different fungal infections in larval zebrafish have previously been covered elsewhere (9, 87, 88). Here we highlight studies exploring the host response to three specific fungal pathogens (*Aspergillus fumigatus* (*A. fumigatus*), *Talaromyces marneffei* (*T. marneffei*), and *Cryptococcus neoformans* (*C. neoformans*) that encompass a range of phagocyte responses, from providing protective niches against host immunity to mediating inter-phagocyte fungal transfer and fungal dissemination.

Macrophages Can Protect Fungal Pathogens From Neutrophil-Mediated Killing

Spores of *A. fumigatus*, an environmental fungus, are inhaled on a daily basis but can cause invasive or pulmonary aspergillosis in immunocompromised individuals (89). Once the dormant spores (conidia) are taken up by a host, a developmental switch to filamentous, invasive hyphae occurs, a process called germination (89). Fungal germination is considered a key event in pathogenesis because neutrophils respond to the hyphal form with the initiation of highly efficient killing mechanisms intracellularly (ROS/RNS and Mpx-dependent) and extracellularly, such as NETosis (90–92). At this point, *A. fumigatus* infection appears contradictory: while hyphae are a necessary virulence factor, germination ultimately entails fungal clearance due to the activation of neutrophils. The role of macrophages in disease progression is less clear. While *in vitro* studies support an important role in killing conidia (93), mouse *in vivo* studies have shown contradicting results (94, 95).

A recent elegant larval zebrafish study was able to shed light on the role of macrophages in *A. fumigatus* infection (**Figure 3A**) (9). The study demonstrated that following infection, macrophages phagocytosed injected conidia (91) and formed tight clusters around the fungus (9). The observed macrophage-driven phagocyte clusters resembled "fungal" granulomas (aspergillomas) (96), which is commonly observed in other infections, such as *M. tuberculosis/M. marinum*. This recent study has revealed that the macrophage clustering creates a protective niche for the spores by inhibiting the switch to fungal germination by an unknown mechanism (9). This delay promotes the persistence of the fungus by preventing neutrophil recruitment and subsequent neutrophil-mediated killing (9). Moreover, the retardation of fungal germination allows certain fungicidal drugs, such as voriconazole, to target and kill predominantly *A. fumigatus* hyphae (97). In light of growing antifungal resistances and inexplicable treatment failures, the larval zebrafish *A. fumigatus* infection model provides an ideal platform for studying drug efficacy and their mechanistic impact on aspergillosis (97). Once the infection progressed further, fungal germination occasionally occured in the late phagosome causing subsequent macrophage necroptosis (98). In some instances, lateral cell-cell transfer from dying to naïve-recipient macrophages was observed using high-resolution confocal microscopy of fluorescently-labeled macrophages and *A. fumigatus*, a process called metaforosis, which further restricted germination of the fungus (99). Elucidating the dichotomous role of macrophages in creating a protective niche for *A. fumigatus,* while simultaneously promoting control of germination (9, 99), may create new avenues for therapeutic strategies.

Another fungal pathogen that uses macrophages as a protective niche to prevent neutrophil-mediated killing is *T. marneffei* (**Figure 3B**). *T. marneffei* (formerly classified as Penicillium) infects predominantly HIV and AIDS patients in southeast Asia and can result in a lethal systemic infection (talaromycosis) (100). This fungus primarily infects macrophages, which has also been demonstrated in the zebrafish infection model using different routes of infection. Even though neutrophils interacted and phagocytosed conidia, the spores were preferentially taken up by macrophages (17). *T. marneffei* is thermally dimorphic, which means it exists as filamentous conidia at moderate temperatures (in the environment) and switches to a more pathogenic yeast form at 37°C (inside the host). Interestingly, once macrophages phagocytosed the conidia in the ectothermic zebrafish model, the transition to the yeast morphology occurred regardless of the lower incubation temperature of the host. This suggests that alternative cues can supersede the requirement for a specific temperature, such as the intracellular milieu of macrophages (17). This might also partially explain why macrophages are the preferred location for the initial infection and the proliferation of *T. marneffei* within the host. As with *A. fumigatus*, *T. marneffei* used macrophages as a protective niche to escape neutrophil-mediated killing, which is primarily achieved through the myeloperoxidase activity abundantly found in their granules.

Shuttling-a New Mechanism of Fungal Transfer Between Phagocytes

Recently, a novel mechanism of pathogen transfer between phagocytes (shuttling) has been identified in zebrafish studies using *A. fumigatus* and *T. marneffei* infections (**Figures 3A,B**) (101), which may be of therapeutic relevance in potential treatments. This transfer of pathogens has been shown to be unidirectional and exclusively from neutrophils to macrophages, while both phagocyte populations remain alive and intact, at the time of the exchange and afterwards. Thus, far, shuttling

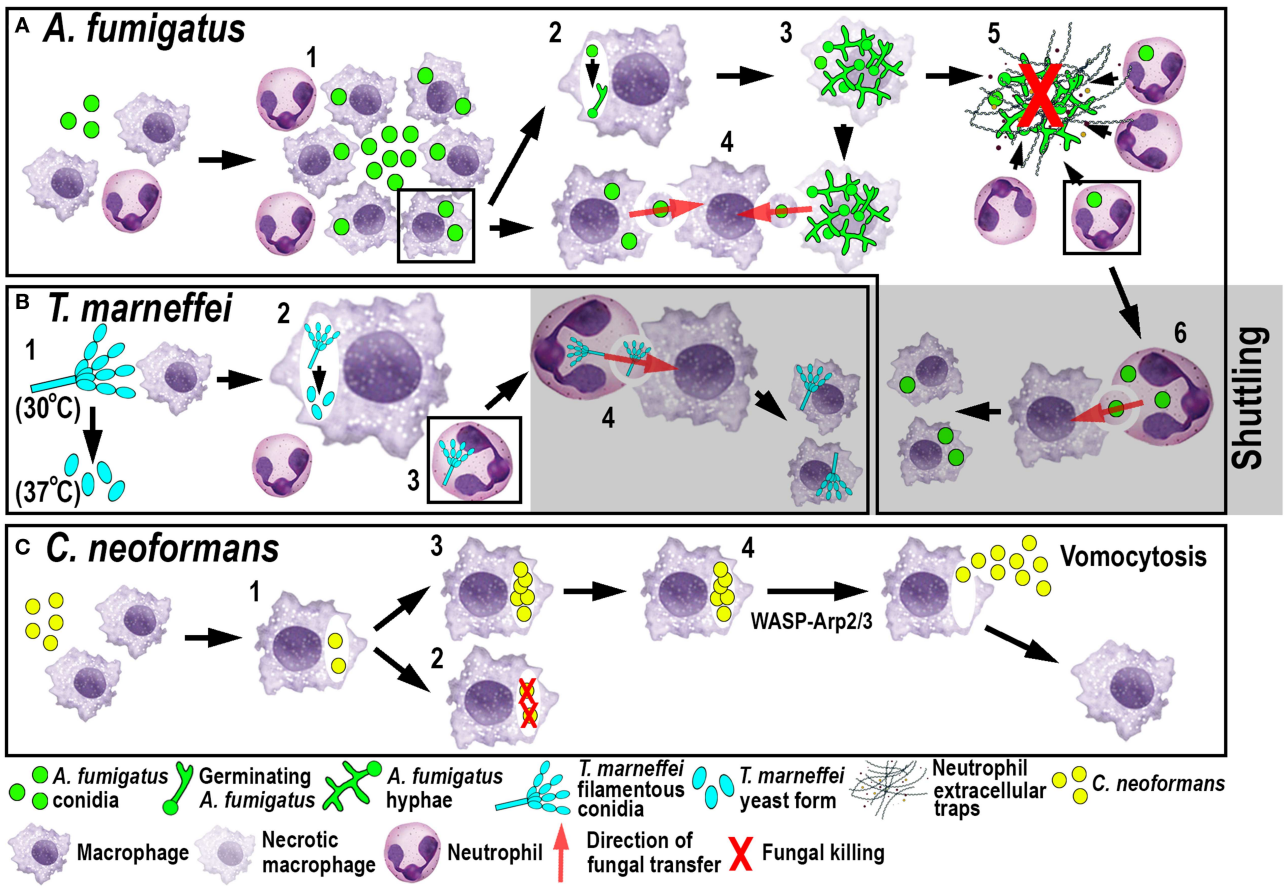

FIGURE 3 | Schematic illustration of phagocyte responses to the fungal pathogens *A. fumigatus* **(A)**, *T. marneffei* **(B)** and *C. neoformans* **(C)** in larval zebrafish. **(A)** Macrophages phagocytose *A. fumigatus* conidia and form tight clusters around the fungus, which inhibits fungal germination (1). Fungal germination can occur in the late phagosomes of infected macrophages (2) causing macrophage necroptosis (3). Transfer of *A. fumigatus* conidia can occur from infected and dying macrophages to recipient macrophages (4). Neutrophils kill *A. fumigatus* hyphae with their effector functions, including phagocytosis and NETosis (5). Infected neutrophils can transfer *A. fumigatus* to recipient macrophages through shuttling (6). **(B)** *T. marneffei* exists as filamentous conidia at 30°C and as pathogenic yeast form at 37°C (1). *T. marneffei* spores can transition to the yeast form within macrophages (2). Neutrophils can also phagocytose *T. marneffei* conidia (3) and transfer them to recipient macrophages through shuttling (4). **(C)** Macrophages phagocytose *C. neoformans* (1) where it can be killed (2) or persist and proliferate (3). WASP-Arp2/3 regulates vomocytosis and fungal dissemination (4).

was only observed within the first 4 h following infection in which single or multiple conidia were transferred to naïve or pre-loaded macrophages. This pathogen exchange mechanism happened through a direct cell-to-cell contact between donor neutrophil and recipient macrophage, which was demonstrated using sophisticated live imaging techniques with differentially labeled phagocyte populations. Phagocytosed conidia resided in a membrane-lined subcellular compartment within the neutrophil and were entirely transferred to the macrophage, suggesting not only pathogen but also phagosome exchange between the phagocytes. This shuttling mechanism was initiated by β-glucan, an integral component of the fungal cell wall. This newly discovered pathogen exchange mechanism was also conserved in isolated mouse neutrophils and macrophages (101). Macrophages recognized β-glucan and participated in shuttling partially through Dectin-1 signaling, which could only be demonstrated *in vitro*, as the zebrafish ortholog of this receptor has not yet been identified. At present, it is unclear if this phenomenon presents a host-defense strategy or a fungal escape mechanism to avoid the unfavorable neutrophil intracellular compartment and access the preferred macrophage niche (9, 17).

Dissemination of Infection by Vomocytosis

The fungus *C. neoformans*, which is also able to persist and proliferate in macrophages, uses a different phagocyte escape mechanism. *C. neoformans* is an environmentally occurring fungus and can cause life-threatening meningitis in immunocompromised patients (102). Even though the phenomenon of non-lytic exocytosis has already been observed previously following mouse and human *in vitro* studies (103), it has only recently been directly visualized for the first time in macrophages using a larval zebrafish *C. neoformans* infection model (20). This phagosome expulsion or "vomocytosis" maintains the pathogen, as well as the phagocyte, alive and intact.

Moreover, in the case of *C. neoformans*, macrophages do not serve as a protective niche but limit the dissemination of the fungus within the host. Thus, vomocytosis from macrophages into the extracellular space helps to promote fungal growth (**Figure 3C**). Moreover, *in vitro* mammalian studies showed that cryptococci-loaded phagosomes formed dynamic actin structures dependent on Wiscott-Aldrich-Syndrome-protein/actin-related protein 2/3 (WASP-Arp2/3) signaling, which were able to counteract non-lytic expulsion and could thereby provide a route for novel pharmacological intervention (103). This non-lytic escape mechanism does not appear to be limited to macrophages and has also recently been described in neutrophils *in vitro* (104). Interestingly, this resembles the observations described earlier in neutrophilic *Bcc* infections (79) suggesting that zebrafish may be a suitable model to investigate further this mechanism of exocytosis, as well as potential interventions.

PHAGOCYTE RESPONSES DURING STERILE INFLAMMATION

In addition to being vital for the host response to microbial challenges, a cellular innate immune response is also essential for tissue and wound repair. Similar to that observed during infection, the host response to such "sterile" insults is dominated by the recruitment of phagocytic cells, in particular neutrophils and macrophages. The zebrafish offers several established models of sterile inflammation, from acute injury and chemical insults to crystal injections (**Figure 1B**) (105–108). The following section describes studies that have utilized zebrafish models of sterile inflammation and uncovered mechanistic insights into how neutrophil numbers are controlled during sterile inflammation and how macrophages help orchestrate neutrophil migration.

Wound-Induced Inflammation

Tissue damage usually triggers a local inflammatory response, which is considered sterile as the host reaction originates from a non-pathogen insult. The recruitment of immune cells, in particular phagocytes, is crucial when physical barriers are compromised to eliminate infiltrating pathogens and clear cellular debris during the process of tissue healing. The timely resolution of this inflammatory response is critical for the restoration of normal tissue function and to avoid prolonged tissue damage. In many inflammatory conditions such as COPD, asthma, rheumatoid arthritis, osteoporosis and atherosclerosis (109), the resolution process is disturbed, which results in a chronic and often incurable manifestation of the disease. The classical wounding model in the zebrafish comprises of tail fin transections or incisions in larvae between 2 and 4 days of development, whereas relatively few studies have induced wounds by needle stabbing at more anterior sites (110). Paired with the use of phagocyte-labeled transgenic zebrafish lines, this model enables the visualization of immune cell behaviors during the initiation and the resolution phase of sterile inflammation. In the initiation phase, neutrophils are typically the first responders to wounding and actively migrate toward the wound following a chemotactic gradient.

An Early Role for Hydrogen Peroxide in Attracting Neutrophils

A significant contribution made to neutrophil biology by exploiting the zebrafish model was uncovering a role for hydrogen peroxide (H_2O_2) as a chemotactic signal for the earliest arriving neutrophils (105). Combining fluorescently-labeled neutrophil transgenic lines with the ability to visually measure H_2O_2 concentrations in real-time using the ratiometric sensor HyPer, a non-myeloid derived H_2O_2 gradient was discovered, for the first time, in and around wounds *in vivo* (105). This elegant study revealed that peak H_2O_2 production, generated via the dual oxidase (Duox) enzyme, was strongest at the wound margin and was necessary for recruitment of the earliest arriving neutrophils. Soon after this discovery, another study employing the zebrafish model revealed that neutrophils sensed the local gradient of H_2O_2 through activation of the Src family kinase (SFK) Lyn by oxidation of the cysteine residue C466 (111). Of significance, these findings were confirmed in mouse and human *in vitro* experiments (111). A further study focussed on understanding the transient nature of the H_2O_2 chemotactic signal. The study discovered that following arrival at the wound, neutrophils immediately begin to reduce the wound-derived H_2O_2 through the intrinsic myeloperoxidase (Mpx) enzyme that catalyzes an H_2O_2-consuming reaction to produce halides (112). This H_2O_2-driven recruitment of neutrophils (**Figure 4A**) has been validated in several *in vitro* and *in vivo* models, ranging from invertebrates to humans (111, 113, 114).

Neutrophil Retrograde Chemotaxis Helps Resolve Neutrophilic Inflammation

Once neutrophils assist with clearing DAMPs, cell debris and invading pathogens, they need to be removed in a timely fashion from the wound site to limit collateral tissue damage. The dominant theory for several decades suggested that macrophages phagocytose and eliminate apoptotic neutrophils, conferring a central role for macrophages in resolving sterile inflammation (115). Through live imaging, a zebrafish study discovered that an alternative mechanism of neutrophil migration away from the wound site (retrograde chemotaxis) also contributed to the resolution of inflammation (13). Many studies have since followed to further elucidate different mechanisms for the initiation of neutrophil retrograde migration from wound sites to the vasculature. The conserved occurrence of this mechanism has since been shown in human neutrophils (116) and mouse models (117), and appears complementary to regulated neutrophil apoptosis during inflammation resolution.

Macrophages play a major role in controlling neutrophil retrograde migration. Although they arrive slightly later than neutrophils at sites of tissue injury, macrophages also sense a chemotactic gradient through the closely related SFK Yes-related kinase Yrk (14). Once macrophages arrived at the wound, they elicited a contact-mediated guidance program toward neutrophils, which was dependent on Yrk and p22phox, an integral component of the NADPH oxidase complex (**Figure 4B**) (14). These findings demonstrated a central role for ROS-activated SFK signaling cascades that involved multiple SFK family members, especially Lyn and Yrk, in the phagocyte

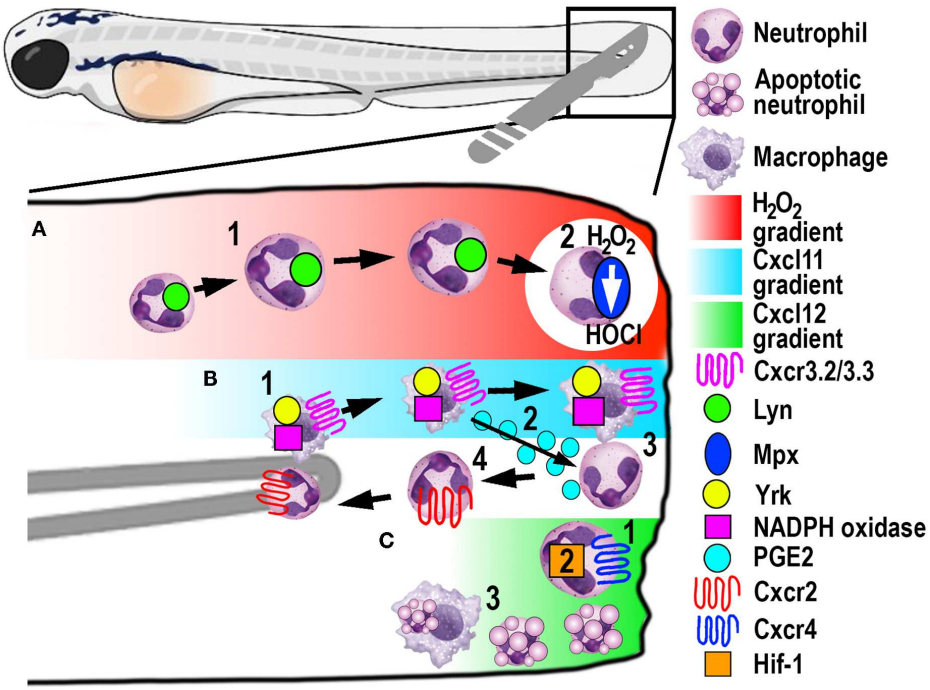

FIGURE 4 | Schematic illustration of the signaling pathways and mechanisms that help control phagocyte migration and abundance during larval zebrafish acute tail fin injury. **(A)** A gradient of H_2O_2, generated at the wound margin, is sensed by neutrophils through oxidation of Lyn, leading to directed neutrophil migration (1). Neutrophil-delivered Mpx consumes H_2O_2 producing hypochlorous acid (HOCl) (2). **(B)** Macrophage arrival at the wound site is promoted by NADPH oxidase activity and Yrk, in addition to Cxcr3.2/Cxcl11(1). In this context, Cxcr3.3 acts as a scavenger receptor to negatively regulate Cxcr3.2 function. Macrophage-delivered PGE2 promotes neutrophil retrograde chemotaxis (2) together with NADPH/Yrk-dependent contact-mediated guidance from macrophages (3). Cxcr2 signaling also contributes to initiate neutrophil retrograde chemotaxis (4). **(C)** Cxcr4/Cxcl12 signaling contributes to the retention of neutrophils at the wound site (1) along with Hif-1 activation (2). Macrophages at the wound site also remove apoptotic neutrophil debris (3).

recruitment and resolution phase of sterile inflammation, respectively (14, 111). Despite the discovery of this contact-mediated mechanism, one of the main roles of macrophages in wound healing, in addition to the clearance of cell debris, is phagocytosis of apoptotic neutrophils (**Figure 4C**). A recent study investigated in more detail the role of macrophages in restoring normal tissue homeostasis (118). Live imaging in larvae depleted of macrophages revealed the accumulation of neutrophil apoptotic bodies at the wound site, which resulted in the persistence of inflammation (118). Moreover, the same study showed the most abundant eicosanoid Prostaglandin E2 (PGE2) was produced by macrophages and was essential for the subsequent promotion of retrograde migration (**Figure 4B**), highlighting the interplay of both mechanisms for efficient resolution of inflammation (118).

Additionally, chemotaxis plays a superordinate role during inflammation resolution, as genetic depletion of chemokines or their receptors abrogated retrograde migration despite the presence of macrophages (107). Even though Cxcr2 was originally implicated in neutrophil migration toward infection, this chemokine receptor showed additional functions in the initiation of retrograde migration in tissue injury (107, 119). The chemokine receptor-ligand pair Cxcl8a (interleukin-8)/Cxcr2 proved to be crucial to orchestrate the initiation of neutrophil migration away from the wound (**Figure 4B**) (107, 119), which has also been shown in human neutrophils (107). Remarkably, another chemokine receptor-ligand pair, Cxcl12/Cxcr4, had the opposite role in this process, as activation of this signaling axis resulted in retention of neutrophils at the wound site (**Figure 4C**) (120). This work is particularly interesting in the context of chronic inflammatory diseases because samples from patients with rheumatoid arthritis or chronic inflammatory lung diseases have been shown to have increased CXCR4 expression on infiltrating neutrophils (121). Hence altered chemokine profiles and receptor expression could play crucial roles in establishing chronic diseases by retaining neutrophils at sites of sterile inflammation and inhibiting retrograde migration.

Recently, a novel chemokine axis has been implicated in the recruitment of macrophages to wounds. The Cxcr3/Cxcl11 receptor-ligand pair was shown to contribute to macrophage migration toward tail wounds using knockouts of the respective receptors in zebrafish (122). The CXCR3 receptor exists as three paralogs in zebrafish (Cxcr3.1, Cxcr3.2, and Cxcr3.3), whereby Cxcr3.2 and Cxcr3.3 antagonistically function during macrophage recruitment. As both receptors share the same ligand, Cxcr3.2 promotes macrophage migration toward the wound, whereas Cxcr3.3 negatively regulates Cxcr3.2 function by acting as a scavenger receptor for Cxcl11 (**Figure 4B**) (122).

In another zebrafish study, the involvement of hypoxia added a further signaling axis to those that regulate retrograde migration (16). Mimicking hypoxic conditions pharmacologically or genetically by manipulating Hif-1α, neutrophil apoptosis at the injury site was decreased, as was the rate of retrograde chemotaxis (**Figure 4C**) (16). Thus, hypoxia/HIF-1 activation delays the resolution of the inflammation after tissue injury and offers a pharmacologically amenable target for potential therapeutic interventions. Because this resolution mechanism includes multiple possibilities for druggable targets, it is noteworthy that neutrophils that underwent retrograde migration did not show a primed inflammatory state or have obvious functional differences to those during steady-state (123). These findings suggest that pharmacological induction of reverse migration may be an attractive new strategy for therapeutic treatments, especially in the context of chronic inflammatory conditions where excessive neutrophil recruitment and retention contribute to tissue destruction.

Chemical and Crystal-Induced Inflammation

One of the major drawbacks of the beforementioned studies involving tail fin transections is the necessity to manipulate every larva individually. This not only exacerbates, and in some instances, precludes high-throughput approaches but can additionally introduce experimental variations within, as well as between, experiments. By immersing larval zebrafish in copper sulfate, a local inflammatory response can be generated in a high-throughput fashion through inducing neuromast cell death (106). Neuromasts are mechanoreceptors that are dispersed superficially along the whole body surface and belong to the lateral line system of fish and amphibia, which senses water pressure and direction. The rapidly induced apoptosis of neuromasts lead to a local inflammatory response characterized by neutrophil and macrophage recruitment, similar to tail fin transection. This experimental setup can be coupled to a (semi-)automatic quantitative readout with transgenic lines possessing fluorescently labeled phagocytic cells to accelerate and facilitate analysis. Using this approach, a vast number of small molecules can be screened for anti-inflammatory properties at multiple steps during the inflammatory response, from the initiation to the resolution phase, depending on the time of drug administration (106).

A further example of sterile inflammation are crystallopathies, which can be caused by the inhalation of airborne micro- or nanoparticles, the endogenous self-aggregation of misfolded proteins or the supersaturation and subsequent deposition of crystals (124). During excretion of organic metabolites, serum urate levels increase, which can lead to hyperuricemia and the formation of monosodium urate (MSU) crystals. The MSU crystals accumulate in and around joints, which leads to the development of the chronic inflammatory disease, gouty arthritis (125). The MSU crystal deposition causes an acute inflammatory reaction, termed a gout flare, which is extremely painful and usually self-resolves within 1–2 weeks (126). Our group has recently developed a larval zebrafish model of gout to provide new insights into how phagocytes become activated in response to crystal-induced sterile inflammation (108). In this novel zebrafish model, MSU crystals, the causative agent in the development of gouty flares, were locally injected into the hindbrain ventricle of zebrafish larvae. The MSU crystals caused an immediate activation of tissue-resident macrophages and a subsequent inflammatory reaction, mimicking the acute gout flare in the joints of gout patients. The acute inflammatory reaction in the human condition is often connected to increased consumption of alcohol and purine-rich foods, which results in the substantial release of fatty acids (FAs) into the circulation (127). By live imaging metabolic processes [such as mitochondrial ROS (mROS) production; (128)] within macrophages during MSU-driven crystal inflammation, we were able to demonstrate that β-oxidation of FAs fueled macrophage activation through elevated mROS production (108). Moreover, this immunometabolic mechanism was conserved in human macrophages. Through performing a drug repositioning screen to identify drugs that inhibit this immunometabolic mechanism of macrophage activation, we uncovered two drugs (chrysin and piperlongumine) that effectively inhibited inflammation in an *in vivo* mouse model of acute gouty inflammation.

CONCLUDING REMARKS AND FUTURE PERSPECTIVES

In this review, we have discussed several examples of modeling infectious and sterile inflammation within larval zebrafish and how these models have been utilized to provide novel mechanistic insights into diverse phagocyte functions. These studies have revealed that the examination of phagocyte-pathogen interactions and microbial evasion strategies are greatly facilitated by the live imaging potential of transparent zebrafish larvae and the ever-expanding number of transgenic reporter lines. This direct observation potential has helped to understand how pathogens can use specific immune cells as intracellular niches or shields, in particular macrophages, and avoid phagolysosomal killing mechanisms (9, 17, 56, 57, 59, 78, 101). Furthermore, specific dissemination or escape strategies have now been successfully demonstrated or validated using zebrafish infection studies, when it was often not possible to observe or dissect such mechanisms previously in an intact animal setting. One such mechanism is non-lytic exocytosis (vomocytosis), which leaves the pathogen as well as the phagocytic cell intact and has only been observed in cell culture studies before (20, 78). Another important example is the discovery of a dissemination mechanism of fungal conidia in a process termed shuttling, where spores are leaving the unfavorable neutrophil environment and are transferred to their preferred macrophage niche (101).

In addition to live imaging, taking advantage of the genetic tractability of the zebrafish system has allowed for the examination of pathogen virulence factors and the discovery of host determinants of susceptibility or resistance toward infections. Several genetic screens for pathogenic elements

(129, 130) or relevant host genes (131) have been successfully performed in zebrafish. The latter study discovered the leukotriene A4 hydrolase (LTA4H) locus as a susceptibility determinant for *M. marinum* and *M. tuberculosis* infections in zebrafish and humans, respectively. In several successive studies, LTA4H has been shown to be ultimately responsible for TNF levels by catalyzing the final reaction in lipid mediator leukotriene B4 (LTB4) synthesis, which could either promote or inhibit TNF production in zebrafish or human tuberculosis (63–65). Analogous to the detrimental effect of imbalanced TNF levels, LTA4H deficiency or excess both resulted in hypersusceptibility toward *M. marinum* and *M. tuberculosis*, as well as increased macrophage necrosis. Importantly, the discovery of this essential genetic host factor using the zebrafish led to the discovery of a single nucleotide polymorphism in the human LTA4H promoter that was associated with phagocyte recruitment, survival and response to anti-inflammatory treatment in patients with tuberculous meningitis.

Not only is the zebrafish model a valuable tool for the initial discovery of novel mechanisms, but it also provides an excellent platform to perform chemical screens to identify drugs that actively target those pathways for therapeutic benefit. As an example, a compound screen searching for small molecules that influence neutrophil retrograde migration and apoptosis identified a drug derived from a Chinese medicinal herb, tanshinone IIA, that was able to accelerate inflammation resolution. The drug was able to simultaneously induce neutrophil apoptosis and promoted retrograde migration in larval zebrafish, an activity that was conserved when examining human neutrophils (15).

Despite the multiple advantages of the zebrafish, there are currently still certain limitations present in this animal model. For one, there is still a prominent lack of available antibodies, which not only hampers advances in zebrafish proteomics but also impedes the discovery and differentiation of phagocyte subsets. Antibody-based staining and selection techniques are routinely used in rodent and human studies, which is currently not possible to the same extent using the zebrafish model. Moreover, the lack of knowledge regarding the degree of functional heterogeneity in immune cell lineages, in particular macrophages and neutrophils, precludes certain in-depth studies on the same level as it is currently possible in mammalian models. However, the zebrafish system is offsetting these limitations with the more recent development of transgenic lines that mark activated phagocytes, which will aid in identifying distinct phagocyte subpopulations. Additionally, rapid advances in single cell RNA-sequencing technology will help to resolve the uncertainty about the functional heterogeneity of larval macrophage and neutrophil subsets and how they compare to their mammalian counterparts. With the recent and advanced CRISPR/Cas9 technology, host-pathogen interactions and tissue inflammation mechanisms can now be studied in-depth on a molecular and genetic level using cutting-edge genomic engineering techniques. Moreover, the CRISPR/Cas9 technology enables zebrafish researchers to recreate human risk alleles for inflammatory diseases using homology-directed repair mechanisms, which may assist in unraveling how such risk alleles contribute to disease.

AUTHOR CONTRIBUTIONS

TL and CH jointly wrote this manuscript.

FUNDING

This work was supported by a Project Grant awarded to CH from the Health Research Council of New Zealand (17/294).

REFERENCES

1. Santoriello C, Zon LI. Hooked! Modeling human disease in zebrafish. *J Clin Invest.* (2012) 122:2337–43. doi: 10.1172/JCI60434
2. White R, Rose K, Zon L. Zebrafish cancer: the state of the art and the path forward. *Nat Rev Cancer.* (2013) 13:624–36. doi: 10.1038/nrc3589
3. Rasighaemi P, Basheer F, Liongue C, Ward AC. Zebrafish as a model for leukemia and other hematopoietic disorders. *J Hematol Oncol.* (2015) 8:29. doi: 10.1186/s13045-015-0126-4
4. Newman M, Ebrahimie E, Lardelli M. Using the zebrafish model for Alzheimer's disease research. *Front Genet.* (2014) 5:189. doi: 10.3389/fgene.2014.00189
5. Bakkers J. Zebrafish as a model to study cardiac development and human cardiac disease. *Cardiovasc Res.* (2011) 91:279–88. doi: 10.1093/cvr/cvr098
6. Seth A, Stemple DL, Barroso I. The emerging use of zebrafish to model metabolic disease. *Dis Model Mech.* (2013) 6:1080–8. doi: 10.1242/dmm.011346
7. Neely MN. The Zebrafish as a model for human bacterial infections. *Methods Mol Biol.* (2017) 1535:245–66. doi: 10.1007/978-1-4939-6673-8_16
8. Varela M, Figueras A, Novoa B. Modeling viral infections using zebrafish: innate immune response and antiviral research. *Antiviral Res.* (2017) 139:59–68. doi: 10.1016/j.antiviral.2016.12.013
9. Rosowski EE, Knox BP, Archambault LS, Huttenlocher A, Keller NP, Wheeler RT, et al. The Zebrafish as a model host for invasive fungal infections. *J Fungi (Basel).* (2018) 4:136. doi: 10.3390/jof4040136
10. Ward AC, Mcphee DO, Condron MM, Varma S, Cody SH, Onnebo SM, et al. The zebrafish spi1 promoter drives myeloid-specific expression in stable transgenic fish. *Blood.* (2003) 102:3238–40. doi: 10.1182/blood-2003-03-0966
11. Hsu K, Traver D, Kutok JL, Hagen A, Liu TX, Paw BH, et al. The pu.1 promoter drives myeloid gene expression in zebrafish. *Blood.* (2004) 104:1291–7. doi: 10.1182/blood-2003-09-3105
12. Renshaw SA, Loynes CA, Trushell DM, Elworthy S, Ingham PW, Whyte MK. A transgenic zebrafish model of neutrophilic inflammation. *Blood.* (2006) 108:3976–8. doi: 10.1182/blood-2006-05-024075
13. Mathias JR, Perrin BJ, Liu TX, Kanki J, Look AT, Huttenlocher A. Resolution of inflammation by retrograde chemotaxis of neutrophils in transgenic zebrafish. *J Leukoc Biol.* (2006) 80:1281–8. doi: 10.1189/jlb.0506346
14. Tauzin S, Starnes TW, Becker FB, Lam PY, Huttenlocher A. Redox and Src family kinase signaling control leukocyte wound attraction and neutrophil reverse migration. *J Cell Biol.* (2014) 207:589–98. doi: 10.1083/jcb.201408090
15. Robertson AL, Holmes GR, Bojarczuk AN, Burgon J, Loynes CA, Chimen M, et al. A zebrafish compound screen reveals modulation of neutrophil reverse migration as an anti-inflammatory mechanism. *Sci Transl Med.* (2014) 6:225ra229. doi: 10.1126/scitranslmed.3007672
16. Elks PM, Van Eeden FJ, Dixon G, Wang X, Reyes-Aldasoro CC, Ingham PW, et al. Activation of hypoxia-inducible factor-1alpha (Hif-1alpha) delays inflammation resolution by reducing neutrophil apoptosis and reverse migration in a zebrafish inflammation model. *Blood.* (2011) 118:712–22. doi: 10.1182/blood-2010-12-324186

17. Ellett F, Pazhakh V, Pase L, Benard EL, Weerasinghe H, Azabdaftari D, et al. Macrophages protect Talaromyces marneffei conidia from myeloperoxidase-dependent neutrophil fungicidal activity during infection establishment in vivo. *PLoS Pathog.* (2018) 14:e1007063. doi: 10.1371/journal.ppat.1007063
18. Hall C, Flores MV, Storm T, Crosier K, Crosier P. The zebrafish lysozyme C promoter drives myeloid-specific expression in transgenic fish. *BMC Dev Biol.* (2007) 7:42. doi: 10.1186/1471-213X-7-42
19. Ellett F, Pase L, Hayman JW, Andrianopoulos A, Lieschke GJ. mpeg1 promoter transgenes direct macrophage-lineage expression in zebrafish. *Blood.* (2011) 117:e49–56. doi: 10.1182/blood-2010-10-314120
20. Bojarczuk A, Miller KA, Hotham R, Lewis A, Ogryzko NV, Kamuyango AA, et al. Cryptococcus neoformans intracellular proliferation and capsule size determines early macrophage control of infection. *Sci Rep.* (2016) 6:21489. doi: 10.1038/srep21489
21. Bernut A, Herrmann JL, Kissa K, Dubremetz JF, Gaillard JL, Lutfalla G, et al. Mycobacterium abscessus cording prevents phagocytosis and promotes abscess formation. *Proc Natl Acad Sci USA.* (2014) 111:E943–52. doi: 10.1073/pnas.1321390111
22. Dee CT, Nagaraju RT, Athanasiadis EI, Gray C, Fernandez Del Ama L, Johnston SA, et al. CD4-transgenic Zebrafish reveal tissue-resident Th2- and regulatory T cell-like populations and diverse mononuclear phagocytes. *J Immunol.* (2016) 197:3520–30. doi: 10.4049/jimmunol.1600959
23. Oehlers SH, Cronan MR, Scott NR, Thomas MI, Okuda KS, Walton EM, et al. Interception of host angiogenic signalling limits mycobacterial growth. *Nature.* (2015) 517:612–5. doi: 10.1038/nature13967
24. Walton EM, Cronan MR, Beerman RW, Tobin DM. The macrophage-specific promoter mfap4 allows live, long-term analysis of macrophage behavior during mycobacterial infection in Zebrafish. *PLoS ONE.* (2015) 10:e0138949. doi: 10.1371/journal.pone.0138949
25. Balla KM, Lugo-Villarino G, Spitsbergen JM, Stachura DL, Hu Y, Banuelos K, et al. Eosinophils in the zebrafish: prospective isolation, characterization, and eosinophilia induction by helminth determinants. *Blood.* (2010) 116:3944–54. doi: 10.1182/blood-2010-03-267419
26. Trede NS, Langenau DM, Traver D, Look AT, Zon LI. The use of zebrafish to understand immunity. *Immunity.* (2004) 20:367–79. doi: 10.1016/S1074-7613(04)00084-6
27. Stein C, Caccamo M, Laird G, Leptin M. Conservation and divergence of gene families encoding components of innate immune response systems in zebrafish. *Genome Biol.* (2007) 8:R251. doi: 10.1186/gb-2007-8-11-r251
28. Dunkelberger JR, Song WC. Complement and its role in innate and adaptive immune responses. *Cell Res.* (2010) 20:34–50. doi: 10.1038/cr.2009.139
29. Aderem A. Phagocytosis and the inflammatory response. *J Infect Dis.* (2003) 187 (Suppl. 2):S340–5. doi: 10.1086/374747
30. Flannagan RS, Jaumouille V, Grinstein S. The cell biology of phagocytosis. *Annu Rev Pathol.* (2012) 7:61–98. doi: 10.1146/annurev-pathol-011811-132445
31. Kinchen JM, Ravichandran KS. Phagosome maturation: going through the acid test. *Nat Rev Mol Cell Biol.* (2008) 9:781–95. doi: 10.1038/nrm2515
32. Kawai T, Akira S. Toll-like receptors and their crosstalk with other innate receptors in infection and immunity. *Immunity.* (2011) 34:637–50. doi: 10.1016/j.immuni.2011.05.006
33. Kawai T, Akira S. Signaling to NF-kappaB by Toll-like receptors. *Trends Mol Med.* (2007) 13:460–9. doi: 10.1016/j.molmed.2007.09.002
34. Ogryzko NV, Lewis A, Wilson HL, Meijer AH, Renshaw SA, Elks PM. Hif-1alpha-Induced expression of Il-1beta protects against mycobacterial infection in Zebrafish. *J Immunol.* (2019) 202:494–502. doi: 10.4049/jimmunol.1801139
35. Nguyen-Chi M, Phan QT, Gonzalez C, Dubremetz JF, Levraud JP, Lutfalla G. Transient infection of the zebrafish notochord with E. coli induces chronic inflammation. *Dis Model Mech.* (2014) 7:871–82. doi: 10.1242/dmm.014498
36. Hasegawa T, Hall CJ, Crosier PS, Abe G, Kawakami K, Kudo A, et al. Transient inflammatory response mediated by interleukin-1beta is required for proper regeneration in zebrafish fin fold. *Elife.* (2017) 6:e22716. doi: 10.7554/eLife.22716.021
37. Sanderson LE, Chien AT, Astin JW, Crosier KE, Crosier PS, Hall CJ. An inducible transgene reports activation of macrophages in live zebrafish larvae. *Dev Comp Immunol.* (2015) 53:63–9. doi: 10.1016/j.dci.2015.06.013
38. Kanther M, Sun X, Muhlbauer M, Mackey LC, Flynn E J III, Bagnat M, Jobin C, et al. Microbial colonization induces dynamic temporal and spatial patterns of NF-kappaB activation in the zebrafish digestive tract. *Gastroenterology.* (2011) 141:197–207. doi: 10.1053/j.gastro.2011.03.042
39. Feng Y, Renshaw S, Martin P. Live imaging of tumor initiation in zebrafish larvae reveals a trophic role for leukocyte-derived PGE(2). *Curr Biol.* (2012) 22:1253–9. doi: 10.1016/j.cub.2012.05.010
40. Kuri P, Ellwanger K, Kufer TA, Leptin M, Bajoghli B. A high-sensitivity bi-directional reporter to monitor NF-kappaB activity in cell culture and zebrafish in real time. *J Cell Sci.* (2017) 130:648–57. doi: 10.1242/jcs.196485
41. Marjoram L, Alvers A, Deerhake ME, Bagwell J, Mankiewicz J, Cocchiaro JL, et al. Epigenetic control of intestinal barrier function and inflammation in zebrafish. *Proc Natl Acad Sci USA.* (2015) 112:2770–5. doi: 10.1073/pnas.1424089112
42. Nguyen-Chi M, Laplace-Builhe B, Travnickova J, Luz-Crawford P, Tejedor G, Phan QT, et al. Identification of polarized macrophage subsets in zebrafish. *Elife.* (2015) 4:e07288. doi: 10.7554/eLife.07288.016
43. Beck-Schimmer B, Schwendener R, Pasch T, Reyes L, Booy C, Schimmer RC. Alveolar macrophages regulate neutrophil recruitment in endotoxin-induced lung injury. *Respir Res.* (2005) 6:61. doi: 10.1186/1465-9921-6-61
44. Fuchs TA, Abed U, Goosmann C, Hurwitz R, Schulze I, Wahn V, et al. Novel cell death program leads to neutrophil extracellular traps. *J Cell Biol.* (2007) 176:231–41. doi: 10.1083/jcb.200606027
45. Summers C, Rankin SM, Condliffe AM, Singh N, Peters AM, Chilvers ER. Neutrophil kinetics in health and disease. *Trends Immunol.* (2010) 31:318–24. doi: 10.1016/j.it.2010.05.006
46. Arango Duque G, Descoteaux A. Macrophage cytokines: involvement in immunity and infectious diseases. *Front Immunol.* (2014) 5:491. doi: 10.3389/fimmu.2014.00491
47. Lam SH, Chua HL, Gong Z, Lam TJ, Sin YM. Development and maturation of the immune system in zebrafish, Danio rerio: a gene expression profiling, *in situ* hybridization and immunological study. *Dev Comp Immunol.* (2004) 28:9–28. doi: 10.1016/S0145-305X(03)00103-4
48. Davison JM, Akitake CM, Goll MG, Rhee JM, Gosse N, Baier H, et al. Transactivation from Gal4-VP16 transgenic insertions for tissue-specific cell labeling and ablation in zebrafish. *Dev Biol.* (2007) 304:811–24. doi: 10.1016/j.ydbio.2007.01.033
49. Gray C, Loynes CA, Whyte MK, Crossman DC, Renshaw SA, Chico TJ. Simultaneous intravital imaging of macrophage and neutrophil behaviour during inflammation using a novel transgenic zebrafish. *Thromb Haemost.* (2011) 105:811–9. doi: 10.1160/TH10-08-0525
50. Okuda KS, Misa JP, Oehlers SH, Hall CJ, Ellett F, Alasmari S, et al. A zebrafish model of inflammatory lymphangiogenesis. *Biol Open.* (2015) 4:1270–80. doi: 10.1242/bio.013540
51. Doro E, Jacobs SH, Hammond FR, Schipper H, Pieters RP, Carrington M, et al. Visualizing trypanosomes in a vertebrate host reveals novel swimming behaviours, adaptations and attachment mechanisms. *Elife.* (2019) 8:e48388. doi: 10.7554/eLife.48388.030
52. Who (2019). *Global Tuberculosis Report*. Available online at: https://www.who.int/tb/publications/global_report/en/ (accessed February 17, 2020).
53. Boros DL. Granulomatous inflammations. *Prog Allergy.* (1978) 24:183–267. doi: 10.1159/000401230
54. Saunders BM, Cooper AM. Restraining mycobacteria: role of granulomas in mycobacterial infections. *Immunol Cell Biol.* (2000) 78:334–41. doi: 10.1046/j.1440-1711.2000.00933.x
55. Saunders BM, Britton WJ. Life and death in the granuloma: immunopathology of tuberculosis. *Immunol Cell Biol.* (2007) 85:103–11. doi: 10.1038/sj.icb.7100027
56. Davis JM, Clay H, Lewis JL, Ghori N, Herbomel P, Ramakrishnan L. Real-time visualization of mycobacterium-macrophage interactions leading to initiation of granuloma formation in zebrafish embryos. *Immunity.* (2002) 17:693–702. doi: 10.1016/S1074-7613(02)00475-2
57. Cambier CJ, Takaki KK, Larson RP, Hernandez RE, Tobin DM, Urdahl KB, et al. Mycobacteria manipulate macrophage recruitment through coordinated use of membrane lipids. *Nature.* (2014) 505:218–22. doi: 10.1038/nature12799
58. Volkman HE, Clay H, Beery D, Chang JC, Sherman DR, Ramakrishnan L. Tuberculous granuloma formation is enhanced

by a mycobacterium virulence determinant. *PLoS Biol.* (2004) 2:e367. doi: 10.1371/journal.pbio.0020367
59. Volkman HE, Pozos TC, Zheng J, Davis JM, Rawls JF, Ramakrishnan L. Tuberculous granuloma induction via interaction of a bacterial secreted protein with host epithelium. *Science.* (2010) 327:466–9. doi: 10.1126/science.1179663
60. Davis JM, Ramakrishnan L. The role of the granuloma in expansion and dissemination of early tuberculous infection. *Cell.* (2009) 136:37–49. doi: 10.1016/j.cell.2008.11.014
61. Pagan AJ, Yang CT, Cameron J, Swaim LE, Ellett F, Lieschke GJ, et al. Myeloid growth factors promote resistance to mycobacterial infection by curtailing granuloma necrosis through macrophage replenishment. *Cell Host Microbe.* (2015) 18:15–26. doi: 10.1016/j.chom.2015.06.008
62. Clay H, Volkman HE, Ramakrishnan L. Tumor necrosis factor signaling mediates resistance to mycobacteria by inhibiting bacterial growth and macrophage death. *Immunity.* (2008) 29:283–94. doi: 10.1016/j.immuni.2008.06.011
63. Tobin DM, Roca FJ, Oh SF, Mcfarland R, Vickery TW, Ray JP, et al. Host genotype-specific therapies can optimize the inflammatory response to mycobacterial infections. *Cell.* (2012) 148:434–46. doi: 10.1016/j.cell.2011.12.023
64. Roca FJ, Ramakrishnan L. TNF dually mediates resistance and susceptibility to mycobacteria via mitochondrial reactive oxygen species. *Cell.* (2013) 153:521–34. doi: 10.1016/j.cell.2013.03.022
65. Roca FJ, Whitworth LJ, Redmond S, Jones AA, Ramakrishnan L. TNF induces pathogenic programmed macrophage necrosis in tuberculosis through a mitochondrial-lysosomal-endoplasmic reticulum circuit. *Cell.* (2019) 178:1344–61.e1311. doi: 10.1016/j.cell.2019.08.004
66. Fenaroli F, Westmoreland D, Benjaminsen J, Kolstad T, Skjeldal FM, Meijer AH, et al. Nanoparticles as drug delivery system against tuberculosis in zebrafish embryos: direct visualization and treatment. *ACS Nano.* (2014) 8:7014–26. doi: 10.1021/nn5019126
67. Wu Z, Koh B, Lawrence LM, Kanamala M, Pool B, Svirskis D, et al. Liposome-mediated drug delivery in larval *Zebrafish* to manipulate macrophage function. *Zebrafish.* (2019) 16:171–81. doi: 10.1089/zeb.2018.1681
68. Pedrosa J, Saunders BM, Appelberg R, Orme IM, Silva MT, Cooper AM. Neutrophils play a protective nonphagocytic role in systemic Mycobacterium tuberculosis infection of mice. *Infect Immun.* (2000) 68:577–83. doi: 10.1128/IAI.68.2.577-583.2000
69. Eruslanov EB, Lyadova IV, Kondratieva TK, Majorov KB, Scheglov IV, Orlova MO, et al. Neutrophil responses to Mycobacterium tuberculosis infection in genetically susceptible and resistant mice. *Infect Immun.* (2005) 73:1744–53. doi: 10.1128/IAI.73.3.1744-1753.2005
70. Yang CT, Cambier CJ, Davis JM, Hall CJ, Crosier PS, Ramakrishnan L. Neutrophils exert protection in the early tuberculous granuloma by oxidative killing of mycobacteria phagocytosed from infected macrophages. *Cell Host Microbe.* (2012) 12:301–12. doi: 10.1016/j.chom.2012.07.009
71. Belon C, Gannoun-Zaki L, Lutfalla G, Kremer L, Blanc-Potard AB. Mycobacterium marinum MgtC plays a role in phagocytosis but is dispensable for intracellular multiplication. *PLoS ONE.* (2014) 9:e116052. doi: 10.1371/journal.pone.0116052
72. Elks PM, Brizee S, Van Der Vaart M, Walmsley SR, Van Eeden FJ, Renshaw SA, et al. Hypoxia inducible factor signaling modulates susceptibility to mycobacterial infection via a nitric oxide dependent mechanism. *PLoS Pathog.* (2013) 9:e1003789. doi: 10.1371/journal.ppat.1003789
73. Madigan CA, Cambier CJ, Kelly-Scumpia KM, Scumpia PO, Cheng TY, Zailaa J, et al. A macrophage response to mycobacterium leprae phenolic glycolipid initiates nerve damage in leprosy. *Cell.* (2017) 170:973–85.e910. doi: 10.1016/j.cell.2017.07.030
74. WHO. *Leprosy.* (2019). Available online at: https://www.who.int/news-room/fact-sheets/detail/leprosy (accessed February 17, 2020).
75. Smith WC. Review of current research in the prevention of nerve damage in leprosy. *Lepr Rev.* (2000) 71 Suppl:S138–45. doi: 10.5935/0305-7518.20000085
76. Klein D, Martini R. Myelin and macrophages in the PNS: an intimate relationship in trauma and disease. *Brain Res.* (2016) 1641:130–8. doi: 10.1016/j.brainres.2015.11.033
77. Drevinek P, Mahenthiralingam E. Burkholderia cenocepacia in cystic fibrosis: epidemiology and molecular mechanisms of virulence. *Clin Microbiol Infect.* (2010) 16:821–30. doi: 10.1111/j.1469-0691.2010.03237.x
78. Vergunst AC, Meijer *AH, Renshaw SA, and O'callaghan D.* Burkholderia cenocepacia creates an intramacrophage replication niche in zebrafish embryos, followed by bacterial dissemination and establishment of systemic infection. *Infect Immun.* (2010) 78:1495–508. doi: 10.1128/IAI.00743-09
79. Mesureur J, Feliciano JR, Wagner N, Gomes MC, Zhang L, Blanco-Gonzalez M, et al. Macrophages, but not neutrophils, are critical for proliferation of Burkholderia cenocepacia and ensuing host-damaging inflammation. *PLoS Pathog.* (2017) 13:e1006437. doi: 10.1371/journal.ppat.1006437
80. Cdc. *Staphylococcus aureus in Healthcare Settings.* (2011). Available online at: https://www.cdc.gov/hai/organisms/staph.html (accessed April 15, 2020).
81. Prajsnar TK, Cunliffe VT, Foster SJ, Renshaw SA. A novel vertebrate model of Staphylococcus aureus infection reveals phagocyte-dependent resistance of zebrafish to non-host specialized pathogens. *Cell Microbiol.* (2008) 10:2312–25. doi: 10.1111/j.1462-5822.2008.01213.x
82. Prajsnar TK, Hamilton R, Garcia-Lara J, Mcvicker G, Williams A, Boots M, et al. A privileged intraphagocyte niche is responsible for disseminated infection of Staphylococcus aureus in a zebrafish model. *Cell Microbiol.* (2012) 14:1600–19. doi: 10.1111/j.1462-5822.2012.01826.x
83. Prajsnar TK, Serba JJ, Dekker BM, Gibson JF, Masud S, Fleming A, et al. The autophagic response to Staphylococcus aureus provides an intracellular niche in neutrophils. *Autophagy.* (2020) 1–15. doi: 10.1080/15548627.2020.1739443
84. Mcvicker G, Prajsnar TK, Williams A, Wagner NL, Boots M, Renshaw SA, et al. Clonal expansion during Staphylococcus aureus infection dynamics reveals the effect of antibiotic intervention. *PLoS Pathog.* (2014) 10:e1003959. doi: 10.1371/journal.ppat.1003959
85. Robert VA, Casadevall A. Vertebrate endothermy restricts most fungi as potential pathogens. *J Infect Dis.* (2009) 200:1623–6. doi: 10.1086/644642
86. Mohan T, Bhatnagar S, Gupta DL, Rao DN. Current understanding of HIV-1 and T-cell adaptive immunity: progress to date. *Microb Pathog.* (2014) 73:60–9. doi: 10.1016/j.micpath.2014.06.003
87. Harwood CG, Rao RP. Host pathogen relations: exploring animal models for fungal pathogens. *Pathogens.* (2014) 3:549–62. doi: 10.3390/pathogens3030549
88. Warris A, Ballou ER. Oxidative responses and fungal infection biology. *Semin Cell Dev Biol.* (2019) 89:34–46. doi: 10.1016/j.semcdb.2018.03.004
89. Latge JP. Aspergillus fumigatus and aspergillosis. *Clin Microbiol Rev.* (1999) 12:310–50. doi: 10.1128/CMR.12.2.310
90. Hogan D, Wheeler RT. The complex roles of NADPH oxidases in fungal infection. *Cell Microbiol.* (2014) 16:1156–67. doi: 10.1111/cmi.12320
91. Knox BP, Deng Q, Rood M, Eickhoff JC, Keller NP, Huttenlocher A. Distinct innate immune phagocyte responses to Aspergillus fumigatus conidia and hyphae in zebrafish larvae. *Eukaryot Cell.* (2014) 13:1266–77. doi: 10.1128/EC.00080-14
92. Gazendam RP, Van De Geer A, Roos D, Van Den Berg TK, Kuijpers TW. How neutrophils kill fungi. *Immunol Rev.* (2016) 273:299–311. doi: 10.1111/imr.12454
93. Philippe B, Ibrahim-Granet O, Prevost MC, Gougerot-Pocidalo MA, Sanchez Perez M, Van Der Meeren A, et al. Killing of Aspergillus fumigatus by alveolar macrophages is mediated by reactive oxidant intermediates. *Infect Immun.* (2003) 71:3034–42. doi: 10.1128/IAI.71.6.3034-3042.2003
94. Mircescu MM, Lipuma L, Van Rooijen N, Pamer EG, Hohl TM. Essential role for neutrophils but not alveolar macrophages at early time points following Aspergillus fumigatus infection. *J Infect Dis.* (2009) 200:647–56. doi: 10.1086/600380
95. Bhatia S, Fei M, Yarlagadda M, Qi Z, Akira S, Saijo S, et al. Rapid host defense against Aspergillus fumigatus involves alveolar macrophages with a predominance of alternatively activated phenotype. *PLoS ONE.* (2011) 6:e15943. doi: 10.1371/journal.pone.0015943
96. Kosmidis C, Denning DW. The clinical spectrum of pulmonary aspergillosis. *Thorax.* (2015) 70:270–7. doi: 10.1136/thoraxjnl-2014-206291
97. Rosowski EE, He J, Huisken J, Keller NP, Huttenlocher A. Efficacy of voriconazole against aspergillus fumigatus infection depends on host immune function. *Antimicrob Agents Chemother.* (2020) 64:e00917–19. doi: 10.1128/AAC.00917-19

98. Koch BEV, Hajdamowicz NH, Lagendijk E, Ram AFJ, Meijer AH. Aspergillus fumigatus establishes infection in zebrafish by germination of phagocytized conidia, while Aspergillus niger relies on extracellular germination. *Sci Rep.* (2019) 9:12791. doi: 10.1038/s41598-019-49284-w
99. Shah A, Kannambath S, Herbst S, Rogers A, Soresi S, Carby M, et al. Calcineurin orchestrates lateral transfer of aspergillus fumigatus during macrophage cell death. *Am J Respir Crit Care Med.* (2016) 194:1127–39. doi: 10.1164/rccm.201601-0070OC
100. Vanittanakom N, Cooper CRJr, Fisher MC, Sirisanthana T. Penicillium marneffei infection and recent advances in the epidemiology and molecular biology aspects. *Clin Microbiol Rev.* (2006) 19:95–110. doi: 10.1128/CMR.19.1.95-110.2006
101. Pazhakh V, Ellett F, Croker BA, O'donnell JA, *Pase L, Schulze KE, et al.* (2019) beta-glucan-dependent shuttling of conidia from neutrophils to macrophages occurs during fungal infection establishment. *PLoS Biol* 17:e3000113. doi: 10.1371/journal.pbio.3000113
102. Clark RA, Greer D, Atkinson W, Valainis GT, Hyslop N. Spectrum of Cryptococcus neoformans infection in 68 patients infected with human immunodeficiency virus. *Rev Infect Dis.* (1990) 12:768–77. doi: 10.1093/clinids/12.5.768
103. Johnston SA, May RC. The human fungal pathogen Cryptococcus neoformans escapes macrophages by a phagosome emptying mechanism that is inhibited by Arp2/3 complex-mediated actin polymerisation. *PLoS Pathog.* (2010) 6:e1001041. doi: 10.1371/journal.ppat.1001041
104. Yang X, Wang H, Hu F, Chen X, Zhang M. Nonlytic exocytosis of Cryptococcus neoformans from neutrophils in the brain vasculature. *Cell Commun Signal.* (2019) 17:117. doi: 10.1186/s12964-019-0429-0
105. Niethammer P, Grabher C, Look AT, Mitchison TJ. A tissue-scale gradient of hydrogen peroxide mediates rapid wound detection in zebrafish. *Nature.* (2009) 459:996–9. doi: 10.1038/nature08119
106. D'alencon CA, Pena OA, Wittmann C, Gallardo VE, Jones RA, Loosli F, et al. A high-throughput chemically induced inflammation assay in zebrafish. *BMC Biol.* (2010) 8:151. doi: 10.1186/1741-7007-8-151
107. Powell D, Tauzin S, Hind LE, Deng Q, Beebe DJ, Huttenlocher A. Chemokine signaling and the regulation of bidirectional leukocyte migration in interstitial tissues. *Cell Rep.* (2017) 19:1572–85. doi: 10.1016/j.celrep.2017.04.078
108. Hall CJ, Sanderson LE, Lawrence LM, Pool B, Van Der Kroef M, Ashimbayeva E, et al. Blocking fatty acid-fueled mROS production within macrophages alleviates acute gouty inflammation. *J Clin Invest.* (2018) 128:1752–71. doi: 10.1172/JCI94584
109. Nathan C, Ding A. Nonresolving inflammation. *Cell.* (2010) 140:871–82. doi: 10.1016/j.cell.2010.02.029
110. Gurevich DB, Severn CE, Twomey C, Greenhough A, Cash J, Toye AM, et al. Live imaging of wound angiogenesis reveals macrophage orchestrated vessel sprouting and regression. *Embo J.* (2018) 37:e97786. doi: 10.15252/embj.201797786
111. Yoo SK, Starnes TW, Deng Q, Huttenlocher A. Lyn is a redox sensor that mediates leukocyte wound attraction in vivo. *Nature.* (2011) 480:109–12. doi: 10.1038/nature10632
112. Pase L, Layton JE, Wittmann C, Ellett F, Nowell CJ, Reyes-Aldasoro CC, et al. Neutrophil-delivered myeloperoxidase dampens the hydrogen peroxide burst after tissue wounding in zebrafish. *Curr Biol.* (2012) 22:1818–24. doi: 10.1016/j.cub.2012.07.060
113. Klyubin IV, Kirpichnikova KM, Gamaley IA. Hydrogen peroxide-induced chemotaxis of mouse peritoneal neutrophils. *Eur J Cell Biol.* (1996) 70:347–51.
114. Moreira S, Stramer B, Evans I, Wood W, Martin P. Prioritization of competing damage and developmental signals by migrating macrophages in the Drosophila embryo. *Curr Biol.* (2010) 20:464–70. doi: 10.1016/j.cub.2010.01.047
115. Bratton DL, Henson PM. Neutrophil clearance: when the party is over, clean-up begins. *Trends Immunol.* (2011) 32:350–7. doi: 10.1016/j.it.2011.04.009
116. Buckley CD, Ross EA, Mcgettrick HM, Osborne CE, Haworth O, Schmutz C, et al. Identification of a phenotypically and functionally distinct population of long-lived neutrophils in a model of reverse endothelial migration. *J Leukoc Biol.* (2006) 79:303–11. doi: 10.1189/jlb.0905496
117. Woodfin A, Voisin MB, Beyrau M, Colom B, Caille D, Diapouli FM, et al. The junctional adhesion molecule JAM-C regulates polarized transendothelial migration of neutrophils in vivo. *Nat Immunol.* (2011) 12:761–9. doi: 10.1038/ni.2062
118. Loynes CA, Lee JA, Robertson AL, Steel MJ, Ellett F, Feng Y, et al. PGE2 production at sites of tissue injury promotes an anti-inflammatory neutrophil phenotype and determines the outcome of inflammation resolution in vivo. *Sci Adv.* (2018) 4:eaar8320. doi: 10.1126/sciadv.aar8320
119. De Oliveira S, Reyes-Aldasoro CC, Candel S, Renshaw SA, Mulero V, Calado A. Cxcl8 (IL-8) mediates neutrophil recruitment and behavior in the zebrafish inflammatory response. *J Immunol.* (2013) 190:4349–59. doi: 10.4049/jimmunol.1203266
120. Isles HM, Herman KD, Robertson AL, Loynes CA, Prince LR, Elks PM, et al. The CXCL12/CXCR4 signaling axis retains neutrophils at inflammatory sites in Zebrafish. *Front Immunol.* (2019) 10:1784. doi: 10.3389/fimmu.2019.01784
121. Hartl D, Krauss-Etschmann S, Koller B, Hordijk PL, Kuijpers TW, Hoffmann F, et al. Infiltrated neutrophils acquire novel chemokine receptor expression and chemokine responsiveness in chronic inflammatory lung diseases. *J Immunol.* (2008) 181:8053–67. doi: 10.4049/jimmunol.181.11.8053
122. Sommer F, Torraca V, Kamel SM, Lombardi A, Meijer AH. Frontline Science: Antagonism between regular and atypical Cxcr3 receptors regulates macrophage migration during infection and injury in zebrafish. *J Leukoc Biol.* (2020) 107:185–203. doi: 10.1002/JLB.2HI0119-006R
123. Ellett F, Elks PM, Robertson AL, Ogryzko NV, Renshaw SA. Defining the phenotype of neutrophils following reverse migration in zebrafish. *J Leukoc Biol.* (2015) 98:975–81. doi: 10.1189/jlb.3MA0315-105R
124. Mulay SR, Anders HJ. Crystallopathies. *N Engl J Med.* (2016) 374:2465–76. doi: 10.1056/NEJMra1601611
125. Zhu Y, Pandya BJ, Choi HK. Prevalence of gout and hyperuricemia in the US general population: the national health and nutrition examination survey 2007-2008. *Arthritis Rheum.* (2011) 63:3136–41. doi: 10.1002/art.30520
126. Dalbeth N, Merriman TR, Stamp LK. Gout. *Lancet.* (2016) 388:2039–52. doi: 10.1016/S0140-6736(16)00346-9
127. Mielants H, Veys EM, De Weerdt A. Gout and its relation to lipid metabolism. I Serum uric acid, lipid, and lipoprotein levels in gout. *Ann Rheum Dis.* (1973) 32:501–5. doi: 10.1136/ard.32.6.501
128. Hall CJ, Boyle RH, Astin JW, Flores MV, Oehlers SH, Sanderson LE, et al. Immunoresponsive gene 1 augments bactericidal activity of macrophage-lineage cells by regulating beta-oxidation-dependent mitochondrial ROS production. *Cell Metab.* (2013) 18:265–78. doi: 10.1016/j.cmet.2013.06.018
129. Kizy AE, Neely MN. First Streptococcus pyogenes signature-tagged mutagenesis screen identifies novel virulence determinants. *Infect Immun.* (2009) 77:1854–65. doi: 10.1128/IAI.01306-08
130. Stoop EJ, Schipper T, Rosendahl Huber SK, Nezhinsky AE, Verbeek FJ, Gurcha SS, et al. Zebrafish embryo screen for mycobacterial genes involved in the initiation of granuloma formation reveals a newly identified ESX-1 component. *Dis Model Mech.* (2011) 4:526–36. doi: 10.1242/dmm.006676
131. Tobin DM, Vary JC Jr, Ray JP, Walsh GS, Dunstan SJ, Bang ND, et al. The lta4h locus modulates susceptibility to mycobacterial infection in zebrafish and humans. *Cell.* (2010) 140:717–30. doi: 10.1016/j.cell.2010.02.013

Conflict of Interest: The authors declare that the research was conducted in the absence of any commercial or financial relationships that could be construed as a potential conflict of interest.

frontiers in Immunology

ORIGINAL RESEARCH
published: 22 July 2020
doi: 10.3389/fimmu.2020.01379

A CD63 Homolog Specially Recruited to the Fungi-Contained Phagosomes Is Involved in the Cellular Immune Response of Oyster *Crassostrea gigas*

Conghui Liu[1,2,3], *Chuanyan Yang*[1,3,4], *Mengqiang Wang*[2], *Shuai Jiang*[2], *Qilin Yi*[1,3,4], *Weilin Wang*[2,3,4], *Lingling Wang*[1,3,4*] *and Linsheng Song*[1,3*]

[1] *Liaoning Key Laboratory of Marine Animal Immunology, Dalian Ocean University, Dalian, China,* [2] *Key Laboratory of Experimental Marine Biology, Institute of Oceanology, Chinese Academy of Sciences, Qingdao, China,* [3] *Liaoning Key Laboratory of Marine Animal Immunology and Disease Control, Dalian Ocean University, Dalian, China,* [4] *Dalian Key Laboratory of Aquatic Animal Disease Prevention and Control, Dalian Ocean University, Dalian, China*

OPEN ACCESS

Edited by:
Xinjiang Lu,
Ningbo University, China

Reviewed by:
Zhen Xu,
Huazhong Agricultural University, China
Linlin Zhang,
Institute of Oceanology (CAS), China
Xian-Wei Wang,
Shandong University, China

***Correspondence:**
Lingling Wang
wanglingling@dlou.edu.cn
Linsheng Song
lshsong@dlou.edu.cn

Specialty section:
This article was submitted to Comparative Immunology, a section of the journal Frontiers in Immunology

Received: *29 February 2020*
Accepted: *29 May 2020*
Published: *22 July 2020*

Citation:
Liu C, Yang C, Wang M, Jiang S, Yi Q, Wang W, Wang L and Song L (2020) A CD63 Homolog Specially Recruited to the Fungi-Contained Phagosomes Is Involved in the Cellular Immune Response of Oyster Crassostrea gigas. Front. Immunol. 11:1379. doi: 10.3389/fimmu.2020.01379

Cluster of differentiation 63 (CD63), a four-transmembrane glycoprotein in the subfamily of tetraspanin, has been widely recognized as a gateway from the infection of foreign invaders to the immune defense of hosts. Its role in Pacific oyster *Crassostrea gigas* is, however, yet to be discovered. This work makes contributions by identifying *Cg*CD63H, a CD63 homolog with four transmembrane domains and one conservative CCG motif, and establishing its role as a receptor that participates in immune recognition and hemocyte phagocytosis. The presence of *Cg*CD63H messenger RNA (mRNA) in hepatopancreas, labial palps, gill, and hemocytes is confirmed. The expression level of mRNA in hemocytes is found significantly ($p < 0.01$) upregulated after the injection of *Vibrio splendidus*. *Cg*CD63H protein, typically distributed over the plasma membrane of oyster hemocytes, is recruited to the *Yarrowia lipolytica*-containing phagosomes after the stimulation of *Y. lipolytica*. The recombinant *Cg*CD63H protein expresses binding capacity to glucan (GLU), peptidoglycan (PGN), and lipopolysaccharide (LPS) in the presence of lyophilized hemolymph. The phagocytic rate of hemocytes toward *V. splendidus* and *Y. lipolytica* is significantly inhibited ($p < 0.01$) after incubation with anti-CgCD63H antibody. Our work further suggests that *Cg*CD63H functions as a receptor involved in the immune recognition and hemocyte phagocytosis against invading pathogen, which can be a marker candidate for the hemocyte typing in *C. gigas*.

Keywords: tetraspanin, phagosomes recruitment, receptor, innate immune response, *Crassostrea gigas*

INTRODUCTION

Tetraspanins establish a conserved superfamily of four-transmembrane glycoproteins involved in a variety of cellular processes, such as cell development, proliferation, activation, adhesion, and motility (1–4). They are ubiquitous in various organisms, sharing a highly conserved architecture with the presence of four transmembrane domains, two extracellular loops containing one Cys–Cys–Gly (CCG) motif, and one intracellular tail containing cysteine palmitoylation sites (5, 6).

Tetraspanins are depicted as a gateway for infection because of the roles in uptaking, trafficking, and spread of viruses as well as intracellular bacteria, fungi, and parasites (7). Extensively studied in mammals, 33 members of tetraspanins have been so far characterized and classified into four major subfamilies, namely, cluster of differentiation (CD), CD63, uroplakin (UPK), and retinal degeneration slow (RDS) subfamily (5–9). CD63, the first characterized tetraspanin, constitutes its own subfamily having a more ancient origin than the other tetraspanins (8, 10). CD63 and other tetraspanins interact with the receptors in the plasma membrane as well as themselves to build an interaction network termed as tetraspanin-enriched microdomains (TEMs) (11, 12). TEMs are always achieved by organizing multiple types of receptors and associated components (6, 7), which provide platforms to control pathogen binding, entry, and invasion, and subsequently the immune responses (13, 14). CD63 can interact directly or indirectly with various proteins, for example integrins, other tetraspanins, cell surface receptors, and kinases (15). CD63 regulates the trafficking of its interaction partners and mediates signal transduction events in the regulation of many membrane-associated processes (16). Growing evidences have demonstrated that tetraspanins also participate in the innate immune response, such as pattern recognition and signal transduction (17, 18). For example, CD63 and other tetraspanins such as CD37, CD9, and CD82 are involved in the pathogen recognition, pattern recognition receptor (PRR) complex formation, and antigen-presentation through their cooperation with other receptors (17, 19–21).

The characterization of CD63 has been recently found in invertebrates, for instance, disk abalone *Haliotis discus discus* (22) and clam *Paphia undulate* (23). Earlier work has observed an interesting phenomenon: under the stimulation with bacteria, virus, and pathogen-associated molecular patterns (PAMPs), the mRNA expressions of these CD63s change significantly. However, the detailed biological roles of CD63 are still not clear. So far, there are many reports on other tetraspanins in nematode, mollusk, arthropod, and ascidian (24–27), which could offer useful leads to the investigation of CD63 subfamily for invertebrates. For instance, invertebrate tetraspanins could be significantly induced by the stimulations of various pathogens (28–33), and they could function as mediators of innate immune response (34, 35). Tetraspanin D76 from insect (*Manduca sexta*) was found to play an important role in cell-mediated immune responses by influencing the encapsulation and clearance of bacteria (35). Tetraspanin from *Crassostrea ariakensis*, Ca-TSP, was also evidenced to associate with phagocytic bodies (25). Although increasing evidences point to the potential roles of invertebrate tetraspanins in innate immunity, most of them are largely limited to the gene diversity and mRNA expression profiles.

As invertebrate, the Pacific oysters (*Crassostrea gigas*) have been deemed as a model to investigate the innate immunity in mollusks (36, 37). The lack of specific cell markers, however, has greatly impeded the cell typing and innate immune research in invertebrates (38). This work investigates the functions of CD63 in Pacific oysters, aiming to offer new insights to understand the possible role of tetraspanins in the innate immune system of invertebrate, and provides a potential candidate marker for the cell typing. Specifically, a homolog of CD63 (designated *Cg*CD63H) is identified and characterized from *C. gigas*; the mRNA transcripts of *Cg*CD63H in different tissues as well as the temporal expression pattern after *V. splendidus* challenge are investigated; the binding ability of *Cg*CD63H to PAMPs is examined; and the roles of *Cg*CD63H during the phagocytosis process of hemocyte are revealed.

MATERIALS AND METHODS

Oysters and Microbes

Adult oysters *C. gigas* (average shell length of 13.0 cm) were collected from a local farm in Qingdao, Shandong Province, China, and acclimatized in aerated fresh seawater at $15 \pm 2^{\circ}$C for 10 days before processing. The oysters were fed with condensed microalgae, and the water was totally replaced daily.

Bacteria *Escherichia coli* Transetta (DE3) (Transgen), *Staphylococcus aureus* (Microbial Culture Collection Center, Beijing, China), *V. splendidus* (39), and fungi *Yarrowia lipolytica* (provided by Dr. Chi) were cultured in Luria–Bertani (LB) medium at 37°C, 2216E medium at 28°C, and Yeast Extract–Peptone–Dextrose (YPD) medium at 28°C, respectively. Then, the microorganisms were harvested and resuspended in sterilized seawater (SSW) and adjusted to the final concentration of 2×10^8 CFU ml^{-1}.

Tissue Collection and Immune Challenge

Tissues including the hepatopancreas, mantle, gonad, labial palps, and gills were collected from six oysters as parallel samples. The hemolymphs were aseptically withdrawn from the posterior adductor muscle sinus of these six oysters by using a syringe and immediately centrifuged at 800 × g, 4°C for 10 min to harvest the hemocytes. All these samples were stored at −80°C after addition of 1 ml TRIzol reagent (TaKaRa) for RNA extraction.

For the bacteria challenge experiment, 200 oysters were randomly assigned into control, challenge, and blank groups. Eighty oysters individually received an injection of 100 μl sterilize seawater (SSW) were employed as the control group, while other 80 oysters that received an injection of 100 μl alive *V. splendidus* suspended in SSW (2×10^8 CFU ml^{-1}) were employed as the challenge group. These treated oysters were maintained in water tanks after injection, and 15 individuals were randomly sampled at 3, 6, 12, 24, and 48 h post-injection. The remaining 40 untreated oysters were employed as the blank group. Hemolymphs collected from three individuals were pooled into one sample, and there were five replicates for each sampling time point. The hemocytes were harvested and stored as described above.

RNA Isolation and cDNA Synthesis

Total RNA was isolated from oyster tissues and hemocytes using Trizol reagent following its protocol (TaKaRa). The first-strand complementary DNA (cDNA) synthesis was carried out based on Promega M-MLV RT Usage information using the DNase I (Promega)-treated total RNA as template and oligo (dT)-adaptor as primer (**Table 1**). The reaction was performed at 42°C

TABLE 1 | Primers used in this study.

Primer name	Sequence (5′-3′)
Clone primers	
Oligo(dT)-adaptor	GGCCACGCGTCGACTAGTACT$_{17}$
T7	GTAATACGACTCACTATAGGGC
*Cg*CD63H-F	ATGGGGTGTCGGGGTACC
*Cg*CD63H-R	AGTGAATGCGGTGGGTAAG
RT-PCR primers	
*Cg*EF1-α-rtF	AGTCACCAAGGCTGCACAGAAAG
*Cg*EF1-α-rtR	TCCGACGTATTTCTTTGCGATGT
*Cg*CD63H-rtF	GCTGGAATGCTGTGGAGGA
*Cg*CD63H-rtR	ACATCTGGCAGGTCTGGTAGT
Recombination primes	
*Cg*CD63H-exF	CGGGGTACCGGTGGAGTACGATGCCTTAG
*Cg*CD63H-exR	ATAAGAATGCGGCCGCAGTGAATGCGGTGGGTAAG

for 1 h, terminated by heating at 95°C for 5 min. The cDNA mix was diluted to 1:100 and stored at −80°C for subsequent gene cloning and SYBR Green fluorescent quantitative real-time PCR (qRT-PCR).

The Cloning and Sequence Analysis of Full-Length cDNA

Sequence information of *Cg*CD63H (XM_011436987.3) was retrieved from the National Center for Biotechnology Information (NCBI) (http://www.ncbi.nlm.gov). A pair of gene-specific primers *Cg*CD63H-F and *Cg*CD63H-R (**Table 1**) was used for cloning of the full-length cDNA sequence. The PCR product was gel purified and cloned into the pMD19-T simple vector (TaKaRa). The resulting sequences were verified and subjected to cluster analysis. The phosphorylation, O-linked glycosylation, N-linked glycosylation, and methylation modifications of *Cg*CD63H were predicted by DISPHOS (http://www.dabi.temple.edu/disphos/), NetOGlyc 4.0 Server (http://www.cbs.dtu.dk/services/NetOGlyc/), NetNGlyc 1.0 Server (http://www.cbs.dtu.dk/services/NetNGlyc/), and GPS-MSP Online Service (http://msp.biocuckoo.org/online.php), respectively.

The tetraspanin homologs of *Cg*CD63H from some other species, including *Mus musculus*, *Xenopus tropicalis*, *Danio rerio*, *Salmo salar,* and *Oplegnathus fasciatus*, *Drosophila melanogaster*, *Tenebrio molitor*, *H. discus*, *Aplysia californica*, *Biomphalaria glabrata*, *Pomacea canaliculata*, and *Mizuhopecten yessoensis* were retrieved from NCBI (**Supplementary Data 1**). The domains of these proteins were predicted using the simple modular architecture research tool (SMART) version 7.0 (http://www.smart.embl-heidelberg.de/). Multiple sequence alignment of *Cg*CD63H and its homologs were performed with the ClustalW multiple alignment program (http://www.ebi.ac.uk/clustalw/). An unrooted phylogenetic tree was constructed based on the sequence alignment by the neighbor-joining (NJ) algorithm using the Mega 6.06 program (http://www.megasoftware.net/).

The qRT-PCR Analysis

The qRT-PCR was carried out to investigate the mRNA expression of *Cg*CD63H. A fragment of 179 bp was amplified using two sequence-specific primers, *Cg*CD63H-rtF and *Cg*CD63H-rtR (**Table 1**), and the PCR products were sequenced to verify the PCR specificity. Two primers (**Table 1**) were used to amplify a 200-bp fragment of elongation factors (*Cg*EF1-α) as an internal control to verify the successful reverse transcription and calibrate the cDNA template. The SYBR Green qRT-PCR assay was carried out in an ABI PRISM 7500 Sequence Detection System (Applied Biosystems) as the previous description (40). All data were given in terms of relative mRNA expression using the $2^{-\Delta\Delta CT}$ method (41).

Preparation of Recombinant Protein and Polyclonal Antibody of *Cg*CD63H

The cDNA fragment encoding the mature peptide of *Cg*CD63H was amplified with specific primers *Cg*CD63H-F and *Cg*CD63H-R (**Table 1**). A *Not*I site and a *Kpn*I site were added to the 5′ end of sense primer *Cg*CD63H-exF and antisense primer *Cg*CD63H-exR with the stop codon deletion, respectively. The PCR fragments were cloned into pMD19-T simple vector (TaKaRa), digested completely by restriction enzymes *Not*I and *Kpn*I (NEB), and then cloned into the *Not*I/*Kpn*I sites of expression vector pET-30a (Novagen).

The strain *E. coli* Transetta (DE3) with recombinant plasmid (pET-30a-CgCD63H) was incubated in LB medium (containing 75 μg ml^{-1} kanamycin), shaken at 220 rpm at 37°C. The control strain with plasmid pET-32a was incubated in the same medium with 100 μg mL^{-1} ampicillin. When the culture media reached OD_{600} of 0.5–0.7, the cells were incubated for an additional 4 h with the induction of isopropyl β-D-1-thiogalactopyranoside (IPTG) at the final concentration of 1 mmol L^{-1}. The recombinant protein *Cg*CD63H (designated r*Cg*CD63H) and the recombinant protein Trx (designated rTrx) were purified by a Ni^{2+} chelating Sepharose column and refolded in gradient urea–Tris-buffered saline (TBS) glycerol buffer as the previous description (40). The resultant proteins were detected by sodium dodecyl sulfate–polyacrylamide gel electrophoresis (SDS-PAGE), and their concentration was quantified by bicinchoninic acid (BCA) kit (Beyotime).

For the preparation of polyclonal antibody anti-*Cg*CD63H, r*Cg*CD63H was injected into mice of 6 weeks of age to acquire polyclonal antibody as previously described (42). The serum from the identical mice before immunization was taken as negative control.

Immunocytochemistry of *Cg*CD63H in Hemocytes

Hemolymphs were collected from the oysters cultured in filtered aerated seawater at 18°C for 1 week and immediately centrifuged at 800 × g, 4°C for 10 min to harvest the hemocytes. Modified Leibovitz L-15 media (Gibco) (43) were used to suspend the hemocytes. The hemocyte suspension was added into confocal dishes precoated with gelatin solution [gelatin, 5 g L^{-1}; $CrK(SO_4)_2{\cdot}12H_2O$, 0.5 g L^{-1}] and allowed them to adhere to the

wall for 3 h. The supernatant was dislodged, and then, 4% paraformaldehyde (PFA; diluted in TBS) was added to fix the hemocytes for 15 min. After rinsing three times with TBST (TBS with 0.1% Tween-20), the dishes were blocked with 200 μl of 3% bovine serum albumin (BSA) [dissolved in phosphate-buffered saline (PBS)] at 37°C for 30 min. The supernatant was removed, and the dishes were incubated with 200 μl anti-*Cg*CD63H (diluted 1:1,000 in blocking buffer) as the primary antibody at 37°C for 1 h. After washing three times with PBST (PBS with 0.1% Tween-20), the dishes were incubated with Alexa Fluer 488-labeled goat-antimouse antibody (diluted 1:1,000 in blocking buffer) as the second antibody at 37°C for 1 h. After another three times of washing with PBST, 4′,6-diamidino-2-phenylindole (DAPI) (diluted 1:10,000 in PBS) was added into the dishes to stain the nucleus. After the last three times of washing, the dishes were mounted in buffered glycerin for observation with a laser scan confocal microscope (ZEISS).

PAMP Binding Assay

The PAMP binding assay was performed according to previous report with modification (44). Briefly, 100 μL (20 mg) of lipopolysaccharides (LPS) from *E. coli* (Sigma-Aldrich, L2630-10MG), peptidoglycan (PGN) from *S. aureus* (Sigma-Aldrich, 77140-10MG), β-glucan (GLU) from *Saccharomyces cerevisiae* (Sigma-Aldrich, 346210-25MG), and mannose (MAN) (Sigma-Aldrich, M2069-25G) were adopted to envelop a 96-well microtiter plate (Costar). The wells were then blocked with 3% BSA (*w*/*v*) in PBS at 37°C for 1 h. After washed with PBS-T, 1/2-fold serial dilutions of r*Cg*CD63H in TBS (50 mmol L^{-1} Tris–HCl, 50 mmol L^{-1} NaCl, pH 7.6) were added in the presence of 0.1 mg mL^{-1} BSA or 1 mg lyophilized hemolymph. The same concentration of rTRX was used as negative control. After incubating at 18°C for 2 h followed by three times of washing, 100 μl mouse anti-His tag monoclonal antibody (Genscript, China) diluted to 1:2,000 was added and incubated at 37°C for 1 h. The plate was washed again, and 100 μl of rabbit-anti-mouse Ig-AP conjugate (Sangon Biotech, China) secondary antibody (diluted 1:2,000) was added and incubated at 37°C for 1 h. After the last washing, 100 μl of 0.1% (*w*/*v*) p-nitrophenyl phosphate (pNPP, Sigma) in 50 mmol L^{-1} carbonate bicarbonate buffer (pH 9.8) containing 0.5 mmol L^{-1} $MgCl_2$ was added and incubated at room temperature in the dark for 30 min. The reaction was stopped by 2 mol L^{-1} NaOH, and the absorbance was measured at 405 nm. The wells with 100 μl of TBS were used as blank. The assay was repeated at least five times under similar procedures. Samples with $P_{sample} - B_{blank}/N_{negative} - B_{blank}$ (P/N value) > 2.1 were considered positive (44, 45).

Phagocytosis Assay

Phagocytosis assay was performed according to previous report with modification (46). Microorganisms including *S. aureus*, *V. splendidus*, and *Y. lipolytica* were labeled with fluorescein isothiocyanate (FITC) to investigate the phagocytosis. All the microorganisms were grown to mid-log phase and harvested by centrifugation at 6,000 × g for 15 min. Cells were fixed with 4% PFA for 10 min, washed with 0.1 M $NaHCO_3$ (pH 9.0) for three times, and then mixed with 1 mg mL^{-1} FITC (Sigma-Aldrich) in 0.1 M $NaHCO_3$ (pH 9.0) buffer at room temperature with continuous gentle stirring overnight.

Briefly, hemolymph was collected from 15 oysters (5 in each group) and then centrifuged at 800 × g for 10 min to harvest hemocytes. The hemocytes were resuspended with 200 μl modified Leibovitz L-15 media. For hemocyte phagocytic rate assay, the hemocytes suspension was mixed with 20 μl of microbe culture ($OD_{600} = 0.6$, suspended in Tris–HCl) together with anti-CgCD63H and incubated in the dark for 1 h. The phagocytosis rate and phagocytosis index (mean FITC fluorescent intensity) were evaluated by FACScan flow cytometry (evaluated by BD, USA) following a previous research (47). PBS was used as blank control, and rTrx and negative serum were employed as negative controls. There were three replicates in each sampling. For the recruitment of *Cg*CD63H to *Y. lipolytica*-containing phagosomes assay, the hemocyte suspension was mixed with 20 μl of microbe culture ($OD_{600} = 0.6$, suspended in Tris–HCl) and incubated in the dark for 1 h. Endogenic *Cg*CD63H was detected by anti-*Cg*CD63H and visualized by DyLight 594-labeled secondary antibody (red). FITC-labeled *Y. lipolytica* (green) was selected to elicit the phagosome in oyster hemocytes. The nucleus stained by DAPI was observed in blue. The signals were investigated via fluorescence confocal microscopy based on previous description.

Statistical Analysis

All data were given as means ± SE. The data were subjected to one-way analysis of variance (one-way ANOVA) followed by an unpaired, two-tailed *t*-test. Differences were considered significant at $p < 0.05$ and extremely significant at $p < 0.01$.

RESULTS

The Molecular Characters and Phylogeny of *Cg*CD63H

A cDNA fragment of 948 bp nucleotides representing the open reading frame (ORF) of *Cg*CD63H was amplified, which encoded a polypeptide of 315 amino acids with a molecular weight of 35.4 kDa and a theoretical isoelectric point of 5.37. There were four characteristic transmembrane (TM) domains, a short extracellular loop and a large extracellular loop identified in *Cg*CD63H (**Supplementary Figures 1, 2**). Additionally, conserved CCG motif and Cys residues were revealed in the large extracellular loop of *Cg*CD63H (**Figure 1B**). In bioinformatics prediction of post-translational modifications, five phosphorylation sites and six O-linked glycosylation sites were detected but no N-linked glycosylation and methylation site (**Supplementary Figures 3–6**).

On the basis of the multiple sequences alignment of tetraspanins, an unrooted phylogenetic tree was constructed by using the neighbor joining (NJ) method (**Figure 1A**). *Cg*CD63H and 37 homologs from other species were clustered into nine groups, including CD63, CD151, CD53, CD82, CD37, CD81, CD9, TSP3, and TSP6 groups (**Figure 1A**). *Cg*CD63H was successively bunched together with CD63s from mollusks and arthropods and then assigned into CD63 subgroup in vertebrates.

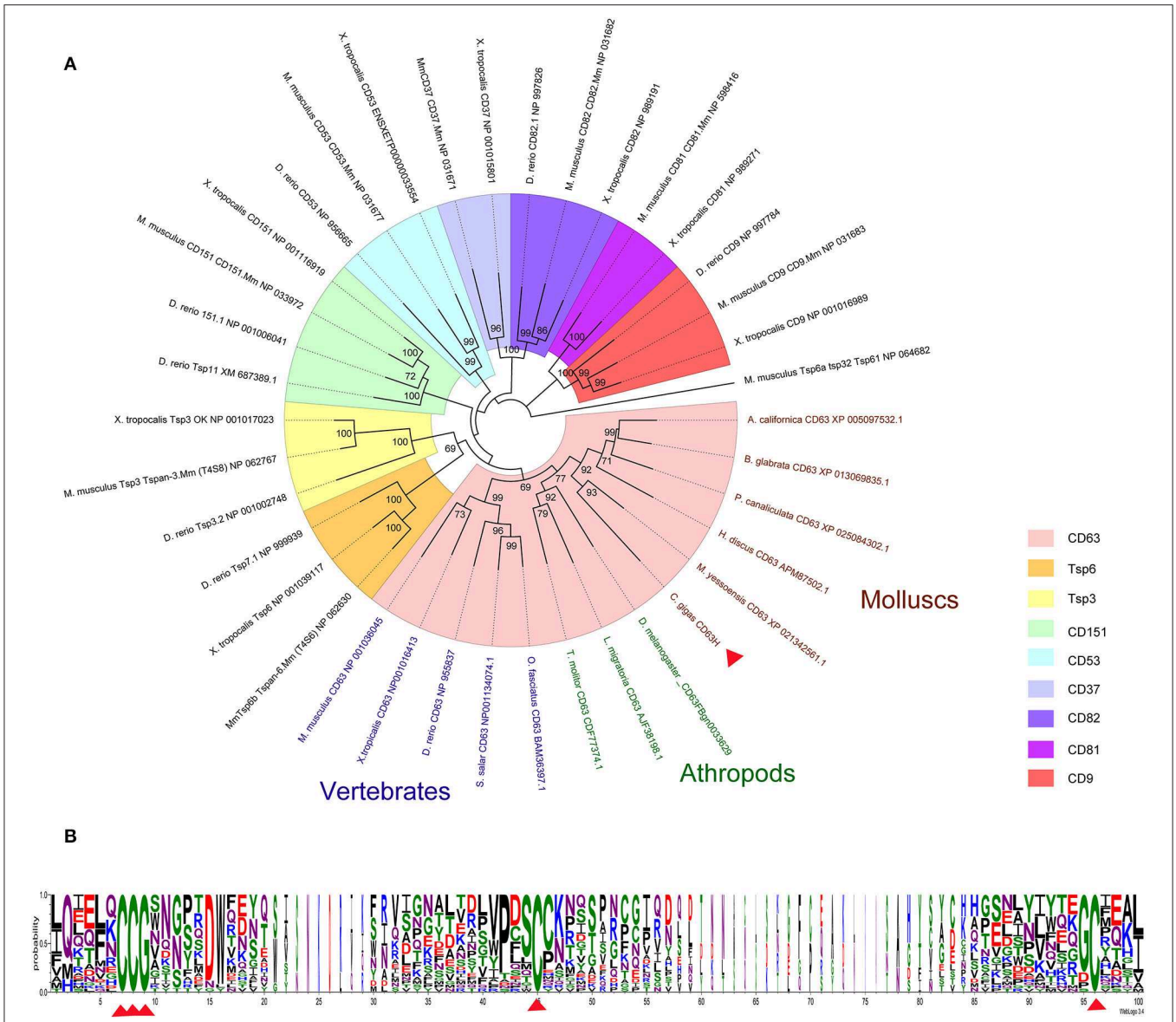

FIGURE 1 | Phylogenetic analysis of *Cg*CD63H. The homologs of *Cg*CD63H from vertebrates (*Mus musculus*, *Xenopus tropicalis*, *Danio rerio*, *Salmo salar*, and *Oplegnathus fasciatus*) and invertebrates (*Drosophila melanogaster*, *Tenebrio molitor*, *Locusta migratoria*, *Haliotis discus discus*, *Aplysia californica*, *Biomphalaria glabrata*, *Pomacea canaliculata*, and *Mizuhopecten yessoensis*) were retrieved from the National Center for Biotechnology Information (**Supplementary Data 1**). **(A)** The unrooted tree was constructed by the neighbor-joining (NJ) algorithm using the Mega 6.06 program based on the multiple sequence alignment by ClustalW. The reliability of the branching was tested by bootstrap (1,000 replicates). Red arrow head indicated *Cg*CD63H. **(B)** The conserved residues and motifs in large extracellular loop were analyzed based on the multiple sequence alignment.

The Tissue Distribution of *Cg*CD63H mRNA

The qRT-PCR was employed to investigate the distribution of *Cg*CD63H mRNA transcripts in different tissues of oysters. A single peak was revealed in the dissociation curve analysis, indicating the amplification specificity for both *Cg*CD63H and *Cg*EF1-α (data not shown). The *Cg*CD63H mRNA transcripts were detected in all the tested tissues (**Figure 2**). A significantly higher *Cg*CD63H expression was observed in hepatopancreas, labial palps, gill, and hemocytes, which was 354.9-fold ($p < 0.01$), 302.7-fold ($p < 0.01$), 279.7-fold ($p < 0.01$), and 240.7-fold ($p < 0.01$) of that in mantle, respectively. The relative expression level of *Cg*CD63H mRNA in the gonad was 1.3-fold ($p < 0.01$) of that in mantle.

The Temporal Expression of *Cg*CD63H mRNA in Hemocytes After *V. splendidus* Stimulation

The qRT-PCR was also used to detect the expression level of *Cg*CD63H mRNA in oyster hemocytes challenged by alive

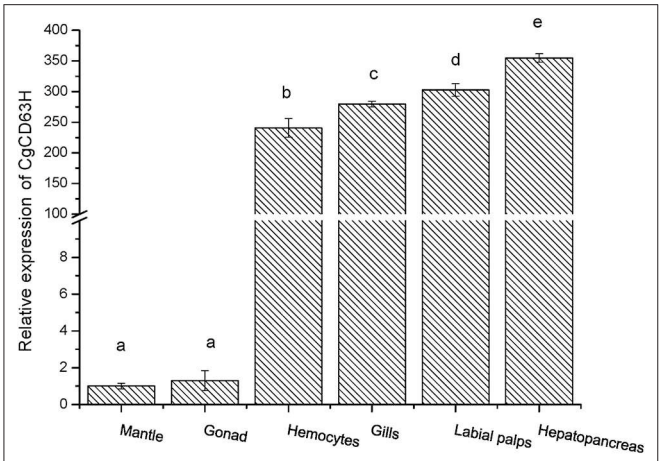

FIGURE 2 | Tissue distribution of the *Cg*CD63H transcripts. *Cg*CD63H relative messenger RNA (mRNA) expression level in mantle, gonad, hemocytes, gills, labial palps, and hepatopancreas was normalized to that of *Cg*EF1-α. Each value was shown as mean ± SE ($N = 6$), and bars with different letters were significantly different ($p < 0.01$).

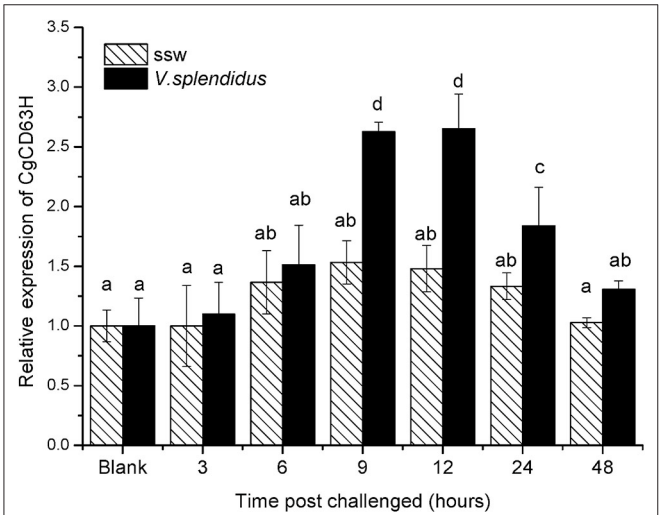

FIGURE 3 | Temporal expression profile of *Cg*CD63H messenger RNA (mRNA) post-*V. splendidus* challenge. Oyster hemocytes were employed to analyze *Cg*CD63H expression, at 0, 3, 6, 12, 24, and 48 h after *V. splendidus* challenge. Comparison of the level of *Cg*CD63H mRNA (relative to *Cg*EF1-α) was normalized to 0 h, which was indicated as "relative expression level of *Cg*CD63H." The values were shown as mean ± SE ($n = 6$), and bars with different letters were significantly different ($p < 0.01$).

V. splendidus (**Figure 3**). The *Cg*CD63H transcripts were significantly upregulated at 9 h after *V. splendidus* challenge (1.71-fold compared to that in the control group, $p < 0.01$) and reached the maximum level (1.79-fold, $p < 0.01$) at 12 h, and then dropped back to the original level at 24 h (1.38-fold, $p < 0.01$). While no significant change on the expression level of *Cg*CD63H mRNA was observed in the control group during the experiment.

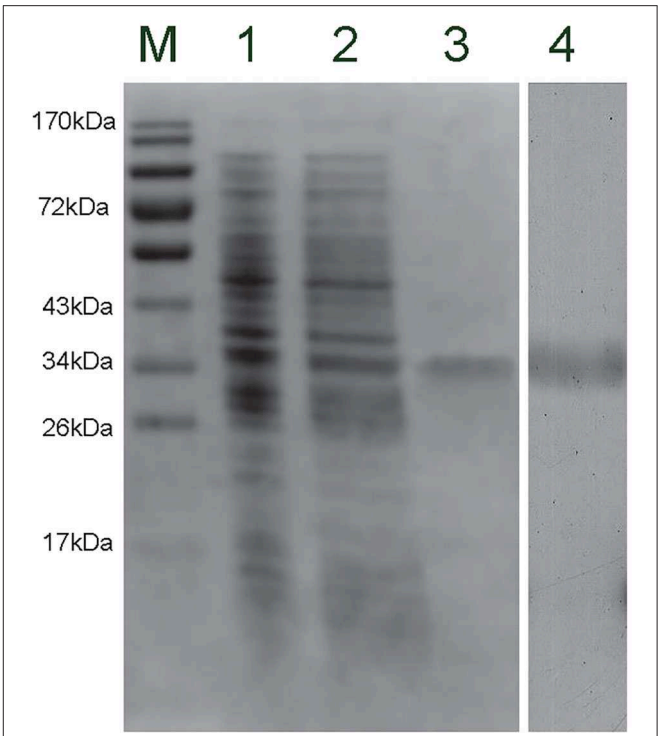

FIGURE 4 | Sodium dodecyl sulfate–polyacrylamide gel electrophoresis (SDS-PAGE) and Western blot analysis of *Cg*CD63H. Lane M, protein molecular standard; lane 1, negative control for *Cg*CD63H (without induction); lane 2, induced r*Cg*CD63H; lane 3, purified r*Cg*CD63H; lane 4, Western blot using purified anti-*Cg*CD63H based on the hemocytes lysate sample.

The Recombinant Protein and Antibody of *Cg*CD63H

The recombinant plasmid (pET-30a-*Cg*CD63H) was transformed into *E. coli* Transetta (DE3). After IPTG induction for 4 h, the whole cell lysate was analyzed by SDS-PAGE, and a distinct band with a molecular mass of 35 kDa was revealed (lane 3), which was in consistence with the predicted molecular mass of fusion recombinant protein of *Cg*CD63H with His-tag (**Figure 4**, lane 3). As control, no visible targeted band was detected in the group of cell lysate without IPTG induction. A polyclonal antibody against r*Cg*CD63H was prepared, and Western blotting analysis revealed a distinct single immune-precipitated band with a similar molecular weight predicted by the target sequence. This result suggested a high binding specificity of the polyclonal antibody against *Cg*CD63H (**Figure 4**, lane 4).

Subcellular Localization of *Cg*CD63H in Oyster Hemocytes

Fluorescence confocal microscopy was employed to detect the localization of endogenous *Cg*CD63H in oyster hemocytes (**Figure 5** and **Supplementary Figure 7**). The nucleus stained by DAPI was observed in blue, and the plasma membrane stained by DiI was observed in red. The *Cg*CD63H immunoreactive area was stained in green.

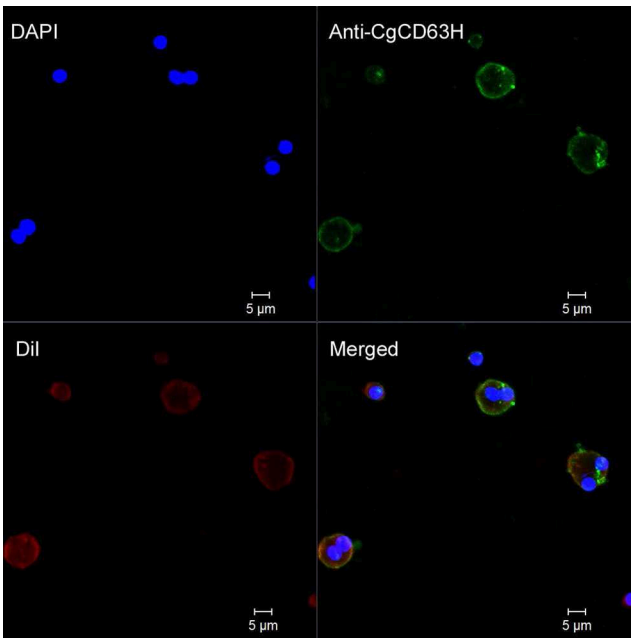

FIGURE 5 | Subcellular localization of *Cg*CD63H protein in oyster hemocytes. Binding of antibody to *Cg*CD63H was visualized by Alexa 488-labeled secondary antibody (green); the nucleus of hemocytes was stained with DAPI (blue), bar = 5 μm.

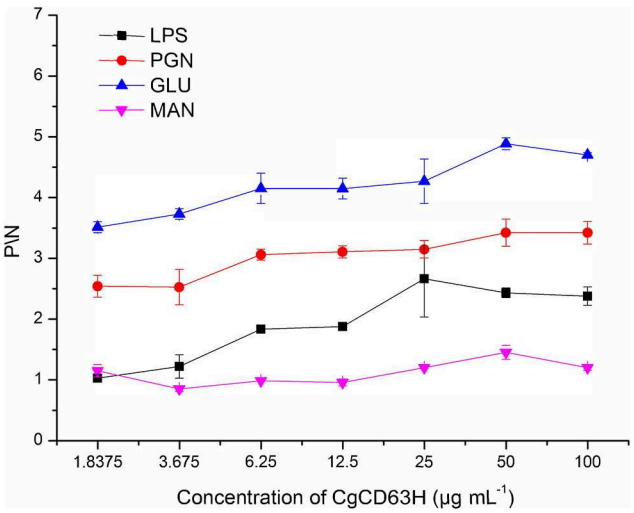

FIGURE 6 | ELISA analysis of the interaction between *Cg*CD63H and the pathogen-associated molecular patterns (PAMPs). Plates were coated with LPS, PGN, GLU, and MAN, and then incubated with a series of concentrations of r*Cg*CD63H and rTrx at the presence of lyophilized hemolymph at 18°C for 2 h. After incubated with anti-*Cg*CD63H, the interaction was detected with goat antimouse Ig-alkaline phosphatase conjugate at 405 nm. Samples with P/N ($P_{sample} - B_{blank}/N_{negative} - B_{blank}$) > 2.1 were considered positive. Results are representative of the mean of three replicates ± SE.

The positive signal of CgCD63H appeared mainly over the plasma membrane of some oyster hemocytes (**Figure 5** and **Supplementary Figure 7**).

Binding Capacity of r*Cg*CD63H to Various PAMPs

The binding assay of r*Cg*CD63H to various PAMPs in the presence of lyophilized hemolymph was performed based on the OD_{405} value. The samples with P/N ($P_{sample} - B_{blank}/N_{negative} - B_{blank}$) > 2.1 were considered as positive (**Figure 6**). No positive value was detected in the absence of lyophilized hemolymph (data not shown). After the addition of lyophilized hemolymph, the P/N values of r*Cg*CD63H toward GLU, PGN, and LPS were all >2.1, under the minimum protein concentration of 1.8375, 1.8375, and 25 μg ml^{-1}, respectively (**Figure 6**). r*Cg*CD63H possessed affinity to GLU, PGN, and LPS in a dose-dependent manner. The r*Cg*CD63H exhibited relatively higher affinity to GLU and PGN while lower affinity to LPS. The P/N values of r*Cg*CD63H for MAN were all <2.1 under the concentration of 1.8375 to 100 μg ml^{-1} (**Figure 6**).

Recruitment of *Cg*CD63H to *Y. lipolytica*-Containing Phagosomes

The recruitment of *Cg*CD63H after a phagocytic stimulus was investigated via fluorescence confocal microscopy (**Figure 7**). FITC-labeled *Y. lipolytica* (green) was selected to elicit the phagosome in oyster hemocytes. The nucleus stained by DAPI was observed in blue. Endogenic *Cg*CD63H was detected by anti-*Cg*CD63H and visualized by DyLight 594-labeled secondary antibody (red). In the absence of phagocytic stimulus, *Cg*CD63H-positive signal was detected on the surface of oyster hemocytes (**Figure 5**). After 1 h incubation with *Y. lipolytica*, *Cg*CD63H was highly enriched on the *Y. lipolytica*-containing phagosomes (**Figure 7**).

The Change of Hemocyte Phagocytic Rate Post-anti-*Cg*CD63H Incubation

Phagocytosis assay was performed on the basis of flow cytometry to test the phagocytic rate and phagocytic index of hemocytes after they were incubated with anti-*Cg*CD63H (**Figure 8**). The phagocytic rates of hemocyte toward Gram-negative bacteria *V. splendidus* and fungi *Y. lipolytica* were significantly down-regulated after they were incubated with anti-*Cg*CD63H, which were 0.60- and 0.86-fold ($p < 0.01$) compared to that of negative control group, respectively. However, in the Gram-positive bacteria *S. aureus* group, no significant change was observed after the hemocytes were incubated with anti-*Cg*CD63H compared to the negative control. The change in phagocytic index (mean FITC fluorescent intensity) indicated the same trend (**Supplementary Figure 8**). The phagocytic indices were 1.67×10^4, 2.15×10^4, and 4.69×10^4 in the negative control group, and 1.78×10^4, 1.30×10^4, and 3.88×10^4 in the anti-*Cg*CD63H blocking group for *S. aureus*, *V. splendidus*, and *Y. lipolytica*, respectively. Significant downregulation of phagocytic index after incubation with anti-*Cg*CD63H was detected in the *V. splendidus* and *Y. lipolytica* group, rather than in the *S. aureus* group.

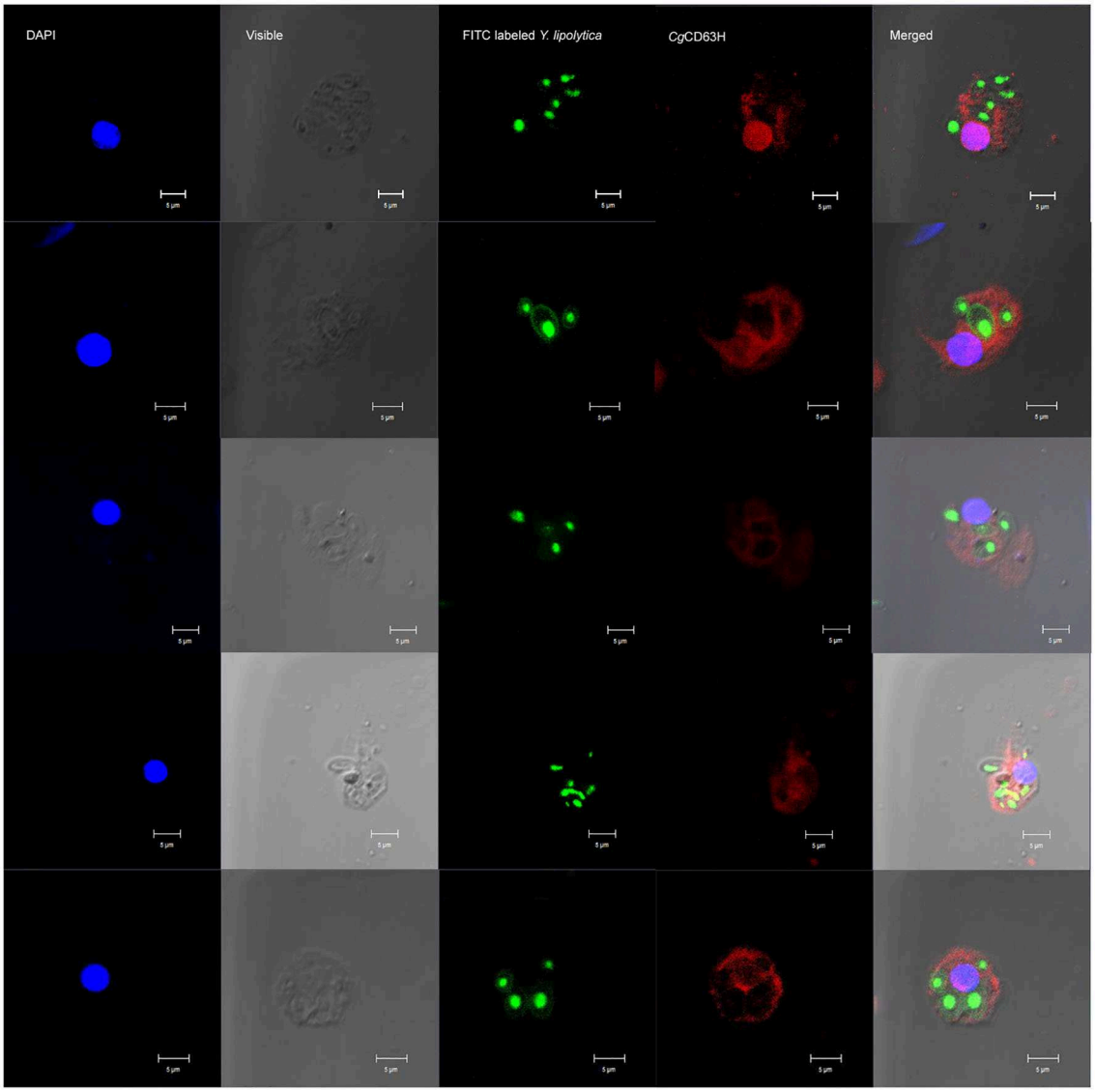

FIGURE 7 | Specific recruitment of *Cg*CD63H to the *Y. lipolytica*-containing phagosomes. Fluorescein isothiocyanate (FITC)-labeled *Y. lipolytica* was selected to investigate the phagosome recruitment; the cell membrane and nucleus of *Y. lipolytica* were indicated with green signal. The hemocyte suspension was mixed with 20 μl of *Y. lipolytica* (OD_{600} = 0.6, suspended in Tris–HCl) and incubated in the dark for 1 h. Antibody anti-*Cg*CD63H was employed to detect the endogenic *Cg*CD63H. Binding of antibody to *Cg*CD63H was visualized by DyLight 594-labeled secondary antibody (red); the nucleus of hemocytes was stained with 4′,6-diamidino-2-phenylindole (DAPI) (blue), bar = 5 μm.

DISCUSSION

CD63, as a member of tetraspanins, is an evolutionarily conserved protein family involved in multiple aspects of cellular physiological regulation (3, 4, 48). Although tetraspanins has been reported in a wide range of organisms, the functions of CD63 in invertebrate are, however, yet to be discovered (8). In the present study, a homolog of CD63 (designated *Cg*CD63H) was identified from genome database of oyster *C. gigas* with an open reading frame (ORF) of 948 bp encoding a polypeptide of 315 amino acids. The predicated amino acid sequence of *Cg*CD63H consists of four typical TM domains, a short extracellular loop, and a large extracellular loop. Additionally, a CCG motif and several Cys residues were identified in the large extracellular loop of *Cg*CD63H, which were highly conserved structural features of the previously reported CD63s (8, 22). Coincidentally, *Cg*CD63H was bunched together with CD63 homologs from invertebrates and vertebrates in an unrooted phylogenetic tree. These similar structure characters and reasonable phylogenetic relationships indicated that *Cg*CD63H was a member of the CD63 subfamily in mollusks, and it might function similarly to other CD63s.

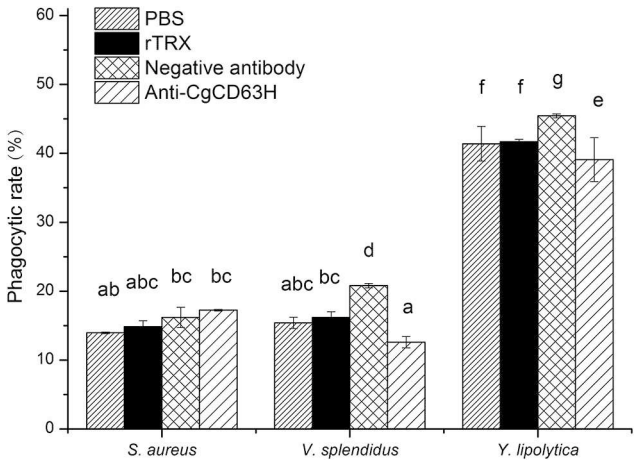

FIGURE 8 | Hemocyte phagocytosis rate post-incubation of anti-*Cg*CD63H. Oyster hemocytes were employed to analyze the change in hemocytes' phagocytosis rate against *S. aureus, V. splendidus*, and *Y. lipolytica* post-incubation of anti-*Cg*CD63H. Fluorescein isothiocyanate (FITC)-labeled microbe, anti-*Cg*CD63H, and hemocytes were mixed and incubated for 1 h in dark. Recombinant protein rTRX and negative antibody were employed as negative controls. For each treatment, assay was performed in three different replicates for statistical analysis ($p < 0.01$).

CD63 has been reported to facilitate the immune response of various organisms (49). In the present study, CgCD63H was found to distribute in a wide range of tissues of *C. gigas* including the hepatopancreas, mantle, gonad, labial palps, gills, as well as hemocytes. The highest expression level of *Cg*CD63H was detected in the hepatopancreas, which was deemed as one of the most important tissues involved in the innate immune defense of mollusks (50). Labial palps, gills, as well as hemocytes were also deemed as important tissues involved in the innate immune defense of mollusks (51–53). The universal distribution of *Cg*CD63H in immune-related tissues led us to further investigate its roles in the immune response. The circulating hemocytes play indispensable roles in the immune response of mollusks against invading pathogens (51). *Cg*CD63H protein was typically distributed over the plasma membrane of oyster hemocytes. Moreover, the expression level of *Cg*CD63H mRNA in hemocytes increased significantly ($p < 0.01$) and reached the highest levels at 12 h after *V. splendidus* stimulation. In our previous publication, the transcriptome profiles of *C. gigas* in response to PAMP treatments were investigated by RNA-seq (54). Based on the published data (NCBI: SRR3110857), the temporal expressions of *Cg*CD63H were found to be significantly upregulated post-LPS stimulation (fold change = 2.07, $q = 0$), PGN (fold change = 1.74, $q = 7.44E\text{-}16$), and GLU (fold change = 1.57, $q = 7.91E\text{-}07$), indicating the potential role of *Cg*CD63H in the immune response against invading Gram-positive bacteria, Gram-negative bacteria, and fungi. The increased expression of CD63 in response to immune stimulation was depicted as its incipient character in immune response by multiple reports (25, 33). These results suggested that *Cg*CD63H could play important roles in immune defense of oysters against invading pathogens.

Immune recognition is the first step of immune response of mollusk which could discriminate non-self- from self-substances (55). Previous work has shown that mutual recognition between membrane receptors and pathogens leads to receptor clustering and membrane protrusions, which eventually enable microbial engulfment. Several mammalian tetraspanins including CD63 are reported to participate in the recognition of PAMPs through the binding activity with PRRs and tetraspanins traffic at the cell surface (11, 56). In invertebrates, CD63 is also suspected to function in recognition process with evidences of the upregulation of mRNA expression after PAMP stimulation (22). Here, *Cg*CD63H was found to bind GLU, PGN, and LPS only in the presence of lyophilized hemolymph, indicating that *Cg*CD63H could combine PAMPs in an indirect manner, possibly with the assistance of other possible PRRs. Earlier reports have demonstrated that CD63 and CD37 could interact with the C-type lectin Dectin-1, identified as fungi-PRR, through "tetraspanin web" and then initiate the antifungal immune responses *in vivo* (17, 57). A CD63 homolog from coleopteran beetle was also reported to possess the possible binding ability to PGN and GLU (49). The results supported that *Cg*CD63H could be involved in the regulation of immune recognition through the interaction of other PRRs within the "tetraspanin web," for instance possible lectins or Ig domain containing cell adhesion molecules (IgCAMs). Since the recognition of the foreign invaders was the first step to initiate the immune response (58), the broad binding spectrum of *Cg*CD63H might endow it with a PRR partner role to organize PRRs on the cell membrane and induce the subsequent downstream immune responses against various intruders in oyster.

The previous reports have confirmed the effect of tetraspanins on phagocytosis in mammals (59–61). As a representative of tetraspanins, CD63 promotes the binding of outer segment particle through the interaction with specific PRRs instead of functioning as a direct receptor (57). In invertebrates, CD63 from calm *P. undulata* also plays roles in hemocyte-mediated phagocytosis (23). In the present study, *Cg*CD63H was recruited to the *Y. lipolytica*-containing phagosomes in the hemocytes of oysters after incubation with *Y. lipolytica*, which was similar to the previous observation in mammalian tetraspanins. The CD63 and CD82 were redistributed after immune stimulation and rapidly recruited to the membrane of nascent *C. neoformans*-containing phagosomes (19, 21). Additionally, in **Figure 5**, some positive signal of CgCD63H was found inside of the cell membrane, which might be caused by the phagocytosis of mixed debris in open circulatory system and resident microbiota, and the recruitment of *Cg*CD63H. Meanwhile, the phagocytosis of hemocytes against *V. splendidus* and *Y. lipolytica* was significantly inhibited after the incubation with anti-*Cg*CD63H. It was suspected that *Cg*CD63H promoted the phagocytosis through the interaction with multiple possible PRRs with its microdomains instead of acting as a direct invader binding receptor. In mammals, the interaction between tetraspanins and PRRs, such as CD81 and Toll-like receptor 4 (TLR-4) (62), was reported to be necessary in macrophage activation. Likewise, in invertebrates, the integrin–tetraspanin interaction was also observed in *M. sexta*, and the monoclonal antibody

of tetraspanin CD76 could disturb the encapsulation of the invader, *Serratia marcescens* (35). An increasing body of evidence suggests that phagocytes play important roles in invertebrate innate immune responses. Cells of phagocytes were classified efficiently from the oyster *C. gigas*, which possess both potent oxidative killing and microbial disintegration capacities (63). Additionally, no significant change of phagocytic rate was found after the hemocytes were incubated with anti-*Cg*CD63H in the Gram-positive bacteria *S. aureus* group. It has been reported that PFAs have effects on some microbes (64). It was suspected that PFA might have impacts on *S. aureus* during FITC labeling, which influenced the immune response of oyster. Moreover, there might be other molecules involved in the phagocytosis toward *S. aureus*, and the phagocytic efficiency did not change significantly even though *Cg*CD63H was blocked by the antibody. As the phagocytosis of oyster hemocytes could be initiated by the recognition of invaders, the recruitment of *Cg*CD63H to the phagosome membrane further suggested the possible interaction between *Cg*CD63H and recognition receptors, as well as the partner roles of *Cg*CD63H in sensing the microbial content of phagosomes and eliciting an appropriate immune response. The difference in the PRRs interacting with CgCD63H may affect the specificity and efficiency in the immune response against different microbes. In the present study, *Cg*CD63H was found to enhance the phagocytosis of *V. splendidus* and *Y. lipolytic* other than *S. aureus*. These results indicated that *Cg*CD63H could interact with the PRRs against *V. splendidus* and *Y. lipolytic* with a higher affinity and promote a more efficient cellular immunity.

In conclusion, a member of the molluscan CD63 subfamily, *Cg*CD63H, was identified from *C. gigas*. *Cg*CD63H mRNA was mainly expressed in immune tissues and induced by the challenge of *V. splendidus*. The *Cg*CD63H exhibited binding activities to a wide spectrum of PAMPs in the presence of lyophilized hemolymph. Moreover, *Cg*CD63H was recruited to the *Y. lipolytica*-containing phagosomes of hemocytes after immune stimulation, and the phagocytosis of hemocytes was significantly inhibited after incubation with anti-*Cg*CD63H. All these results collectively indicated that *Cg*CD63H might function as a "gateway" between the pattern recognition of foreign invaders and the subsequent immune responses in oysters. CgCD63H could also be a promising marker in cell typing of phagocytic lines in *C. gigas*.

DATA AVAILABILITY STATEMENT

The raw data supporting the conclusions of this article will be made available by the authors, without undue reservation, to any qualified researcher.

ETHICS STATEMENT

This animal study was reviewed and approved by Ethics Committee of the Institute of Oceanology, Chinese Academy of Sciences.

AUTHOR CONTRIBUTIONS

CL carried out cloning, expression, and purification of recombinant proteins as well as PAMP binding analyses. CY and SJ performed phagocytosis and flow cell cytometry analysis, while QY, WW, and MW carried out bioinformatics analyses. CL, LW, and LS designed the research and wrote the manuscript. All authors contributed to the article and approved the submitted version.

FUNDING

This research was supported by the National Key R&D Program (2018YFD0900606), grants (Nos. U1706204 and 41961124009) from the National Science Foundation of China, earmarked fund from Modern Agro-Industry Technology Research System (CARS-49) and the Fund for Outstanding Talents and Innovative Team of Agricultural Scientific Research from the Ministry of Agriculture and Rural Affairs in China, the Distinguished Professor of Liaoning (to LS), AoShan Talents Cultivation Program Supported by Qingdao National Laboratory for Marine Science and Technology (No. 2017ASTCP-OS13), Liaoning Climbing Scholar (to LS), the Distinguished Professor of Liaoning (XLYC1902012), Dalian High Level Talent Innovation Support Program (2015R020), and the Research Foundation for Talented Scholars in Dalian Ocean University (to LW).

SUPPLEMENTARY MATERIAL

The Supplementary Material for this article can be found online at: https://www.frontiersin.org/articles/10.3389/fimmu.2020.01379/full#supplementary-material

REFERENCES

1. Berditchevski F. Complexes of tetraspanins with integrins: more than meets the eye. *J Cell Sci*. (2001) 114(Pt 23):4143–51.
2. Wright M, Moseley G, Van Spriel A. Tetraspanin microdomains in immune cell signalling and malignant disease. *Tissue Antigens*. (2004) 64:533–42. doi: 10.1111/j.1399-0039.2004.00321.x
3. Wright MD, Ni J, Rudy GB. The L6 membrane proteins a new four-transmembrane superfamily. *Protein Sci*. (2000) 9:1594–600. doi: 10.1110/ps.9.8.1594
4. Wright MD, Tomlinson MG. The ins and outs of the transmembrane 4 superfamily. *Immunol Today*. (1994) 15:588–94. doi: 10.1016/0167-5699(94)90222-4
5. Charrin S, Le Naour F, Silvie O, Milhiet P, Boucheix C, Rubinstein E. Lateral organization of membrane proteins: tetraspanins spin their web. *Biochem J*. (2009) 420:133–54. doi: 10.1042/BJ20082422
6. Hemler ME. Tetraspanin functions and associated microdomains. *Nat Rev Mol Cell Bio*. (2005) 6:801–11. doi: 10.1038/nrm1736
7. Monk PN, Partridge LJ. Tetraspanins-gateways for infection. *Infect Disord Drug Targets*. (2012) 12:4–17. doi: 10.2174/187152612798994957
8. Garcia-España A, Chung PJ, Sarkar IN, Stiner E, Sun TT, DeSalle R. Appearance of new tetraspanin genes during vertebrate evolution. *Genomics*. (2008) 91:326–34. doi: 10.1016/j.ygeno.2007.12.005
9. Huang S, Yuan S, Dong M, Su J, Yu C, Shen Y, et al. The phylogenetic analysis of tetraspanins projects the evolution of cell-cell interactions

from unicellular to multicellular organisms. *Genomics*. (2005) 86:674–84. doi: 10.1016/j.ygeno.2005.08.004
10. Hemler ME. Tetraspanin proteins mediate cellular penetration, invasion, and fusion events and define a novel type of membrane microdomain. *Annu Rev Cell Dev Biol.* (2003) 19:397–422. doi: 10.1146/annurev.cellbio.19.111301.153609
11. Rubinstein E, Le Naour F, Lagaudrière-Gesbert C, Billard M, Conjeaud H, Boucheix C. CD9, CD63, CD81, and CD82 are components of a surface tetraspan network connected to HLA-DR and VLA integrins. *Eur J Immunol.* (1996) 26:2657–65. doi: 10.1002/eji.1830261117
12. Sanyal M, Fernandez R, Levy S. Enhanced B cell activation in the absence of CD81. *Int Immunol.* (2009) 21:1225–37. doi: 10.1093/intimm/dxp090
13. Figdor CG, van Spriel AB. Fungal pattern-recognition receptors and tetraspanins: partners on antigen-presenting cells. *Trends Immunol.* (2010) 31:91–6. doi: 10.1016/j.it.2009.11.005
14. Levy S, Shoham T. The tetraspanin web modulates immune-signalling complexes. *Nat Rev Immunol.* (2005) 5:136–48. doi: 10.1038/nri1548
15. Pols MS, Klumperman J. Trafficking and function of the tetraspanin CD63. *Exp cell Res.* (2009) 315:1584–92. doi: 10.1016/j.yexcr.2008.09.020
16. Bonifacino JS, Traub LM. Signals for sorting of transmembrane proteins to endosomes and lysosomes. *Ann Rev Biochem.* (2003) 72:395–447. doi: 10.1146/annurev.biochem.72.121801.161800
17. Meyer-Wentrup F, Figdor CG, Ansems M, Brossart P, Wright MD, Adema GJ, et al. Dectin-1 interaction with tetraspanin CD37 inhibits IL-6 production. *J Immunol*. (2007) 178:154–62. doi: 10.4049/jimmunol.178.1.154
18. Jones E, Demaria M, Wright M. Tetraspanins in cellular immunity. *Biochem Soc Trans.* (2011) 39:506. doi: 10.1042/BST0390506
19. Artavanis-Tsakonas K, Love JC, Ploegh HL, Vyas JM. Recruitment of CD63 to *Cryptococcus neoformans* phagosomes requires acidification. *Proc Natl Acad Sci USA*. (2006) 103:15945–50. doi: 10.1073/pnas.0607528103
20. Suzuki M, Tachibana I, Takeda Y, He P, Minami S, Iwasaki T, et al. Tetraspanin CD9 negatively regulates lipopolysaccharide-induced macrophage activation and lung inflammation. *J Immunol.* (2009) 182:6485–93. doi: 10.4049/jimmunol.0802797
21. Artavanis-Tsakonas K, Kasperkovitz PV, Papa E, Cardenas ML, Khan NS, Van der Veen AG, et al. The tetraspanin CD82 is specifically recruited to fungal and bacterial phagosomes prior to acidification. *Infect Immun*. (2011) 79:1098–106. doi: 10.1128/IAI.01135-10
22. Priyathilaka TT, Bathige SDNK, Herath HMLPB, Lee S, Lee J. Molecular identification of disk abalone (Haliotis discus discus) tetraspanin 33 and CD63: Insights into potent players in the disk abalone host defense system. *Fish Shellfish Immunol.* (2017) 69:173–84. doi: 10.1016/j.fsi.2017.08.020
23. Yu M, Yang S, Sun H, Xia Q. CD63 promotes Hemocyte-mediated phagocytosis in the clam, *Paphia undulata. J. Immunol. Res.* (2016) 2016:7893490. doi: 10.1155/2016/7893490
24. Moribe H, Yochem J, Yamada H, Tabuse Y, Fujimoto T, Mekada E. Tetraspanin protein (TSP-15) is required for epidermal integrity in *Caenorhabditis elegans*. *J Cell Sci.* (2004) 117:5209–20. doi: 10.1242/jcs.01403
25. Luo M, Ye S, Xu T, Wu X, Yang P. Molecular characterization of a novel tetraspanin from the oyster, *Crassostrea ariakensis*: variation, localization and relationship to oyster host defense. *Fish Shellfish Immunol*. (2012) 33:294–304. doi: 10.1016/j.fsi.2012.05.009
26. Todres E, Nardi J, Robertson H. The tetraspanin superfamily in insects. *Insect Mol Biol.* (2000) 9:581–90. doi: 10.1046/j.1365-2583.2000.00222.x
27. Konno A, Padma P, Ushimaru Y, Inaba K. Multidimensional analysis of uncharacterized sperm proteins in *Ciona intestinalis*: EST-based analysis and functional immunoscreening of testis-expressed genes. *Zool Sci.* (2010) 27:204–15. doi: 10.2108/zsj.27.204
28. Wang Y, Wang M, Wang B, Liu M, Jiang K, Hou X, et al. A preliminary attempt to explore the potential functions of a tetraspanin gene (MmTSPAN) in the innate immunity of hard clam *Meretrix meretrix*: sequence features and expression profiles. *Fish Shellfish Immunol.* (2019) 88:135–41. doi: 10.1016/j.fsi.2019.01.048
29. Zhu XJ, Yang X, He W, Xiong Y, Liu J, Dai ZM. Involvement of tetraspanin 8 in the innate immune response of the giant prawn, *Macrobrachium rosenbergii*. *Fish Shellfish Immunol*. (2019) 86:459–64. doi: 10.1016/j.fsi.2018.11.055
30. Lau YT, Gambino L, Santos B, Espinosa EP, Allam B. Regulation of oyster (*Crassostrea virginica*) hemocyte motility by the intracellular parasite *Perkinsus marinus*: a possible mechanism for host infection. *Fish Shellfish Immunol.* (2018) 78:18–25. doi: 10.1016/j.fsi.2018.04.019
31. Morga B, Arzul I, Faury N, Segarra A, Chollet B, Renault T. Molecular responses of *Ostrea edulis* haemocytes to an *in vitro* infection with *Bonamia ostreae*. *Dev Comp Immunol.* (2011) 35:323–33. doi: 10.1016/j.dci.2010.10.005
32. Tanguy A, Guo X, Ford SE. Discovery of genes expressed in response to Perkinsus marinus challenge in Eastern (*Crassostrea virginica*) and Pacific (*C. gigas)* oysters. *Gene*. (2004) 338:121–31. doi: 10.1016/j.gene.2004.05.019
33. Wang B, Li F, Xiang J, Gui L, Luo Z, Yan H. Three tetraspanins from Chinese shrimp, *Fenneropenaeus chinensis*, may play important roles in WSSV infection. *J Fish Dis*. (2010) 33:15–29. doi: 10.1111/j.1365-2761.2009.01079.x
34. Boucheix C, Rubinstein E. Tetraspanins. *Cell Mol Life Sci*. (2001) 58:1189–205. doi: 10.1007/PL00000933
35. Zhuang S, Kelo L, Nardi JB, Kanost MR. An integrin-tetraspanin interaction required for cellular innate immune responses of an insect, *Manduca sexta*. *J Biol Chem.* (2007) 282:22563–72. doi: 10.1074/jbc.M700341200
36. Gueguen Y, Herpin A, Aumelas A, Garnier J, Fievet J, Escoubas JM, et al. Characterization of a defensin from the oyster *Crassostrea gigas* recombinant production, folding, solution structure, antimicrobial activities, and gene expression. *J Biol Chem*. (2006) 281:313–23. doi: 10.1074/jbc.M510850200
37. Yang S, Wu X. Identification and functional characterization of a human sTRAIL homolog, CasTRAIL, in an invertebrate oyster *Crassostrea ariakensis*. *Dev Comp Immunol.* (2010) 34:538–45. doi: 10.1016/j.dci.2009.12.014
38. Jiang S, Jia Z, Zhang T, Wang L, Qiu L, Sun J, et al. Functional characterisation of phagocytes in the Pacific oyster *Crassostrea gigas*. *PeerJ*. (2016) 4:e2590. doi: 10.7717/peerj.2590
39. Liu R, Qiu L, Yu Z, Zi J, Yue F, Wang L, et al. Identification and characterisation of pathogenic *Vibrio splendidus* from Yesso scallop (*Patinopecten yessoensis*) cultured in a low temperature environment. *J Invertebr Pathol*. (2013) 114:144–50. doi: 10.1016/j.jip.2013.07.005
40. Zhang H, Kong P, Wang L, Zhou Z, Yang J, Zhang Y, et al. Cflec-5, a pattern recognition receptor in scallop Chlamys farreri agglutinating yeast *Pichia pastoris*. *Fish Shellfish Immunol*. (2010) 29:149–56. doi: 10.1016/j.fsi.2010.02.024
41. Livak KJ, Schmittgen TD. Analysis of relative gene expression data using real-time quantitative PCR and the 2– ΔΔCT method. *Methods*. (2001) 25:402–8. doi: 10.1006/meth.2001.1262
42. Cheng S, Zhan W, Xing J, Sheng X. Development and characterization of monoclonal antibody to the lymphocystis disease virus of Japanese flounder *Paralichthys olivaceus* isolated from China. *J Virol Methods*. (2006) 135:173–80. doi: 10.1016/j.jviromet.2006.03.016
43. Cao A, Mercado L, Ramos-Martinez JI, Barcia R. Primary cultures of hemocytes from *Mytilus galloprovincialis Lmk.*: expression of IL-2Rα subunit. *Aquaculture.* (2003) 216:1–8. doi: 10.1016/S0044-8486(02)00140-0
44. Yu Y, Yu Y, Huang H, Feng K, Pan M, Yuan S, et al. A short-form C-type lectin from amphioxus acts as a direct microbial killing protein via interaction with peptidoglycan and glucan. *J Immunol.* (2007) 179:8425–34. doi: 10.4049/jimmunol.179.12.8425
45. Xu J, Jiang S, Li Y, Li M, Cheng Q, Zhao D, et al. Caspase-3 serves as an intracellular immune receptor specific for lipopolysaccharide in oyster Crassostrea gigas. *Dev Comp Immunol.* (2016) 61:1–12. doi: 10.1016/j.dci.2016.03.015
46. Wootton E, Dyrynda E, Ratcliffe N. Bivalve immunity: comparisons between the marine mussel (*Mytilus edulis*), the edible cockle (*Cerastoderma edule*) and the razor-shell (*Ensis siliqua*). *Fish Shellfish Immunol*. (2003) 15:195–210. doi: 10.1016/S1050-4648(02)00161-4
47. Lv Z, Wang L, Jia Z, Sun J, Wang W, Liu Z, et al. Hemolymph C1qDC promotes the phagocytosis of oyster *Crassostrea gigas* hemocytes by interacting with the membrane receptor β-integrin. *Dev Comp Immunol*. (2019) 98:42–53. doi: 10.1016/j.dci.2019.04.004
48. Green LR, Monk PN, Partridge LJ, Morris P, Gorringe AR, Read RC. Cooperative role for tetraspanins in adhesin-mediated attachment of bacterial species to human epithelial cells. *Infect Immun.* (2011) 79:2241–9. doi: 10.1128/IAI.01354-10
49. Patnaik BB, Kang SM, Seo GW, Lee HJ, Patnaik HH, Jo YH, et al. Molecular cloning, sequence characterization and expression analysis of a CD63 homologue from the coleopteran beetle, *Tenebrio molitor*. *Int J Mol Sci.* (2013) 14:20744–67. doi: 10.3390/ijms141020744

50. Zhang H, Song X, Wang L, Kong P, Yang J, Liu L, et al. AiCTL-6, a novel C-type lectin from bay scallop *Argopecten irradians* with a long C-type lectin-like domain. *Fish Shellfish Immunol.* (2011) 30:17–26. doi: 10.1016/j.fsi.2009.12.019
51. Costa M, Prado-Álvarez M, Gestal C, Li H, Roch P, Novoa B, et al. Functional and molecular immune response of Mediterranean mussel (*Mytilus galloprovincialis*) haemocytes against pathogen-associated molecular patterns and bacteria. *Fish Shellfish Immunol.* (2009) 26:515–23. doi: 10.1016/j.fsi.2009.02.001
52. Yang C, Wang L, Zhang H, Wang L, Huang M, Sun Z, et al. A new fibrinogen-related protein from *Argopecten irradians* (*Ai*frep-2) with broad recognition spectrum and bacteria agglutination activity. *Fish Shellfish Immunol.* (2014) 38:221–9. doi: 10.1016/j.fsi.2014.03.025
53. Jing X, Espinosa EP, Perrigault M, Allam B. Identification, molecular characterization and expression analysis of a mucosal c-type lectin in the eastern oyster, *crassostrea virginica*. *Fish Shellfish Immunol.* (2011) 30:0–858. doi: 10.1016/j.fsi.2011.01.007
54. Wang L, Zhang H, Wang M, Zhou Z, Wang W, Liu R, et al. The transcriptomic expression of pattern recognition receptors: insight into molecular recognition of various invading pathogens in Oyster *Crassostrea gigas*. *Dev Comp Immunol.* (2019) 91:1–7. doi: 10.1016/j.dci.2018.09.021
55. Song L, Wang L, Zhang H, Wang M. The immune system and its modulation mechanism in scallop. *Fish Shellfish Immunol.* (2015) 46:65–78. doi: 10.1016/j.fsi.2015.03.013
56. Little KD, Hemler ME, Stipp CS. Dynamic regulation of a GPCR-tetraspanin-G protein complex on intact cells: central role of CD81 in facilitating GPR56-Gαq/11 association. *Mol Biol Cell.* (2004) 15:2375–87. doi: 10.1091/mbc.e03-12-0886
57. Mantegazza AR, Barrio MM, Moutel S, Bover L, Weck M, Brossart P, et al. CD63 tetraspanin slows down cell migration and translocates to the endosomal-lysosomal-MIICs route after extracellular stimuli in human immature dendritic cells. *Blood*. (2004) 104:1183–90. doi: 10.1182/blood-2004-01-0104
58. Wang XW, Wang JX. Diversity and multiple functions of lectins in shrimp immunity. *Dev Comp Immunol.* (2013) 39:27–38. doi: 10.1016/j.dci.2012.04.009
59. Dijkstra S, Geisert E, Dijkstra C, Bär P, Joosten E. CD81 and microglial activation in vitro: proliferation, phagocytosis and nitric oxide production. *J Neuroimmunol.* (2001) 114:151–9. doi: 10.1016/S0165-5728(01)00240-5
60. Chang Y, Finnemann SC. Tetraspanin CD81 is required for the αvβ5-integrin-dependent particle-binding step of RPE phagocytosis. *J Cell Sci.* (2007) 120:3053–63. doi: 10.1242/jcs.006361
61. Takeda Y, Tachibana I, Miyado K, Kobayashi M, Miyazaki T, Funakoshi T, et al. Tetraspanins CD9 and CD81 function to prevent the fusion of mononuclear phagocytes. *J Cell Biol.* (2003) 161:945–56. doi: 10.1083/jcb.200212031
62. Pfeiffer A, Böttcher A, Ors,ó E, Kapinsky M, Nagy P, Bodnár A, et al. Lipopolysaccharide and ceramide docking to CD14 provokes ligand-specific receptor clustering in rafts. *Eur J Immunol.* (2001) 31:3153–64. doi: 10.1002/1521-4141(200111)31:11<3153::AID-IMMU3153>3.0.CO;2-0
63. Jiang S, Qiu L, Wang L, Jia Z, Lv Z, Wang M, et al. Transcriptomic and quantitative proteomic analyses provide insights into the phagocytic killing of hemocytes in the oyster *Crassostrea gigas*. *Front Immunol.* (2018) 9:1280. doi: 10.3389/fimmu.2018.01280
64. Ribeiro-Sobrinho AP, Rabelo FL, Figueiredo CB, Alvarez-Leite JI, Nicoli JR, Uzeda M, et al. Bacteria recovered from dental pulp induce apoptosis of lymph node cells. *J Med Microbiol.* (2005) 54:413–6. doi: 10.1099/jmm.0.45728-0

Conflict of Interest: The authors declare that the research was conducted in the absence of any commercial or financial relationships that could be construed as a potential conflict of interest.

The reviewer LZ declared a shared affiliation, with no collaboration, with several of the authors CL, MW, and SJ, to the handling editor at the time of the review.

frontiers in Immunology

ORIGINAL RESEARCH
published: 12 November 2020
doi: 10.3389/fimmu.2020.544718

Non-Specific Antibodies Induce Lysosomal Activation in Atlantic Salmon Macrophages Infected by *Piscirickettsia salmonis*

*Diego Pérez-Stuardo[1], Allison Espinoza[1], Sebastián Tapia[1,2], Jonathan Morales-Reyes[2], Claudio Barrientos[2], Eva Vallejos-Vidal[3,4], Ana M. Sandino[2,4], Eugenio Spencer[2,4], Daniela Toro-Ascuy[5], J. Andrés Rivas-Pardo[1,6], Felipe E. Reyes-López[3] and Sebastián Reyes-Cerpa[1,6]**

[1] Centro de Genómica y Bioinformática, Facultad de Ciencias, Universidad Mayor, Santiago, Chile, [2] Consorcio Tecnológico de Sanidad Acuícola, Ictio Biotechnologies S.A., Santiago, Chile, [3] Department of Cell Biology, Physiology and Immunology, Universitat Autonoma de Barcelona, Bellaterra, Spain, [4] Centro de Biotecnología Acuícola, Facultad de Química y Biología, Universidad de Santiago de Chile, Santiago, Chile, [5] Laboratorio de Virología, Instituto de Ciencias Biomedicas, Facultad de Ciencias de la Salud, Universidad Autónoma de Chile, Santiago, Chile, [6] Escuela de Biotecnología, Facultad de Ciencias, Universidad Mayor, Santiago, Chile

OPEN ACCESS

Edited by:
Kim Dawn Thompson, Moredun Research Institute, United Kingdom

Reviewed by:
Irene Cano Cejas, Centre for Environment, Fisheries and Aquaculture Science (CEFAS), United Kingdom
Javier Santander, Memorial University of Newfoundland, Canada

***Correspondence:**
Sebastián Reyes-Cerpa
sebastian.reyes@umayor.cl

Specialty section:
This article was submitted to Comparative Immunology, a section of the journal Frontiers in Immunology

Received: *22 March 2020*
Accepted: *14 October 2020*
Published: *12 November 2020*

Citation:
Pérez-Stuardo D, Espinoza A, Tapia S, Morales-Reyes J, Barrientos C, Vallejos-Vidal E, Sandino AM, Spencer E, Toro-Ascuy D, Rivas-Pardo JA, Reyes-López FE and Reyes-Cerpa S (2020) Non-Specific Antibodies Induce Lysosomal Activation in Atlantic Salmon Macrophages Infected by Piscirickettsia salmonis. Front. Immunol. 11:544718. doi: 10.3389/fimmu.2020.544718

Piscirickettsia salmonis, an aggressive intracellular pathogen, is the etiological agent of salmonid rickettsial septicemia (SRS). This is a chronic multisystemic disease that generates high mortalities and large losses in Chilean salmon farming, threatening the sustainability of the salmon industry. Previous reports suggest that *P. salmonis* is able to survive and replicate in salmonid macrophages, inducing an anti-inflammatory environment and a limited lysosomal response that may be associated with host immune evasion mechanisms favoring bacterial survival. Current control and prophylaxis strategies against *P. salmonis* (based on the use of antibiotics and vaccines) have not had the expected success against infection. This makes it urgent to unravel the host-pathogen interaction to develop more effective therapeutic strategies. In this study, we evaluated the effect of treatment with IgM-beads on lysosomal activity in Atlantic salmon macrophage-enriched cell cultures infected with *P. salmonis* by analyzing the lysosomal pH and proteolytic ability through confocal microscopy. The impact of IgM-beads on cytotoxicity induced by *P. salmonis* in infected cells was evaluated by quantification of cell lysis through release of Lactate Dehydrogenase (LDH) activity. Bacterial load was determined by quantification of *16S* rDNA copy number by qPCR, and counting of colony-forming units (CFU) present in the extracellular and intracellular environment. Our results suggest that stimulation with antibodies promotes lysosomal activity by lowering lysosomal pH and increasing the proteolytic activity within this organelle. Additionally, incubation with IgM-beads elicits a decrease in bacterial-induced cytotoxicity in infected Atlantic salmon macrophages and reduces the bacterial load. Overall, our results suggest that stimulation of cells infected by *P. salmonis* with IgM-beads reverses the modulation of the lysosomal activity induced by bacterial infection,

promoting macrophage survival and bacterial elimination. This work represents a new important evidence to understand the bacterial evasion mechanisms established by *P. salmonis* and contribute to the development of new effective therapeutic strategies against SRS.

Keywords: macrophages, Atlantic salmon, IgM, *P. salmonis*, lysosome activity

INTRODUCTION

Piscirickettsia salmonis is the etiological agent of piscirickettsiosis or salmonid rickettsial septicemia (SRS), which mostly affects farmed salmonid species (1, 2). *Piscirickettsia salmonis* is a Gram-negative, non-motile, unencapsulated, pleomorphic, and usually coccoid bacterium, between 0.2 and 1.5 μm in diameter (1, 3, 4). It is an intracellular pathogen, classified phylogenetically as a *Gammaproteobacteria* in the family *Piscirickettsiaceae*, and closely related order to *Legionella*, *Francisella*, and *Coxiella* (1).

In Chile, the National Fisheries Service (SERNAPESCA, Servicio Nacional de Pesca) has identified SRS as the most serious health problem facing the Chilean salmon industry (5) owing to its highly aggressive nature, recurrent outbreaks, and widespread transmission among other cultivated salmonid species (6–9). In 2018, mortalities associated with *P. salmonis* represented 54.7% and 83.3% of the total mortalities attributed to infectious causes in Atlantic salmon (*Salmo salar* L.) and rainbow trout (*Oncorhynchus mykiss*), respectively (9). The control and prophylactic strategies against *P. salmonis* have relied on antibiotics and vaccines to date; however, both are inadequate. Antibiotics have been used indiscriminately to control outbreaks of infection. In 2018, the Chilean aquaculture industry alone utilized over 322 tons of antibiotics, mainly florfenicol and oxytetracycline (10). Moreover, infected salmonids respond poorly to these treatments, likely because of the intracellular characteristics of the infective cycle of *P. salmonis* and the insufficient concentrations of antibiotics that reach the intracellular niche to eliminate the bacterium (11). This situation is further complicated by the lack of effective vaccines against *P. salmonis* (12), because prophylactic vaccines do not provide acceptable levels of protection (11).

Despite the severe impact of *P. salmonis* on the Chilean aquaculture industry, key aspects of this bacterium, such as its life cycle and pathogenic mechanisms, are poorly characterized (13). It is reported that *P. salmonis* survives and replicates inside macrophage vacuoles (14) that do not mature to fuse them with lysosomes to degrade the pathogen (13, 15). Recently, we observed that macrophages infected by *P. salmonis* have a lower number of lysosomes in comparison with those incubated with inactivated *P. salmonis*; as a consequence, these infected macrophages exhibited fewer proteolytic foci and also had a pH close to neutral (16). Moreover, it has been suggested that *P. salmonis* induces an anti-inflammatory milieu when it infects macrophages, by manipulating the host cytokine profile to promote an environment that is favorable for its survival and replication in salmonid macrophage-like cells (17).

The low effectiveness of antibiotic treatment is not only observed against *P. salmonis*, but also against other intracellular pathogens, such as *Legionella pneumophila*, for which erythromycin (antibiotic most commonly used for 25 years to treat infections with this bacterium) is no longer effective in *in vivo* models (18). In this scenario, the passive immunization strategy against infection with *L. pneumophila* proposed by Joller et al. (19) offers new prospects in the development of antimicrobials against intracellular pathogens. Joller et al. used non-specific antibodies that form IgG-beads that stimulate the intracellular immune response in macrophages infected with *L. pneumophila*, promoting their degradation within lysosomes of infected cells. The underlying mechanism is suggested to involve induction of the signaling cascade that counteracts the modulation of the endocytic vacuolar traffic (19). The activation of the response of cells infected by *L. pneumophila* due to the IgG-beads stimulation is dependent on the interaction of the Fc region of non-specific antibodies with the Fc receptor (FcR) present in macrophages (20).

In salmonids, antibody-mediated opsonization of particles enhances phagocytosis and respiratory burst by phagocytes, providing functional evidence for the presence of antibody receptors on leukocytes (21–24). In Atlantic salmon, this mechanism is potentially mediated by receptors that may be similar to Fc receptors, which are widely distributed on leukocytes in mammals (25, 26). The utilization of antibodies bound to antigens as a passive immunization strategy against infectious diseases has been poorly explored. In the context of strategies against bacteria such as *Flavobacterium psychrophilum* and *Vibrio anguillarum* in rainbow trout, the delivery of specific antibodies attenuates the mortality rates and aggressiveness associated with infectious outbreaks, suggesting a protective role and a putative immune stimulatory effect (27, 28).

Previously, our group reported that *P. salmonis* survives at least 120 h within Atlantic salmon macrophages-enriched cell cultures. During this time, the intracellular bacterial load rises, as evidenced by an increase in the number of copies of the bacterial *16S* rDNA ribosomal gene. Additionally, we suggest that the survival of the *P. salmonis* is favored by perturbations in lysosomal activity, as evidenced by a limited lysosomal proteolytic activity observed in infected cells (16). The aim of this study was to evaluate whether the use of non-specific antibodies forming IgM-beads activate the lysosomal response of macrophage-enriched cell cultures infected by *P. salmonis*. The effectiveness of the treatment was analyzed in terms of the effect that non-specific antibodies forming IgM-beads would have on the modulation of both lysosomal acidification and proteolytic activity induced by the bacterium when it infects macrophages-like cells of Atlantic salmon. Additionally, we evaluated the effect on bacterial load and survival of infected macrophages.

MATERIALS AND METHODS

Experimental Fish

Atlantic salmon with an average weight of 55 ± 15 g were obtained from a local farm and maintained in tanks with freshwater at a biomass of 10–12 kg/m^3, with controlled temperature (14–16°C) and continuous aeration. Water quality parameters, such as oxygen, pH, and levels of nitrogen compounds (i.e., nitrate, nitrite, and ammonia) were monitored daily and maintained at constant values. The fish were fed with commercial pellet twice daily (Golden Optima, Biomar, Puerto Montt, Chile), and acclimatized for 3 weeks prior to the experiments. The maintenance of fish was performed in accordance with the ethical standards of the Institutional Ethics Committee of Universidad de Santiago de Chile (approved in internal report n°364) and the relevant legislation in force.

Isolation of Macrophages and Cell Cultures

Macrophage-enriched cell cultures were obtained from Atlantic salmon head kidneys, as described by Braun-Nesje et al. (29) and by our group in Pérez-Stuardo et al. (16) with slight modifications. Briefly, Atlantic salmon head kidney were aseptically extracted and disaggregated using a cell strainer (pore size: 70 µm) (BD Falcon, Seaton Delaval, England) suspended in Leibovitz-15 medium (L-15; Corning, New York, USA) with supplement 1 (**Supplementary Table 1**). Mechanical disaggregation was performed until a homogeneous cell suspension was obtained. The leukocyte fraction was isolated through a discontinuous gradient in densities of 34 and 51% of Percoll (GE Healthcare) diluted in miliQ water, supplemented with 1× Hank's Balanced Salt Solution (HBSS, Gibco). The cell suspension was placed on the Percoll gradient, and centrifuged at 400 g for 40 min at 16°C. The leukocyte interface was collected and resuspended in L-15 medium with supplement 1 (**Supplementary Table 1**). To eliminate the traces of Percoll, the cell suspension was centrifuged twice for 7 min at 250 g at 16°C. The cell suspension was seeded at 40,000 cells/cm^2 in L-15 medium with supplement 2 (**Supplementary Table 1**) at 16°C.

To enrich the primary cell culture with monocytic/macrophage adherent cell population, the primary culture was washed the following day with three washes of 1× phosphate-buffered saline (PBS) at pH 7.4. Non-adherent cells were discarded and the remaining cells were cultivated with fresh L-15 medium with supplement 2 (**Supplementary Table 1**). At 3, 5, and 7 days of cultivation, the cells were washed three times with 1× PBS. Non-adherent cells were discarded, and fresh L-15 medium with supplement 3 (**Supplementary Table 1**) was added to the cultures.

SHK-1 cells (*Salmo salar*; ATCC, American Type Culture Collection, Manassas, VA, USA), which are described as macrophage-like cells (30), were grown at 16°C in L-15 medium with supplement 4 (**Supplementary Table 1**).

Piscirickettsia salmonis and Infection

Culture and propagation of *P. salmonis* (strain 9734, ETECMA, Puerto Montt, Chile) was performed in salmonid cell line CHSE-214 (ATCC N°CRL-1682), as previously described by Fryer et al., 1992 (30). The CHSE-214 cell line was maintained in minimal essential medium (MEM; Corning) with supplement 5 (**Supplementary Table 1**) at 16°C. The infected cells were observed using conventional inverted light microscopy (Motic AE31E, Leica Microsystems, Wetzlar, Germany) after 4 to 6 days post-infection (dpi) to observe any cytopathic effect (CPE) (31).

Piscirickettsia salmonis was extracted from the supernatant of infected CHSE-214 cells displaying CPE. Bacterial quantification was performed in a Petroff-Hausser chamber (Hausser Scientific, PA, USA) according to the instructions provided by the manufacturer. Cellular debris was eliminated through centrifugation for 5 min at 500 g. Subsequently, *P. salmonis* was centrifuged at 7,500 *g* for 15 min at 16°C. Macrophage-enriched cell cultures from Atlantic salmon head kidneys were seeded at 6,000 cells/cm^2 in six-well flat bottom plates and were incubated for 2 h with *P. salmonis* at a multiplicity of infection (MOI) of 10 bacteria/cell in L-15 medium with supplement 3 (**Supplementary Table 1**). Infection was synchronized by centrifugation at 150 g for 3 min at 16°C, and the infected cells were incubated at 16°C. Then, cells were washed twice with 1× PBS and incubated with L-15 medium with supplement 3 (**Supplementary Table 1**). As a control, *P. salmonis* was inactivated by incubation of the pellet in 4% paraformaldehyde (PFA; Sigma Aldrich, MO, USA), diluted in 1× PBS and incubated overnight at 4°C. The bacterial suspension was centrifuged for 15 min at 7,500 *g* at 16°C; then, the supernatant was discarded and the pellet was washed three times with 1× PBS. Finally, the bacterial suspension was centrifuged for 15 min at 7,500 g at 16°C; the supernatant was discarded and the pellet was resuspended in L-15 medium with supplement 3 (**Supplementary Table 1**).

Evaluation of Lysosomal Acidification

Evaluation of lysosomal acidification in macrophage-enriched cell cultures was performed by fluorescence analysis using the LysoSensor™ Yellow/Blue probe (LSYB; Thermo Scientific). This ratiometric probe can be used to measure the pH of acidic organelles. The LysoSensor™ dye produces blue and yellow fluorescence in neutral and acidic environments, respectively. Therefore, a fluorescence shift from blue (maximum emission at 430 nm) to yellow (maximum emission at 535 nm) indicates a decrease in lysosomal pH (16, 32).

The IgM-beads were prepared with latex beads coated with immunoglobulin M (IgM). IgM was purified from the serum of Atlantic salmon (weighing 80 to 100 g) by an affinity protein A sepharose column. The presence of IgM was confirmed by western blotting and ELISA based on a monoclonal antibody (I-14 hybridoma) (33). Additionally, the homogeneity of the IgM preparation was evaluated by SDS-PAGE. In order to assess the short-term effect of the IgM-beads on lysosomal acidification, the macrophage-enriched cell cultures were seeded at 6,000 cells/cm^2 in 12-well flat bottom plates with glass coverslips and infected with *P. salmonis* at MOI 10 for 2 h, as previously described. Then, infected macrophage-enriched cell culture was incubated for 1 h with 30 beads/cell. After incubation, the cells were washed twice with 1× PBS and cultivated in fresh L-15 medium with

supplement 3 (**Supplementary Table 1**). The analysis of lysosomal acidification was performed at 1 and 3 h post-treatment (hpt), according to the described by Pérez-Stuardo et al. (16). Additionally, we evaluated the effect of Bovine Serum Albumin (BSA)-beads in infected cells as protein-beads control. To evaluate the lysosomal acidification in macrophage-enriched cell cultures infected by *P. salmonis*, we incubated the cells with bacteria for 2 h as was previously described and maintained in L-15 medium with supplement 3 for 3 and 5 h post-infection (hpi) (equivalent to 1 and 3 hpt). Similarly, as a control for lysosomal activation, macrophage-enriched cell cultures were incubated with inactivated *P. salmonis* and evaluated at the same times as the experimental group.

At each time point, the infected cells were incubated for 5 min with 10 μM LSYB. Subsequently, the cells were washed three times with 1× PBS and fixed for 10 min with 4% (w/v) PFA (Sigma Aldrich), followed by three additional washes with 1× PBS. Finally, the cells were stained by incubating for 1 min with 1 μg/mL propidium iodide (PI); then, the cells were washed twice with 1× PBS and once with MilliQ water to remove the residual salts. The samples were mounted on slides with Fluoromount^{TM} (Sigma Aldrich), and images were obtained using a Leica SP8 confocal microscope (Leica, Wetzlar, Germany). Results were obtained by the division of the emission spectrum of the LSYB probe, specifically to obtain an acidic indicator channel (acquired between 500 and 580 nm) and a neutral-basic indicator channel (acquired between 450 and 495 nm). According to instructions provided by the manufacturer. The fluorescence intensity obtained in the acidic indicator channel had to be ≥2-fold that obtained in the neutral-basic indicator channel for a lysosome to be considered as acidic. The analysis of lysosomal acidity was performed using the software LAS X (version 3.3.0). Briefly, the average fluorescence intensity for each indicator channel was obtained for each lysosome present in the micrographs obtained from the samples. Subsequently, the ratio between the fluorescence intensity values obtained from the two indicator channels was used as the acidity index. An acidic index of $x \geq 2$ denoted an acidic pH, while an acidity index between $0<x<2$ represented a neutral-basic pH. The number of lysosomes per sample was normalized to the number of cells per sample. For each condition, four random micrographs were obtained with a z-stack containing 30 cells mean. The micrographs were processed using the software Fiji (ImageJ 1.52g) (34). The results are represented as the number of lysosomes/cell and percentage of acidic lysosomes per condition.

Evaluation of Lysosomal Activity

In order to assess the short-term effect on the lysosomal activity in *P. salmonis*-infected macrophage-enriched cell cultures, fluorescence analysis using the DQ^{TM} Green BSA probe was performed in a similar way as previously described by our group in Pérez-Stuardo et al. (16). The DQ^{TM} Green BSA probe is composed of albumin derivatized with a self-quenching fluorochrome. The degradation of DQ^{TM} Green BSA in acidic lysosomes results in smaller protein fragments than those of isolated fluorophores. Once the quencher is released, brightly fluorescent products are observed. The cleavage of DQ^{TM} Green BSA results in the release of fragments with maximum excitation and emission at 505 and 515 nm, respectively (35–37).

The macrophage-enriched cell cultures were established at 6,000 cells/cm^2 in 12-well flat bottom plates with glass coverslips and infected with *P. salmonis*, as described in the previous section. Subsequently, analysis of lysosomal activity was performed at 1 and 3 hpt from IgM-beads incubation. The macrophage-enriched cells were treated with IgM-beads (or BSA-beads as control) in the same way as described in the previous section. Lysosomal activity was also evaluated in infected macrophage-enriched cell cultures incubated with BSA-beads. To evaluate the lysosomal activity in macrophage-enriched cell cultures infected by *P. salmonis*, we incubated the cells with bacteria for 2 h as was previously described and maintained in L-15 medium containing supplement 3 for 3 and 5 hpi (equivalent to 1 and 3 hpt). As positive control for lysosomal activation, macrophage-enriched cell cultures were incubated with inactivated *P. salmonis*, and lysosomal activity was evaluated at the same times as in the experimental group.

Two hours prior to each time point for IgM-beads incubation, DQ^{TM} Green BSA 10 μg/mL in L-15 medium containing supplement 3 (**Supplementary Table 1**) was added to the evaluated cells. Then, the cells were washed three times with 1× PBS and fixed using 4% (w/v) PFA, followed by three additional washes with 1× PBS. The cells were stained with 1 μg/mL PI as previously described. The samples were mounted on slides using the mounting solution Fluoromount^{TM} (Thermo Scientific). Micrographs were obtained using a Leica SP 8 confocal microscope, and processed and analyzed using Fiji software (ImageJ 1.52g) (34). The analysis was performed by counting each positive event per cell due to the fluorescence of DQ^{TM} Green BSA, from four micrographs, with a merge of the images from z-stack, containing an average of 30 cells per micrograph for each experimental condition. The data were normalized to the number of cells on the micrograph, and the results are represented as the number of proteolytic events/cell.

Evaluation of the Effect of Non-specific Antibodies Forming IgM-Beads on Cytotoxicity Induced by *P. salmonis*

To evaluate the effect of IgM-beads on cytotoxicity induced by *P. salmonis*, we quantified lactate dehydrogenase (LDH) release into the extracellular medium. The macrophage-enriched cell cultures were seeded at 10,000 cells/well in 96-well flat bottom plates. Cells were incubated with *P. salmonis* at MOI 10 for 2 h, as previously described. Then, cells were incubated for 1 h with 30 IgM-beads/cell. After incubation, cells were washed twice with 1× PBS and cultivated in fresh L-15 medium with supplement 3 (**Supplementary Table 1**). Cytotoxicity was evaluated in macrophage-enriched cell culture at 3, 5, and 7 days post-treatment (dpt) using the Pierce LDH Cytotoxicity Assay Kit (Thermo Scientific), according to the instructions of the manufacturer. As the control, we evaluated the cytotoxicity induced by *P. salmonis* and the effect of BSA-beads and non-coupled-beads on infected cells.

Gentamicin Protection Assay and Quantification of Bacterial Load

In order to recover intracellular bacteria from the infected macrophage-like cells, a gentamicin protection assay was performed. Briefly, macrophage-like cells (SHK-1 cell line) were seeded at a density of 150,000 cells/well in 6-well flat bottom plates. Cells were infected with *P. salmonis* at MOI 10 for 24 h. Infection was synchronized by centrifugation, and the infected cells were incubated at 16°C. Then, cells were washed twice with 1× PBS and incubated with L-15 medium with supplement 3 (**Supplementary Table 1**). SHK-1-infected cells were incubated with 30 IgM-beads/cell, and the infection was maintained until 72 and 120 hpi. Recovery of the intracellular bacterium was performed following the protocol described by Pérez-Stuardo et al. (16). As control, bacterial load was also evaluated in infected macrophage-enriched cell cultures incubated with BSA-beads.

To quantify the extracellular bacterial load, the supernatant from SHK-1 cells infected with *P. salmonis* was recovered and centrifuged for 15 min at 7,500 *g* at 16°C. The supernatant was discarded, and the pellet was resuspended in 1× PBS. Accordingly, the sample was subdivided to (i) isolate DNA in order to quantify the bacterial load by qPCR, and (ii) determine the bacterial viability by plating on serial dilutions (from 10^{-1} to 10^{-5}) in CHAB agar which includes: Cystine heart agar [25 g/L Bacto heart Infusion broth (BD Difco), 10g/L Glucose (Merck), 1 g/L L-cysteine (Merck), 15 g/L agar (Sigma Aldrich), 2g/L hemoglobin from bovine blood (Sigma Aldrich)] supplemented with 5% bovine blood (Health Public Institute Chile) (38). To quantify the intracellular bacteria, macrophage-enriched cell cultures infected with *P. salmonis* were incubated with 100 µg/mL gentamicin for 60 min to eliminate bacteria from the extracellular environment. Subsequently, the cells were washed three times with cold 1× PBS, and incubated for 15 min with 1% (w/v) saponin (Sigma Aldrich) in 1× PBS at 16°C. Finally, the permeabilized cells were suspended in 1× PBS and centrifuged at 7,500 g for 10 min at 4°C. The supernatant was then discarded, and the pellet was resuspended in 1× PBS. The sample was subdivided to (i) isolate DNA in order to quantify the bacterial load by qPCR, and (ii) determine bacterial viability by plating on serial dilutions (from 10^{-1} to 10^{-5}) in CHAB agar, as described above.

Detection of *P. salmonis* Using Quantitative Polymerase Chain Reaction (qPCR)

The gene encoding *16S* rRNA (primers, Fw: 5'-AGG-GAG-ACT-GCC-GGT-GAT-A-3'; Rv: 5'-ACT-ACG-AGG-CGC-TTT-CTC-A-3') was amplified as described by Karatas et al. (2008) in order to detect the presence of *P. salmonis* in the infected cell cultures (39). Genomic DNA was obtained using the Wizard™ Genomic DNA Purification kit (Promega, WI, USA) according to the instructions provided by the manufacturer. PCR amplification was performed using the PowerUp™ SYBR® Green Master Mix (Thermo Scientific) according to the manufacturer's instructions. The primers were added to a final concentration of 0.4 µM, and 12 ng of template was used. The qPCR was performed on a QuantStudio 3 Real-Time PCR system (Thermo Scientific). Quantification of *16S* rDNA copies was performed through interpolation from the standard curve with the cycle threshold (Ct) value obtained for each sample. The results are expressed as *16S* rDNA copy/cell.

Statistical Analysis

Statistical analysis for each experiment was performed between all the conditions, for each timepoint analyzed. Statistical differences were determined using one-way analysis of variance (ANOVA) with a Tukey multiple comparison test. We used GraphPad Prism v6.0 for Windows software (GraphPad Software Inc.) to calculate the mean, the standard error of the mean (SEM), and to perform the statistical tests. A value of $p < 0.05$ denoted statistical significance.

RESULTS

IgM-Beads Favor Lysosomal Acidification in Macrophage-Enriched Cell Cultures Infected by *P. salmonis*

To determine if IgM-beads reverses the modulation of the lysosomal activity induced by bacterial infection, the number of lysosomes and their acidification level were evaluated. In non-infected cells, either 1 or 3 hpt, there is a punctate pattern of yellow/green and cyan fluorescent signal (**Figures 1A, E**). This result suggests the presence of acidic and neutral vesicles along the macrophage-like cell. When we imaged *P. salmonis*-infected macrophage-enriched cell cultures, we also observed at 1 hpt a yellow/green fluorescent punctate pattern (**Figure 1B**). However, only at 3 hpt we found both yellow/green and cyan fluorescent dots (**Figure 1F**), suggesting the presence of acidic and neutral vesicles after treatment. When incubating macrophage-enriched cell cultures with inactivated *P. salmonis*, we observed a pattern of dots of yellow/green fluorescent (**Figures 1C, G**) at both times assayed. This result suggests the presence of acid vesicles generated against inactivated *P. salmonis*. Finally, in macrophage-enriched cells cultures infected with *P. salmonis* and then incubated with IgM-beads (**Figure 1D**), we observed at 1 hpt a punctate pattern of yellow/green fluorescence and at 3 hpt we observed both dots of yellow/green and cyan fluorescence (**Figure 1H**), in a similar way to the observed in infected cells (**Figures 1B, F**).

When we quantified the number of lysosomes/cell in macrophage-enriched cell cultures infected with *P. salmonis*, we observed a significant increase in comparison to non-infected cells at 1 hpt. However, this difference was not maintained with longer infection times (**Figure 2A** and **Supplementary Table 2**). When we used inactivated *P. salmonis* during the incubation, we observed a significant increase in comparison to non-infected cells at both times assayed. Nevertheless, the larger effect was found at 3 hpt (**Figure 2A** and **Supplementary Table 2**). On the other hand, when the macrophage-enriched cell cultures infected with *P. salmonis* were incubated with IgM-beads, the results show

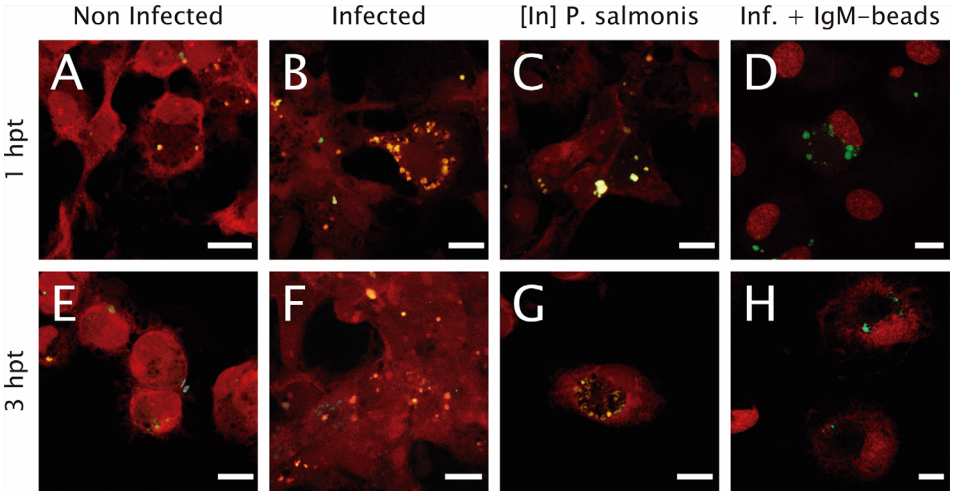

FIGURE 1 | Lysosomal acidification in infected macrophage-enriched cell cultures treated with IgM-beads. Macrophage-enriched cell cultures obtained from Atlantic salmon head kidneys were incubated with *P. salmonis* at a MOI of 10 bacteria/cell. The infected cells were treated with IgM-beads and analyzed at 1 and 3 hpt. The macrophage-enriched cell cultures were treated with the LSYB probe (green and blue) to stain lysosomes and analyze their pH. **(A, E)** Non-infected macrophages analyzed at 1 and 3 hpt. Macrophages-enriched cell cultures infected with *P. salmonis* for 1 hpt **(B)**, and 3 hpt **(F)**. Macrophage-enriched cell cultures incubated with inactivated (In) *P. salmonis* for 1 hpt **(C)** and 3 hpt **(G)**. Macrophage-enriched cultures infected with *P. salmonis* and treated with IgM-beads for 1 hpt **(D)** and 3 hpt **(H)**. Scale bar: 10 μm.

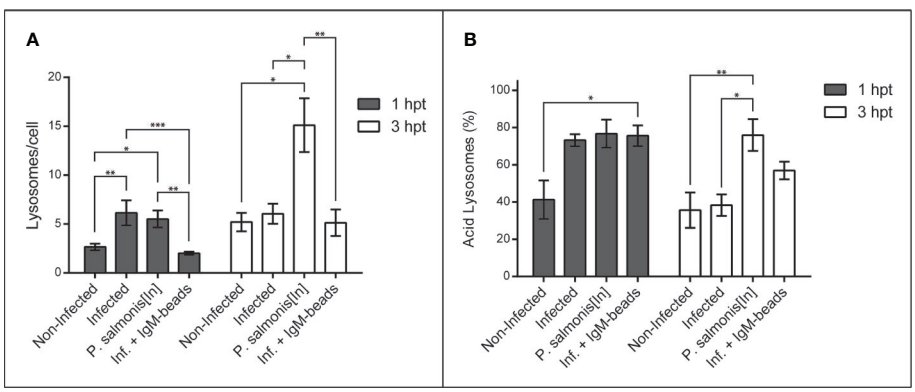

FIGURE 2 | Lysosomal quantification in infected macrophage-enriched cell cultures treated with IgM-beads. Macrophage-enriched cell cultures were infected with *P. salmonis* at a MOI of 10 bacteria/cell and analyzed at 1 and 3 hpt. The lysosomes were stained with the LSYB probe and quantified as acidic lysosomes or neutral-basic (NB) lysosomes. The data were normalized to the number of cells analyzed. **(A)** Total number of lysosomes per cell. **(B)** Percentage of acidic lysosomes for each condition. The statistical analysis was performed through parametric ANOVA with a Tukey multiple comparison test. Significant differences: *$p < 0.05$, **$p < 0.01$, ***$p < 0.001$.

no difference in the number of lysosomes/cell compared to the non-infected cells (**Figure 2A** and **Supplementary Table 2**). Similarly, when we used the BSA-beads we found no difference compared with the infected macrophage-enriched cell cultures incubated at 1 and 3 hpt (**Supplementary Figure 1A** and **Supplementary Table 2**).

Subsequently, we determined the percentage of acid lysosomes in macrophage-enriched cell cultures. This analysis showed that, despite the slight increase in the number of lysosomes at the first timepoint evaluated, the macrophage-enriched cell cultures infected with *P. salmonis* exhibited a higher percentage of acidic lysosomes in comparison with non-infected cells (**Figure 2B** and **Supplementary Table 3**), although, not significantly different. This increase was even greater in magnitude in macrophage-enriched cell cultures incubated with inactivated *P. salmonis*, and macrophage-enriched cell cultures infected with *P. salmonis* and incubated with IgM-beads at 1 hpt. However, the only group to show significant differences to non-infected cells, were cells infected with *P. salmonis* and incubated with IgM-beads. At longer infection

times with *P. salmonis*, the percentage of acid lysosomes decreased by almost half. Nonetheless, the macrophage-enriched cell cultures infected with *P. salmonis* and incubated with IgM-beads at 3 hpt, showed a decrease in the percentage of acid lysosomes, but not enough to reach a statistical difference (**Figure 2B** and **Supplementary Table 3**). Similar percentages of acid lysosomes was observed in macrophage-enriched cell cultures infected with *P. salmonis* and incubated with BSA-beads (**Supplementary Figure 1B** and **Supplementary Table 3**). In contrast, in macrophage-enriched cell cultures incubated with inactivated *P. salmonis*, the percentage of acid lysosomes at both times analyzed was higher than 75% of the total lysosomes in the samples (**Figure 2B** and **Supplementary Table 3**). In summary, the results suggest that the infection of *P. salmonis* prevents the lysosomal acidification, but the effect is attenuated after treatment with protein-beads.

Incubation With IgM-Beads Reverses the Weak Hydrolytic Activity Induced by *P. salmonis* During Infection of Macrophage-Enriched Cell Cultures

The proteolytic activity was assessed using the fluorescent degrading event marker DQ™ Green BSA. In non-infected macrophage-enriched cell cultures, either 1 or 3 hpt, fluorescent events were evident (**Figures 3A, E**), suggesting proteolytic activity in non-infected cells. Similarly, in infected *P. salmonis* macrophage-enriched cell cultures we observed fluorescent dots due to proteolytic events/cell at both time points evaluated (**Figures 3B, F**). Nevertheless, when we imaged macrophage-enriched cell cultures with inactivated *P. salmonis*, at 1 and 3 hpt, we observed larger clusters with an intense green fluorescent signal due to proteolytic activity at (**Figures 3C, G**). A similar result was observed when IgM-beads were incubated with infected macrophage-enriched cell cultures (**Figures 3D, H**), suggesting that incubation with IgM-beads induced proteolytic activity in infected cells at both times evaluated.

In order to determine whether IgM-beads reverse the inhibition of proteolytic activity induced by *P. salmonis* during infection, we quantified the fluorescence events of DQ™ Green BSA degradation using confocal microscopy. At 1 hpt, macrophage-enriched cell cultures infected by *P. salmonis* showed less than half of the proteolytic activity foci compared to non-infected cells. Despite this decrease in activity, statistical analysis suggested non-significant differences between both conditions. In the case of macrophage-enriched cell cultures infected with *P. salmonis* and incubated with IgM-beads, the proteolytic foci were similar to those observed in non-infected cells and in macrophage-enriched cell cultures incubated with inactivated *P. salmonis* (**Figure 4** and **Supplementary Table 4**).

At the second timepoint evaluated (3 hpt), the number of proteolytic foci observed in macrophage-enriched cell cultures infected by *P. salmonis* was significantly lower in comparison to proteolytic events/cell observed in infected cells incubated with IgM-beads. This induction is similar to that observed in macrophage-enriched cell cultures incubated with inactivated *P. salmonis* (**Figure 4** and **Supplementary Table 4**). The increase in proteolytic foci was not observed in the infected macrophage-enriched cell cultures incubated with BSA-beads, at either timepoint analyzed (**Supplementary Figure 2** and **Supplementary Table 4**). Collectively, these results suggest that IgM-beads reversed the inhibition of lysosomal hydrolytic activity induced by *P. salmonis* during infection of macrophage-enriched cell cultures derived from Atlantic salmon head kidney.

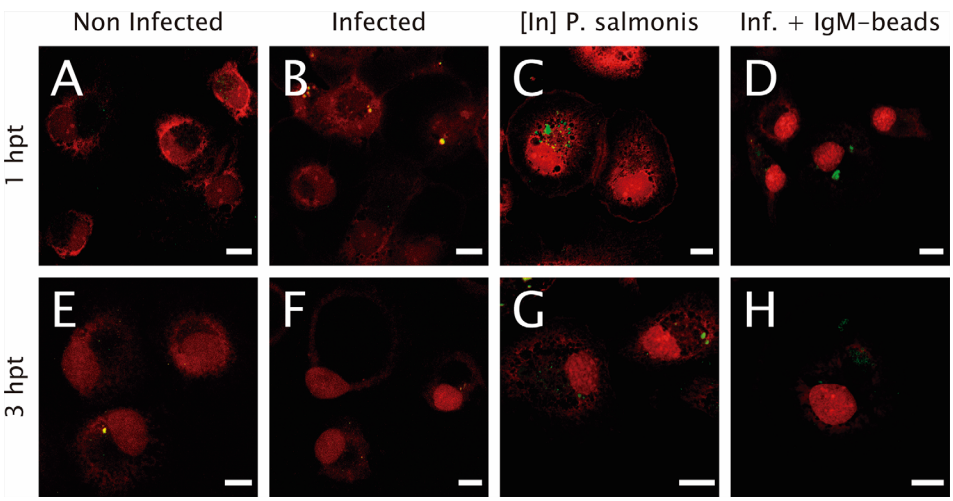

FIGURE 3 | Lysosomal functionality in infected macrophage-enriched cell cultures treated with IgM beads. Macrophage-enriched cell cultures were infected with P. salmonis at a MOI 10 of bacteria/cell, treated with IgM beads and analyzed at 1 and 3 hpt. Cells were treated with the DQ BSA™ Green probe to stain the proteolytic focusses; the nucleus was stained with PI (red). **(A, E)** Non-infected macrophages analyzed at 1 and 3 hpt. Macrophage-enriched cell cultures incubated with P. salmonis for 1 hpt **(B)** and 3 hpt **(F)**. Macrophage-enriched cell cultures incubated with inactivated (In) P. salmonis for 1 hpt **(C)** and 3 hpt **(G)**. Macrophage enriched cell cultures infected with P. salmonis and treated with IgM-beads for 1 hpt **(D)** and 3 hpt **(H)**. Scale bar: 10 μm.

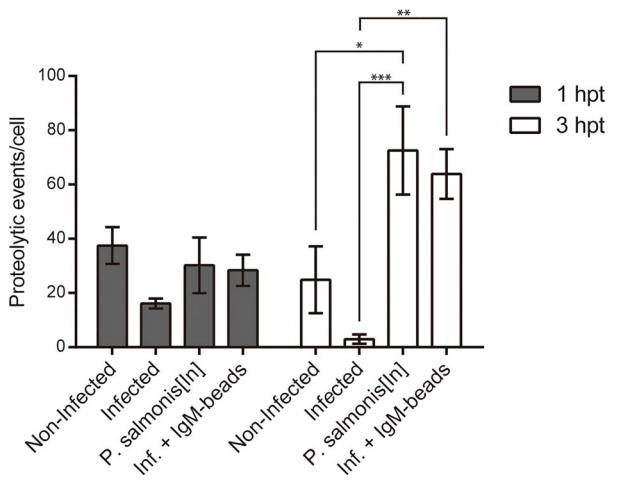

FIGURE 4 | Quantification of proteolytic events in infected macrophage-enriched cell cultures treated with igM-beads. Macrophage-enriched cell cultures were infected with *P. salmonis* at a MOI of 10 bacteria/cell and analyzed at 1 and 3 hpt. The proteolytic events were detected using the DQ-BSA™ Green probe and data were quantified and normalized to the number of cells analyzed for each condition. The statistical analysis was performed through a parametric ANOVA with a Tukey multiple comparison test. Significant differences: *p <0.05, **p < 0.01, ***p<0.001.

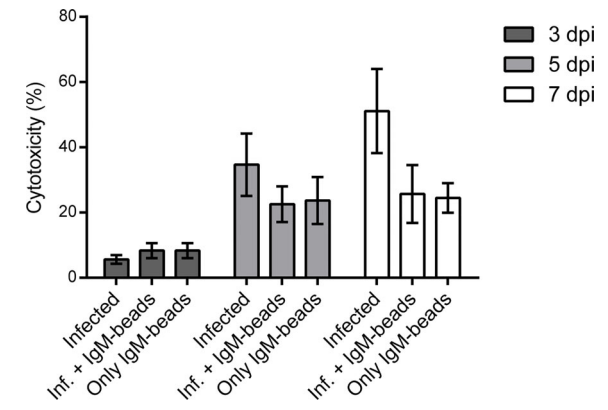

FIGURE 5 | Evaluation of cytotoxicity induced by IgM-beads. Macrophage-enriched cell cultures were infected with *P. salmonis* at MOI of 10 bacteria/cell and treated with IgM-beads. The cytotoxicity was evaluated at 3, 5, and 7 dpi by the detection LDH release into the extracellular medium. The statistic test was performed using ANOVA with a Tukey multiple comparison test, the analysis was performed individually for each evaluated time.

IgM-Beads Decrease the Cytotoxicity in Macrophage-Enriched Cell Cultures Infected by *P. salmonis*

We used the LDH assay as a reporter for cell death to evaluate the cytotoxicity induced by *P. salmonis* when it infects macrophage-enriched cell cultures and the possible effect that the IgM-beads triggers. The cytotoxicity induced by *P. salmonis* in infecting macrophage-enriched cell cultures 3 dpi, was similar to that observed in infected cells incubated with IgM-beads (**Figure 5**, left panel, and **Supplementary Table 5**), although not significantly different. In the same way, a similar cytotoxicity was observed in macrophage-enriched cell cultures incubated with only IgM-beads. At 5 dpi, the cytotoxicity induced by *P. salmonis* was higher than the effect obtained with *P. salmonis* infection and IgM-beads. However, no significant differences were observed between both conditions. As control, the cytotoxicity induced by incubation with only IgM-beads was similar to the infected group, but neither reach significant differences with the other conditions evaluated (**Figure 5**, middle panel, and **Supplementary Table 5**). At 7 dpi, the higher cytotoxicity was induced by *P. salmonis*, which was higher than in macrophage-enriched cell cultures infected by *P. salmonis* and incubated with IgM-beads. However, despite that the treatment with IgM-beads produces half the level of cytotoxicity to that observed in infected cells, although there is no significant difference between both conditions. Similarly, the cytotoxicity induced by the incubation with only IgM-beads reached ~25% (**Figure 5**, right panel, and **Supplementary Table 5**). Additionally, we evaluated the effect of BSA-beads on the cytotoxicity induced by *P. salmonis* during infection of macrophage-enriched cell cultures, and we observed that it was similar to the cells infected by *P. salmonis* at 5 and 7 dpi (**Supplementary Figure 3** and **Supplementary Table 5**). These results suggest that the effect of IgM-beads on the cytotoxicity of macrophage-enriched cell cultures is due to the presence of IgM.

IgM-Beads Promote Bacterial Clearance in Macrophage-Enriched Cell Cultures Infected by *P. salmonis*

To evaluate the effect of IgM-beads on the survival and replication of *P. salmonis* when it infected Atlantic salmon macrophages, we used the SHK-1 cell line, which is derived from leukocytes and possesses the properties of macrophages (40). The bacterial load was evaluated by quantification of *16S* rDNA copies/cell and CFU/cell. In both cases, quantification was performed from the supernatant and intracellular medium of *P. salmonis*-incubated macrophages. At 72 hpi the incubation of SHK-1 cells infected by *P. salmonis* with IgM-beads resulted in a significant decrease in about 50% of the number of copies of *16S* rDNA/cell, in comparison with that in infected cells that were not incubated with IgM-beads (**Figure 6A** and **Supplementary Table 6**). As control, infected cells were incubated with BSA-beads, which have no effect over the number of copies of *16S* rDNA/cell (**Figure 6A** and **Supplementary Table 6**). A similar result was observed at 120 hpi, incubation of infected SHK-1 cells with IgM-beads resulting in a significant decrease of bacterial load, both intracellular and extracellular, in comparison with that observed in infected cells that had not been treated with IgM-beads. As control, infected SHK-1 cells were incubated with BSA-beads, although no effect were observed on bacterial load (**Figure 6B** and **Supplementary Table 6**).

On the other hand, the effects of IgM-beads on bacterial load were evaluated by recovery of CFU present inside as well as

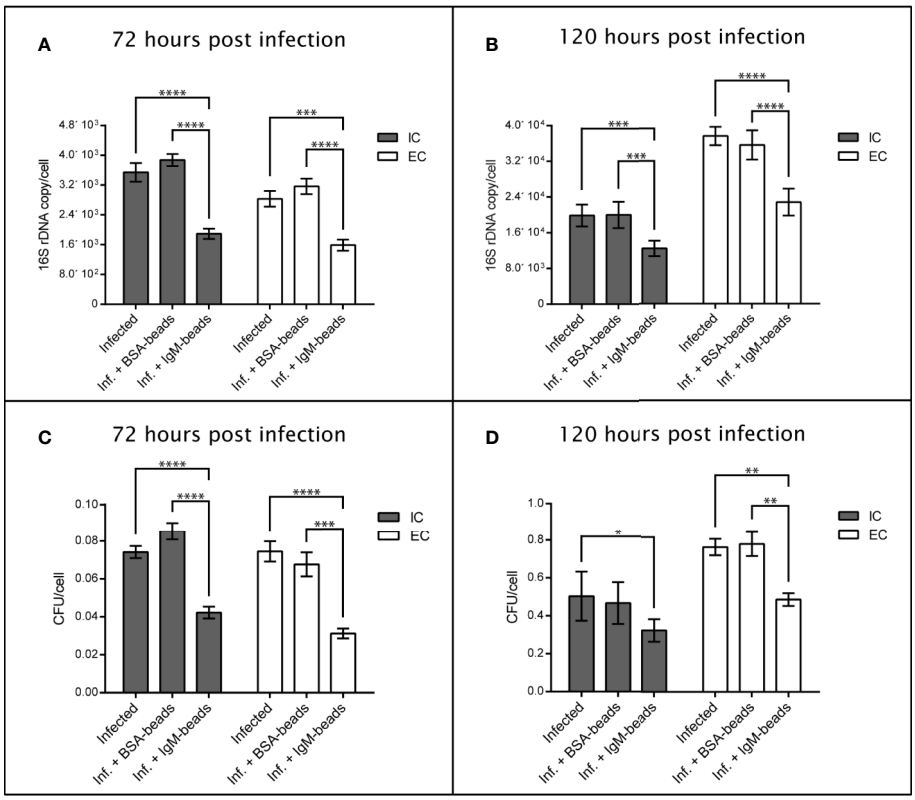

FIGURE 6 | Quantification of extracellular and intracellular P. salmonis recovered from SHK-1 infected cells treated with IgM-beads. SHK-1 cells were infected with P. salmonis at a MOI of 10 bacteria/cell and treated with IgM-beads. SHK-1 cells incubated with BSA-beads were used as controls for each time point. The bacterial load was determined by quantification of 16S rDNA copy/cell at 72 hpi **(A)** and 120 hpi **(B)**, and also by quantification of CFU/cell at 72 hpi **(C)** and 120 hpi **(D)**. The statistical analysis was performed through a parametric ANOVA with a Tukey multiple comparison test. Significant differences: *p < 0.05, **p < 0.01, ***p < 0.001, ****p < 0.0001.

outside the SHK-1 cells. We observed that, at 72 and 120 hpi, incubation of IgM-beads in infected SHK-1 cells induced a significant decrease in recovered CFU both intracellularly as well as in the infection supernatant, in comparison with SHK-1 cells infected by *P. salmonis* (**Figures 6C, D** and **Supplementary Table 6**). As control, CFU/cell were quantified from intracellular medium and infection supernatant of infected SHK-1 cells incubated with BSA-beads, however these protein beads control do not decrease the bacterial load (**Figures 6C, D** and **Supplementary Table 6**).

Together, these results suggest that incubation with IgM-beads affects the viability and replication of *P. salmonis* when it infects macrophage-like cells. This effect was not observed when we utilized BSA-beads, in all cases evaluated (**Figure 6** and **Supplementary Table 6**).

DISCUSSION

Antibody-based therapies, which have been widely used as a passive immunization strategy against various pathogens (19, 20, 41–44), are capable of stimulating the endocytic pathway through the interaction between Fc and FcR (45). In mammals, this binding activates a phosphoinositol 3-kinase (PI3-K) protein-dependent signal and downstream signaling pathways that lead to a wide variety of effector mechanisms including oxidative burst, increased phagocytosis, cytokine release, and increased antigen presentation and routing. In addition, the Fc-FcR interaction is responsible for routing the vesicular traffic that is altered by intracellular pathogens, which allows the bacteria to undergo degradation in the lysosome (19, 20, 46).

Antibody-based therapies using beads coated with immunoglobulins have been previously reported in treatment against *L. pneumophila* and *Streptococcus dysgalactiae*; these treatments stimulate the intracellular response by inducing bacterial clearance (19, 42). IgG-beads against *L. pneumophila* infection stimulate the intracellular response of murine macrophages (19). These IgG-beads induce host cells to become non-permissive for intracellular replication; as a result, intracellular pathogens are targeted to the lysosome for degradation. The use of IgY-beads against *S. dysgalactiae*, the causal agent of cow mastitis, have been demonstrated to be

effective in inhibiting propagation and inducing the phagocytosis of bacteria (42). In fish, although stimulation of the endocytic pathway through the Fc-FcR interaction has not been described to date, passive immunization strategies based on the intraperitoneal delivery of specific antibodies against bacteria such as *Flavobacterium psychrophilum*, *Yersinia ruckerii*, and *Vibrio anguillarum* have been reported in rainbow trout. In all of these strategies, a reduction in the mortality and aggressiveness index of infectious outbreaks was observed (27, 28, 47), suggesting that these passive immunization strategies are capable of stimulating a protective response in fish.

Recently, it has been described that *P. salmonis* is able to persist in macrophage-enriched cell cultures for at least 120 hpi, where it evades the host response by reducing lysosomal acidification and its proteolytic activity in the first hpi (16). In the current work, we evaluated the functionality of this organelle by assessing lysosomal acidity and proteolytic activity of macrophages infected with *P. salmonis* and stimulated with IgM-beads. Results showed that incubation of infected cells with IgM-beads promotes an increase in the acidity of lysosomes as well as an increase of about 2 folds in the number of proteolytic foci per cell, in comparison with cells infected with *P. salmonis* that were not incubated with IgM-beads. In the latter, the pH was maintained in a neutral–basic range similar to that observed in non-infected macrophages.

The mechanisms of cell death induced by *P. salmonis* are poorly described. However, it is reported that in early, intermediate, and late stages of infection of *P. salmonis* in trout monocytes/macrophages like cells, apoptosis was induced in about 22–30% of infected cells; this represents a mechanism of *P. salmonis* to promote apoptosis in a fraction of phagocytic cells. Rojas et al. (48) suggested that apoptosis may allow the majority of the macrophage population to be productively infected by the bacterium, and ensure the initiation of bacterial infection and subsequent spread to other tissues (48). Furthermore, *P. salmonis* is able to infect various salmonid cell lines, such as CHSE-214, RTS-11, RTG-2, ASK, and SHK-1 (4, 14, 31, 49–52). In all of them, *P. salmonis* induces a CPE characterized by the production of clusters of rounded and vacuolated cells, which culminated with the detachment of the monolayer and delayed cell lysis (49, 51, 52). In our results, we observed that infection by *P. salmonis* induced cell lysis in about 50% of infected cells after 7 dpi. Similar results were reported by Oliver et al. (53), who reported cell lysis in about 60% of infected cells after 8 dpi and also by Hernández et al. (54), who observed cell lysis in almost 60% of infected cells after 9 dpi. In our work, we use the same strategy implemented by Oliver et al. (53) and Hernandez et al. (54), where cell lysis was determined by the quantification of LDH leakage (53, 54). The enzyme activity is an indicator of irreversible damage to the plasma membrane and the inability of cells to retain intracellular enzymes (55). Together, these results suggest that a fraction of the infected macrophages can be driven to apoptosis, while other fraction eventually could evolve to necrosis since both routes of cell death can be independently regulated. These parallel running pathways are the case of infection of alveolar macrophages by *Mycobacterium tuberculosis*, where bacteria can control cell death pathways: apoptotic cell death is bactericidal, whereas necrotic cell death may facilitate bacterial dissemination and transmission (56). However, the mechanisms of host cell death in Atlantic salmon macrophages infected by *P. salmonis* are not well understood and require further studies.

Recently, Oliver et al. (53) described a protective effect of both IgY antibody against a whole protein extract of *P. salmonis*, as also IgY antibody against *P. salmonis* Hsp60, when SHK-1 cells are incubated with these antibodies previous to be infected with *P. salmonis*, observing a cell lysis similar to non-infected cells (~20%) at 8 dpi. Interestingly, in our work the incubation of infected cells with IgM-beads decreased cell lysis to 25% of total cells, suggesting a protective effect of incubation with non-specific antibodies. This effect was not observed when infected macrophage-enriched cell cultures were incubated with BSA-beads, suggesting that, in a similar way to that in the work of Joller et al. (19), this protection would involve FcR signaling. However, further studies are needed to validate this hypothesis.

The classical treatment of pathogenic infection by passive immunization includes the use of soluble antibodies, which bind to the pathogen and promote its phagocytosis and lysis by the complement pathway. However, the utilization of a carrier loaded with antibodies induces phagocytosis of macrophages and neutrophils *via* FcR. Thus, increasing bacterial uptake by phagocytes is expected to contribute to reduce the inflammation (42). Confirmation that IgM-beads induce protection against infection with *P. salmonis* was obtained by analysis of bacterial load in infected cells. After stimulating macrophage-like cells infected by *P. salmonis* with IgM-beads, we observed a reduction in bacterial load after 72 and 120 hpi. This was evidenced by quantifying the bacterial load in the extracellular medium and inside the cell through the determination of the number of copies of *16S* rDNA gene by qPCR and CFU counting. These results are similar to those obtained by Joller et al. (19), where the authors described a decrease in the viable bacterial load after incubating murine macrophages infected by *L. pneumophila* with IgG-beads. Joller et al. (19) proposed that treatment with IgG-beads mediates host cell protection against intracellular pathogens that reside in vacuoles and evade phagolysosomal fusion, by re-routing the pathogens to undergo lysosomal degradation.

The quantification of bacterial load recovered in agar CHAB was inconsistent with the number of *P. salmonis* utilized to infect SHK-1 cells (10 bacteria for each cell). This discrepancy is probably due to that *P. salmonis* is considered be highly fastidious—even previously was considered to be cultivable only in eukaryotic cell lines—than may be cultured on cell-free agar, but with demanding nutritional requirements which could hinder the growth of recovered bacteria, according to the facultative intracellular nature of this fish pathogen (2, 57). Similar results were observed in Yañez et al. (50), where the authors described that efficiency of recovering of *P. salmonis* in cell-free agar media is not suitable to determine the CFU concentration, mainly because the bacterial growth is extremely low.

Intracellular pathogens invade their hosts *via* a cell entry process that culminates in the formation of a pathogen-

containing vacuoles, where it replicates and prevents their fusion with lysosomes. This evasion requires to modulation of the membrane Rab proteins (58). Rab proteins are small GTPases of the endocytic pathway that participate in the maturation of the endosome prior to fusion and delivery of their contents for lysosomal degradation, where Rab4 and Rab5 proteins are characteristic of early endosomes and Rab7 is indicative to late endosomes (59). In fish, the presence of 52 Rab GTPases have been described in channel catfish (60), and have also been described in the cellular distribution and transcriptional regulation of Rab5c and Rab7a in CHSE-214 cells, where both have the same function as those described in mammals (61). In our work, we have observed that IgM-beads promotes the lysosomal activity in infected macrophage-enriched cell cultures, as well as decreasing the bacterial load, suggesting that the IgM-beads effect over the macrophage-enriched cells could be mediated by reversing the lysosomal evasion from *P. salmonis*, opening an interesting question to further research about the mechanism promoted by IgM-beads over the exchange of Rab proteins.

In this *in vitro* approach, we observed that treatment with IgM-beads resulted in a decrease in the bacterial load. However, the mechanism by which this occurs is not yet understood, because it is necessary to determine whether IgM-beads can lead *P. salmonis* to cause lysosomal degradation, as is the case against *L. pneumophila*, another intracellular pathogen. Although our results suggest this to be the case, but further verification of this is required.

DATA AVAILABILITY STATEMENT

The original contributions presented in the study are included in the article/**Supplementary Material**. Further inquiries can be directed to the corresponding author.

ETHICS STATEMENT

The animal study was reviewed and approved by Institutional Ethics Committee of Universidad de Santiago de Chile.

AUTHOR CONTRIBUTIONS

DP-S, AE, and ST performed most of the experiments, analyzed data, and prepared figures. JM-R and CB performed any experiments. EV-V, DT-A, JR-P, AS, and ES contributed to review the manuscript. SR-C conceived and supervised the study. DP-S, FR-L, JR-P, and SR-C wrote the manuscript. All authors contributed to the article and approved the submitted version.

FUNDING

This work was financially supported by FONDECYT Iniciación grant 11150807 (SR-C), 11180621 (DT-A), and 11180705 (JR-P), Start-Up UMayor 101205 (SR-C), CORFO 13CTI-21527, FDP UMayor PEP-I 2019082 (SR-C), and PCI-ANID REDES180097 (SR-C). The authors also acknowledge the fellowship support DYCIT USACH 041831MH-Postdoc (JR-P) and 022043IB-Postdoc (EV-V), National Agency for Research and Development (ANID)/Scholarship Program/DOCTORADO BECAS CHILE/2019 – 21191135 fellowship to DP-S, UMayor-Ph.D. fellowships to DP-S.

SUPPLEMENTARY MATERIAL

The Supplementary Material for this article can be found online at: https://www.frontiersin.org/articles/10.3389/fimmu.2020.544718/full#supplementary-material

SUPPLEMENTARY FIGURE 1 | Lysosomal quantification in infected macrophage-enriched cell cultures treated with IgM-beads and BSA-beads. Macrophage-enriched cell cultures were infected with *P. salmonis* at MOI of 10 bacteria/cell and analyzed at 1 and 3 hpt. The lysosomes were stained with the LSYB probe and quantified as acidic lysosomes or neutral-basic (NB) lysosomes. The data were normalized to the number of cells analyzed. **(A)** Total number of lysosomes per cell. **(B)** Percentage of acidic lysosomes for each condition. The statistical analysis was performed through parametric ANOVA with a Tukey multiple comparison test. Significant differences: *p < 0.05.

SUPPLEMENTARY FIGURE 2 | Quantification of proteolytic events in infected macrophage-enriched cell cultures treated with IgM-beads and BSA-beads. Macrophage-enriched cell cultures were infected with *P. salmonis* at MOI of 10 bacteria/cell and analyzed at 1 and 3 hpt. The proteolytic events were detected using the DQ-BSA^{TM} Green probe and data were quantified and normalized to the number of cells analyzed for each condition. The statistical analysis was performed through a parametric ANOVA with a Tukey multiple comparison test. Significant differences: *p <0.05, **p < 0.01.

SUPPLEMENTARY FIGURE 3 | Evaluation of cytotoxicity in infected macrophage-enriched cell cultures treated with IgM-beads and BSA-beads. Macrophage-enriched cell cultures obtained from *S. salar* were infected with *P. salmonis* at MOI of 10 bacteria/cell and treated with IgM-beads. The cytotoxicity was evaluated at 3, 5 and 7 dpi by the detection of LDH release into the extracellular medium. The statistical analysis was performed through a parametric ANOVA with a Tukey multiple comparison test. Significant differences: *p <0.05, **p < 0.01, ***p<0.001, **** p<0.0001.

REFERENCES

1. Fryer JL, Hedrick RP. Piscirickettsia salmonis: a Gram-negative intracellular bacterial pathogen of fish. *J Fish Dis* (2003) 26(5):251–62. doi: 10.1046/j.1365-2761.2003.00460.x
2. Rozas M, Enriquez R. Piscirickettsiosis and Piscirickettsia salmonis in fish: a review. *J Fish Dis* (2014) 37(3):163–88. doi: 10.1111/jfd.12211
3. Branson EJ, Nieto-Diaz Muñoz D. Description of a new disease condition occurring in farmed coho salmon, Oncorhynchus kisutch (Walbaum), in South America. *J Fish Dis* (1991) 14:147–56. doi: 10.1111/j.1365-2761.1991.tb00585.x
4. Cvitanich JD, O. Garate N, Smith CE. The isolation of a rickettsial-like organism causing disease and mortality in Chilean salmonids and its confirmation by Koch's postulate. *J Fish Dis* (1991) 14:121–45. doi: 10.1111/j.1365-2761.1991.tb00584.x

5. Aqua. *Sernapesca: "El SRS sigue siendo el mayor problema sanitario que enfrenta la salmonicultura"*. Editorial group Editec SpA (2012). Available at: http://www.aqua.cl/2012/11/23/sernapesca-el-srs-sigue-siendo-el-mayor-problema-sanitario-que-enfrenta-la-salmonicultura/#.
6. SERNAPESCA. *Informe Sanitario Acuícola año 2017*. Chile: Departamento de Salud Animal, Subdirección de Acuicultura, Servicio Nacional de Pesca y Acuicultura (2018).
7. Marshall SH, Conejeros P, Zahr M, Olivares J, Gómez FA, Cataldo P, et al. Immunological characterization of a bacterial protein isolated from salmonid fish naturally infected with Piscirickettsia salmonis. *Vaccine* (2007) 25 (11):2095–102. doi: 10.1016/j.vaccine.2006.11.035
8. SERNAPESCA. *Informe Sanitario Acuícola año 2012, Unidad de Salud Animal, Subdirección de Acuicultura, Servicio Nacional de Pesca y Acuicultura*. Chile: Servicio Nacional de Pesca y Acuicultura, Gobierno de Chile (2013).
9. SERNAPESCA. *Informe Sanitario Acuícola año 2018*. Chile: Departamento de Salud Animal, Subdirección de Acuicultura, Servicio Nacional de Pesca y Acuicultura (2019).
10. SERNAPESCA. Informe sobre uso de antimicrobianos en la salmonicultura nacional. In: D Animal, editor. *Sudirección de Acuicultura*. Valparaíso: National Fishing Service dependent on the Ministry of Economy, Development and Tourism of the Government of Chile (2019).
11. Maisey K, Montero R, Christodoulides M. Vaccines for piscirickettsiosis (salmonid rickettsial septicaemia, SRS): the Chile perspective. *Expert Rev Vaccines* (2017) 16(3):215–28. doi: 10.1080/14760584.2017.1244483
12. Figueroa J, Castro D, Lagos F, Cartes C, Isla A, Yáñez AJ, et al. Analysis of single nucleotide polymorphisms (SNPs) associated with antibiotic resistance genes in Chilean Piscirickettsia salmonis strains. *J Fish Dis* (2019) 42 (12):1645–55. doi: 10.1111/jfd.13089
13. Gomez FA, Tobar JA, Henríquez V, Sola M, Altamirano C, Marshall SH. Evidence of the presence of a functional Dot/Icm type IV-B secretion system in the fish bacterial pathogen Piscirickettsia salmonis. *PloS One* (2013) 8(1): e54934. doi: 10.1371/journal.pone.0054934
14. Rojas V, Galanti N, Bols NC, Marshall SH. Productive infection of Piscirickettsia salmonis in macrophages and monocyte-like cells from rainbow trout, a possible survival strategy. *J Cell Biochem* (2009) 108 (3):631–7. doi: 10.1002/jcb.22295
15. McCarthy UM, Bron JE, Brown L, Pourahmad F, Bricknell IR, Thompson KD, et al. Survival and replication of Piscirickettsia salmonis in rainbow trout head kidney macrophages. *Fish Shellfish Immunol* (2008) 25(5):477–84. doi: 10.1016/j.fsi.2008.07.005
16. Perez-Stuardo D, Morales-Reyes J, Tapia S, Ahumada DE, Espinoza A, Soto-Herrera V, et al. Non-lysosomal Activation in Macrophages of Atlantic Salmon (Salmo salar) After Infection With Piscirickettsia salmonis. *Front Immunol* (2019) 10:434. doi: 10.3389/fimmu.2019.00434
17. Álvarez CA, Gomez FA, Mercado L, Ramírez R, Marshall SH. Piscirickettsia salmonis Imbalances the Innate Immune Response to Succeed in a Productive Infection in a Salmonid Cell Line Model. *PloS One* (2016) 11(10):e0163943. doi: 10.1371/journal.pone.0163943
18. Roig J, Rello J. Legionnaires' disease: a rational approach to therapy. *J Antimicrob Chemother* (2003) 51(5):1119–29. doi: 10.1093/jac/dkg191
19. Joller N, Weber SS, Müller AJ, Spörri R, Selchow P, Sander P, et al. Antibodies protect against intracellular bacteria by Fc receptor-mediated lysosomal targeting. *Proc Natl Acad Sci U S A* (2010) 107(47):20441–6. doi: 10.1073/pnas.1013827107
20. Joller N, Weber SS, Oxenius A. Antibody-Fc receptor interactions in protection against intracellular pathogens. *Eur J Immunol* (2011) 41(4):889–97. doi: 10.1002/eji.201041340
21. Griffin BR. Opsonic effect of rainbow trout (Salmo gairdneri) antibody on phagocytosis of Yersinia ruckeri by trout leukocytes. *Dev Comp Immunol* (1983) 7(2):253–9. doi: 10.1016/0145-305X(83)90006-X
22. Kodama H, Yamada F, Murai T, Nakanishi Y, Mikami T, Izawa H. Response of rainbow trout immunized with formalin-killed Vibrio anguillarum: Activity of phagocytosis of fish macrophages and opsonising effect of antibody. *Fish Pathol* (1985) 20(2/3):395–402. doi: 10.3147/jsfp.20.395
23. Honda A, Kodama H, Moustafa M, Yamada F, Mikami T, Izawa H. Phagocytic activity of macrophages of rainbow trout against Vibrio anguillarum and the opsonising effect of antibody and complement. *Res Vet Sci* (1986) 40(3):328–32. doi: 10.1016/S0034-5288(18)30544-7
24. Sakai DK. Opsonization by fish antibody and complement in the immune phagocytosis by peritoneal exudate cells isolated from salmonid fishes. *J Fish Dis* (1984) 7(1):29–38. doi: 10.1111/j.1365-2761.1984.tb00904.x
25. O'Dowd AM, Ellis AE, Secombes CJ. Binding of soluble immune complexes to fractionated Atlantic salmon (Salmo salar L.) leucocytes. *Vet Immunol Immunopathol* (1999) 68(2-4):149–57. doi: 10.1016/S0165-2427(99)00018-5
26. O'Dowd AM, Ellis AE, Secombes CJ. Binding of immune complexes to Atlantic salmon peripheral blood leucocytes. *Dev Comp Immunol* (1998) 22 (4):439–48. doi: 10.1016/S0145-305X(98)00018-4
27. Arasteh N, Aminirissehei A-H, Yousif AN, Albright LJ, Durance TD. Passive immunization of rainbow trout (Oncorhynchus mykiss) with chicken egg yolk immunoglobulins (IgY). *Aquaculture* (2004) 231(1-4):23–36. doi: 10.1016/j.aquaculture.2003.11.004
28. LaFrentz BR, LaPatra SE, Jones GR, Cain KD. Passive immunization of rainbow trout, Oncorhynchus mykiss (Walbaum), against Flavobacterium psychrophilum, the causative agent of bacterial coldwater disease and rainbow trout fry syndrome. *J Fish Dis* (2003) 26(7):371–84. doi: 10.1046/j.1365-2761.2003.00468.x
29. Braun-Nesje R, Bertheussen K, Kaplan G, Seljelid R. Salmonid macrophages: separation, in vitro culture and characterization. *J Fish Dis* (1981) 4:141–51. doi: 10.1111/j.1365-2761.1981.tb01118.x
30. Fryer JL, Lannan CN, Giovannoni SJ, Wood ND. Piscirickettsia salmonis gen. nov., sp. nov., the causative agent of an epizootic disease in salmonid fishes. *Int J Syst Bacteriol* (1992) 42(1):120–6. doi: 10.1099/00207713-42-1-120
31. Henriquez M, González E, Marshall SH, Henríquez V, Gómez FA, Martínez I, et al. A novel liquid medium for the efficient growth of the salmonid pathogen Piscirickettsia salmonis and optimization of culture conditions. *PloS One* (2013) 8(9):e71830. doi: 10.1371/journal.pone.0071830
32. Wang MX, Cheng XY, Jin M, Cao YL, Yang YP, Wang JD, et al. TNF compromises lysosome acidification and reduces alpha-synuclein degradation via autophagy in dopaminergic cells. *Exp Neurol* (2015) 271:112–21. doi: 10.1016/j.expneurol.2015.05.008
33. DeLuca D, Wilson M, Warr GW. Lymphocyte heterogeneity in the trout, Salmo gairdneri, defined with monoclonal antibodies to IgM. *Eur J Immunol* (1983) 13(7):546–51. doi: 10.1002/eji.1830130706
34. Schindelin J, Arganda-Carreras I, Frise E, Kaynig V, Longair M, Pietzsch T, et al. Fiji: an open-source platform for biological-image analysis. *Nat Methods* (2012) 9(7):676–82. doi: 10.1038/nmeth.2019
35. Marwaha R, Sharma M. DQ-Red BSA Trafficking Assay in Cultured Cells to Assess Cargo Delivery to Lysosomes. *Bio Protoc* (2017) 7(19):e2571. doi: 10.21769/BioProtoc.2571
36. Frost LS, Dhingra A, Reyes-Reveles J, Boesze-Battaglia K. The Use of DQ-BSA to Monitor the Turnover of Autophagy-Associated Cargo. *Methods Enzymol* (2017) 587:43–54. doi: 10.1016/bs.mie.2016.09.052
37. Russell DG, Vanderven BC, Glennie S, Mwandumba H, Heyderman RS. The macrophage marches on its phagosome: dynamic assays of phagosome function. *Nat Rev Immunol* (2009) 9(8):594–600. doi: 10.1038/nri2591
38. Mikalsen J, Skjaervik O, Wiik-Nielsen J, Wasmuth MA, Colquhoun DJ. Agar culture of Piscirickettsia salmonis, a serious pathogen of farmed salmonid and marine fish. *FEMS Microbiol Lett* (2008) 278(1):43–7. doi: 10.1111/j.1574-6968.2007.00977.x
39. Karatas S, Mikalsen J, Steinum TM, Taksdal T, Bordevik M, Colquhoun DJ. Real time PCR detection of Piscirickettsia salmonis from formalin-fixed paraffin-embedded tissues. *J Fish Dis* (2008) 31(10):747–53. doi: 10.1111/j.1365-2761.2008.00948.x
40. Dannevig BH, Brudeseth BE, GjØen T, Rode M, Wergeland HI, Evensen Ø, et al. Characterisation of a long-term cell line (SHK-1) developed from the head kidney of Atlantic salmon (Salmo salar L.). *Fish Shellffish Immunol* (1997) 7:213–26. doi: 10.1006/fsim.1996.0076
41. Casadevall A, Scharff MD. Serum therapy revisited: animal models of infection and development of passive antibody therapy. *Antimicrob Agents Chemother* (1994) 38(8):1695–702. doi: 10.1128/AAC.38.8.1695
42. Aizenshtein E, Pinchasov Y, Morag E, Leitner G, Shpanir Y, Reimond D, et al. Immunological complex for enhancement of innate immune response in passive vaccination. *Vaccine* (2013) 31(4):626–31. doi: 10.1016/j.vaccine.2012.11.058
43. Herrada AA, Contreras FJ, Tobar JA, Pacheco R, Kalergis AM. Immune complex-induced enhancement of bacterial antigen presentation requires

Fcgamma receptor III expression on dendritic cells. *Proc Natl Acad Sci U S A* (2007) 104(33):13402–7. doi: 10.1073/pnas.0700999104
44. Casadevall A, Dadachova E, Pirofski LA. Passive antibody therapy for infectious diseases. *Nat Rev Microbiol* (2004) 2(9):695–703. doi: 10.1038/nrmicro974
45. Nimmerjahn F, Ravetch JV. Antibody-mediated modulation of immune responses. *Immunol Rev* (2010) 236:265–75. doi: 10.1111/j.1600-065X.2010.00910.x
46. Pincetic A, Bournazos S, DiLillo DJ, Maamary J, Wang TT, Dahan R, et al. Type I and type II Fc receptors regulate innate and adaptive immunity. *Nat Immunol* (2014) 15(8):707–16. doi: 10.1038/ni.2939
47. Lee SB, Mine Y, Stevenson RM. Effects of hen egg yolk immunoglobulin in passive protection of rainbow trout against Yersinia ruckeri. *J Agric Food Chem* (2000) 48(1):110–5. doi: 10.1021/jf9906073
48. Rojas V, Galanti N, Bols NC, Jiménez V, Paredes R, Marshall SH. Piscirickettsia salmonis induces apoptosis in macrophages and monocyte-like cells from rainbow trout. *J Cell Biochem* (2010) 110(2):468–76. doi: 10.1002/jcb.22560
49. Fryer JL, Lannan CN, Garcés LH, Larenas JJ, Smith PA. Isolation of a Rickettsiales-Like Organism from Diseased Coho Salmon (Oncorhynchus kisutch)in Chile. *Fish Pathol* (1990) 25(2):107–14. doi: 10.3147/jsfp.25.107
50. Yanez AJ, Valenzuela K, Silva H, Retamales J, Romero A, Enriquez R, et al. Broth medium for the successful culture of the fish pathogen Piscirickettsia salmonis. *Dis Aquat Organ* (2012) 97(3):197–205. doi: 10.3354/dao02403
51. Smith PA, Díaz FE, Rojas ME, Díaz S, Galleguillos M, Carbonero A. Effect of Piscirickettsia salmonis inoculation on the ASK continuous cell line. *J Fish Dis* (2015) 38(3):321–4. doi: 10.1111/jfd.12248
52. Ramirez R, Gomez FA, Marshall SH. The infection process of Piscirickettsia salmonis in fish macrophages is dependent upon interaction with host-cell clathrin and actin. *FEMS Microbiol Lett* (2015) 362(1):1–8. doi: 10.1093/femsle/fnu012
53. Oliver C, Sánchez P, Valenzuela K, Hernández M, Pontigo JP, Rauch MC. Subcellular Location of Piscirickettsia salmonis Heat Shock Protein 60 (Hsp60) Chaperone by Using Immunogold Labeling and Proteomic Analysis. *Microorganisms* (2020) 8(1):117. doi: 10.3390/microorganisms8010117
54. Hernandez AJ, Romero A, Gonzalez-Stegmaier R, Dantagnan P. The effects of supplemented diets with a phytopharmaceutical preparation from herbal and macroalgal origin on disease resistance in rainbow trout against Piscirickettsia salmonis. *Aquaculture* (2015) 454(1):109–17. doi: 10.1016/j.aquaculture.2015.12.016
55. Mickuviene I, Kirveliene V, Juodka B. Experimental survey of non-clonogenic viability assays for adherent cells in vitro. *Toxicol Vitro* (2004) 18(5):639–48. doi: 10.1016/j.tiv.2004.02.001
56. Butler RE, Brodin P, Jang J, Jang MS, Robertson BD, Gicquel B, et al. The balance of apoptotic and necrotic cell death in Mycobacterium tuberculosis infected macrophages is not dependent on bacterial virulence. *PloS One* (2012) 7(10):e47573. doi: 10.1371/journal.pone.0047573
57. Yanez AJ, Silva H, Valenzuela K, Pontigo JP, Godoy M, Troncoso J, et al. Two novel blood-free solid media for the culture of the salmonid pathogen Piscirickettsia salmonis. *J Fish Dis* (2013) 36(6):587–91. doi: 10.1111/jfd.12034
58. Kumar Y, Valdivia RH. Leading a sheltered life: intracellular pathogens and maintenance of vacuolar compartments. *Cell Host Microbe* (2009) 5(6):593–601. doi: 10.1016/j.chom.2009.05.014
59. Elkin SR, Lakoduk AM, Schmid SL. Endocytic pathways and endosomal trafficking: a primer. *Wien Med Wochenschr* (2016) 166(7-8):196–204. doi: 10.1007/s10354-016-0432-7
60. Wang R, Zhang Y, Liu S, Li C, Sun L, Bao L, et al. Analysis of 52 Rab GTPases from channel catfish and their involvement in immune responses after bacterial infections. *Dev Comp Immunol* (2014) 45(1):21–34. doi: 10.1016/j.dci.2014.01.026
61. Nepal A, Wolfson DL, Ahluwalia BS, Jensen I, Jørgensen J, Iliev DB. Intracellular distribution and transcriptional regulation of Atlantic salmon (Salmo salar) Rab5c, 7a and 27a homologs by immune stimuli. *Fish Shellfish Immunol* (2020) 99:119–29. doi: 10.1016/j.fsi.2020.01.058

Conflict of Interest: ST, JM-R, CB, AS and ES were employed by Ictio Biotechnologies S.A.

The remaining authors declare that the research was conducted in the absence of any commercial or financial relationships that could be construed as a potential conflict of interest.

Advantages of publishing in Frontiers

OPEN ACCESS
Articles are free to read for greatest visibility and readership

FAST PUBLICATION
Around 90 days from submission to decision

HIGH QUALITY PEER-REVIEW
Rigorous, collaborative, and constructive peer-review

TRANSPARENT PEER-REVIEW
Editors and reviewers acknowledged by name on published articles

Frontiers
Avenue du Tribunal-Fédéral 34
1005 Lausanne | Switzerland

Visit us: www.frontiersin.org
Contact us: frontiersin.org/about/contact

REPRODUCIBILITY OF RESEARCH
Support open data and methods to enhance research reproducibility

DIGITAL PUBLISHING
Articles designed for optimal readership across devices

FOLLOW US
@frontiersin

IMPACT METRICS
Advanced article metrics track visibility across digital media

EXTENSIVE PROMOTION
Marketing and promotion of impactful research

LOOP RESEARCH NETWORK
Our network increases your article's readership